OXIDATION OF RICE HUSK, PALM FIBRE AND PALM FIBRE CHAR

A thesis submitted in total fulfilment of the requirements

of the degree of Doctor of Philosophy

by

Azil Bahari ALIAS ALES

DEPARTMENT OF CHEMICAL AND BIOMOLECULAR ENGINEERING

UNIVERSITY OF MELBOURNE

AUSTRALIA

OCTOBER, 2012

ABSTRACT

The selection and design of any biomass combustion system is primarily determined by the combustion characteristics of the fuel. It is the thermal energy released by the combustion reactions which drives the entire process. Thus, understanding of the combustion characteristics or oxidation behaviour of the biomass may lead to successful biomass combustion process at larger scale.

This study investigates the oxidation of rice husk, palm fibre and palm fibre char using an evolved gas analysis (EGA) technique. This EGA technique involves heating the biomass and char from 100°C to 500°C at a controlled rate with a constant flow of air. The evolved gas was continually analysed for its oxygen, carbon monoxide and carbon dioxide contents. A series of EGA experiments was carried out using rice husk, palm fibre and palm fibre char. By studying how the evolved gas composition varies with temperature, the many oxidation reactions occurring may be grouped into just three simultaneous and competing reaction regimes known as low, medium and high temperature oxidation. The different reaction regimes may be decoupled and the key kinetic parameters such as activation energy for each regime were determined. These not only demonstrated the potential of the EGA technique as a tool to study the biomass oxidation but also provide insights into the effects of variations in pressure, oxygen partial pressure and heating rate for both of the biomass and biomass char.

The oxidation behaviour of both the rice husk and palm fibre was found to be substantially different to that observed for the palm fibre char. The principle difference observed was the number of peaks present in a plot of oxygen consumption versus temperature - two peaks were formed for the both of biomass but EGA experiments consistently shows only one peak for palm fibre char. It was found that the oxygen partial pressure of the oxidising gas in the combustion cell significantly influences the oxidation behaviour. Increasing the partial pressure of the oxygen typically moved the reactions to lower temperatures. The activation energies and peak oxygen consumption temperatures were all found to be linear functions of the oxygen partial pressure of the

gas supplied to the reactor. varying the total pressure of the reaction vessel while keeping the oxygen partial pressure constant did not lead to any significant variations in the reactions parameters.

CANDIDATE'S DECLARATION

This is to declare that this thesis does not exceed 100,000 words in length, exclusive of tables, references and appendices. This thesis comprises the original work towards the degree except where indicated in the preface and due acknowledgment has been made in the text to all other material used.

Azil Bahari ALIAS ALES

ACKNOWLEDGEMENT

First and foremost I offer my sincerest gratitude to my supervisors, Associate Professor David Shallcross and Professor Sharifah Aishah who have supported throughout my thesis with their immense knowledge, guidance, motivation and enthusiasm throughout the project.

I warmly thank Mr. K. Smeaton and the workshop staff for their expert advice and skilful workmanship in the maintenance of the experimental equipment. Dr. Sharif Abdul Bari Ali who helped me in the modelling software. Mr. Mohd Jindra Aris who taught me the biomass chemical reaction.

I would like to thank The Ministry of Higher Education, Malaysia and Universiti Teknologi MARA, Shah Alam, Selangor, Malaysia for funding my study.

I would also like to thank The University of Melbourne, particularly Department of Chemical and Biomolecular Engineering for important support throughout this work.

My sincere thanks are due to my colleagues for their discussions and friendship throughout my study

Last but not least, I wish to express my warm and sincere gratitude and dedicate this thesis to my parents (Alias and Hasnah), my wife (Wan Azlina) and our three precious jewels, Faris Erhan, Fahmiey Erhan and Faerell Erhan for their support, sacrifice and encouragement over the years.

Azil Bahari Alias Ales

October, 2012

TABLE OF CONTENTS

Page

LIST OF TABLES

LIST OF FIGURES

NOMENCLATURE

Symbol

A	Cross-sectional area of packed bed
a	Variable defined by equation (4.18)
a_1,a_2,a_3,a_4	Approximation constant of the exponential integral of the first kind as used in equation (4.36)
b_1,b_2,b_3,b_4	Approximation constant of the exponential integral of the first kind as used in equation (4.36)
C_f	Fuel concentration
DTG	Derivative thermogravimetric
E	Activation energy
EFB	Empty fruit bunches
EGA	Evolved gas analysis
HTO	High Temperature Oxidation
I_1	Exponential integral of the first kind as defined in equation (4.35)
I_{LTO}	Total integral under low temperature oxidation curve with respect to time
k	Reaction constant
L	Length of packed bed
LTO	Low temperature oxidation
m	Number of data points used in equation (4.15)
MTO	Medium Temperature Oxidation
MTOE	Million tonnes of oil equivalent
n	Reaction order with respect to fuel concentration
P	Pressure
P_{O_2}	Oxygen partial pressure
PKS	Palm kernel shell
q	Volumetric flow rate of the injected gas

R	Universal gas constant
RDF	Refuse derived fuel
R_r	Reaction rate
Rrr	Relative reaction rate
T	Absolute temperature
t	Time
TGA	Thermogravimetric analysis
T_{max}	Peak temperature
u	Simplify notation defined by equation (4.32)
V	Volume
w	Pre-Arrhenius constant
x,y,z	Chemical formula used in equation (4.1)

Greek Symbol

α	Proportionality factor
β	A lumped group parameter which includes the pre-Arrhenius constant defined in equation (4.11)
δ	Uncertainty
ε	Error term defined in equation (4.36)
Θ	Expression of temperature as a function of time in equation (4.30)
σ^2	Variance
χ	Simplify notation defined in equation (4.26)
ψ	Expression of temperature as a function of time in equation (4.29)
ΔO_2	Difference in oxygen concentration between the inlet and outlet gases

Subscripts

i	Reaction regimes (HTO, MTO, LTO)
j	Numbering of data points

Superscripts

m	Reaction order with respect to oxygen partial pressure
n	Reaction order with respect to fuel concentration

CHAPTER 1

INTRODUCTION

1.1 Overview

Depletion of fossil fuel and tighter environmental regulations have forced the world to consider adopting alternative renewable fuel sources such as solar, hydro, wind and biomass (Guan, 2003). The energy and oil crisis worldwide will increase demand for renewable energy resources for power and transportation into the future. Hence, due to current demands for fuel and with recent developments in the energy sector, alternative renewable fuels such as biomass must be recognised as an important energy source for the foreseeable future.

Biomass may broadly be defined as being organic material that has stored sunlight in the form of chemical energy. Biomass is largely produced by plants converting sunlight into plant material through photosynthesis. The use of biomass fuels provides substantial benefits as far as the environment is concerned. Biomass absorbs carbon dioxide during growth, and emits it during combustion. Therefore, biomass helps the atmospheric carbon dioxide recycling and does not make a net contribution to the greenhouse effect. This is because biomass consumes the same amount of carbon dioxide from the atmosphere during growth as is released during combustion (i.e. biomass is considered a carbon dioxide neutral fuel). Further, biomass is also considered a sustainable renewable energy source that may be used to meet a significant proportion of the energy demand in the future.

It is an environmentally-friendly renewable energy sources. Its use has a lower impact on the environment than fossil fuel sources and reduces the amount of waste required to be sent to landfills (Gokcol *et al.*, 2009).

Palm oil wastes (empty fruit bunch, fibre and palm oil shell) are the main biomass resources in ASEAN countries. In Malaysia, the second largest palm oil producing country in the world, 30 million tonnes of palm oil wastes were generated in the year 2000 with the rate of palm oil waste production increasing rapidly due to the expansion of the food and manufacturing industries (Yang *et al.*, 2006). As of the year 2012, approximately 368 palm oil mills operate in the country, which produced substantial amount of biomass waste in the form of fibre, empty fruit bunches and palm kernel shell. It was estimated that the amount of biomass waste produced may reach 39 million tonnes by the year 2020 (Yusoff, 2006). In order to treat this tremendous amount of waste, novel technologies with improved efficiencies and reduced environmental impacts need to be established in the future. At present, most Malaysian oil palm waste is disposed by means of open burning which contribute significantly to waste management issues. They have also been used as mulching around the plants so as to prevent excessive evaporation or erosion, producing medium density fibre board in furniture and used as material for mattresses, seats, insulation and paper making industries (Chuah *et al.*, 2006 and Kelly-Yong *et al.*, 2007). Oil palm biomasses are highly potential materials for energy resources. That they are renewable and abundantly available are amongst the attractive reasons of employing them as the major source for renewable energy (Yusoff, 2006). In practice, about half of the agricultural residues are consumed for energy generation. This amount contributes to about 20% of the primary energy demand of industries in Malaysia. It is estimated that by year 2050 biomass may provide nearly 38% of the world's direct fuel use and 17% of the world's electricity (Idris *et al.*, 2010).

Combustion technologies produce about ninety percent of their energy from biomass. the biomass fuels are convert into several forms of useful energy including hot air, hot water, steam and electricity. Commercial and industrial combustion plants may burn many types of biomass ranging from woody biomass to municipal solid wastes.

Biomass combustion facilities that generate electricity from steam-driven turbine generators have conversion efficiencies of between 17 and 25%. The selection and design of any biomass combustion system is primarily determined by the combustion characteristics of the fuel, the environmental constraints, and the cost of equipment and the size of the plant (Gokcol *et al.*, 2009).

To date no significant work has been conducted to study in detail the combustion characteristics of rice husk, palm fibre and palm fibre char using an evolved gas analysis (EGA) technique. By studying how the evolved gas composition varies with temperature, the many oxidation reactions occurring may be grouped into three simultaneous and competing reaction regimes known as high, medium and low temperature oxidation. The different reaction regimes may be decoupled and the key kinetic parameters for each regime determined. This research is important as knowledge associated with such kinetics gives insight into the viability of these biomass and biomass char to be utilised as energy resources.

1.2 Research scope

This research focuses on the combustion characteristics of the rice husk, palm fibre and palm fibre char using an evolved gas analysis (EGA) experiments. A three regime model was used to decouple the oxygen consumption data into its component contributing reactions: low, medium and high temperature oxidations. The effect of the oxidation kinetics of variables such as pressure and heating rate are examined. The outcomes of the research will be useful in subsequent biomass and biomass char combustion reactor design studies.

1.3 Research objectives

1) To improve the understanding of the combustion characteristics of rice husk, palm fibre and palm fibre char using an evolved gas analysis (EGA) experiments over a range of operating conditions (i.e. pressure, heating rate and oxygen partial pressure).

2) To validate the novel model predictions using the experimental results of the oxygen consumption under different operating conditions such as heating rate and pressure for rice husk, palm fibre and palm fibre char.

3) To compare the experimental results and the calculated kinetic parameters of the reaction order, the activation energy (E/R) and the natural log of beta group, ln β for the rice husk, the palm fibre and the palm fibre char.

1.4 Thesis outline

Chapter 2 reviews the literature of the biomass and biomass char combustion processes and the experimental techniques used to study the combustion characteristics. Descriptions of the materials, the experimental apparatus and the operating procedure are then presented in Chapter 3. Chapter 4 presents the development of the theoretical model. This model is based on the assumption that the oxidation kinetics may be described by a number of overlapping and competing reaction regimes known as high, medium and low temperature oxidation. The reaction regimes may be decoupled and the key kinetic parameters of the reaction order, the activation energy and the natural log of beta group for each regime may be calculated. This model is relating to crude oil combustion but with several modifications before being implemented to biomass and biomass char studies. The major modification proposed in this study allows the low temperature oxidation (LTO) and medium temperature oxidation (MTO) reactions to be solved simultaneously.

Results of the experimental work are discussed in Chapters 5 to 7. Chapter 5 presents the results of the study with rice husk. Chapters 6 and 7 present the EGA works using palm fibre and palm fibre char, respectively. The accuracy and the reproducibility of the experimental data and the calculated kinetic parameters are also examined in Chapters 5 to 7.

Further, the effect of varying the heating rate and pressure on the EGA experimental results and the calculated kinetic parameters will be also be examined. Chapter 8 presents a comparison study of the rice husk, the palm fibre and the palm fibre char. Finally in Chapter 9, the conclusions that may be drawn from this study are presented. Recommendations are also given for further reseach.

CHAPTER 2

LITERATURE REVIEW

2.1 Biomass

In general, any organic fuel derived from growing plants or animal manure may be considered as biomass (Sami *et al.,* 2001). It is the term for all organic materials that originates from the natural waste products (e.g. saw dust, wood chips, corn husks, sewage sludge) and dedicated energy crops (e.g. short rotation woody and herbaceous crops). The main components of biomass are cellulose, hemicellulose, lignin, extractives, lipids, proteins, simple sugars, starches, water and ash (Mansaray and Ghaly, 1998). The polymers of the hemicellulose, cellulose and lignin as displayed in Figure 2.1 that constitute of the macromolecular structure of the biomass and other woody materials, are linked together with relatively weak ether bonds (R-O-R, bond energy of 380-420 kJ/mol).

These bonds are less resistant to heat at intermediate temperatures of 400°C to 500°C (Blazej *et al.*, 1993). Biomass properties differ in many important ways to coal, including the organic, inorganic and energy content and the physical properties. Normally, biomass has less carbon, more oxygen, more silica and potassium, less aluminum and iron, lower heating value, higher moisture content, lower density and friability in comparison to coal (Tewfik, 2004).

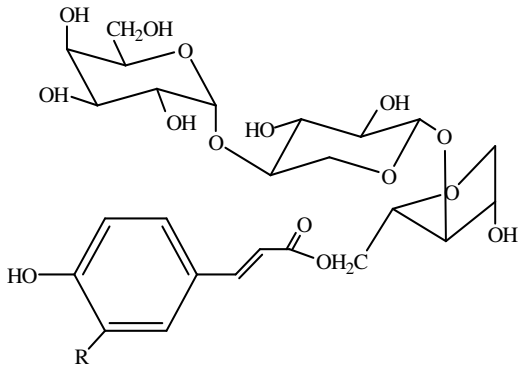

(a)

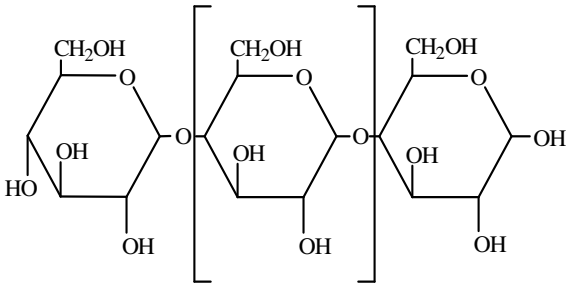

(b)

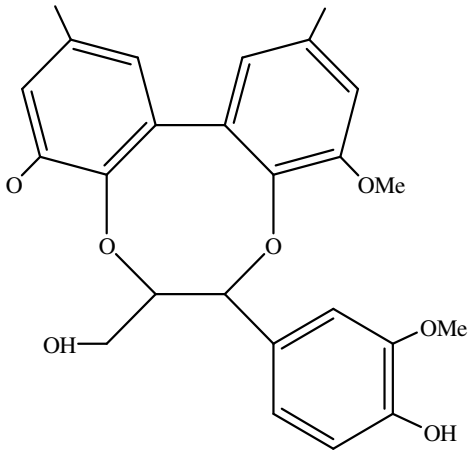

(c)

Figure 2.1 - Chemical structures of (a) hemicellulose, (b) cellulose and (c) lignin (Blazej *et al.*, 1993).

Biomass is an alternative energy source and currently provides approximately 14% of the world's total energy, predominantly in developing countries. The process of liberating biomass energy through combustion is non-polluting and offers significant protection for the environment as it is carbon neutral. This is because the carbon emitted to the atmosphere is equal to the carbon taken in by the biomass plant during the photosynthesis. Furthermore, biomass offers important advantages as a combustion feedstock because of the high volatility and reactivity during conversion. In combustion applications, biomass has been fired directly, either alone or along with a primary fuel, where the co-firing with coal has been found to be a promising method in the near future (Demirbas, 2005).

In Malaysia, biomass may be a very promising alternative source of renewable energy. The government of Malaysia has embarked on this ideology by drafting a fuel policy that states "To supplement the conventional energy supply, new sources such as renewable energy will be encouraged and biomass such as oil palm, wood waste as well as rice husk will be used on the wider basis" (Shuit *et al.*, 2009). Figure 2.2 shows the energy demand in Malaysia that foresees a rapid increase in demand. As may be seen in Figure 2.2, energy demand in Malaysia is expected to reach almost 100 million tonnes of oil equivalent (MTOE) in 2030. In order to meet the increasing demand of energy and to reduce emission of carbon dioxide while ensuring energy security, Malaysia needs to have an effective and sustainable source of energy. Although the use of renewable energy as an alternative energy source is growing rapidly to date it provides only 3% of the world's primary energy consumption.

Table 2.1 shows that based on the 2005 data, about 93% of Malaysian energy consumption depended heavily on the fossil fuels such as natural gas, coal diesel and oil, with only 0.5% of energy came from the renewable sources such as biomass (excluding hydropower).

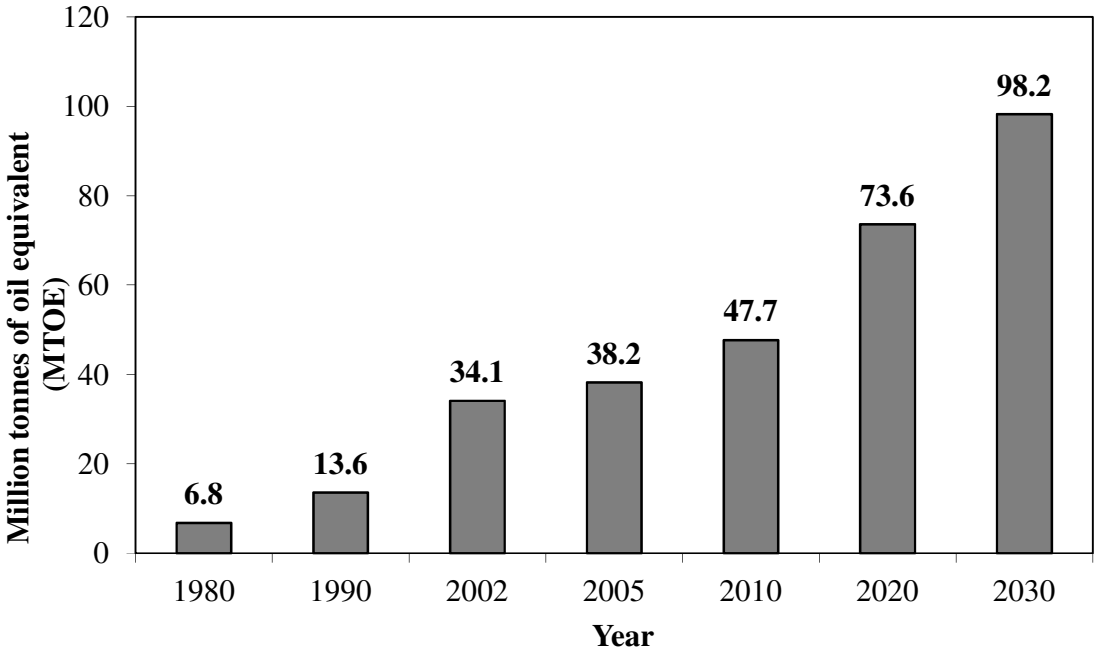

Figure 2.2 - Historical and projected energy demand in Malaysia (Shuit *et al.*, 2009).

Table 2.1 - Malaysia's energy mix in year 2005 (Shuit *et al.*, 2009).

Source	Percentage (%)
Gas	72.5
Coal	16.5
Hydropower	6.2
Diesel	3.2
Oil	0.8
Biomass	0.5
Others	0.3

If this trend was to continue Malaysia would suffer from a lack of energy security as Malaysian fossil fuel reserves are predicted to last only for another 30 to 40 years. Beyond that, Malaysia will become a net importer of fossil fuel. Therefore, it is inevitable that the Malaysian government has to start looking for reliable sources of renewable energy urgently (Shuit, *et al.*, 2009).

2.1.1 Rice husks

Rice husk is a major agricultural waste, constituting to about 20% of total agricultural waste (Shackley *et al*., 2012). The world annual production of the rice husk amounts to more than 120 million tonnes. The rice husk is the outer cover of the rice grain and is in the form of hull. It is also called rice hull or paddy husk/hull. It accounts for 14% to 35% of the weight of the paddy harvested depending on the paddy variety. In general, the rice husk has a low energy density and high ash content, and silica accounts for 95% of the elements in the rice husk ash. The rice husk heating value is about one-third that of furnace oil, one-half that of good quality coal and comparable with that of the sawdust, low rank coal and peat (Natarajan *et al.,* 1998). Rice husk is also renewable in nature and has low sulphur and heavy metal contents. Currently rice husk wastes are widely used as mats, compost and fillers.

Due to the increasing demands for the utilisation of waste to energy, many researchers are actively involved in researching ways to use the rice husk as fuel. Presently the average annual production of rice husk of about 471 000 tonnes is sufficient to provide fuel to generate electric power of 72MW (Armesto *et al.*, 2002). Rice husks typically have heating values in between 15MJ/kg and 17MJ/kg, a volatile matter content in the range of 60% to 80% and ash content approximately 13% to 18%. These parameters influence the combustion characteristics of the fuel. Rice husks are easier to ignite and to burn than coal due to the high volatile matter, although their combustion is expected to be more rapid and difficult to control (Armesto *et al.*, 2002). These characteristics indicate that the rice husk could be a good fuel.

2.1.2 Oil palm and oil palm biomass

Oil palm, also known as *Elaeis guineensis*, is the most important species in *Elaeis genus* which belongs to the family of *Palmae*. Figure 2.3 presents the world's oil production in the 2007. As may be seen in Figure 2.3, palm oil which is generated from the oil palm tree has now become the world's largest source of edible oil with 38.5 million tones or 25% of the world total edible oil and fat production. Thus, oil palm has now become a major economic crop which has triggered expansion of the plantation areas in Malaysia and Indonesia. In 2009, Malaysia was the second largest producer of palm oil with 43% of the total world supply (Shuit *et al.*, 2009).

The oil palm industry currently produces the largest amount of biomass in Malaysia with 85.5% out of more than 70 million tonnes. Other types of biomass generated in Malaysia are from the wood, sugarcane industry and municipal solid waste (Shuit *et al.*, 2009). In 2010, over 83 million tonnes of the oil palm biomass was produced (Kheang *et al.*, 2012). Types of biomass produced by the oil palm industry includes the empty fruit bunches (EFB), the mesocarp fibre (palm fibre), the palm kernel shell (PKS), oil palm fronds (OPF) and oil palm trunks (OPT). These biomasses may be used to produce steam for the process industries and for electricity generation. Of the 83 million tonnes of the oil palm biomass produced in 2010, the estimated oil palm biomass generated comprised:

- 21.8 million tonnes of oil palm fronds
- 6.4 million tonnes of empty fruit bunches
- 10.6 million tonnes of palm fibre and palm kernel shell

It has long been envisaged that renewable energy from oil palm biomass could be one of the most beneficial approaches in overall environmental improvement to sustain the palm oil industry. Their potential energy available for power generation is summarised in Table 2.2.

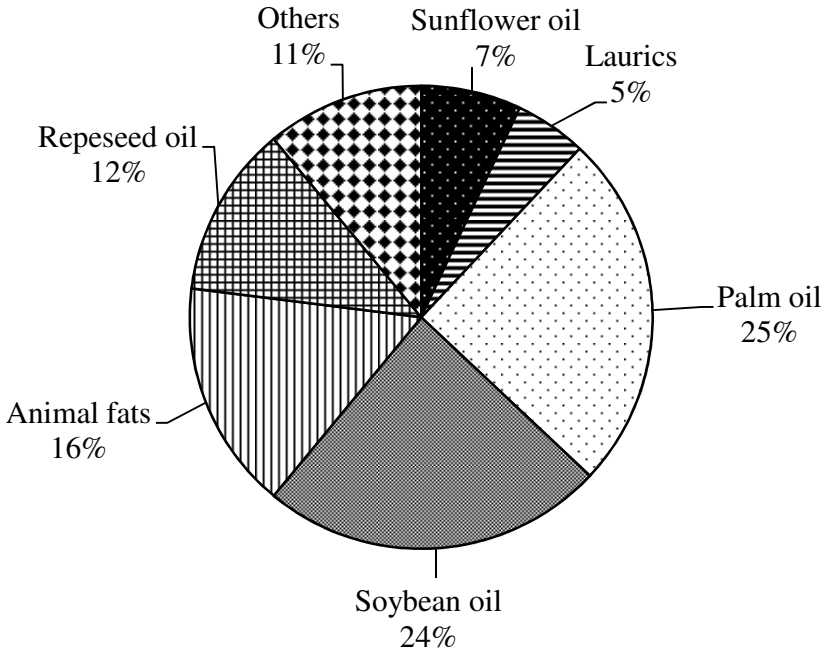

Figure 2.3 - World's non-petroleum oil production in the year 2007 (Shuit et *al.*, 2009).

Table 2.2 - Potential renewable energy from oil palm biomass. Mtoe is million tonnes of oil equivalent. Figures based on 83.1 million tonnes of oil palm biomass generated (Kheang *et al.*, 2012).

Source	**Energy sector**	**Total potential quantity for renewable energy generation**
Empty fruit bunches (EFB)	Electricity for industrial sector	6.4 million tonnes (dry basis) 2.7 Mtoe
Shell and fibre	Electricity for industrial sector	10.6 million tonnes (dry basis) 4.8 Mtoe
Fronds and trunks	Electricity for industrial sector	10.2 million tonnes (dry basis) 3.5 Mtoe
Total		**11 Mtoe**

The easily accessible oil palm biomass in Malaysia totaling around 27.2 million tonnes on a dry weight basis could produce an estimated 11 million tonnes of oil equivalent (see Table 2.3).

Typically palm fibre is characterised by high volatility (76%) and moisture (40%) but low ash content (5.8%). Further, the carbon content and heating values are considerable being 50wt% and 19.0MJ/kg, respectively (Kheang *et al.*, 2012). Oil palm biomass contains about 18% to 21% lignin and 65% to 80% hemicellulose and cellulose (Wahid *et al.*, 2009). These values indicate that the palm fibre has potential as a fuel.

2.1.3 Biomass char

Biomass char is a carbon-rich, fine-grained and porous substance obtained when biomass is heated or naturally burned under oxygen-limited condition and at relatively low temperatures of (<700°C) (Sohi *et al.*, 2010). Biomass char is considered a promising renewable resources that may be utilised in many applications. It has been reported by Kastanaki *et al.* (2006) that biomass char obtained after partial devolatilization are more reactive than those obtained from coal. It has a porous and highly disordered carbon structure and belongs to the class of most reactive carbon materials. The porosity within the biomass char increases the accessibility of the reactive gas to active sites resulting in the very good combustion reactivity (Sahu *et al.*, 2010).

The quality of the biomass char produced mainly depends upon the origin of the biomass feedstock. The biomass feedstock currently used at a commercial scale or at research facilities include wood chip and wood pellets, tree bark, crop residues (including straw, nut shell and rice husk), switch grass, organic wastes including distillers grain, bagasse from sugarcane industry and olive waste (Yaman, 2004), chicken litter (Das *et al.*, 2008), dairy manure, sewage sludge (Shinogi *et al*., 2002) and paper sludge. In Malaysia, more than two million tonnes of agricultural wastes are produced annually and potentially an attractive feedstock for producing energy as its use contributes little or no nett carbon dioxide to the

atmosphere. Major agricultural products are of the palm-based industries. There are significant amounts of wastes and residues also known as agricultural wastes or residues produced from the post-processing of these products (Ghani *et al.*, 2011).

There are various technologies available to produce biomass char from the raw biomass such as pyrolysis, carbonisation and gasification. However, pyrolysis which consists of the thermal decomposition in the absence of oxygen, is the most preferable technique due to the low cost and the high biomass char yield. The pyrolysis process converts biomass into solid biomass char, liquid bio-oil and combustible gas product. The solid biomass char product comprising of carbon and ash may be a potential absorbent material for catalyst or fertiliser support (Boateng *et al.*, 2007). Furthermore, biomass char may be used as a field fertiliser to improve soil physical and biological properties. Also due to its high stability, it may be considered for carbon sequestration with consequent removal of carbon from the atmosphere (Xu *et al.*, 2011). In addition, due to its low sulphur and phosphorus contents, as well as its structural and reactivity properties, the solid biomass char product can be used in the chemical, pharmaceutical and food industries. The co-product liquid bio-oil and gases, have a high energy content and can be combusted to thermally sustain the endothermic pyrolysis process.

A number of workers have reported on biomass char production from various biomass using a pyrolysis process. Among them are Purevsuren *et al.* (2003), Cao *et al.* (2009), Brown *et al.* (2006), Masek, *et al.* (2011) and Xu *et al.* (2011). Slow pyrolysis is characterised by moderate heating rates in the range of about 20°C/min to 100°C/min. Maximum temperatures of 600°C give an approximately equal distribution of oils, char and gasses because the residence times of vapors is long enough that most of the biomass is cracked (Brown *et al.*, 2006). Table 2.3 summarises the product distribution of the pyrolysis process. Other important criteria are the proportions of hemicellulose, cellulose and lignin content of the feedstock which will determined the ratios of volatile carbon (bio-oil and fuel gas) and stabilised carbon (biomass char) in the pyrolysis products.

Table 2.3 - Products distribution of the pyrolysis process (Ghani *et al.*, 2011).

Process	Liquid (Bio-oil)	Solid (Biomass char)	Gas (syngas)
Fast pyrolysis Moderate temperature (~500°C) Short vapour residence time (<2 seconds) Fast heating rates (>2°Cs^{-1})	75% (25% water)	10%	15%
Slow pyrolysis Low-moderate temperature (400-650°C) Long vapour residence times (>5 seconds) Low heating rates (0.01-2°Cs^{-1})	30% (70% water)	35%	35%
Gasification High temperature (>800°C) Long vapour residence time	5% tar (5% water)	10%	85%

Table 2.4 - Chemical composition of oil palm biomass (% dry matter) (Yang *et al.*, 2004 and Wan Rosli *et al.*, 2004).

Components	Empty fruit bunch	Shell	Frond	Fibre	Trunk
Cellulose	62.9	31.8	30.4	33.9	34.5
Hemicellulose	28	22.7	40.4	26.1	31.8
Lignin	36.6	22.1	21.7	27.7	25.7

Table 2.4 indicates the chemical composition of the oil palm biomass in percents of dry matter. Feedstock with high lignin content produce the highest biomass char yield when pyrolysed at moderate temperatures (~500°C) (Dermibas, 2004).

Demirbas (2004) studied the effects of temperature and particle size on the biomass char yield from the pyrolysis of the agricultural residues of olive husk, corncob and tea waste. The reactor was a cylindrical vessel of height 95.1mm, internal diameter of 17.0mm, and outside diameter of 19.0mm. The reactor was heated externally by an electric furnace with the temperature being controlled by a thermocouple inside the reactor. The samples were subjected to pyrolyse for obtaining biomass chars at high temperatures of 450K to 1250K in a cylindrical batch reactor. The pyrolysis process was carried out at 10K/s heating rate for obtaining the biomass char products from the samples at different temperatures: 470K, 550K, 650K, 750K, 850K, 950K and 1050K. He found that the biomass char yield increased with increasing sample particle sizes. For a high biomass char production, a low temperature between 750K and 850K and a low heating rate process would be chosen.

Masek *et al.,* (2011) studied the influence of the production conditions on the yield and environmental stability of biomass char using a pyrolysis process. The raw materials used were pine wood chips, mixed larch and spruce wood chips and softwood pellets. The pyrolysis apparatus used was a fixed bed reactor comprising of a borosilicate glass sample tube (50mm internal diameter) with a sintered glass plate at the base. The sample tube is sealed into a porcela in work-tube heated by an electrical split-tube furnace with cascade control of temperature based on a thermocouple within the test sample. The biomass sample was heated at an average heating rate of 8°C/min to the required temperature of 350°C, 450°C and 550°C. The temperature was maintained for 60 minutes before the heating was stopped and the sample cooled naturally to below 100°C in approximately 1 hour. They found that the carbon content of biomass char increased with increasing pyrolysis temperature as more and more oxygen, hydrogen and nitrogen is released in the gaseous phase.

Xu *et al.,* (2011) investigated the pyrolysis behaviour for the sustainable production of biomass char from several agricultural residues of sugarcane, palm oil and forestry. The reactor used was a highly automated and instrumented fast pyrolysis pilot plant to convert solid biomass over temperature range 250°C to 700°C and under near atmospheric pressures in the absence of oxygen. The heart of the plant was an atmospheric fluidised bed reactor, 0.078m in diameter, with a 0.52m long cylindrical section. The reactor was equipped with thermo wells for temperature measurements and control. The reactor body is fitted with an electric band heaters, covering all sections of the reactor body and its extension. The feed injection system was a biomass "slug injector" which discharged into the bed, 10cm above the gas distributor plate. They reported that the most favourable pyrolysis condition for biomass char production is to operate between the temperature of 450°C and 550°C.

As for this present study, the palm fibre was pyrolysed in a fluidised bed reactor to produce biomass char (palm fibre char). Based on the literature, in order to obtain a large amount of biomass char, the pyrolysis process was conducted at temperature of 550°C and at a slow heating rate of 10°C/min. This condition would gives a high carbon content of the biomass char and a high biomass char yield. The palm fibre char was then subjected to a series of evolved gas analysis (EGA) experiments for its combustion characteristics study and the results are discussed in Chapter 7.

2.2 Experimental techniques

Many approaches have been taken to the laboratory scale study of biomass combustion characteristics. The main techniques involve the use of either thermogravimetric analysis (TGA) or evolved gas analysis (EGA).

Thermogravimetric analysis (TGA) is a type of testing performed on samples that determines changes in weight in relation to change in temperature. This analysis relies on a high degree of precision in three measurements: weight, temperature, and temperature

change. When the temperature increases, the weight change and the rate of weight change of the sample are measured. Both the thermogravimetric (TGA) curve and the derivative thermogravimetric (DTG) curve can identify the point where weight loss is most apparent. The TGA curve is where the sample weight loss is plotted against temperature. The DTG curve is the sample derivative weight loss with respect to time (%/min) that is plotted against temperature. TGA is commonly employed in research and testing to determine characteristics of materials such as biomass to determine degradation temperatures. Another approach for biomass combustion characteristics study is using the evolved gas analysis (EGA) technique. The evolved gas analysis (EGA) technique studies the gas evolved from a heated sample that undergoes decomposition or desorption. The EGA procedure is performed by injecting air at a controlled flow rate and pressure into a sample. The sample is heated at a programmed heating rate and the measured exit gases are oxygen, carbon dioxide and carbon monoxide. With the gas composition measurement data recorded at a high frequency and at a slow heating rate, the biomass decomposition curves may be obtained. Further, the types of oxidation reactions are determined by examining the variation in carbon oxides production and the oxygen consumption with temperature.

2.2.1 TGA combustion characteristic studies on biomass materials

Several researchers have investigated the combustion characteristics of biomass using the TGA technique. Among them are Zheng and Kozinski (2000) who studied the thermal events occurring during the combustion of the biomass sludge residue. A sample of approximately 1.1mg of the bio-sludge was used in each experiment with a heating rate of 40°C/min until a maximum temperature of 1500°C was reached. They observed four stages occurring during the bio-sludge residue combustion. The stages are initial burning, transition, sintering and melting (cooling/quenching) occurring at temperature ranges of 25°C to 600°C, 600°C to 1100°C, 1100°C to 1400°C and 1400°C to 1500°C, respectively.

Biagini *et al.* (2008) investigated the effect of heating rate on the devolatilization of biomass residues. Three biomass fuels are used in their study: rice husks, olive cake and

cacao shell. For each experiments, 5mg to 6mg samples were used and the temperature range was from ambient to 1270K with a heating rate from 0.1K/min to 100K/min. They reported that the devolatilization profile of rice husk exhibits a complex peak with a well defined main peak, a shoulder at earlier temperatures and a long tail zone. The higher the heating rate, the higher the values of the peak temperatures. The derivative thermogravimetric (DTG) curve revealed that the reactivity of the first two components (hemicellulose and cellulose) was differently influenced by the heating rate. At the low heating rate, the DTG curve of hemicellulose was almost incorporated in the main peak of cellulose while at high heating rate, the relative distance is larger and the separation of peaks more evident.

Yorulmaz and Atimtay (2009) studied the combustion mechanisms of the wood samples using the TGA technique. Approximately 5mg sample was used in each experiments and was combusted in air at 10°C/min, 20°C/min and 30°C/min heating rates from temperature range of 30°C to 900°C. Considering the TGA results, three regions were determined on thermographs. These regions were identified according to the approximate starting and end points of the derivative thermogravimetric (DTG) curve which shows thermal breakdown of the organic matters and volatile matters in the samples. The first region on the DTG curve was due to the moisture and highly volatile matters in the samples. The second region was due to the oxidation and removal of the volatile matters of the samples. The third region was due to the oxidation of the char remaining after the volatiles were removed from the samples. As the heating rate increased, a higher peak temperature was detected for all the biomass samples. The peak temperature in the DTG curve depends on the heating regime. A lower peak temperature shows an easier ignition.

Sung and Seo (2009) reported the work on the non-isothermal combustion behaviour of the *Nicotiana Tabacum* stem using a TGA technique. The sample weighing approximately 10mg was used for each kind of tobacco stem with a heating rate of 10°C/min from the room temperature up to 900°C. The thermal behaviour of the tobacco stem showed different patterns depending on the decomposition conditions as well as the tobacco

varieties. The higher content of the volatile components and simple sugar in the bright stem resulted in the greater thermal decomposing in the temperature range of 120°C to 250°C. The structural differences in the hemicellulose and the cellulose that vary with the differing tobacco varieties were also detected by the temperature difference in the results.

Darvell *et al.* (2010) studied the combustion properties of three of the United Kingdom commonly imported biomass fuels for co-firing, which are palm kernel expellers (PKE), shea residue, and waste from olive oil production and its char. The fuels were characterised and their thermal decomposition properties were studied by thermogravimetric analysis (TGA) technique. Approximately 10mg of biomass were heated at a heating rate of 10°C/min from room temperature to a final temperature of 600°C. They found that two main mass losses can be observed for all the fuels. The first mass loss at $T < 120°C$ is from moisture evaporation, followed by a larger mass loss due to the volatile matter being released. The remaining residue is char. It can be noted that higher total mass losses were obtained for the fuels with higher volatile contents i.e. PKE. Differences in their pyrolysis behaviour can also be observed on their derivative thermogravimetric (DTG) curves, with the PKE sample presenting a single peak with a flat tailing section at higher temperatures, whilst two partially unresolved peaks can be observed for the shea residue. The olive residue samples show a single peak each, with a shoulder at lower temperatures. This shoulder at lower temperatures has often been ascribed to the decomposition of hemicellulose, whilst the main peak at higher temperatures is due mostly to cellulose decomposition. Lignin decomposes very slowly over a broad temperature range, resulting in an unresolved band with a flat trailing section at higher temperatures. Peak height and peak temperature have been taken as a measure of the reactivity of the fuel. Peak temperature is the temperature at which the rate of mass loss is at its maximum. Therefore the fuels presenting the lowest peak temperatures are considered most reactive. It can be noted that PKE is the most reactive of the fuels studied here, whilst the shea residue and olive residue are the least reactive; these latter two fuels also have the lowest volatile contents. A single peak can be observed for the combustion of the PKE and olive residues chars, whilst two overlapping peaks are obtained for the combustion of shea residue char.

This two-stage char combustion process indicates the existence of at least two types of char reacting due to the nature of the biomass components of the shea meal (i.e. soft fleshy material and shell/skin).

Idris *et al.* (2010) investigated the thermochemical behaviour of the low rank Malaysian coal, oil palm biomass of palm fibre (PMF), empty fruit bunch (EFB), palm kernel shell (PKS) and their blends during pyrolysis via thermogravimetric analysis (TGA). In their TGA experiments, a 20mg sample was used for each experiment at various heating rates of 10°C/min, 20°C/min, 40°C/min and 60°C/min and was heated from the room temperature to 900°C. The PMF and EFB samples exhibit three peaks in their derivative thermogravimetric (DTG) curves. The first peak corresponds to the moisture drying. The second and third peaks correspond to the hemicellulose and the cellulose decompositions, respectively. The PMF sample starts to degrade first at a temperature of around 180°C and followed by the EFB and PKS samples at degradation temperature of approximately 200°C. There is no obvious weight loss observed beyond temperature of 550°C for both the PMF and the EFB samples. Nevertheless, the PKS sample continues to decompose until beyond a temperature of 750°C with maximum decomposition at temperature of 704°C. The fourth peak of the PKS sample was due to the decomposition of lignin which is known to decompose slowly at this temperature region. Further, they also found that the DTG peaks for the oil palm biomass were systematically shifted to higher temperatures as the heating rate increased.

Skreiberg *et al.* (2011) reported on the thermal behaviour of selected biomass fuels and mixtures as wood, demolition wood, coffee waste and glossy paper using thermogravimteric analyser (TGA) and macro-thermobalance (macro-TGA). Two sets of TGA experiments were carried out. The behaviour of biomass samples under inert (argon) atmosphere was studied in the first series. For the second series of TGA experiments with biomass samples under an oxidising atmosphere; a mixture of 21% oxygen in argon was used. A constant flow rate of 100ml/min was applied both for argon and oxygen/argon (21% oxygen/ 79% argon). Each of the biomass samples (~10mg ± 3mg, except for glossy

paper: ~2.75 ± 0.4mg) was subjected to three different dynamic runs performed at heating rates of 5K/min, 20K/min and 100K/min at temperature ranging from 60°C to 900°C under inert and oxidising atmosphere. They observed that the pyrolysis of hemicellulose started at a temperature above 200°C and the cellulose started to decompose at a temperature above 300°C, i.e., close to the derivative thermogravimetric (DTG) pyrolysis peak of hemicellulose. In comparison to the sharper DTG peaks of cellulose and hemicellulose, lignin has wide and flat DTG peaks. Lignin started to decompose at about the same temperature as hemicellulose and showed gradual weight loss until temperature of 900°C. They concluded that the thermogravimetric analysis for each single fuel had pyrolysis and combustion characteristics based on its own main pseudo-components (hemicellulose, cellulose and lignin).

Most recently, Fernandez *et al.* (2012) studied the main combustion characteristics of biomass fuels used in boilers using TGA technique. Six of the more common biomass fuels used in their study were almond shell, rice husks, rice straws, wine pornace, wood pellets and vegetable coal. The TGA program involved increasing the temperature to 50°C then purging the system with nitrogen for one minute. Once this had occurred, the gas was changed to air and the temperature increases until 900°C is reached using a heating rate of 10°C/min. They observed that general biomass derivative thermogravimetric (DTG) profile consists of three peaks occurring at slightly different temperatures. The first of these peaks corresponds to drying by moisture evaporation, and is situated generally at a temperature near to 105°C. The second phase change corresponds to biomass volatilization and volatile matter release due to hemicelluloses, cellulose and lignin decompositions, this usually occurs in a range between 190°C and 450°C (190°C to 320°C for hemicellulose, 280°C to 400°C for cellulose and 320°C to 450°C for lignin). The last peak, beginning in the range of 550°C to 600°C and concluding around 900°C when constant weight is reached, corresponds to char oxidation or combustion of carbonaceous residue without flame.

In summary, most of the combustion characteristic studies of biomass using TGA techniques involve using a small sample sizes of 5mg to 10mg of each experimental run.

Even though extensive results have been reported, the small biomass sample sizes of each TGA experiment may produces a large error. The fact that biomass is a heterogeneous materials would further increase the error.

2.2.2 TGA combustion characteristic studies on biomass char materials

Combustion characteristic studies of biomass char sample have been reported by various researchers. Maiti *et al.* (2006) reported the thermochemical characterisation of the rice husk char using TGA. The rice husk char samples (10mg) were subjected to TGA in air using a heating rate of 10°C/min and was heated from ambient to 1000°C. They observed a three steps of weight loss. The first weight loss step from ambient to temperature of around 150°C was associated with the loss of water present in the biomass char and the external water bound by surface tension. The second weight loss step occurred at temperature of 325°C to 425°C and was correlated with decomposition of lignin in the biomass char. The third step of combustion observed over a temperature range of 425°C to 490°C was referred to as the active zone.

Daood *et al.* (2010) investigated the char oxidation of sugar cane bagasse, cotton stalk and Pakistani coal under 1% and 3% oxygen concentrations using TGA. The samples were heated from 105°C to 950°C at a heating rate of 20°C/min for the both oxygen concentrations. They found that all the biomass chars exhibited higher reactivity towards oxygen in the conditions studied. In 3% oxygen concentration average rate of weight loss was found to be doubled compared to 1% oxygen concentration. The biomass chars were more reactive as compared to the Pakistani coal in the both oxygen concentrations. It is also found that the rate of reaction during char oxidation is dependent on the temperature and the oxygen partial pressure. An increase in the oxygen partial pressure may significantly enhance the rate of weight loss.

Haykiri-Acma *et al.* (2012) investigated the combustion characteristics of sodium-free pyrolytic char from hazelnut shells using the TGA technique. The hazelnut shells were

pyrolysed under nitrogen to eliminate sodium and then the burning characteristics of the obtained sodium-free pyrolytic char were investigated up to 900°C by heating rates of 5, 10, 20, 30, 40 and 50°C/min under dry air flow. They found that char burning reactivity was higher at the low heating rate conditions, Further, heating rate has an influence on burning of char in such a way that the increasing heating rate shifted the temperatures of maximum burning rates to higher temperatures.

Meng *et al.* (2012) studied the combustion behaviour of dried distiller's grains with solubles (DDGS) and willow chars using TGA technique. The effects of combustion temperature (400°C, 600°C, 750°C and 900°C), oxygen concentration (7%, 5%, 10%, 15%, 21%) and heating rate (10°C/min, 30°C/min, 50°C/min) on the char-oxygen reaction rate were reported. They observed that the char combustion rate increased with the increasing of either the oxygen concentrations or the combustion temperatures.

Park and Jang (2012) studied the effects of pyrolysis temperature on changes in fuel characteristics of biomass char using TGA technique. The fuel characteristics and the combustion profile of biomass char that had been pyrolysed at 300°C to 500°C were investigated for the rice husk, wood chip and wood pellet. They observed that at the higher pyrolysis temperatures, the calorific value became proportional to the fuel ratio and inversely proportional to that of the volatile matter. Further, as the pyrolysis temperature increased, the number of peaks decreased from two (pyrolysis temperature of 300°C) to one (pyrolysis temperature of 400°C and 500°C) for all the biomass chars.

In conclusion, many studies have been reported on biomass char combustion characteristics using TGA technique. However, very small sample sizes are involved in the experiments.

2.2.3 EGA combustion characteristic studies on non-biomass materials

The EGA technique has been widely used for the oxidation study of crude oil. Many studies have been carried out to study the oxidation behaviour of various types of crude oils. Among them are the study by Shallcross (1991). He investigated the oxidation behaviour of heavy and light crude oils using an EGA technique. A heavy crude oil from California (943kg/m^3) and a light crude oil from Bass Strait (800kg/m^3) were used. Figures 2.4 and 2.5 show the typical EGA data for Californian and Bass Strait crude oils, respectively. As observed in Figure 2.4, there are two peaks each for oxygen consumption, carbon dioxide production and carbon monoxide production. Based on Fassihi *et al.* (1984) and Mamora *et al.* (1993), this curve trend is followed for all heavy crude oils although variations are expected in peak temperatures and heights that are fully depends on the crude and experimental conditions. Figure 2.5 displays three oxygen consumption peaks at temperatures 240°C, 290°C and 420°C with each having a corresponding carbon dioxide production and carbon monoxide production peaks.

Later, Kisler (1995) continued the study on the oxidation behaviour of light Australian crude oil using EGA technique. Mixtures of 824kg/m^3 crude oil, water and sand were subjected to a constant flow of an oxidising gas and a linear heating schedule. He found that the principle difference observed between light and heavy oil was the number of peaks present in a plot of oxygen consumption against temperature. Three peaks were observed for light crude oil rather than two peaks for heavy crude oil. Figure 2.6 shows the typical EGA results of Australian light crude oil. He also reported the oxidation of activated carbon using an EGA technique that constantly show one peak (see Figure 2.7). Further, he reported that high pressures increases the oxygen consumption throughout the run.

Nguyen (2004) investigated the oxidation kinetics of Vietnamese crude oil using an EGA technique. Mixtures of crude oil (853kg/m^3), sand and water were heated at a programmed heating rate while an oxidising gas, typically air was injected continuously into the mixtures.

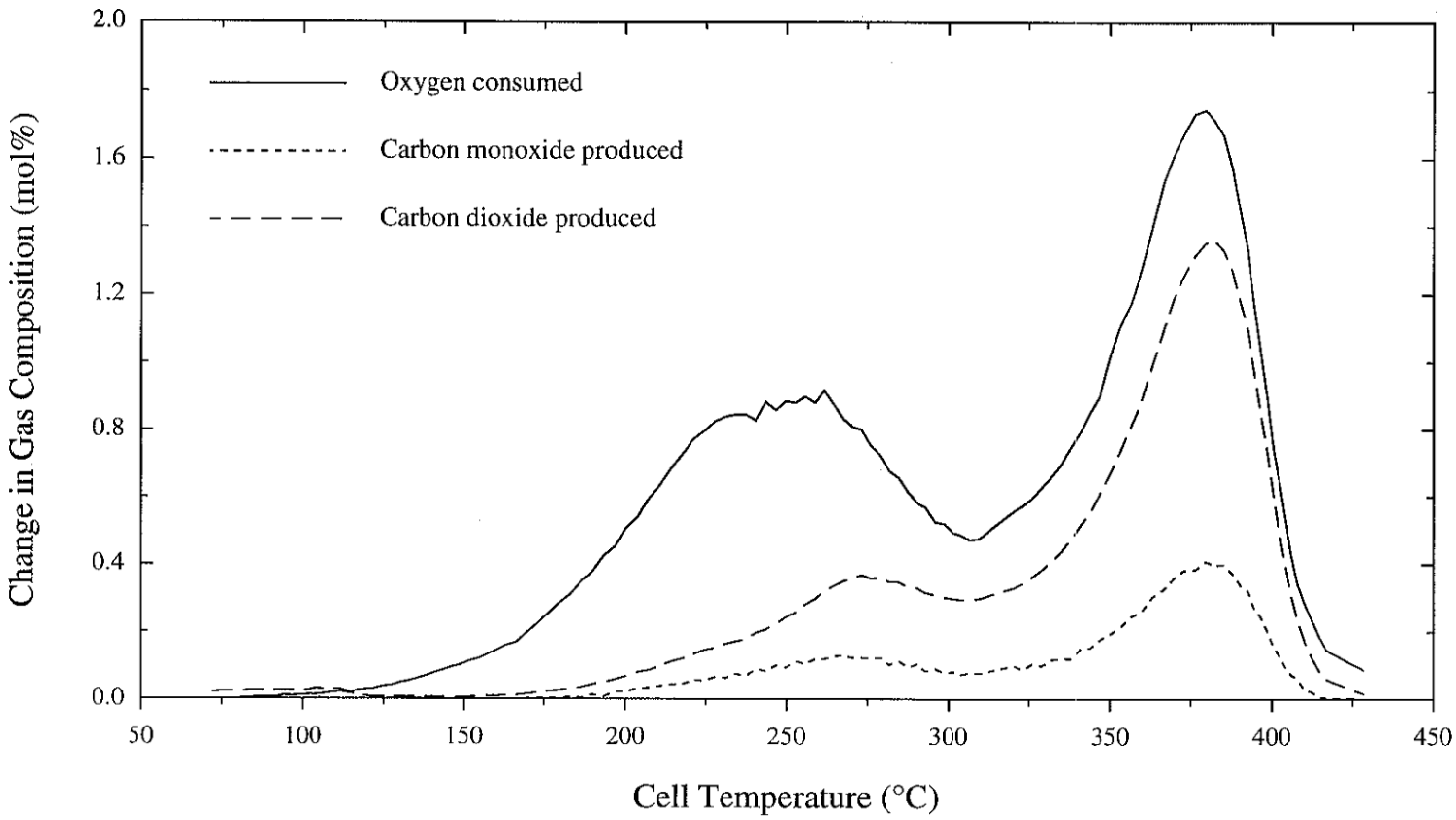

Figure 2.4 - Evolved gas analysis (EGA) data for a typical experiment with California heavy crude oil (943kg/m^3). Data reproduced from the work of Shallcross (1991).

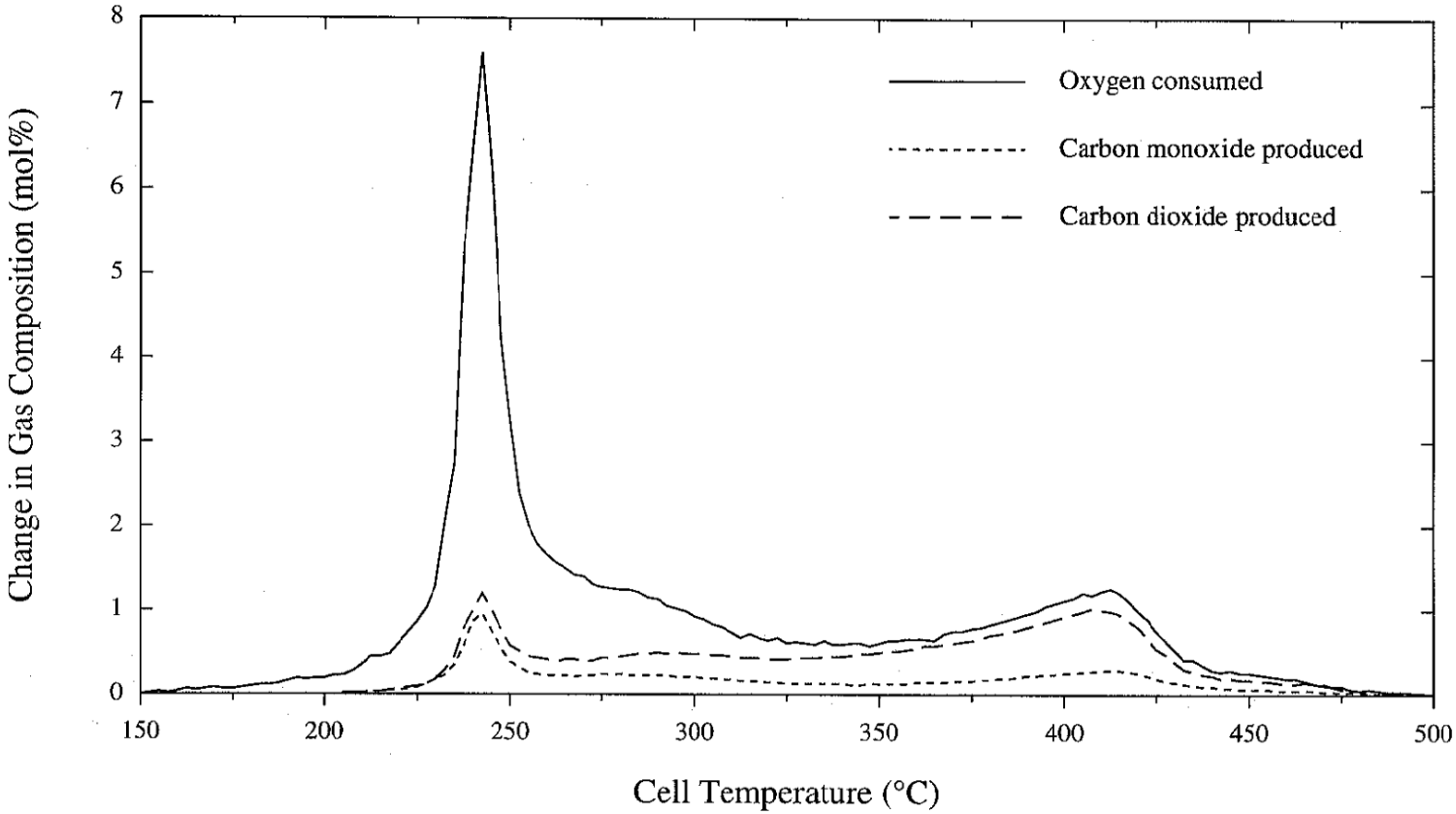

Figure 2.5 - Evolved gas analysis (EGA) data for a typical experiment with Bass Strait light crude oil (800kg/m^3). Data reproduced from the work of Shallcross (1991).

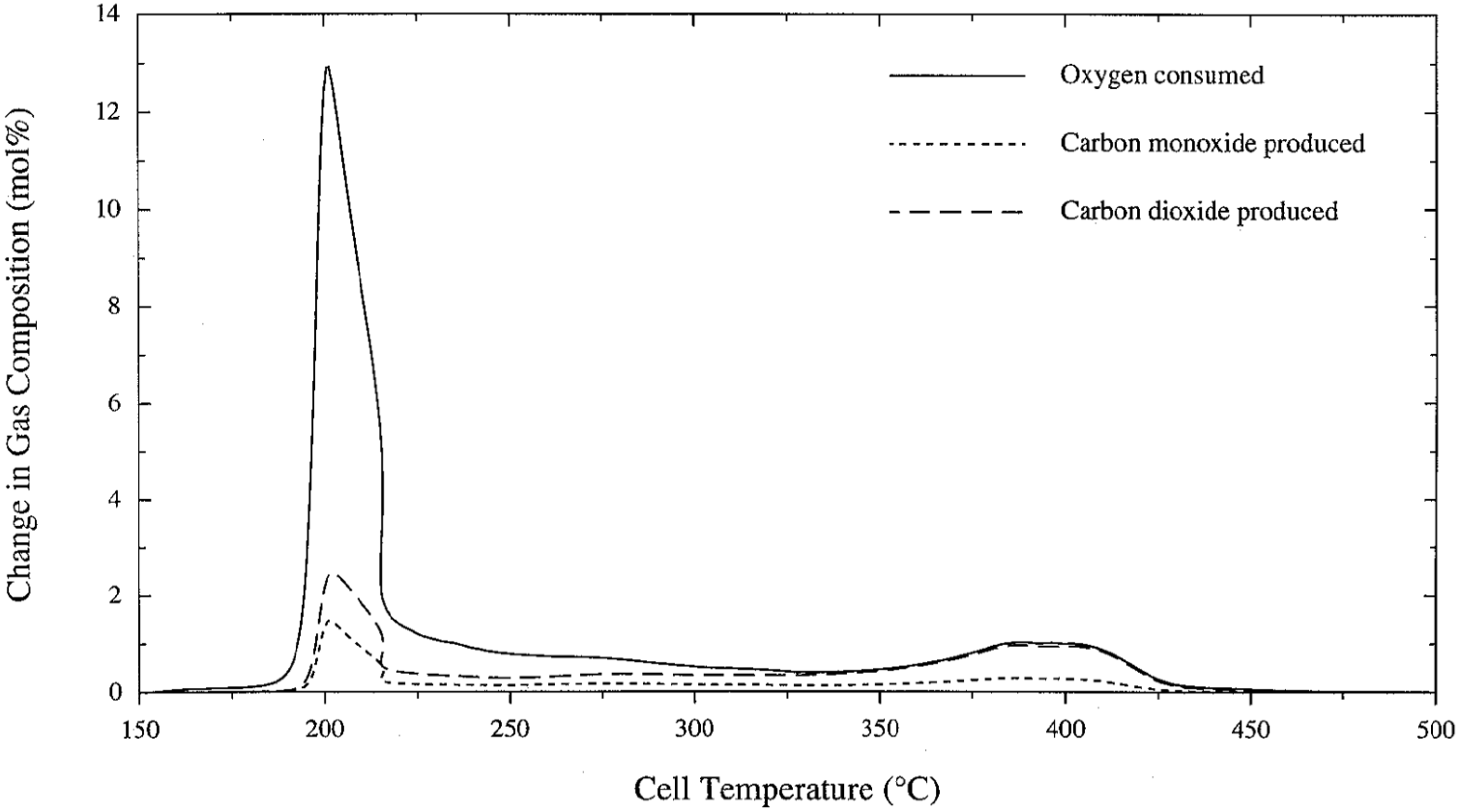

Figure 2.6 - Evolved gas analysis (EGA) data for a typical experiment with Australian light crude oil (824kg/m^3). Data reproduced from the work of Kisler (1995).

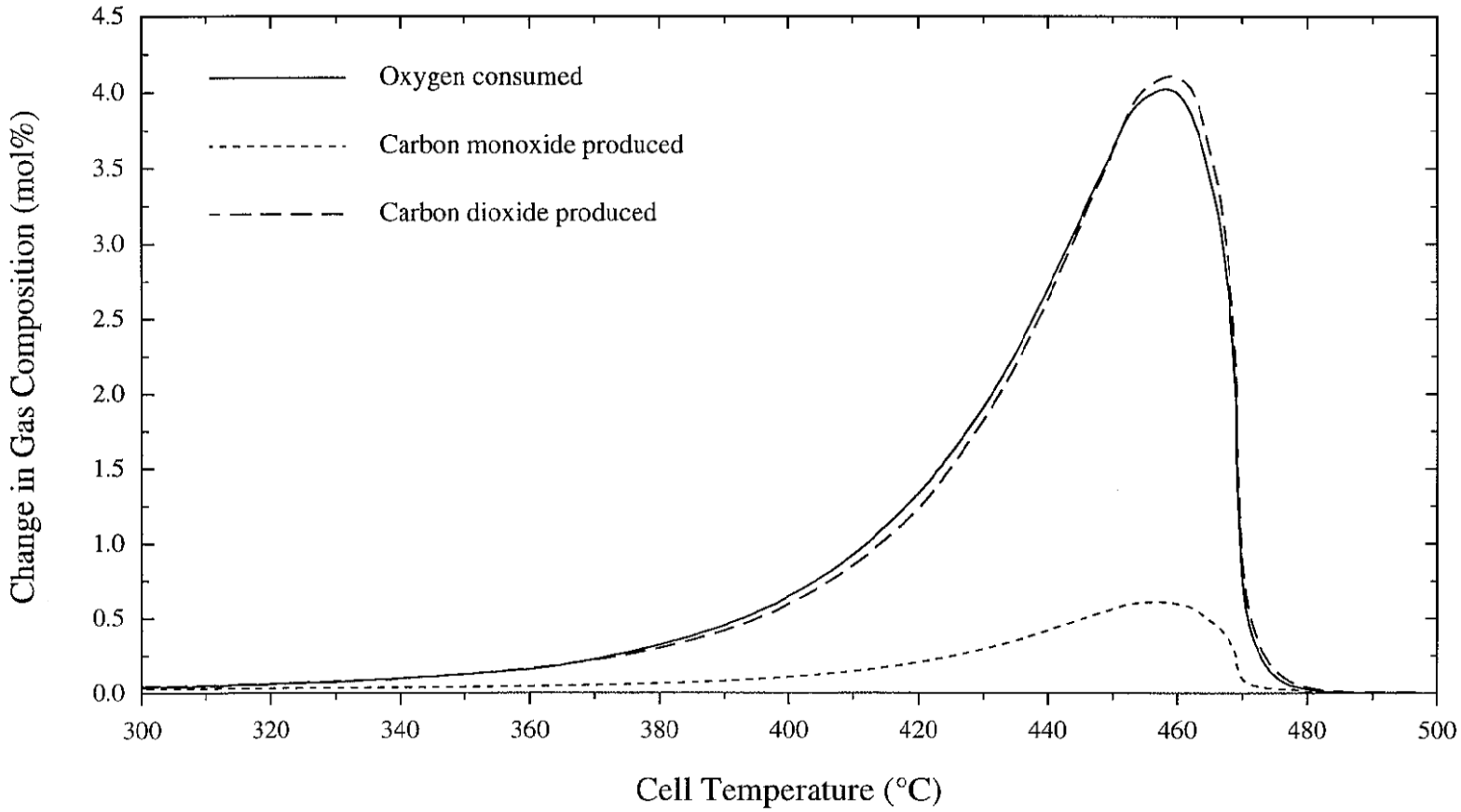

Figure 2.7 - Evolved gas analysis (EGA) data for a typical experiment using activated carbon. Data reproduced from the work of Kisler (1995).

The oxygen consumption, carbon dioxide production and carbon monoxide production were measured against temperature. She found that the oxidation behaviour of Vietnamese crude oil has similar characteristics of some light and heavy crude oils. The similarities observed for the number of oxygen consumption peaks between Vietnamese and light Australian crude oils (three peaks), and the number of carbon oxides production peaks between Vietnamese and heavy crude oils (two peaks). She also found that the oxygen consumption increases with increasing pressure. All three oxygen consumption peaks shifted to lower temperatures as oxygen partial pressure increases (Nguyen, 2004).

2.2.4 EGA combustion characteristic studies on biomass materials

A limited number of studies have been conducted to investigate biomass combustion characteristic study using EGA technique. Bridgwater and Boocock (1997) studied the pyrolytic decomposition and subsequent combustion of rice husk using an evolved gas analysis (EGA) technique. The EGA rig used was similar to the one of the present study. The cell was loaded with a mixture of the rice husk and sand. The cell was then heated so as to give a constant rate of temperature increase. At the same time, air or another oxidising gas of known composition was passed through the cell at a known flow rate. The pressure in the cell is maintained at a preset value. The gas leaving the cell have their composition of oxygen, carbon dioxide and carbon monoxide analysed on a continuous basis. Approximately 0.5g sample was used in each experiments and was combusted in air at 50°C/h and 75°C/h of heating rate from room temperature to 500°C with pressure ranging from 200kPa to 700kPa and various oxygen concentrations in the feed gas. They found that the total system pressure has no effect on patterns of rice husk decomposition whereas varying the oxygen partial pressure does. The influence of oxygen partial pressure is predominantly on gas phase oxidation reactions. Exposure of rice husk to water leads to the dissolution of alkali metals in the husks and to slower rate of pyrolytic decompositions. They also observed that the peak temperature increased with increasing heating rates. The increment could be linked to the existence of slightly larger temperature gradients within the rice husk at the higher heating rate and/or to response times at the temperature sensors.

They reported that grinding the rice husk would also facilitate the transfer of heat into the husk interior and increase the rate at which volatile pyrolytic decomposition products from within the husk to the surface and react with oxygen in the surrounding gases. They believed that the combustion of rice husk is affected by the diffusion limitations but no report on the rice husk pore size to confirm the statement. This paper is the only work published using EGA to study biomass combustion characteristics.

In summary, the EGA technique offers several advantages compared to the TGA approach. The advantages are:

- EGA provides an insight into the types of reactions occurring (e.g. amounts of carbon oxides produced and oxygen consumed) which is not available from the TGA methods.
- EGA uses larger sample sizes (typically 100 times larger than corresponding TGA samples) and longer experimental running times. The longer run times allow the gathering of more experimental data. Hence, will reduce the impact of short term fluctuations in the data. The larger sample sizes generally lead to increased precision. When handling a heterogeneous sample such as biomass, a larger sample size would have more accurate results.

Despite a range of investigations into the combustion characteristic studies of the biomass and biomass char using TGA technique, no work has been conducted on the devolatilisation of palm fibre and palm fibre char particularly using an EGA technique. Thus, this technique is emphasized in this study through detailed investigations on the combustion characteristics of a range of biomass materials and various operating parameters such as particle sizes, absolute total pressures, oxygen partial pressures and heating rates.

2.3 Mathematical modeling of fuel combustion kinetics

Extensive experimental validation of both detailed and simplified kinetic models have been performed in only a few cases (Blasi, 2008). The comparison between the kinetic model

predictions and the experimental measurements usually are considered to concern the conversion time, sample weight loss characteristics and the thermal profiles. Many researchers have reported the biomass combustion kinetics using TGA technique (Kastanaki *et al.*, 2002, Vuthaluru, 2004 and Idris *et al.*, 2010). Several researchers also reported on the modeling of a combustor such as the work by Kadir (1995), Kaer (2005) and Zhou *et al.* (2005). However, no detailed study of the biomass combustion kinetics using EGA technique has been conducted. This thesis aims to provide a detailed investigation on biomass combustion characteristics study using EGA technique. The oxidation kinetic model is adapted from the EGA crude oil study with several modifications and will be discussed in the following sections.

2.3.1 EGA modeling on non-biomass materials

The crude oil oxidation model was developed earlier by Fassihi *et al*. (1984) and de los Rios *et al.* (1988) and further modified by Shallcross (1991) and Kisler (1995). The modified model was applied in studies by Kisler and Shallcross (1997) and Nguyen (2004). In their work, rather than considering individual reactions they grouped them together. The lumped groups or reaction regimes consist of numerous reactions of similar types. For example, all the high temperature oxidation reactions involve the combustion of a solid hydrocarbon fuel. The kinetic parameters such as reaction order, activation energy and the natural log of the beta group are to be calculated for each of the reaction groups or reaction regimes. A similar approach of modeling will be further improved and applied to the combustion of the rice husk, palm fibre and palm fibre char. The improved model will be used in this study to predict the oxygen consumption of the biomass combustion process. The predicted oxygen consumption model shall be validated with the actual EGA experimental data. The calculated kinetic parameters data from the EGA experiments will enable the influence of several experimental variables to be studied.

Fassihi *et al.* (1984) and later de los Rios *et al.* (1988) developed a model to analyse and differentiate between crude oil/oxygen reactions at different temperatures. The oxygen

consumption data from the experiments were analysed by decoupling the total oxygen consumption curve into three parts representing the oxygen consumed by the three competing and overlapping reactions known as low temperature oxidation (LTO), medium temperature oxidation (MTO) and high temperature oxidation (HTO). This model assumed a constant heating rate throughout and a reaction order of one. Generally, de los Rios *et al.* (1988) found that the oxygen consumption between medium and high temperature oxidation reactions were not well matched. However, the quality of resultant data matches was quite good near the reaction peaks. Shallcross (1991) made an improvement to the model previously developed by Fassihi *et al.* (1984). The improvement allowed the non-constant heating rates to be considered and the enabled the reaction order with respect to the fuel concentration to be calculated. The calculation procedure of Shallcross (1991) produced repeatable results and was successfully applied to model heavy crude oil EGA data. The calculation procedure requires the carbon oxides production data for the MTO calculation. The model was least accurate for the LTO parameters since any errors in the high temperature calculations are transmitted to the low temperature data. Therefore, the fitted curves at the low temperatures are inherently less accurate than the curves fitted at the high temperatures. Figure 2.8 shows a typical EGA model of using Californian heavy crude oil from the work of Shallcross (1991). The overall model was obtained by summation of the low, medium and high temperature oxidations. The model uses a calculation procedure that starts with the high temperature data and progressively moves to lower temperatures.

Later, Kisler (1995) and Kisler and Shallcross (1997) used the same model but with minor modifications and applied to the Australian light crude oil. They suggested that calculation should be based only on the oxygen consumption data. The use of the carbon dioxide production and carbon monoxide production data increases both the inaccuracy and complexity of the calculations. Further, Kisler (1995) and Kisler and Shallcross (1997) also improved the curve fitting for the LTO reaction by working from the low temperature end of the data instead of working from the high temperature end of the data. Figure 2.9 shows the typical EGA model of Australian light crude oil reported by Kisler (1995).

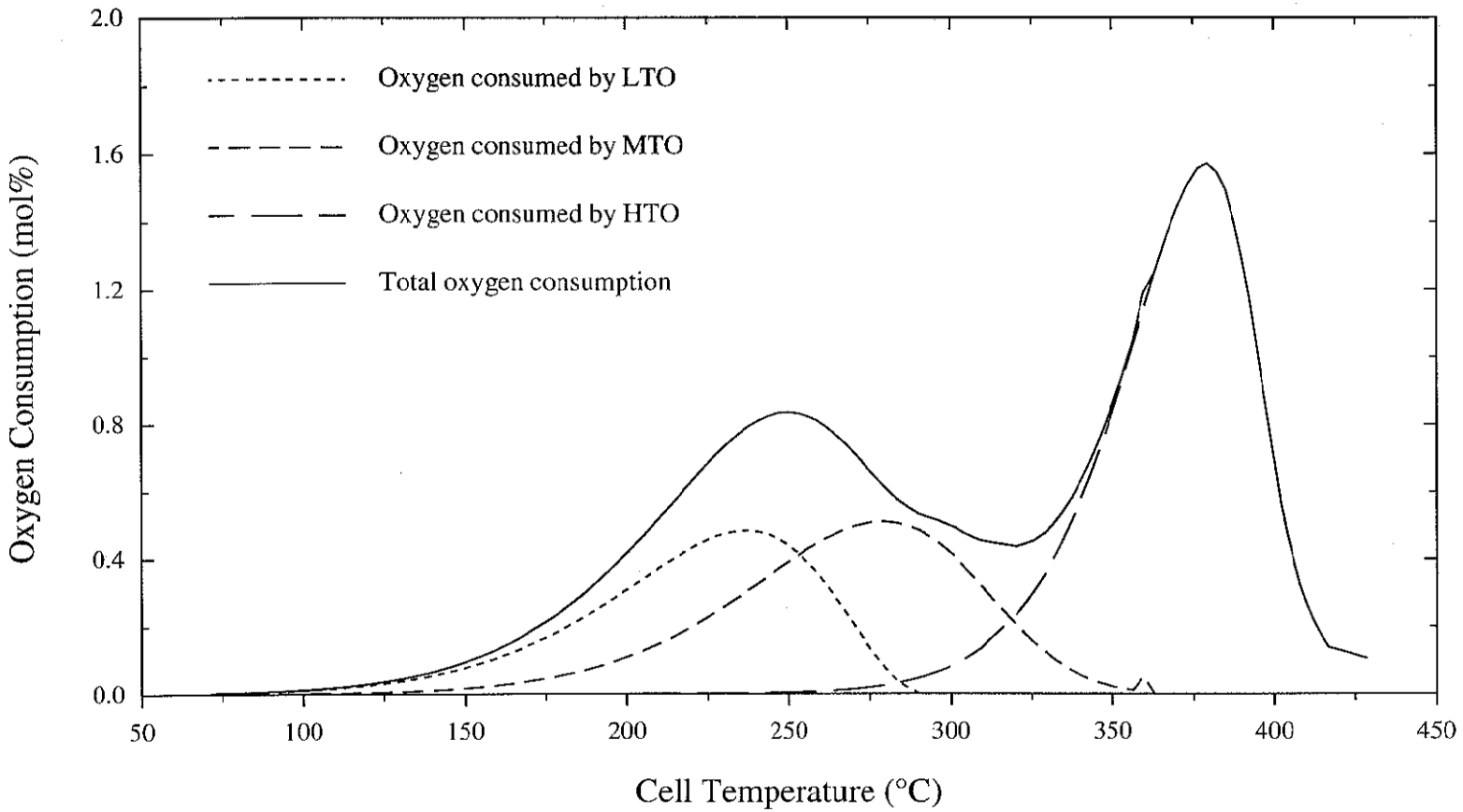

Figure 2.8 - The evolved gas analysis data model for a typical experiment with California heavy crude oil (943kg/m^3). The overall model was obtained by summation of the low, medium and high temperature oxidations. The model represents the calculation technique working from high to low temperature data. Data reproduced from the work of Shallcross (1991).

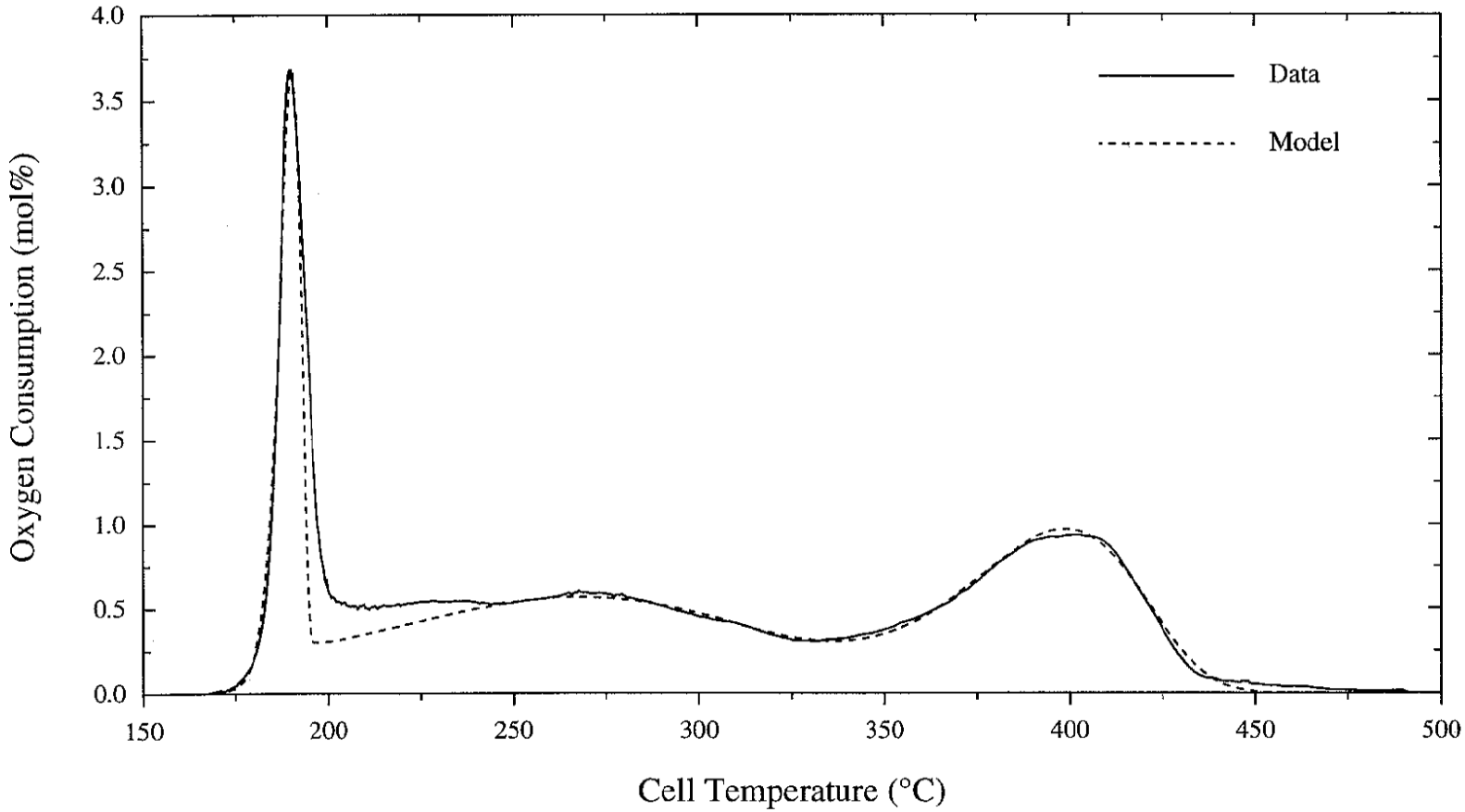

Figure 2.9 - The evolved gas analysis data model for a typical experiment with Australian light crude oil (824kg/m^3). The overall model was obtained by summation of the contributions of the low, medium and high temperature oxidations. The HTO and MTO models represent the calculation technique of working from high temperature data towards the low temperature data. The LTO model uses the low to high temperature calculation method. Data reproduced from the work of Kisler (1995).

The HTO and MTO reactions were modeled using a calculation procedure of working from high temperature data to low temperature data. The LTO reaction was calculated using the low temperature data first working to the high temperature oxidation data. The overall model was obtained by summation of the low, medium and high temperature oxidations. They reported that the LTO and MTO reactions were influenced by the oxygen partial pressure and the HTO reaction was dependant on the total system pressure. They also reported that furnace heating rate had no influence on the oxidation kinetics other than on the reaction rate via the Arrhenius law. Kisler (1995) also modeled the EGA work on the activated carbon (see Figure 2.10) assuming just a single reaction.

Nguyen (2004) also applied the same model calculation procedure as both Kisler (1995) and Kisler and Shallcross (1997) to Vietnamese crude oil. She found that fitting the model to the LTO and MTO reaction regimes were less accurate than the corresponding fit for the HTO reaction regime. This was due to the temperature range of the MTO peak that developed from the right edge of the LTO peak. The extent of the overlap between the two reactions made it difficult to differentiate between the LTO and MTO regimes. She also found that increasing the oxygen partial pressure results in all three oxygen consumption peaks (LTO, MTO and HTO) shifting to lower temperatures. Generally, the calculated kinetic parameters showed that the LTO reaction was mainly controlled by the oxygen partial pressure while the MTO and HTO reactions were affected by both the oxygen partial pressure and total system pressure.

Most researchers generally assumed three competing reaction regimes of the oxidation kinetics known as the low, medium and high temperature oxidations (e.g. Fassihi *et al*., 1984, de los Rios *et al*., 1988, Shallcross, 1991, Kisler, 1995, Kisler and Shallcross, 1997 and Nguyen, 2004). Mamora *et al.* (1993) suggested using just two oxidation reactions of HTO and LTO. They investigated the different findings of combustion tube and EGA work.

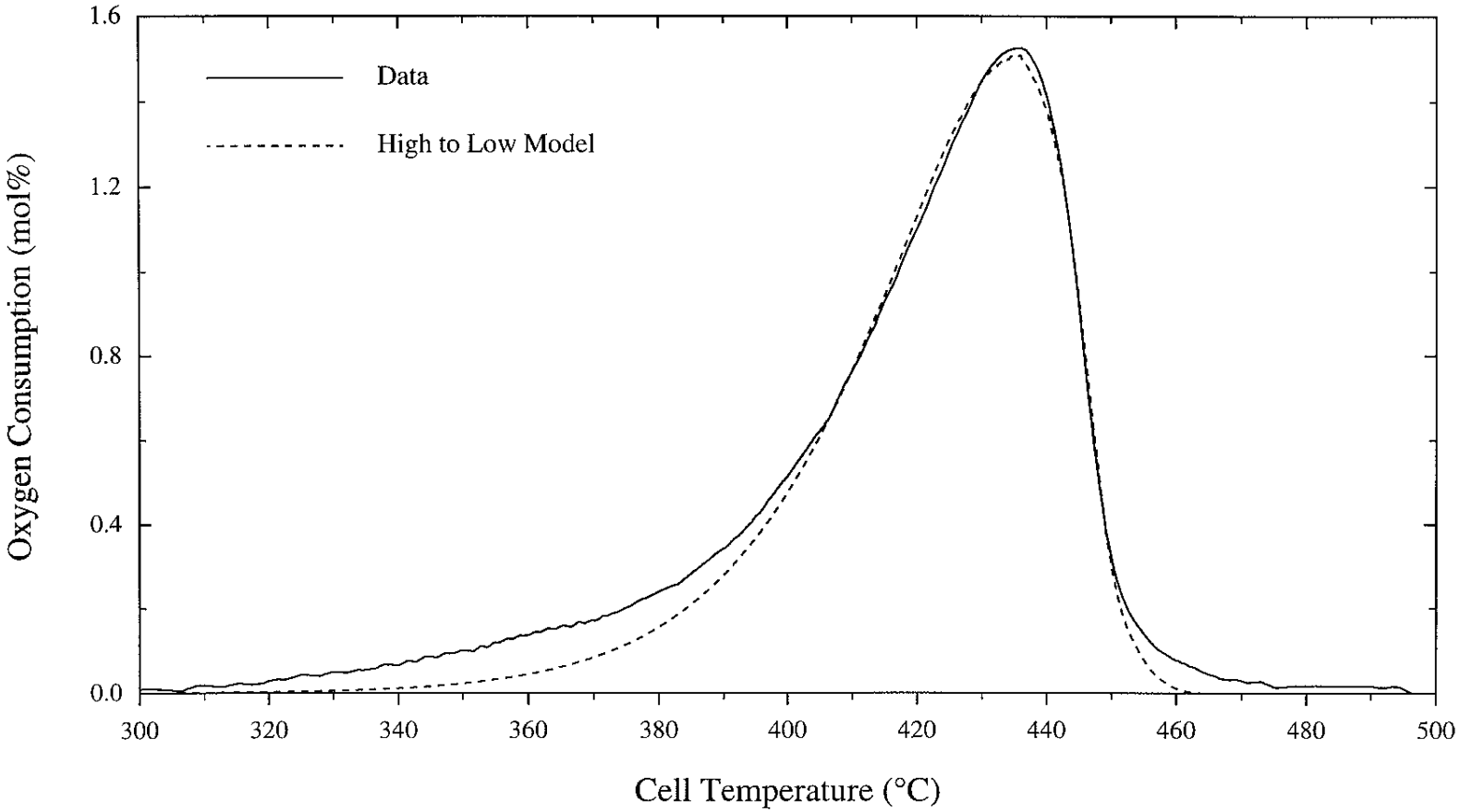

Figure 2.10 - The evolved gas analysis data model for a typical activated carbon experiment. The model represents the calculation technique of starting with high temperature data and working towards the low temperature data. Data reproduced from the work of Kisler (1995).

Allowance was made for the inclusion of the size of the sand grains in the model by considering the change to the fuel geometry. The MTO and HTO reactions were represented by the HTO reaction alone (Mamora *et. al.*, 1993). However, the model calculation procedure is more complicated than that of the Shallcross (1991), Kisler (1995), Kisler and Shallcross (1997) and Nguyen (2004). The information of the average sand grain size and effluent gas flow rate are required in the calculation procedure. The accuracy to which the average grain size estimated has a significant effect on the calculated kinetic parameters.

Mamora *et al.* (1993) assumed that the reaction occurring within an EGA cell is similar to those in a combustion tube. However, in the combustion tube, the majority of the injected oxygen is consumed at the combustion front and a very little oxygen is present in the low temperature zones ahead of the combustion front. On the other hand, a large excess of oxygen is present throughout an EGA cell. Therefore, assumptions made by Mamora *et al.* (1993) were incorrect. Further Kisler (1995) argued that the LTO model proposed by Mamora *et al.* (1993) only works for regions where the temperature is not constant.

Al-Saffar *et al.* (2000) used a flow reactor operated at high pressures to study the oxidation kinetics of selected North Sea light crude oils. An approach of decoupling of just two reaction regimes (LTO and HTO) was suggested and they determined the boundary between the both reaction regimes. They found that LTO reactions were important as a precursor for the formation of fuel for the combustion. The LTO results either when oxygen bypasses the combustion front due to reservoir heterogeneities or because of insufficient combustion rates to consume oxygen. The presence of LTO reaction was identified in the non-isothermal experiments. However, the LTO reactions are still occurring to some extent together with HTO and there is a degree of interaction between the LTO and HTO reactions. However, oxygen by-passing does not to occur during an evolved gas analysis (EGA) experiment (Nguyen, 2004).

De los Rios (1988) suggested that it is possible to fit the data better mathematically by introducing an additional reaction between the medium and high temperature reactions. However, they found that the procedure would have been burdened with even more uncertainty and thus the results would have been more suspect with no guarantee that the matches would have been any better.

In conclusion, in the present study, the many oxidation reactions occurring may be grouped into three simultaneous and competing reaction regimes of HTO, MTO and LTO. The previous model developed by Shallcross (1991) and further modified by Kisler (1995) thus will be used as a starting point for the development of a model for the biomass oxidation in this thesis.

2.3.2 The oxidation regimes

The three oxidation regimes involve quite different chemical reactions but occur across overlapping temperature ranges. The low temperature oxidation (LTO) reactions are generally heterogeneous reactions for hydrocarbons. The LTO reactions consume oxygen but produce no carbon oxides (de los Rios *et al.*, 1988). Based on Dabbous and Fulton (1974), LTO reactions typically occur at temperatures below 300°C. At very low temperatures below 90°C, the oxygen conversion is too small for accurate use in the data analysis. The LTO products of hydrocarbon combustion are water and partially oxygenated compounds such as the carboxylic acids, aldehydes, ketones, alcohols and hydroperoxides. The LTO products are not feasible to determine experimentally due to any reactive intermediates rapidly reacting and thus would not appear in an analysis of the remaining compounds (Kisler, 1995). Further, the other reactions are occurring at similar temperatures such as the pyrolysis which consume the LTO products. Fassihi *et al.* (1984) found that the LTO reactions are kinetic controlled and not diffusion controlled due to the oxygen diffusion to hydrocarbon molecules is faster than the oxidation process. Further, spontaneous ignition may occur because of the LTO reactions.

Medium temperature oxidation (MTO) reactions are caused mainly by the oxidation of the products of distillation and pyrolysis (Fassihi *et al.*, 1984). The MTO reaction is indicated by the oxygen consumption at the intermediate temperatures with an associated production of the carbon oxides. Since in EGA experiments excess oxygen is present throughout the entire range of temperature, any light hydrocarbons produced by the pyrolysis will generally undergo MTO reactions (Kisler, 1995).

High temperature oxidation (HTO) reactions are generally exothermic and heterogeneous reactions that involve the combustion of the solid residue deposited by the pyrolysis (Fassihi *et al.*, 1984). The main products of the HTO reactions are carbon monoxide, carbon dioxide and steam. The HTO reaction take place in the high temperature zone above 316°C (Dabbous and Fulton, 1974). Based on Burger and Sahuquet (1972), the temperature in the HTO region is higher than 250°C to 300°C. Alexander *et al.* (1962) reported that the temperature of the HTO zone is dependent on the types of fuel but typically starts at 340°C. Fassihi *et al*. (1984), Kisler and Shallcross (1997) reported that in the HTO region, the oxygen consumption is nearly equal to the carbon oxides productions whereas at the low temperature, the oxygen is consumed more than the carbon oxide productions.

In summary, the oxidation of hydrocarbon oils may be adequately represented by considering three overlapping oxidation regimes. Each class of reaction is a lumped group of many similar reactions. Only oxidation reactions are monitored by the EGA experimental technique but other non-oxidation reactions also occur within the EGA cell. The pyrolysis reactions are responsible for depositing a solid fuel on the sand grains. Note that the discussion on the oxidation regimes is based on the crude oil oxidation study. No equivalent model has been developed for the oxidation of biomass fuel.

2.4 Concluding remarks

The EGA technique is the most appropriate method for studying biomass oxidation processes since it provides an insight into the types of reactions occurring (e.g. amounts of

carbon oxides produced and oxygen consumed) which is not available from the other cited methods. Further, the EGA technique uses larger sample sizes and longer experimental running times. The longer run time will allow the gathering of more experimental data. Hence, it will reduce the impact of short term fluctuations in the data. The larger sample sizes generally lead to increased precision and better handling of the heterogeneous sample such as typically found with biomass samples.

Based on the literature, no work has been conducted on the combustion characteristics of palm fibre and palm fibre char using an EGA technique. The only biomass EGA work is by using rice husk as reported by Bridgwater and Boocock (1997).

Several workers have developed a method of decoupling the EGA data into three competing and overlapping reaction regimes known as low temperature oxidation (LTO), medium temperature oxidation (MTO) and high temperature oxidation (HTO). In Chapter 4, a reaction model is presented which is a refinement on this work. Note that the model is limited to the behavior observed for the heavy and the light crude oils oxidations. The literature does not contain any detailed study for the palm fibre and palm fibre char oxidations using the equivalent model.

This thesis will provide the first detailed study of the palm fibre and palm fibre char using EGA experiments. The EGA study using rice husk will also be conducted. Further, the oxidation reactions kinetic model is adapted from the EGA crude oil study with several modifications and apply to the biomass and biomass char oxidation studies. Once the kinetic parameters are known, a predicted oxygen consumption curve may be plotted and compared with the actual experimental data.

CHAPTER 3

EXPERIMENTAL MATERIALS, APPARATUS AND PROCEDURE

3.1 Introduction

In the evolved gas analysis (EGA) technique, a sample combustion cell is loaded with a mixture of combustion biomass material and sand. Air or any oxidising gas of known composition is passed through the cell at a known flow rate. At the same time, the temperature of the cell is gradually increased at a constant and known rate. The gas leaving the cell is analysed on a continuous basis for its oxygen and carbon oxides content. From the results of these analyses, the rate and nature of the decomposition or devolatilisation reactions undergone by the biomass material may be studied.

This Chapter describes the materials and apparatus used to study the oxidation kinetics of biomass. The first section provides a detailed description and the specifications of the apparatus used in the research. The second section discusses in details the test materials. Next, details description of the instrumental analyses. Following this is the step by step experimental procedures. Concluding this Chapter is a summary of the experimental work performed.

3.2 Apparatus and control systems

This section discusses the experimental apparatus and control system which includes the specification of the major equipment items.

3.2.1 Apparatus

A schematic diagram of the apparatus is presented in Figure 3.1. The apparatus consists of a combustion cell located inside a tube furnace. The gas flow rate, system pressure and temperature of the furnace may all be controlled. The produced gas is fed to three continuous gas analysers, connected in series. This equipment is similar to that used by Kisler (1995) on his light crude oil oxidation study but with minor improvement. Table 3.1 summarised the specification of the major equipment items.

Throughout the experiments, one of three gases having different compositions was used as the feed to the combustion cell. The compositions of the gases are:

- Air (20.96 mol% O_2 and balance nitrogen)
- Gas mixture 1 (15.10 mol% O_2, 2.01 mol% CO_2, 0.983 mol% CO and balance nitrogen)
- Gas mixture 2 (18.10 mol% O_2, 4.99 mol% CO_2, 2.51 mol% CO and balance nitrogen)

By switching between the different feed gases it was possible to operate the experiments at constant pressure but different oxygen partial pressure.

The flow of gases through the apparatus starts as the gas leaves the cylinders and flows through a mass flow controller and into the combustion cell via a preheating coil. This arrangement allows the gas flow rate to the combustion cell inlet to be held constant while the pressure within the cell is continuously monitored. The combustion cell and preheating coil are both located inside a tube furnace.

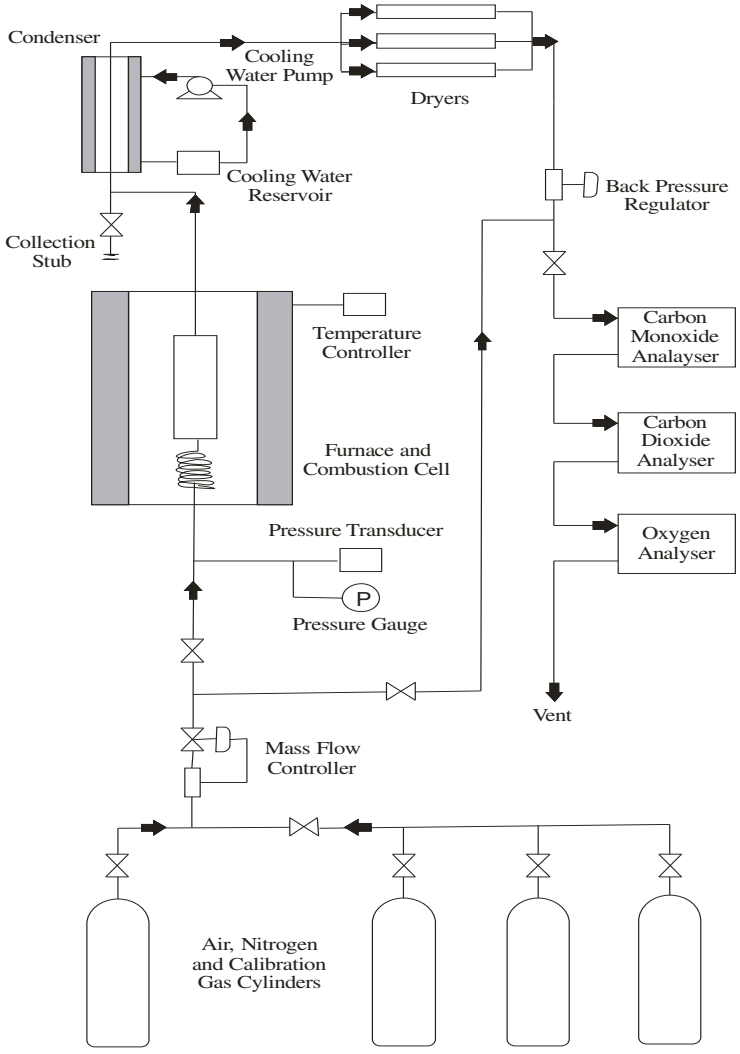

Figure 3.1 - Schematic flow diagram of the evolved gas analysis experimental rig.

Table 3.1 - Specifications of major equipment items.

Item	Model	Range
Mass flow controller	Brooks 5850E	0-500 smL/min
Temperature controller	Eurotherm 815P	0-1200°C
Pressure regulator	Tescon back pressure regulator	Up to 800 kPa
Gas analyser	Rosemount 870 Hartman and Barun, Uras 10E	0-5 mol% CO Accuracy: ±0.025 mol% CO 0-20 mol% CO_2 Accuracy: ±0.025 mol% CO_2 0-25 mol% O_2 Accuracy: ±0.025 mol% O_2
Vertical tube furnace	Tetlow Kilns & Furnaces	1200°C
Data logger	Datataker DT80 Series 2 with channel expansion module CEM20	15 channels
Submersible pump	Slaterpumps (Model: 3E-12NY)	240 volt
Dryer	10-mm outside diameter × 150-mm long stainless steel pipe	

Gases leaving the cell pass through a cleaning system comprising of a condenser and three dryers. The cooled and dried gases then flow to a back pressure regulator which is used to control the pressure within the combustion cell. The gases then pass through three gas analysers (O_2, CO and CO_2) connected in series. Finally the gases are vented to the atmosphere. Figure 3.2 features the photograph of the gas analysers and control panel. In Figure 3.3 the furnace and gas cleaning systems are shown.

3.2.2 Combustion cell

Figures 3.4 and 3.5 show a cross-section and the photographs of the combustion cell, respectively. The combustion cell and preheating coil are placed at the heart of the tube furnace with the water-cooled condenser above and to one side. The stainless steel preheating coil of nominal 3mm diameter is wound in a spiral shape to form the coil. Gas passes through the preheating coil and then into the base of the cell. The function of the preheating coil is to ensure that the gas entering the cell is preheated to the same temperature as the cell. The combustion cell is a cylindrical steel vessel, designed to handle pressure up to 900kPa, closed at both ends with plugs, O-rings and screwed on end caps. The O-rings are made of copper to provide an effective high temperature pressure seal. Within the cell are two thin-walled stainless steel cups with perforated bases to allow gas to pass through. The bottom cup is filled with sand and acts as both a flow distributor and a final preheater for the gas passing through the cell. The upper cup is 27.0mm in diameter and 70.7mm high. This is the sample cup which holds the mixture of biomass material and sand used in the study. A sample cup of 27.0mm diameter was selected in this study as recommended by Fassihi *et al.* (1984) in order to minimise the radial temperature gradient. The sand in the upper cup functions both as flow distributor and as a thermal capacitance, damping out temperature fluctuations associated with endothermic and exothermic decomposition or oxidation reactions ensuring that all temperature follow a linear rate of increase. Quartz sand with a size range of 425-500μm and the bed porosity of 40 ± 0.5% was used. Screens of wire mesh are placed on the bottoms of both cups and on top of the sample cup to contain the sand.

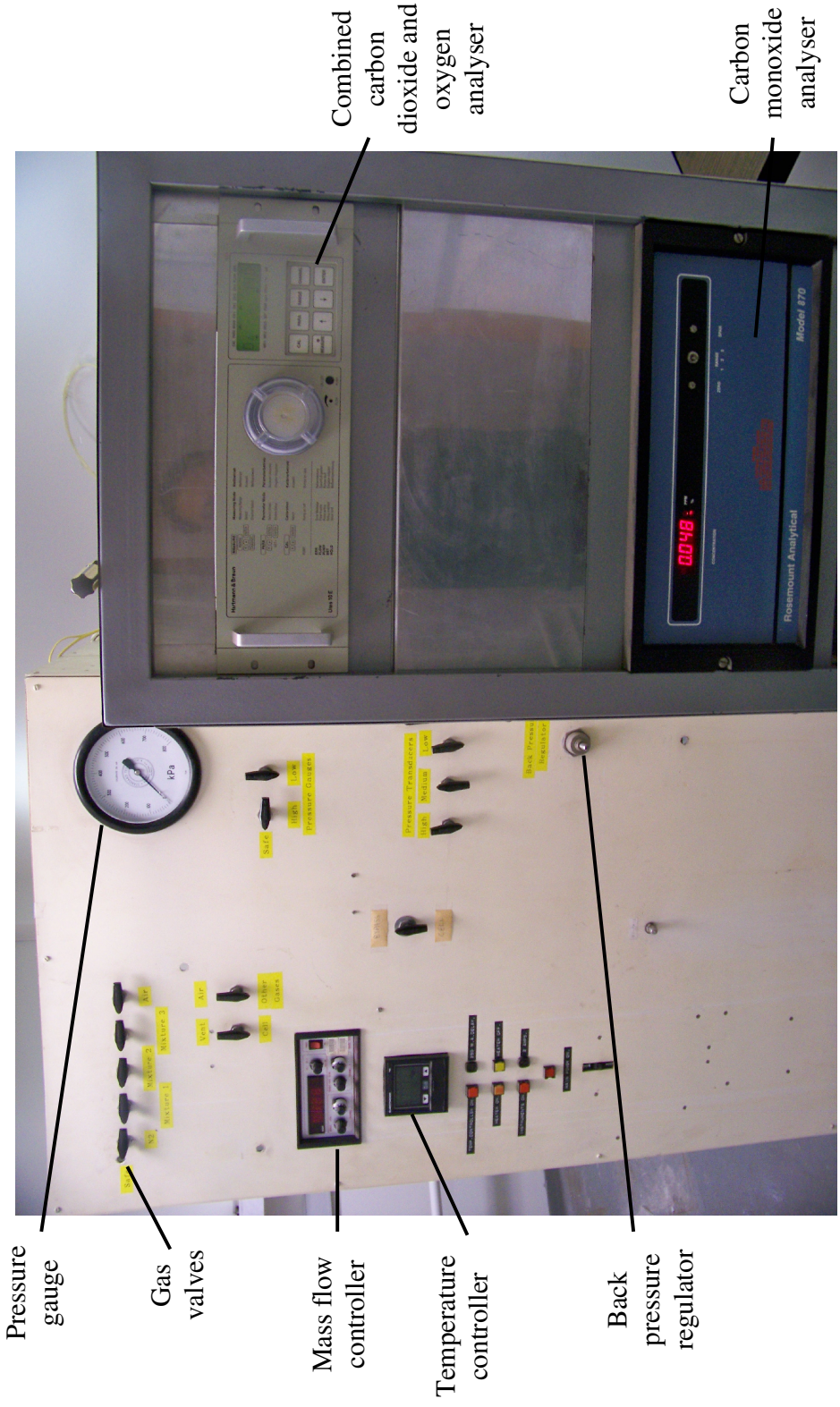

Figure 3.2 - Photograph of experimental rig showing the control panel and gas analysers.

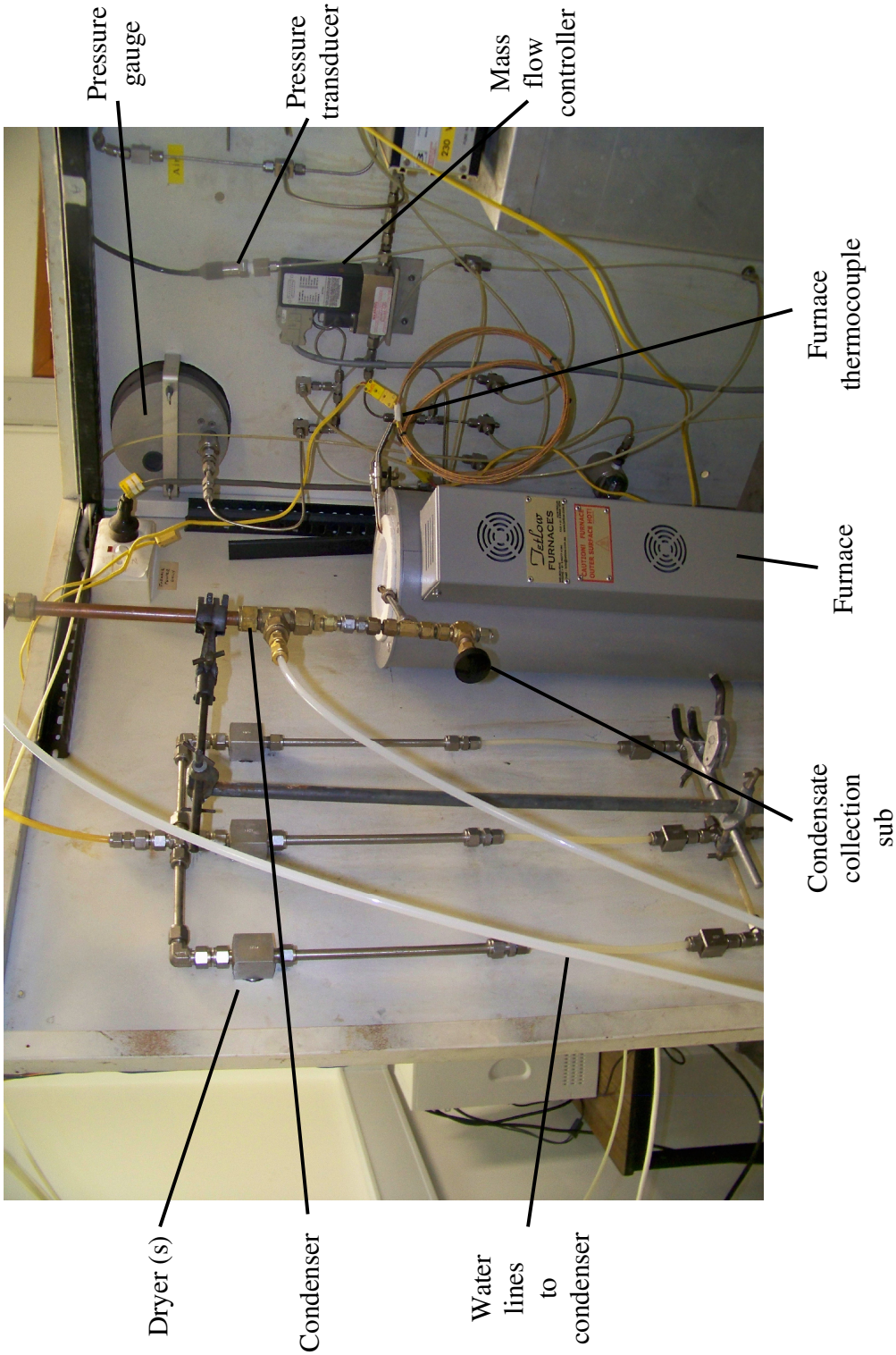

Figure 3.3 - Photograph of the experimental rig showing furnace and gas cleaning system.

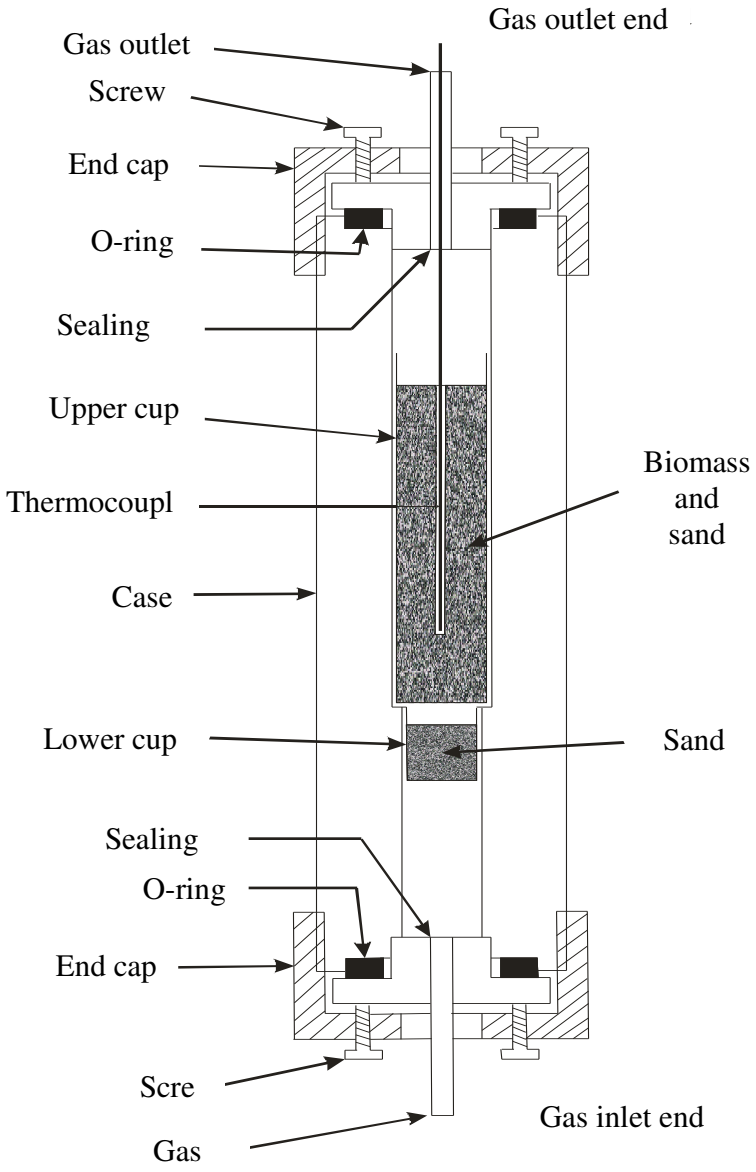

Figure 3.4 - A cross-section of the combustion cell showing the two cups and thermocouple position (not to scale).

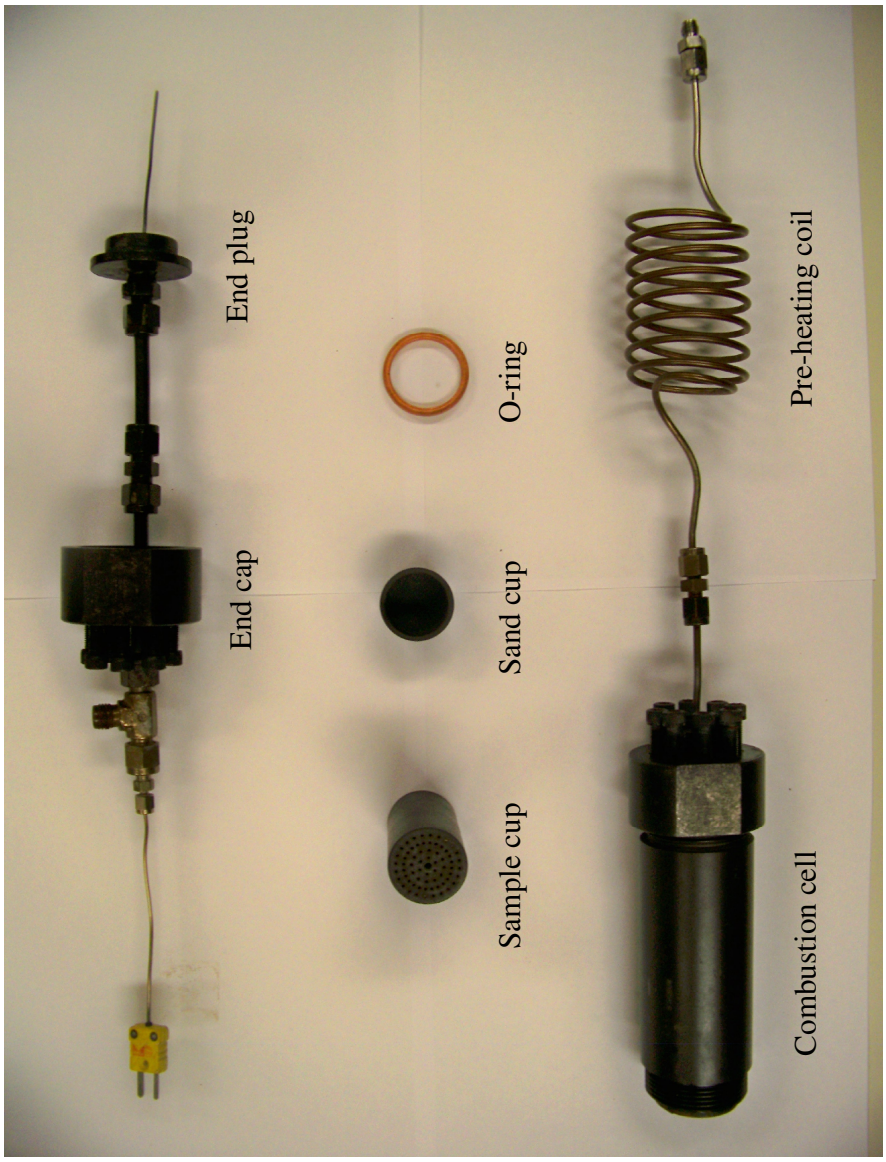

Figure 3.5 - Photographs showing the combustion cell, pre-heating coil and the two cups.

Gas flowing from the sample cup exits through the top of the cell into the condenser. The condenser is fitted with a small collection stub so that any condensed material does not drain back into the cell.

Initial work by Kisler (1995) with the condenser directly above the cell resulted in inconsistent results as condensed hydrocarbons would drain back into the cell and would re-ignite thus producing sharp changes in gas concentrations. For this reason the condenser is offset to one side of the cell by about 150mm. Table 3.2 presents the specifications of the combustion cell.

3.2.3 Temperature control

Two K-type thermocouples are used to monitor the temperature in the experiments with the measurement errors typically ±0.5°C of the reading. One thermocouple is placed vertically in the cell with the tip just above the upper cup base (see Figure 3.4). A second thermocouple is positioned within the furnace but outside the cell in order to monitor the furnace temperature. Based on the experience of Kisler (1995), there is usually a lag between the furnace and the cell temperature of about 20°C throughout an experimental run. The lag is caused by the time taken for heat to be conducted from the furnace wall to the sample cup since both the air surrounding the combustion cell and the cell wall need to be heated.

Typically, in this study, a heating rate of 50˚C/hour was chosen since it provides both a reasonable length experiment (7 hours from 150˚C to 500˚C) and significant gas production levels (1 to 2 mol% oxygen consumption and carbon oxides production). During some experimental runs the cell temperature reaches a peak, of up to 20°C above the heating schedule, at the point where oxygen consumption is greatest. This temperature peak is due to the heat generated by the exothermic oxidation reactions that occur within the cell. After this peak the cell temperature slowly drops back to below the furnace temperature. The cell and furnace temperatures then increase according to the heating schedule. The data analysis is based on cell temperature and not the furnace temperature.

Table 3.2 - Combustion cell specifications.

Item	Material	Dimensions
Case	Steel	48.20-mm outside diameter 30.05-mm inside diameter at top 28.5-mm at base 133-mm long
End cap	Steel	
Sealing Plug	Steel	
O-ring	Copper	Top - 4.94-mm thickness 30.42-mm inside diameter 36.65-mm outside diameter Base- 5.06-mm thickness 28.63-mm inside diameter 36.55-mm outside diameter
Lower Cup (sand)	Steel	28.50-mm outside diameter 25.32-mm inside diameter 27.04-mm long
Upper cup (sample)	Steel	30.10-mm outside diameter 27.00-mm inside diameter 70.72-mm long
Thermocouple	K-type	1.52-mm diameter 755-mm long
Piping	Plastic and stainless steel	3-mm diameter Swagelok fittings

3.2.4 Flow control

The gas mass flow rate controller controls the inlet gas flow rate into the combustion cell. The inlet gas flow rate during experiments is relatively stable and typically does not vary by more than ±0.4mL/min over a 12 hours period. The standard typical flow rate is 400 standard milliliters (smL/min) measured under standard conditions (1 atm and 25°C). This flow rate was selected as the flow rate is high enough to reduce the lag time between the combustion cell and the gas analyser but low enough for a considerable amount of carbon oxides to be observed.

3.2.5 Pressure control

A manual back pressure regulator is used to maintain the cell at the desired pressure. It is located downstream of the cell, condenser and dryer (see Figure 3.1). The regulator allows the pressure in the system to be maintained within ±5kPa of the desired value under normal condition but it can fluctuate by ±10kPa and sometimes up to ±20kPa depending on the oxidation reactions with the produced gas hanging rapidly (Kisler, 1995). The maximum working pressure of the system is 800kPa and typically the experiments are performed at a pressure of 400kPa to 700kPa. The system pressure is measured by a pressure transducer or pressure sensing device with a voltage output that has an accuracy of 0.25% of full scale. The actual output is directly proportional to the pressure transducer input power or excitation. The measured pressure is relative to ambient atmosphere pressure. All pressures quoted in the report are absolute pressures unless otherwise stated.

3.2.6 Condenser system

The condenser system consists of a single shell and tube heat exchanger, a submersible pump and a water reservoir. The purpose of the condenser is to cool down the gases and prevent any liquids such as water and light hydrocarbons from entering or any vapour from condensing into the gas analysers. The condenser is placed downstream from the combustion cell in order to condense the vapours leaving just the CO, CO_2, N_2 and O_2

to pass through the gas analysers. The hot gas from the cell flows through the tubeside while the cooling water is recirculated through the shellside of the exchanger. The location of the condenser system may be seen in Figure 3.3.

3.2.7 Dryer system

The dryer system consists of three steel tubes containing calcium sulphate anhydrous (drierite) and a glass wool with three inlet and outlet valves. The tubes are connected in parallel with only one in operation at any one time. Each column is 150mm in length and 10mm in outside diameter. The sizes of the column are chosen to minimise the dead volume between the cell and the gas analysers. The purpose of the dryer system is to absorb water, water vapour and liquids produced after the gas passes through the condenser. It acts to protect to the gas analysers from these compounds which could impair their operations. The location of the dryer system may be seen in Figure 3.3. All three dryers outlet valves are always opened during the experiment. Just one dryer inlet valve is opened while the two other dryers inlet valves are closed to allow the gas to pass through one column at a time. When drierite crystals in the first dryer become saturated with water, the second dryer is used by opening the second dryer inlet valve while immediately closing the first dryer inlet valve. A similar manner is employed for the third dryer. This sequence is selected to restrict the fluctuation in flow rate when changing over dryer. It is found experimentally that the change from the first dryer to second dryer are best to take place when the cell temperature reaches 250˚C and 350˚C, respectively. The short time in changing between the second to the third dryer is due to a considerable amount of water produced by biomass decomposition at that temperature range.

3.2.8 Analyser system

The gas analyser system consists of two units arranged in series. The first unit measures the carbon monoxide content of the gases and the second unit is for both carbon dioxide and oxygen measurement. The measurement ranges and accuracy of the analysers are presented in Table 3.3.

Table 3.3 - Range and accuracy of the gas analysers.

Analyser	Range (mol%)	Accuracy (% of full scale value)	Accuracy (% of reading)
Oxygen	0-25	± 0.5	± 0.125 mol% O_2
Carbon monoxide	0-5	± 0.5	± 0.025 mol% CO
Carbon dioxide	0-20	± 0.5	± 0.10 mol% CO_2

The lag time is the time taken for the gases to travel from the combustion cell outlet through the back pressure regulator and through the dryer tubes to reach the analysers. The recorded CO, CO_2 and O_2 data at particular temperature are not the actual concentrations of the gases at that temperature. They are actually the concentrations of CO, CO_2 and O_2 in the gases at an earlier time. A correction must therefore be performed by shifting the gas analyser data to compensate for this lag time.

The combustion cell lag time is determined by changing the concentration of the gas flowing through the cell until the gas analysers record 95% of its final value. The process is applied to all the analysers. The response curves are shown in Figure 3.6, 3.7 and 3.8 for an operating pressure of 500kPa and flow rate of 400smL/min. As expected the order of response is CO, CO_2 and O_2 since this is the order in which the gas flows through the analysers. The lag time of the combustion cell depends on the operating pressure. For an operating pressure of 500kPa and a flow rate of 400smL/min, the response times of CO, CO_2 and O_2 analysers are 116, 118 and 138 seconds, respectively.

Kisler (1995) in his work with light crude oil oxidation study logged the data at 30 seconds interval rounded the data to the nearest tenths of the CO, CO_2 and O_2 response times. Based on Kisler (1995), even though interpolating the experimental data to get more accurate residence time may be performed, it was not considered worthwhile.

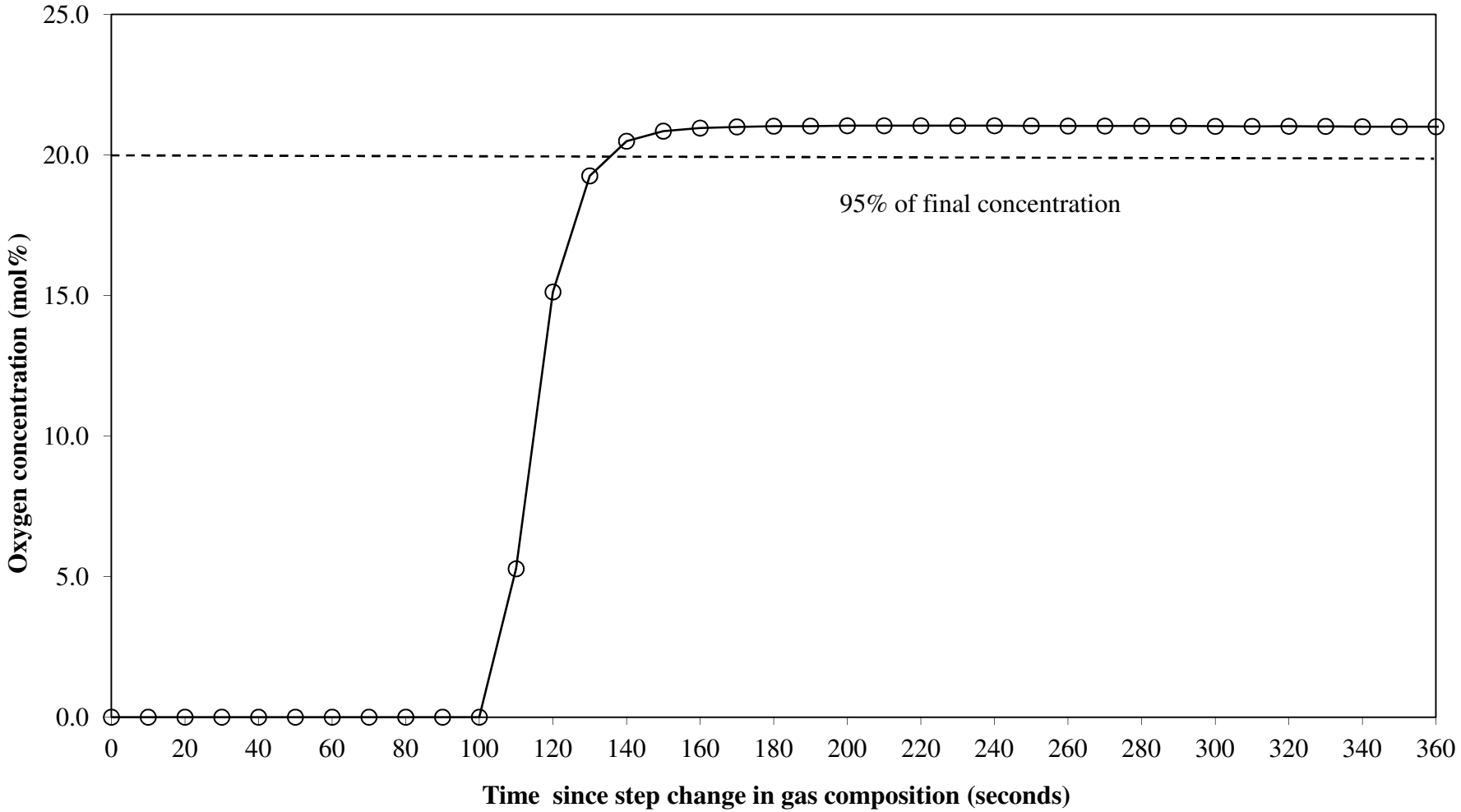

Figure 3.6 - Response of the oxygen analyser to a step change from 0.00 mol% to 20.96 mol% oxygen (air) for an operating absolute pressure of 500kPa and injection flow rate of 400smL/min.

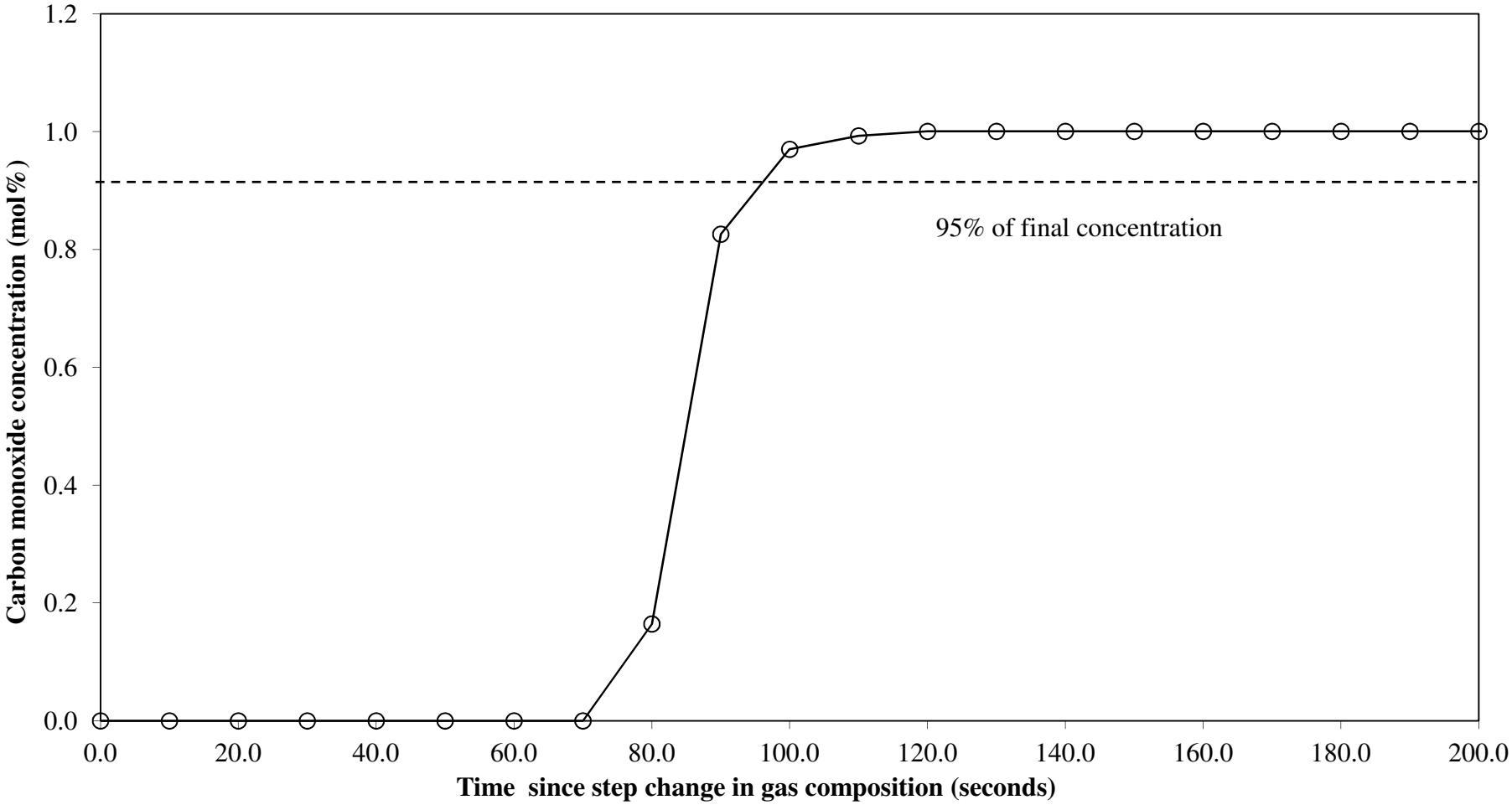

Figure 3.7 - Response of the carbon monoxide analyser to a step change from 0.00 mol% to 0.98 mol% carbon monoxide for an operating absolute pressure of 500kPa and injection flow rate of 400smL/min.

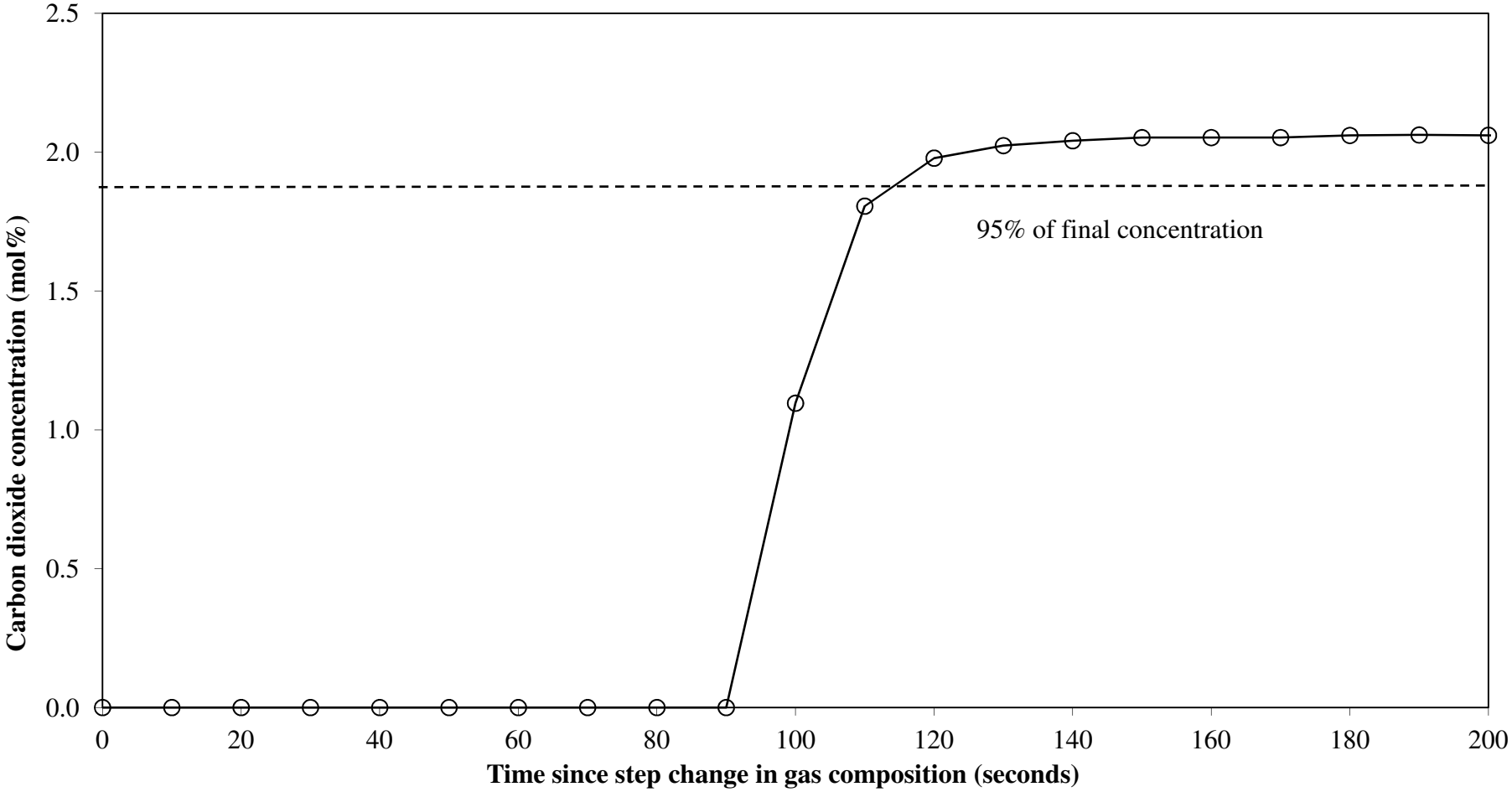

Figure 3.8 - Response of the carbon dioxide analyser to a step change from 0.00 mol% to 2.01 mol% carbon dioxide for an operating absolute pressure of 500kPa and injection flow rate of 400smL/min.

A typical run takes over 9 hours and involves 1000 readings, hence, a residence time of ±10 seconds is sufficiently accurate. The error introduced was very minimal with the overall total experimental readings error was reported at below 0.5%. In this study the data were recorded to regular 10 seconds intervals and with typical run taking over 9 hours and involving 3000 readings the combustion cell lag times may be rounded to the nearest tenths. The error introduced was three times lower than Kisler (1995) since the data are recorded at 10 seconds interval. The combustion lag time may be taken as 120, 120 and 140 seconds for CO, CO_2 and O_2 analysers, respectively.

3.2.9 Data acquisition

A data logger and personal computer are used to record and monitor the experimental runs. Seven channels are logged:

- cell temperature,
- furnace temperature,
- cell pressure gauge,
- inlet gas flow rate,
- O_2 content,
- CO_2 content,
- CO content.

The gas mass flow controller and the three gas analysers produce voltage signals which are measured by the data logger. The pressure transducer returns a voltage signal to the logger. A K-type thermocouple which is connected directly to the data logger is used to monitor the temperature. The data logging program allows the data sampling interval of 1 second to 1000 seconds. For the experiments of the present study, the data is recorded at 10 seconds intervals.

3.3 Test materials

A mixture of sand and biomass was prepared for each run. As repeatability is vital when dealing with biomass material, which is a heterogeneous substance, it is important to ensure that materials are taken from the same known source.

3.3.1 Palm fibre

The palm fibre was obtained from a palm oil factory located in Labu, Negeri Sembilan, Malaysia. It is a biomass waste and sometimes being used as a boiler fuel or for composting. Figure 3.9 shows a photograph of the palm fibre. Typical samples of palm fibre are relatively heterogeneous as may be seen in Figure 3.9. It was concluded that it was necessary to segregate the samples From the segregation process, it was concluded that there are three sample types of the palm fibre. They are loose fibre, clump fibre and kernel. The photographs of these samples are presented in Figures 3.10 to 3.12. The proportions of loose fibre, clump fibre and kernel that expected to present in the palm fibre sample are 60:30:10, respectively.

Figure 3.9 - Photograph showing the palm fibre.

Figure 3.10 - Photograph showing the loose fibre (Scale: 1 cm × 1 cm).

Figure 3.11 - Photograph showing the clump fibre (Scale: 1 cm × 1 cm).

Figure 3.12 - Photograph showing the kernel (Scale: 1cm × 1 cm).

3.3.2 Palm fibre char

The palm fibre char was produced from the raw sample using a fluidised bed reactor (see Figure 3.13) located at the Department of Chemical and Environmental Engineering, Faculty of Engineering, Universiti Putra Malaysia. The reactor was made of stainless steel pipe and externally heated by the electrical furnace. The total height of reactor was 850mm with the bed diameter of 55mm. Thermocouples set at three zones along the total height of the reactor for control and temperature adjustment to the desire temperature for the pyrolysis process. The palm fibre sample was pyrolysed in the fluidised bed reactor and heated from room temperature to 550°C at 10°C/min under the nitrogen flow. These were based on literature studies that the optimum biomass char may be obtained by heating the biomass to a temperature ranges of 400°C to 650°C and at low heating rate of 0.01°C/s to 2°C/s (up to 35% biomass char yield) in the absence of oxygen (Ghani *et al.*, 2011). The fluidisation velocity of the nitrogen gas was 0.1 m/s and the bed material consisted of sand. The temperature (550°C) was maintained for 60 minutes before the heating was stopped and the sample cooled naturally to below 100°C. the biomass char was collected from the inside of the rig. The palm fibre char produced from the pyrolysis process was then subjected to a series of evolved gas analysis (EGA) experiments. Figure 3.14 shows the photograph of the palm fibre char.

Figure 3.13 - Photograph showing the fluidised bed reactor used for palm fibre char production.

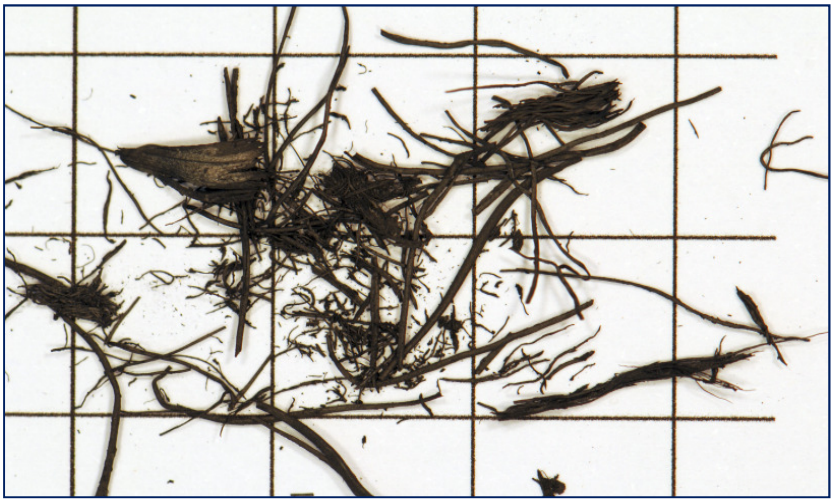

Figure 3.14 - Photograph showing the palm fibre char (Scale: 1cm × 1 cm).

3.3.3 Rice husk

The rice husk used in this study is originated from the State of New South Wales. This biomass waste currently is incinerated or utilised as boiler fuels for steam generation. Some of the husk was also used in the cement industry. Figure 3.15 shows a photograph of the rice husk.

3.3.4 Sand

Quartz sand was obtained from commercial minerals, Victoria, Australia. This sand was nominal grade 300µm to 600µm (*i.e.* 300µm < Grain size < 600µm) and typically experiments were conducted using sand from 425-500µm size range. Using a density flask the sand was experimentally determined to be 2.641g/cm^3 (Kisler, 1995).

Figure 3.15 - Photograph showing the rice husk.

3.4 Instrumental analyses

Instrumental analyses used in this research are the elemental analyser, thermogravimetric analyser (TGA) and bomb-calorimeter for the determination of calorific values. These instruments are used in the ultimate and proximate analyses of the biomasses. The proximate analysis was carried out according to ASTM standards (ASTM D5142-02a) using thermobalance TGA/SDRA51e manufactured by Mettler Toledo while the ultimate analysis was performed using a Thermo Finnigan Flashed 1112 analyser according to ASTM D5373-02. The calorific value was achieved based on ASTM D2015-96 using Ika-works C5000 calorimeter.

3.4.1 Elemental analyser (CHNSO analyser)

By using this analyser for ultimate analysis, the percents of carbon, hydrogen, nitrogen and sulphur in biomass is obtained with oxygen being calculated by difference from the four elements. The elemental analyser used is Thermo Finnigan Flashed 1112 model with helium gas as carrier. The ultimate analysis was carried out according to ASTM standards (ASTM D5373-02).

Figure 3.16 - Photograph showing the elemental analyser.

This instrument is located at the Faculty of Chemical Engineering, Universiti Teknologi MARA, Shah Alam, Malaysia. The CHNSO series instruments may determine the carbon, hydrogen, nitrogen and sulphur for homogeneous organic material. High temperature combustion is used as the means of removing the elements from the material. In the combustion process, a nominal 2mg sample is encapsulated in a tin or silver capsule. The sample is placed in the sample loading chamber and held there until a dose of oxygen has been released. The sample is then dropped into the furnace at the same time the oxygen arrives. The sample is combusted by the heated oxygen-rich environment. The products of CHNSO analysis are CO_2, H_2O, NO_x and SO_x. These gases, which are carried through the system by the helium carrier are swept through the oxidation tube packed with copper sticks (which removes oxygen), to complete the conversion to SO_2. These gases were passed through four infrared detectors of C, H, N and S and the results are displayed as weight percent C, H, N and S. Figure 3.16 shows a photograph of the elemental analyser.

3.4.2 Thermogravimetric analyser

The percents of moisture, volatile matter, fixed carbon and ash were determined using thermobalance TGA/SDRA51e manufactured by Mettler Toledo for proximate analysis that is located at the Faculty of Chemical Engineering, Universiti Teknologi MARA, Shah Alam, Malaysia. Proximate analysis was carried out according to ASTM standards (ASTM D5142-02a). For each analysis, about 10 - 15mg biomass sample was weight and placed inside of ceramic furnace, cylindrical shape inside of the analyser. The heating rate was set at 35°C/min. Nitrogen gas was used at the beginning. When the mass loss plateau was established in the temperature range of 600°C to 950°C, the gas was switched over from nitrogen to air to determine the ash and fixed carbon content. The temperature reached 1300°C by the end of analysis. During the analysis, a thermogravimteric analysis (TGA) graph appears on the monitor screen and data will be transferred to the computer and calculated based on weight loss procedure by given software. Figure 3.17 shows the photograph of the thermogravimetric analyser.

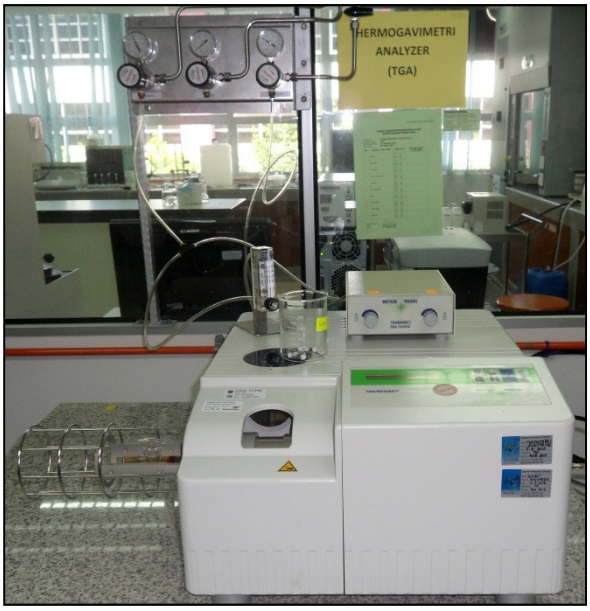

Figure 3.17 - Photograph showing the thermogravimetric analyser.

3.4.3 Bomb-calorimeter

Calorific values analyses of biomass samples were conducted at the Faculty of Chemical Engineering, Universiti Teknologi MARA, Shah Alam, Malaysia using Ika-works C5000 Calorimeter model. The C5000 Calorimeter is a Digital Signal Processing (DSP) microprocessor based instrument; developed to measure the calorific content of various organic materials such as biomass and other polymerise materials. The calorific value was determined based on ASTM standards (ASTM D2015-96). The calorific value of a sample is determined by burning the sample in a controlled environment. The heat released by combustion is proportional to the calorific value of the substance. In the C5000 calorimeter, the sample being analysed is placed in a high-pressure environment called a combustion vessel. The combustion vessel is surrounded by water and the sample is ignited. The temperature of the water is then measured by an electronic thermometer with a resolution of 1/10000 of a degree. During analysis, the fan speed is modulated to control the jacket temperature. In this isoperibol system, there may be some energy exchange between the outside environment and the water surrounding the combustion vessel. This is accounted for by continuously monitoring the bucket and jacket temperature during analysis. The heat exchange due to environmental conditions is then calculated. The microprocessor measures the temperature of the water surrounding the combustion vessel every six seconds. The analog to digital converter converts this output into a binary number that is stored in memory. The computer processes the difference in water temperature between pre-fired and post-fired where the results is corrected for the length of the fuse wire. Figure 3.18 shows the photograph of the bomb calorimeter.

3.5 Experimental procedure

The experimental procedure is adapted from Kisler (1995) in his light crude oil oxidation study and further improved and modified for the use with biomass materials. It is important to follow the experimental procedure in order to minimise the error and obtain reproducible results.

Figure 3.18 - Photograph showing the bomb calorimeter.

The experimental procedure may be divided into four parts; preparation of sample, during the experiments, conclusion of the experiments and rig recovery. Due to length of time required for each experimental run the biomass material and sand sample was prepared on the previous day. Several other items could also be set up ahead of time. The summarised steps taken are, in order:

3.5.1 Sample Preparation

1) The sample is prepared by placing 40.5g consisting of 40g of sand and 0.5g of biomass materials of well mixed sample into the upper cup. The lower cup is filled with fresh sand. A layer of sand is created at the top and the bottom of the sample cup out of the 40g sand. The mixture of biomass and the rest of sand are put in the middle between the layers. By covering the biomass with sand, the temperature follows a linear rate of increase.
2) The two cups are placed inside the combustion cell. The cell thermocouple is inserted into the upper cell and the cell is sealed with screw on caps. A pressure test is performed on the combustion cell to ensure that it does not leak.

3) The combustion cell is placed within the annular furnace and connected to the inlet and outlet tubings.
4) The dryers are packed with fresh drierite and the end of each tube is packed with glass wool to contain drierite.
5) The dryers and condenser are connected to the system.
6) The system is tested for leakage under pressure.

3.5.2 During the run

1) The power is turned on to all instruments and to the computer.
2) The nitrogen flow is commenced through the system and the flow rate is set to 400 mL/min at the desired pressure and at bypass mode.
3) The heating rate is commenced and the heating rate is set to 50°C/hour. The temperature is held at 130°C for 10 minutes allowing the cell temperature to heat up. Oxygen consumption typically does not start until a temperature of at least 160°C.
4) The data logging program is started.
5) The first gas calibration is started using a range of concentrations of CO, CO_2 and O_2 and ensuring that at least 10 minutes is allowed for each mixture gas to reach stable data.
6) The cooling water pump is turned on when the condenser external surface begins to heat up, typically at a cell temperature of about 100°C.
7) After finishing the first calibration, the cell mode is switched and nitrogen is purged for about 10 minutes.
8) Air is switched and the heating schedule is re-commenced at the appropriate heating rate.
9) The barometric pressure is recorded.
10) The pump, pressure gauge, mass flow controller and gas analysers are checked regularly to identify any problems.

3.5.3 Conclusion of runs

1) The heater and temperature controller are switched off.
2) The nitrogen is swapped and run through cell for about 20 minutes.
3) The bypass mode is switched on.
4) The second calibration gases are run to calibrate the analysers with the nitrogen to be the last gas.
5) The gas flow is stopped and pressure is released.
6) The data logger is stopped.
7) The data files are backed up for security.
8) The power to rig is shut down.
9) Thermocouple and cell are removed from the furnace after the cell has cooled for at least several hours.
10) The following items are checked for modification, repairs or replacement prior to the next run – gas cylinders, drierite, pump, data acquisition program, condenser and thermocouples.

3.5.4 Rig cleaning and recovery

1) Test cell is removed from furnace and opened.
2) The samples are removed from cell. Ash and sand are retained.
3) The O-rings are checked and cleaned using wire brush.
4) The cell is water cleaned and dried.
5) The spent drierite is removed and regenerated.

3.6 Details of experimental runs

A total of forty-eight experimental runs were performed throughout the study. Thirty-nine experiments out of forty-eight will be discussed in this thesis. The other nine runs were considered unusable due to the sample preparation error, commissioning problems and equipment failure. These unsuccessful runs are discussed in Section 3.6.1 with the successful runs summarised in Section 3.6.2.

3.6.1 Unsuccessful runs

A number of preliminary experiments were conducted to establish an appropriate biomass to sand ratio. This experiments showed that if too much biomass were present, carbon monoxide levels in the effluent gas could exceed the upper limit of the range set on the measuring instruments. In addition, during periods when exothermic reactions were occurring, the cell temperature could rise above the desired level; this had the effect of increasing reaction rates, further accelerating rates of heat generation and leading to unwanted temperature and carbon oxide concentration “spikes”. On the other hand, too low a biomass content was found to give very low carbon monoxide readings on the measuring instrument, thereby introducing larger than desirable inaccuracies into measured gas compositions. A sample size of 40.5g consisting of 40g of sand and 0.5g of biomass materials was settled on; for this mixture the rate of temperature increase in the cell remained linear while at the same time effective use was made of the measuring instrument ranges.

Other experimental runs had to be aborted due to equipment failure. The failed runs include blockage in the dryer which resulted in it becoming impossible to control the cell pressure. Based on these unsuccessful runs, a suitable changeover dryer time was successfully devised. It was further found that the equipment must be cleaned thoroughly to avoid any blockage at the condenser, regulator and along the gas lines.

Several experiments were also aborted due to sample preparation error. Biomass materials needed to be well mixed with sand in the sample cup. The sand in the sample cup acts both as flow distributor and as a thermal capacitance, damping out temperature fluctuations associated with endothermic and exothermic decomposition or oxidation reactions ensuring that all temperature follow a linear rate of increase. If the biomass and sand were not mixed properly, the temperature will not follow a linear rate and the data could not be used.

3.6.2 Successful runs

The thirty-nine successful experiments have been divided into three groups: rice husk, palm fibre and palm fibre char. For the rice husk oxidation study, eight experiments were performed including reproducibility study, heating rates effect and pressures effect (total and oxygen partial pressure). For the palm fibre, the twenty-two experiments were conducted to study the reproducibility, heating rates effect and pressures effect (total and oxygen partial pressure). Further study on various types of palm fibre (i.e. clumped fibre, loose fibre and kernel) were also performed. The remaining nine experiments were conducted for the palm fibre char to study the reproducibility and pressure effect.

These runs are summarised in Table 3.4. Rice husk, palm fibre and palm fibre char are discussed in a separate chapter of this thesis, starting at Chapter 5.

3.7 Concluding remarks

The apparatus and experimental procedure used to study the oxidation kinetics of the three biomasses has been described and discussed. The evolved gas analysis (EGA) experimental data may be decoupled into a number of competing oxidation reactions. A reaction model is developed in Chapter 4 that will allow decoupling of EGA data into its constituent reactions. The model will enable kinetic parameters to be calculated for each of the competing oxidation regimes.

Table 3.4 - Summary of successful experimental runs.

Run type	No. of runs
Rice husk	8
Palm fibre – Loose fibre	17
Palm fibre – Clump fibre	4
Palm fibre – Kernel	1
Palm fibre char	9

CHAPTER 4

THE REACTION MODEL

4.1 Introduction

The total amount of oxygen consumed during an evolved gas analysis (EGA) experiment is the summation of the oxygen consumed by a number of competing and overlapping oxidation reactions. It is not possible to study individual oxidation reactions due to the chemical complexity of biomass. Previous workers such as Kisler (1995) and Nguyen (2004) have established that the overall mechanism may be represented by grouping the reactions into three classes referred to as low temperature oxidation (LTO), medium temperature oxidation (MTO) and high temperature oxidation (HTO). Each of these reaction regimes consist of a large number of similar competing oxidation reactions. In order to obtain the kinetic parameters for each of these competing reaction classes, the total amount of oxygen consumed in the EGA experiments must be decoupled into its constituent reaction regimes.

The primary kinetic parameters of interest are the pre-Arrhenius constant, activation energy, reaction order with respect to the fuel concentration and the partial pressure of oxygen for each class of oxidation reactions. Determining these parameters from the experimental EGA data will enable the influence of several experimental variables to be studied.

Investigation of the experimental variables will involve comparing the kinetic parameters calculated from a series of EGA experiments conducted under slightly different experimental conditions (Kisler, 1995). The mathematical model used in the research is that previously developed by de los Rios *et al.* (1988) and modified by Shallcross (1991). The model was also used by Kisler (1995) and Nguyen (2004) in their studies of the oxidation of crude oil. The aim is to develop a model that may be used to calculate the kinetic parameters from biomass EGA data, a material fundamentally different to crude oil. Once these parameters are known, a predicted oxygen consumption curve may be plotted and compared with the experimental data.

Typically, the oxidation reaction mechanism for biomass is assumed to involve three competing reaction regimes, known as low, medium and high temperature oxidation. Each class of oxidation reaction lumps together countless similar reactions. A low temperature oxidation (LTO) reaction involves the production of partially oxygenated compounds such as aldehydes and ketones. Medium temperature oxidation (MTO) reaction involves the oxidation of light hydrocarbons formed by pyrolysis of the LTO reaction products. High temperature oxidation (HTO) reaction involves the combustion of the solid fuel formed by the pyrolysis of the LTO reaction products (Kisler, 1995). Modeling of EGA experiments by most of the previous researchers considered three competing oxidation classes (de los Rios *et al*., 1988, Shallcross, 1991, Kisler, 1995, Nguyen, 2004). The three-stage model is based on the two oxygen peaks referred to as hemicellulose and cellulose. The three reaction regimes (LTO, MTO and HTO) add together to produce the total oxygen consumption curve. Previously, all reaction regimes are handled one at a time in a similar manner. The reaction model developed in this Chapter is assumed independent of the number of oxidation regimes and the reaction regimes of LTO and MTO are considered simultaneously. Previous researchers attempted to use both the oxygen consumption and carbon oxides production data as part of their modeling process. Fassihi *et al*. (1984) found that only total carbon oxides production data could be used but only applied to the MTO reaction alone. The modeling presented in this thesis relies only on oxygen consumption data.

The model derived in this Chapter is a modified and improved version of that developed by Fassihi *et al.* (1984) and further improved by Kisler (1995). The experimental technique has also been improved to allow data logging at 10 second intervals rather than 30 second intervals used by Kisler (1995).

This Chapter begins with a definition and derivation of a relative reaction rate term. Next, using weighted linear regression, the kinetic parameters may be calculated from a plot of relative reaction rate versus inverse temperature. Once the kinetic parameters have been obtained, a predicted oxygen consumption curve may be plotted using the equations derived in Section 4.4.

4.2 Relative reaction rate

The typical stoichiometric equation for biomass fuel combustion may be represented by:

$$CH_xO_yN_z \; + \; \alpha O_2 \; \rightarrow \; \beta CO_2 \; + \; (1-\beta)CO \; + \; \frac{x}{2} H_2O \; + \; \frac{z}{2} N_2 \qquad (4.1)$$

This reaction assumes the biomass fuel contains carbon, hydrogen, oxygen and nitrogen and that only carbon oxides, water and the inert nitrogen are left after reactions. The relationship between α and oxygen balance is given by:

$$y = \beta + 1 + {}^{x}/_{2} - 2\alpha \qquad (4.2)$$

The stoichiometric coefficient and ratio may be calculated by elemental analysis of the biomass fuel and from the composition of the effluent gas. In an EGA experiment the oxygen, carbon monoxide and carbon dioxide contents of the effluent gas are measured at regular time intervals.

The reaction rates of the three reaction regimes are assumed to be functions of the fuel concentration and the oxygen partial pressure:

$$R_{r_i} = k_i P_{O_2}{}^{m_i} C_{f\,i}{}^{n_i} \tag{4.3}$$

where, R_{r_i} is the reaction rate,

k_i is the reaction constant,

P_{O_2} is the oxygen partial pressure,

C_{fi} is the fuel concentration,

m_i is the reaction order with respect to oxygen partial pressure,

and, n_i is the reaction order with the respect to fuel concentration.

The subscript i represents the reaction regime considered, either for low temperature oxidation (LTO), medium temperature oxidation (MTO) or high temperature oxidation (HTO). Note that the fuel being consumed is different for each class of oxidation reaction. For example in a two stage model the fuel for LTO reaction involve the combustion of hemicellulose and the HTO reaction are supposed to involve the combustion of cellulose. Hence, the fuel for each reaction regime is dependent on what has occurred previously.

The reaction constants, k_i, for each reaction are assumed to follow the Arrhenius law behaviour:

$$k_i = w_i e^{-E_i/RT} \tag{4.4}$$

where, w_i is the pre-Arrhenius constant,

E_i is the activation energy of the particular oxidation reaction,

R is the Universal gas constant,

and, T is the absolute temperature.

It is further assumed that the difference in oxygen contents between the inlet and outlet gas streams across the reaction cell is due solely to the oxidation reactions. The oxidation reactions are also considered to involve only two reactants: oxygen and biomass fuel.

The rate of oxygen consumption by each oxidation regimes may be defined in terms of the injection gas flow rate and the change in oxygen content of the gas between the combustion cell inlet and outlet. The reaction rate of equation (4.3) and reaction constants of equation (4.4), may be equated to the rate of oxygen consumption:

$$\frac{q\Delta O_{2_i}}{AL} = w_i P_{O_2}^{m_i} C_{f_i}^{n_i} e^{-E_i/RT} \tag{4.5}$$

where, q is the volumetric flow rate of the injected gas,

ΔO_{2_i} is the increase in oxygen between the inlet and outlet gases expressed as a percentage of the inlet gas flow,

A is the cross-sectional area of the packed bed,

and, L is the length of the packed bed.

This assumes that the packed bed has a constant cross-section and a bed depth that does not change with the time. Rearrangement of equation (4.5) yields an expression for the instantaneous fuel concentration:

$$C_{f_i}^{n_i} = \frac{q\Delta O_{2_i}}{ALw_i P_{O_2}^{m_i} e^{-E_i/RT}} \tag{4.6}$$

The oxygen consumption rate is proportional to the rate of fuel consumption due to the oxidation reactions depend only the availability of biomass fuel and oxygen:

$$\frac{q\Delta O_{2_i}}{AL} = -\alpha \frac{dC_{f_i}}{dt} \tag{4.7}$$

where α is a proportionality factor and t is the time.

Equation relating E_i and w_i to ΔO_{2_i} may be derived from equation (4.6) and (4.7) excluding C_{f_i} since it cannot easily be measured experimentally.

At any time, *t*, the fuel concentration is C_{f_i}. However as *t* approaches infinity the fuel concentration drops to zero because all of the fuel will have been consumed. Integrating equation (4.7) between time, *t* and infinity yields:

$$-\alpha \int_{C_{f_i}}^{0} dC_{f_i} = \int_t^{\infty} \frac{q}{AL} \Delta O_{2_i} dt \tag{4.8}$$

The instantaneous fuel concentration is given by:

$$C_{f_i} = \frac{q}{AL\alpha} \int_t^{\infty} \Delta O_{2_i} dt \tag{4.9}$$

This assumes that the volumetric flow rate does not vary with time. Raising equation (4.9) to the power n_i and equating this with equation (4.6) produces an expression independent of C_{f_i}.

$$\left(\frac{q}{AL\,\alpha} \int_t^{\infty} \Delta O_{2_i} dt \right)^{n_i} = \frac{q \Delta O_{2_i}}{ALw_{\,i} P_{O_2}^{m_i} e^{-E_i/RT}} \tag{4.10}$$

β_i may be defined as equation (4.11) as:

$$\beta_i = \left(\frac{q}{AL} \right)^{n_i - 1} \frac{w_i P_{O_2}^{\ m_i}}{\alpha^{n_i}} \tag{4.11}$$

Combining equations (4.10) and (4.11):

$$\frac{\Delta O_{2_i}}{\left(\int_t^{\infty} \Delta O_{2_i} dt \right)^{n_i}} = \beta_i e^{-E_i/RT} \tag{4.12}$$

The relative reaction rate, R_{rr_i}, may be defined as:

$$R_{rr_i} = \frac{\Delta O_{2_i}}{\left(\int_t^{\infty} \Delta O_{2_i} dt \right)^{n_i}} \tag{4.13}$$

Combining equations (4.12) and (4.13) and taking the natural logarithms of both sides yields:

$$\ln R_{rr_i} = \ln \beta_i - \frac{E_i}{RT} \tag{4.14}$$

This equation shows a linear relationship between the logarithm of the relative reaction rate and inverse temperature.

The oxygen consumption data produced by an EGA experiment, ΔO_{2i}, is the sum of all competing reactions and not the oxygen consumed by just one of the reactions, ΔO_{2i}, as required by equation (4.12). In order to solve this problem it is assumed that at high temperatures only one reaction is occurring, typically known as the high temperature oxidation or HTO reaction. This implies that the oxygen consumption data at the end of a run, usually at 350°C to 450°C, is due solely to HTO reaction. Similarly, at very low temperatures of 150°C to 250°C, only low temperature oxidation (LTO) reaction will occur. At intermediate temperatures (250°C to 350°C) other competing and overlapping reactions will take place and grouped as the medium temperature oxidation (MTO) reaction. The decoupling of the total oxygen consumption curve for the HTO and MTO reactions is achieved by working from the high temperature end of the data to the low temperature data. As for the LTO reaction, the calculation starts at low temperature end of the data and moves to the high temperature data.

Considering equation (4.14) a plot of ln (R_{rr}) against inverse temperature should produce straight line region with a gradient of E_i / R and a y axis intercept of $\ln \beta_i$. An example of this plot is shown in Figure 4.1. Note that at low temperature (high inverse temperature) the straight line segment ends due to the influence of another oxidation reaction, i.e., the oxygen consumption data is no longer solely due to the HTO reaction. However, in order to

plot equation (4.14) the reaction order n_i must be known. Theoretically it is possible to use non-linear regression on equation (4.14) to determine E_i, β_i and n_i. Practically it is easier to use linear regression to obtain E_i and β_i and to iterate to find n_i (Kisler, 1995).

4.3 Linear regression of the relative reaction rate data

By plotting the log of the relative reaction rate against inverse temperature a straight line should be produced in the temperature range in which only one reaction is occurring (see Figure 4.1). Values for the kinetic parameters E_i and β_i may then be determined. In order to maximise the closeness of fit of the model, a weighted linear regression may be used. A weighted linear regression approach allows the more accurate data to be given a greater emphasis than the less accurate data (Kisler, 1995). The model is validated with the actual experimental oxygen consumption data.

4.3.1 Optimising the linear regression

Figure 4.2 shows a series of fitted lines to the one set of data. The parameters calculated by the linear regression are highly dependent on the choice of data points to be included in the analysis. The fitted lines were all obtained by linear regression but use a different ranges of data points. A procedure to standardise the curve fitting is required to determine the optimum line of best fit.

Kisler (1995) initially fitted straight lines using 10 adjacent data points at higher temperature. For his work, the data sampling interval was 30 seconds, i.e. ten points is equivalent to $4\frac{1}{2}$ minutes. From the fitted line the kinetic parameters E_i and βi could be determined by assuming $n_i = 1$. Next, a predicted oxygen consumption curve was plotted and a variance calculated by:

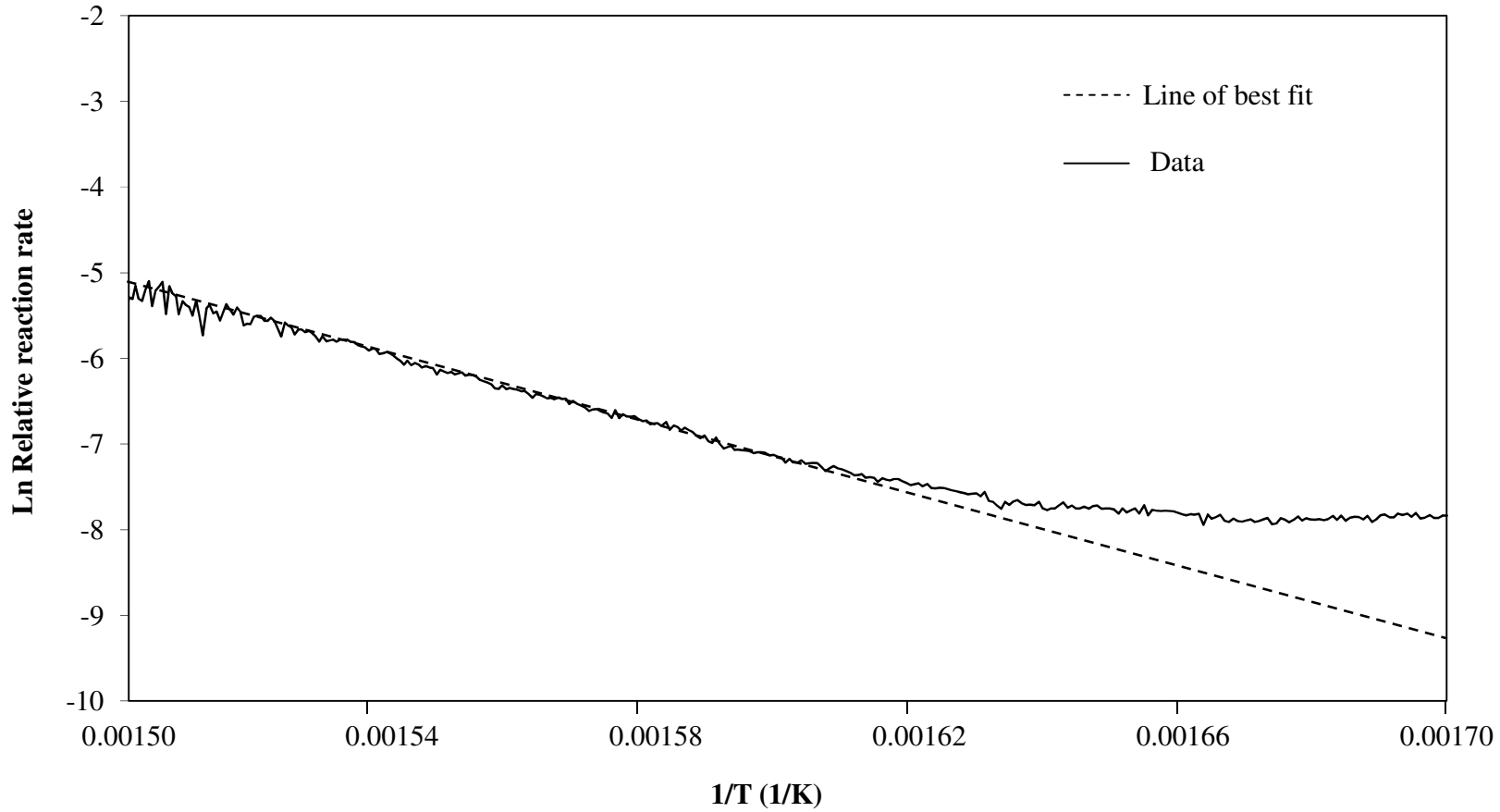

Figure 4.1 - Natural log of relative reaction rate plotted against inverse temperature. The data is for experiment F6. The straight line section represents the region where only high temperature oxidation (HTO) is occurring.

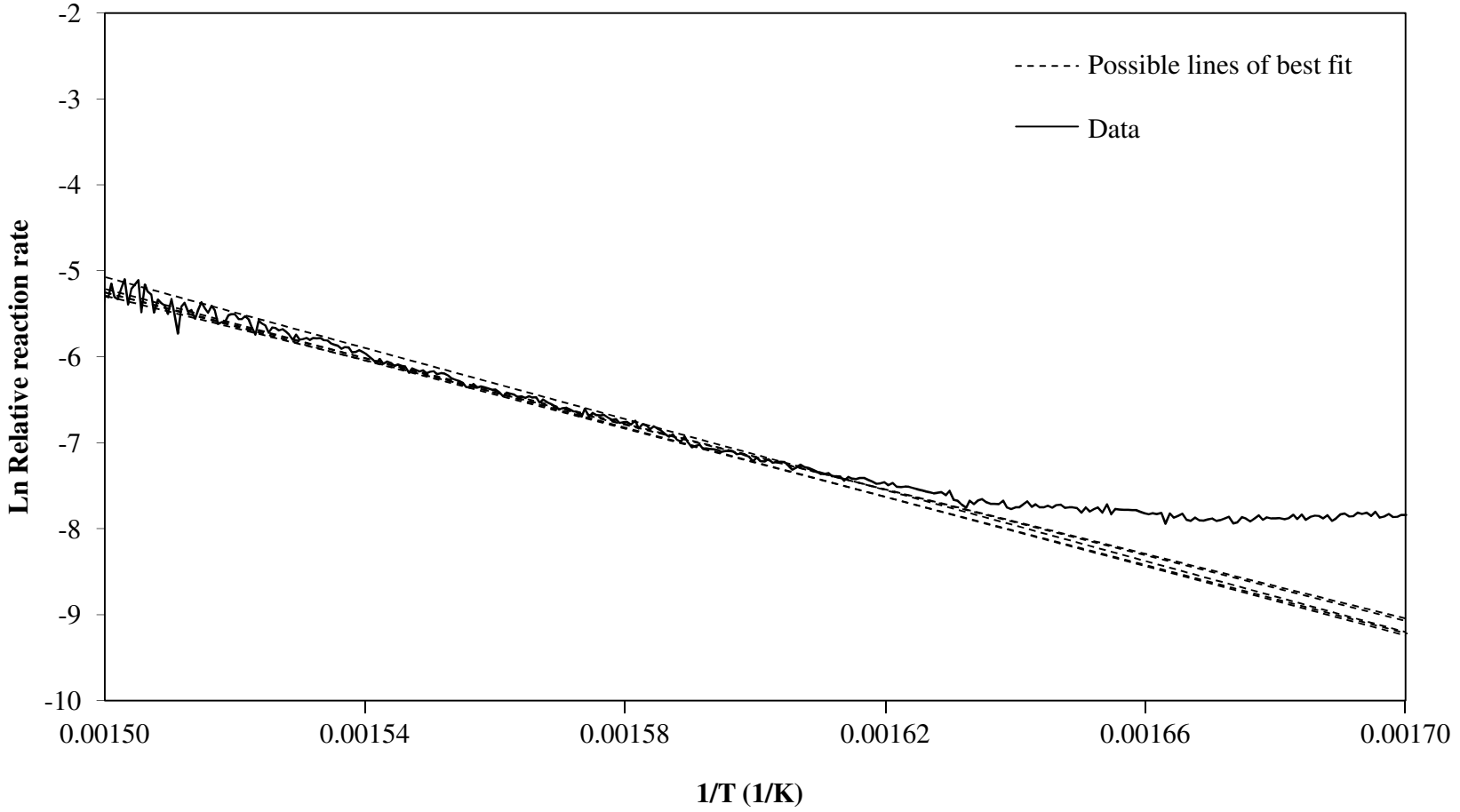

Figure 4.2 - Natural log of relative reaction rate plotted against inverse temperature. The data is for experiment F6. The straight lines were fitted by linear regression using a range of different data points.

$$\sigma^2 = \frac{\sum_{j=1}^{m} \left(\Delta O_{2\,j} - \Delta O_{2\,calc} \right)^2}{(m-2)} \qquad (4.15)$$

where, σ^2 is the variance,

m is the number of data points used in the regression, first point at time t_1 , and last point at time t_m,

and, m-2 is the degree of freedom.

Fitted lines which involve data around the ΔO_{2i} peak or large numbers of data points were therefore favoured. Once the variance had been calculated, one more data point was added to the previous 10 points. A new linear regression was performed on this set of eleven data points and the variance calculated again. More points were added at higher temperature until the minimum variance was found. By adding more data points in this manner an expanding number of points are being fitted around a constant starting point. The entire procedure is then repeated by moving the starting point to the next higher temperature data point.

The procedure used in this Thesis was similar except that the starting point and the next 30 higher temperature adjacent data points initially selected. Typically, the data points were at 10 seconds interval, i.e., 31 data points corresponds to 5 minutes. An additional data point was added to the higher temperature end for each iteration. The choice of the initial number of data points and whether to add one or two points at a time is arbitrary. It was decided to add only one point at a time to maximise the number of fitted lines tested (i.e., try 31, 32, 33, etc points instead of 31, 33, 35, etc).

Thirty-one data points were selected as the minimum number to be used since they cover a reasonable time period (five minutes), i.e., longer than any short terms fluctuations in the data. The choices made for this thesis were arrived at by trial and error using EGA data for biomass oxidation.

The curve fitting procedure may be summarised as follows:

1. select a starting point on the low temperature side of the oxygen consumption peak that is being considered;
2. perform linear regression, with equation (4.14) , using the next 30 adjacent points at higher temperature;
3. calculate the predicted oxygen consumption curve and the variance using equation (4.15);
4. add another data point to the previous 31 points (moving to higher temperature) and repeat calculation of variance;
5. keep adding points until the minimum variance is found and then moved the starting position by one data point (to higher temperature);
6. repeat steps 1 to 5 until the overall minimum variance has been found; and
7. repeat entire process for a range of reaction orders.

4.4 Calculation of oxygen consumption at any temperature working from high to low temperatures

Since the kinetic parameters E_i , β_i and $n_{i.}$ may be derived from the experimental data, the next task is to calculate the predicted ΔO_{2_i} curve over a range of temperatures. Shallcross (1991) derived a mathematical expression for calculating ΔO_{2_i} at any temperature. Later, Kisler (1995) used the same mathematical expression in calculating ΔO_{2_i}. The same approach of the mathematical expression is reproduced in this section. It assumes that the kinetic parameters and a series of regular time and temperature readings are known. A single known value of ΔO_{2_i} is also required to begin the calculations.

Recalling equation (4.12):

$$\frac{\Delta O_{2_i}}{\left(\int_t^{\infty} \Delta O_{2_i}\, dt\right)^{n_i}} = \beta_i e^{-E_i/RT} \tag{4.12}$$

From the definition of an integral and since ΔO_{2_i} approaches zero at large *t*:

$$\Delta O_{2_i} = -\frac{d}{dt}\left(\int_t^{\infty} \Delta O_{2_i}\, dt\right) \tag{4.16}$$

Substituting (4.16) in (4.12) produces:

$$\frac{-\frac{d}{dt}\left(\int_t^{\infty} \Delta O_{2_i}\, dt\right)}{\left(\int_t^{\infty} \Delta O_{2_i}\, dt\right)^{n_i}} = \beta_i e^{-E_i/RT} \tag{4.17}$$

Simplifying the notation let:

$$a(t) = \int_t^{\infty} \Delta O_{2_i}\, dt \tag{4.18}$$

Hence equation (4.18) becomes:

$$-\frac{da(t)}{dt} a(t)^{-n_i} = \beta_i e^{-E_i/RT} \tag{4.19}$$

Integrating both sides (4.19) between time t_1 *and* t_2:

$$\int_{t_1}^{t_2} \frac{-da(t)}{dt} a(t)^{-n_i} dt = \int_{t_1}^{t_2} \beta_i e^{-E_i/RT} dt \tag{4.20}$$

The right hand side of (4.20) cannot be simplified further at this stage, but the left hand side, LHS (4.20) becomes:

$$\text{LHS (4.20)} = \int_{t_1}^{\infty} \frac{-da(t)}{dt} a(t)^{-n_i} dt - \int_{t_2}^{\infty} \frac{-da(t)}{dt} a(t)^{-n_i} dt \tag{4.21}$$

Integrating by parts, this becomes:

$$\text{LHS (4.20)} = \frac{1}{1-n_i} a(t_1)^{1-n_i} - \frac{1}{1-n_i} a(t_2)^{1-n_i} \tag{4.22}$$

Equation (4.20) can now be written as:

$$\left(\int_{t_1}^{\infty} \Delta O_{2_i}\, dt\right)^{1-n_i} - \left(\int_{t_2}^{\infty} \Delta O_{2_i}\, dt\right)^{1-n_i} = (1-n_i)\int_{t_1}^{t_2} \beta_i\, e^{-E_i/RT} \tag{4.23}$$

From equation (4.12):

$$\left(\int_{t}^{\infty} \Delta O_{2_i}\, dt\right)^{1-n_i} = \left(\frac{\Delta O_{2_i}(t)}{\beta_i e^{-E_i/RT}}\right)^{\frac{1-n_i}{n_i}} \tag{4.24}$$

Substituting (4.24) in (4.23) and rearranging becomes**:**

$$\Delta O_{2_i}(t_1) = \beta_i e^{-E_i/RT_1}\left[\left(\frac{\left(\Delta O_{2_i}(t_2)\right)}{\beta_i e^{-E_i/RT_2}}\right)^{\frac{1-n_i}{n_i}} + (1-n_i)\int_{t_1}^{t_2} \beta_i e^{-E_i/RT_1} dt\right]^{\frac{n_i}{1-n_i}} \tag{4.25}$$

where, the subscripts *1* and *2* denote two adjacent data points,

T_1 and T_2 are the absolute temperatures at times t_1 and t_2 respectively,

$\Delta O_{2_i}(t_1)$ is the calculated oxygen consumption at time t_1,

and, $\Delta O_{2_i}(t_2)$ is the known oxygen consumption at time t_2.

According to the equation (4.25) all terms known except for the integral term. So, let the integral term be represented by χ :

$$\chi = \int_{t_1}^{t_2} \beta_i e^{-E_i/RT} \tag{4.26}$$

Assuming that temperature is a function of time and that between any two data points it may be approximated by a linear function:

$$T(t) = \Theta + \psi\, t \tag{4.27}$$

This assumption is valid since the experimental data readings are at 10 second intervals. For a heating rate of 50°C/hour the temperature change between any two readings is less than 0.1°C.

At times t_1 and t_2 the temperature may be defined as:

$$T(t_1) = T_1 = \Theta + \psi\, t_1 \tag{4.28a}$$
$$T(t_2) = T_2 = \Theta + \psi\, t_2 \tag{4.28b}$$

From equations (4.28a) and (4.28b):

$$\psi = \frac{T_1 - T_2}{t_1 - t_2} \tag{4.29}$$
$$\Theta = T_1 - \psi\, t_1 \tag{4.30}$$

Substituting into (4.26) yields:

$$\chi = \int_{t_1}^{t_2} \beta_i e^{-E_i/R\,(\Theta + \psi\, t)} dt \tag{4.31}$$

Simplifying the notation by define u as:

$$u = \frac{E_i}{RT} = \frac{E_i}{R(\Theta + \psi\, t)} \tag{4.32}$$

Changing variables from t to u in equation (4.31) using:

$$t = \frac{1}{\psi}\left(\frac{E_i}{R\,u} - \Theta\right) \text{ and } dt = -\frac{E_i}{R\psi\, u^2} du$$

Hence equation (4.31) becomes:

$$\chi = -\frac{E_i \beta_i}{R\psi} \int_{u_1}^{u_2} \frac{e^{-u}}{u^2} du \tag{4.33}$$

Integrating (4.33) by parts yields:

$$\chi = -\frac{E_i \beta_i}{R\psi}\left(\frac{e^{-u_1}}{u_1} - \frac{e^{-u_2}}{u_2} - \int_{u_1}^{u_2} \frac{e^{-u}}{u} du\right) \tag{4.34}$$

The integral term in (4.34) cannot be solved by integration but it may be approximated. Based on Abramowitz and Stegun (1972) an exponential integral of the first kind, I_1 is defined as:

$$I_1(u) = \int_t^{\infty} \frac{e^{-u}}{u} du \tag{4.35}$$

where,

$$ue^u I_1(u) = \frac{u^4 + a_1 u^3 + a_2 u^2 + a_3 u + a_4}{u^4 + b_1 u^3 + b_2 u^2 + b_3 u + b_4} + \varepsilon(u) \tag{4.36}$$

and

$a_1 = 8.573\ 322\ 874\ 01$	$b_1 = 9.573\ 322\ 345\ 4$
$a_2 = 18.059\ 016\ 973\ 0$	$b_2 = 25.632\ 956\ 148\ 6$
$a_3 = 8.634\ 760\ 892\ 5$	$b_3 = 21.099\ 653\ 082\ 7$
$a_4 = 0.267\ 773\ 734\ 3$	$b_4 = 3.958\ 496\ 922\ 8$

The error term, $\varepsilon(u)$, is less than 2×10^{-8} for values of u greater than or equal to one.
Substituting (4.34) and (4.35) into (4.26) becomes:

$$\chi = -\frac{E_i \beta_i}{R\psi}\left[\frac{e^{-u_1}}{u_1} - \frac{e^{-u_2}}{u_2} I_1(u_1) + I_1(u_2)\right] \tag{4.37}$$

Changing variables from u to E_i / RT using equation (4.32) becomes:

$$\chi = -\frac{E_i \beta_i}{R\psi}\left[\frac{RT_1}{E_i} e^{-E_i/RT_1} - \frac{RT_2}{E_i} e^{-E_i/RT_2} - I_1\left(\frac{E_i}{RT_1}\right) + I_1\left(\frac{E_i}{RT_2}\right)\right] \tag{4.38}$$

Substituting (4.26) into (4.24) produces:

$$\Delta O_{2_i}(t_1) = \beta_i e^{-E_i/RT_1}\left[\left(\frac{\Delta O_{2_i}(t_2)}{\beta_i e^{-E_i/RT_2}}\right)^{\frac{1-n_i}{n_i}} + (1-n_i)\chi\right]^{\frac{n_i}{1-n_i}} \tag{4.39}$$

Hence, if n_i, E_i and β_i are known then ΔO_{2_i} may be calculated using equations (4.38) and (4.39), provided that regular time and temperature readings are available. A single known of ΔO_{2_i} value is also required to start off the calculations.

4.4.1 Derivation of equations for a reaction order of one

The derivation of equation (4.39) does not hold if n_i is one.

From equation (4.21) with $n_i = 1$:

$$\int_{t_1}^{t_2} \frac{-da(t)}{dt}\frac{1}{a(t)}dt = \int_{t_1}^{t_2} \beta_i e^{-E_i/RT}\,dt \tag{4.40}$$

Due to the right hand side of (4.40) was defined as χ, by (4.26), then left hand side simplifies using (4.16):

$$\ln a(t_1) - \ln a(t_2) = \chi \tag{4.41}$$

Using (4.12) and (4.18) with $n_i = 1$ yields:

$$\Delta O_{2_i}(t_1) = \Delta O_{2_i}(t_2)e^{\chi} e^{-\frac{E_i}{R}\left(\frac{1}{T_1}-\frac{1}{T_2}\right)} \tag{4.42}$$

Hence, when n_i=1 equations (4.42) and (4.38) may be used to calculate ΔO_{2i} at any temperature.

4.5 Calculation of oxygen consumption at any temperature working from low to high temperatures

As mentioned earlier in Section 4.1, Shallcross (1991) starts the model calculation at the high temperature end of the data and work backwards for all reactions regimes. They found that the curve fitting at low temperatures was inherently less accurate than at high temperatures due to the method of working backwards from high temperature. Any errors in fitting the high and intermediate oxidation reactions will be passed on to the final curve fitted. It was also observed that the greatest differences between the model and the data occurred in the region of the local minimum between the oxygen consumption peaks since two overlapping reactions are occurring and no single reaction dominates. Kisler (1995) improved the curve fitting for the LTO reaction by working from the low temperature end of the data instead of working from high temperature.

Recalling equation (4.12):

$$\frac{\Delta \mathrm{O}_{2_i}}{\left(\int_t^{\infty} \Delta O_{2_i}\, dt\right)^{n_i}} = \beta_i e^{-E_i/RT} \tag{4.12}$$

At very low temperatures the ΔO_{2_i} data is only due to the LTO reaction. This means that the integral from time 0 to any time t may be calculated but not the integral from t to infinity as required by equation (4.12).

Let the total area under the LTO curve be equal to I_{LTO} where:

$$I_{LTO} = \int_0^{\infty} \Delta O_{2,_{LTO}}\, dt \tag{4.43}$$

Therefore:

$$\int_0^{\infty} \Delta O_{2,LTO}\, dt = I_{LTO} - \int_0^{t} \Delta O_{2,LTO}\, dt \tag{4.44}$$

Substituting (4.44) into (4.12) produces:

$$\frac{\Delta O_{2,LTO}}{\left(I_{LTO} - \int_0^{t} \Delta O_{2,LTO}\, dt \right)^{n_{LTO}}} = \beta_{LTO} e^{-E_{LTO}/RT} \tag{4.45}$$

I_{LTO} cannot be calculated at this stage since the kinetic parameters are unknown. However, by estimating an initial value for I_{LTO} and performing the regression, the values for E_{LTO}, β_{LTO} and n_{LTO} may be obtained. From these parameters a predicted $\Delta O_{2,LTO}$ curve may be plotted and the integral I_{LTO} may be calculated. The estimated value for I_{LTO} should be iterated until it matches the value calculated from the predicted $\Delta O_{2,LTO}$ curve. The integral term I_{LTO} was iterated to give the minimum variance between the predicted and data curves. In any case the final value of I_{LTO} and the calculated area under the $\Delta O_{2,LTO}$ curve should not differ by more than 5% for any run.

The method of working from low to high temperature is most appropriate for the LTO reaction only as it enables the use of data from low temperature where no significant MTO occurs, i.e., where LTO is the dominant oxidation regime. Similarly, the HTO reaction is best modeled by working from high to low temperature. Working from low to high temperature and fitting the HTO curve last would introduce significant uncertainties into the calculations.

As for this thesis, the HTO reaction is modeled first and followed by the LTO reaction and lastly the MTO reaction. The method for modeling the HTO and MTO reactions are working from high to low temperature. However, when the LTO reaction is considered, the data is modeled by working from low to high temperature.

4.6 An innovative approach of solving the LTO and MTO reactions simultaneously

Previous models, such as Shallcross (1991) and Kisler (1995) assumed that the reaction model is independent of the number of oxidation regimes and all reaction regimes are handled one at a time. Kisler (1995) also uses a fixed reaction order for calculation of all the oxidation regimes in order to standardise the curve fitting procedure. To improve the curve fitting for all the oxidation regimes, it would be advantageous to not fixing the reaction order in the calculation. Further a new approach of solving the LTO and MTO reactions simultaneously will further improve the curve fitting. In this new approach, the HTO reaction is first modeled and calculated from high to low temperatures. The optimum of predicted HTO curve was based on the minimum value of variance with a range of reaction orders. Figure 4.3 shows a predicted HTO curves over a range of reaction orders for experiment F6 (palm fibre). Based on the Figure 4.3, obviously the reaction order of 1.01 gave the closenest fit to the HTO oxygen consumption experimental data with the minimum value of variance (0.007). Next, the same procedure is applied to the LTO reaction with the calculation started from low to high temperatures instead. Figure 4.4 displays a predicted LTO curves at various reaction orders for experiment F6. The optimum predicted LTO curve was at the reaction order of 1.15 (see Figure 4.4) that gives the lowest variance of 3.824. Next, is the model of MTO curve using the same approach calculation as the HTO reaction (working from high to low temperatures) and applied at the LTO reaction optimum order of 1.15.

Figure 4.5 shows both the experimental oxygen consumption data and the sum up of all the reaction regimes of HTO, LTO and MTO (H+L+M) at the optimum reaction order. From Figure 4.5 it may be seen clearly that at the LTO regimes (250°C – 270°C), the predicted oxygen consumption curve (H+L+M) was high (overshoot) in comparison with the experimental data and the overall variance is 0.867. In order to increase the closeness of fit of the predicted oxygen consumption curve with the experimental data particularly in the LTO regime, a higher LTO reaction order was chosen by trial.

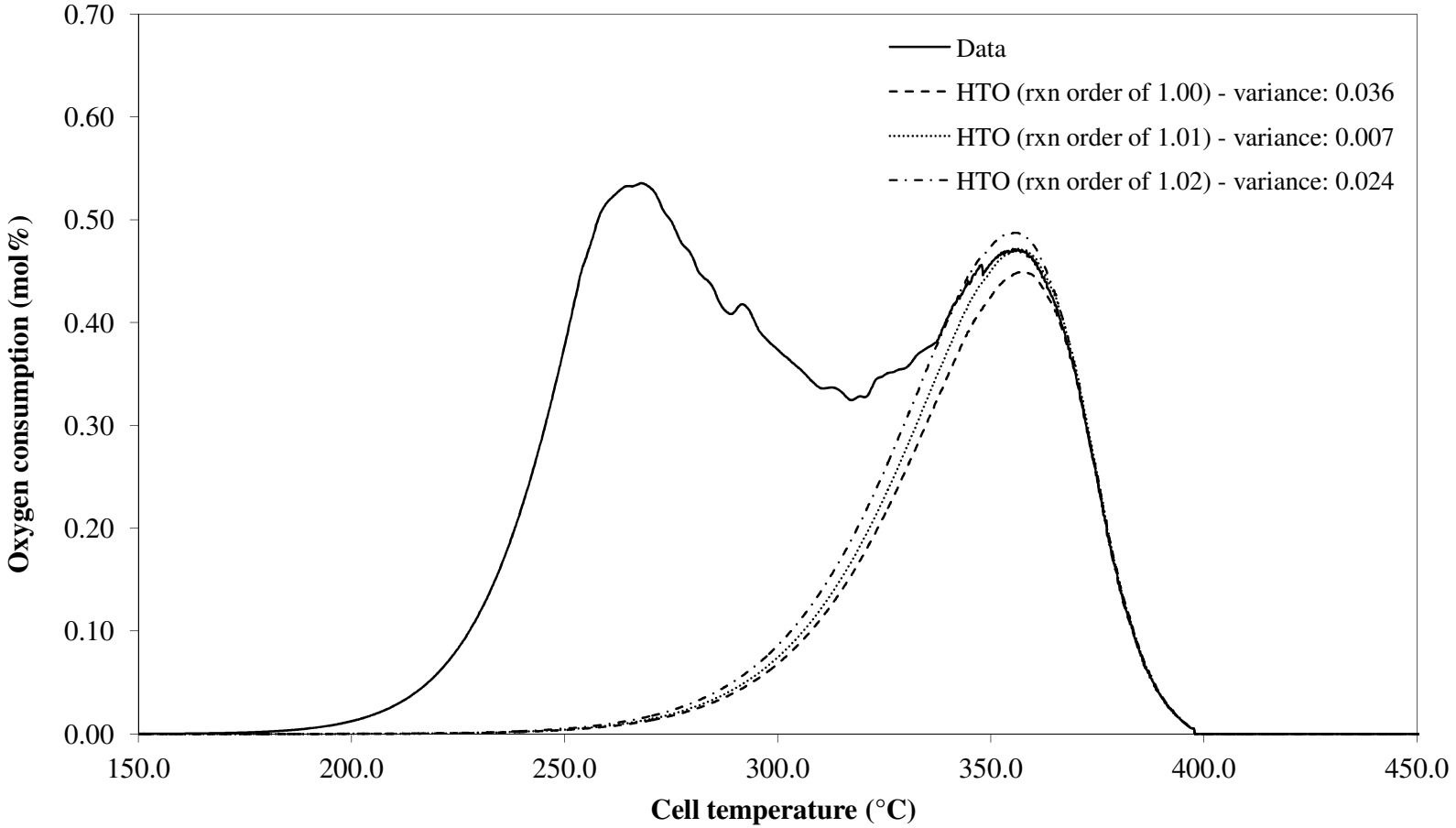

Figure 4.3 - A predicted HTO curves over a range of reaction orders for experiment F6 (palm fibre). The experimental was conducted at 500kPa absolute total system pressure, injection flow rate of 400smL/min and 50°C/hour heating rate.

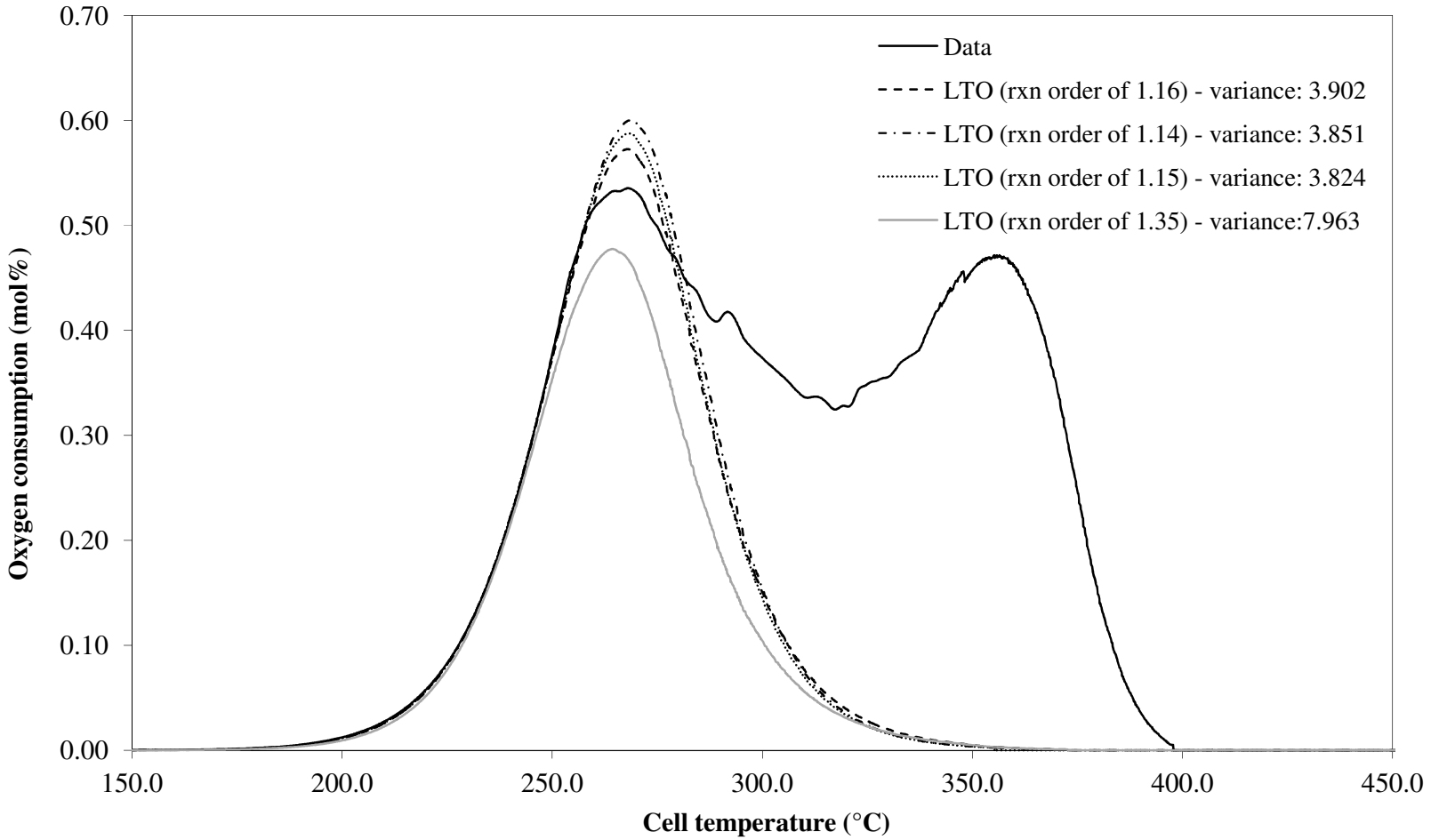

Figure 4.4 - A predicted LTO curves over a range of reaction orders for experiment F6 (palm fibre). The experimental was conducted at 500kPa absolute total system pressure, injection flow rate of 400smL/min and 50°C/hour heating rate.

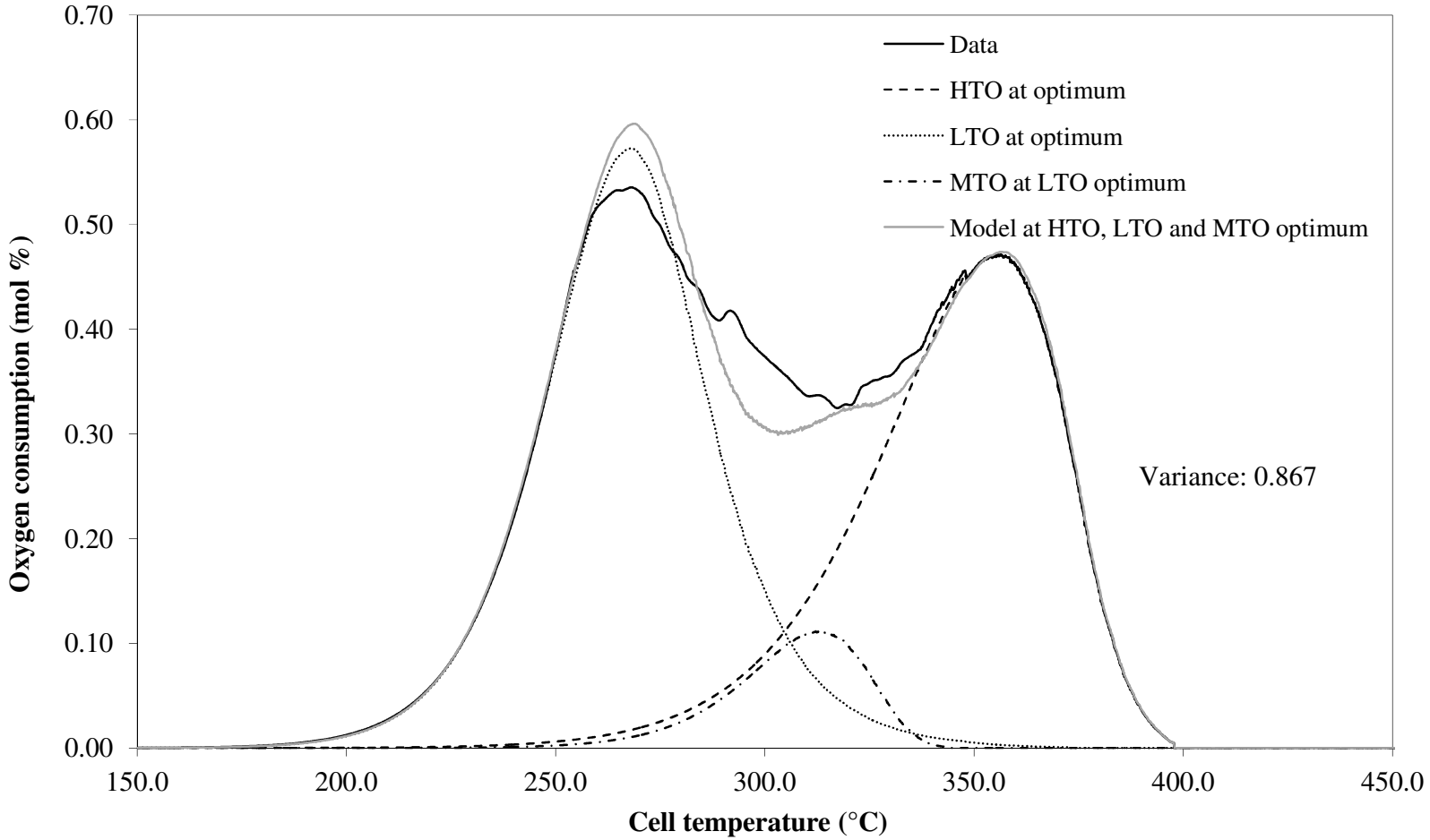

Figure 4.5 - An oxygen consumption experimental data and the predicted oxygen consumption (H+L+M) at the optimum reaction order. The experiment F6 was conducted at 500kPa absolute total system pressure, injection flow rate of 400smL/min and 50°C/hour heating rate.

Figures 4.6, 4.7 and 4.8 show the both predicted and the experimental data of oxygen consumption for experiment F6 with LTO reaction order taken at 1.35, 1.36 and 1.37, respectively. From Figures 4.6 to 4.8 it may be seen that LTO reaction order of 1.36 gives the best fit with variance of 0.112 (see Figure 4.7). This confirms that by solving the LTO and MTO reactions simultaneously, model best fit the oxygen consumption experimental data.

4.7 Summary of calculation procedure

The modeling technique developed in this chapter may be summarised as:

1. Starting at the high temperature end of the data use linear regression to obtain E_{HTO}, and β_{HTO} and iterate to get n_{HTO}. Linear regression is covered in Section 4.3.
2. Calculate a predicted oxygen consumption curve for HTO reaction using the equations developed in Section 4.4
3. Subtract the predicted ΔO_{2_i} ,$_{HTO}$ curve from the ΔO_{2_i} ,$_{TOTAL}$ curve.
4. From the ΔO_2 , $_{TOTAL\text{-}HTO}$ curve, use linear regression to obtain E_{LTO}, and β_{LTO} and iterate to get n_{LTO} starting from low temperature end of the data.
5. Calculate a predicted oxygen consumption curve for the LTO reaction using the equations developed in Section 4.5.
6. Subtract the predicted ΔO_{2_i} ,$_{LTO}$ curve from the ΔO_{2_i} ,$_{TOTAL\text{-}HTO}$ curve
7. From the ΔO_{2_i} ,$_{TOTAL\text{-}HTO\text{-}LTO}$ curve, repeat steps 1 and 2 to get the ΔO_{2_i} ,$_{MTO}$ parameters.
8. Add ΔO_{2_i} ,$_{HTO}$, ΔO_{2_i} ,$_{LTO}$ and ΔO_{2_i} ,$_{MTO}$ and calculate the total error value of ΔO_{2_i} ,$_{HTO+LTO+MTO}$ from the ΔO_{2_i} , $_{TOTAL}$ curve.
9. Repeat steps 4 to 9 by choosing a different value of n_{LTO} until the total minimum error value is found.

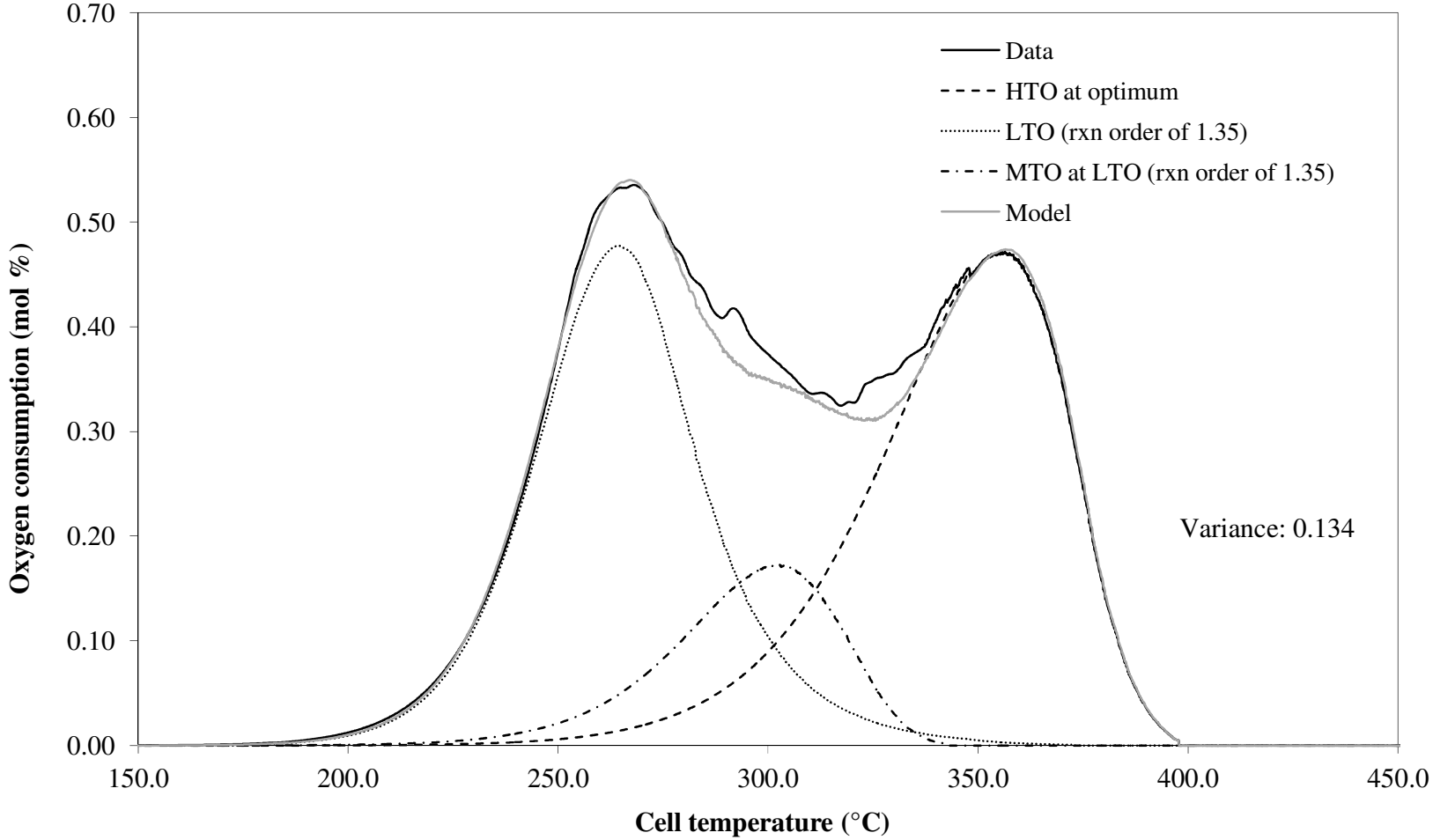

Figure 4.6 - An oxygen consumption experimental data and the predicted oxygen consumption (H+L+M) at the LTO reaction order of 1.35. The experiment F6 was conducted at 500kPa absolute total system pressure, injection flow rate of 400smL/min and 50°C/hour heating rate.

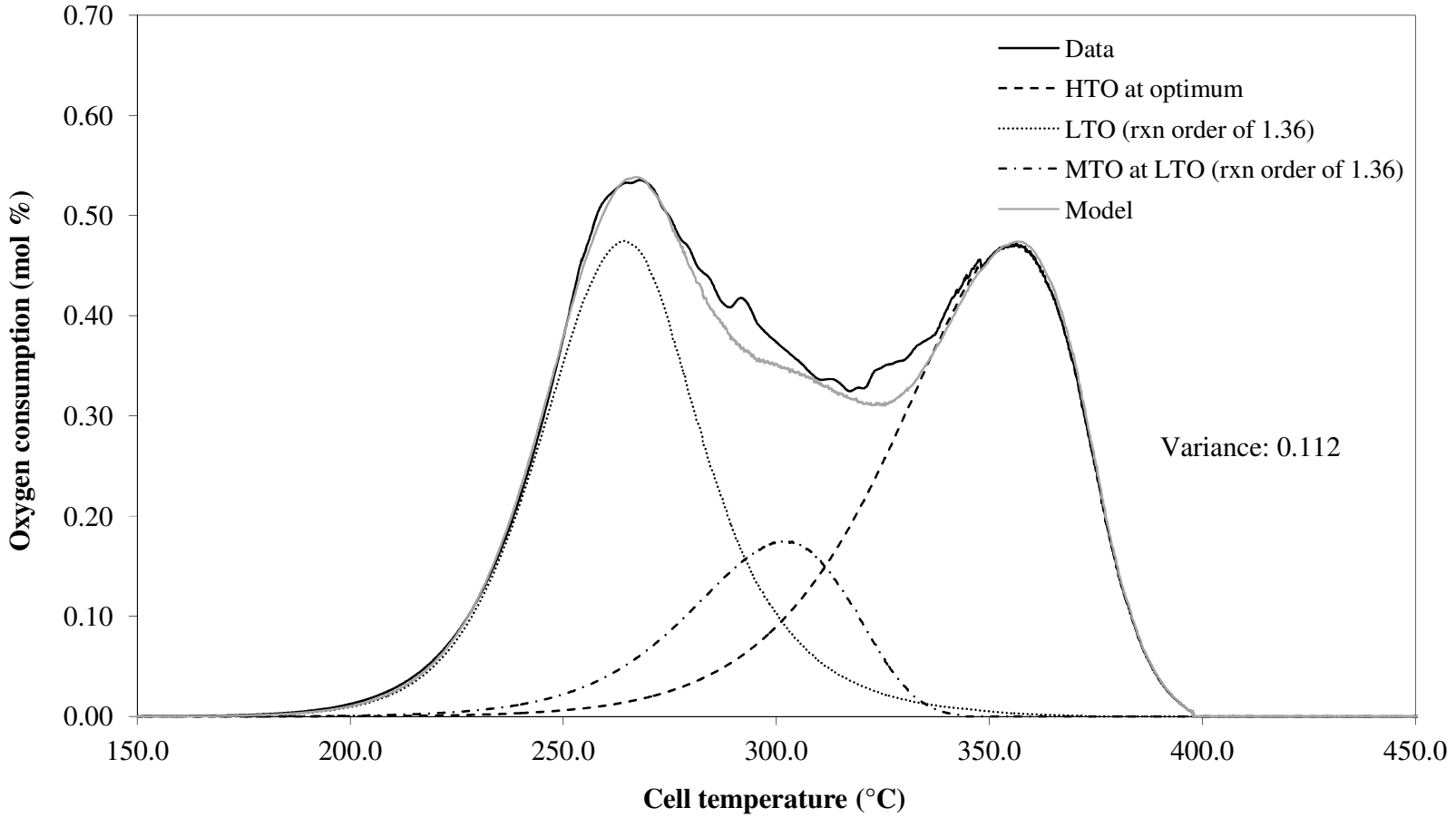

Figure 4.7 - An oxygen consumption experimental data and the predicted oxygen consumption (H+L+M) at the LTO reaction order of 1.36. The experiment F6 was conducted at 500kPa absolute total system pressure, injection flow rate of 400smL/min and 50°C/hour heating rate.

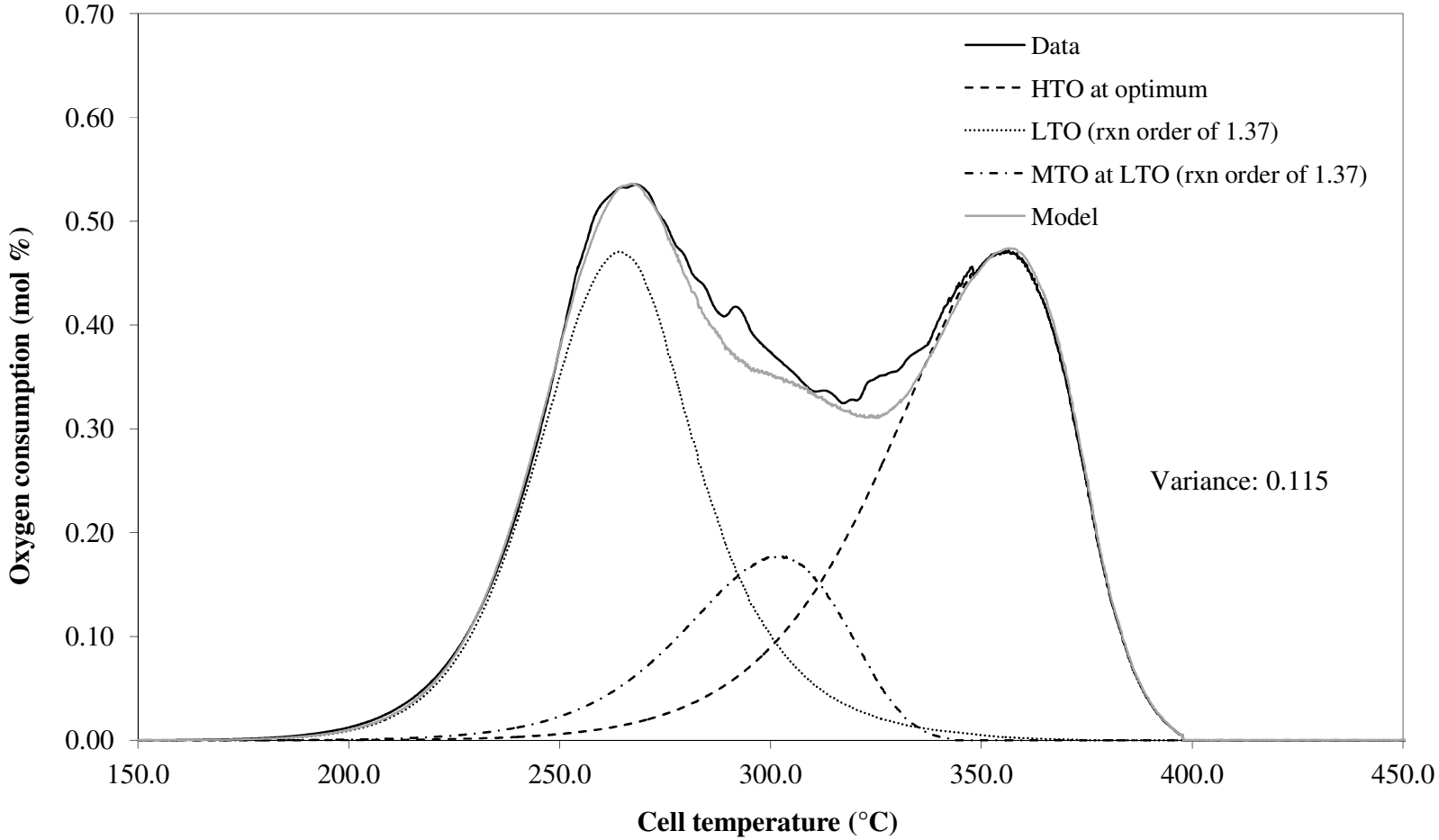

Figure 4.8 - An oxygen consumption experimental data and the predicted oxygen consumption (H+L+M) at the LTO reaction order of 1.37. The experiment F6 was conducted at 500kPa absolute total system pressure, injection flow rate of 400smL/min and 50°C/hour heating rate.

4.8 Concluding remarks

This Chapter describes in detail the reaction model development. The major features of the model are:

1. The many oxidation reactions occurring may be grouped into just three simultaneous and competing reaction regimes known as high temperature oxidation (HTO), medium temperature oxidation (MTO) and low temperature oxidation (LTO).
2. The reaction order with respect to fuel concentration is calculated by iteration rather than assuming it to be equal to one.
3. A new technique was developed of solving the LTO and MTO reactions simultaneously that further improved the curve fitting between the prediction model and the actual experimental data of oxygen consumption.
4. Calculations are based solely on the ΔO_{2_i} curve and did not involve the use of carbon oxides production data.
5. Given regular time and temperature readings a predicted ΔO_{2_i} curve may be plotted using the calculated kinetics parameters. This calculated curve takes into account any deviations from the linear heating schedule.

The model developed so far is a general method for any EGA work. It does apply for any fuels whether it is crude oil or biomass materials. The model will be used in the oxidation of biomass material throughout the study.

CHAPTER 5

RICE HUSK OXIDATION

5.1 Introduction

Biomass has become one of the most commonly used renewable sources of energy. Rice husk is a biomass and was selected for this study as it is a readily available biomass and it provides an excellence comparison to the palm fibre due to its physically consistent size and shape. This Chapter reports the results of an experimental investigation into the combustion characteristics of rice husk. The first section provide a detailed discussion on the results of a typical rice husk evolved gas analysis (EGA) experiment and is followed by a discussion on the kinetic parameter results. Next, detail discussions are presented of the experimental results and the calculated kinetic parameters of the effect of heating rate, total system pressure and oxygen partial pressure.

5.2 Typical rice husk experimental and kinetic parameter results

Eight experimental runs were performed using rice husk. Experiments R1, R2 and R3 were conducted under similar experimental conditions in order to study the reproducibility of the experimental technique. Experiment R4 was used to study the effect of heating rate. Experiments R7 and R8 were conducted to study the effect of total system pressure at the same oxygen partial pressure.

Table 5.1 - Ultimate and proximate analyses of rice husk. Note that db is dry basis and daf is dry ash free.

Analyses	Rice husk
Proximate analysis (db) (wt.%)	
Volatile matter	64.2
Fixed carbon	17.4
Ash	18.4
Ultimate analysis (daf) (wt.%)	
Carbon	40.90
Hydrogen	4.82
Nitrogen	0.43
Sulphur	0.17
Oxygen	53.68
Calorific value (MJ/kg)	15.50

Experiments R4 and R7 were performed to study the effect of oxygen partial pressure at the same total system pressure. Finally, experiments R5 and R6 were performed at low and high total system and oxygen partial pressures, respectively with air as the oxidising gas. Table 5.1 presents the results of ultimate and proximate analyses of the rice husk used in this study. As shown in Table 5.1, the volatile matter of the rice husk is almost 65% and the carbon content of nearly 41%. The rice husk also has a relatively high heating value of 15.5MJ/kg. These values confirm the suitability of using rice husk as a boiler fuel. The summary of the experimental conditions for these rice husk experiments is presented in Table 5.2.

Figure 5.1 shows the results from a typical rice husk evolved gas analysis (EGA) experiment. Experiment R4 was selected for this purpose. The actual carbon monoxide and carbon dioxide levels in the evolved gas are shown together with the oxygen consumption curves. As observed in Figure 5.1, the plots are of similar forms, exhibiting two main peaks, one in the 230°C to 270°C region and the other in the 330°C to 370°C region except for the carbon monoxide production curve. The carbon monoxide production curve appears to have only one peak in the 240°C to 270°C region. This evolved gas analysis (EGA) experiment was conducted at a heating rate of 50°C/h.

Table 5.2 - Experimental conditions for the rice husk experiments. M1 is gas mixture 1 that consists of 15.10 mol% O_2, 2.01 mol% CO_2, 0.983 mol% CO and balance nitrogen.

Experiment	**R1**	**R2**	**R3**	**R4**	**R5**	**R6**	**R7**	**R8**
Absolute total system pressure (kPa)	500	500	500	500	300	700	500	363
Oxygen partial pressure (kPa)	105	105	105	105	63	147	76	76
Injection gas (mol% Oxygen)	20.96 (Air)	20.96 (Air)	20.96 (Air)	20.96 (Air)	20.96 (Air)	20.96 (Air)	15.10 (M1)	20.96 (Air)
Injection flow rate (smL/min)	400	400	400	400	400	400	400	400
Heating rate (°C/h)	80	80	80	50	50	50	50	50

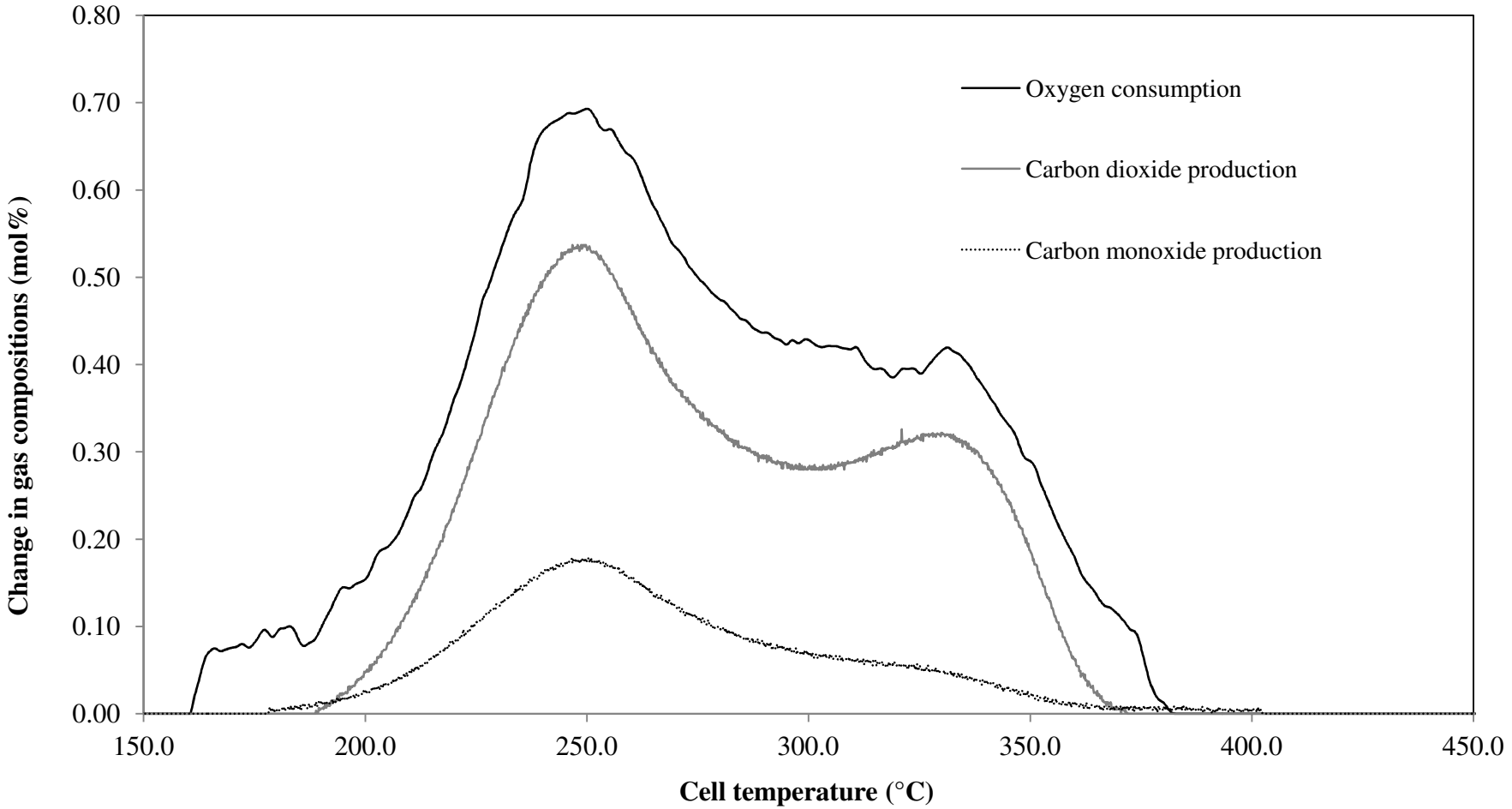

Figure 5.1 - Typical rice husk evolved gas analysis (EGA) experimental results with air as the oxidising gas, an absolute total system pressure of 500kPa, an air flow rate of 400smL/min and a heating rate of 50°C/h (Experiment R4).

The gas composition measurement data were recorded at a frequency of once every ten seconds. As a result, the peak temperatures and heights of all the exit gas compositions were accurately determined. The first peak occurred at a temperature of 248.0°C ± 1°C for all the three curves.

The second peak temperature for the oxygen consumption and the carbon dioxide production curves coincide at 329.8°C ± 1.0°C. However, the peak heights vary between the peaks and the gas compositions. The peak height of the first peak was higher than the second peak for all three gas components.

The results agree reasonably well with those of similar studies using thermogravimetric analysis (TGA) techniques (Fernandez *et al.*, 2012, Skreiberg *et al.*, 2011, Sung and Seo, 2009 and Biagini *et al.*, 2008). On the basis of these similarities, the two peaks may be taken to define the periods of hemicellulose and cellulose decompositions. The first and second peaks may be referred to as the hemicellulose and cellulose peaks, respectively. A slight bump in the oxygen consumption curve may be observed at the high temperature of 370°C to 380°C due to the lignin decomposition. It is believed that lignin decomposition overlaps with cellulose decomposition. Because of that, the small bump that is represented by lignin decomposition at high temperatures may not appear at some experiments. Hence, the discussion will only focus on the hemicellulose and cellulose decompositions of rice husk. Referring to Figure 5.1 and Table 5.1, out of total 65% volatile matter, the rice husk samples had higher hemicellulose in comparison to the cellulose.

The kinetic parameters calculated for each of the oxidation regimes (LTO, MTO and HTO reactions) are the natural log of beta group (ln β), the activation energy expressed as the activation energy divided by Universal gas constant (E/R) and the reaction order (n). The procedure used to calculate kinetic parameters has been described in detail in the previous Chapter 4. The typical rice husk experimental results of experiment R4 are modeled against the three overlapping reaction regimes of the HTO, MTO and LTO. The LTO and MTO regimes are decoupled simultaneously. Each of the experimental data are decoupled into their constituent oxidation reactions and kinetic parameters such

as activation energy are calculated for each reaction regime. As in Chapter 4, the variance is calculated by:

$$\sigma^2 = \frac{\sum_{j=1}^{m} \left(\Delta O_{2\,j} - \Delta O_{2\,calc} \right)^2}{(m-2)} \tag{5.1}$$

where, σ^2 is the variance,

m is the number of data points used in the regression, first point at time t_1 , and last point at time t_m,

and, m-2 is the degree of freedom.

The level of agreement between the predicted oxygen consumption curve with the actual oxygen consumption curve was based on the calculated variance. For ease of discussion, we define a good fit to be when the value of the variance is below than 0.001 whereas if the value of the variance is between 0.001 and 0.003, we define this to be acceptable. A poor fit is defined when the value of variance is higher than 0.003. Figure 5.2 presents the predicted oxygen consumption curve in comparison with the actual oxygen consumption curve of the experimental data of experiment R4.

As may be seen in Figure 5.2, a good fit (variance of 0.0006) between the predicted oxygen consumption curve with the experimental data was obtained for experiment R4. There are a few noticeable differences between the observed data and modeled behaviour at the low temperature range of 150°C to 200°C, medium temperature range of 270°C to 320°C and at the high temperature range of 350°C to 380°C. The discrepancy at the higher temperature range of 350°C to 380°C is due to the error in the experimental data at higher temperatures. At very high temperature, the experimental data seems to be unstable and makes a poor match to the predicted oxygen consumption curve. Likewise, at very low temperature of 150°C to 200°C, the experimental data was unstable and hence, gives a poor match of the predicted oxygen consumption curve with the actual oxygen consumption curve. The oxygen consumption data for the medium temperature oxidation (MTO) reaction is obtained by subtracting the predicted $\Delta O_{2,HTO}$ and $\Delta O_{2,LTO}$ curves from the $\Delta O_{2,TOTAL}$ data.

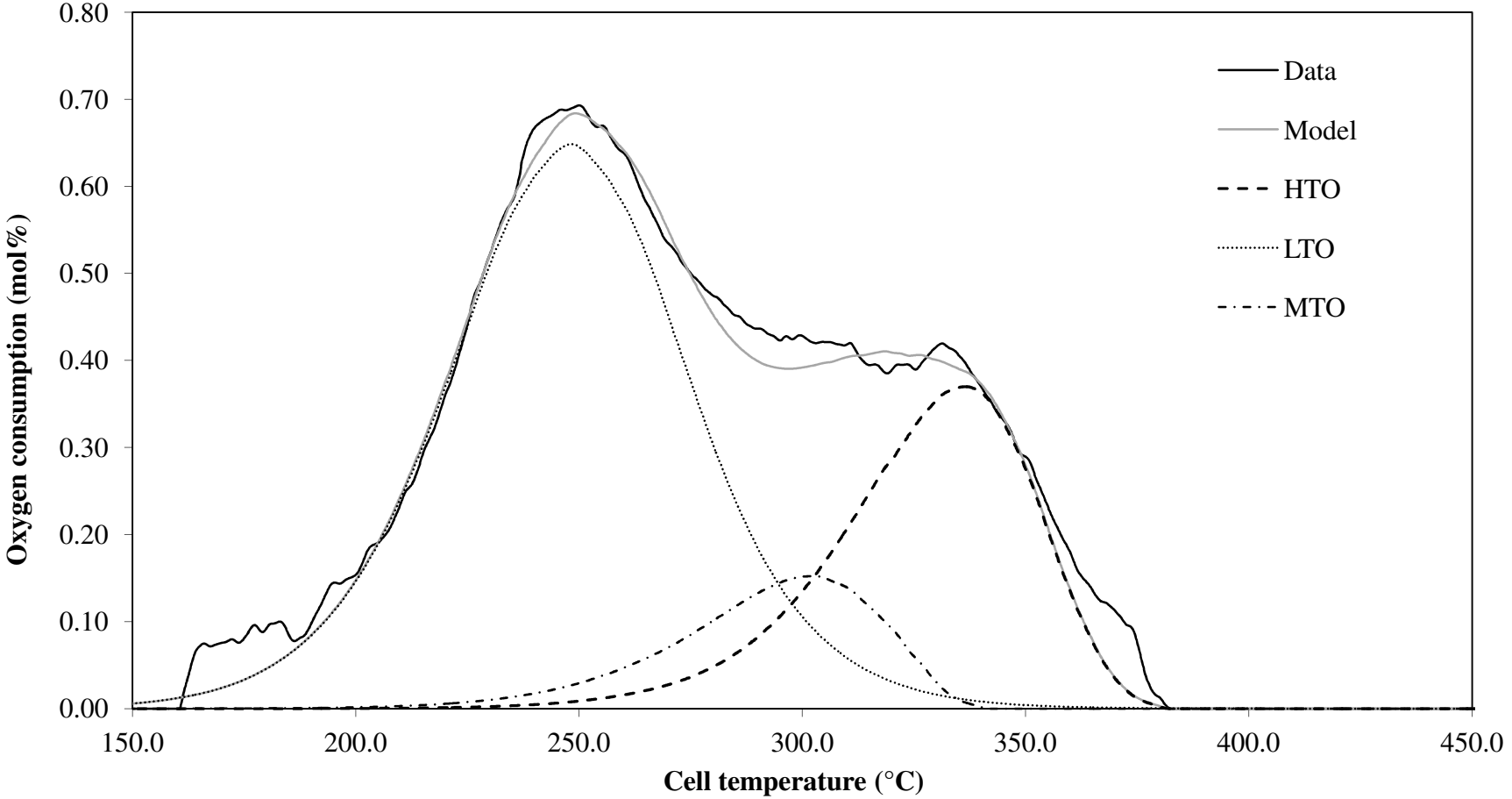

Figure 5.2 - Typical rice husk decoupled evolved gas analysis for the oxidation of rice husk (Experiment R4). The oxygen consumption curve was decoupled using the three regimes (HTO, MTO and LTO) model. The LTO and the MTO reactions were decoupled simultaneously.

Any differences or errors in the HTO and LTO calculations are potentially passed on to the MTO calculation. Further, the overlap between the LTO and MTO peaks and the MTO and HTO peak may contributes to the disagreement at the medium temperature range of 270°C to 320°C. The overlap between the three regimes can make it difficult to obtain a good fit.

The same approach of kinetic parameters calculation is applied to all the rice husk experiments. Next, Section 5.3 discusses in details of the reproducibility of the rice husk experimental data. The discussion is based on the peak temperatures and heights for the exit gas oxygen, carbon dioxide and carbon monoxide compositions. Following that is the discussion on the calculated kinetic parameters of the rice husk reproducibility study.

5.3 Rice husk reproducibility study

In order to examine the reproducibility of the evolved gas analysis (EGA) experiments, three rice husk experiments, R1 to R3, were conducted under identical conditions with air as the oxidising gas, an absolute system pressure of 500kPa, an air flow rate of 400smL/min and a heating rate of 80°C/h. The results of these three experimental rice husk experiments are presented in Table 5.3. Figures 5.3 to 5.5 are plots showing the variation in the exit gas compositions versus cell temperature for experiments R1 to R3, respectively. Note that the oxygen curves in these diagrams refers to the decrease in oxygen content between the inlet and exit gases. As observed in Table 5.3, the peak temperature for the hemicellulose decomposition lies at an average peak temperature of 270.7°C ± 0.5°C for all the gas compositions of the three runs. For the cellulose decompositions, the average peak temperature obtained is 358.1°C ± 3.1°C for the oxygen consumption and the carbon dioxide production curves of all the three experiments.

Individually, as for the hemicellulose of the oxygen consumption curve, the average peak temperature for the three identical rice husk experiments was obtained at 270.8°C ± 0.3°C.

Table 5.3 - Summary of the evolved gas analysis (EGA) experimental results of the rice husk. The $\Delta O_{2,\,max}$, $\Delta CO_{2,\,max}$ and $\Delta CO_{,\,max}$ (in mol%) is the peak height and the T (in °C) is cell temperature at which the peak occurs. M1 is gas mixture 1 that consist of 15.10 mol% O_2, 2.01 mol% CO_2, 0.983 mol% CO and balance nitrogen.

Experiment		**R1**	**R2**	**R3**	**R4**	**R5**	**R6**	**R7**	**R8**
Total system pressure (kPa) (a)		500	500	500	500	300	700	500	363
Oxygen partial pressure (kPa)		105	105	105	105	63	147	76	76
Oxygen concentration in feed gas (mol%)		20.96 (Air)	20.96 (Air)	20.96 (Air)	20.96 (Air)	20.96 (Air)	20.96 (Air)	15.10 (M1)	20.96 (Air)
Heating rate (°C/h)		80	80	80	50	50	50	50	50
Oxygen consumption peaks									
First peak	$\Delta O_{2,\,max}$ (mol%)	0.96	0.95	0.95	0.69	0.62	0.66	0.68	0.62
	T (°C)	271.1	270.7	270.7	247.8	274.3	233.3	258.2	261.2
Second peak	$\Delta O_{2,\,max}$ (mol%)	0.42	0.42	0.45	0.42	0.37	0.35	0.37	0.32
	T (°C)	360.8	361.2	357.7	329.5	350.7	316.5	347.5	342.5
Carbon dioxide production peaks									
First peak	$\Delta CO_{2,\,max}$ (mol%)	0.90	0.85	0.82	0.54	0.48	0.55	0.53	0.47
	T (°C)	271.1	270.7	270.9	247.9	273.5	233.3	258.0	261.5
Second peak	$\Delta CO_{2,\,max}$ (mol%)	0.33	0.33	0.35	0.32	0.34	0.32	0.34	0.27
	T (°C)	355.0	360.8	356.7	330.2	351.7	314.9	345.8	346.8
Carbon monoxide production peak									
Peak	$\Delta CO_{,\,max}$ (mol%)	0.27	0.29	0.28	0.16	0.16	0.18	0.20	0.18
	T (°C)	271.6	271.2	271.4	248.3	273.8	233.3	260.2	262.4

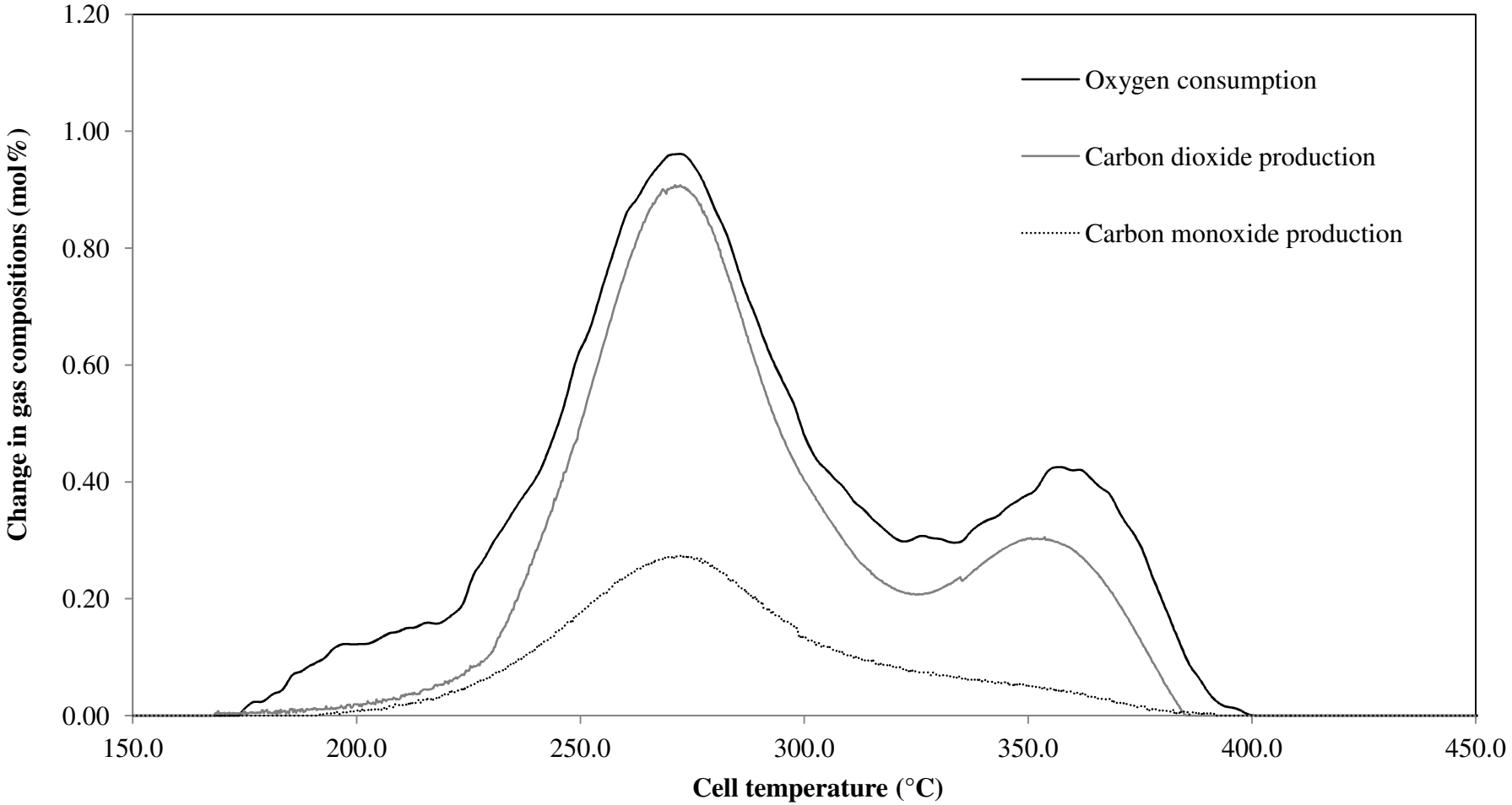

Figure 5.3 - Evolved gas analysis data with respects to the cell temperature for the oxidation of rice husk with air as the oxidising gas, an absolute total system pressure of 500kPa, an air flow rate of 400smL/min and a heating rate of 80°C/h (Experiment R1).

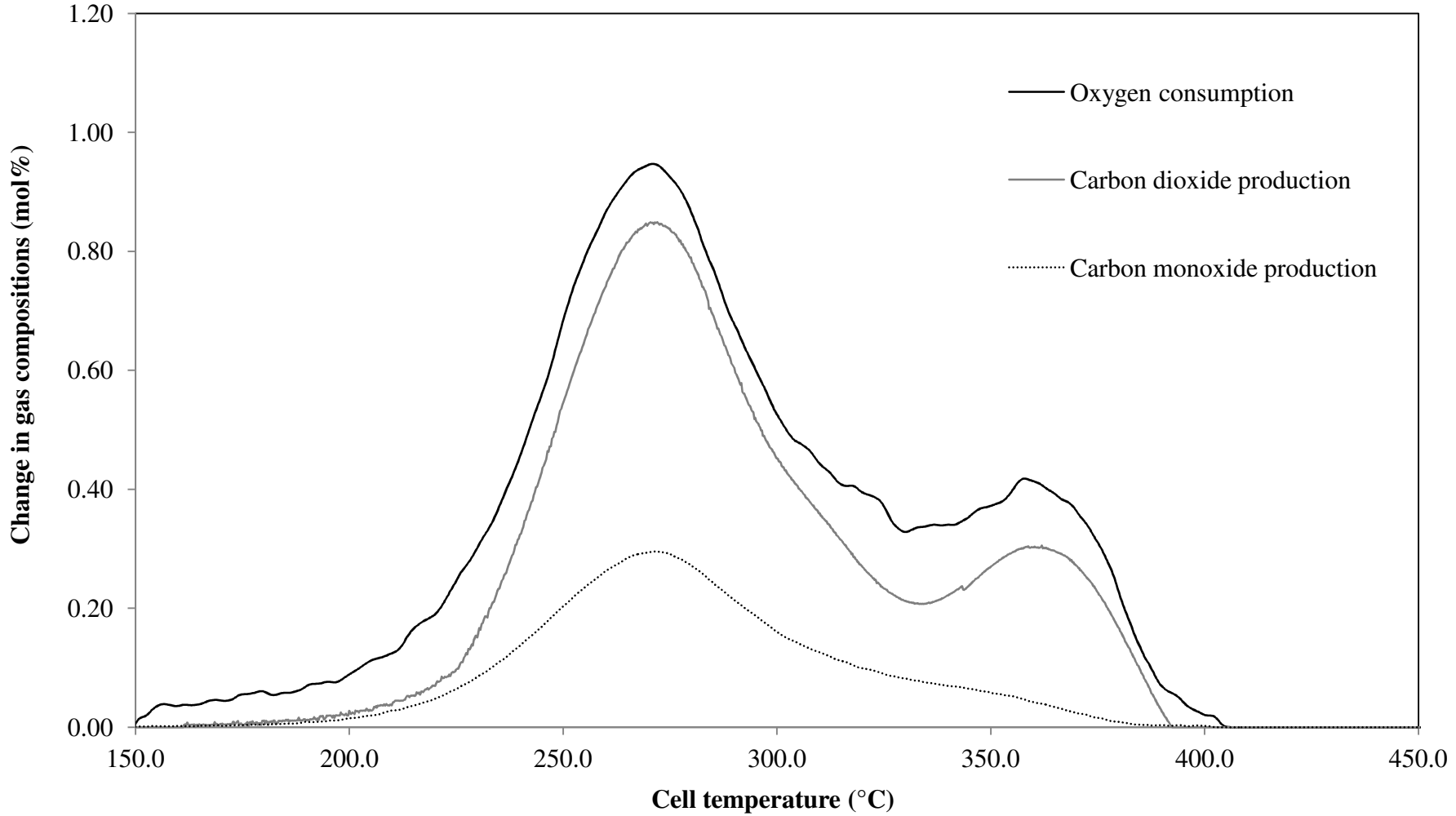

Figure 5.4 - Evolved gas analysis data with respects to the cell temperature for the oxidation of rice husk with air as the oxidising gas, an absolute total system pressure of 500kPa, an air flow rate of 400smL/min and a heating rate of 80°C/h (Experiment R2).

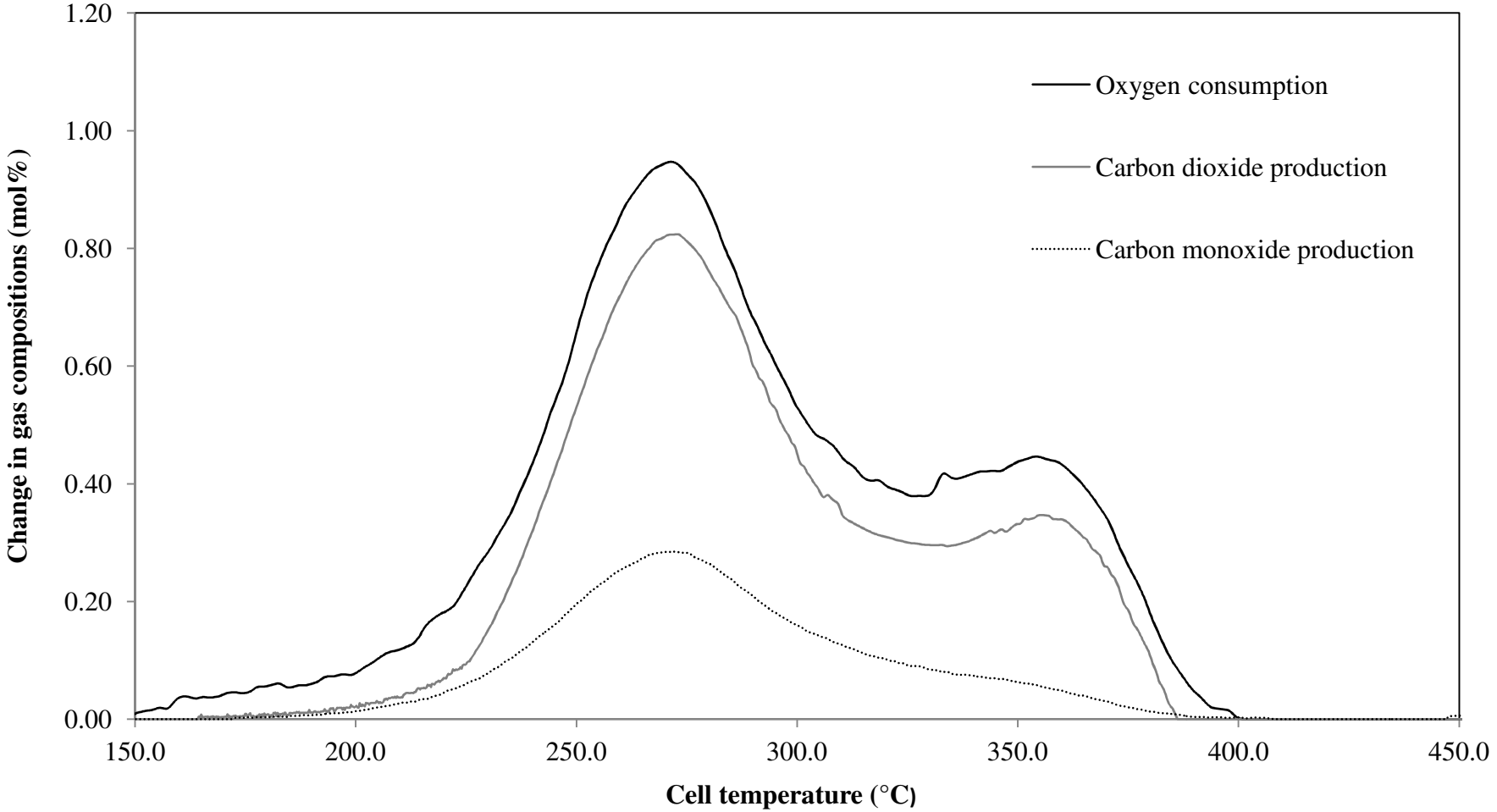

Figure 5.5 - Evolved gas analysis data with respects to the cell temperature for the oxidation of rice husk with air as the oxidising gas, an absolute total system pressure of 500kPa, an air flow rate of 400smL/min and a heating rate of 80°C/h (Experiment R3).

The cellulose average peak temperature for the oxygen consumption curve coincide at 359.9°C ± 2.2°C. For the carbon dioxide production curve, the average peak temperature for the three identical rice husk experiments, R1 to R3, was obtained at 270.9°C ± 0.2°C for the hemicellulose peak. Considering the cellulose peak, the average peak temperature was 357.5°C ± 2.5°C. The average peak temperature for the carbon monoxide production curve which display a single peak also shows a good agreement with an average peak temperature obtained of 271.4°C ± 0.2°C. By comparison, Table 5.3 shows an agreement to ±3°C. The error is due to the small differences in the experimental conditions, the technique and the measurement errors. For the remainder of the rice husk experiments, the level of reproducibility may be taken as agreement to be within ±3°C.

Figure 5.6 allows a comparison between the oxygen consumption curves as functions of cell temperature for the three identical rice husk experiments. Figures 5.7 and 5.8 allow similar comparisons for carbon dioxide production and carbon monoxide production curves, respectively. As shown in Figure 5.6, for the oxygen consumption of the hemicellulose peak, a close agreement of the peak height between the three experiments is observed. The peak height ranges from 0.95 mol% to 0.96 mol% oxygen for the three identical rice husk experiments. Likewise, a close agreement of the hemicellulose peak height was also observed for the both carbon dioxide production and carbon monoxide production curves (see Figures 5.7 and 5.8). The hemicellulose peak height of these three identical rice husk experiments ranges from 0.82 mol% to 0.90 mol% carbon dioxide. For the carbon monoxide production curves, the variation of the hemicellulose peak height is 6.9% from 0.27 mol% to 0.29 mol% carbon monoxide. Considering the cellulose peak of the oxygen consumption curve for the three identical rice husk experiments, the peak heights range from 0.42 mol% to 0.45 mol% oxygen. For the cellulose peak height of the carbon dioxide production curve, the variation of the three identical rice husk experiments is from 0.33 mol% to 0.35 mol% carbon dioxide. There is no second peak observed for carbon monoxide production curve (see Figure 5.8).

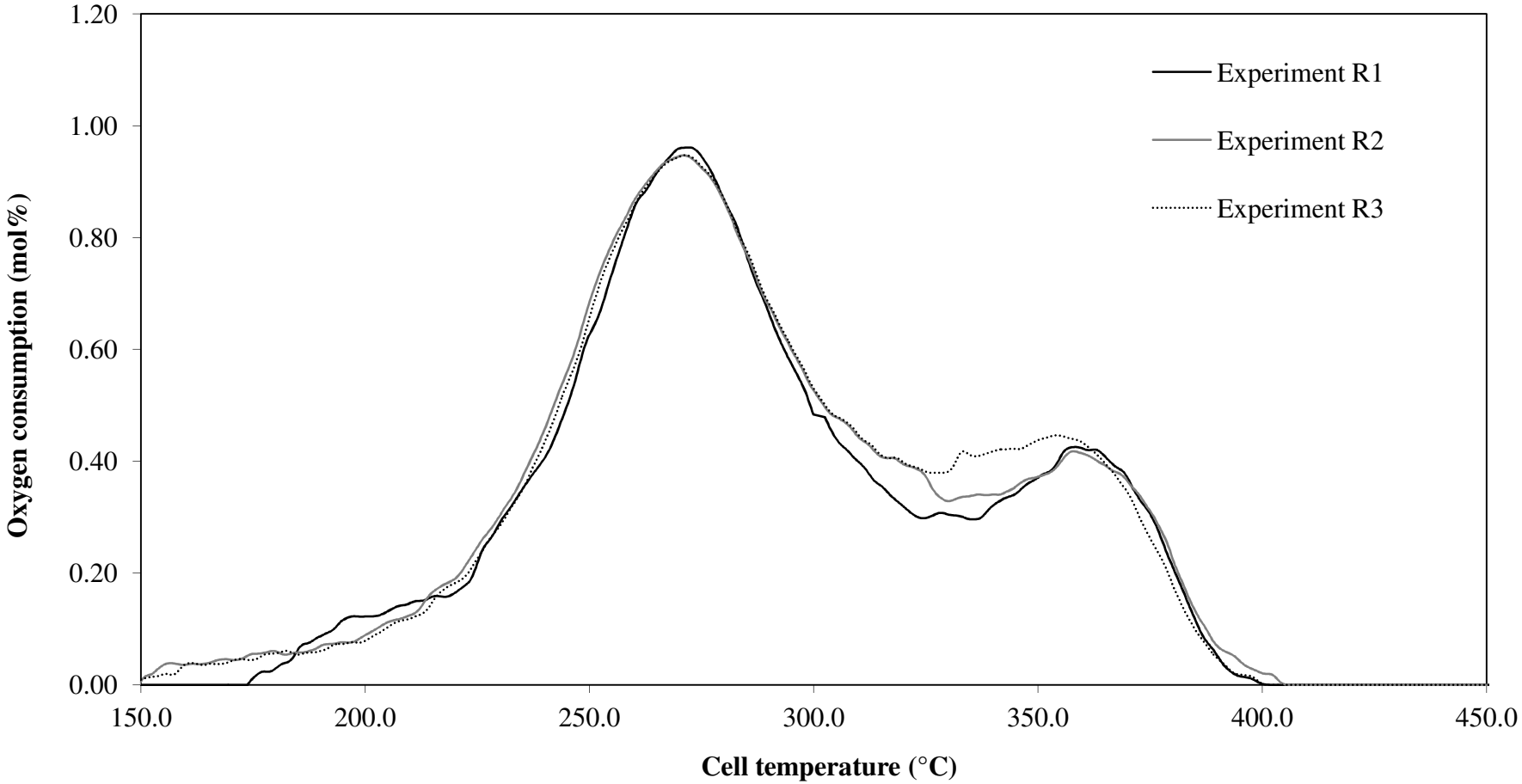

Figure 5.6 - Comparison of the oxygen consumption data with respects to the cell temperature for the three rice husk experimental runs conducted under identical conditions with air as the oxidising gas, an absolute total system pressure of 500kPa, an air flow rate of 400smL/min and a heating rate of 80°C/h.

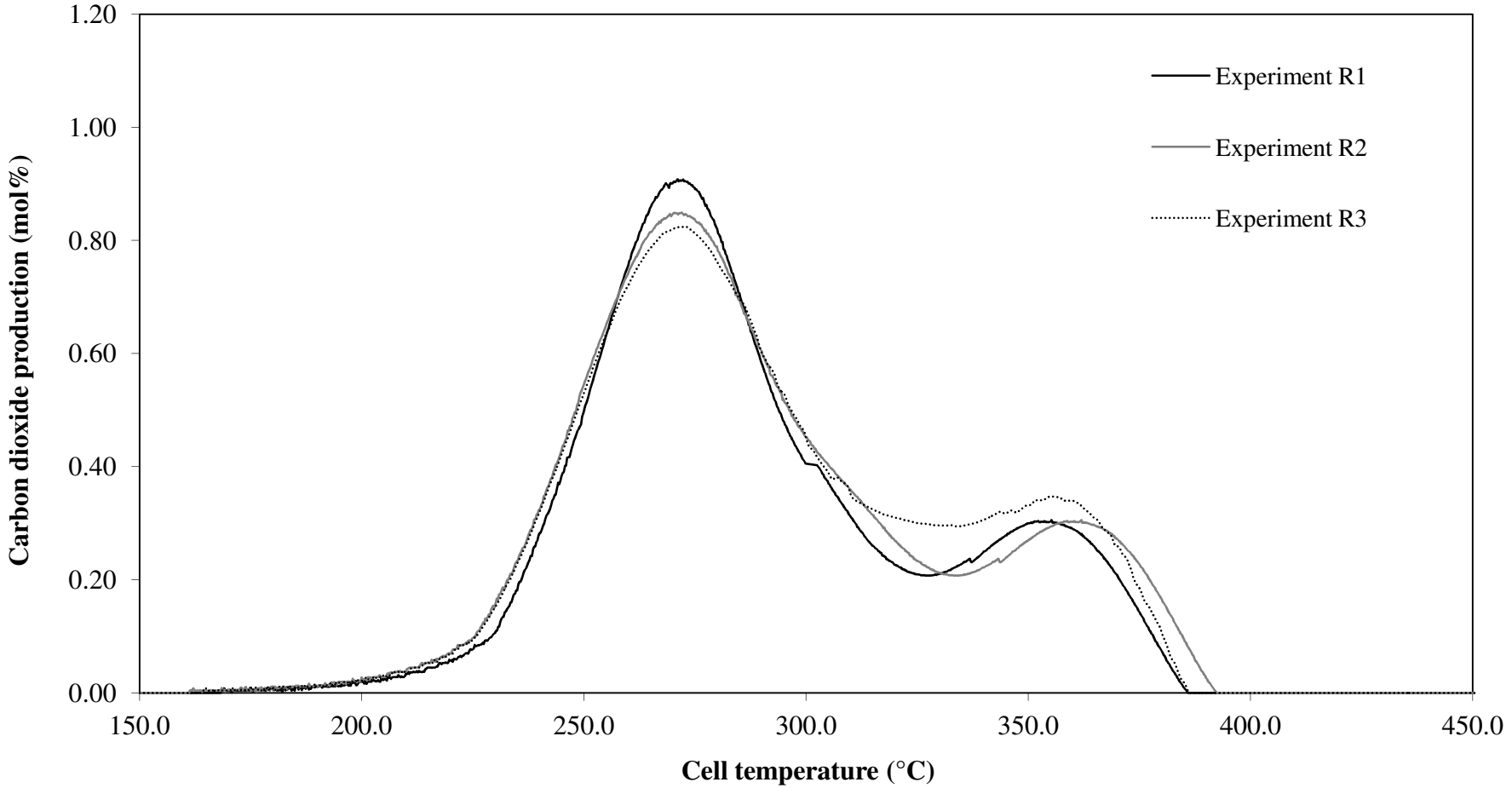

Figure 5.7 - Comparison of the carbon dioxide production data with respects to the cell temperature for the three rice husk experimental runs conducted under identical conditions with air as the oxidising gas, an absolute total system pressure of 500kPa, an air flow rate of 400smL/min and a heating rate of 80°C/h.

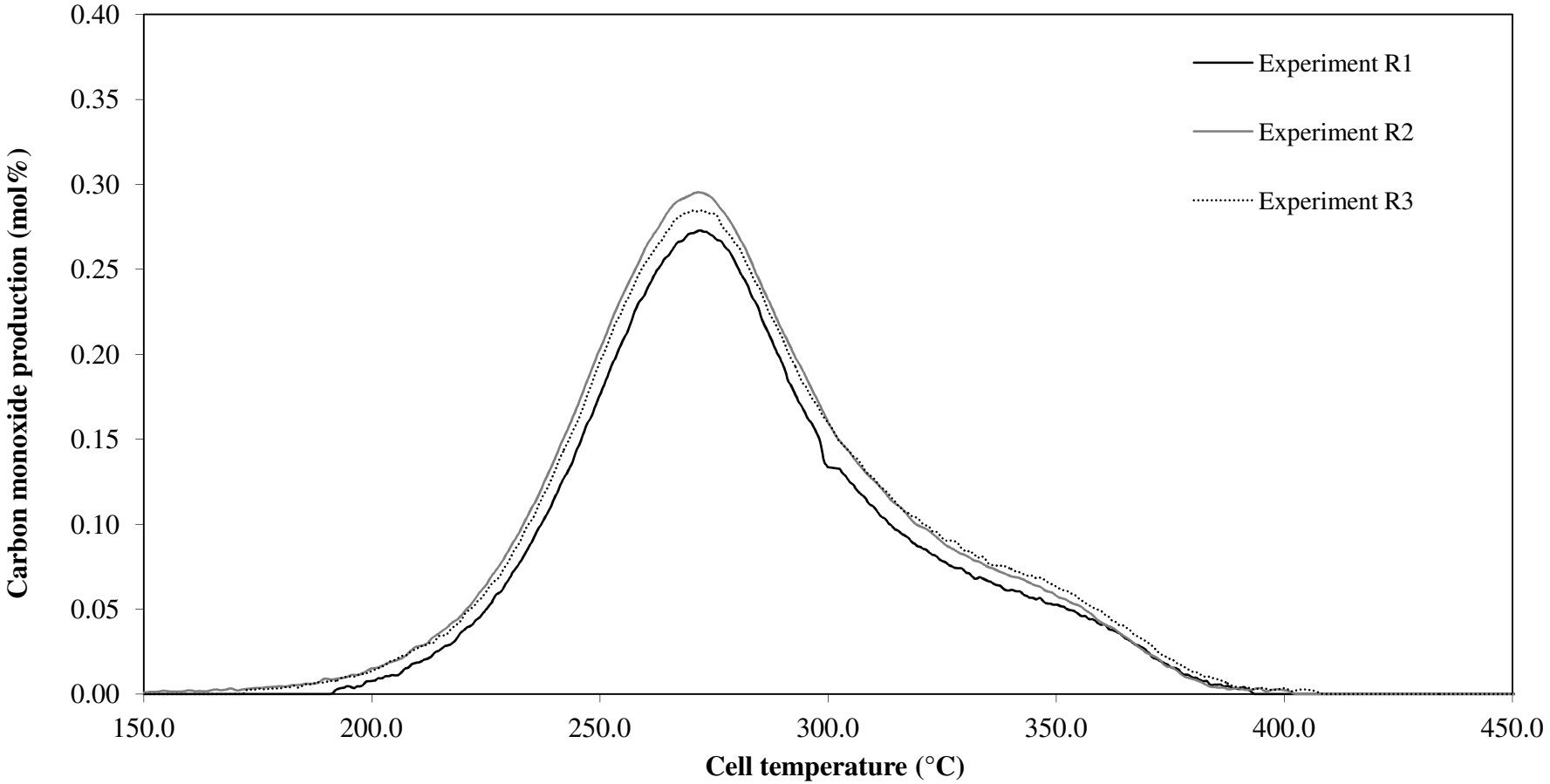

Figure 5.8 - Comparison of the carbon monoxide production data with respects to the cell temperature for the three rice husk experimental runs conducted under identical conditions with air as the oxidising gas, an absolute total system pressure of 500kPa, an air flow rate of 400smL/min and a heating rate of 80°C/h.

The overall comparison of the peak height in Table 5.3 presents an agreement to within ±10% of the actual values. The peak height depends on the quantity of sample presents in each of experiments. The small differences observed for the three runs may be due to the amount of the rice husk initially present in the reaction cell. In this case, the sample weight of the three identical rice husk experiments varied by around ±5%. A significant error during the preparation of the sample may contribute to the variation in the results. Because rice husk is a heterogeneous material, a small variation should be expected in the values of the calculated parameters. The same observation was also been reported by Nguyen (2004) in the evolved gas analysis (EGA) experiments of Vietnamese crude oil. In her study, larger variations in the results were observed for the experimental runs performed under identical conditions.

The calculated kinetic parameters of these three runs, R1 to R3, are presented in Table 5.4. The predicted oxygen consumption curve in comparison with the actual oxygen consumption curve of the experimental data are presented in Figures 5.9 to 5.11 for experiments R1 to R3, respectively. A good fit with the variance below 0.001 was observed for experiments R2 and R3 of the predicted oxygen consumption curve with the experimental data. The calculated variance for experiments R2 and R3 were 0.0004 and 0.0002, respectively. However, an acceptable fit of the predicted curve with the experimental data is achieved for experiment R1 with the variance of 0.0029. For all the three identical rice husk experiments, there are a few discrepancies observed at the low temperature range of 150°C to 230°C, at the medium temperature range of 270°C to 320°C and at the high temperature range of 370°C to 400°C. The reasons of the discrepancies were explained in details in the previous Section 5.2. In terms of the calculated kinetic parameters for the HTO, MTO and LTO reactions, there are no significant differences observed for all the three identical rice husk experiments (see Table 5.4).

Considering Table 5.4, for the high temperature oxidation (HTO) reaction, the reaction order varied by 0.01 for all the three identical rice husk experiments. The activation energy varied from 17.3×10^3K to 17.5×10^3K. The ln β for the HTO reaction varied in the range of 19.8 to 20.2 for all the three identical rice husk experiments.

Table 5.4 - Summary of the calculated kinetic parameters of the rice husk oxidation. The E/R is the activation energy (in K) and the ln β is the natural log of beta group (dimensionless). M1 is gas mixture 1 that consist of 15.10 mol% O_2, 2.01 mol% CO_2, 0.983 mol% CO and balance nitrogen.

Experiment		**R1**	**R2**	**R3**	**R4**	**R5**	**R6**	**R7**	**R8**
Absolute total system pressure (kPa)		500	500	500	500	300	700	500	363
Oxygen partial pressure (kPa)		105	105	105	105	63	147	76	76
Oxygen concentration in feed gas (mol%)		20.96 (Air)	20.96 (Air)	20.96 (Air)	20.96 (Air)	20.96 (Air)	20.96 (Air)	15.10 (M1)	20.96 (Air)
Heating rate (°C/h)		80	80	80	50	50	50	50	50
HTO	Reaction order, n	0.99	0.98	0.99	1.01	1.00	1.01	1.00	1.00
	E/R ($\times 10^{-3}$)	17.5	17.3	17.3	17.5	19.8	17.2	19.0	19.1
	ln β	20.2	19.8	19.8	21.3	24.6	20.4	24.0	23.8
MTO	Reaction order, n	1.00	0.99	0.97	0.98	0.97	1.01	0.99	0.98
	E/R ($\times 10^{-3}$)	19.6	19.0	19.1	19.5	13.7	20.1	14.4	14.1
	ln β	26.9	25.8	25.7	26.1	16.9	26.4	17.0	17.2
LTO	Reaction order, n	1.39	1.36	1.36	1.35	1.16	1.57	1.27	1.27
	E/R ($\times 10^{-3}$)	14.9	14.6	14.5	14.8	18.7	5.2	17.6	17.8
	ln β	16.7	16.1	16.2	16.2	22.8	7.4	22.0	22.4
Variance, σ^2		0.0029	0.0004	0.0002	0.0006	0.0001	0.0005	0.0002	0.0001

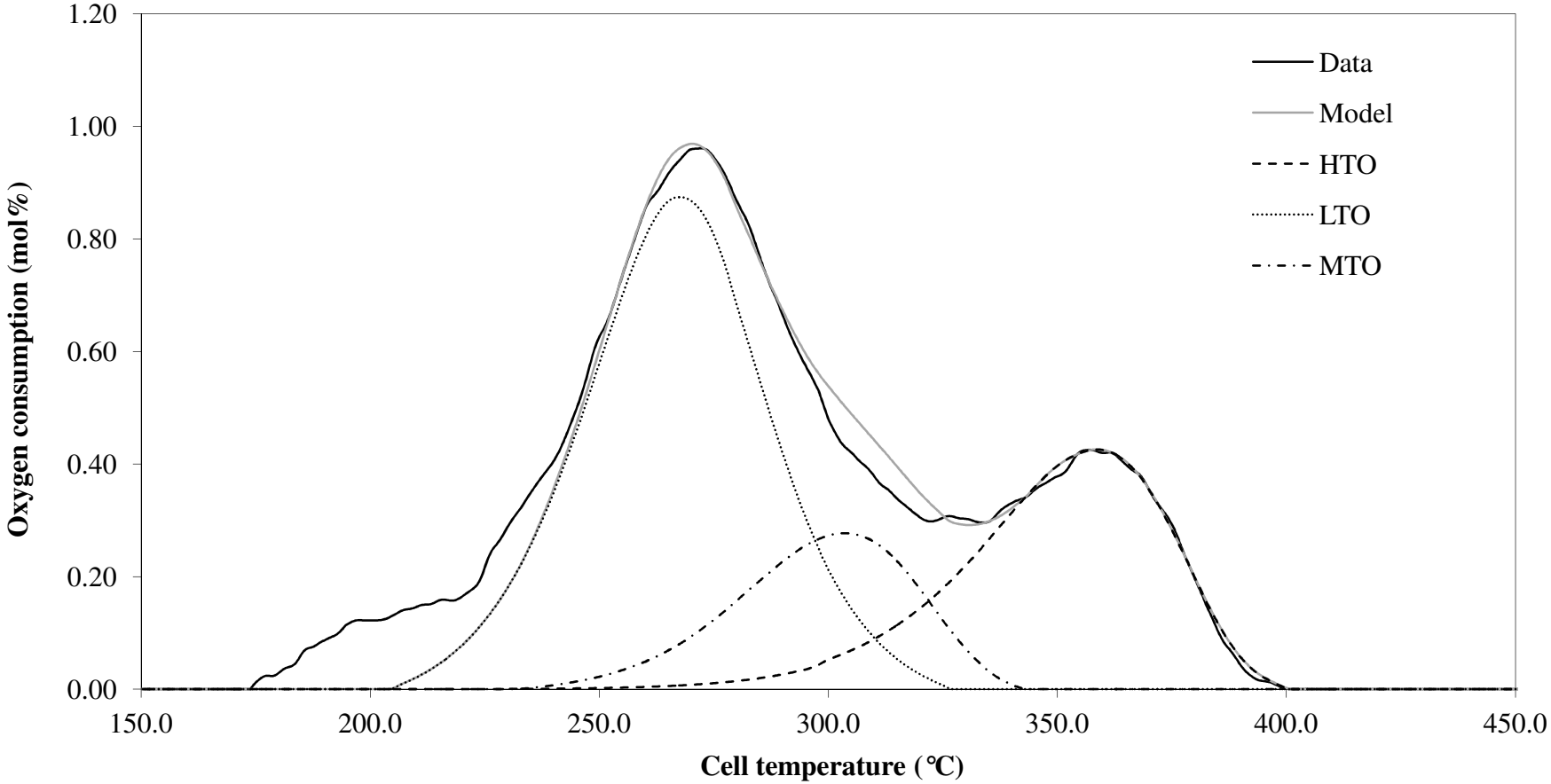

Figure 5.9 - Comparison of the oxygen consumption data and the model predictions with respects to the cell temperature for the oxidation of rice husk with air as the oxidising gas, an absolute total system pressure of 500kPa, an air flow rate of 400smL/min and a heating rate of 80°C/h (Experiment R1).

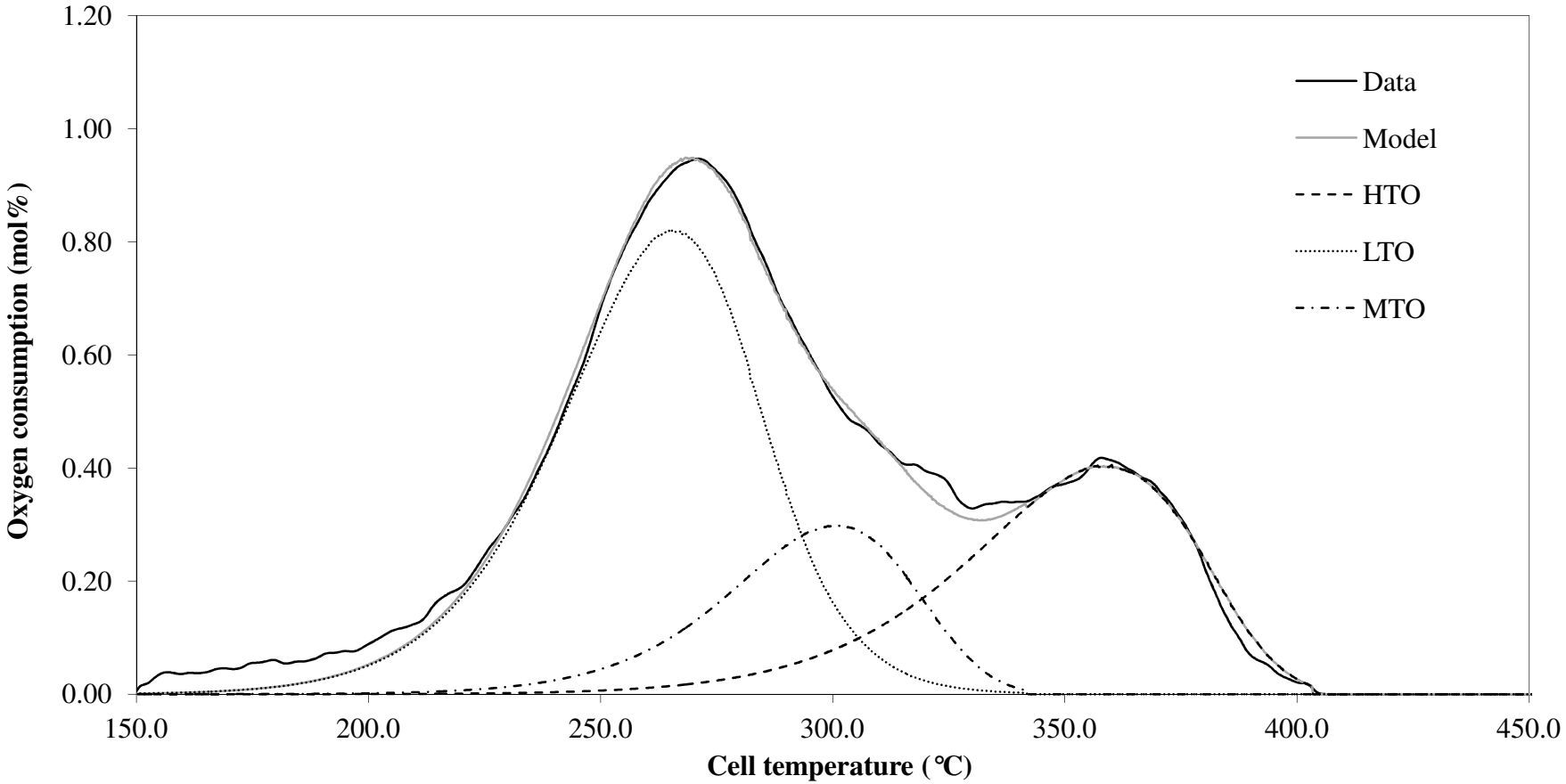

Figure 5.10 - Comparison of the oxygen consumption data and the model predictions with respects to the cell temperature for the oxidation of rice husk with air as the oxidising gas, an absolute total system pressure of 500kPa, an air flow rate of 400smL/min and a heating rate of 80°C/h (Experiment R2).

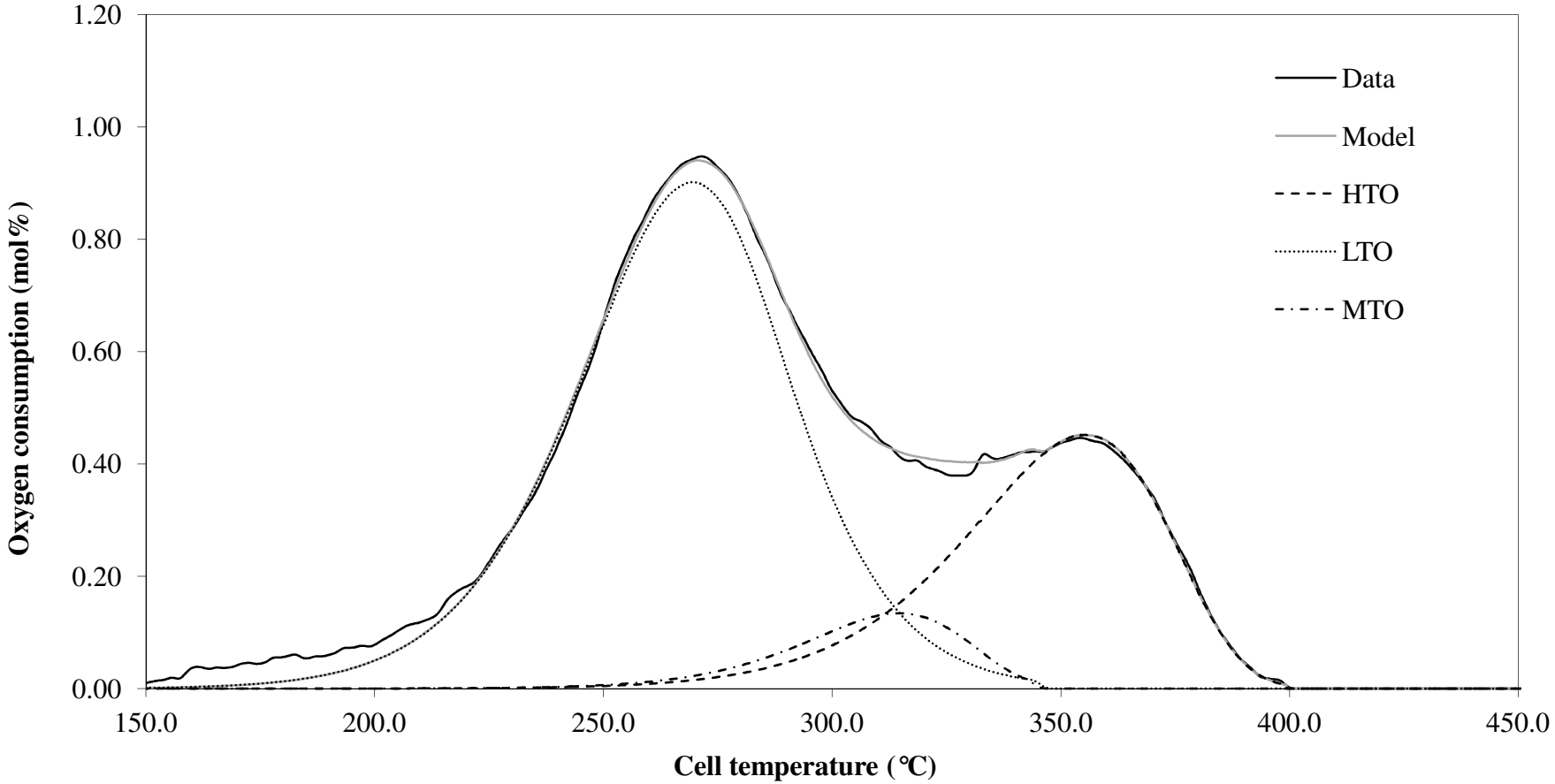

Figure 5.11 - Comparison of the oxygen consumption data and the model predictions with respects to the cell temperature for the oxidation of rice husk with air as the oxidising gas, an absolute total system pressure of 500kPa, an air flow rate of 400smL/min and a heating rate of 80°C/h (Experiment R3).

For the medium temperature oxidation (MTO) reaction of the three identical rice husk experiments, the reaction order varied by 0.03. The activation energy varied from 19.0 × 10^3K to 19.6 × 10^3K for these rice husk experiments. The ln β varied in the range of 25.7 to 26.9 for the MTO reaction of the three identical rice husk experiments. For the low temperature oxidation (LTO) reaction of the three identical rice husk experiments, the reaction order varied by 0.03 while the activation energy varied in the range of 14.5 × 10^3K to 14.9 × 10^3K. For the ln β of the LTO reaction for the three identical rice husk experiments, the variation is 3.6% from 16.1 to 16.7. The HTO reaction shows the lowest variations and followed by the LTO reaction and eventually the MTO reaction. This is well expected since the errors from the HTO calculation were transferred to the LTO calculation and the errors from the LTO calculation were then transferred to MTO calculation.

In summary, the overall reproducibility of the data is good between the three rice husk experiments made at identical conditions. There are no significant differences in the peak temperatures and heights observed for all the three identical rice husk experiments for the exit gas oxygen, carbon dioxide and carbon monoxide compositions.

Further, there are also no significant differences in the calculated kinetic parameters of the three identical rice husk experiments. These observations show that the evolved gas analysis (EGA) results of the rice husk experiments are reproducible. This also confirms that the kinetic model of decoupling procedure may successfully be applied to the rice husk oxidation data and provides a good fit between the predicted oxygen consumption curve with the experimental data.

5.4 Effect of the heating rate

One of the purposes in conducting experiment R4 was to determine the influence of heating rate on the rice husk combustion characteristics. Experiment R4 was conducted with a lower heating rate of 50°C/h compared to the rate of 80°C/h used in experiments R1 to R3. Details of the experimental conditions are provided in Table 5.1. The evolved gas analysis (EGA) experimental results of these runs are presented in Table 5.3. Figure

5.1 presents the variation in the exit gas compositions with respects to cell temperature for experiment R4.

In order to ease the discussion on the influence of the heating rate on the peak heights and peak temperatures of the rice husk combustion characteristics, Figures 5.12 to 5.14 allow a comparison between the observations of experiment R4 with those of experiments R1 to R3 conducted at different heating rate for the oxygen consumption, the carbon dioxide production and the carbon monoxide production curves, respectively. As observed in Figures 5.12 to 5.14, the peak shifts to lower temperatures as the heating rate decreases from 80°C/h to 50°C/h for all the exit gas composition curves. The hemicellulose peak temperature is shifted 23°C lower as the heating rate changed from 80°C/h to 50°C/h for the carbon dioxide production, the carbon monoxide production and the oxygen consumption curves. Similarly, the cellulose peak temperature for the exit gas composition curves is shifted 30°C lower as the heating rate reduced. A significant influence was also observed for the peak height as the heating rate changed from 80°C/h to 50°C/h. As observed in Figure 5.12, the hemicellulose peak height of the oxygen consumption curve reduced from 0.95 mol% to 0.69 mol% oxygen as the heating rate changed from 80°C/h to 50°C/h. However, the cellulose peak height of the oxygen consumption curves show no noticeable changes as the heating rate changed. A similar trend regarding the peak heights was also observed for the carbon dioxide production curve (see Figure 5.13).

As the heating rate decreased from 80°C/h to 50°C/h, the hemicellulose peak height of the carbon dioxide production curve reduced from 0.86 mol% to 0.54 mol% carbon dioxide. There is a small change to the cellulose peak height for the carbon dioxide production curves as the heating rate reduced. Similarly to the oxygen consumption curve, there are no significant differences in the cellulose peak height of the carbon dioxide production curve as the heating rate reduced from 80°C/h to 50°C/h. For the carbon monoxide production curve, the hemicellulose peak height reduced from 0.28 mol% to 0.16 mol% carbon monoxide as the heating rate reduced (see Figure 5.14). There is no cellulose peak observed for the carbon monoxide production curve.

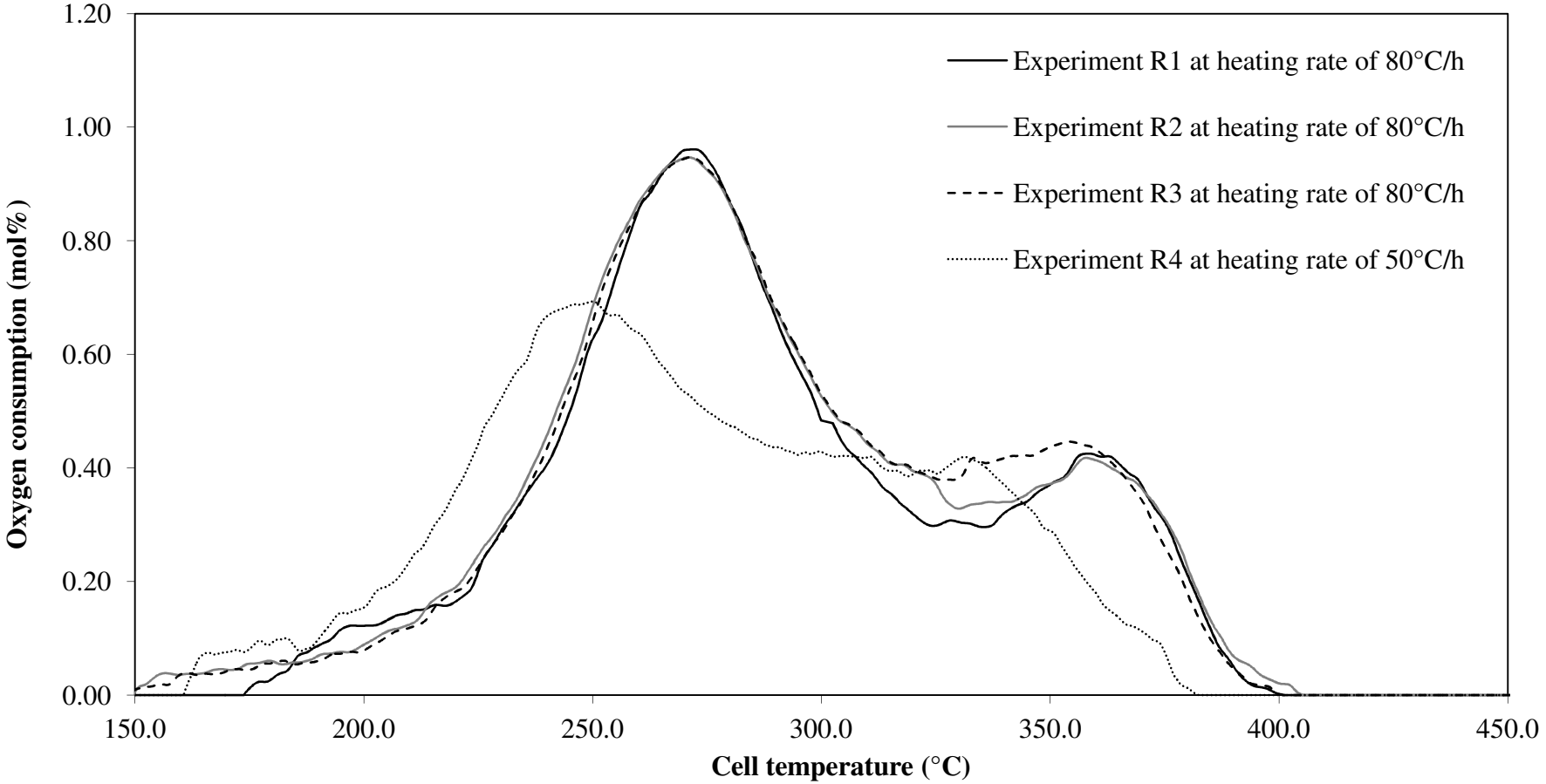

Figure 5.12 - Comparison of the oxygen consumption data with respects to the cell temperature for experiments R1 to R3 conducted at heating rate of 80°C/h with experiment R4 performed at heating rate of 50°C/h at an absolute total system pressure of 500kPa and an air flow rate of 400smL/min.

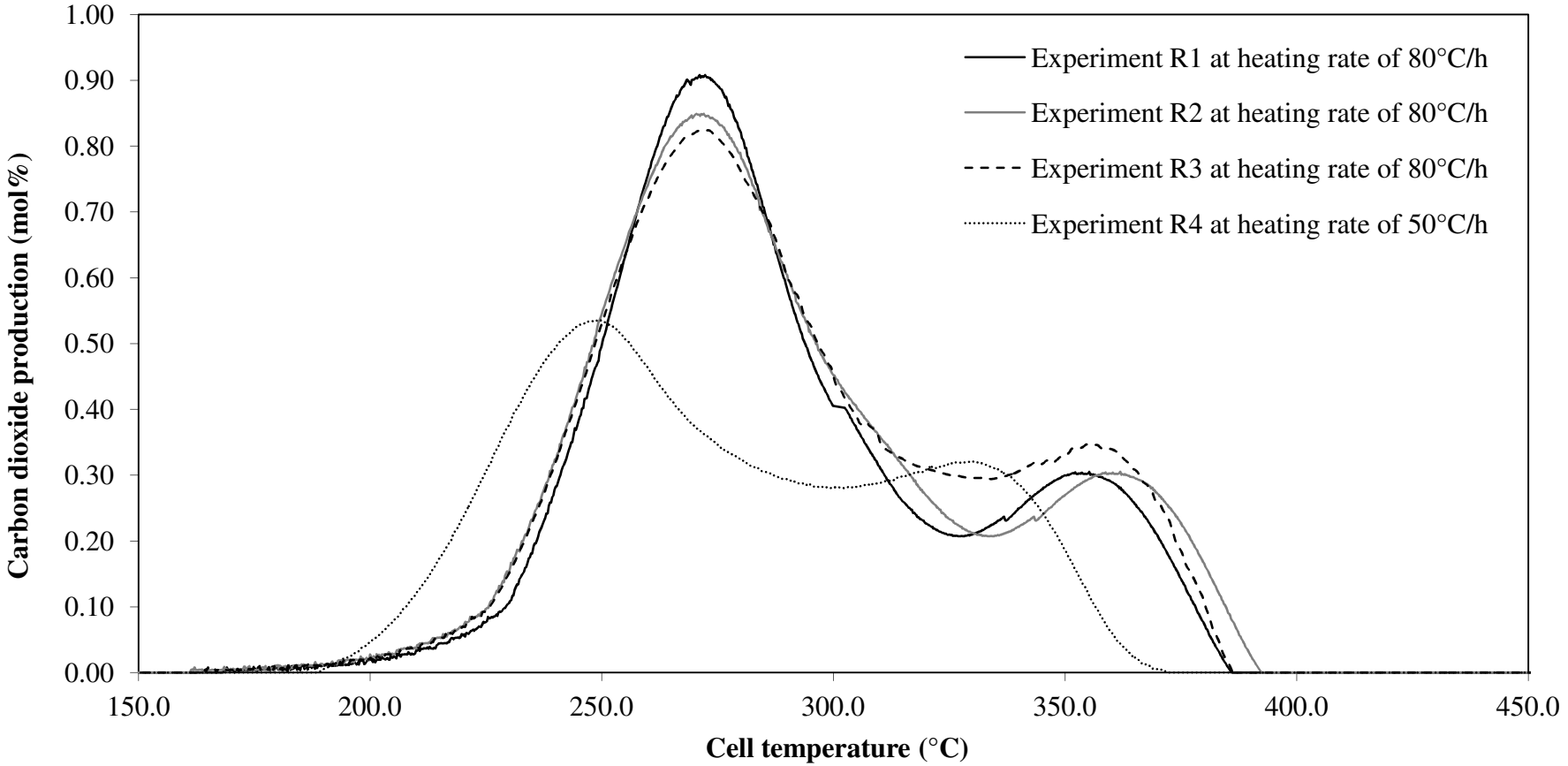

Figure 5.13 - Comparison of the carbon dioxide production data with respects to the cell temperature for experiments R1 to R3 conducted at heating rate of 80°C/h with experiment R4 performed at heating rate of 50°C/h at an absolute total system pressure of 500kPa and an air flow rate of 400smL/min.

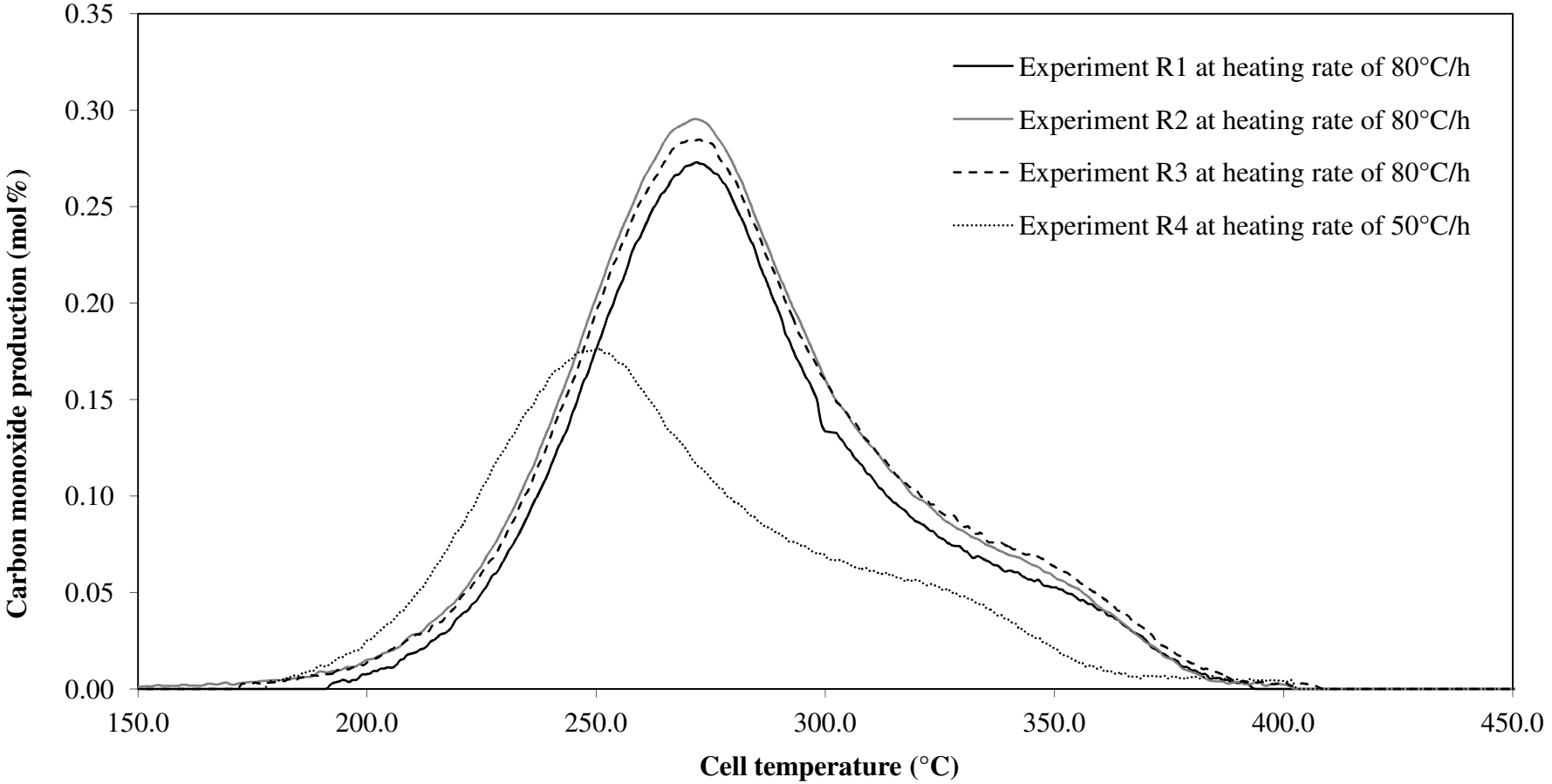

Figure 5.14 - Comparison of the carbon monoxide production data with respects to the cell temperature for experiments R1 to R3 conducted at heating rate of 80°C/h with experiment R4 performed at heating rate of 50°C/h at an absolute total system pressure of 500kPa and an air flow rate of 400smL/min.

Kisler (1995) reported similar observations in his study of the oxidation of Australian light crude oil. Kisler (1995) noted that slower heating rates produced shorter and broader peaks with respect to time. Idris *et al.* (2010) performed a thermogravimetric analysis (TGA) experiments with an oil palm biomass. They found that as the heating rate increased from 10°C/min to 60°C/min, the decomposition of oil palm biomass increased hence, the peak was systematically shifted to higher temperatures. They noted that the reason for these temperature shifts is that less heat is required for cracking of the biomass materials. By comparison of the high and the low heating rates, at the lower heating rates, the heating of the biomass material occurred more gradually leading to an improved and more effective heat transfer to the inner portions and among the biomass particles. As a result, the lower heating rate is more effective and efficient compared to the higher heating rate for oil palm biomass combustion characteristics study using TGA. The same observation was also been reported by Skreiberg *et al.* (2011) and Yorulmaz and Atimtay (2009) in their wood waste combustion characteristics study using TGA technique.

In this study, it was found that the slower heating rate of an evolved gas analysis (EGA) experiments may avoid the exothermic decomposition reaction in the cell temperature. It is important to ensure that the entire cell is always at a uniform temperature. Hence, for the next study on the effect of the total system and oxygen partial pressures (Section 5.5), the standard heating rate is applied at 50°C/h.

Considering the influence of the heating rate on the calculated kinetic parameters of the reaction order (n), the activation energy (E/R) and the ln β, Table 5.4 presents the calculated kinetic parameters obtained for experiment R4 which was performed at a heating rate of 50°C/h with comparison to experiments R1 to R3 that were performed at a heating rate of 80°C/h. A plot of the oxygen consumption data and the model predictions with respect to cell temperature for the combustion characteristics of experiment R4 was shown and discussed previously in Figure 5.2. Table 5.4 shows that the heating rate does not significantly influence the calculated kinetic parameter values. The calculated kinetic parameter values for experiment R4 are consistent with those obtained for experiments R1 to R3 which are conducted at the higher heating rate of

80°C/h. For the high temperature oxidation (HTO) reaction, the reaction order was in the range of 0.98 to 1.01 for experiments R1 to R4. The activation energy varied from 17.3 × 10^3K to 17.5 × 10^3K while the ln β was in the range of 19.8 to 21.3 for experiments R1 to R4. Considering the medium temperature oxidation (MTO) reaction, the reaction order varied from 0.97 to 1.00 for experiments R1 to R4 conducted at different heating rate. The activation energy was in the range of 19.0 × 10^3K to 19.5 × 10^3K. The ln β varied from 25.7 to 26.1 for experiments R1 to R4. For the low temperature oxidation (LTO) reaction of the four experiments, the reaction order varied by 0.04. The activation energy was in the range of 14.5 × 10^3K to 14.9 × 10^3K and the ln β varied by 0.6. The variations in the calculated kinetic parameters are consistent with the level of accuracy of the rice husk experiments. A similar observation was reported by Kisler (1995) in the oxidation study of the light Australian oils using essentially the same equipment as the present study.

In conclusion, the heating rate of the combustion cell has a significant influence on the oxidation behaviour of the rice husk. As the heating rate decreases, the peaks of the exit gas oxygen, carbon dioxide and carbon monoxide compositions shift to lower temperatures. Likewise, as the heating rate decreases, the peak heights of all the effluent gas compositions are also decrease. More importantly, there is no significant effect on the calculated kinetic parameter values over the differing heating rates. This is evidence that the reaction model adequately accounts for varieties in the heating rates in the reactor.

5.5 Effect of the total system and the oxygen partial pressures

A major advantage of the evolved gas analysis (EGA) technique is the ease with which the influence of the total system and the oxygen partial pressures on the combustion characteristics of biomass materials may be studied. The EGA experimental rigs has a back pressure regulator that is used to maintain the combustion cell at the desired pressure. Hence, the study on the effect of pressure may be performed. The total system pressures ranging from 300kPa to 700kPa and the oxygen partial pressures ranging from 63kPa to 147kPa were investigated. The oxygen concentrations of the inlet gas

were varied appropriately in order to study the influence of the total system and the oxygen partial pressures on the rice husk combustion characteristics.

Experiments R5 to R8 were conducted at various total system and oxygen partial pressures at a heating rate of 50°C/h and with a feed gas flow rate of 400smL/min. For all experiments in this Section, the feed gas flow rate was 400smL/min and the heating rate was 50°C/h. Experiments R5 and R6 were conducted at a lower and a higher total system pressures, respectively with air as the oxidising gas. Experiment R7 was performed with an absolute total system pressure of 500kPa and with a feed gas composition with a 15.10 mol% of oxygen concentration. The oxygen partial pressure for experiment R7 was 76kPa. Experiment R8 was conducted at an absolute total system pressure of 363kPa with air as the oxidising gas. The oxygen partial pressure for experiment R8 was 76kPa. Comparison of experiments R7 and R8 allows the influence of the total system pressures on the rice husk combustion characteristics. Experiments R7 and R4 were performed at the same absolute total system pressure of 500kPa but with different oxygen partial pressure. Comparison of experiments R4 and R7 allows the effect of oxygen partial pressure on the rice husk combustion characteristics to be observed. The summary of the experimental conditions is presented in Table 5.1. The evolved gas analysis (EGA) experimental results are shown in Table 5.3. Figures 5.15 to 5.18 present the variation in exit gas compositions with respects to cell temperature for experiments R5 to R8. These figures exhibit similar features to those observed for experiments R1 to R4. The oxygen consumption and the carbon dioxide production curves have two peaks of the hemicellulose and the cellulose decompositions. The carbon monoxide production curve has only one peak.

Figure 5.19 presents the effect of the total system pressure and the oxygen partial pressure on the oxygen consumption of the rice husk combustion characteristics. Figures 5.20 and 5.21 present the corresponding information for the carbon dioxide production and the carbon monoxide production curves.

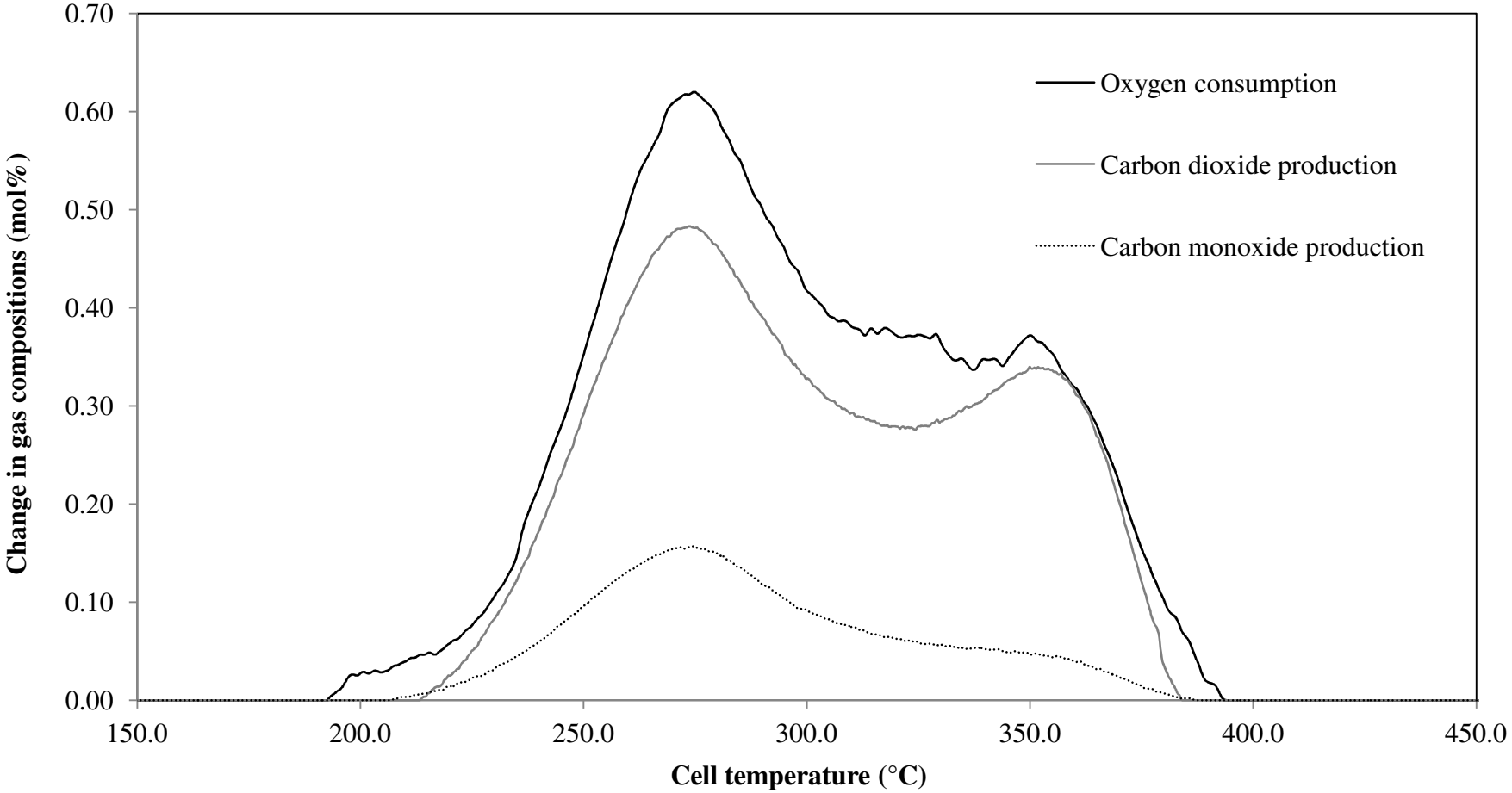

Figure 5.15 - Evolved gas analysis data with respects to the cell temperature for the oxidation of rice husk with air as the oxidising gas, an absolute total system pressure of 300kPa, an air flow rate of 400smL/min and a heating rate of 50°C/h (Experiment R5).

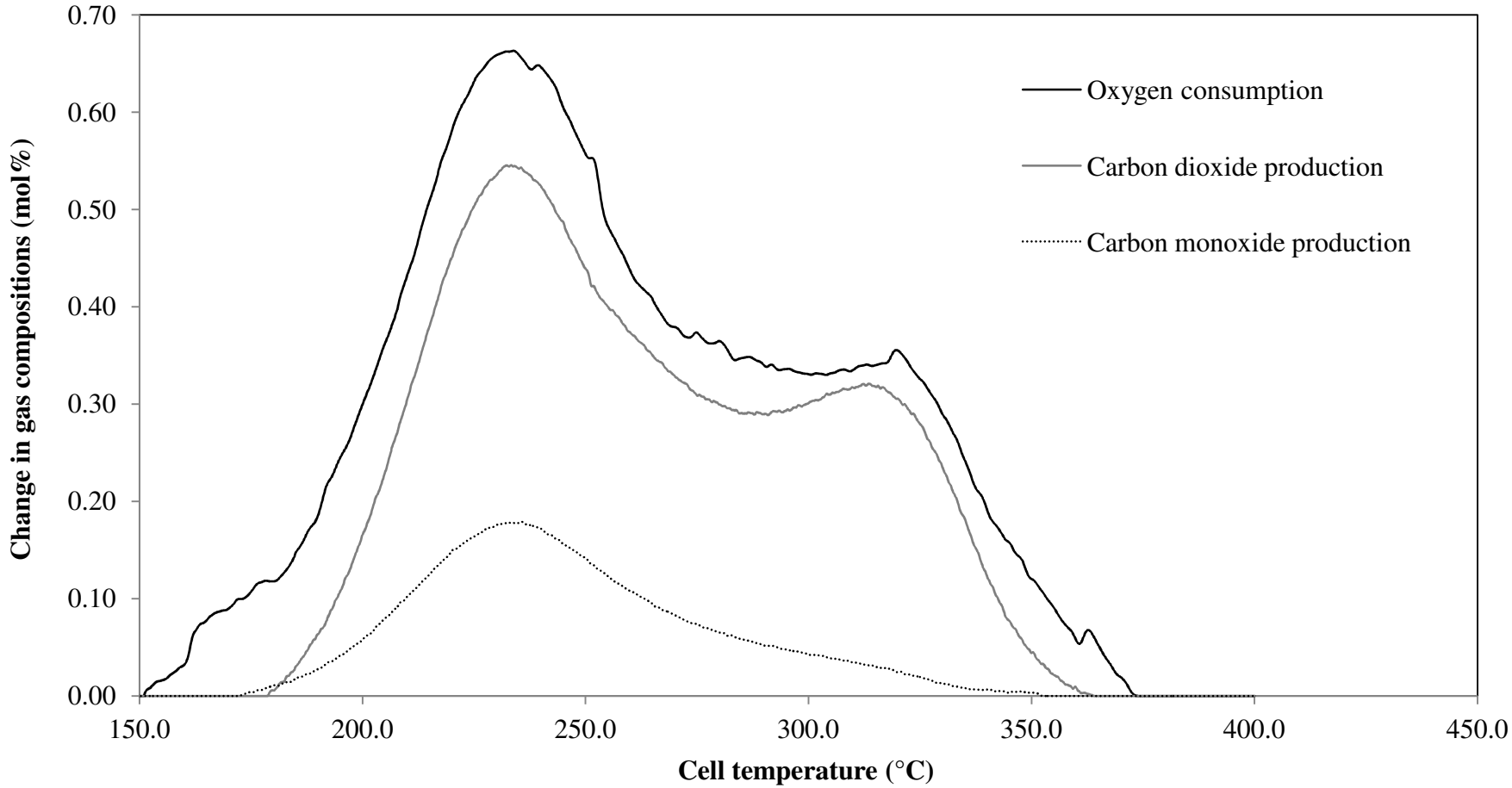

Figure 5.16 - Evolved gas analysis data with respects to the cell temperature for the oxidation of rice husk with air as the oxidising gas, an absolute total system pressure of 700kPa, an air flow rate of 400smL/min and a heating rate of 50°C/h (Experiment R6).

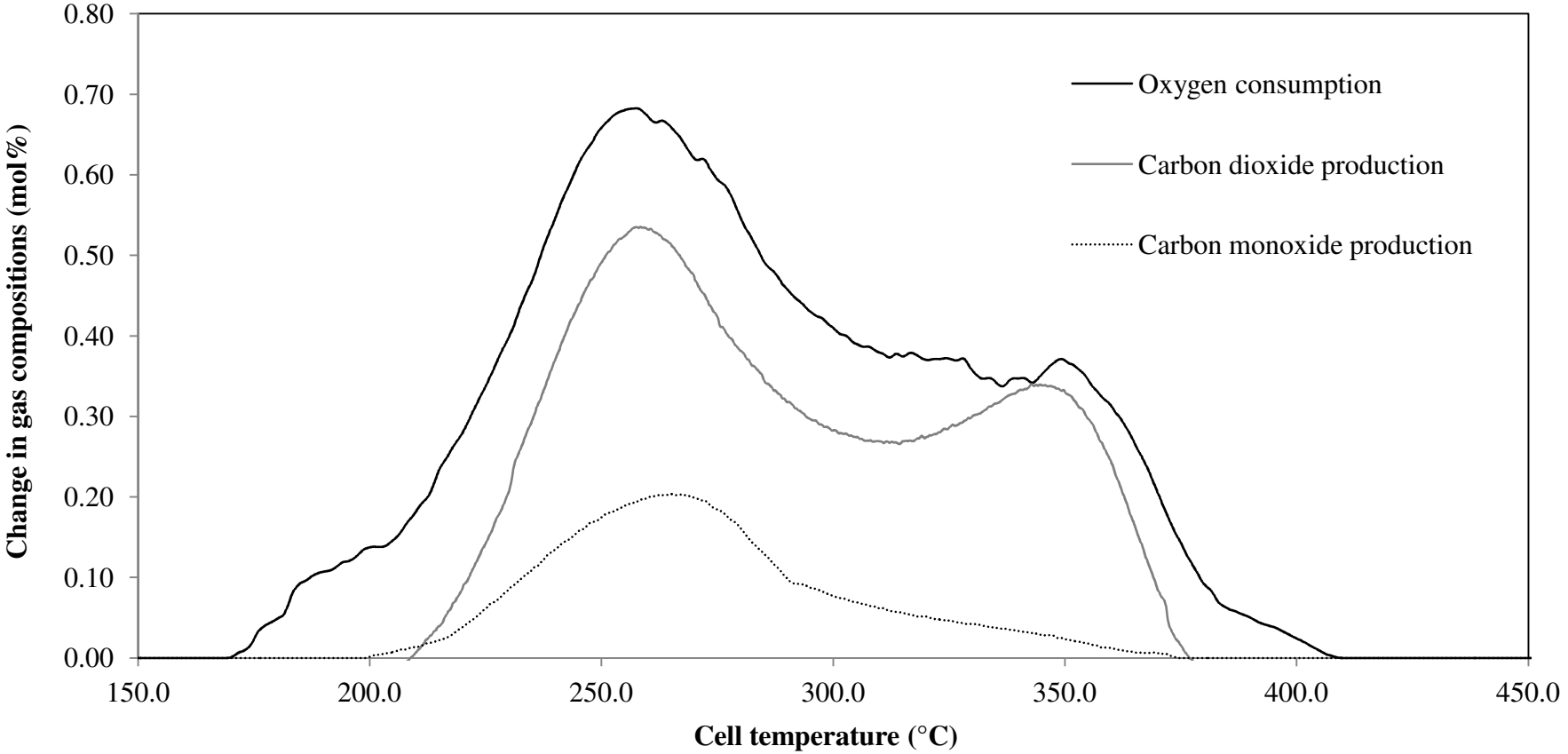

Figure 5.17 - Evolved gas analysis data with respects to the cell temperature for the oxidation of rice husk with 15.10 mol% oxygen concentration in feed gas (gas mixture 1), an absolute total system pressure of 500kPa, an oxygen partial pressure of 76kPa, a flow rate of 400smL/min and a heating rate of 50°C/h (Experiment R7).

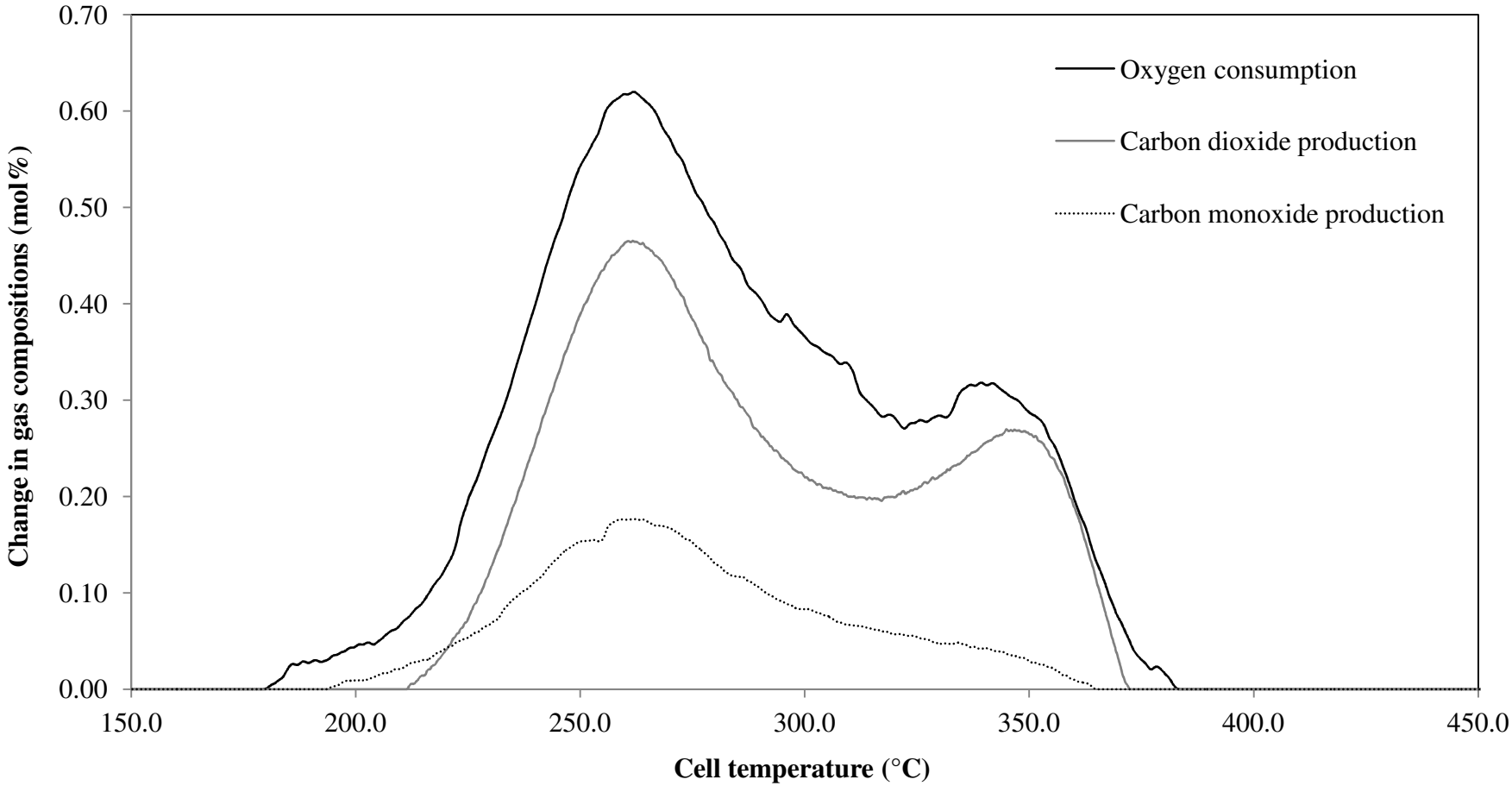

Figure 5.18 - Evolved gas analysis data with respects to the cell temperature for the oxidation of rice husk with air as the oxidising gas, an absolute total system pressure of 363kPa, an air flow rate of 400smL/min and a heating rate of 50°C/h (Experiment R8).

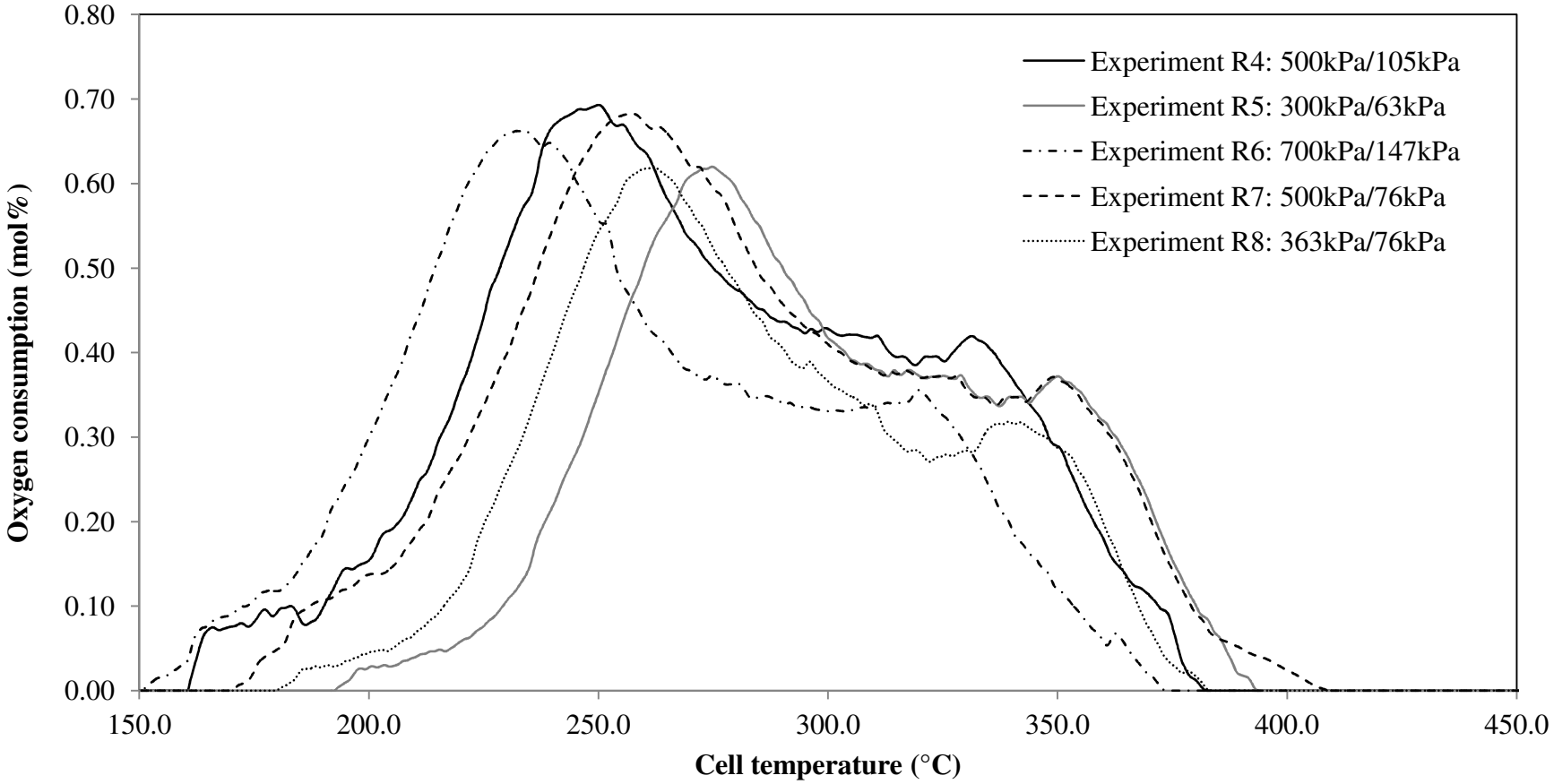

Figure 5.19 - Comparison of the oxygen consumption data with respects to the cell temperature for various system and oxygen partial pressures conducted at heating rate of 50°C/h and gas flow rate of 400smL/min. The pressures shown refer to the absolute total system pressure and oxygen partial pressure, respectively.

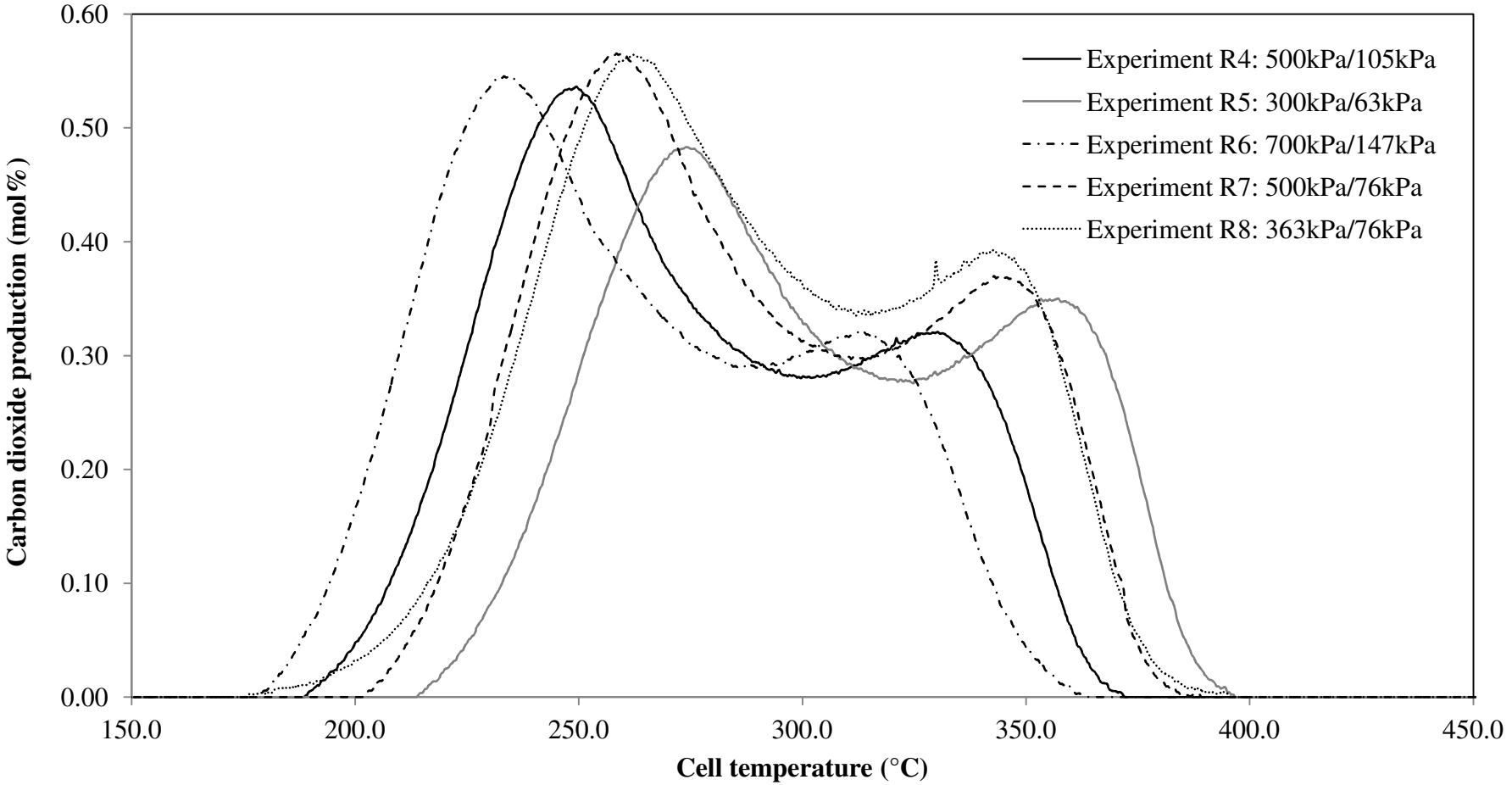

Figure 5.20 - Comparison of the carbon dioxide production data with respects to the cell temperature for various system and oxygen partial pressures conducted at heating rate of 50°C/h and gas flow rate of 400smL/min. The pressures shown refer to the absolute total system pressure and oxygen partial pressure, respectively.

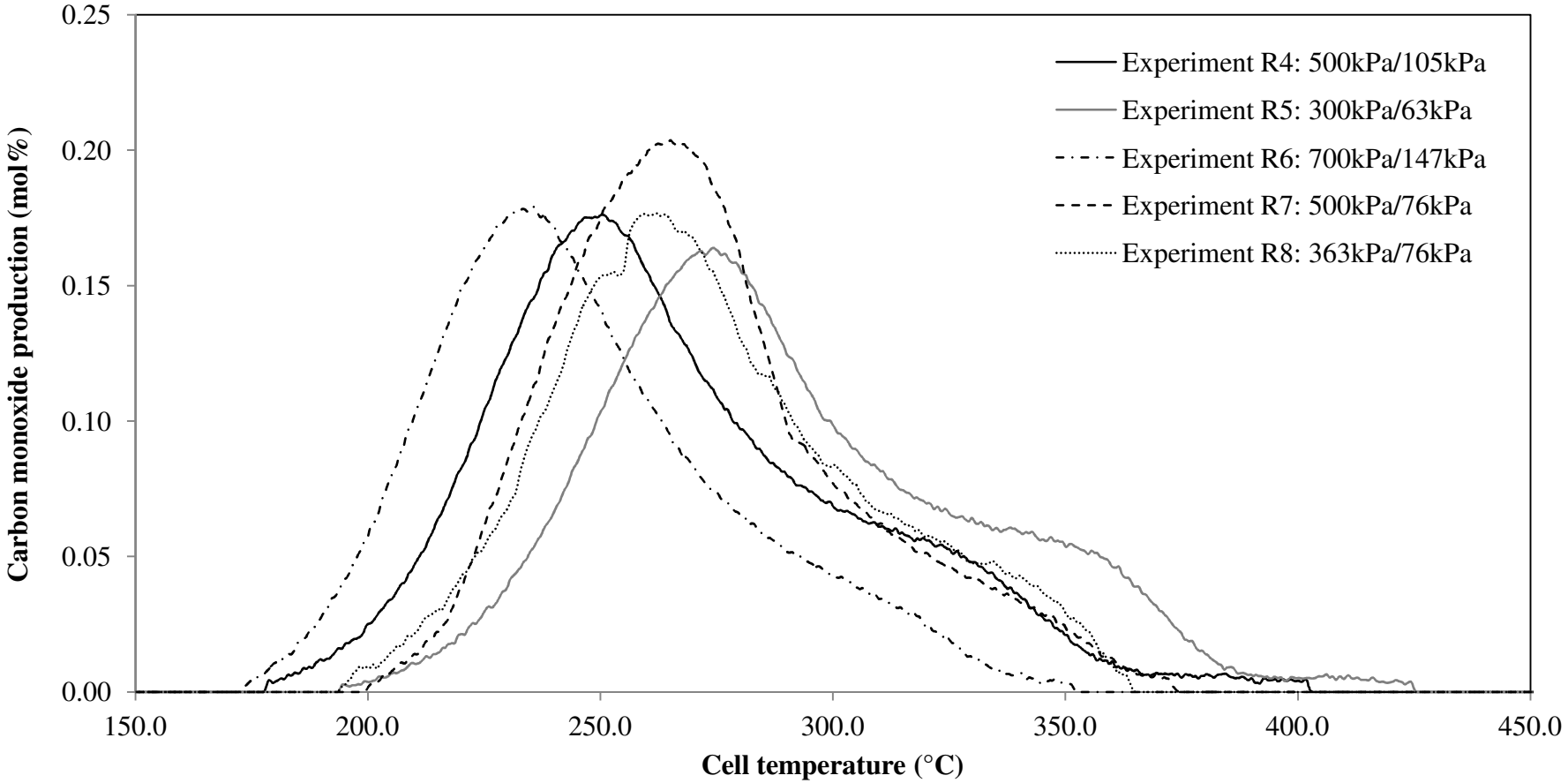

Figure 5.21 - Comparison of the carbon monoxide production data with respects to the cell temperature for various system and oxygen partial pressures conducted at heating rate of 50°C/h and gas flow rate of 400smL/min. The pressures shown refer to the absolute total system pressure and oxygen partial pressure, respectively.

As observed in Figure 5.19, the peaks shift to lower temperatures as the total system and the oxygen partial pressures increased. The hemicellulose peak temperature for the oxygen consumption curve was reduced approximately 40°C as the total system pressure increased from 300kPa to 700kPa (see experiments R5 and R6 in Table 5.3).

Likewise, the cellulose peak temperature of the oxygen consumption also shows a similar trend as the hemicellulose peak. The cellulose peak temperature of the oxygen consumption curve was reduced by 34°C as the total system pressure increased from 300kPa to 700kPa. A similar reduction of 40°C for the hemicellulose peaks was observed for both the carbon dioxide and carbon monoxide production curves (see Figures 5.20 and 5.21). The cellulose peak temperature for the carbon dioxide production curve was also in agreement with the oxygen consumption curve with a reduction of around 34°C as the total system pressure increased from 300kPa to 700kPa. However there were no significant changes in the peak heights of all the exit gas composition curves when pressure is applied.

In order to examine whether it is the total system pressure or the oxygen partial pressure that has the more significant influence on the rice husk combustion characteristics, a comparison between experiments R7 and R8 (effect of the total system pressure) and experiments R4 and R7 (effect of the oxygen partial pressure) was conducted. Figures 5.22 to 5.23 present the effect of the total system pressure on the peak temperatures of the oxygen consumption and the both carbon dioxide and carbon monoxide productions.

Considering Table 5.3 and Figure 5.22 for the oxygen consumption curve under similar oxygen partial pressures of 76kPa, the total system pressure has no significant influences on the measured peak temperatures (see experiments R7 and R8). Likewise, a similar observation is observed for the carbon dioxide and the carbon monoxide production curves (see Figure 5.23).

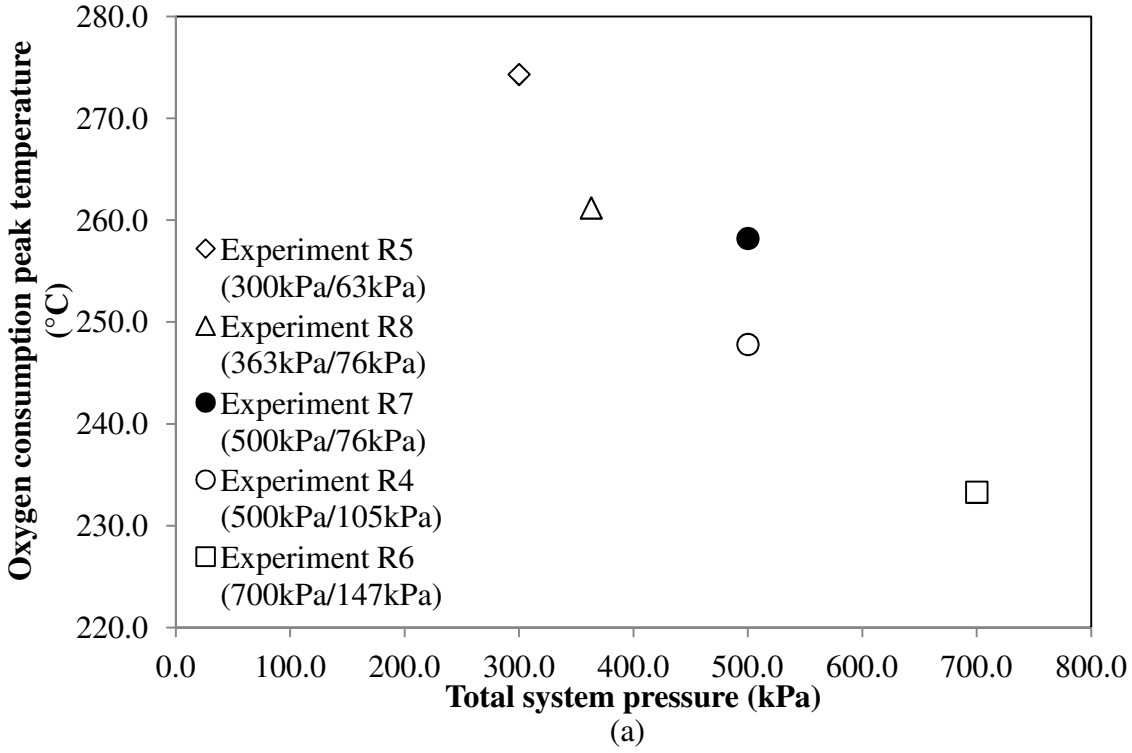

(a)

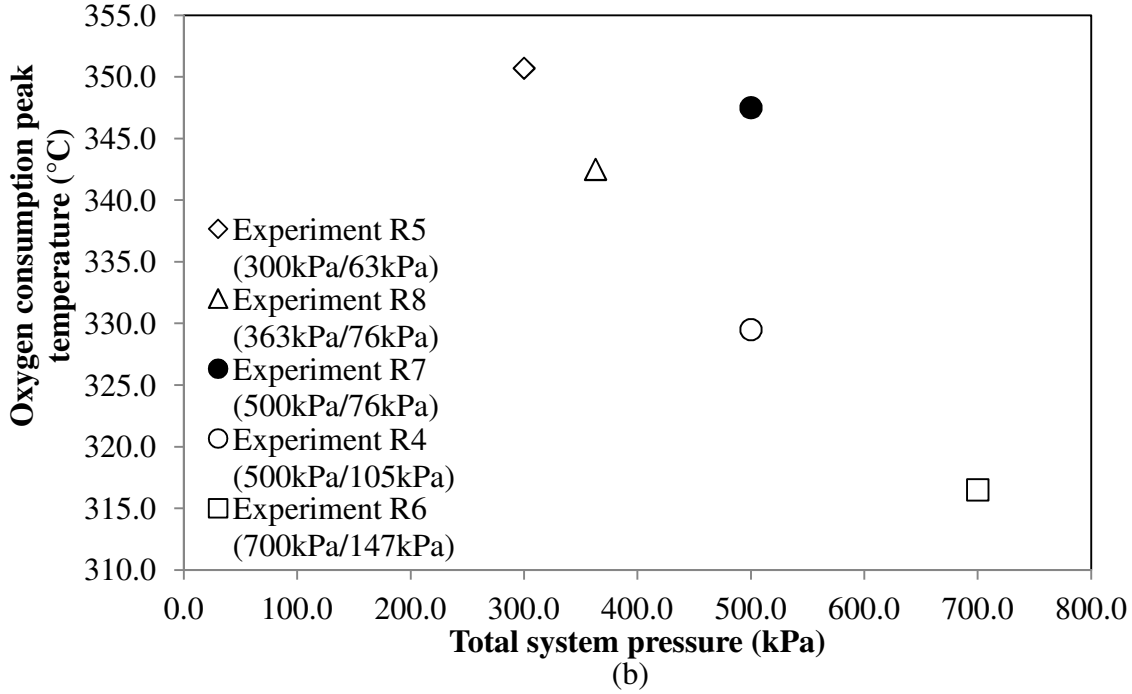

(b)

Figure 5.22 - Effect of the total system pressure on (a) the hemicellulose peak temperature (b) the cellulose peak temperature of the oxygen consumption. The pressures shown refer to the absolute total system pressure and oxygen partial pressure, respectively.

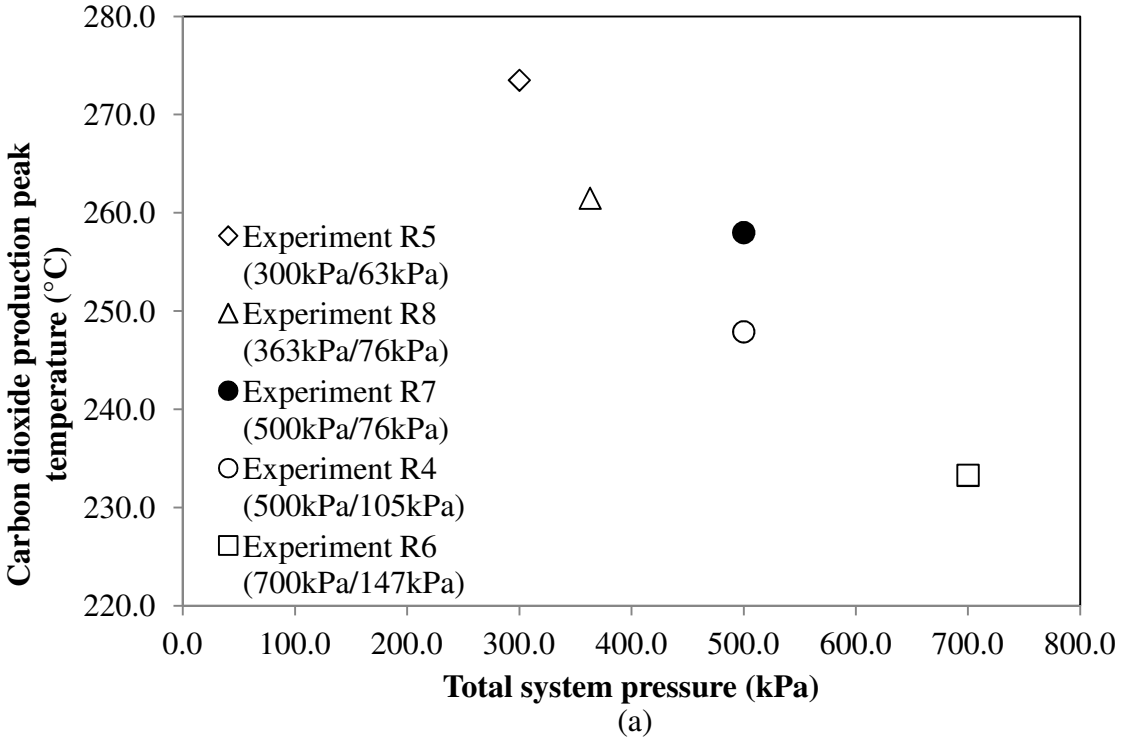

(a)

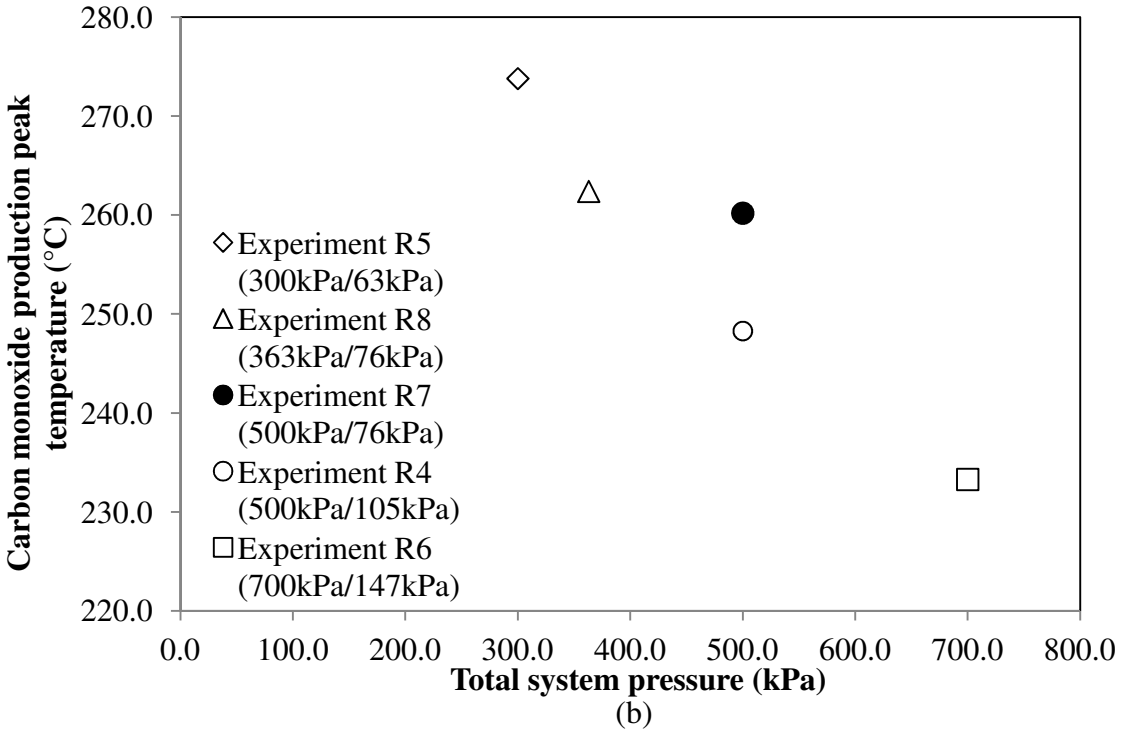

(b)

Figure 5.23 - Effect of the total system pressure on the hemicellulose peak temperatures of (a) the carbon dioxide production (b) the carbon monoxide production. The pressures shown refer to the absolute total system pressure and oxygen partial pressure, respectively.

The difference is only 1°C to 3°C of the peak temperatures and 10% of the peak heights, for the exit gas oxygen, carbon dioxide and carbon monoxide compositions. A similar observation has also been reported by Bridgwater and Boocock (1997) in their rice husk decomposition study using EGA technique. The same margin of 1°C to 3°C was reported for the oxygen consumption curves for experimental runs at various total system pressures while holding the oxygen partial pressure constant at 42kPa. They believed that the combustion of rice husk is affected by the diffusion limitations. This may be due to the fact that heat transfer into the rice husk is not materially affected by a change of gas pressure. The heat transfer occurring predominantly by conduction through the solid portion rather than by conduction and convection of the gases into the internal pores of the husks. Further, the evolution of volatiles from the surface of the rice husk into the surrounding gas phase is not affected by the external pressure which implies that internal mass transfer resistances are small compared to the quantities of gas seeking to migrate to the surface. This would be consistent with rates of decomposition within the biomass being heat transfer limited. However, there is no reports on the pore sizes of the rice husk to support the findings. For this study, it is believed that the effect was more to the volumetric reaction rather than surface and internal reactions. The molecules react as a whole with oxygen and temperature would be the important factor rather than mass transfer resistance.

Figures 5.24 and 5.25 present the effect of the oxygen partial pressure on the peak temperatures of the oxygen consumption and the both carbon dioxide and carbon monoxide productions. For the same total system pressure of 500kPa, the oxygen partial pressure shows a significant influences on the measured peak temperatures (see experiments R4 and R7 in Table 5.3 and Figure 5.24). As the oxygen partial pressure increased from 76kPa to 105kPa at the same total system pressure of 500kPa, the peak temperatures shifted towards lower temperatures for the hemicellulose oxygen consumption curve. The hemicellulose peak was reduced approximately 10°C as the oxygen partial pressure increased from 76kPa to 105kPa for the exit gas oxygen, carbon dioxide and carbon monoxide compositions (see Figures 5.24 and 5.25).

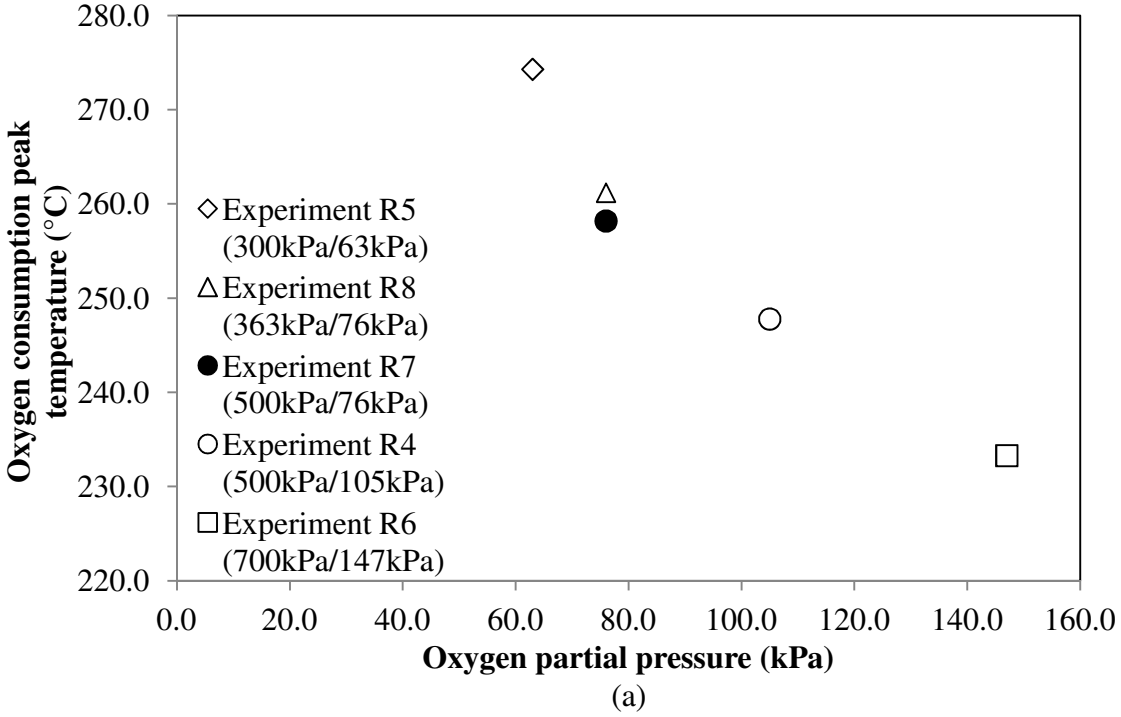

(a)

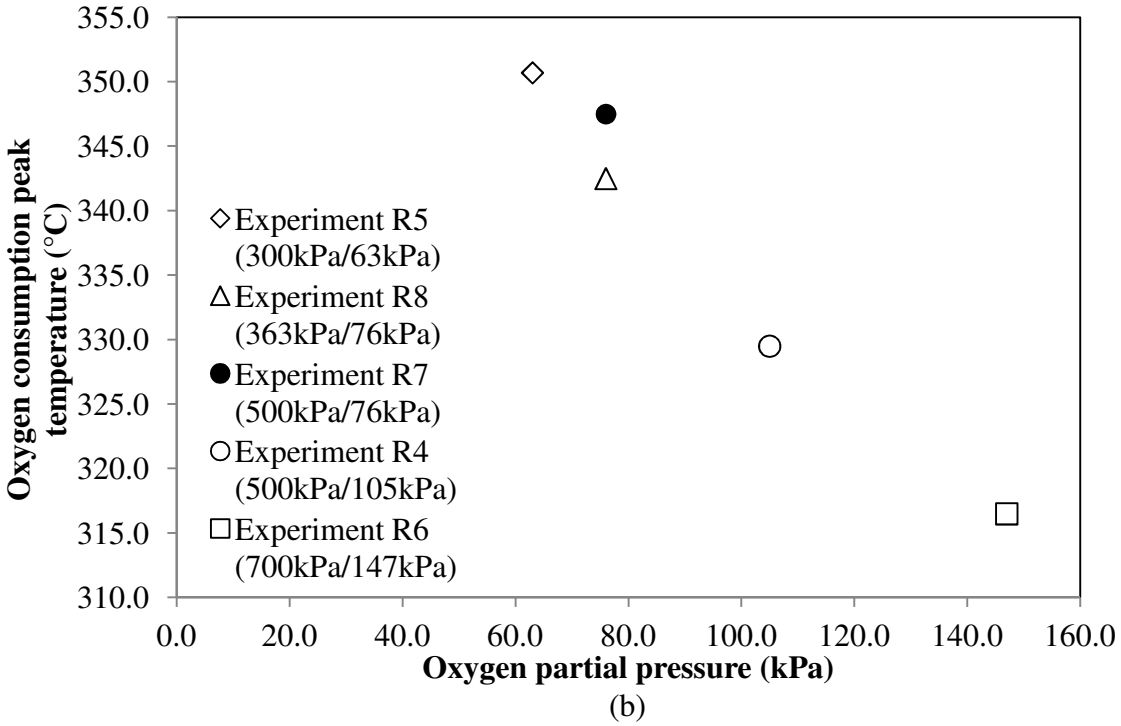

(b)

Figure 5.24 - Effect of the oxygen partial pressure on (a) the hemicellulose peak temperature (b) the cellulose peak temperature of the oxygen consumption. The pressures shown refer to the absolute total system pressure and oxygen partial pressure, respectively.

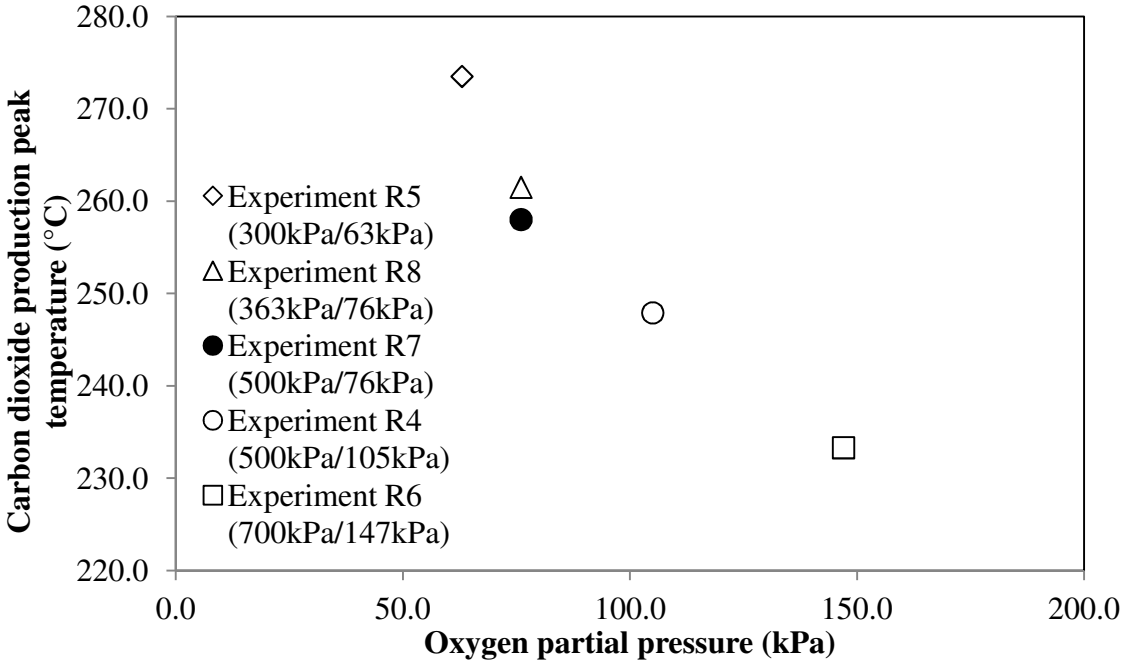

(a)

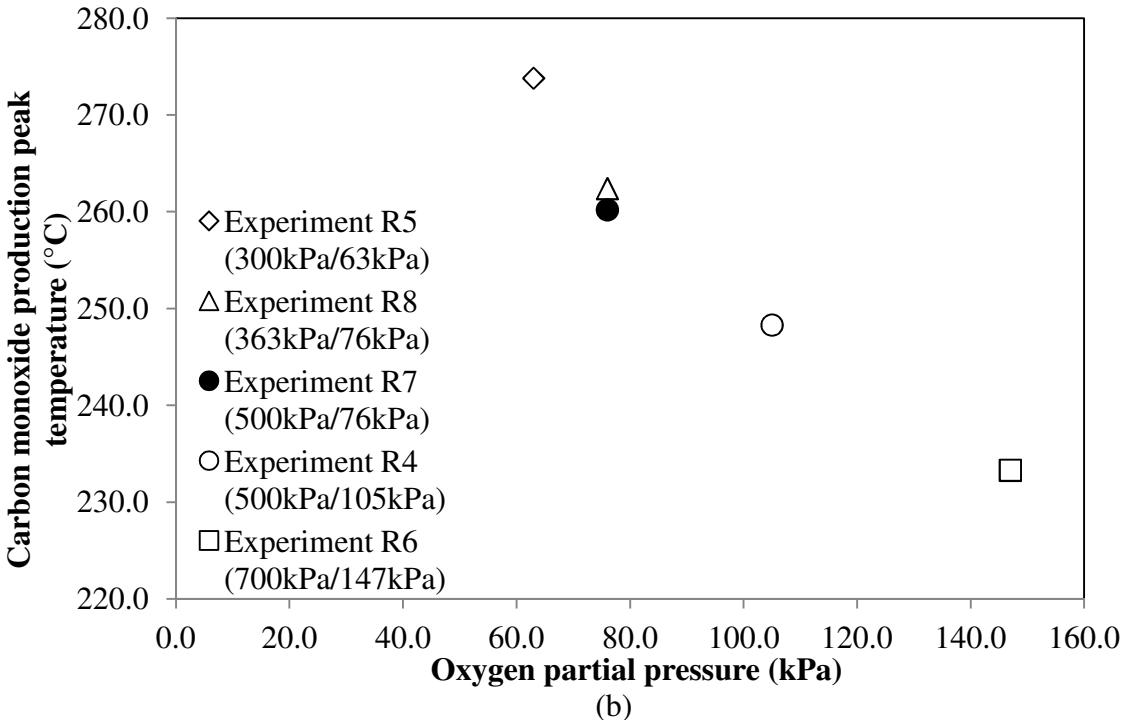

(b)

Figure 5.25 - Effect of the oxygen partial pressure on the hemicellulose peak temperatures of (a) the carbon dioxide production (b) the carbon monoxide production. The pressures shown refer to the absolute total system pressure and oxygen partial pressure, respectively.

Similarly, the reduction of the cellulose peak temperature was in the range of 15°C to 20°C for both the oxygen consumption and carbon dioxide production curves as the oxygen partial pressure increased from 76kPa to 105kPa. However, the oxygen partial pressure has no significant influence on the peak heights for the three exit gas components.

The results agree well with Bridgwater and Boocock (1997) in their rice husk decomposition study using an EGA technique. The oxidation reactions are predominantly gas phase reactions until the efflux of volatile, combustible decomposition products from the rice husk fall to a fairly low level which is after the cellulose decomposition products have been evolved. The effect of varying the oxygen partial pressure may be inferred to reflect a change in the rate of the gas phase oxidation reactions (Bridgwater and Boocock, 1997).

Table 5.4 presents the calculated kinetic parameters for a series of EGA runs conducted in order to study the effect of the total system and the oxygen partial pressures. Figures 5.26 to 5.29 present a plotted of the oxygen consumption data and the model predictions of experiments R5 to R8. From these Figures, all four experiments display a good fit having variances below 0.001. The calculated variance for experiments R5 to R8 were 0.0001, 0.0005, 0.0002 and 0.0001, respectively. Considering Table 5.4, in comparison between experiments R5 and R6 (air as the oxidising gas), the activation energy of the high temperature oxidation (HTO) reaction decreased from 19.8×10^3K to 17.2×10^3K as the total system pressure increased from 300kPa to 700kPa. The ln β for the HTO reaction was also decreased from 24.6 to 20.4 as the total system pressure increased. However, the reaction order for the HTO reaction was unaffected by the variation in pressure. A similar trend for the calculated kinetic parameters was observed for the low temperature oxidation (LTO) reaction. The activation energy of the LTO reaction decreased 72% from 18.7×10^3K to 5.2×10^3K as the total system pressure increased from 300kPa to 700kPa. The ln β of the LTO reaction was decreased by 67.5% from 22.8 to 7.4 as the pressure increased. An increment of 0.41 in the reaction order was also observed for the LTO reaction as the pressure increased from 300kPa to 700kPa.

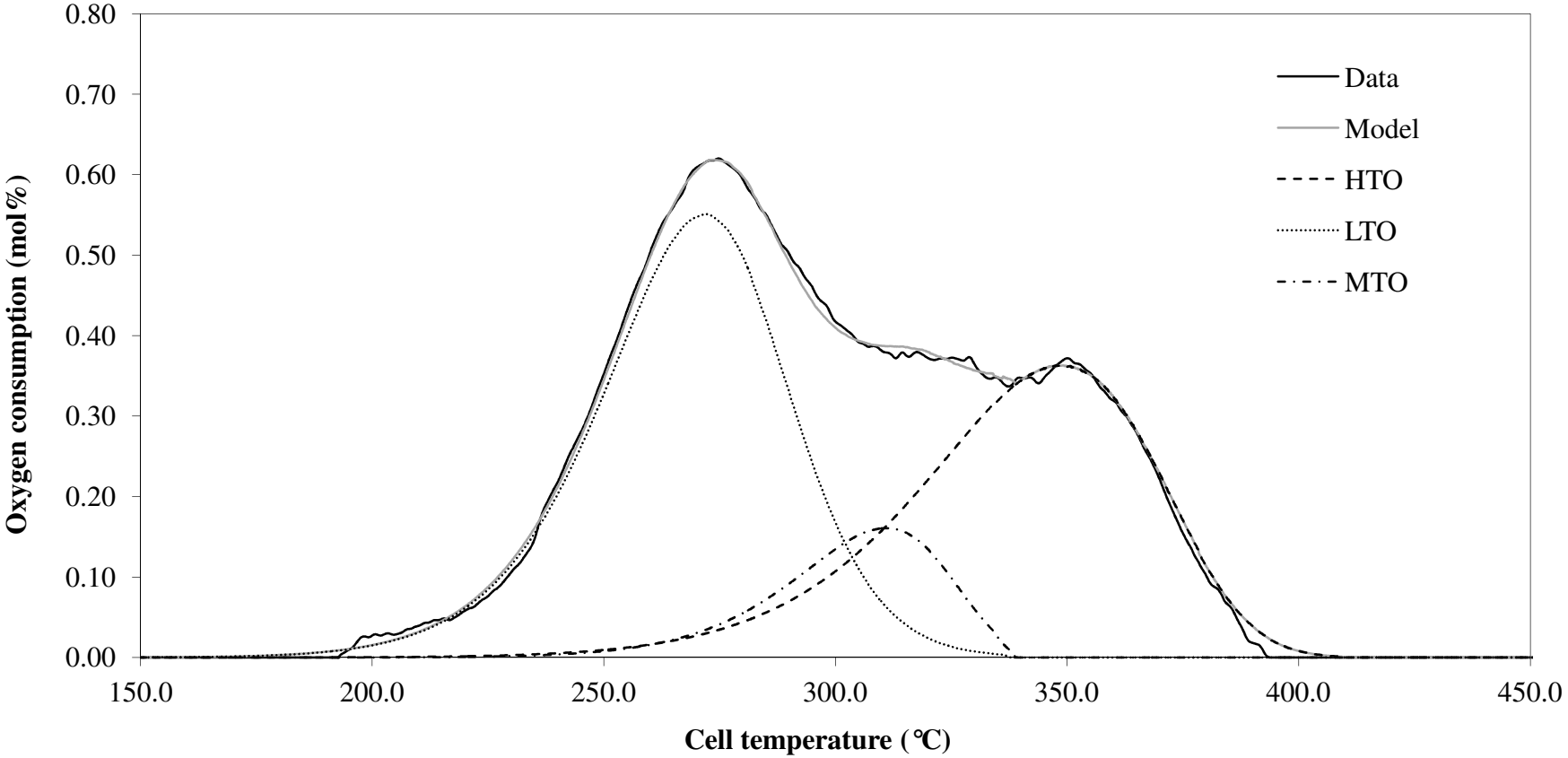

Figure 5.26 - Comparison of the oxygen consumption data and the model predictions with respects to the cell temperature for the oxidation of rice husk with air as the oxidising gas, an absolute total system pressure of 300kPa, an air flow rate of 400smL/min and a heating rate of 50°C/h (Experiment R5).

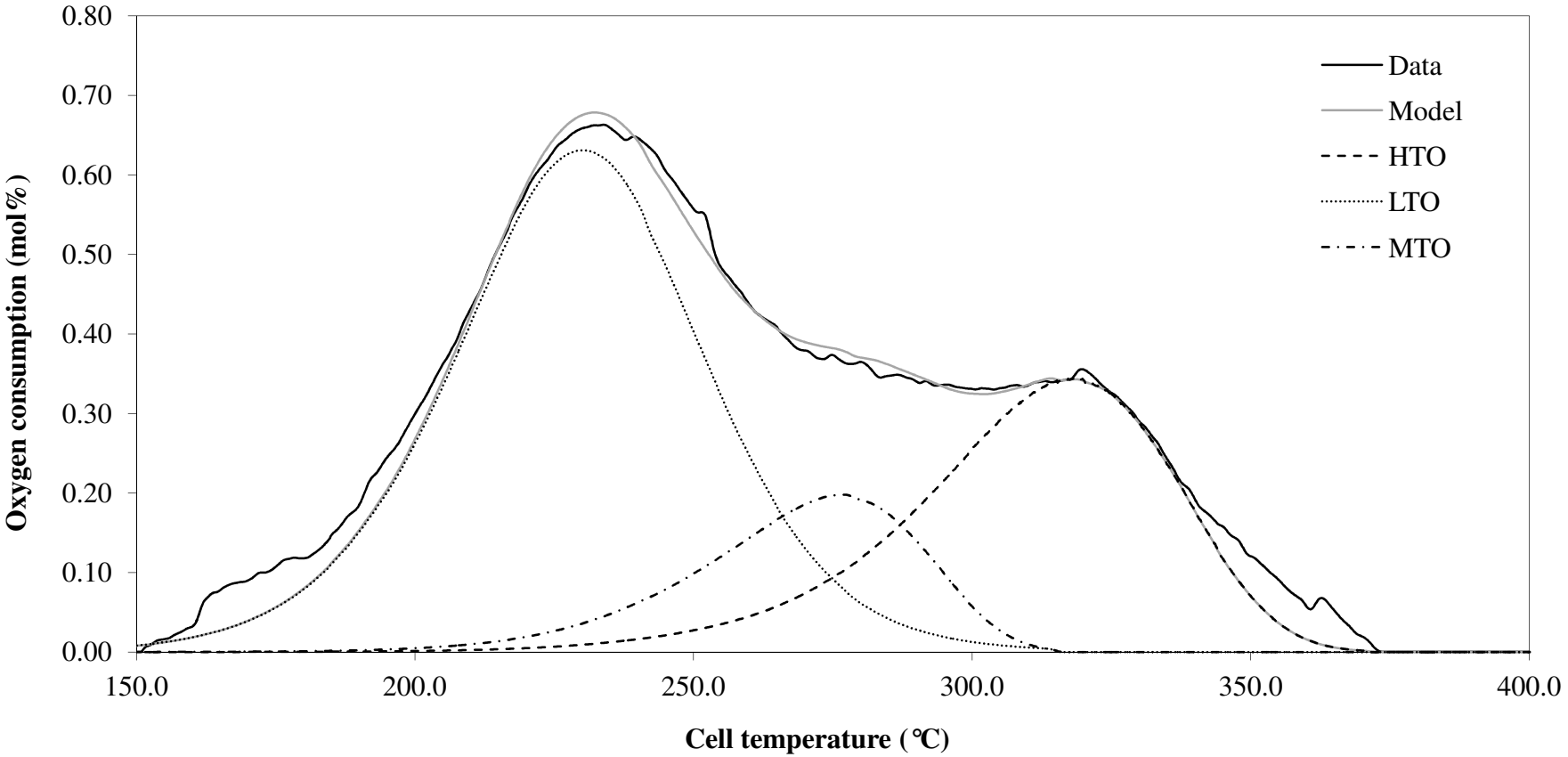

Figure 5.27 - Comparison of the oxygen consumption data and the model predictions with respects to the cell temperature for the oxidation of rice husk with air as the oxidising gas, an absolute total system pressure of 700kPa, an air flow rate of 400smL/min and a heating rate of 50°C/h (Experiment R6).

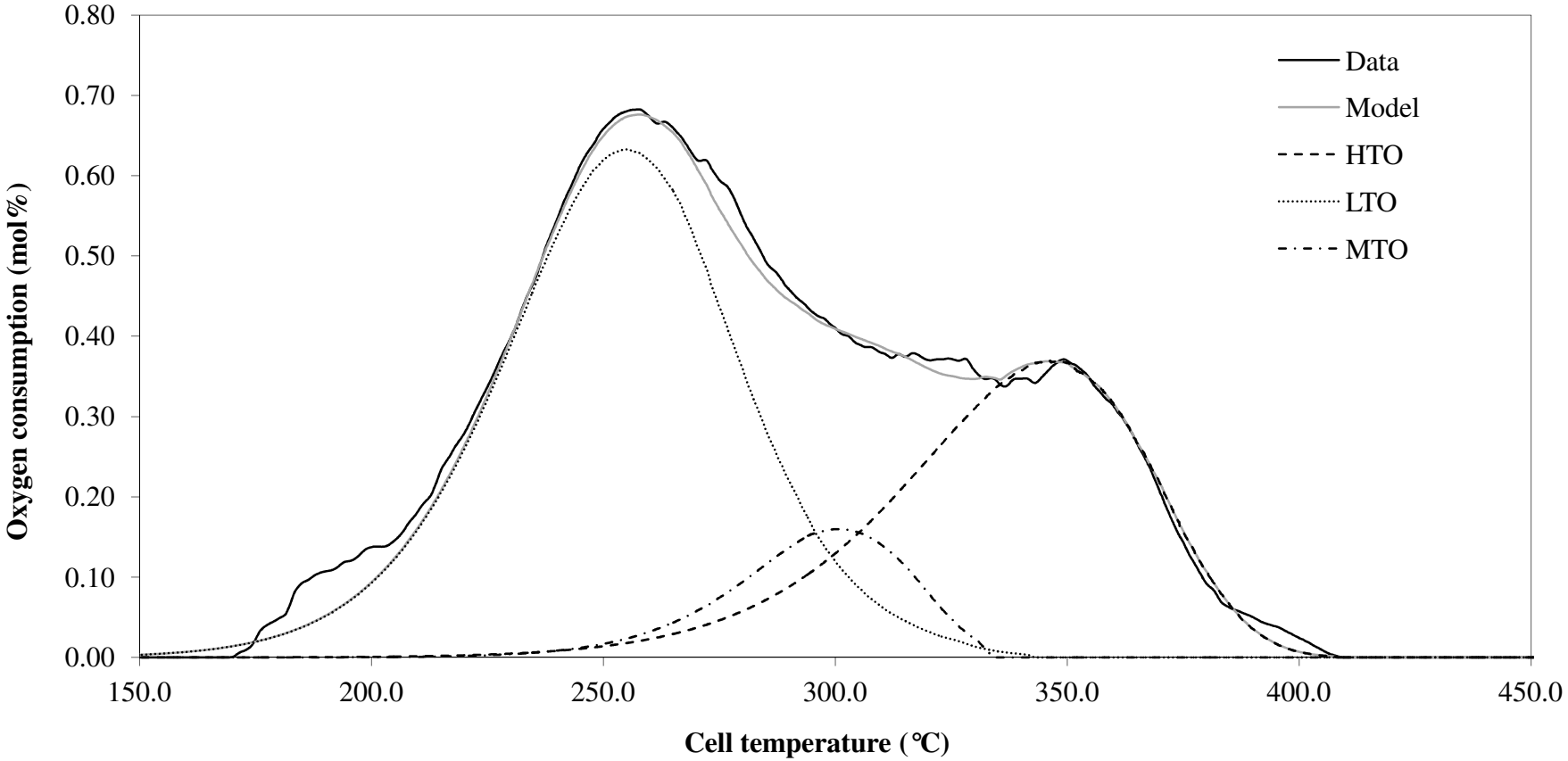

Figure 5.28 - Comparison of the oxygen consumption data and the model predictions with respects to the cell temperature for the oxidation of rice husk with 15.10 mol% oxygen concentration in feed gas (gas mixture 1), an absolute total system pressure of 500kPa, an oxygen partial pressure of 76kPa, a flow rate of 400smL/min and a heating rate of 50°C/h (Experiment R7).

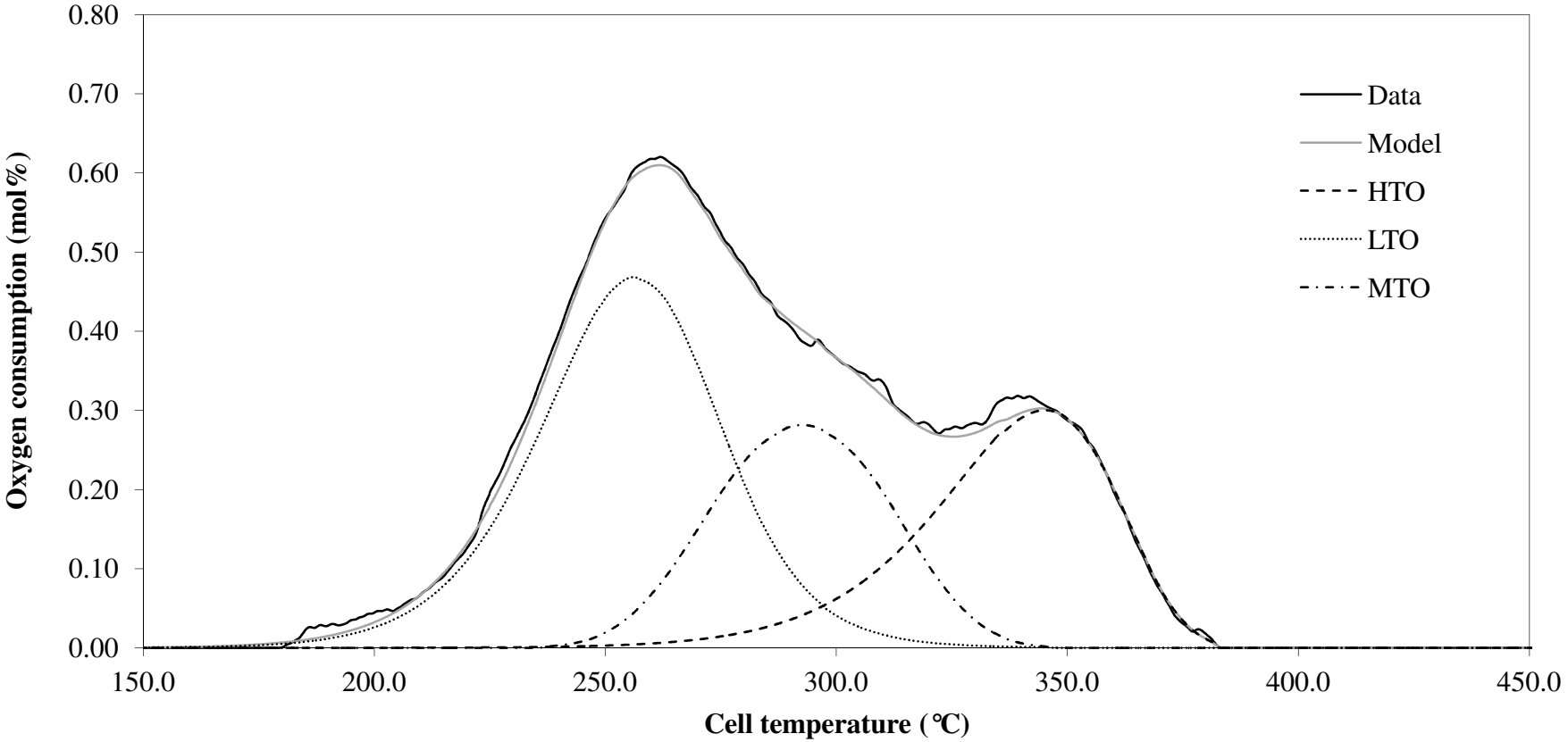

Figure 5.29 - Comparison of the oxygen consumption data and the model predictions with respects to the cell temperature for the oxidation of rice husk with air as the oxidising gas, an absolute total system pressure of 363kPa, an air flow rate of 400smL/min and a heating rate of 50°C/h (Experiment R8).

Unlike the HTO and LTO reactions, the calculated kinetic parameter values for the medium temperature oxidation (MTO) reaction display an opposing trend as the total system pressure increased from 300kPa to 700kPa. The activation energy increased from 13.7×10^3K to 20.1×10^3K as the total system pressure increased.

The value of ln β for the MTO reaction also increased from 16.9 to 26.4 as the total system pressure increased. A noticeable increment of 0.04 in the reaction order of the MTO reaction was also observed as the total system pressure increased from 300kPa to 700kPa. These results are presented in Figures 5.30 to 5.32 for the HTO, MTO and LTO reactions. In these Figures, the kinetic parameters of the activation energy (E/R) and the ln β are plotted against the total system pressure. Figures 5.33 to 5.35 present plots of the kinetic parameters of the activation energy (E/R) and the ln β with respect to the oxygen partial pressure for the HTO, MTO and LTO reactions. As seen in all the Figures 5.30 to 5.35 for the reaction regimes representing HTO, MTO and LTO, the calculated kinetic parameters of the activation energy (E/R) and the ln β for experiment R7 correspond better with that for experiment R8 (same oxygen partial pressure of 76kPa) rather than experiment R4 (same total system pressure of 500kPa). From this we infer that all the reaction regimes are influenced by the oxygen partial pressure rather than by the total system pressure. These findings are in good agreement with the experimental data discussed in the Section 5.5.1. For the rice husk combustion characteristics, the oxygen partial pressure is dominant in comparison to the total system pressure.

These findings was also consistent with the reaction model derived in Chapter 4 that assumed that the reaction rate was proportional to the oxygen partial pressure and the fuel concentration:

$$R_{r_i} = k_i P_{O_2}{}^{m_i} C_{f_i}{}^{n_i} \tag{5.2}$$

where, R_{r_i} is the reaction rate,
k_i is the reaction constant,
P_{O_2} is the oxygen partial pressure,
C_{fi} is the fuel concentration,
m_i is the reaction order with respect to oxygen partial pressure,
and, n_i is the reaction order with the respect to fuel concentration.

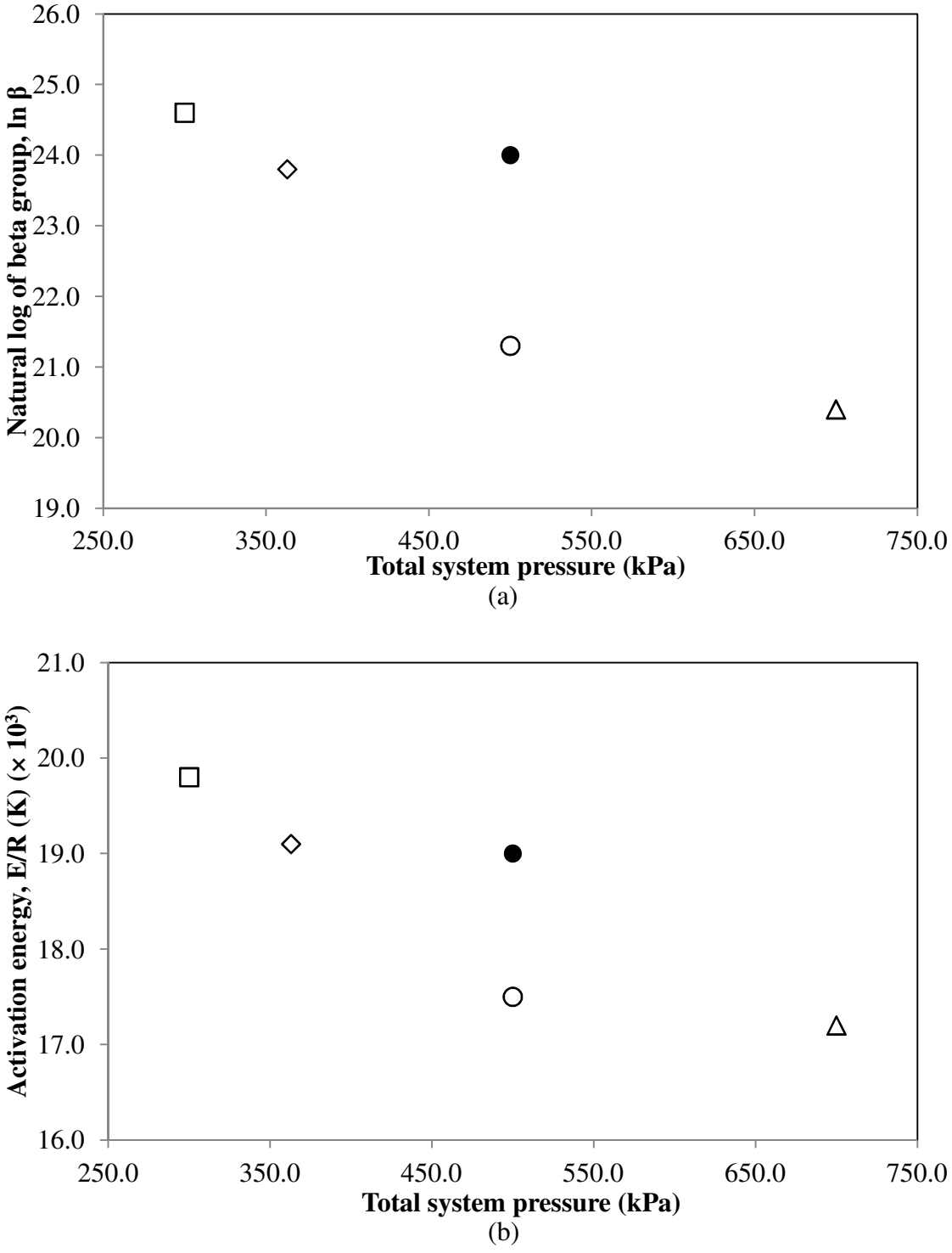

Figure 5.30 - Effect of the total system pressure on (a) the natural log of beta group, ln β (b) the activation energy, E/R for the high temperature oxidation, HTO. The pressure shown refer to the oxygen partial pressure.

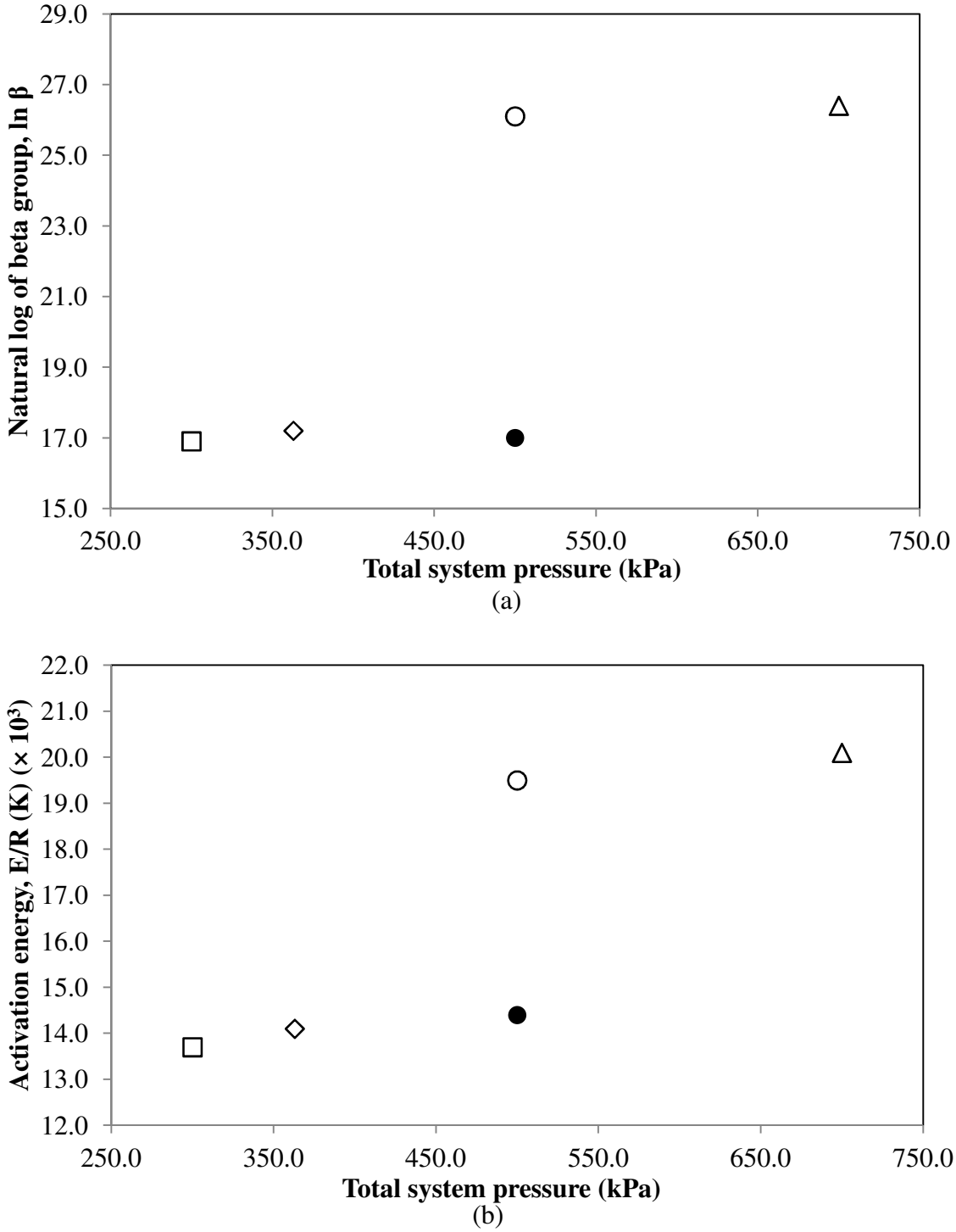

Figure 5.31 - Effect of the total system pressure on (a) the natural log of beta group, ln β (b) the activation energy, E/R for the medium temperature oxidation, MTO. The pressure shown refer to the oxygen partial pressure.

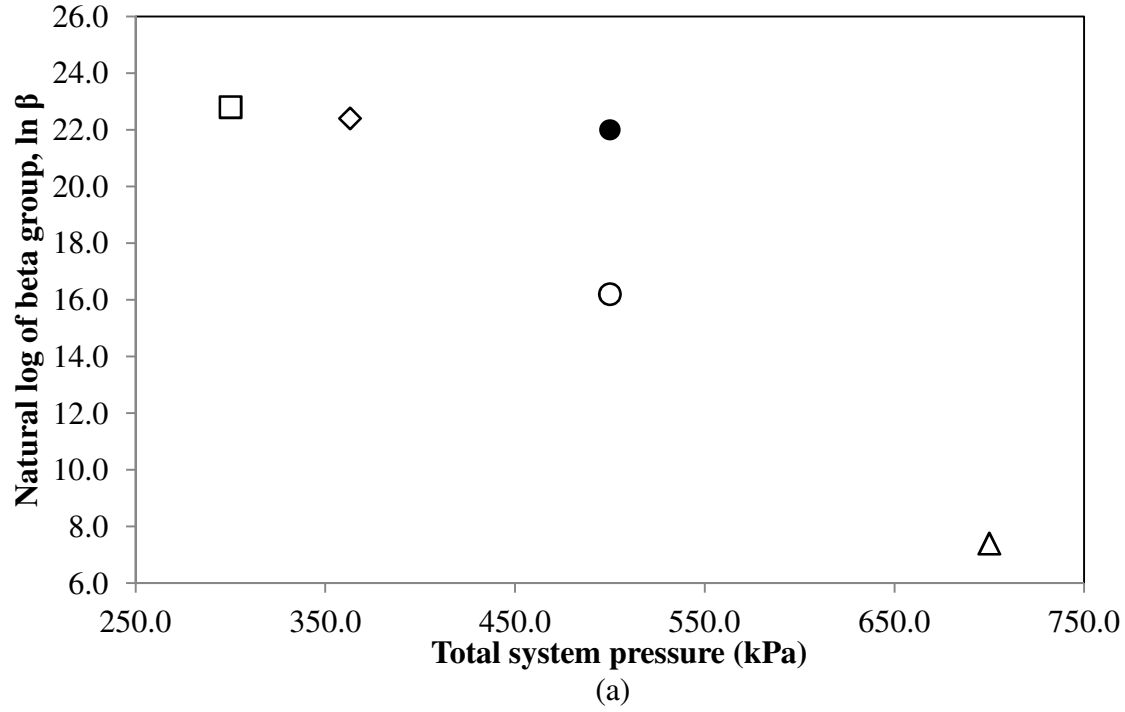

(a)

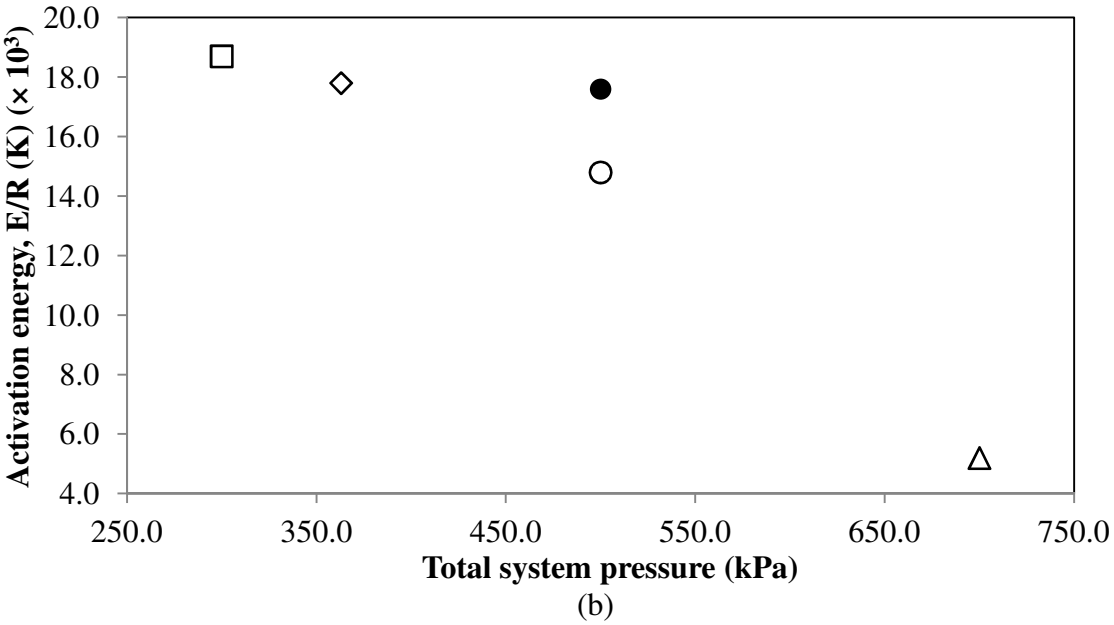

(b)

□Experiment R5 (63kPa) ◇Experiment R8 (76kPa) ●Experiment R7 (76kPa)
○Experiment R4 (105kPa) △Experiment R6 (147kPa)

Figure 5.32 - Effect of the total system pressure on (a) the natural log of beta group, ln β (b) the activation energy, E/R for the low temperature oxidation, LTO. The pressure shown refer to the oxygen partial pressure.

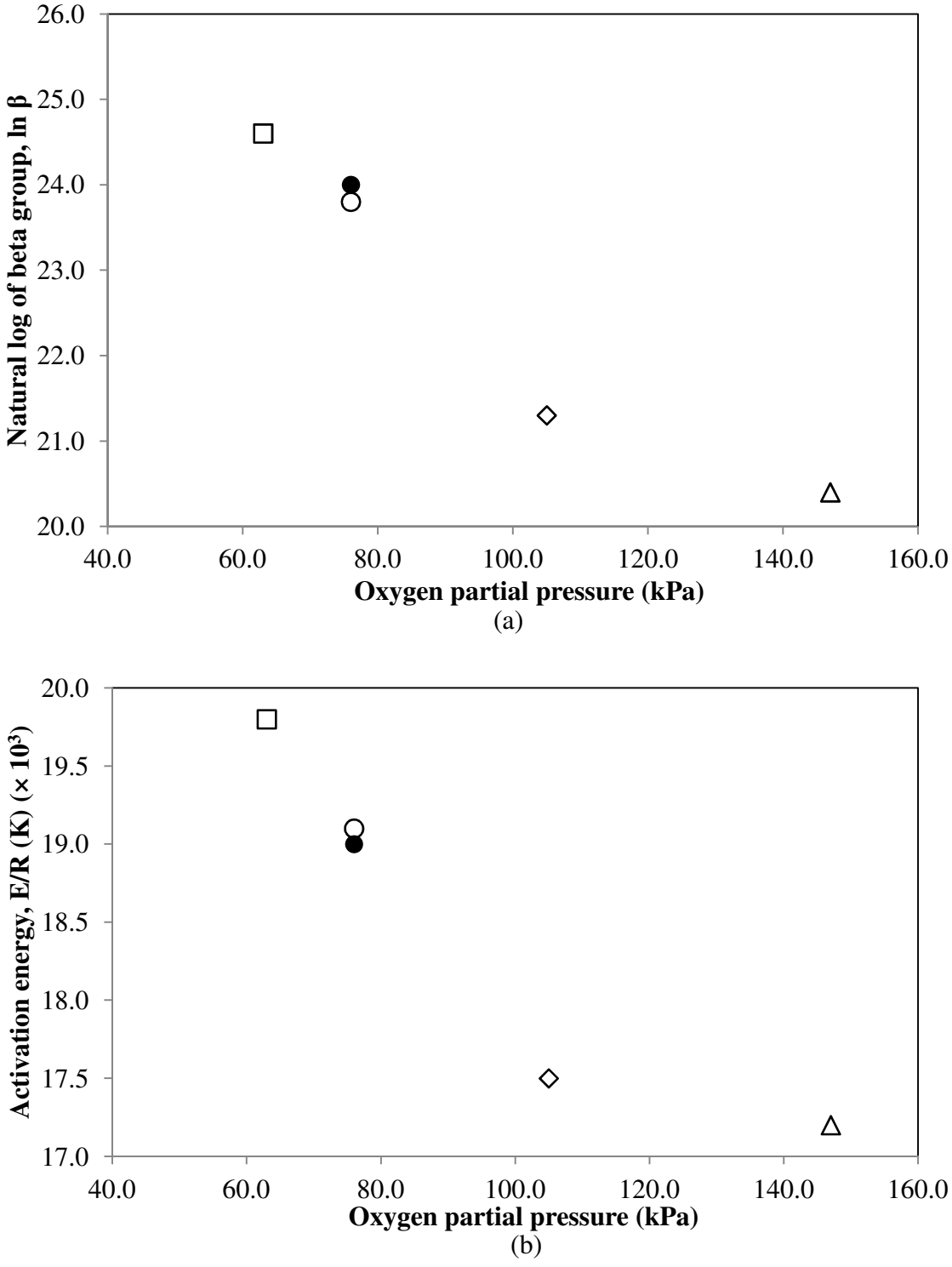

Figure 5.33 - Effect of the oxygen partial pressure on (a) the natural log of beta group, ln β (b) the activation energy, E/R for the high temperature oxidation, HTO. The pressure shown refer to the total system pressure.

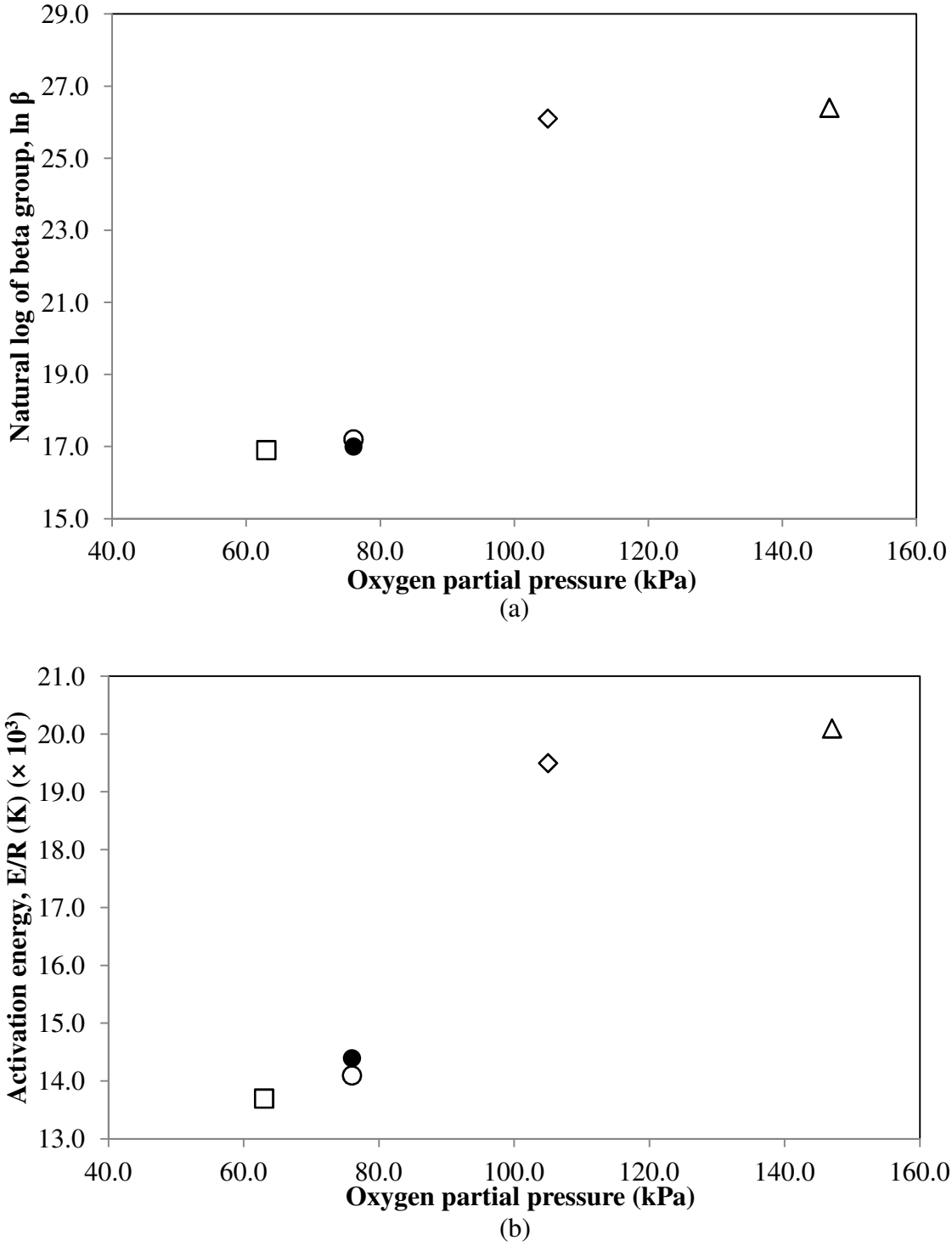

Figure 5.34 - Effect of the oxygen partial pressure on (a) the natural log of beta group, ln β (b) the activation energy, E/R for the medium temperature oxidation, MTO. The pressure shown refer to the total system pressure.

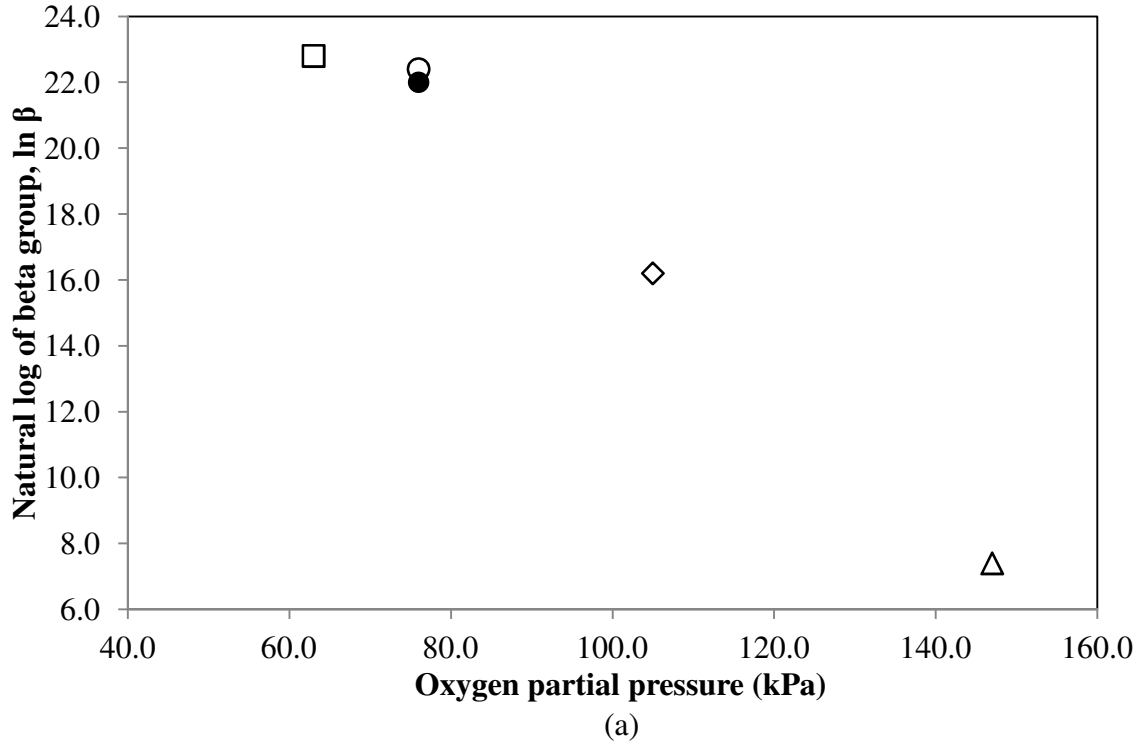

(a)

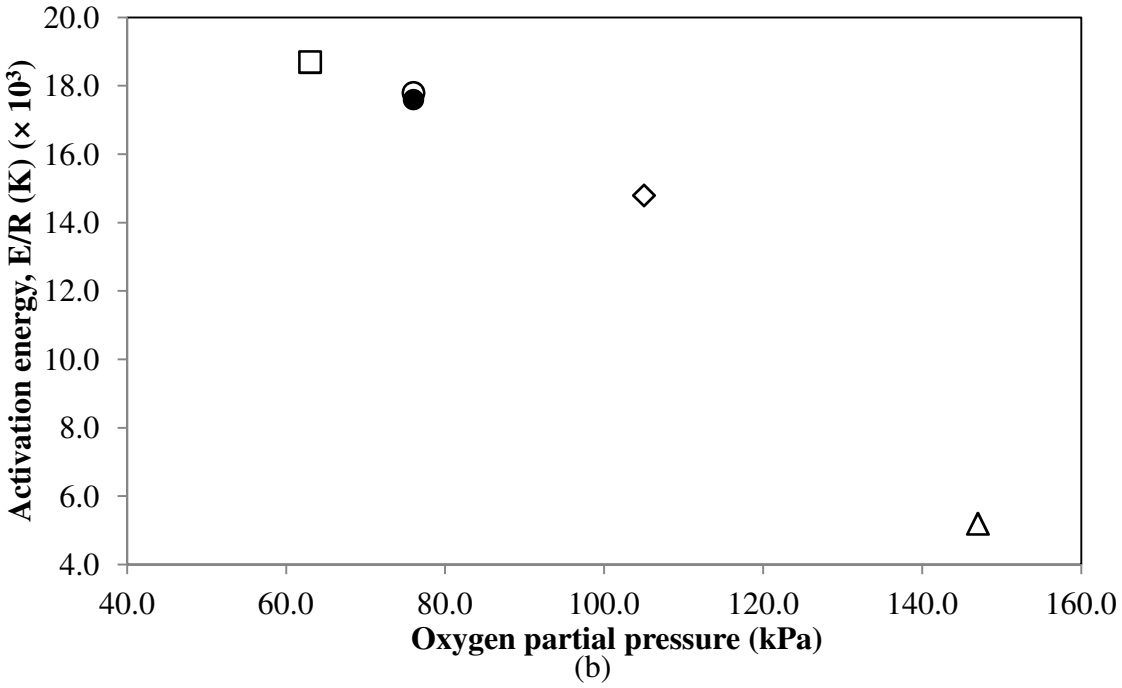

(b)

□Experiment R5 (300kPa) ○Experiment R8 (363kPa) ●Experiment R7 (500kPa)
◇Experiment R4 (500kPa) △Experiment R6 (700kPa)

Figure 5.35 - Effect of the oxygen partial pressure on (a) the natural log of beta group, ln β (b) the activation energy, E/R for the low temperature oxidation, LTO. The pressure shown refer to the total system pressure.

Even though no studies have been reported on the effect of pressure on the calculated kinetic parameters of the rice husk combustion characteristics, many authors have studied the effect of pressure on the various types of crude oil oxidations (Nguyen, 2004, Al-Saffar *et al.*, 2000, Kisler, 1995, Shallcross, 1991). Shallcross (1991) performed an EGA experiments with a heavy crude oil. They found that the natural log of beta group increased with pressure for the LTO and MTO reactions but decreased for the HTO reaction. The activation energy was not affected by pressure as Nguyen (2004) reported for the oxidation kinetics of Vietnamese crude oil. She found that the LTO reaction was controlled by the oxygen partial pressure rather than by the total system pressure while the MTO reaction was affected by the total system pressure. For the HTO reaction, an increase in the calculated kinetic parameters is observed with a rise in both the total system and the oxygen partial pressures. Hence, the HTO reaction is controlled by both pressures. Kisler (1995) reported that the LTO and MTO reactions were influenced by the oxygen partial pressure while HTO reaction was dependant on the total system pressure in his light crude oil oxidation study. Al-Saffar *et al.* (2000) found that the total system pressure influences the calculated activation energy in their crude oil oxidation study. The variation of findings are due to the different types of oil used in each of the study.

In summary, the oxygen partial pressure has a significant influence on the rice husk combustion characteristics. Increasing the oxygen partial pressure results in the peak temperatures shifting to lower temperatures for the exit gas oxygen, carbon dioxide and carbon monoxide compositions. However, the heights of these peaks appear not to be significantly affected by the total system and the oxygen partial pressures. The oxygen partial pressure of the EGA experiments using rice husk were seen to have a significant influence on the calculated kinetic parameters of the reaction regimes of the HTO, MTO and LTO. It appears that all the reaction regimes are controlled by the oxygen partial pressure rather than by the total system pressure. Overall, the calculated kinetic parameters of the activation energy (E/R) and the ln β decreased with the increasing of pressure for the HTO and LTO reactions while for the MTO reaction shows the opposing trend. A review of the literature showed that the effects of pressure are dependent on the materials used.

5.6 Analysis of error in calculating the rice husk kinetic parameters

The modeling procedure developed in Chapter 4 involves a series of calculations based on the data obtained from a series of EGA experiments. Any uncertainty in the raw experimental data will be passed on to the values calculated for the kinetic parameters. Hence, the kinetic parameters calculated from the EGA data will fall within a range of confidence limits which are dependent on the accuracy of the raw data. These confidence limits for the results may be determined by considering the contributions made by the various data points and the uncertainty associated with each data point. Each step of the calculation algorithm involves the propagation of the uncertainties in the experimental data. If a final result, R is a function of several experimental parameters (a and b), then the error in R, ΔR, due to the experimental uncertainties Δa and Δb is given by:

$$\Delta R = \frac{\partial R}{\partial a}\,\Delta a + \frac{\partial R}{\partial b}\,\Delta b \tag{5.3}$$

This relationship holds provided that the uncertainties are relatively small, i.e. $\Delta a \ll a$. Equation 5.3 may be simplified for many common mathematical operations such as for the calculation of the inverse absolute temperature from cell temperature. The inverse absolute temperature is calculated directly from the cell temperature. The uncertainties in the inverse absolute temperature are given by:

$$\delta\left(\frac{1}{T}\right) = \frac{1}{T}\left(\frac{\Delta T}{T}\right) = \frac{\Delta T}{T^2} \tag{5.4}$$

where, δ denotes the uncertainty in calculated quantities and T is temperature

The mathematical operations may be considered for calculation of the uncertainties involve the calculation of the following:

- the inverse temperature from the cell temperature;
- the oxygen consumption (ΔO_2) from the evolved gas compositions data;
- the integral of the ΔO_2 with respects to the time data;

- the relative reaction rate; and,
- the activation energy and the natural log of beta group by the linear regression which involves a series of summation terms.

The uncertainties in the experimental data were quantified and their influence followed through the entire calculation process.

The evolved gas analysis (EGA) experimental technique is subject to a number of sources of error. These include the experimental technique, the limitations of the equipment and the design of the experimental rig. Based on Kisler (1995), the major factors which have an influence on the reproducibility of the EGA experimental work and the accuracy of the calculated kinetic parameters are:

- the radial position of the combustion cell within the furnace;
- the accuracy of the gas analyser calibration and the assumption of a linear drift with time;
- the composition and the amount of the sand and biomass mixture initially packed into the cell and the homogeneity of the mixture;
- the accuracy of the cell thermocouple and the gas analysers;
- the residence time of the combustion cell;
- the short term fluctuations in the injection gas flow rate and the operating pressure;
- the assumption that no hydrocarbons, hydrogen or water vapour passes through the gas analysers; and,
- the mixing of the combustion gases before they reach the gas analysers, i.e. so that analysed gas is actually a mixture corresponding to a range of temperatures.

Table 5.5 presents the uncertainty in the calculated kinetic parameter values of the rice husk combustion characteristics for the peak temperature of the high temperature oxidation (HTO) reaction. The absolute error was obtained by considering the change in the variable between each data reading of 10 seconds intervals.

Table 5.5 - Uncertainty in the calculated values for the rice husk EGA experiments. The relative error is refer to the peak temperature of the high temperature oxidation (HTO) reactions.

Variable	Absolute error	Relative error (%)							
		R1	**R2**	**R3**	**R4**	**R5**	**R6**	**R7**	**R8**
ΔO_2 (mol%)	0.004	0.95	0.95	0.89	0.95	1.08	1.14	1.08	1.25
Inverse temperature (K^{-1})	0.000001	0.04	0.04	0.04	0.03	0.04	0.03	0.04	0.03
Integral (ΔO_2 vs t)	6	0.18	0.19	0.19	0.11	0.15	0.13	0.12	0.15
Ln (RRR)	0.009	0.12	0.12	0.12	0.11	0.11	0.11	0.11	0.11
E_i/R	700	4.00	4.05	4.05	4.00	3.54	4.07	3.68	3.67
$\ln \beta_i$	1.3	6.44	6.57	6.57	6.10	5.29	6.37	5.42	5.46

The level of uncertainty in the activation energy is in the range of 3.5% to 4.1% for all the rice husk oxidation reactions. The error in the calculated ln β for all the rice husk EGA experiments are in the range of 5.3% to 6.6%. Hence, the level of uncertainty in the activation energy is about ±4.1% while the error for the ln β is approximately ±6.6% for all the rice husk experiments.

The kinetic parameters for a typical experiment R4 were calculated to be an activation energy of 17.5×10^3K and a ln β value of 21.3. Allowing for the calculated uncertainty, this yields activation energies of between 16.8×10^3K and 18.2×10^3K. The natural log of beta group, ln β ranges from 19.9 to 22.7. Most of the calculated kinetic parameters for rice husk oxidation fall under these ranges. Shallcross (1991) calculated the activation energy (E/R) and natural log of beta group (ln β) of between 6×10^3K to 18×10^3K and 6 to 19, respectively for their work on heavy crude oil. Kisler (1995) reported the calculated kinetic parameters of 12×10^3K to 14×10^3K for the activation energy and 10.3 to 12.9 for the natural log of beta group, ln β in the work of light crude oil. From this review of the literature it may be concluded that the value of activation energy and the natural log of beta group for the rice husk were comparatively similar with the crude oil especially for the heavy crude oil.

5.7 Concluding remarks

A series of evolved gas analysis (EGA) experiments involving the combustion characteristics of dried rice husk was conducted. The heating rate used had a significant influence on the peak temperatures and heights for the exit gas oxygen, carbon dioxide and carbon monoxide compositions. As the heating rate increases, the peaks of the exit gas composition curves shift to higher temperatures. The peak heights increase as the heating rate increases. A slower heating rate may ensure the entire cell is always at a uniform temperature by avoiding the exothermic reactions in the combustion cell. As a result, heating rate of 50°C/h is settled on for the remaining experiments. The series of rice husk EGA experiments conducted at the various total system pressures and oxygen partial pressures show that the total system pressure has no effect on the exit gas composition curves other than through the oxygen partial pressure. As the oxygen

partial pressure increases, the peak temperatures of the exit gas composition curves shift to lower temperatures. The heights of these peaks appear not to be significantly affected by either the total system and the oxygen partial pressures.

The model of the three oxidation regimes developed in Chapter 4 that was previously applied to the crude oil was improved for the application of the rice husk. The predictions of the reaction model is compared with the oxygen consumption data from the rice husk experimental runs and found to be able to model the oxygen consumption of the experimental data.

The calculated kinetic parameters from the model are also highly reproducible. The effect of the furnace heating rate on the calculated kinetic parameters is also investigated. The results show that the values of the calculated kinetic parameters from the experiments are independent of the heating rate used. The three reaction regimes of HTO, MTO and LTO are found to be significantly affected by the oxygen partial pressure of the feed gas. It is found that it is this oxygen partial pressure rather than the total system pressure that affected the reactions. Overall, the calculated kinetic parameters of the activation energy (E/R) and the natural log of beta group (ln β) decrease with increasing pressure for the HTO and LTO reactions. However, the MTO reaction shows the opposing trend. The calculated parameters increase with increasing pressure for the MTO reaction.

The level of uncertainty for the rice husk experiments are calculated for the kinetic parameters of the activation energy (E/R) and the natural log of beta group (ln β) and are found to be ±4.1% and ±6.6%, respectively. This yields the activation energies of between 16.8×10^3K and 18.2×10^3K. The natural log of beta group ranges from 19.9 to 22.7. The calculated kinetic parameter values of the activation energy and the ln β are comparable with the values obtained for heavy crude oil. The best conditions obtained for the rice husk combustion characteristics are at the absolute total system pressure of 700kPa, an oxygen partial pressure of 147kPa, a heating rate of 50°C/h and a flow rate of 400smL/min. At this condition, the activation energy is at the lowest within the range of 16.2×10^3K to 17.9×10^3K. Further, at this best condition, the peak temperature is

recorded at the lowest. Hence, the carbon conversion efficiency at this best condition must be at the highest in the scope of the study using the present EGA rig.

The results of the rice husk combustion characteristics using the EGA apparatus will provide a basis for comparison to the palm fibre and palm fibre char. The study will now move to consider the combustion of palm fiber and palm fibre char.

CHAPTER 6

PALM FIBRE OXIDATION

6.1 Introduction

A series of evolved gas analysis (EGA) experiments was conducted using palm fibre as the biofuel. The experimental results presented in this Chapter 6 examine the reproducibility of the palm fibre experimental technique. The effect of the heating rate and the effect of the total system and the oxygen partial pressures are also observed. The experimental EGA data are decoupled into their constituent oxidation reactions. Values for the kinetic parameters including the reaction order (n), the activation energy (E/R), and the natural log of beta group (ln β) are calculated for each of the three reaction regimes, namely, high temperature oxidation (HTO), low temperature oxidation (LTO) and medium temperature oxidation (MTO).

Typical samples of palm fibre are relatively heterogeneous as may be seen in Figure 3.9 in Chapter 3. It was concluded that it was necessary to segregate the samples and observe the combustion characteristics of each of the different types of fibre samples. From the segregation process, it was concluded that there are three sample types of the palm fibre. They are loose fibre, clump fibre and kernel. The photographs of these samples are presented in Figures 3.10 to 3.12. The proportions of loose fibre, clump fibre and kernel that expected to present in palm fibre sample are 60:30:10, respectively. Section 6.2 discusses the typical EGA experimental results for the three types of palm fibre samples.

Next, a discussion of the calculated kinetic parameters of each of these sample types is presented. Section 6.3 considers the reproducibility of the experimental procedure applies to the palm fibre. Section 6.4 determines the influence of the heating rates on the experimental results and the calculated kinetic parameters of the palm fibre. Section 6.5 and 6.6 examine the influence of the total system and the oxygen partial pressures on the experimental results and the calculated kinetic parameters. Section 6.7 discusses the effect of pressure on the experimental results and the calculated kinetic parameters of the clump fibre, respectively. Next, Section 6.8 examines the influence of particle size on the experimental results and the calculated kinetic parameters. Section 6.9 discusses the analysis of error in calculating the kinetic parameters for the palm fibre experiments. Finally, Section 6.10 presents the conclusion that may be drawn from the palm fibre oxidation reactions study using the EGA technique.

6.2 Typical palm fibre types experimental and kinetic parameter results

A total of twenty-one EGA experiments were conducted using the palm fibre. Table 6.1 presents a summary of the experimental conditions for the palm fibre. Table 6.2 shows the results of the ultimate and proximate analyses of the three types of the palm fibre. As observed in Table 6.2 the values of the proximate analysis and the ultimate analysis were comparatively similar for the loose fibre and the clump fibre. However slight differences are observed for the kernel especially for the ultimate analysis values. The calorific value for the kernel was significantly lower than for both the loose and clump fibres.

A series of an EGA experiments was conducted using the palm fibre. Experiments F1, F3 and F6 were selected as representing typical runs for the clump fibre, the kernel and the loose fibre, respectively. These experiments were conducted using air as the oxidising gas, an absolute total system pressure of 500kPa, a heating rate of 50°C/h and an air flow rate of 400smL/min. Table 6.3 shows the summary of the evolved gas analysis (EGA) experimental results of the palm fibre. Figures 6.1 to 6.3 present typical clump fibre, kernel and loose fibre EGA results of experiments F1, F3 and F6, respectively.

Table 6.1 - Experimental conditions for the palm fibre experiments. M1 is gas mixture 1 that consists of 15.10 mol% O_2, 2.01 mol% CO_2, 0.983 mol% CO and balance nitrogen. M2 is gas mixture 2 that contains of 18.10 mol% O_2, 4.99 mol% CO_2, 2.51 mol% CO and balance nitrogen.

Experiment	**F1**	**F2**	**F3**	**F4**	**F5**	**F6**	**F7**	**F8**	**F9**
Sample type	Clump fibre	Clump fibre	Kernel	Loose fibre	Loose fibre	Loose fibre	Loose fibre	Loose fibre	Loose fibre
Absolute total system pressure (kPa)	500	500	500	500	500	500	500	500	700
Oxygen partial pressure (kPa)	105	105	105	105	105	105	105	105	147
Injection gas (mol% Oxygen)	20.96 (Air)	20.96 (Air)	20.96 (Air)	20.96 (Air)	20.96 (Air)	20.96 (Air)	20.96 (Air)	20.96 (Air)	20.96 (Air)
Injection flow rate (smL/min)	400	400	400	400	400	400	400	400	400
Heating rate (°C/h)	50	50	50	50	50	50	70	30	50

Table 6.1 (continued) - Experimental conditions for the palm fibre experiments. M1 is gas mixture 1 that consists of 15.10 mol% O_2, 2.01 mol% CO_2, 0.983 mol% CO and balance nitrogen. M2 is gas mixture 2 that contains of 18.10 mol% O_2, 4.99 mol% CO_2, 2.51 mol% CO and balance nitrogen.

Experiment	**F10**	**F11**	**F12**	**F13**	**F14**	**F15**	**F16**	**F17**	**F18**
Sample type	Loose fibre	Loose fibre	Loose fibre	Loose fibre	Loose fibre	Loose fibre	Loose fibre	Loose fibre	Loose fibre
Absolute total system pressure (kPa)	232	500	200	278	700	700	200	200	420
Oxygen partial pressure (kPa)	42	76	42	42	106	127	30	36	76
Injection gas (mol% Oxygen)	18.10 (M2)	15.10 (M1)	20.96 (Air)	15.10 (M1)	15.10 (M1)	18.10 (M2)	15.10 (M1)	18.10 (M2)	18.10 (M2)
Injection flow rate (smL/min)	400	400	400	400	400	400	400	400	400
Heating rate (°C/h)	50	50	50	50	50	50	50	50	50

Table 6.1 (continued) - Experimental conditions for the palm fibre experiments. M1 is gas mixture 1 that consists of 15.10 mol% O_2, 2.01 mol% CO_2, 0.983 mol% CO and balance nitrogen. M2 is gas mixture 2 that contains of 18.10 mol% O_2, 4.99 mol% CO_2, 2.51 mol% CO and balance nitrogen.

Experiment	**F19**	**F20**	**F21**	**F22**
Sample type	Loose fibre	Clump fibre	Clump fibre	Loose fibre (ground)
Absolute total system pressure (kPa)	362	700	362	500
Oxygen partial pressure (kPa)	76	147	76	105
Injection gas (mol% Oxygen)	20.96 (Air)	20.96 (Air)	20.96 (Air)	20.96 (Air)
Injection flow rate (smL/min)	400	400	400	400
Heating rate (°C/h)	50	50	50	50

Table 6.2 - Ultimate and proximate analyses of various types of palm fibre. Note that db is dry basis and daf is dry ash free.

Analyses	Palm fibre (loose fibre)	Palm fibre (clump fibre)	Palm fibre (kernel)
Proximate analysis (db) (wt.%)			
Volatile matter	68.8	68.6	69.2
Fixed carbon	15.2	15.4	16.0
Ash	10.2	10.1	10.5
Ultimate analysis (daf) (wt.%)			
Carbon	43.19	42.85	41.33
Hydrogen	5.24	5.33	4.57
Nitrogen	1.59	1.59	0.99
Sulphur	0.19	0.21	0.09
Oxygen	49.79	50.02	53.02
Calorific value (MJ/kg)	19.00	18.82	16.30

In these figures, the oxygen consumption curve is plotted with the actual carbon monoxide production and the carbon dioxide production curves with respect to the cell temperature. As observed in Figures 6.1 and 6.3, the figures were all in the same form having two main peaks in the regions of 260°C to 280°C and 340°C to 380°C. The first peak temperature for the clump fibre sample (Experiment F1) was recorded at an average temperature of 267.6°C ± 0.5°C for all the three curves.

The second peak temperature of the clump fibre sample for the oxygen consumption and the carbon dioxide production curves was at the average of 357.1°C ± 0.1°C. However, the second peak temperature for the clump fibre samples of the carbon monoxide production curve was 352.1°C, 5°C lower than the both oxygen consumption and carbon dioxide production curves. The first peak temperature for the loose fibre sample (Experiment F6) for all the exit gas composition curves was at an average temperature of 265.2°C ± 0.8°C and the second peak temperature was at average of 355.4°C ± 0.2°C.

Table 6.3 - Summary of the evolved gas analysis (EGA) experimental results of the palm fibre. The $\Delta O_{2,\,max}$, $\Delta CO_{2,\,max}$ and $\Delta CO_{,\,max}$ (in mol%) is the peak height and the T (in °C) is cell temperature at which the peak occurs. M1 is gas mixture 1 that consists of 15.10 mol% O_2, 2.01 mol% CO_2, 0.983 mol% CO and balance nitrogen. M2 is gas mixture 2 that contains of 18.10 mol% O_2, 4.99 mol% CO_2, 2.51 mol% CO and balance nitrogen.

Experiment		**F1**	**F2**	**F3**	**F4**	**F5**	**F6**	**F7**	**F8**	**F9**
Sample type		Clump fibre	Clump fibre	Kernel	Loose fibre	Loose fibre	Loose fibre	Loose fibre	Loose fibre	Loose fibre
Absolute total system pressure (kPa)		500	500	500	500	500	500	500	500	700
Oxygen partial pressure (kPa)		105	105	105	105	105	105	105	105	147
Oxygen concentration in feed gas (mol%)		20.96 (Air)	20.96 (Air)	20.96 (Air)	20.96 (Air)	20.96 (Air)	20.96 (Air)	20.96 (Air)	20.96 (Air)	20.96 (Air)
Heating rate (°C/h)		50	50	50	50	50	50	70	30	50
Oxygen consumption peaks										
First peak	$\Delta O_{2,\,max}$ (mol%)	0.55	0.54	0.41	0.53	0.53	0.53	0.74	0.38	0.74
	T (°C)	267.4	267.1	267.4	267.8	265.2	265.0	279.2	251.3	253.6
Second peak	$\Delta O_{2,\,max}$ (mol%)	0.51	0.51	0.88	0.46	0.47	0.47	0.57	0.31	0.55
	T (°C)	357.1	359.9	372.7	353.0	356.0	355.6	375.4	342.5	344.8
Carbon dioxide production peaks										
First peak	$\Delta CO_{2,\,max}$ (mol%)	0.29	0.29	0.13	0.30	0.31	0.30	0.36	0.20	0.53
	T (°C)	268.1	267.8	268.5	265.1	265.6	266.0	280.4	251.4	254.7
Second peak	$\Delta CO_{2,\,max}$ (mol%)	0.39	0.39	0.71	0.30	0.29	0.30	0.36	0.22	0.44
	T (°C)	357.0	359.6	372.9	352.8	357.5	355.3	373.2	342.8	345.7
Carbon monoxide production peaks										
First peak	$\Delta CO_{,\,max}$ (mol%)	0.13	0.13	0.11	0.13	0.13	0.13	0.17	0.09	0.22
	T (°C)	267.3	267.6	268.8	264.3	264.3	264.5	279.6	250.7	254.6
Second peak	$\Delta CO_{,\,max}$ (mol%)	0.06	0.07	0.14	0.06	0.05	0.06	0.09	0.04	0.13
	T (°C)	352.1	352.6	371.8	350.9	355.7	355.3	372.7	341.8	346.1

Table 6.3 (continued) - Summary of the evolved gas analysis (EGA) experimental results of the palm fibre. The $\Delta O_{2,\,max}$, $\Delta CO_{2,\,max}$ and $\Delta CO_{,\,max}$ (in mol%) is the peak height and the T (in °C) is cell temperature at which the peak occurs. M1 is gas mixture 1 that consists of 15.10 mol% O_2, 2.01 mol% CO_2, 0.983 mol% CO and balance nitrogen. M2 is gas mixture 2 that contains of 18.10 mol% O_2, 4.99 mol% CO_2, 2.51 mol% CO and balance nitrogen.

Experiment		**F10**	**F11**	**F12**	**F13**	**F14**	**F15**	**F16**	**F17**	**F18**
Sample type		Loose fibre	Loose fibre	Loose fibre	Loose fibre	Loose fibre	Loose fibre	Loose fibre	Loose fibre	Loose fibre
Absolute total system pressure (kPa)		232	500	200	278	700	700	200	200	420
Oxygen partial pressure (kPa)		42	76	42	42	106	127	30	36	76
Oxygen concentration in feed gas (mol%)		18.10 (M2)	15.10 (M1)	20.96 (Air)	15.10 (M1)	15.10 (M1)	18.10 (M2)	15.10 (M1)	18.10 (M2)	18.10 (M2)
Heating rate (°C/h)		50	50	50	50	50	50	50	50	50
Oxygen consumption peaks										
First peak	$\Delta O_{2,\,max}$ (mol%)	0.38	0.59	0.29	0.37	0.70	0.67	0.33	0.33	0.55
	T (°C)	289.0	277.1	288.1	290.3	276.7	267.0	331.7	322.5	273.0
Second peak	$\Delta O_{2,\,max}$ (mol%)	0.31	0.58	0.30	0.34	0.50	0.56	0.32	0.31	0.51
	T (°C)	381.8	366.7	385.4	387.5	369.3	359.1	419.4	418.3	365.9
Carbon dioxide production peaks										
First peak	$\Delta CO_{2,\,max}$ (mol%)	0.20	0.26	0.12	0.20	0.46	0.46	0.12	0.11	0.25
	T (°C)	290.6	277.7	294.3	291.2	278.2	267.9	332.0	331.5	275.0
Second peak	$\Delta CO_{2,\,max}$ (mol%)	0.22	0.38	0.22	0.22	0.45	0.45	0.26	0.26	0.37
	T (°C)	381.2	365.4	385.1	388.7	369.4	359.6	418.5	417.6	364.2
Carbon monoxide production peaks										
First peak	$\Delta CO_{,\,max}$ (mol%)	0.09	0.11	0.08	0.08	0.20	0.21	0.06	0.06	0.11
	T (°C)	289.6	278.0	288.8	290.0	278.9	267.3	333.9	332.2	274.5
Second peak	$\Delta CO_{,\,max}$ (mol%)	0.04	0.09	0.03	0.03	0.11	0.14	0.05	0.05	0.10
	T (°C)	381.0	366.8	381.7	387.7	369.3	360.1	420.0	417.6	366.0

Table 6.3 (continued) - Summary of the evolved gas analysis (EGA) experimental results of the palm fibre. The $\Delta O_{2,\,max}$, $\Delta CO_{2,\,max}$ and $\Delta CO_{,\,max}$ (in mol%) is the peak height and the T (in °C) is cell temperature at which the peak occurs. M1 is gas mixture 1 that consists of 15.10 mol% O_2, 2.01 mol% CO_2, 0.983 mol% CO and balance nitrogen. M2 is gas mixture 2 that contains of 18.10 mol% O_2, 4.99 mol% CO_2, 2.51 mol% CO and balance nitrogen.

Experiment		**F19**	**F20**	**F21**	**F22**
Sample type		Loose fibre	Clump fibre	Clump fibre	Loose fibre (ground)
Absolute total system pressure (kPa)		362	700	362	500
Oxygen partial pressure (kPa)		76	147	76	105
Oxygen concentration in feed gas (mol%)		20.96 (Air)	20.96 (Air)	20.96 (Air)	20.96 (Air)
Heating rate (°C/h)		50	50	50	50
Oxygen consumption peaks					
First peak	$\Delta O_{2,\,max}$ (mol%)	0.44	0.73	0.40	0.55
	T (°C)	276.0	252.3	274.8	263.0
Second peak	$\Delta O_{2,\,max}$ (mol%)	0.47	0.55	0.43	0.47
	T (°C)	366.9	343.5	367.7	356.0
Carbon dioxide production peaks					
First peak	$\Delta CO_{2,\,max}$ (mol%)	0.23	0.52	0.19	0.30
	T (°C)	275.0	254.2	274.1	263.2
Second peak	$\Delta CO_{2,\,max}$ (mol%)	0.40	0.49	0.36	0.30
	T (°C)	367.3	345.0	367.5	355.0
Carbon monoxide production peaks					
First peak	$\Delta CO_{,\,max}$ (mol%)	0.10	0.21	0.08	0.13
	T (°C)	274.8	254.2	276.0	263.0
Second peak	$\Delta CO_{,\,max}$ (mol%)	0.09	0.15	0.04	0.07
	T (°C)	367.0	345.0	361.3	350.0

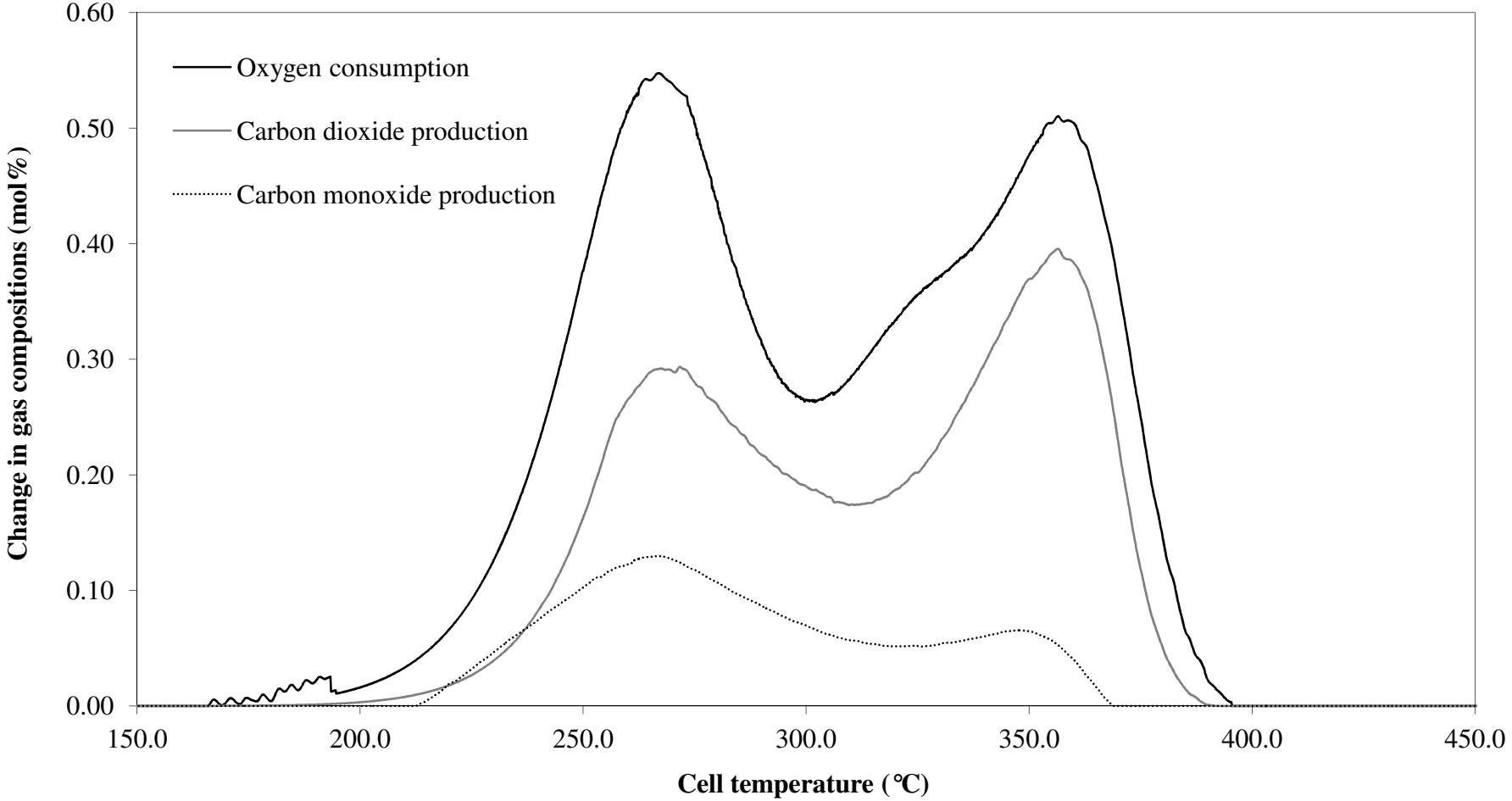

Figure 6.1 - Typical palm fibre (clump fibre) evolved gas analysis (EGA) experimental results with air as the oxidising gas, an absolute total system pressure of 500kPa, an air flow rate of 400smL/min and a heating rate of 50°C/h (Experiment F1).

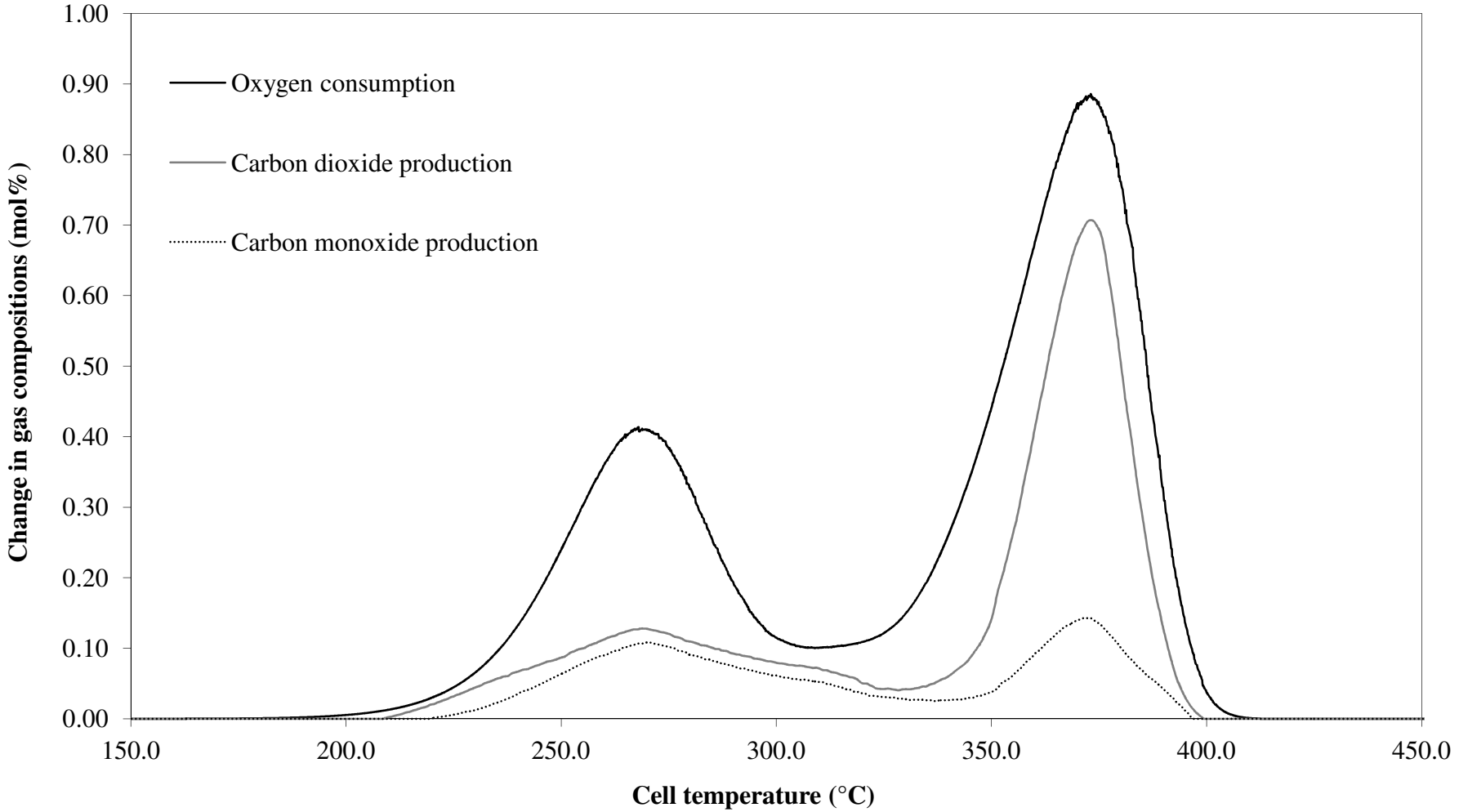

Figure 6.2 - Typical palm fibre (kernel) evolved gas analysis (EGA) experimental results with air as the oxidising gas, an absolute total system pressure of 500kPa, an air flow rate of 400smL/min and a heating rate of 50°C/h (Experiment F3).

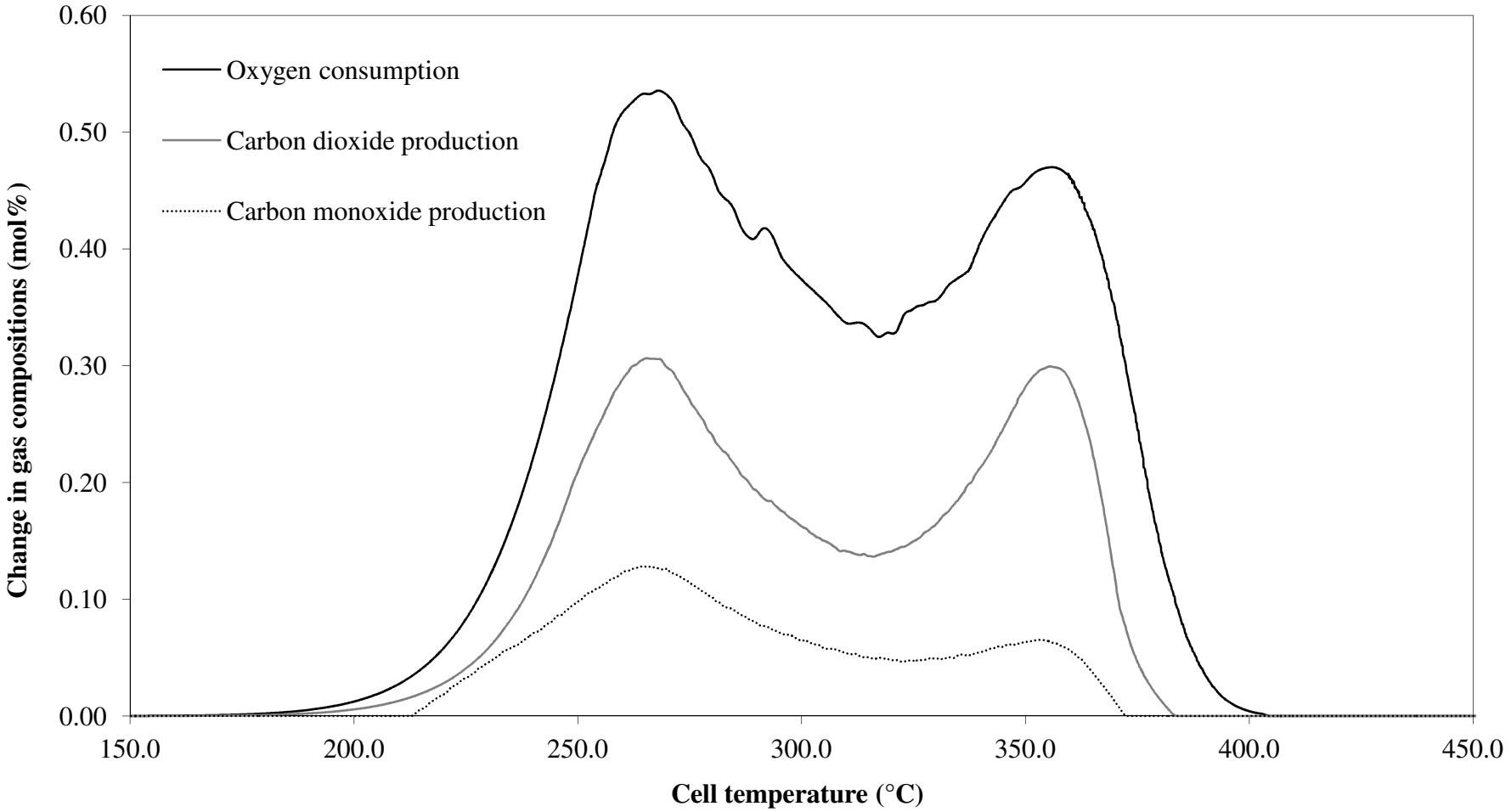

Figure 6.3 - Typical palm fibre (loose fibre) evolved gas analysis (EGA) experimental results with air as the oxidising gas, an absolute total system pressure of 500kPa, an air flow rate of 400smL/min and a heating rate of 50°C/h (Experiment F6).

Considering the kernel sample (Experiment F3), the average first peak temperature was 268.2°C ± 0.8°C for the exit gas oxygen, carbon dioxide and carbon monoxide compositions. The average second peak temperature for the oxygen, carbon dioxide and carbon monoxide curves of the kernel sample coincide at 372.5°C ± 0.7°C. The two peaks may be taken to define periods during which decomposition of hemicellulose and cellulose escape from the palm fibre during combustion (Idris *et al.*, 2010 and Darvell *et al.*, 2010). Hence, the first and second peaks may be referred to as the hemicellulose and the cellulose peaks, respectively. A small bump in the oxygen consumption curve may be observed at the high temperature of 370°C to 380°C for clump fibre sample (see Figure 6.1). This was due to the lignin decomposition that might overlap with cellulose decomposition. In some experiments, there is no noticeable bump over the same temperature range (see Figures 6.2 and 6.3). because of that, the discussion that follows will only consider the hemicellulose and cellulose decompositions for palm fibre samples. The hemicellulose and the cellulose peak heights of the oxygen consumption curve for the clump and the loose fibres, are comparatively similar. However, in comparison of the hemicellulose and cellulose peaks, the peak height of the hemicellulose was slightly higher than the cellulose peak. However, both the hemicellulose and the cellulose peak heights for the kernel samples display a large differences in comparison to the clump and the loose fibres for the three curves. The cellulose peak height for the kernel was larger than the hemicellulose peak. The ratio of the hemicellulose to cellulose peak heights of the oxygen consumption for the kernel sample (experiment F3) was 1 to 2.2. A similar trend was observed for the carbon dioxide and the carbon monoxide production curves for experiments F1, F3 and F6.

Figures 6.4 to 6.6 present the comparison between the experiments F1, F3 and F6 for the oxygen consumption, the carbon dioxide production and the carbon monoxide production curves, respectively. As observed in Figures 6.4 to 6.6, the loose fibre and the clump fibre exhibit comparatively similar features to each other for the exit gas oxygen, carbon dioxide and carbon monoxide compositions. The exit gas composition curve features for the kernel sample show a large number differences to those observed for the loose and the clump fibres.

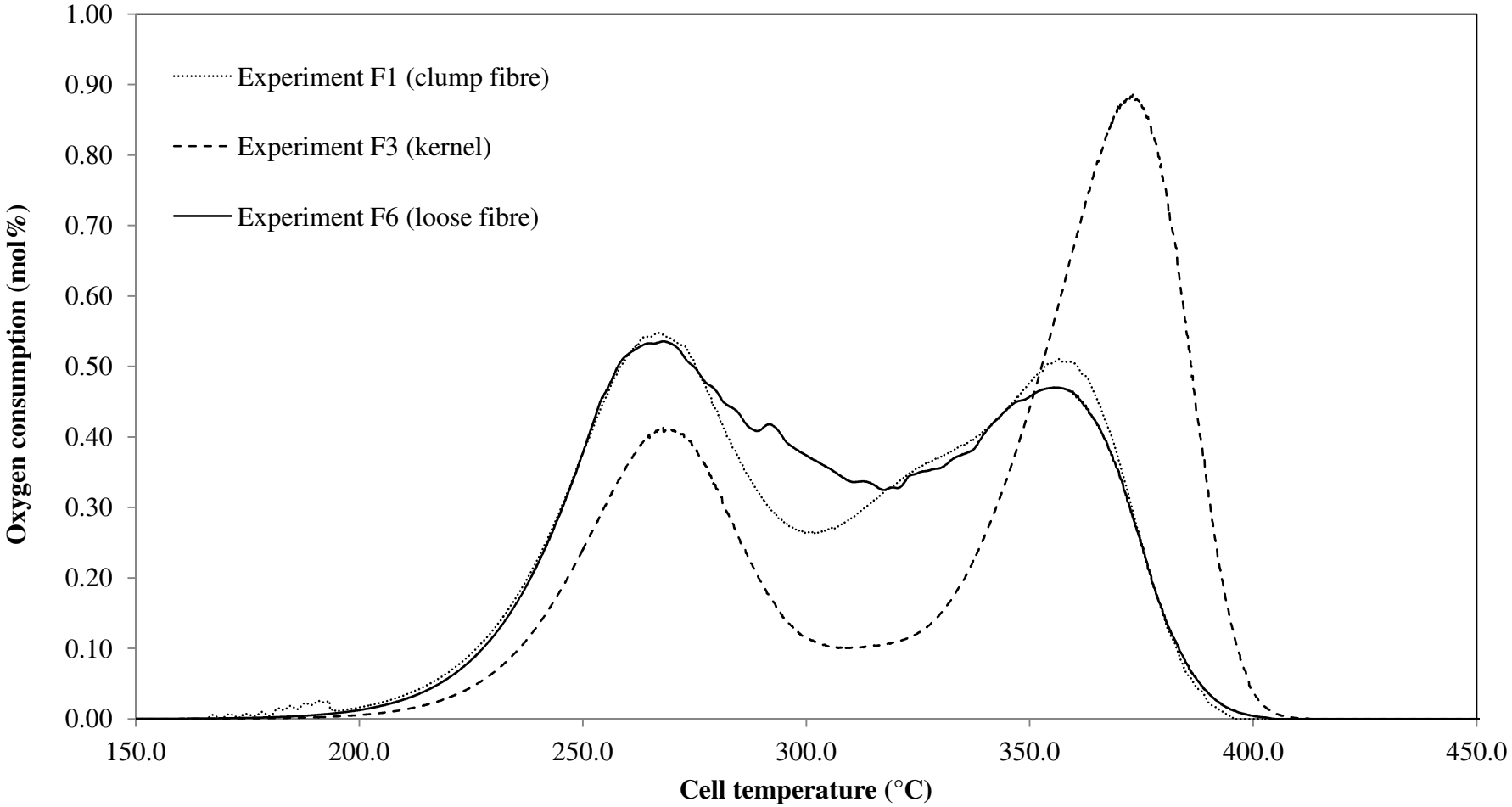

Figure 6.4 - Comparison of the oxygen consumption data with respects to the cell temperature for various types of palm fibre experiments of F1 (clump fibre), F3 (kernel) and F6 (loose fibre) with air as the oxidising gas, an absolute total system pressure of 500kPa, an air flow rate of 400smL/min and a heating rate of 50°C/h.

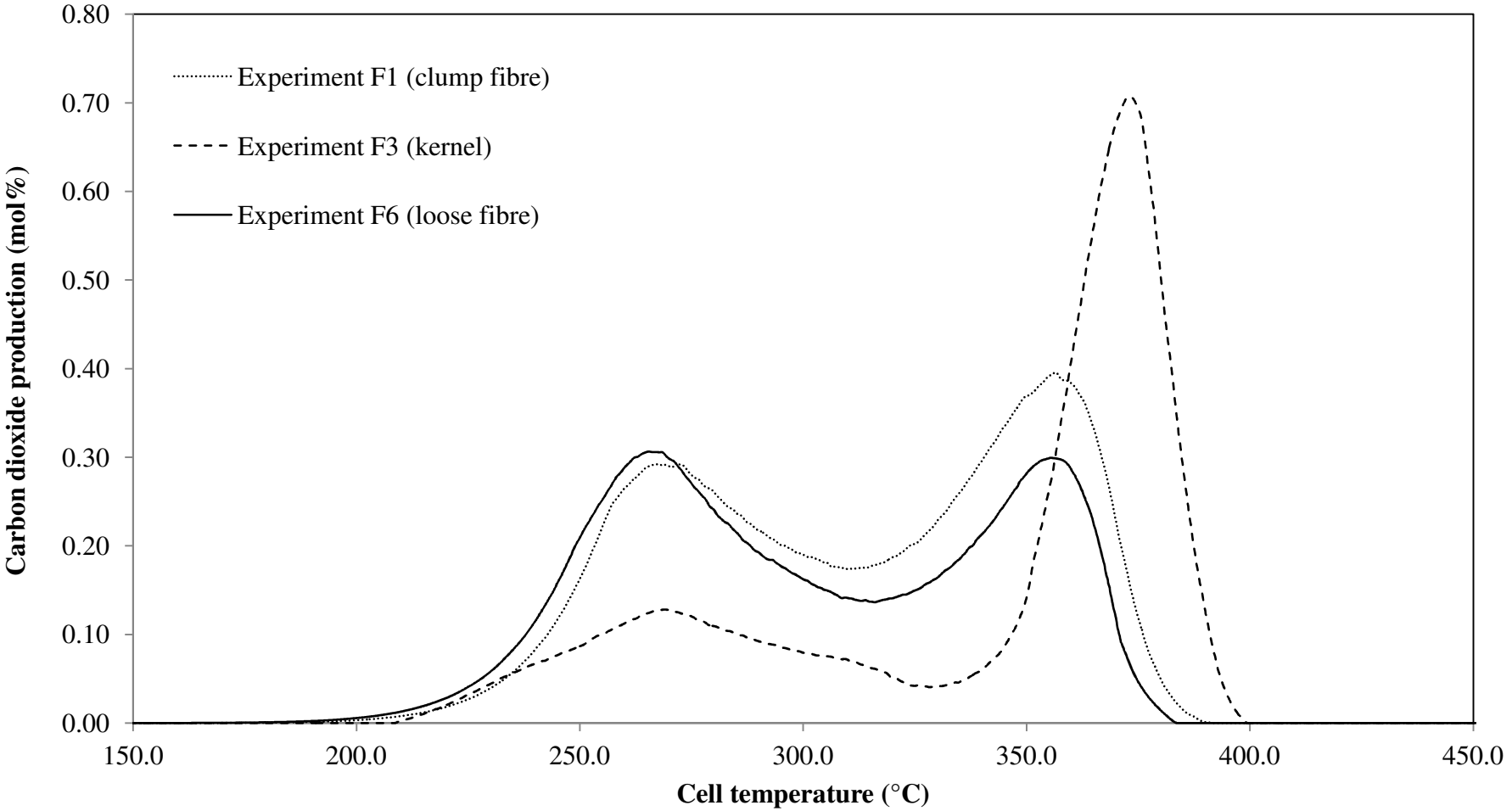

Figure 6.5 - Comparison of the carbon dioxide production data with respects to the cell temperature for various types of palm fibre experiments of F1 (clump fibre), F3 (kernel) and F6 (loose fibre) with air as the oxidising gas, an absolute total system pressure of 500kPa, an air flow rate of 400smL/min and a heating rate of 50°C/h.

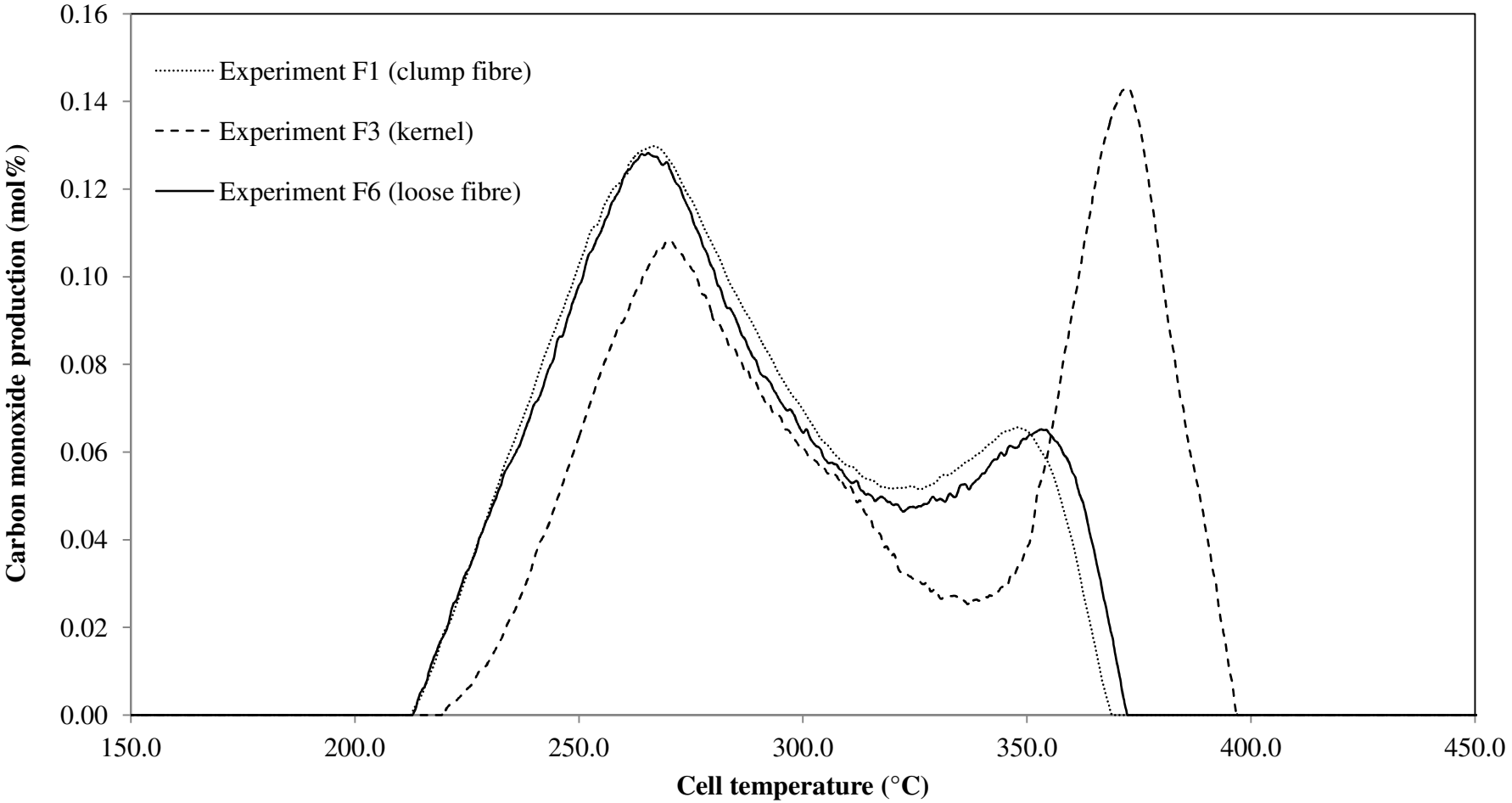

Figure 6.6 - Comparison of the carbon monoxide production data with respects to the cell temperature for various types of palm fibre experiments of F1 (clump fibre), F3 (kernel) and F6 (loose fibre) with air as the oxidising gas, an absolute total system pressure of 500kPa, an air flow rate of 400smL/min and a heating rate of 50°C/h.

The kernel samples have a relatively higher proportion of cellulose rather than hemicellulose (see Figure 6.2) in comparison to those observed for the clump and loose fibres. Both the clump and loose fibres have equally balance hemicellulose and cellulose. The observation was in good agreement to the results obtained for the ultimate and proximate analyses in Table 6.2. The loose and clump fibre are comparatively similar between the samples.

The palm fibre evolved gas analysis (EGA) experiments are modeled by considering three overlapping reaction regimes, namely, high temperature oxidation (HTO), low temperature oxidation (LTO) and medium temperature oxidation (MTO) reactions. The calculated kinetic parameters of the reaction order (n), the activation energy (E/R) and the natural log of beta group (ln β) are obtained for each of the oxidation regimes. The procedure as described in Chapter 4 was used to calculate the kinetic parameters. The calculated values obtained for the kinetic parameters indicate the accuracy of the experimental technique and the data analysis procedure.

The level of agreement between the predicted and the actual oxygen consumption may be measured by the calculated variance. The variance is defined by:

$$\sigma^2 = \frac{\sum_{j=1}^{m} \left(\Delta O_{2\,j} - \Delta O_{2\,calc} \right)^2}{\left(m - 2 \right)} \tag{6.1}$$

where, σ^2 is the variance,

m is the number of data points used in the regression, first point at time t_1 , and last point at time t_m,

and, m-2 is the degree of freedom.

Similar to the rice husks oxidation study, we define a good fit if the value of the variance is below than 0.001. If the value of the variance in between 0.001 and 0.003, an acceptable fit is defined. A poor fit is defined if the value of variance is higher than 0.003. Figures 6.7 to 6.9 show the predicted oxygen consumption curve together with the actual oxygen consumption curve with respects to the cell temperature for the clump fibre (experiment F1), the kernel (experiment F3) and the loose fibre (experiment F6).

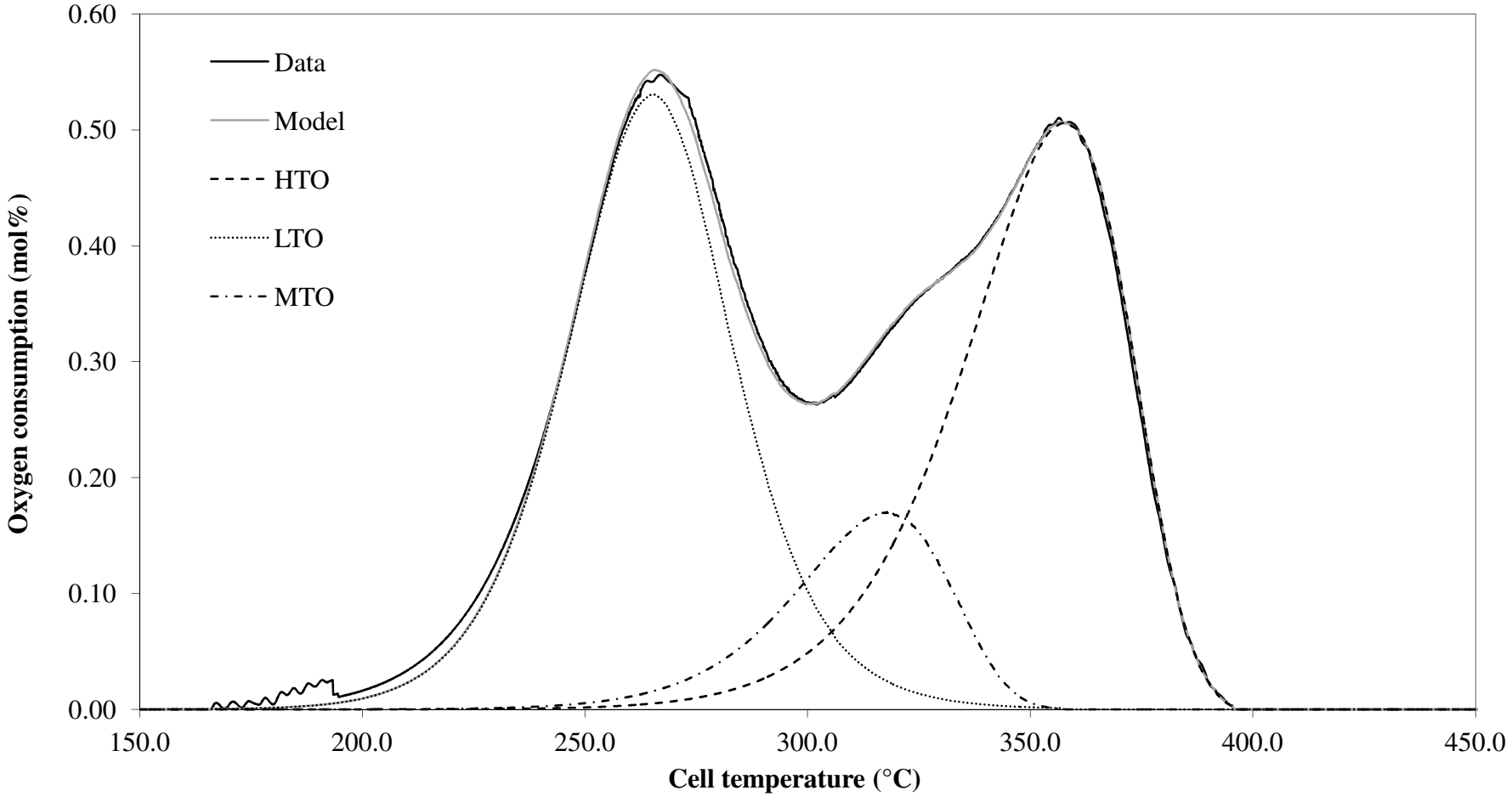

Figure 6.7 - Comparison of the oxygen consumption data and the model prediction with respects to the cell temperature for the combustion characteristics of palm fibre - clump fibre with air as the oxidising gas, an absolute total system pressure of 500kPa, an air flow rate of 400smL/min and a heating rate of 50°C/h (Experiment F1).

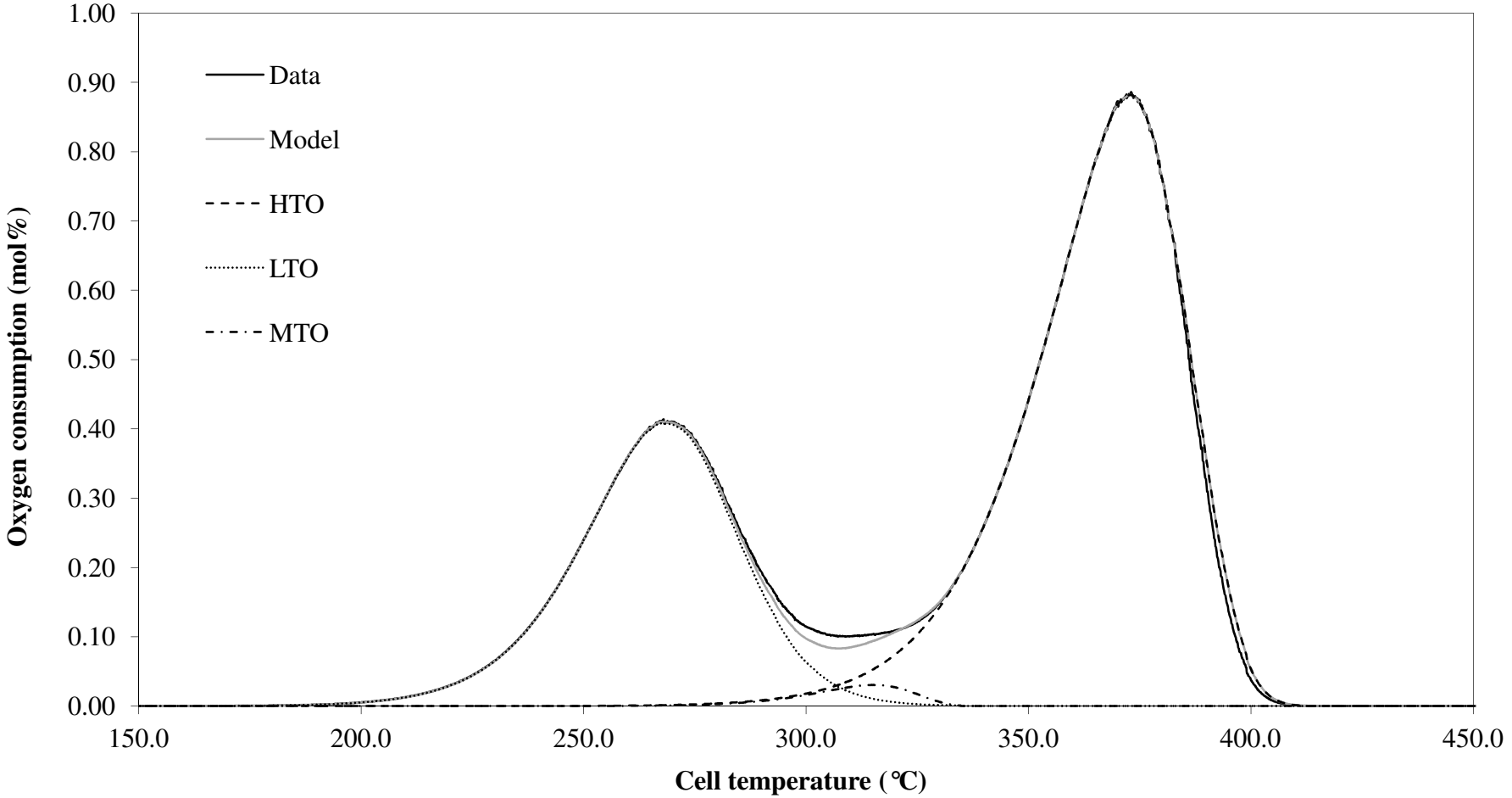

Figure 6.8 - Comparison of the oxygen consumption data and the model prediction with respects to the cell temperature for the combustion characteristics of palm fibre - kernel with air as the oxidising gas, an absolute total system pressure of 500kPa, an air flow rate of 400smL/min and a heating rate of 50°C/h (Experiment F3).

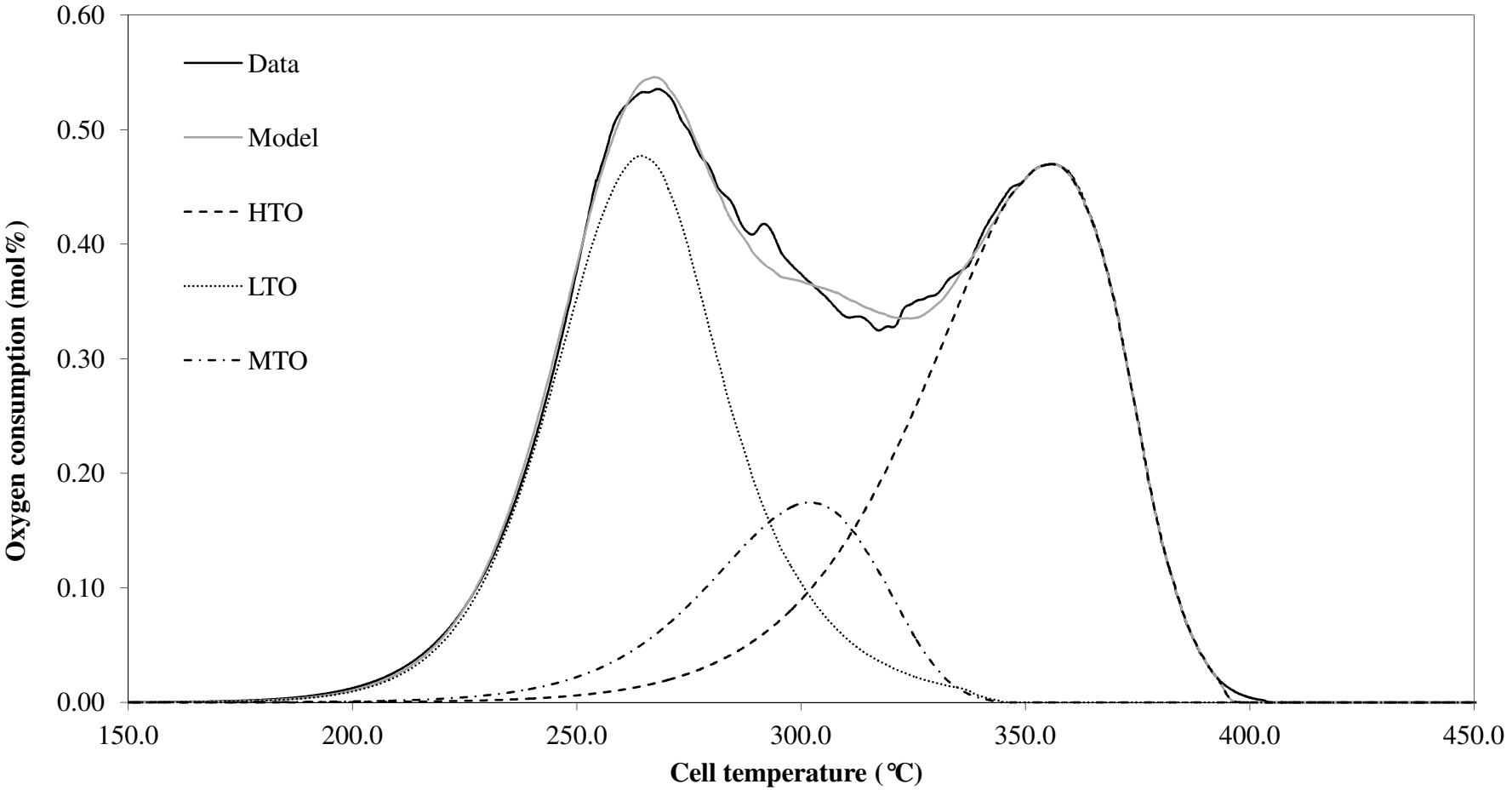

Figure 6.9 - Comparison of the oxygen consumption data and the model prediction with respects to cell temperature for the combustion characteristics of palm fibre - loose fibre with air as the oxidising gas, an absolute total system pressure of 500kPa, an air flow rate of 400smL/min and a heating rate of 50°C/h (Experiment F6).

Table 6.4 - Summary of the calculated kinetic parameters of the palm fibre oxidations. The E/R is the activation energy (in K) and the ln β is the natural log of beta group (dimensionless). M1 is gas mixture 1 that consists of 15.10 mol% O_2, 2.01 mol% CO_2, 0.983 mol% CO and balance nitrogen. M2 is gas mixture 2 that contains of 18.10 mol% O_2, 4.99 mol% CO_2, 2.51 mol% CO and balance nitrogen.

Experiment		**F1**	**F2**	**F3**	**F4**	**F5**	**F6**	**F7**	**F8**	**F9**
Sample		Clump fibre	Clump fibre	Kernel	Loose fibre	Loose fibre	Loose fibre	Loose fibre	Loose fibre	Loose fibre
Absolute total system pressure (kPa)		500	500	500	500	500	500	500	500	700
Oxygen partial pressure (kPa)		105	105	105	105	105	105	105	105	147
Oxygen concentration in feed gas (mol%)		20.96 (Air)	20.96 (Air)	20.96 (Air)	20.96 (Air)	20.96 (Air)	20.96 (Air)	20.96 (Air)	20.96 (Air)	20.96 (Air)
Heating rate (°C/h)		50	50	50	50	50	50	70	30	50
HTO	Reaction order, n	1.01	1.00	0.99	1.01	1.01	1.01	1.01	1.00	1.05
	E/R ($\times 10^{-3}$)	20.0	19.8	24.4	20.0	19.8	19.6	20.5	20.3	11.0
	ln β	21.2	21.0	30.8	21.0	21.5	21.2	21.8	21.6	13.2
MTO	Reaction order, n	1.00	0.99	0.96	1.01	1.00	0.99	1.01	0.99	1.02
	E/R ($\times 10^{-3}$)	22.1	22.2	26.7	23.0	22.4	22.1	22.8	22.9	18.7
	ln β	22.9	22.5	39.0	22.6	22.6	22.5	22.9	22.1	15.3
LTO	Reaction order, n	1.37	1.38	1.44	1.37	1.37	1.36	1.37	1.36	1.86
	E/R ($\times 10^{-3}$)	22.4	22.7	20.4	22.7	22.6	22.5	22.7	22.1	15.0
	ln β	23.5	23.9	27.7	24.7	24.4	23.8	24.6	24.0	19.0
Variance, σ^2		0.0001	0.0001	0.0001	0.0005	0.0013	0.0001	0.0001	0.0001	0.0003

Table 6.4 (continued) - Summary of the calculated kinetic parameters of the palm fibre oxidations. The E/R is the activation energy (in K) and the ln β is the natural log of beta group (dimensionless). M1 is gas mixture 1 that consists of 15.10 mol% O_2, 2.01 mol% CO_2, 0.983 mol% CO and balance nitrogen. M2 is gas mixture 2 that contains of 18.10 mol% O_2, 4.99 mol% CO_2, 2.51 mol% CO and balance nitrogen.

Experiment		**F10**	**F11**	**F12**	**F13**	**F14**	**F15**	**F16**	**F17**	**F18**
Sample type		Loose fibre	Loose fibre	Loose fibre	Loose fibre	Loose fibre	Loose fibre	Loose fibre	Loose fibre	Loose fibre
Absolute total system pressure (kPa)		232	500	200	278	700	700	200	200	420
Oxygen partial pressure (kPa)		42	76	42	42	106	127	30	36	76
Oxygen concentration in feed gas (mol%)		18.10 (M2)	15.10 (M1)	20.96 (Air)	15.10 (M1)	15.10 (M1)	18.10 (M2)	15.10 (M1)	18.10 (M2)	18.10 (M2)
Heating rate (°C/h)		50	50	50	50	50	50	50	50	50
HTO	Reaction order, n	0.99	1.02	0.99	1.00	1.00	1.01	0.97	0.99	1.01
	E/R ($\times 10^{-3}$)	35.2	26.2	34.0	35.1	19.8	16.3	36.7	35.8	27.9
	ln β	38.9	26.4	36.4	37.3	21.4	18.9	38.9	38.2	28.8
MTO	Reaction order, n	1.00	1.02	0.99	1.01	0.97	0.98	0.95	0.98	1.00
	E/R ($\times 10^{-3}$)	33.5	28.2	31.8	29.1	23.0	24.0	36.6	32.2	27.6
	ln β	34.8	31.1	34.9	36.6	24.8	24.1	49.4	46.1	30.6
LTO	Reaction order, n	1.33	1.66	1.33	1.34	1.36	1.54	1.22	1.23	1.43
	E/R ($\times 10^{-3}$)	33.0	28.3	32.4	32.2	20.7	17.8	39.8	37.0	27.2
	ln β	31.6	30.7	30.8	29.9	25.5	23.2	34.6	32.3	29.3
Variance, σ^2		0.0001	0.0013	0.0001	0.0001	0.0001	0.0002	0.0001	0.0001	0.0002

Table 6.4 (continued) - Summary of the calculated kinetic parameters of the palm fibre oxidations. The E/R is the activation energy (in K) and the ln β is the natural log of beta group (dimensionless). M1 is gas mixture 1 that consists of 15.10 mol% O_2, 2.01 mol% CO_2, 0.983 mol% CO and balance nitrogen. M2 is gas mixture 2 that contains of 18.10 mol% O_2, 4.99 mol% CO_2, 2.51 mol% CO and balance nitrogen.

Experiment		**F19**	**F20**	**F21**	**F22**
Sample type		Loose fibre	Clump fibre	Clump fibre	Loose fibre (ground)
Absolute total system pressure (kPa)		362	700	362	500
Oxygen partial pressure (kPa)		76	147	76	105
Oxygen concentration in feed gas (mol%)		20.96 (Air)	20.96 (Air)	20.96 (Air)	20.96 (Air)
Heating rate (°C/h)		50	50	50	50
HTO	Reaction order, n	1.00	1.06	1.00	1.01
	E/R ($\times 10^{-3}$)	27.0	11.7	27.2	19.9
	ln β	28.7	13.5	28.0	21.2
MTO	Reaction order, n	0.99	1.01	1.01	0.99
	E/R ($\times 10^{-3}$)	28.1	19.2	28.8	22.2
	ln β	33.4	15.3	33.1	22.6
LTO	Reaction order, n	1.37	1.84	1.37	1.36
	E/R ($\times 10^{-3}$)	26.8	14.9	26.6	22.5
	ln β	28.9	19.2	28.5	24.0
Variance, σ^2		0.0002	0.0002	0.0005	0.0001

As observed in Figures 6.7 to 6.9, all the three types of palm fibre samples show a good fit between the predicted oxygen consumption curve and the actual experimental data. Table 6.4 presents the summary of the calculated kinetic parameters of the palm fibre oxidations. As shown in Table 6.4, the calculated variance was 0.0001 for all the sample types of the experiments F1, F3 and F6. The discrepancies observed for the clump fibre sample were at the low temperature region of 170°C to 250°C and at the medium temperature region of 270°C to 300°C (see Figure 6.7). A very good agreement between the predicted and the actual oxygen consumption curve was observed for the high temperature oxidation (HTO) reactions. The discrepancy at the low temperature region was due to the instability of the experimental data at very low temperature, this is because the gas analysers are most accurate at higher temperatures. This will gives a poor match of the predicted oxygen consumption curve and the actual experimental data. The discrepancy at the medium temperature region was due to the overlapping of the LTO and MTO regimes which made it difficult to obtain a good fit.

Considering the kernel sample results presented in Figure 6.8, the disagreement between the predicted and the actual oxygen consumption curves is mainly at the medium temperature range of 270°C to 330°C. The disagreement at this medium temperature range of 270°C to 330°C was due to the overlapping of the MTO and LTO reactions. Similarly to the kernel and the clump fibre samples, the discrepancy observed for the loose fibre samples was at the medium temperature range of 260°C to 350°C (see Figure 6.9). Considering Table 6.4, the calculated kinetic parameters of the activation energy, the natural log of beta group and the reaction order of the HTO, LTO and MTO reactions for the loose and clump fibres were comparatively similar to each other. However, significant differences are observed for the kernel sample calculated kinetic parameters in comparison to the loose and clump fibres. The observation was in agreement to the experimental results reported earlier for the clump fibre, the kernel and the loose fibre samples.

In summary, the clump and the loose fibres sample were comparatively similar to each other as revealed by the EGA experimental results and the calculated kinetic parameters of the both samples. However, there is a difference observed for the kernel sample. This

is due to the heterogeneity of the palm fibre samples. From this findings, throughout the study, the loose fibre was selected to represents the palm fibre samples.

6.3 Palm fibre reproducibility study

In order to examine the reproducibility of the palm fibre experimental data, three evolved gas analysis (EGA) experiments (F4 to F6) were conducted under similar experimental conditions. The details of the experimental conditions are presented in Table 6.1. The variations in the exit gas compositions with respects to cell temperature for the three identical runs of experiments F6, F5 and F4 are shown in Figures 6.3, 6.10 and 6.11, respectively. The EGA results of these three experimental palm fibre experiments are presented in Table 6.3.

Figures 6.10 and 6.11, for experiments F4 and F5, exhibit similar features to those observed for the typical palm fibre run of experiment F6 exhibiting two main peaks in the region of 260°C to 280°C and 340°C to 380°C. The first peak corresponds to the hemicellulose decomposition while the second peak is referred to the cellulose decomposition.

As presented in Table 6.3, the hemicellulose peak temperature lies at the average peak temperature of 266.0°C within ±1.8°C for the oxygen consumption of the three identical experimental runs F4 to F6. The cellulose average peak temperature for the oxygen consumption curve coincide at 354.9°C ± 1.9°C. For the carbon dioxide production curve, the hemicellulose average peak temperature for the three identical palm fibre experimental runs was obtained at 265.6°C within ±0.5°C. For the cellulose peak, the average peak temperature for the carbon dioxide production curve was 355.2°C within ±2.4°C. Further, the hemicellulose average peak temperature for the carbon monoxide production curve was obtained at 264.4°C within ±0.1°C. The cellulose average peak temperature for the carbon monoxide production curve coincide at 354.0°C ± 3.1°C. By comparison, Table 6.3 shows an agreement to within ±3.1°C for the peak temperatures. For the remainder of the palm fibre experiments, the level of reproducibility may be taken as agreement to within ±3.1°C.

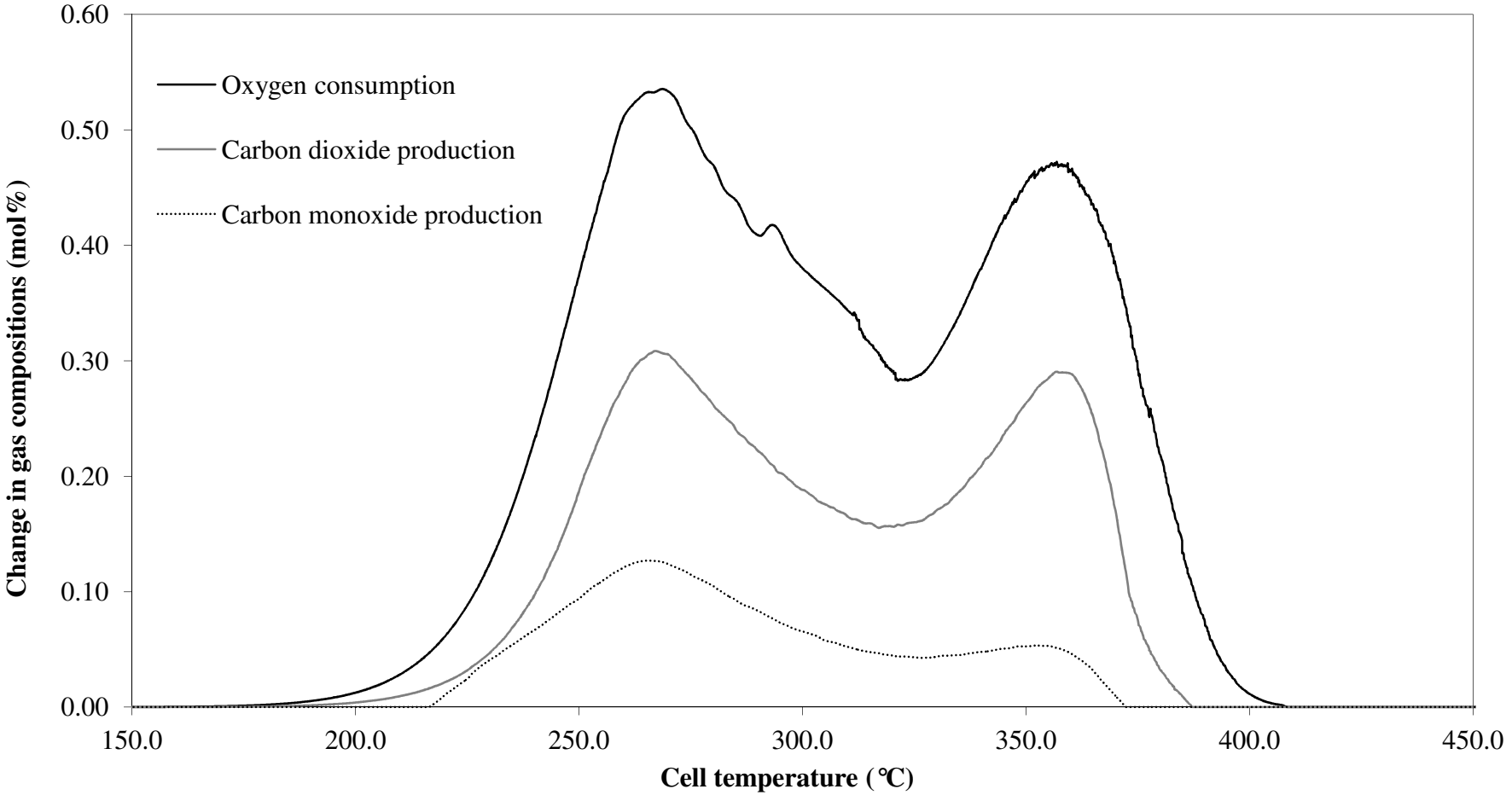

Figure 6.10 - Evolved gas analysis data with respects to the cell temperature for the oxidation of palm fibre with air as the oxidising gas, an absolute total system pressure of 500kPa, an air flow rate of 400smL/min and a heating rate of 50°C/h (Experiment F5).

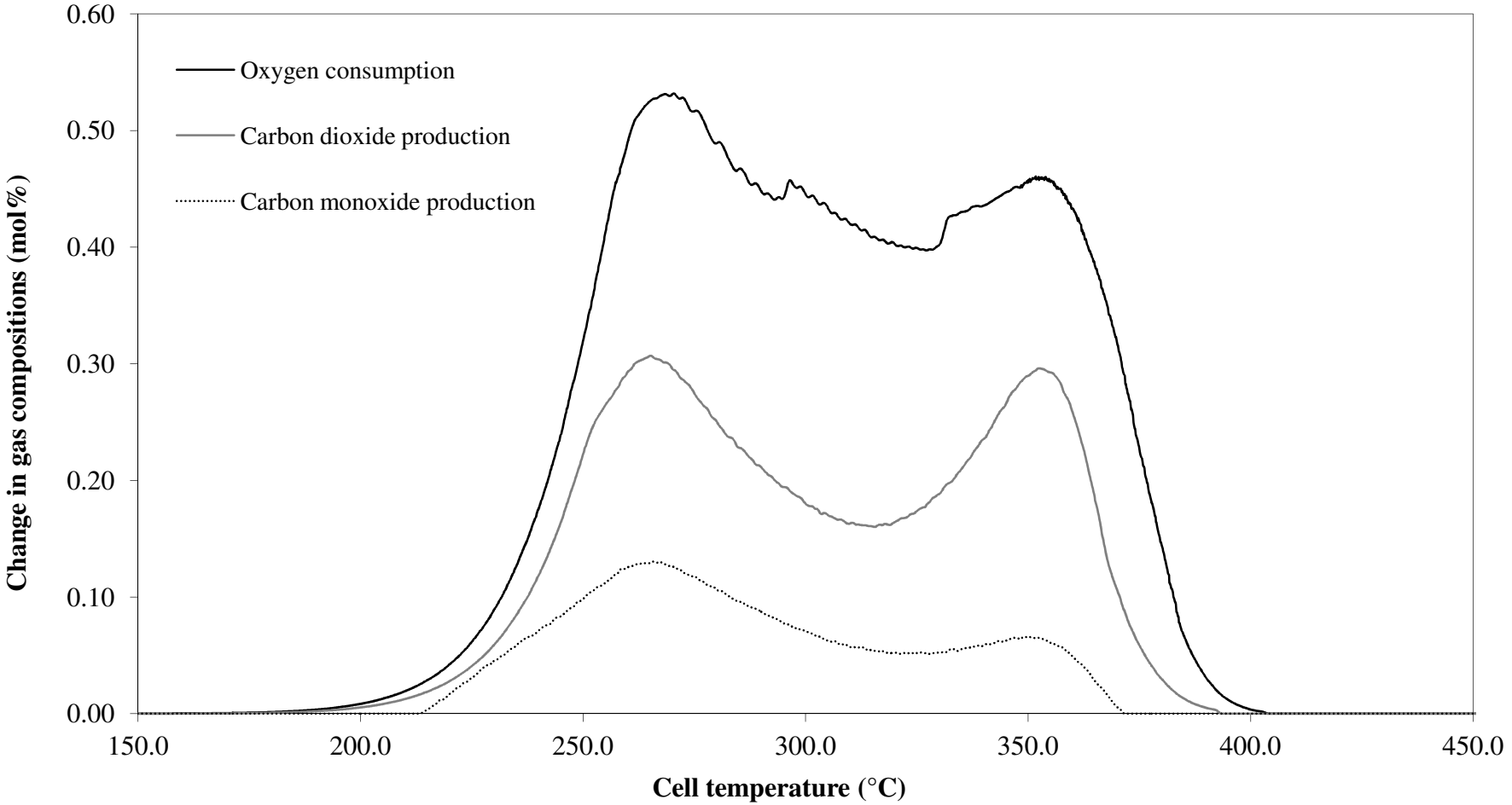

Figure 6.11 - Evolved gas analysis data with respects to the cell temperature for the oxidation of palm fibre with air as the oxidising gas, an absolute total system pressure of 500kPa, an air flow rate of 400smL/min and a heating rate of 50°C/h (Experiment F4).

In order to examine the peak height of the reproducibility study of palm fibre, Figure 6.12 presents the comparison of the oxygen consumption curve as a functions of the cell temperature for the three identical palm fibre experimental runs of F4 to F6. Figures 6.13 and 6.14 display a similar comparison for the carbon dioxide production and the carbon monoxide production curves, respectively. As observed in Figure 6.12, the hemicellulose peak height of the oxygen consumption curve shows a close agreement between the three identical experimental runs of F4 to F6. The hemicellulose peak height obtained at 0.53 mol% oxygen for all the three identical experimental runs. As for the cellulose peak height of the oxygen consumption curve, a close agreement was also observed with the peak height ranges from 0.46 mol% to 0.47 mol% oxygen for these experiments. Similar to the oxygen consumption curve, a close agreement of the hemicellulose peak height was also observed for the both carbon dioxide production and carbon monoxide production curves (see Figures 6.13 and 6.14).

The variations in the hemicellulose and cellulose peak heights between the carbon dioxide production curves of these three identical palm fibre experimental runs was just 0.02 mol% carbon dioxide. For the carbon monoxide production curve, the peak height for the hemicellulose was the same for the three identical experimental runs of F4 to F6. The variations of the cellulose peak height of the carbon monoxide production curves was 0.01 mol% carbon monoxide for the three identical experimental runs.

The overall comparison of the peak heights in Table 6.3 presents an agreement to within ±0.01 mol%. The peak height was much depending on the quantity of the sample presents in each of the experiments. The small differences observed for the three runs are due to the amount of palm fibre initially present in the reaction cell. Similar to the rice husks, a significant error during the preparation of the sample may have contributed to the variation in the results. Because palm fibre is a heterogeneous material, a small variation should be expected but in an acceptable value of the expected experimental error. In comparison to the rice husks experimental results, the variations in the peak temperatures and heights for the palm fibre experiments are higher. This indicates that the palm fibre samples are more heterogeneous compared to the rice husks.

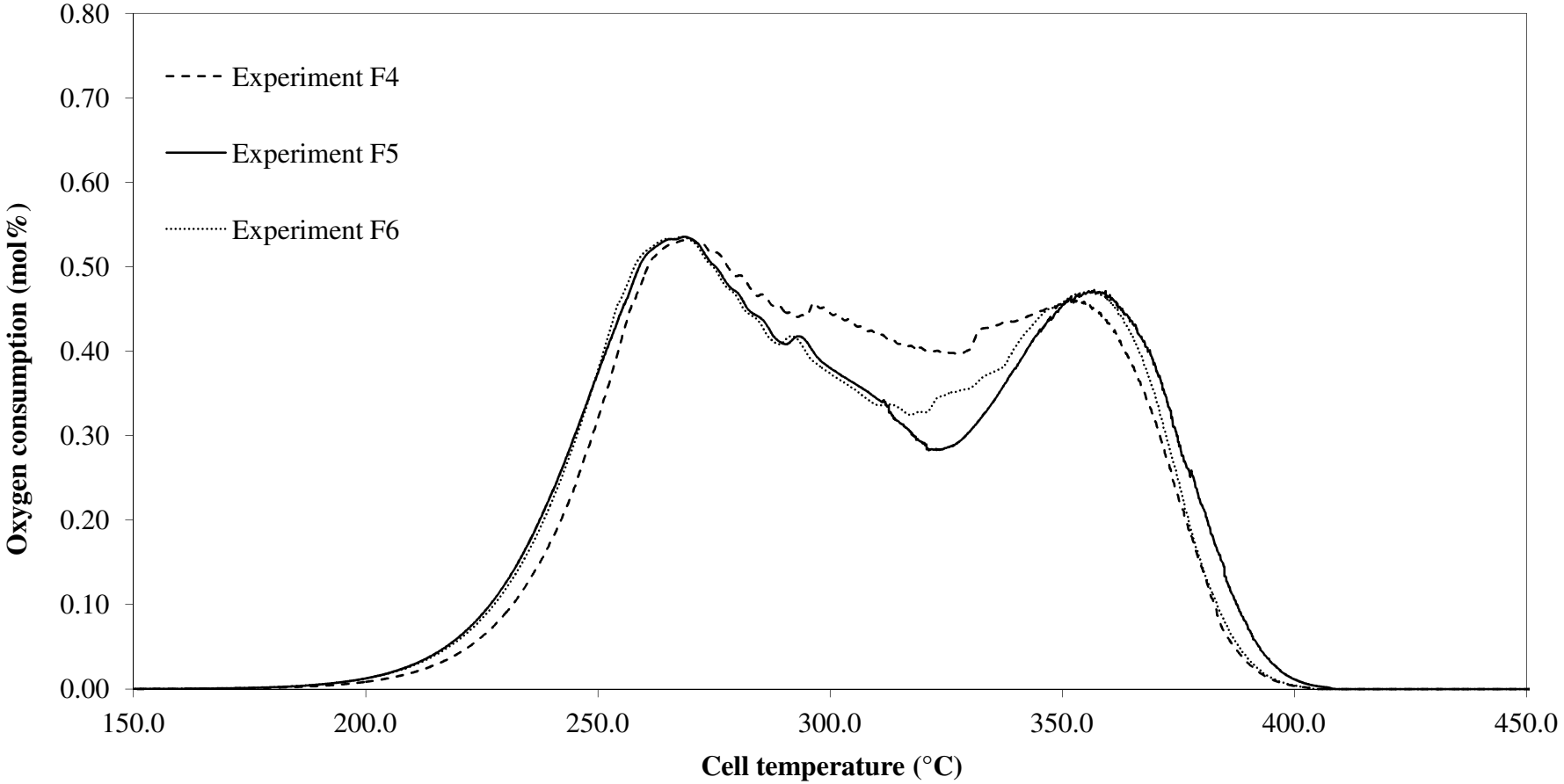

Figure 6.12 - Comparison of the oxygen consumption data with respects to the cell temperature for the three palm fibre experiments conducted under identical conditions with air as the oxidising gas, an absolute total system pressure of 500kPa, an air flow rate of 400smL/min and a heating rate of 50°C/h.

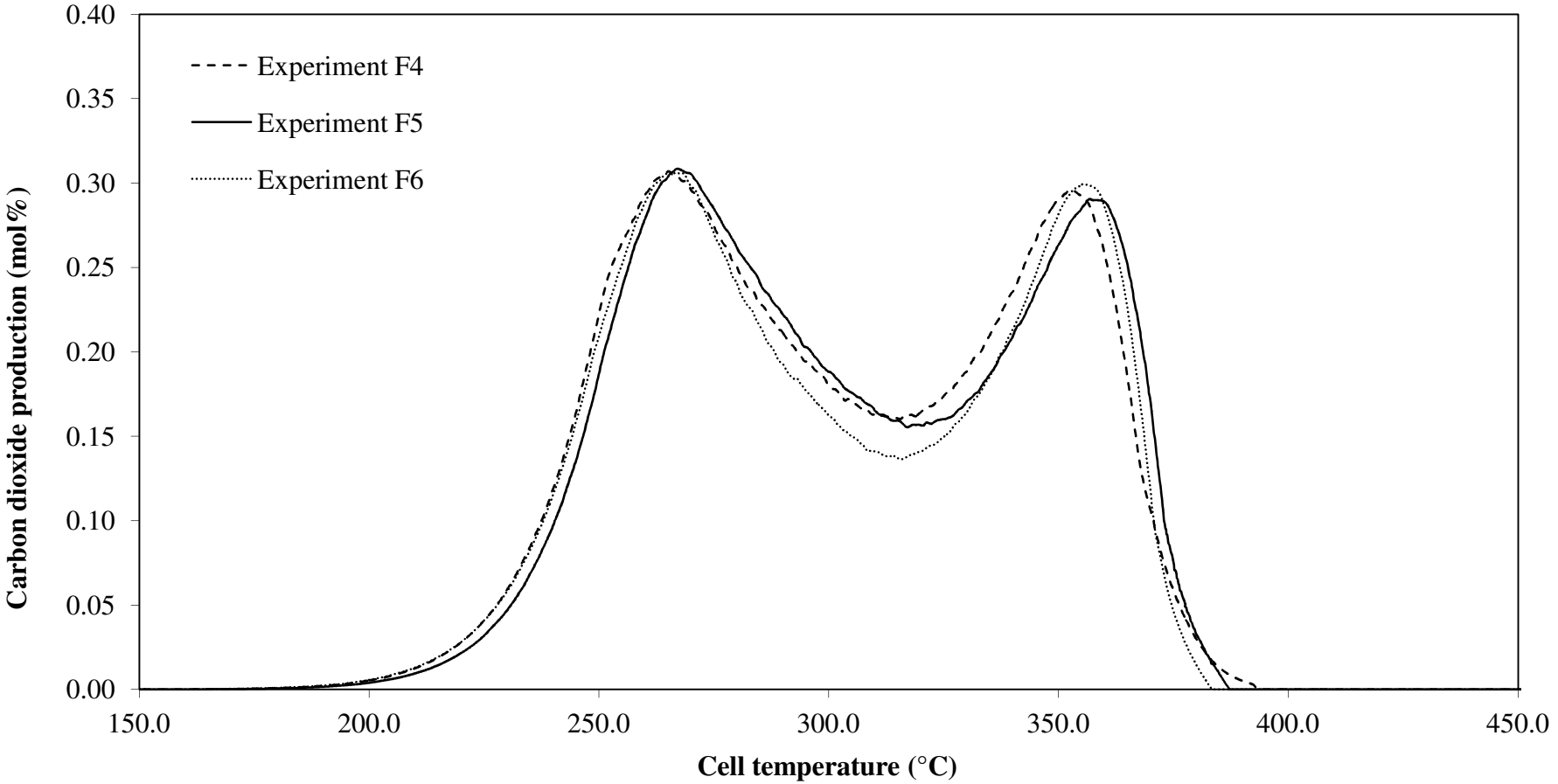

Figure 6.13 - Comparison of the carbon dioxide production data with respects to the cell temperature for the three palm fibre experiments conducted under identical conditions with air as the oxidising gas, an absolute total system pressure of 500kPa, an air flow rate of 400smL/min and a heating rate of 50°C/h.

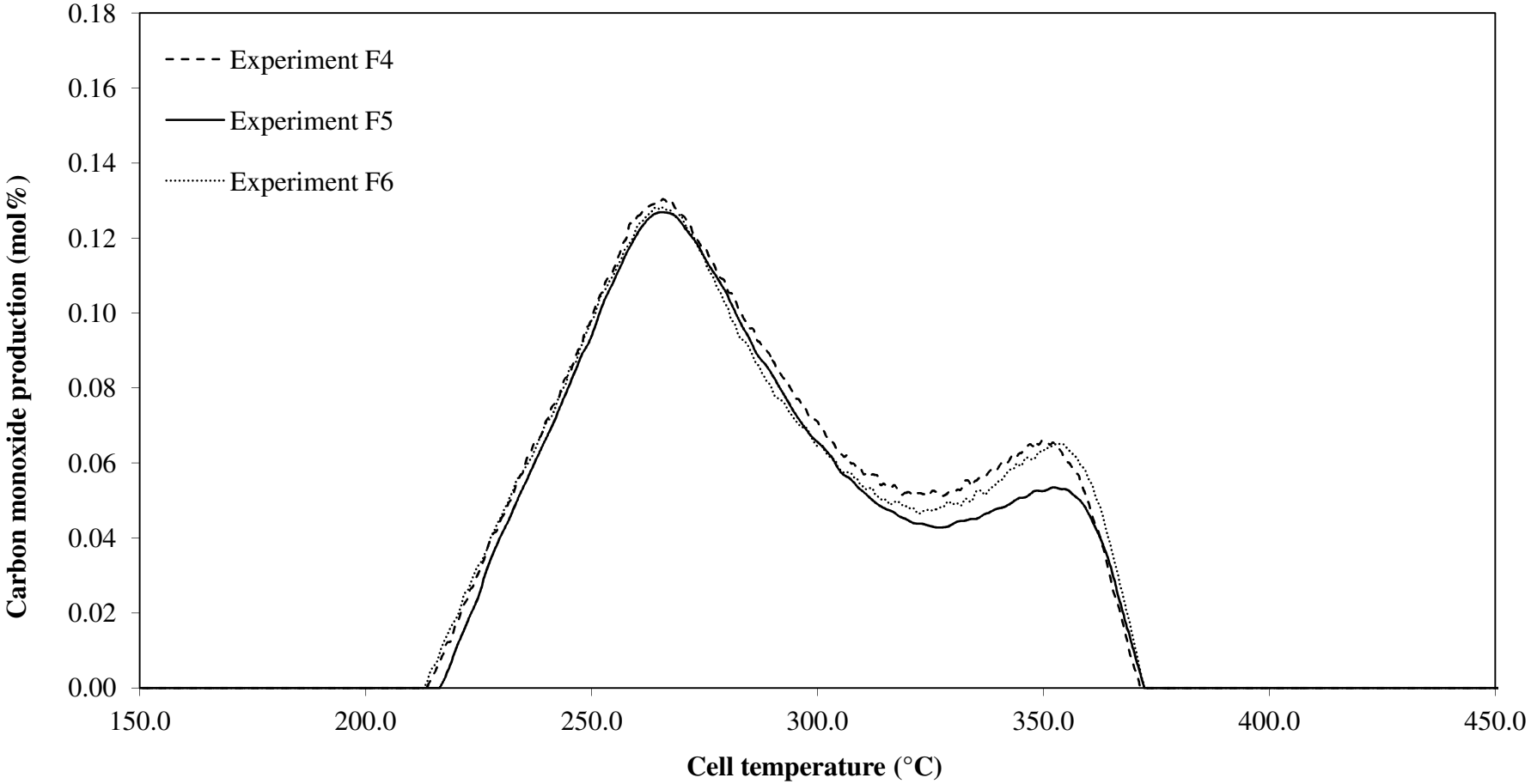

Figure 6.14 - Comparison of the carbon monoxide production data with respects to the cell temperature for the three palm fibre experiments conducted under identical conditions with air as the oxidising gas, an absolute total system pressure of 500kPa, an air flow rate of 400smL/min and a heating rate of 50°C/h.

The summary of the calculated kinetic parameters of the palm fibre oxidations are shown in Table 6.4. The predicted oxygen consumption curve with the actual experimental data for experiment F6 was presented earlier in Figure 6.9. Figures 6.15 and 6.16 present the predicted oxygen consumption curve with the actual experimental data for the experiments F5 and F4.

As shown in Table 6.4, experiments F4 and F6 display a good fit between the predicted oxygen consumption curve and the actual experimental data. The calculated variances obtained were below 0.001 for both samples. The calculated variance for experiments F4 and F6 were 0.0005 and 0.0001, respectively. However, an acceptable fit between the predicted oxygen consumption curve and the actual experimental data was observed for the experiment F5 with the calculated variance of 0.0013.

Similar to experiment F6, there were a few discrepancies observed at the medium temperature range of 260°C to 350°C between the predicted and the actual oxygen consumption curve for both experiments F4 and F5 due to the overlapping of the MTO, LTO and HTO reactions (see Figures 6.15 and 6.16).

Considering the calculated kinetic parameters of the reaction order, the activation energy and the natural log of beta group for the HTO, MTO and LTO reactions, no significant differences are observed for all the three identical palm fibre runs of experiments F4 to F6 (see Table 6.4). For the high temperature oxidation (HTO) reaction, the same reaction order was observed for the three identical palm fibre experiments. However, the activation energy for the HTO reaction between the three experiments agreed within 2.0% and for the ln β within 2.3%. Considering the medium temperature oxidation (MTO) reaction, the reaction order was in the range of 0.99 to 1.01. The values calculated for the activation energies for the three experiments agreed within 3.9% and for the ln β within 0.4%. The variation of the reaction order for the low temperature oxidation (LTO) reaction is 0.01. The values calculated for the activation energies and the ln β for the three experiments were within 0.9% and 3.6%, respectively. Hence, Table 6.4 shows an agreement to 2% of the reaction order, 4% of the activation energy and 4% of the ln β.

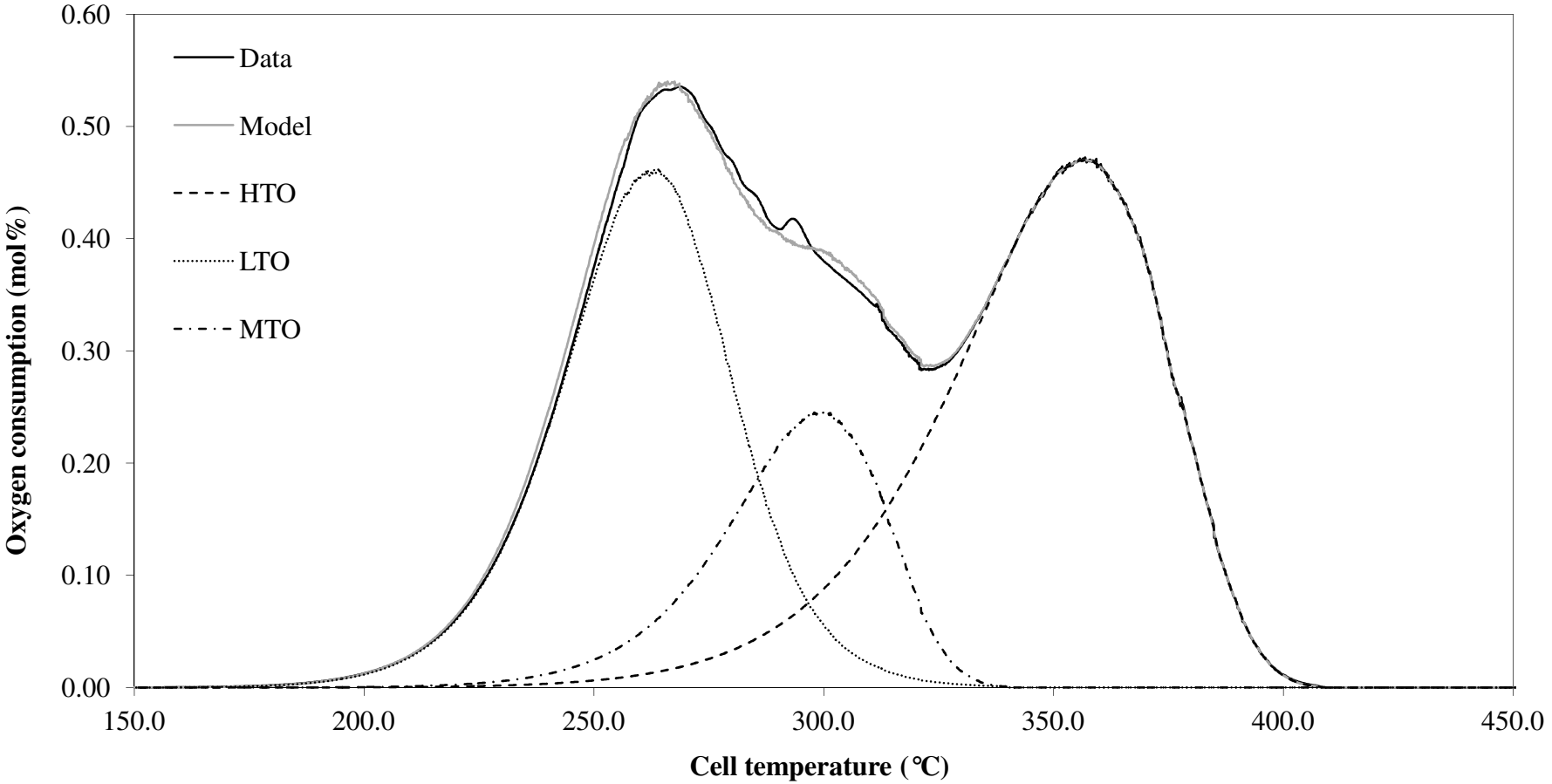

Figure 6.15 - Comparison of the oxygen consumption data and the model predictions with respects to the cell temperature for the oxidation of palm fibre with air as the oxidising gas, an absolute total system pressure of 500kPa, an air flow rate of 400smL/min and a heating rate of 50°C/h (Experiment F5).

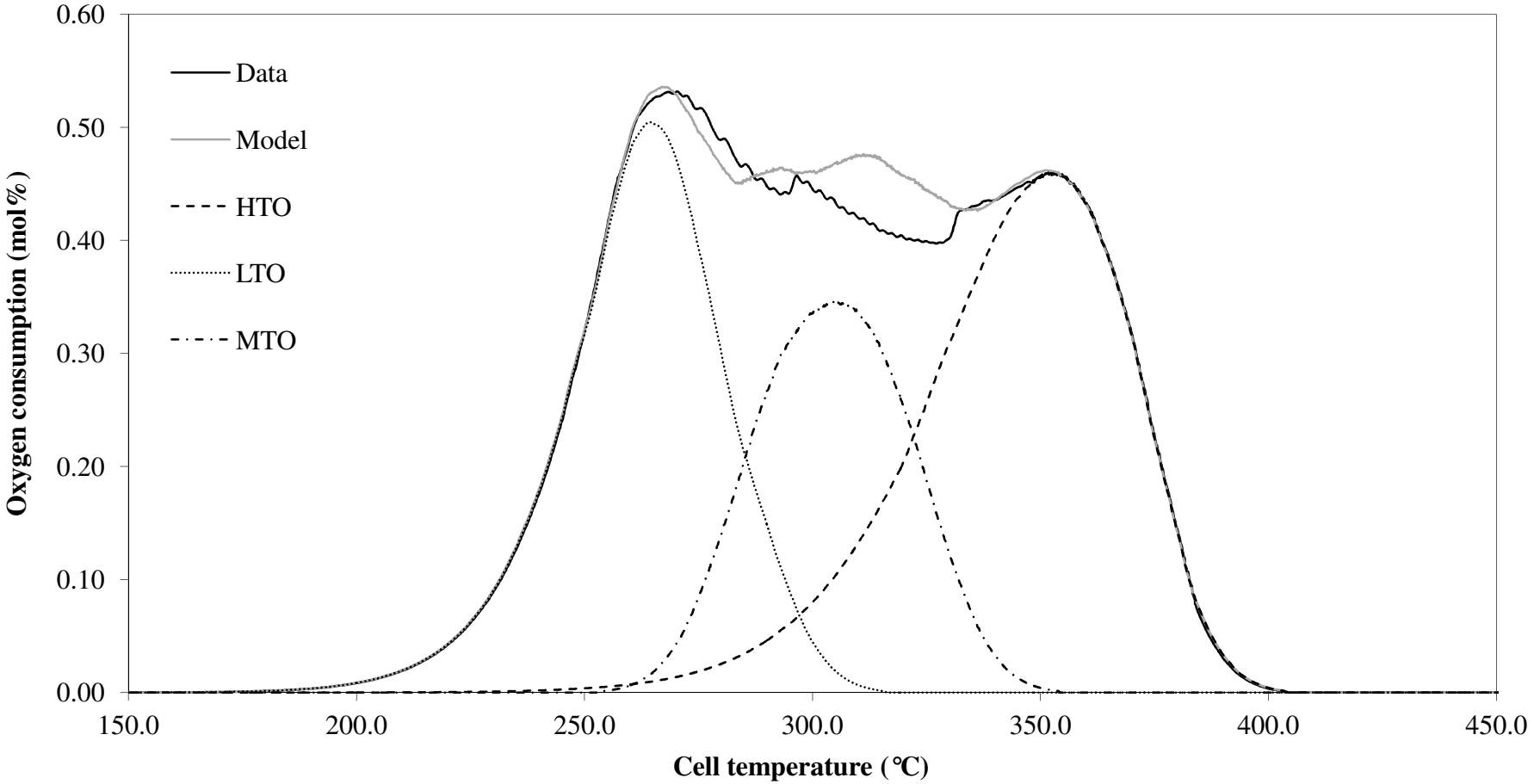

Figure 6.16 - Comparison of the oxygen consumption data and the model predictions with respects to the cell temperature for the oxidation of palm fibre with air as the oxidising gas, an absolute total system pressure of 500kPa, an air flow rate of 400smL/min and a heating rate of 50°C/h (Experiment F4).

In summary, there are no significant differences in the peak temperatures and heights observed for the oxygen consumption, the carbon dioxide production and the carbon monoxide production curves of the three palm fibre experimental runs conducted under similar conditions. The peak temperatures shows an agreement to about ±3.1°C and peak heights to about 0.01 mol% of the exit gas oxygen, carbon dioxide and carbon monoxide compositions of the three identical palm fibre experimental runs. Further, there are no significant differences for the calculated kinetic parameters of the reaction order, the activation energy and the natural log of beta group of the three palm fibre experiments conducted under similar conditions. The calculated kinetic parameters show an agreement to within 2% of the reaction order, 4% of the activation energy and 4% of the ln β. Overall, the evolved gas analysis (EGA) experiments for the palm fibre are reproducible.

6.4 Effect of the heating rate

Experiments F7 and F8 were conducted at different heating rate in comparison to experiments F4 to F6, in order to determine the influences of the heating rate on the palm fibre oxidation reactions. Experiment F7 was conducted at the heating rate of 70°C/h and experiment F8 was performed at the heating rate of 30°C/h. These values compare to the standard heating rate of 50°C/h as used in experiments F4 to F6. The experimental conditions of these runs were provided in Table 6.1.

Figures 6.17 and 6.18 present the variation in the exit gas compositions with respects to the cell temperature for experiments F7 and F8, respectively. The evolved gas analysis (EGA) experimental results of experiments F7 and F8 may be seen in Table 6.3. Figures 6.17 and 6.18 exhibit similar features to those observed for experiments F4 to F6. There are two main peaks for the oxygen consumption, the carbon dioxide production and the carbon monoxide production curves. However, there are variations in the peak temperatures and heights between the experiments F7, F8 and F4 to F6. Figures 6.19 to 6.21 allows comparisons to be made between the experiments F7 and F8 and the experiments F4 to F6 conducted at different heating rate for the oxygen consumption, the carbon dioxide production and the carbon monoxide production, respectively.

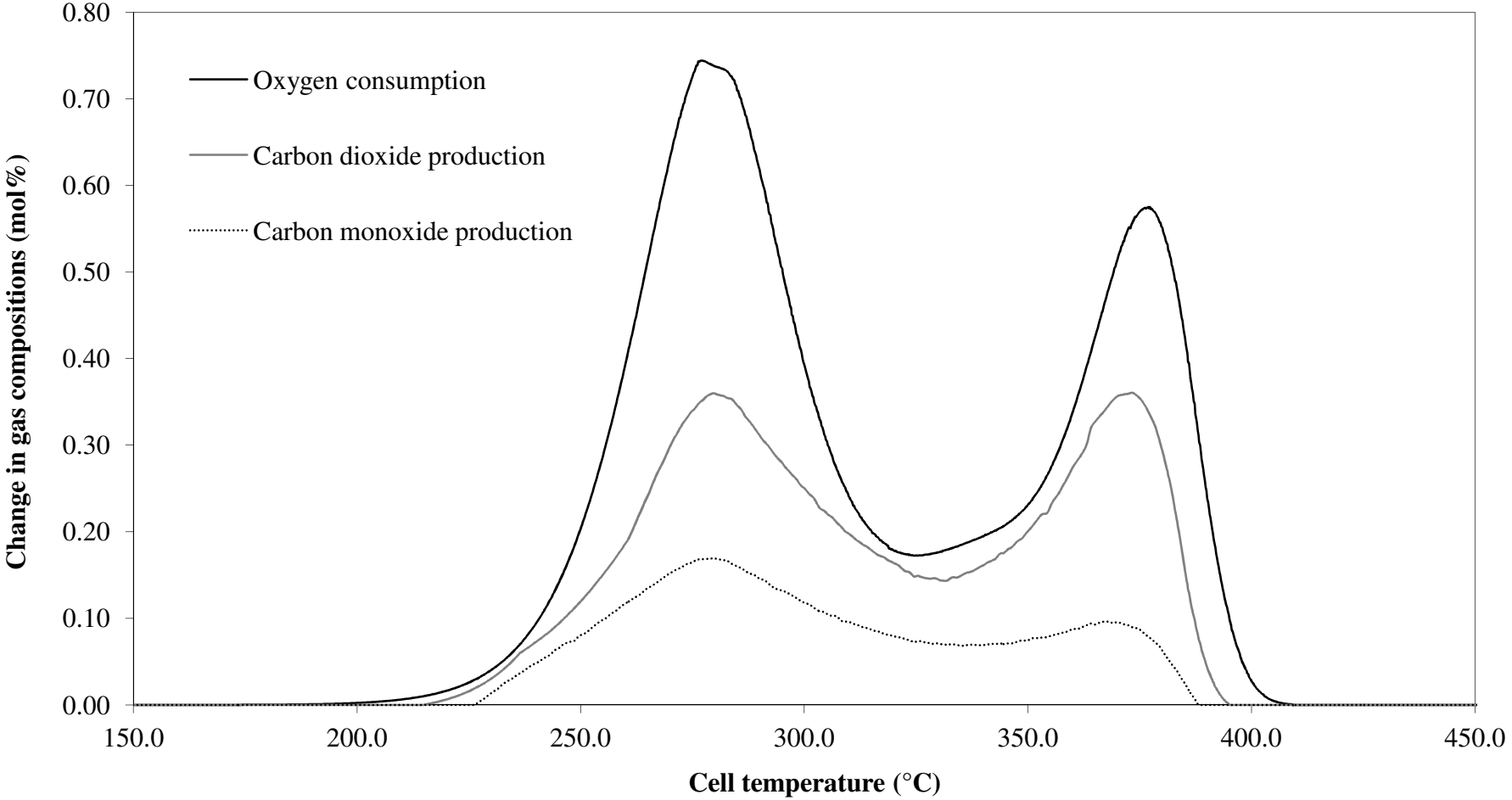

Figure 6.17 - Evolved gas analysis data with respects to the cell temperature for the oxidation of palm fibre with air as the oxidising gas, an absolute total system pressure of 500kPa, an air flow rate of 400smL/min and a heating rate of 70°C/h (Experiment F7).

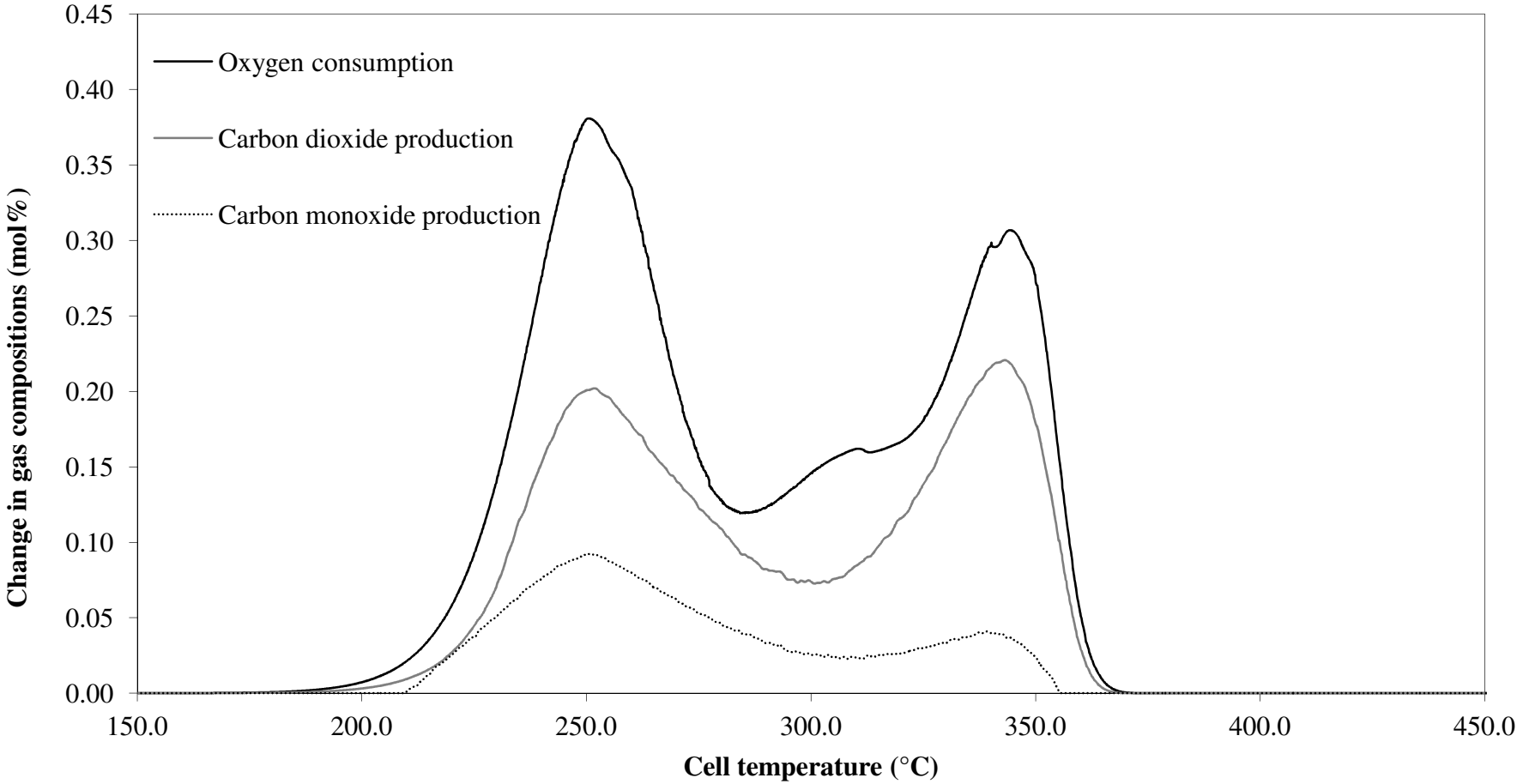

Figure 6.18 - Evolved gas analysis data with respects to the cell temperature for the oxidation of palm fibre with air as the oxidising gas, an absolute total system pressure of 500kPa, an air flow rate of 400smL/min and a heating rate of 30°C/h (Experiment F8).

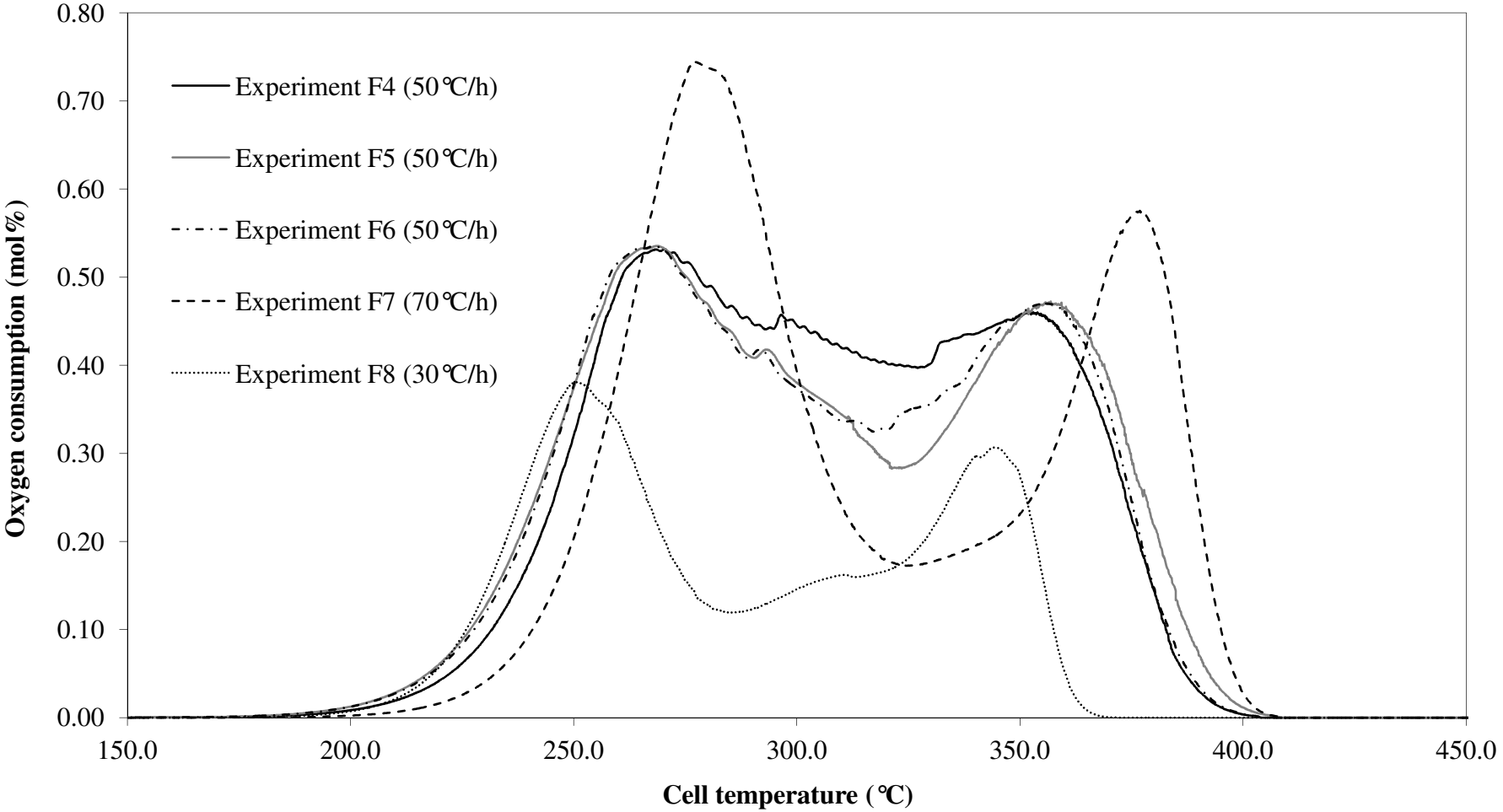

Figure 6.19 - Comparison of the oxygen consumption data with respects to the cell temperature for experiments F4 to F8 conducted at various heating rates, with an absolute total system pressure of 500kPa and an air flow rate of 400smL/min.

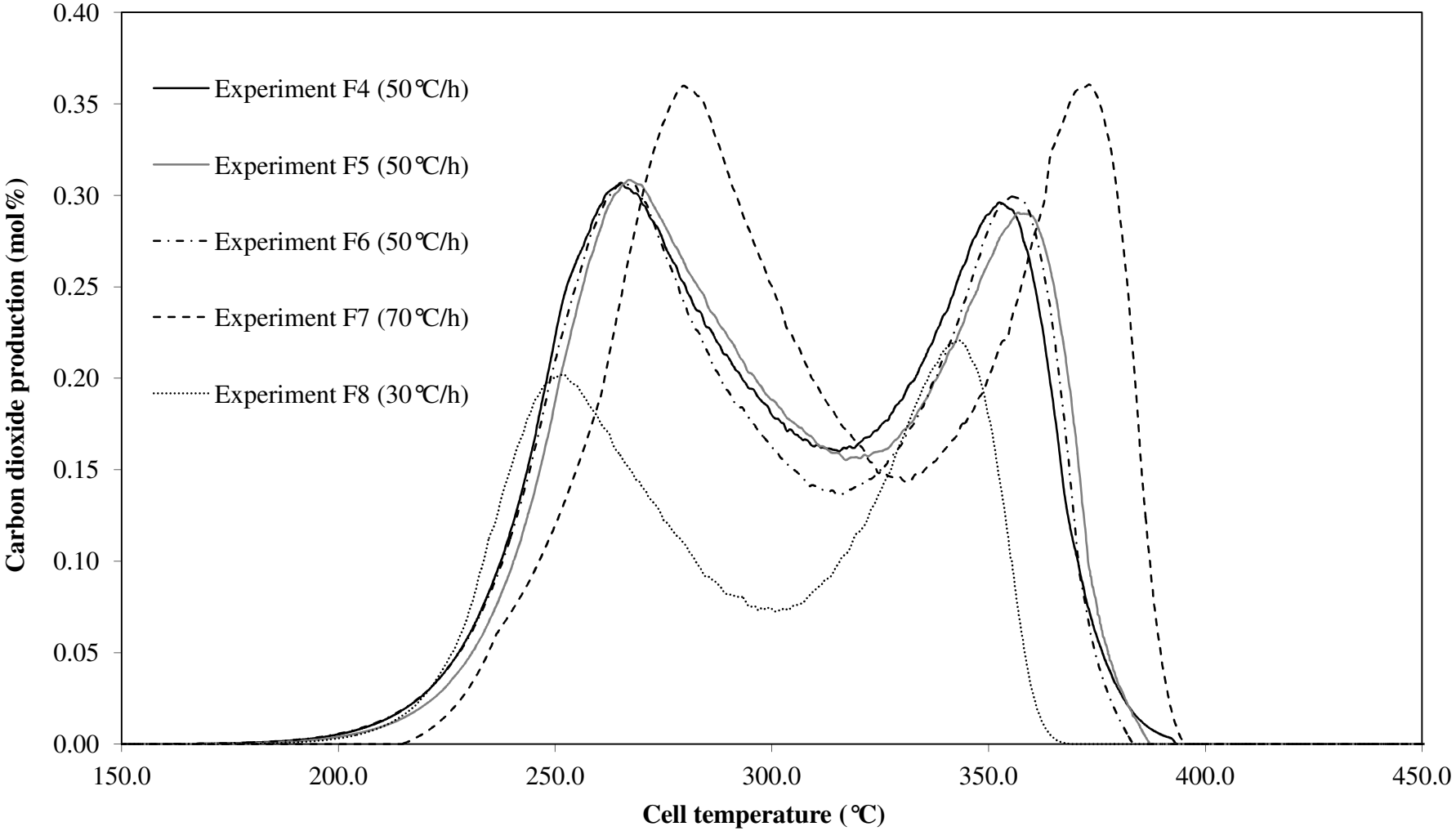

Figure 6.20 - Comparison of the carbon dioxide production data with respects to the cell temperature for experiments F4 to F8 conducted at various heating rates, with an absolute total system pressure of 500kPa and an air flow rate of 400smL/min.

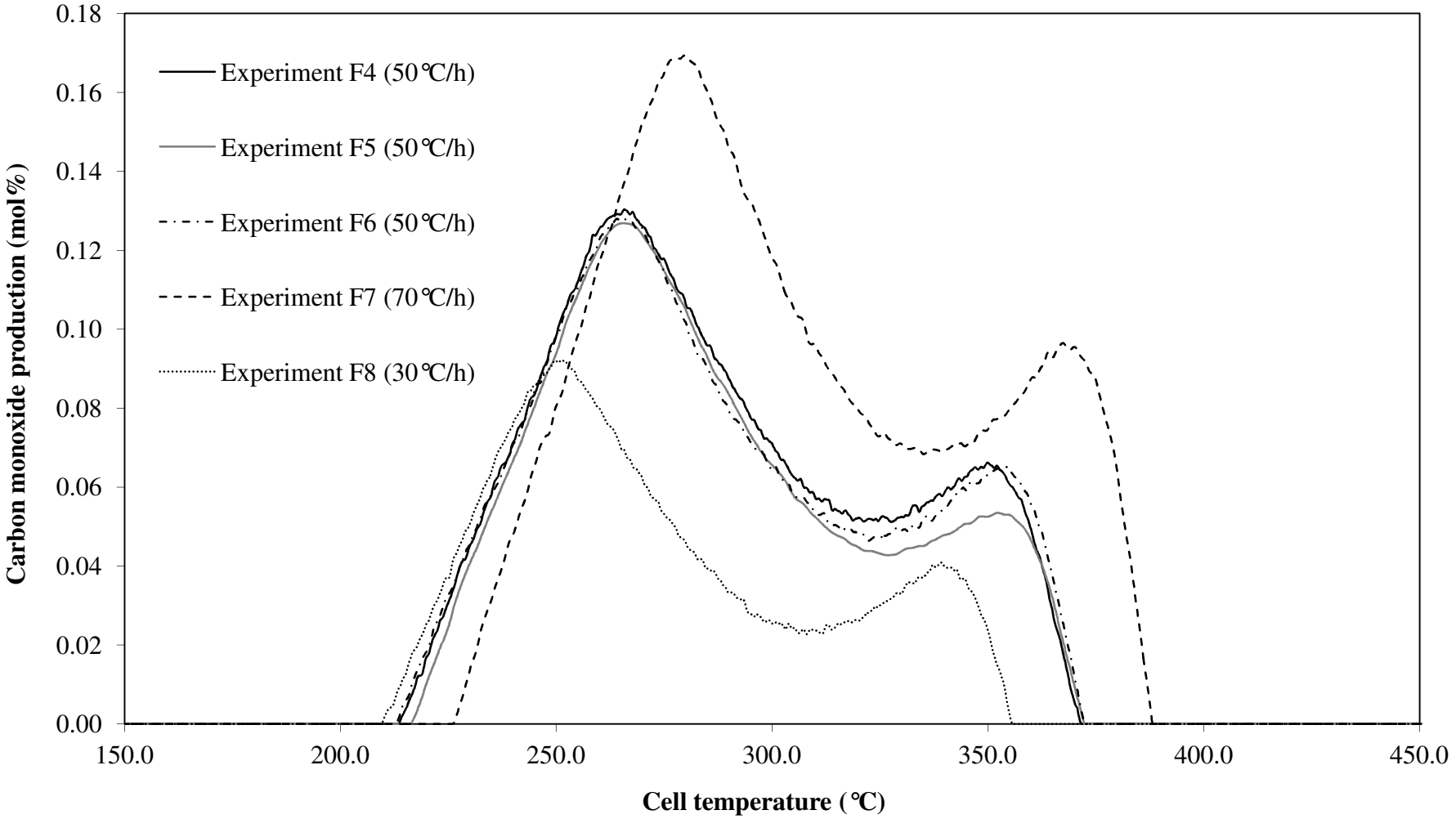

Figure 6.21 - Comparison of the carbon monoxide production data with respects to the cell temperature for experiments F4 to F8 conducted at various heating rates, with an absolute total system pressure of 500kPa and an air flow rate of 400smL/min.

As observed in Figures 6.19 to 6.21, the peak temperature increased with increasing heating rate from 30°C/h to 70°C/h. Likewise, the peak height also increased with increasing heating rates. The hemicellulose peak temperature decreased in the range of 27°C to 29°C as the heating rate decreased from 70°C/h to 30°C/h for the exit gas oxygen, carbon dioxide and carbon monoxide compositions. Likewise, the cellulose peak temperature for all the exit gas composition curves decreased by 30°C to 33°C as the heating rate decreased. Considering the peak height of the oxygen consumption curve for experiments F7 and F8, the peak heights were reduced in the range of 0.26 mol% to 0.36 mol% oxygen for both the hemicellulose and the cellulose peaks. Similar to the oxygen consumption curve, the peak heights for both the hemicellulose and the cellulose for the carbon dioxide production curve also show a decreased in the range of 0.14 mol% to 0.16 mol% carbon dioxide as the heating rates reduced from 70°C/h to 30°C/h.

A similar reduction in peak heights for both the hemicellulose and the cellulose is also observed for the carbon monoxide production curve as the heating rates reduced. This observation is in agreement to the rice husk combustion characteristics study discussed in previous Chapter 5. Further, Idris *et al.* (2010) also reported a similar observations in their combustion characteristics study of oil palm biomass using thermogravimetric analysis (TGA) experiments. They observed that as heating rate increased from 10°C/min to 60°C/min, the decomposition of oil palm biomass increased hence, the peak was systematically shifted to higher temperature regime. Skreiberg *et al.* (2011) and Biagini *et al.* (2008) also reported a similar observations in their oxidation behaviour study of wood waste and rice husk, respectively using TGA technique.

Experiments F4 to F8 were performed at various heating rates and the calculated kinetic parameters of these experiments may be seen in Table 6.4. Figures 6.22 and 6.23 present a plot of the oxygen consumption data and the model prediction with respect to the cell temperature for the experiments F7 and F8, respectively. Considering Figures 6.22 and 6.23, a good fit between the predicted oxygen consumption and the actual experimental data was obtained for the both experiments F7 and F8.

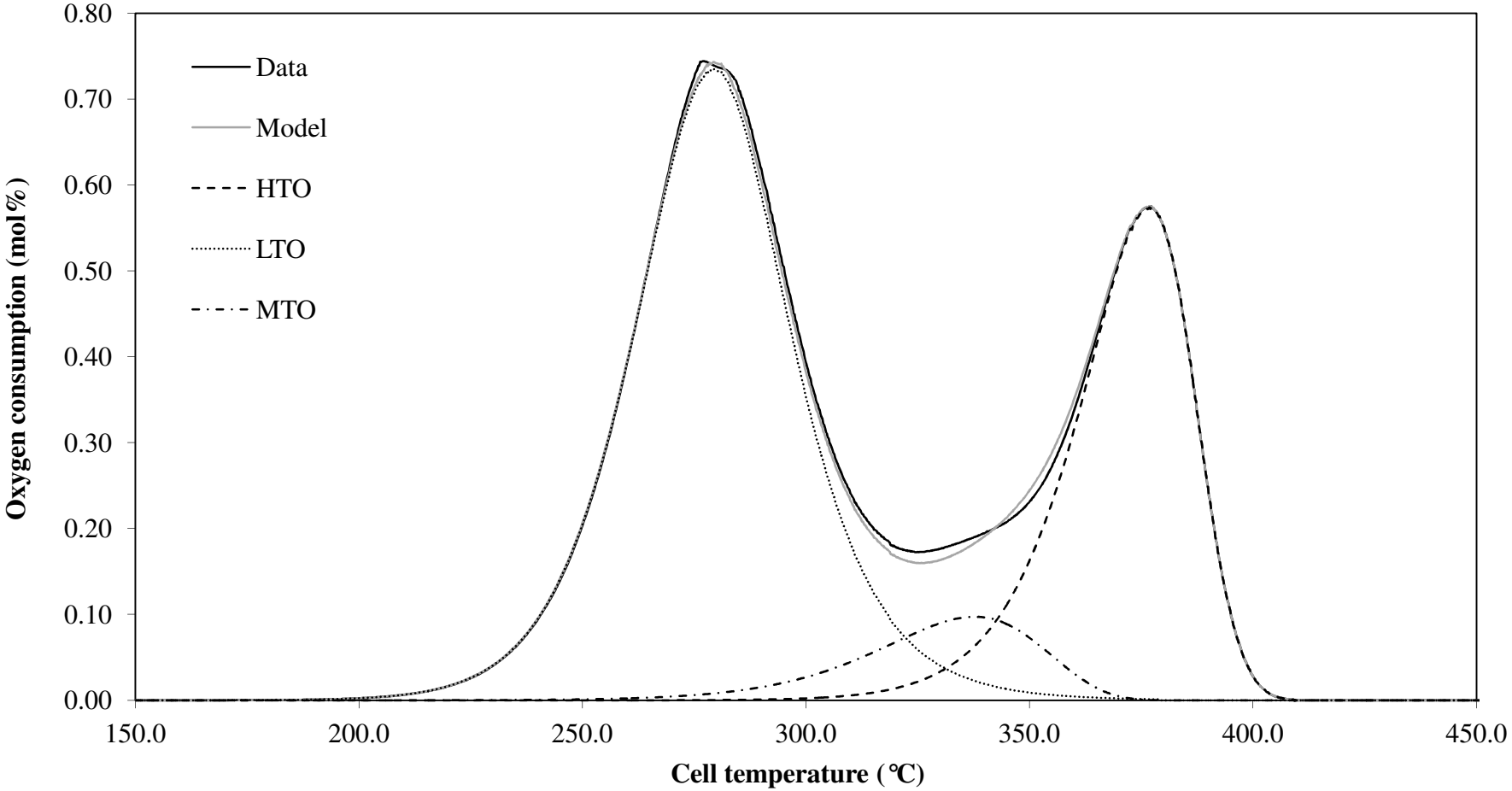

Figure 6.22 - Comparison of the oxygen consumption data and the model prediction with respects to the cell temperature for the oxidation of palm fibre with air as the oxidising gas, an absolute total system pressure of 500kPa, an air flow rate of 400smL/min and a heating rate of 70°C/h (Experiment F7).

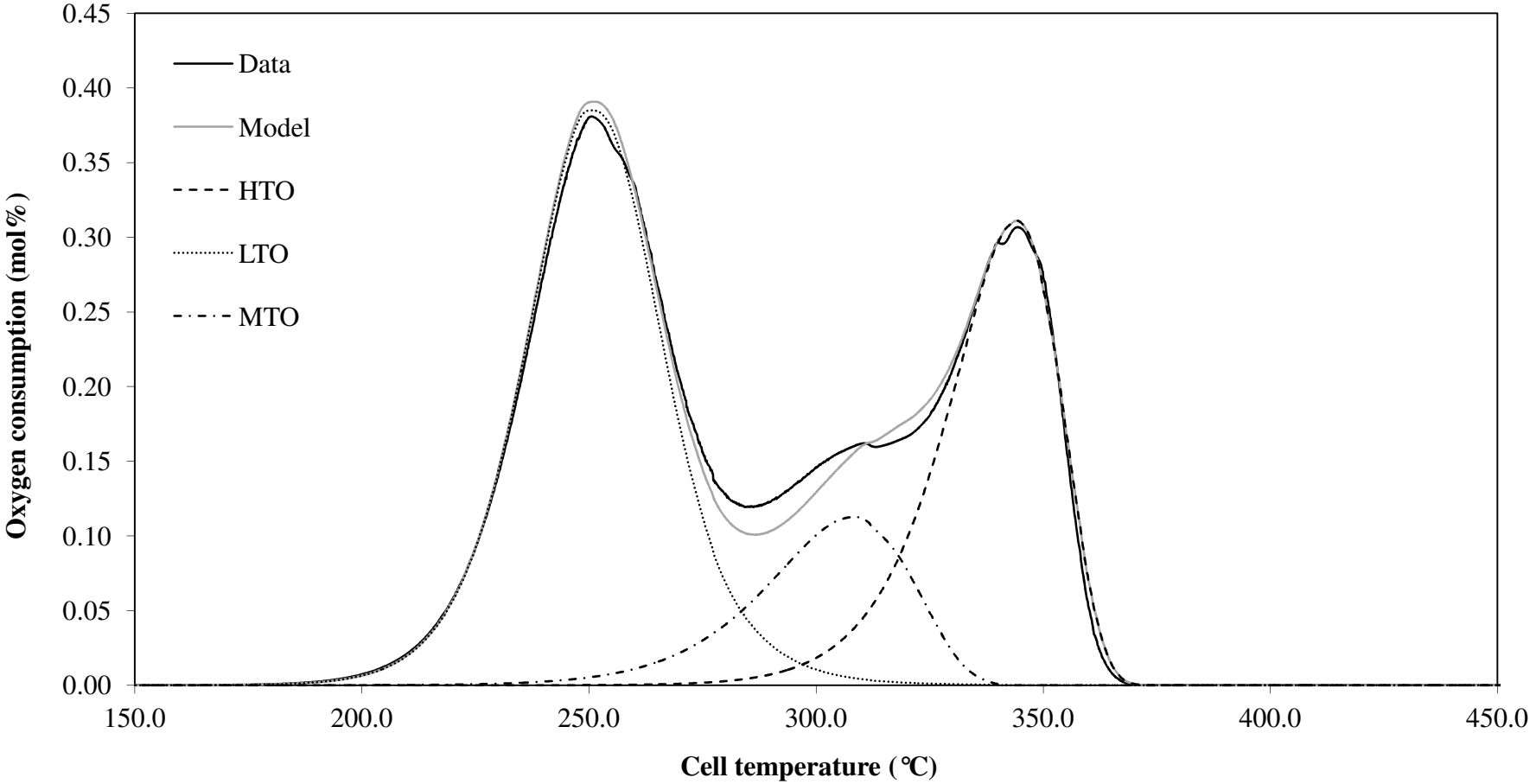

Figure 6.23 - Comparison of the oxygen consumption data and the model prediction with respects to the cell temperature for the oxidation of palm fibre with air as the oxidising gas, an absolute total system pressure of 500kPa, an air flow rate of 400smL/min and a heating rate of 30°C/h (Experiment F8).

The calculated variance for both samples was 0.0001. As observed in Figures 6.22 and 6.23, the discrepancy observed at the medium temperature range for both samples due to the overlapping of the MTO, LTO and HTO reactions.

Considering Table 6.4 for experiments F4 to F8, there are no significant differences in the calculated kinetic parameter values as the heating rate reduced from 70°C/h to 30°C/h. The reaction order varied by 0.01 for the HTO and LTO regimes and by 0.02 for the MTO regime. The variation in the activation energy and ln β were in the range of 0.6×10^3K to 0.8×10^3K and 0.6 to 0.8, respectively for all the reaction regimes. The differences are consistent with the level of accuracy shown in Table 6.4 for the kinetic parameters from three identical experiments. The heating rate was not expected to affect the kinetic parameters since the calculation procedure allows for changes in the heating rate. Kisler (1995) also reported a similar observation in his oxidation study of light Australian oils using an EGA experiments.

In summary, the heating rate of the combustion cell has a significant influence on the both peak temperatures and heights for all the exit gas composition curves. The peak temperatures and heights of the exit gas oxygen, carbon dioxide and carbon monoxide compositions increase with increasing heating rates. Further, there is no significant difference in the calculated kinetic parameters observed for the experimental runs conducted at the various heating rates. The differences are consistent with the level of accuracy of the palm fibre experiments. Thus, the values determined for the kinetics parameters of the proposed reaction model are found to be independent of the heat rate used in the experimental program.

6.5 Effect of the total system pressure

The influence of the total system pressure on the palm fibre combustion characteristics may be examined using an evolved gas analysis (EGA) experiments. A series of EGA experiments (F6, F9 to F13, F18 to F19) were conducted to determine the influences of the pressure on the combustion characteristics. In this series of EGA experimental runs, the absolute total system pressure was varied from 200kPa to 700kP with various

oxygen concentrations in the feed gas. The details of the experimental conditions are provided in Table 6.1. Note that the absolute pressures that could be used were limited by the design of the experimental rig to below 900kPa.

Experiments F6, F9 to F13, F18 to F19 were performed at the various total system pressures and oxygen concentrations in the feed gas with a heating rate of 50°C/h and a flow rate of 400smL/min. The experimental results of these runs are presented in Table 6.3. The variation in the exit gas compositions with respect to the cell temperature for experiment F6 is shown in Figure 6.3 and discussed in detail in Section 6.2.

Figures 6.24 to 6.30 plot the change in the exit gas composition with respect to the cell temperature for the experiments F9 to F13 and F18 to F19, respectively. These figures show that they are two main peaks of the hemicellulose and the cellulose peaks. These features are similar to those observed for the typical palm fibre experiment F6. However, there are variations in the peak temperatures and heights between the experiments.

Figure 6.31 presents the effect of the total system pressure at the same oxygen partial pressure on the oxygen consumption of the palm fibre combustion characteristics. Figures 6.32 and 6.33 present the corresponding information for the carbon dioxide production and the carbon monoxide production curves. As observed in Figures 6.31 to 6.33, the peak temperatures decreased as the total system pressure increased from 200kPa to 700kPa. However, the peak heights show an opposing trends. The peak height increased as the total system pressure increased from 200kPa to 700kPa. Further, it may be seen that the peak temperatures for the exit gas oxygen, carbon dioxide and carbon monoxide composition curves were similar at the various total system pressures but at the same oxygen partial pressure. However, the peak heights of the three exit gas composition curves decreased as the total system pressure decreased at the same oxygen partial pressure.

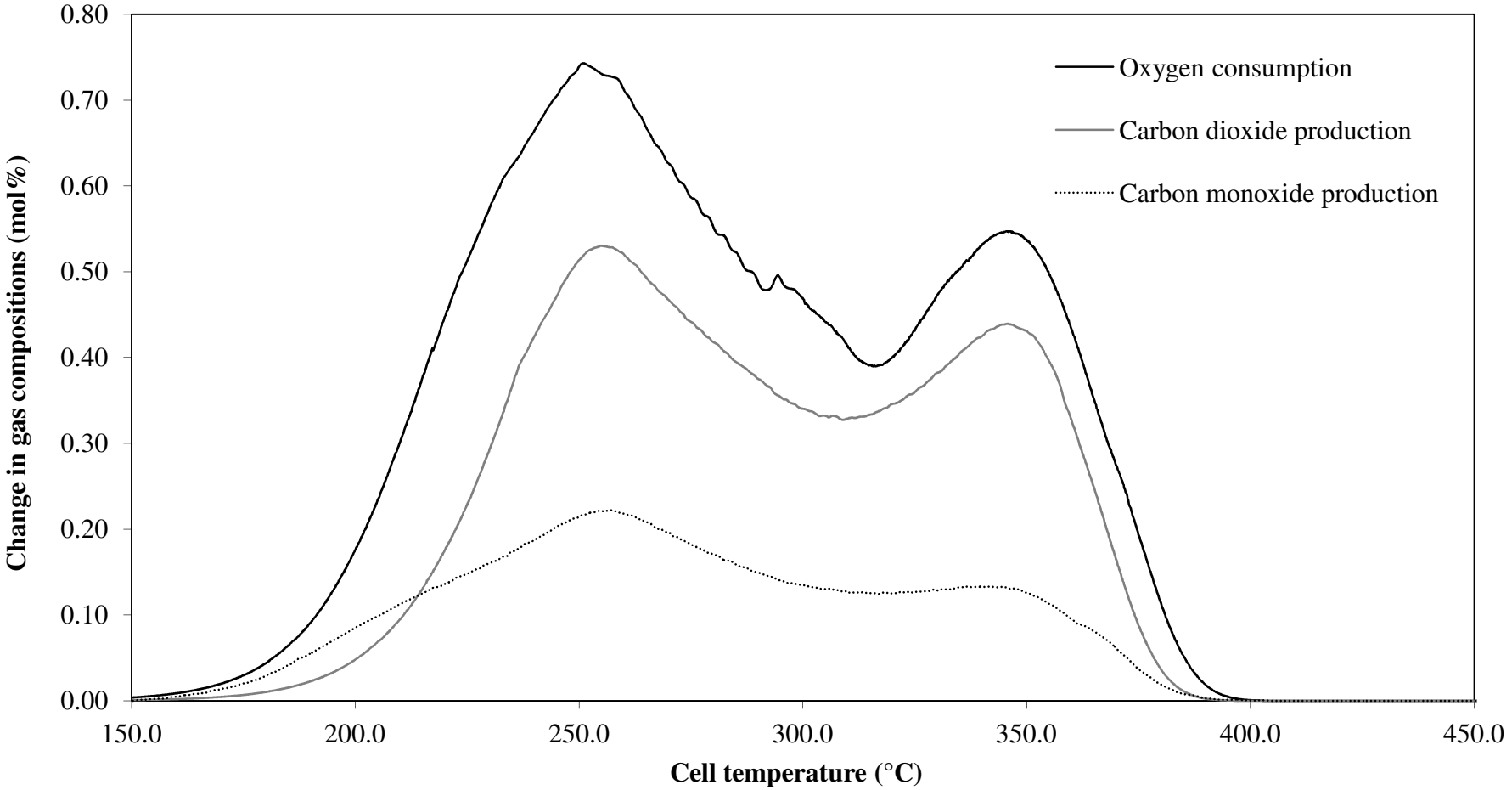

Figure 6.24 - Evolved gas analysis data with respects to the cell temperature for the oxidation of palm fibre with air as the oxidising gas, an absolute total system pressure of 700kPa, an air flow rate of 400smL/min and a heating rate of 50°C/h (Experiment F9).

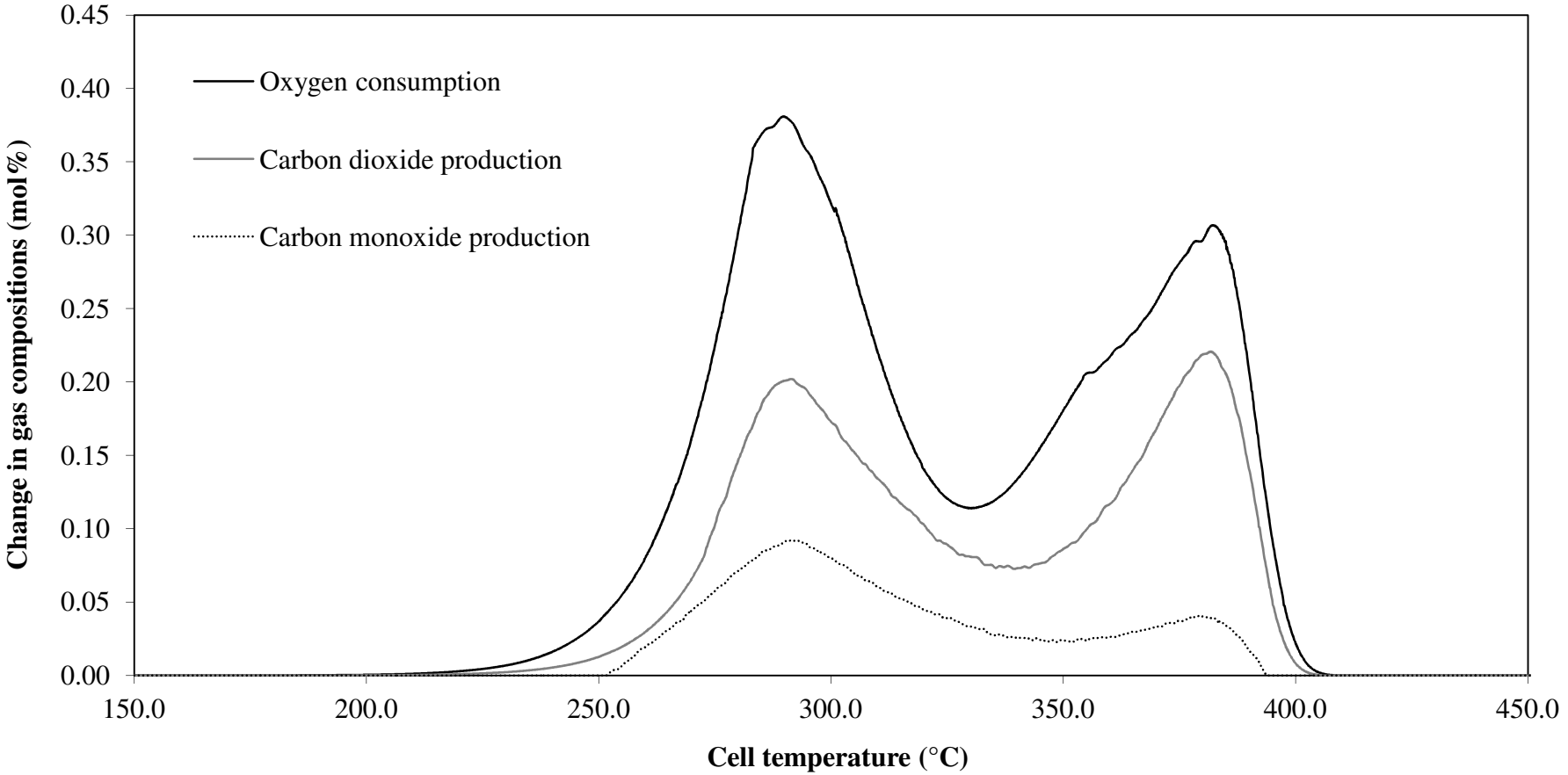

Figure 6.25 - Evolved gas analysis data with respects to the cell temperature for the oxidation of palm fibre with 18.10 mol% oxygen concentration in feed gas, an absolute total system pressure of 232kPa, an oxygen partial pressure of 42kPa, a flow rate of 400smL/min and a heating rate of 50°C/h (Experiment F10).

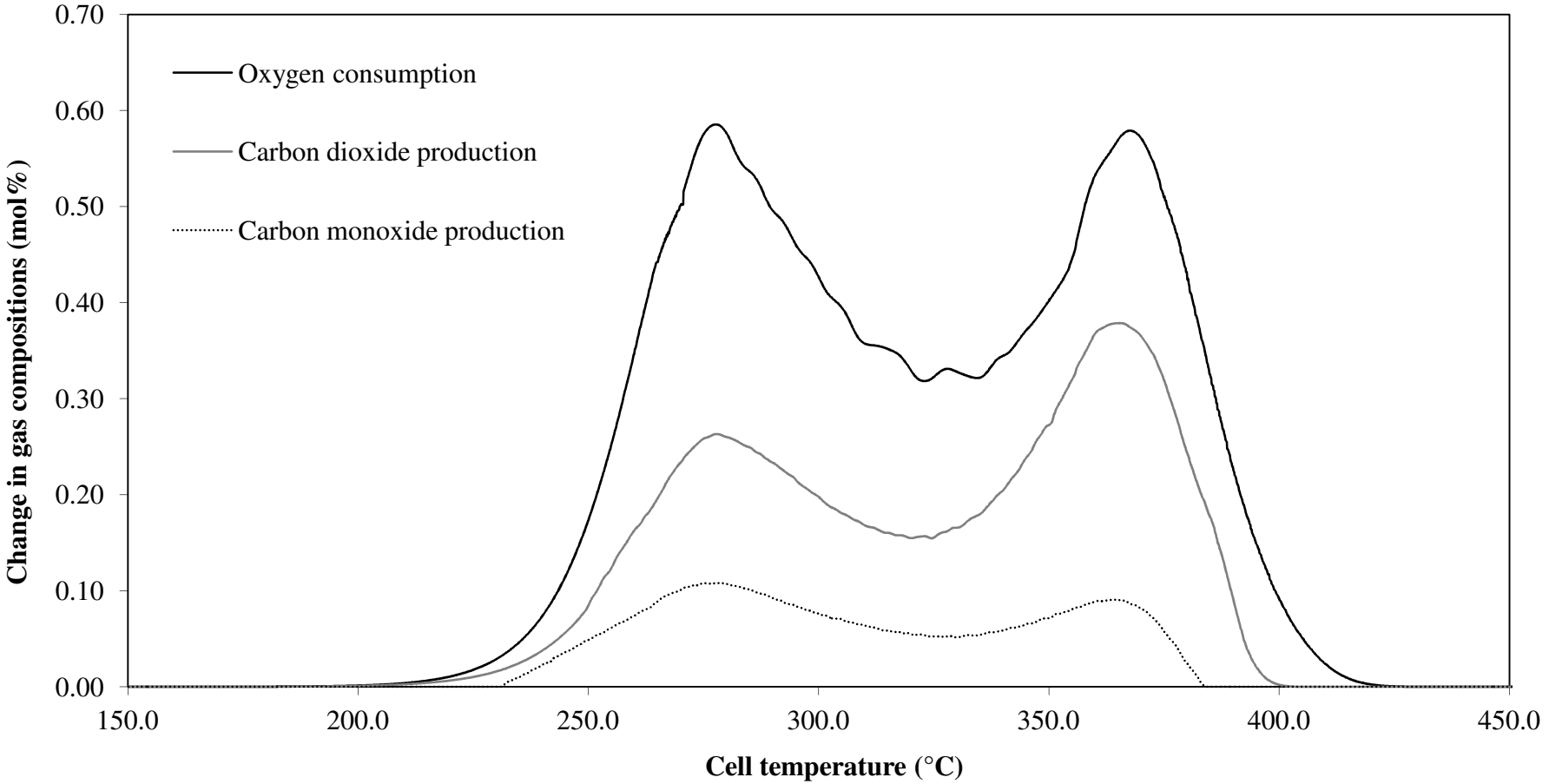

Figure 6.26 - Evolved gas analysis data with respects to the cell temperature for the oxidation of palm fibre with 15.10 mol% oxygen concentration in feed gas, an absolute total system pressure of 500kPa, an oxygen partial pressure of 76kPa, a flow rate of 400smL/min and a heating rate of 50°C/h (Experiment F11).

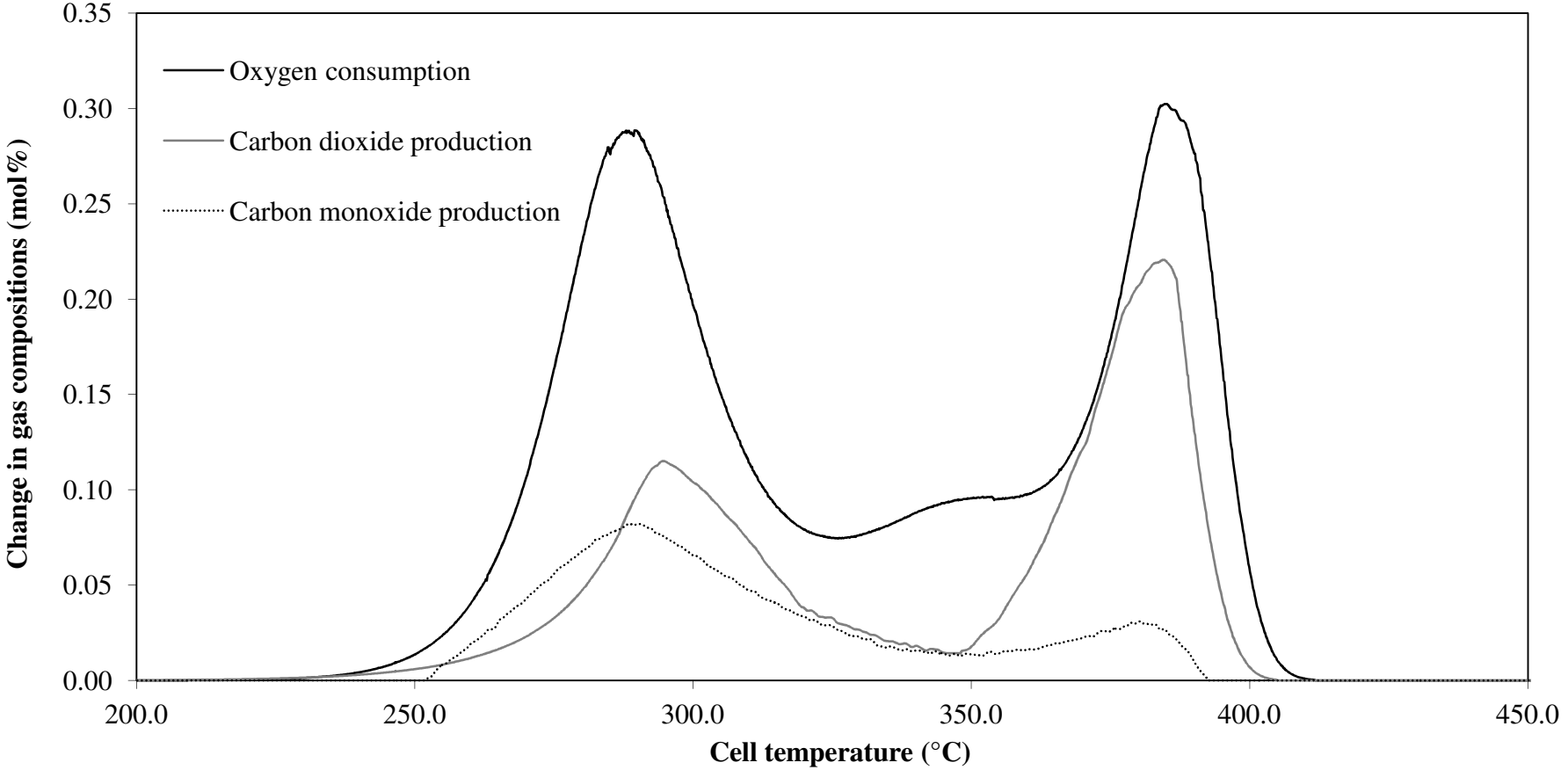

Figure 6.27 - Evolved gas analysis data with respects to the cell temperature for the oxidation of palm fibre with air as the oxidising gas, an absolute total system pressure of 200kPa, an air flow rate of 400smL/min and a heating rate of 50°C/h (Experiment F12).

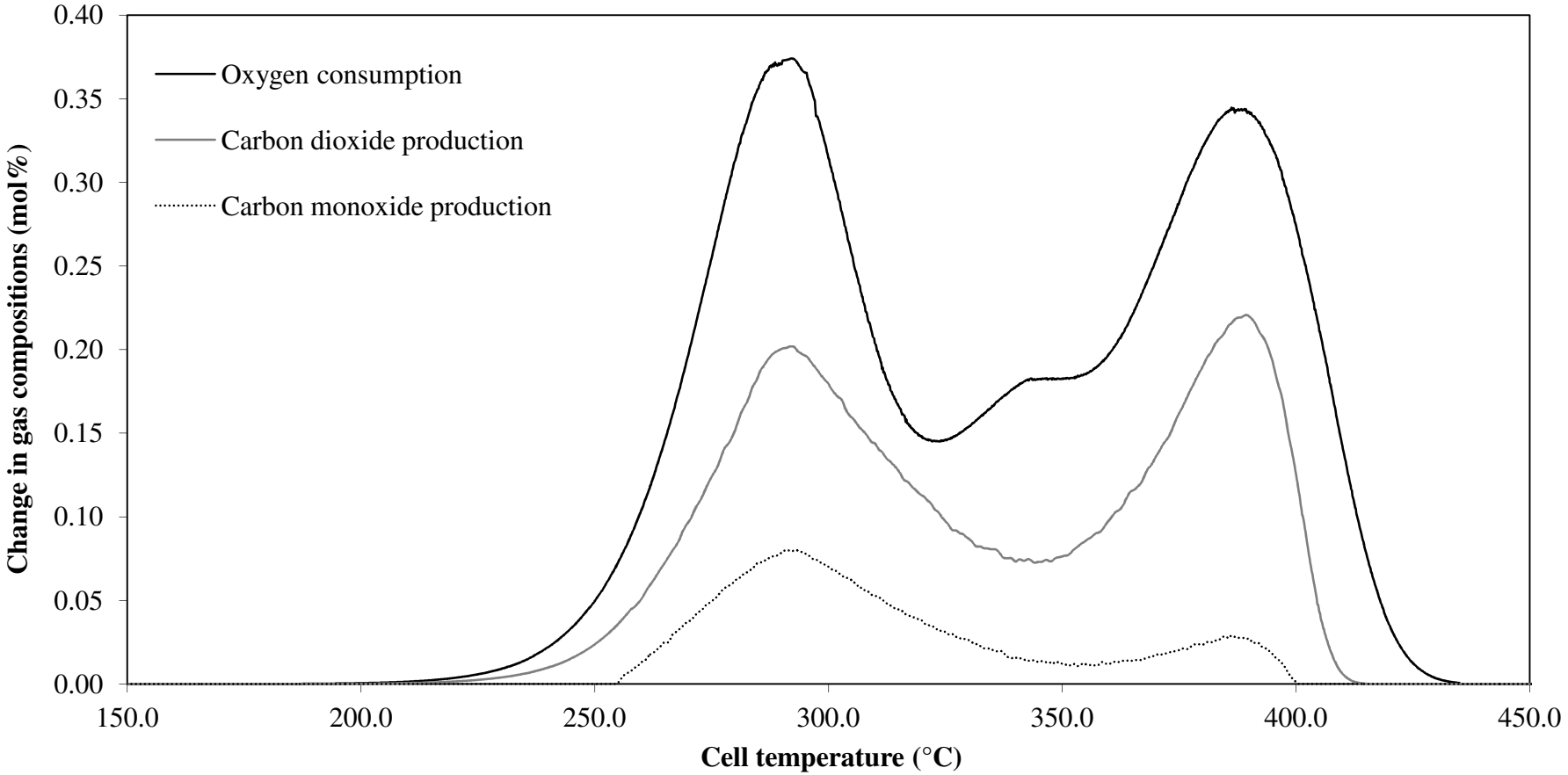

Figure 6.28 - Evolved gas analysis data with respects to the cell temperature for the oxidation of palm fibre with 15.10 mol% oxygen concentration in feed gas, an absolute total system pressure of 278kPa, an oxygen partial pressure of 42kPa, a flow rate of 400smL/min and a heating rate of 50°C/h (Experiment F13).

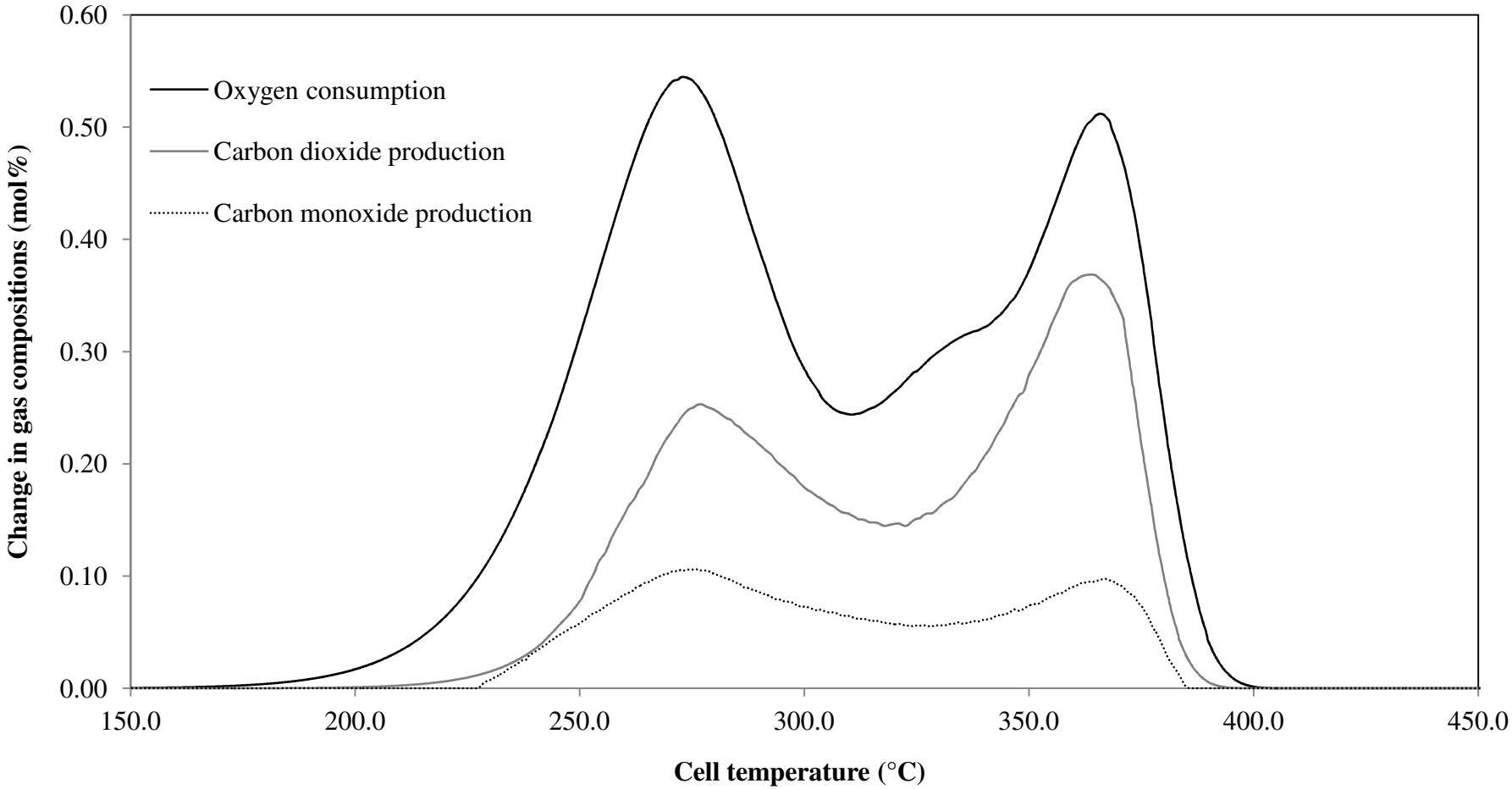

Figure 6.29 - Evolved gas analysis data with respects to the cell temperature for the oxidation of palm fibre with 18.10 mol% oxygen concentration in feed gas, an absolute total system pressure of 420kPa, an oxygen partial pressure of 76kPa, a flow rate of 400smL/min and a heating rate of 50°C/h (Experiment F18).

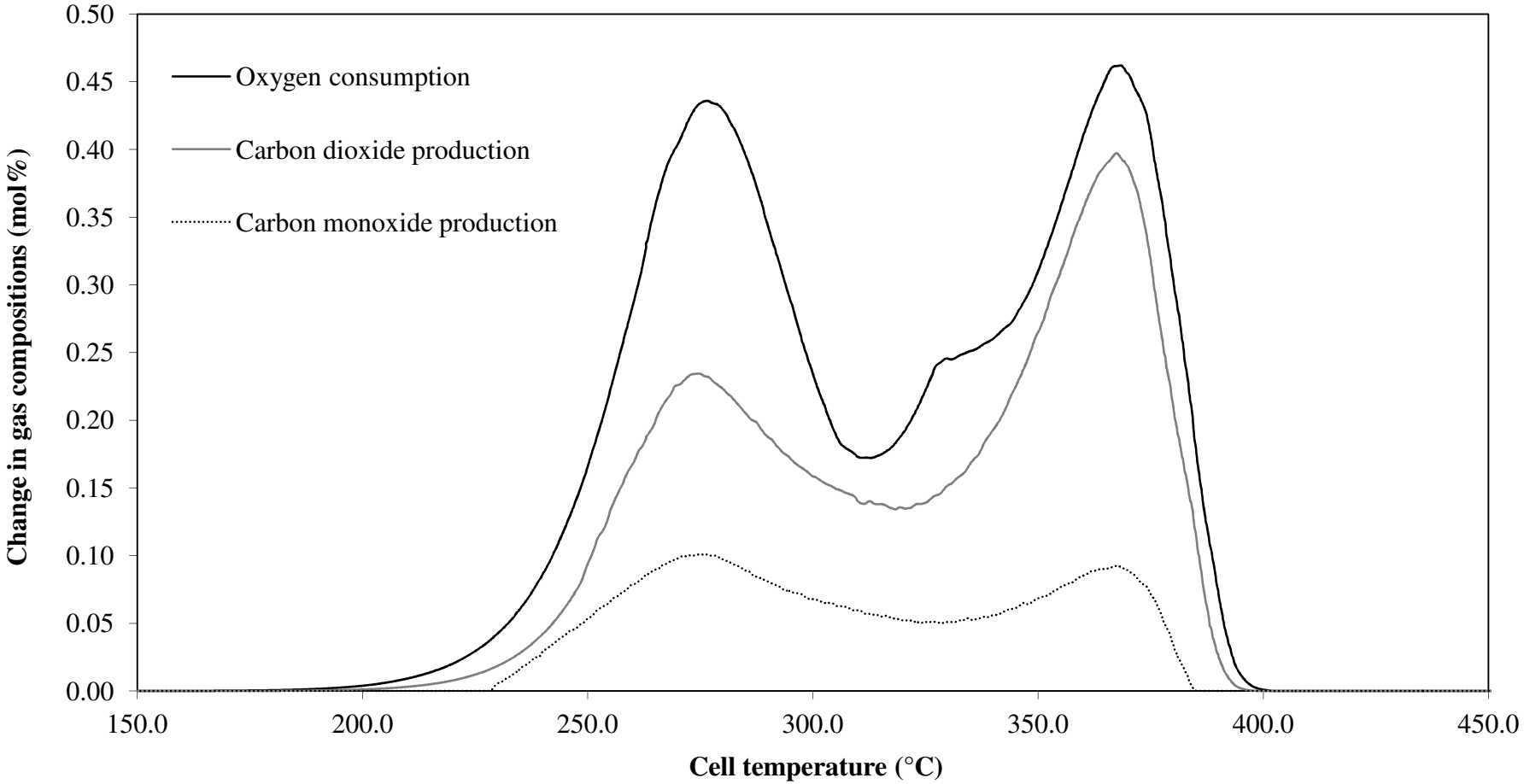

Figure 6.30 - Evolved gas analysis data with respects to the cell temperature for the oxidation of palm fibre with air as the oxidising gas, an absolute total system pressure of 362kPa, an air flow rate of 400smL/min and a heating rate of 50°C/h (Experiment F19).

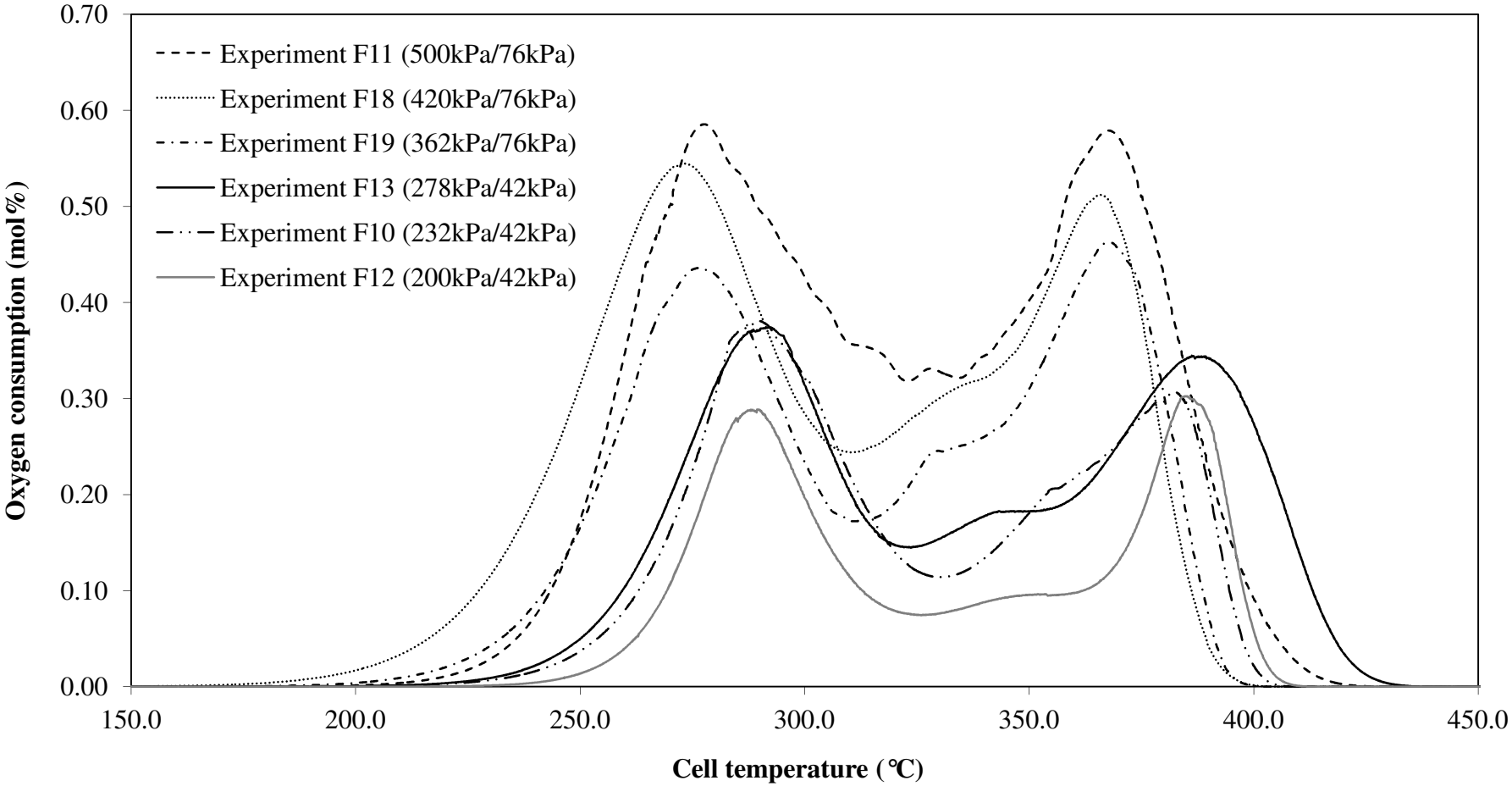

Figure 6.31 - Comparison of the oxygen consumption data with respects to the cell temperature for various system and oxygen partial pressures conducted at heating rate of 50°C/h and gas flow rate of 400smL/min. The pressures shown refer to the absolute total system pressure and oxygen partial pressure, respectively.

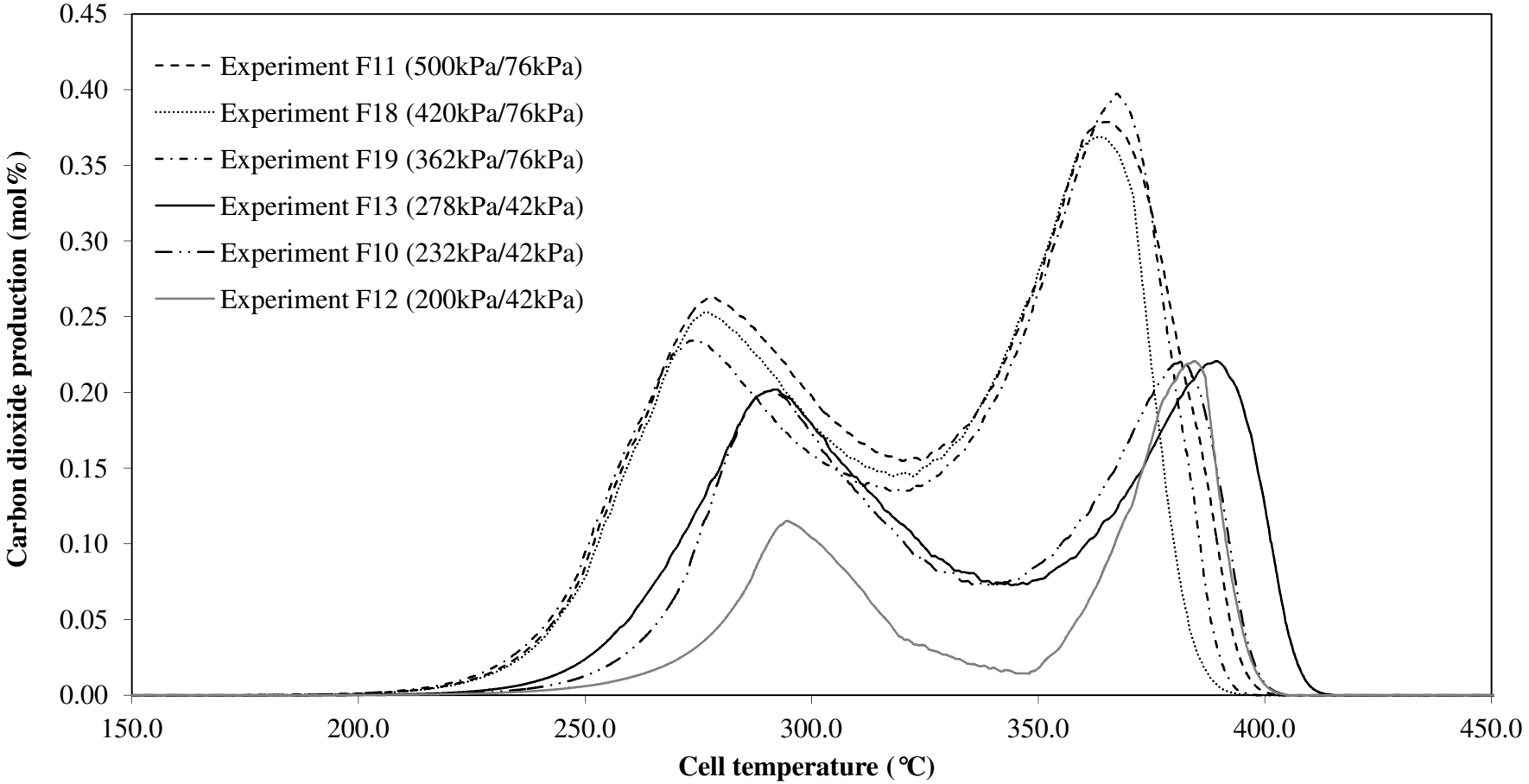

Figure 6.32 - Comparison of the carbon dioxide production data with respects to the cell temperature for various system and oxygen partial pressures conducted at heating rate of 50°C/h and gas flow rate of 400smL/min. The pressures shown refer to the absolute total system pressure and oxygen partial pressure, respectively.

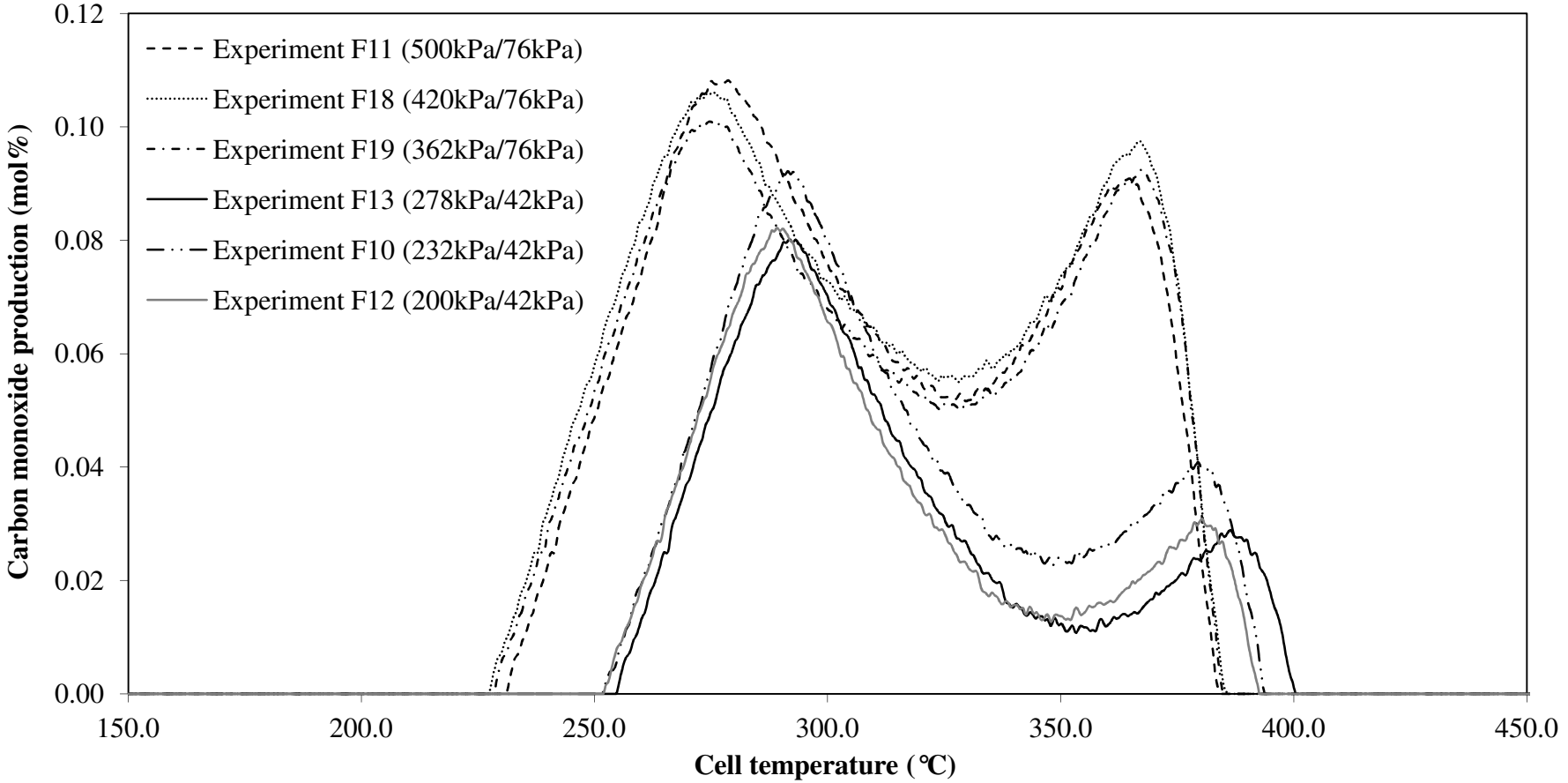

Figure 6.33 - Comparison of the carbon monoxide production data with respects to the cell temperature for various system and oxygen partial pressures conducted at heating rate of 50°C/h and gas flow rate of 400smL/min. The pressures shown refer to the absolute total system pressure and oxygen partial pressure, respectively.

Figure 6.34 presents the influence of the total system pressure at the same oxygen partial pressure on the hemicellulose peak temperatures and heights of the oxygen consumption curve. Figure 6.35 shows the corresponding information for the cellulose peak temperatures and heights. Figure 6.36 and 6.37 show the influences of the total system pressure at the same oxygen partial pressure on the hemicellulose and cellulose peak temperatures for the both carbon oxides, respectively.

Considering Figure 6.34, the hemicellulose peak temperature decreased with increasing pressure. However, at the various total system pressures but at the same oxygen partial pressure (experiments F10, F12 and F13 conducted at the oxygen partial pressure of 42kPa; experiments F11, F18 and F19 conducted at the oxygen partial pressure of 76kPa), there are no significant differences in the hemicellulose peak temperatures of the oxygen consumption. However, the hemicellulose peak height increased with increasing pressure.

Likewise, as observed in Figures 6.36 and 6.37, there is no significant difference observed for the hemicellulose and the cellulose peak temperatures for the both carbon oxides at the various total system pressures but at the same oxygen partial pressure. Hence, the peak temperatures for the exit gas oxygen, carbon dioxide and carbon monoxide composition curves was not affected by the total system pressure. However, the peak heights of the effluent gas oxygen, carbon dioxide and carbon monoxide curves increased with increasing total system pressure. This observation is in an agreement to the EGA experimental results reported for the rice husk combustion characteristics. The same observation is also reported by Nguyen (2005) in her oxidation study of Vietnamese crude oil. She reported that more oxygen consumption is observed at higher total system pressures. The heights of the oxygen consumption peaks depend considerably on the total system pressure. In this study, it is believed that the pressure actually suppress the amount of distillation hence more fuel remains for oxidation. Further, the external pressure has no influence to the decomposition of palm fibre which implies that internal mass transfer resistances are small.

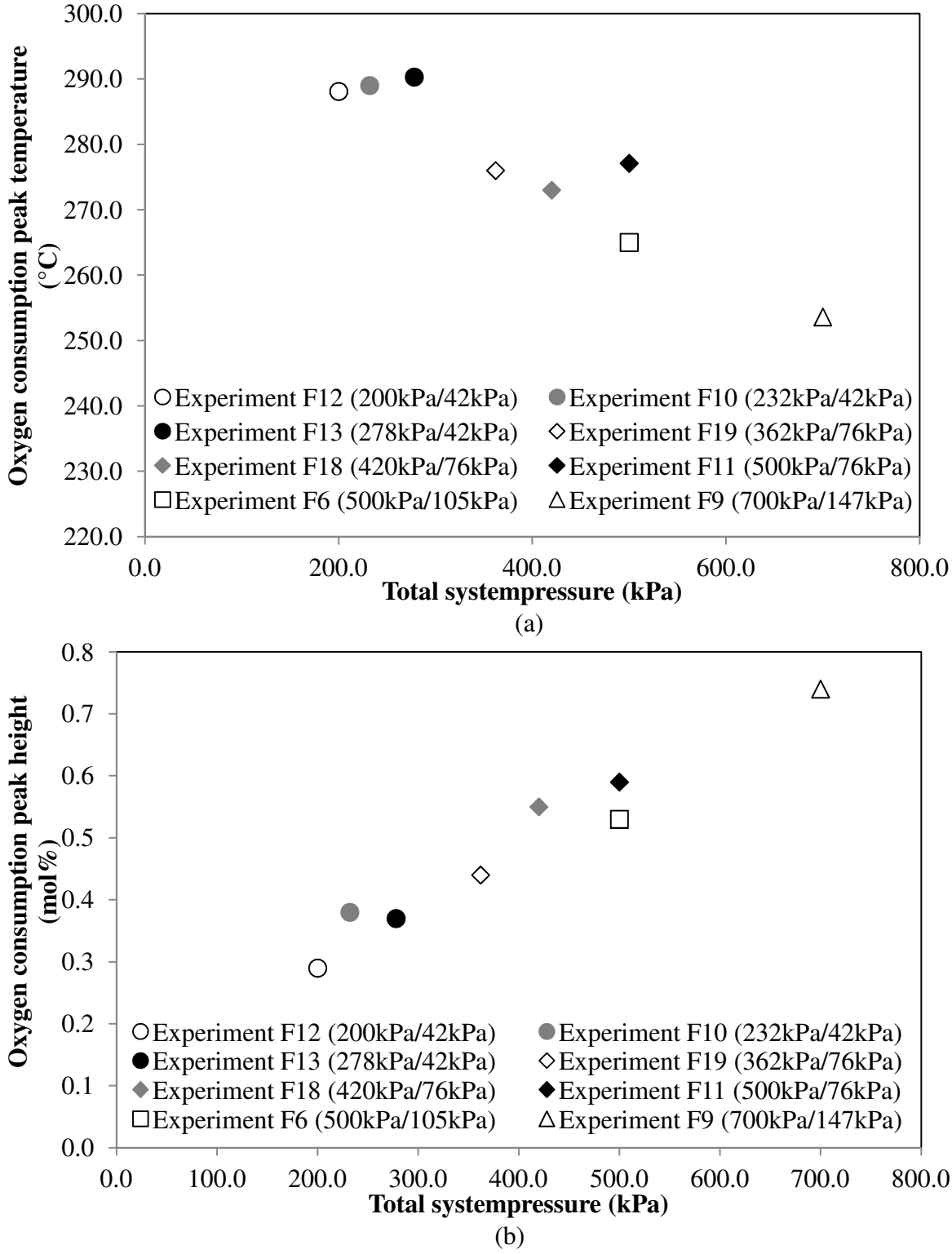

Figure 6.34 - Effect of the total system pressure of the hemicellulose (a) peak temperature (b) peak height of the oxygen consumption. The pressures shown refer to the absolute total system pressure and oxygen partial pressure, respectively.

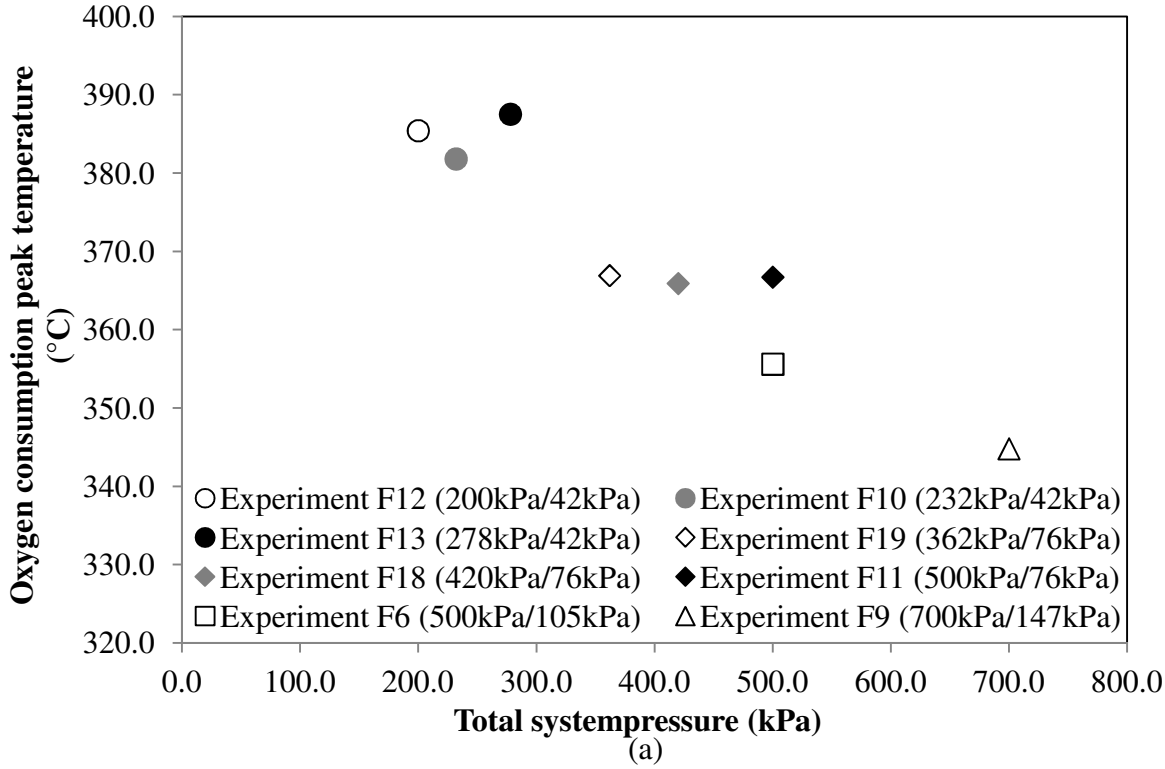

(a)

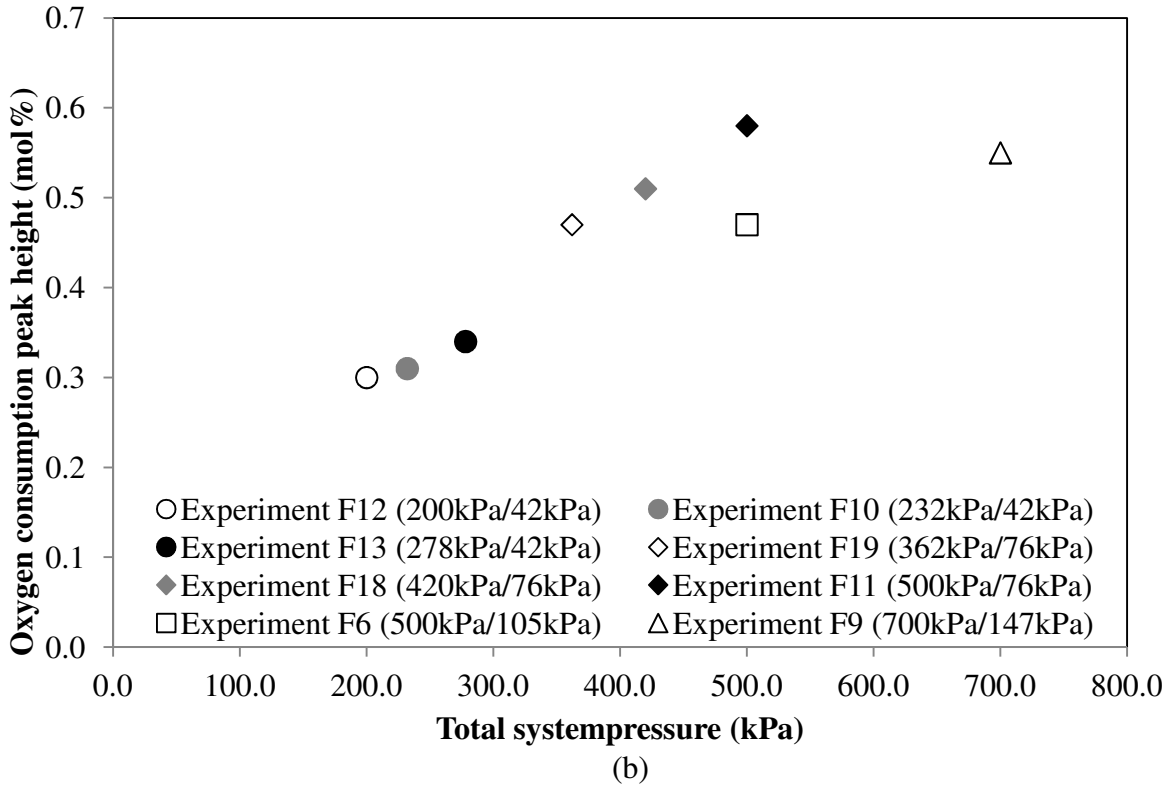

(b)

Figure 6.35 - Effect of the total system pressure of the cellulose (a) peak temperature (b) peak height of the oxygen consumption. The pressures shown refer to the total system pressure and the oxygen partial pressure, respectively.

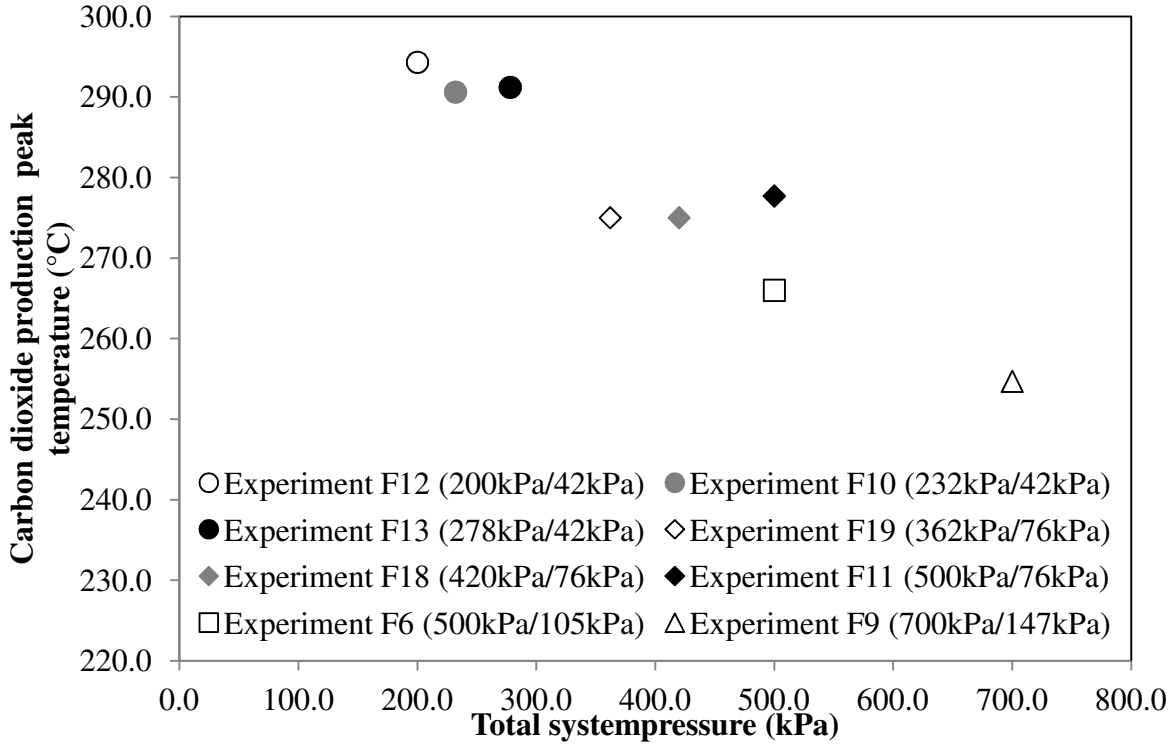

(a)

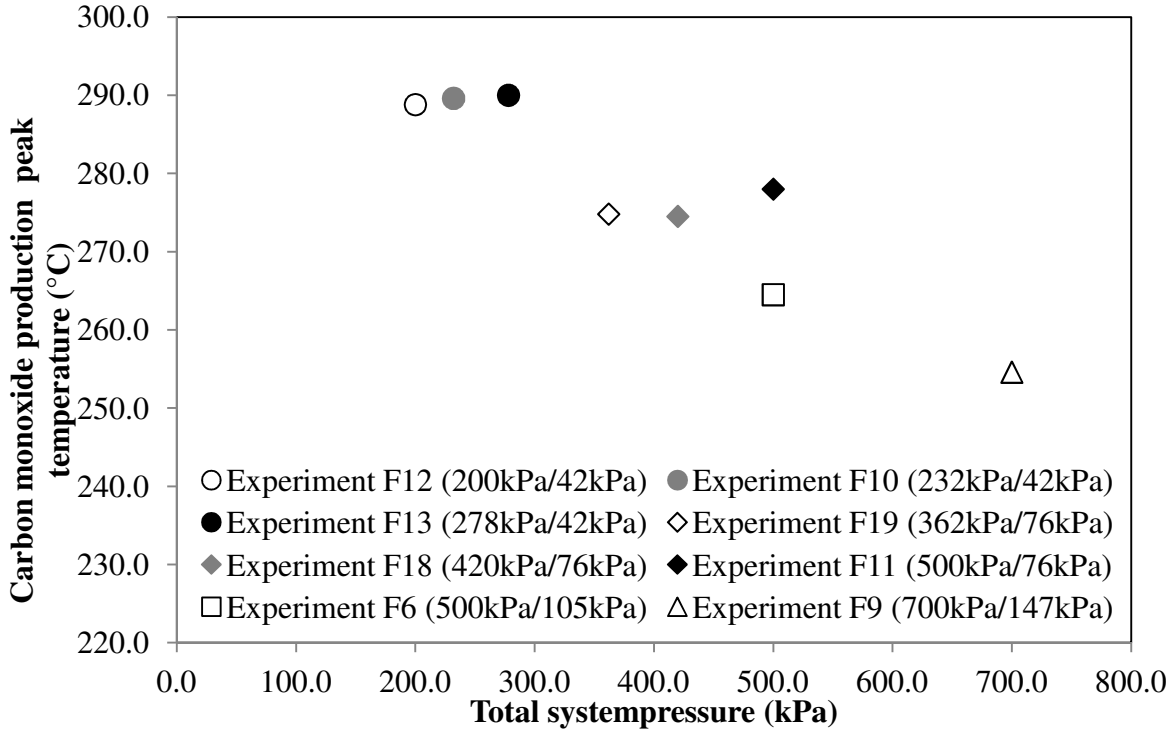

(b)

Figure 6.36 - Effect of the total system pressure on the hemicellulose peak temperatures of the (a) carbon dioxide production (b) carbon monoxide production. The pressure shown refer to the total pressure and the oxygen partial pressure.

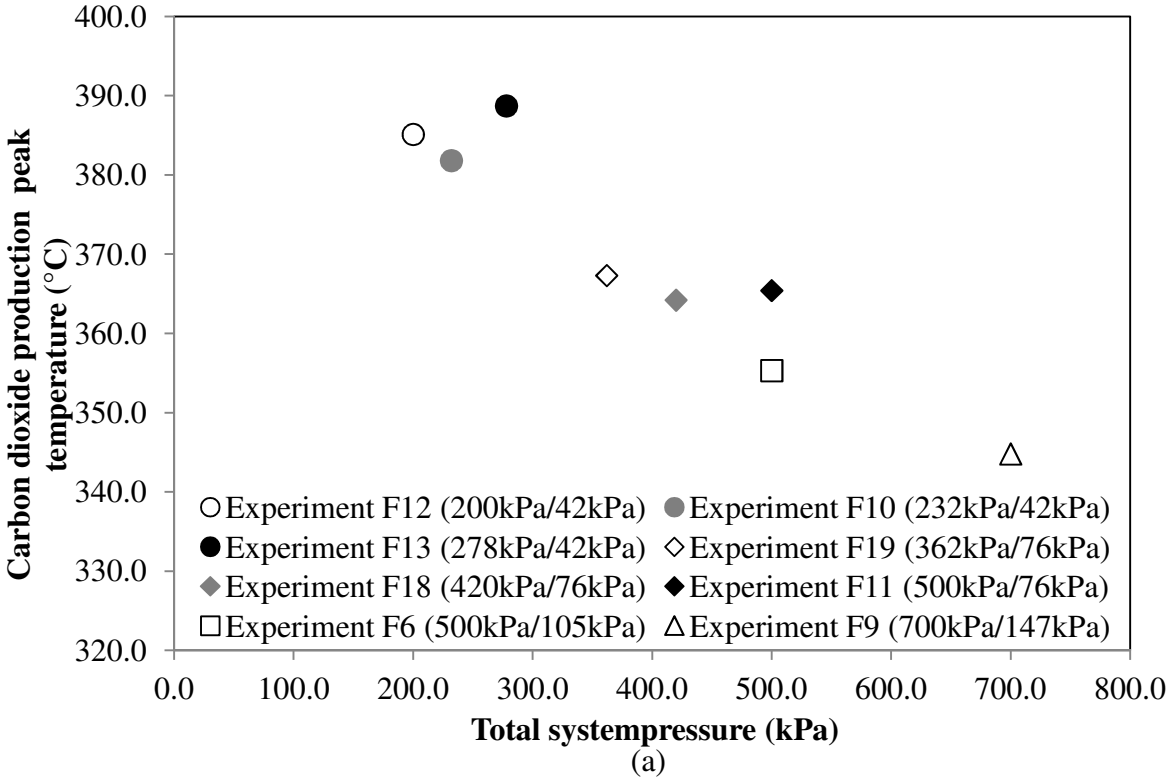

(a)

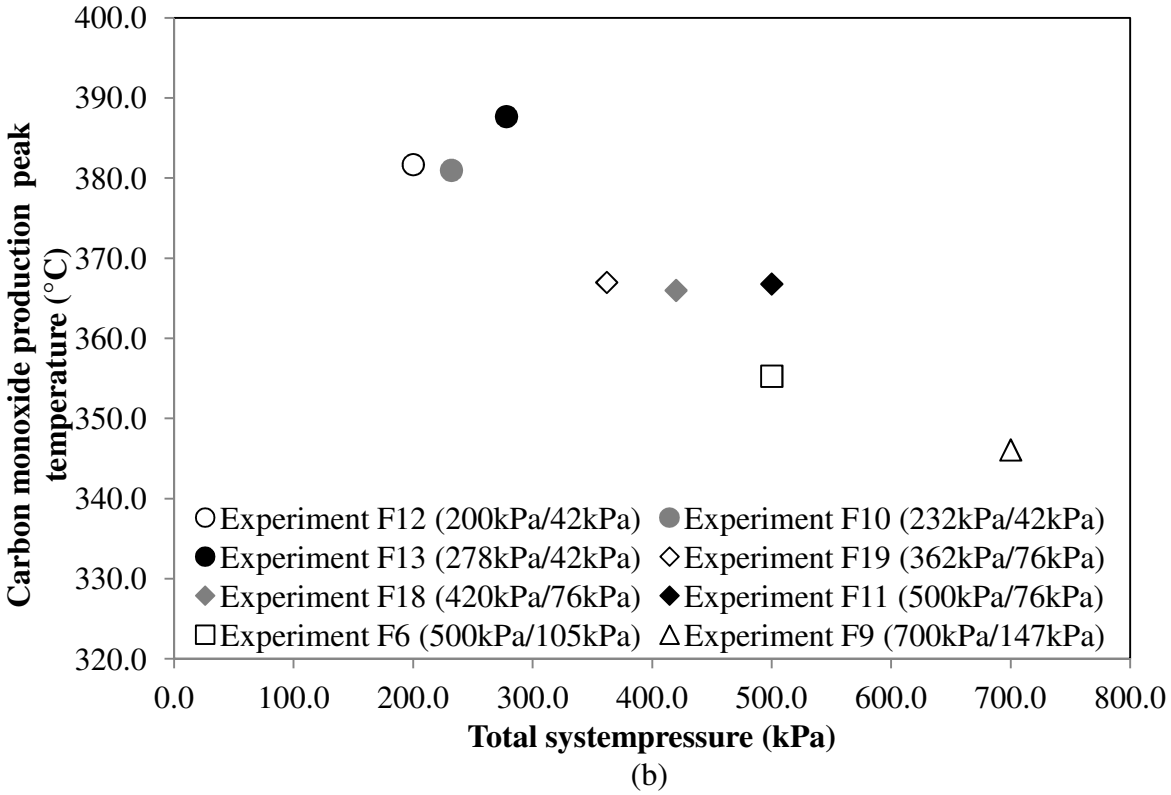

(b)

Figure 6.37 - Effect of the oxygen partial pressure on the cellulose peak temperatures of the (a) carbon dioxide production (b) carbon monoxide production. The pressure shown refer to the total pressure and the oxygen partial pressure.

The calculated kinetic parameters of experiments F6, F9 to F13 and experiments F18 to F19 are presented in Table 6.4. The comparison of the model prediction and the actual oxygen consumption data of experiment F6 was previously shown in Figure 6.9 and discussed in Section 6.2. Figures 6.38 to 6.44 plot the oxygen consumption data and the model prediction of experiments F9 to F13 and experiments F18 to F19, respectively.

Considering Table 6.4 and Figures 6.38 to 6.44, all experiments except for the experiment F11 show a good fit between the predicted curve and the actual oxygen consumption experimental data at various pressures. The variance was calculated to be below 0.001 for all these experiments except for the experiment F11. Experiment F11 displays an acceptable fit between the predicted curve with the actual oxygen consumption experimental data with the calculated variance of 0.0013. Most of the discrepancies were observed at the medium temperature range due to the overlapping of the MTO, LTO and HTO reactions. The discrepancy was also mostly observed at the LTO reaction. The disagreement for the LTO reaction was due to the poor match of the experimental data since the gas analysis results are most accurate at higher temperature. As for the experiment F11, the discrepancies were more obvious observed at the medium temperature range and at the low temperature range as the other experiments. Apart from that, the disagreement was also observed at the high temperature range of 340°C to 370°C. The predicted oxygen consumption curve for the HTO reaction for experiment F11 is broad compared to the actual experimental data at that temperature range. The error in the experimental data of experiment F11 was larger hence gives a poor match to the predicted model of oxygen consumption. Further, because of the heterogeneity of the palm fibre samples, it may be that the sample may be mixed with some kernel fragments.

Experiments F6, F9, F12 and F19 were conducted using air as the oxidising gas and at various absolute pressures ranging from 200kPa to 700kPa. Comparison of these samples over the calculated kinetic parameters determines the effect of pressure on the palm fibre combustion characteristics.

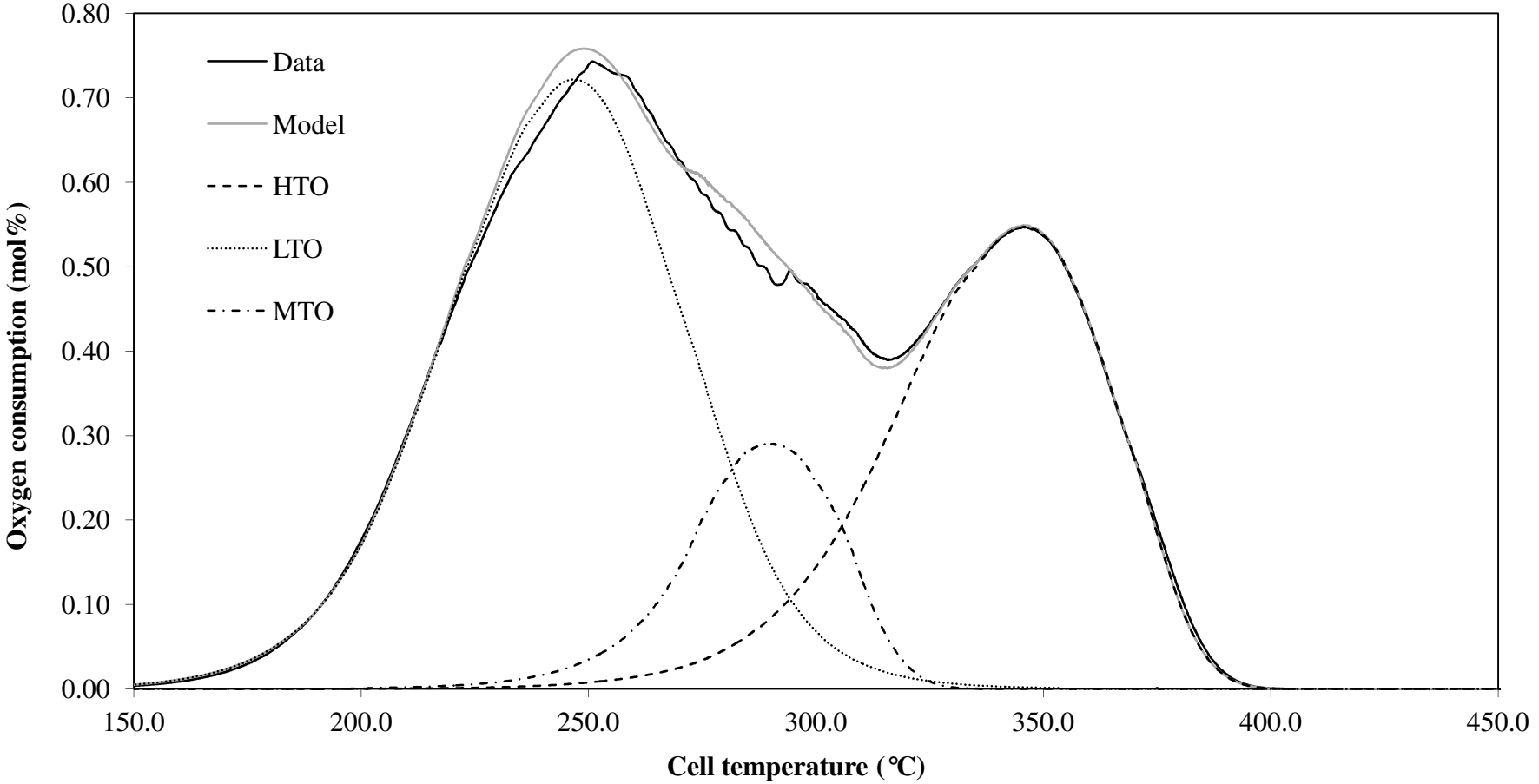

Figure 6.38 - Comparison of the oxygen consumption data and the model prediction with respects to the cell temperature for the oxidation of palm fibre with air as the oxidising gas, an absolute total system pressure of 700kPa, an air flow rate of 400smL/min and a heating rate of 50°C/h (Experiment F9).

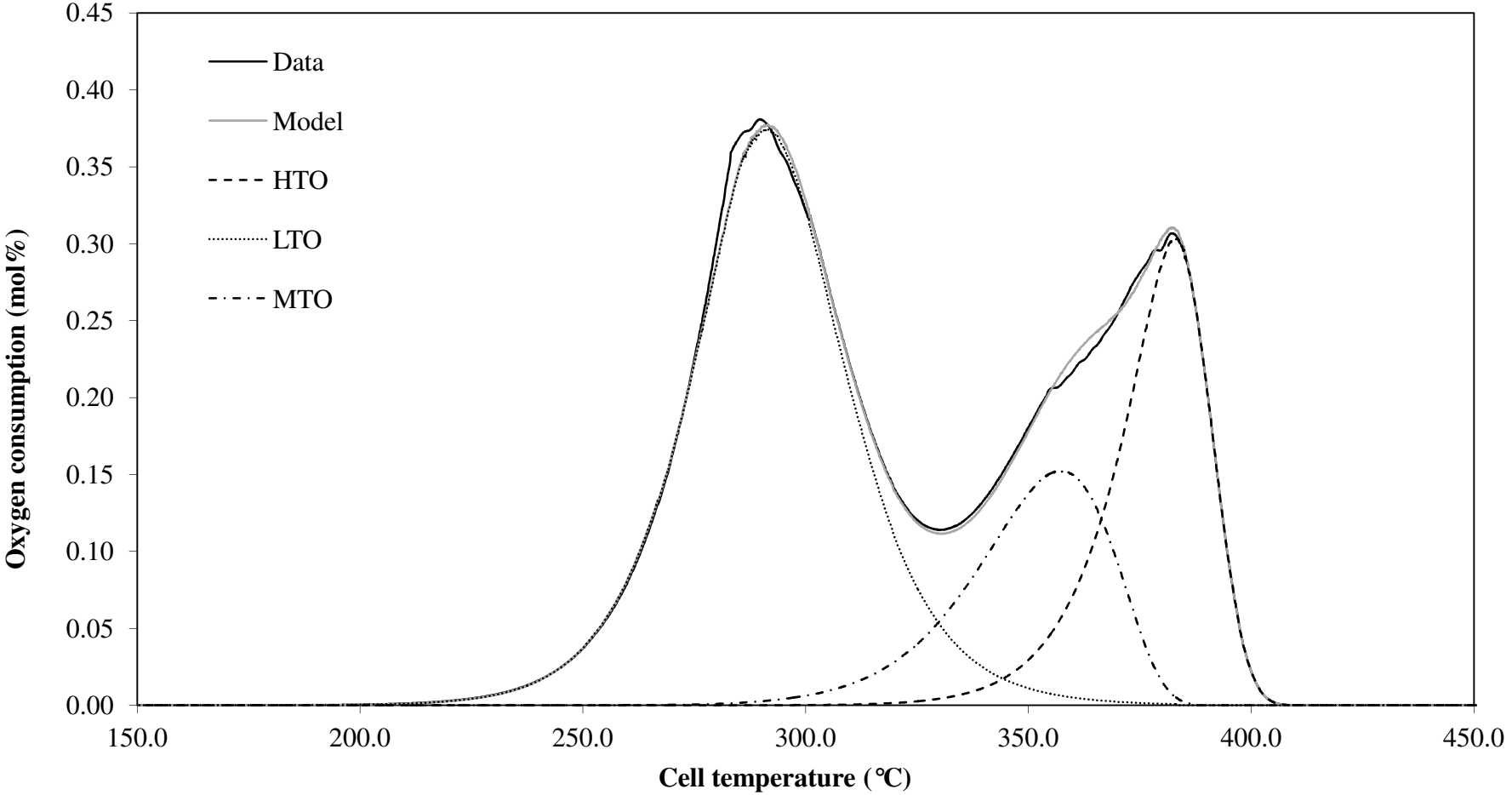

Figure 6.39 - Comparison of the oxygen consumption data and the model prediction with respects to the cell temperature for the oxidation of palm fibre with 18.10 mol% oxygen concentration in feed gas, an absolute total system pressure of 232kPa, an oxygen partial pressure of 42kPa, a flow rate of 400smL/min and a heating rate of 50°C/h (Experiment F10).

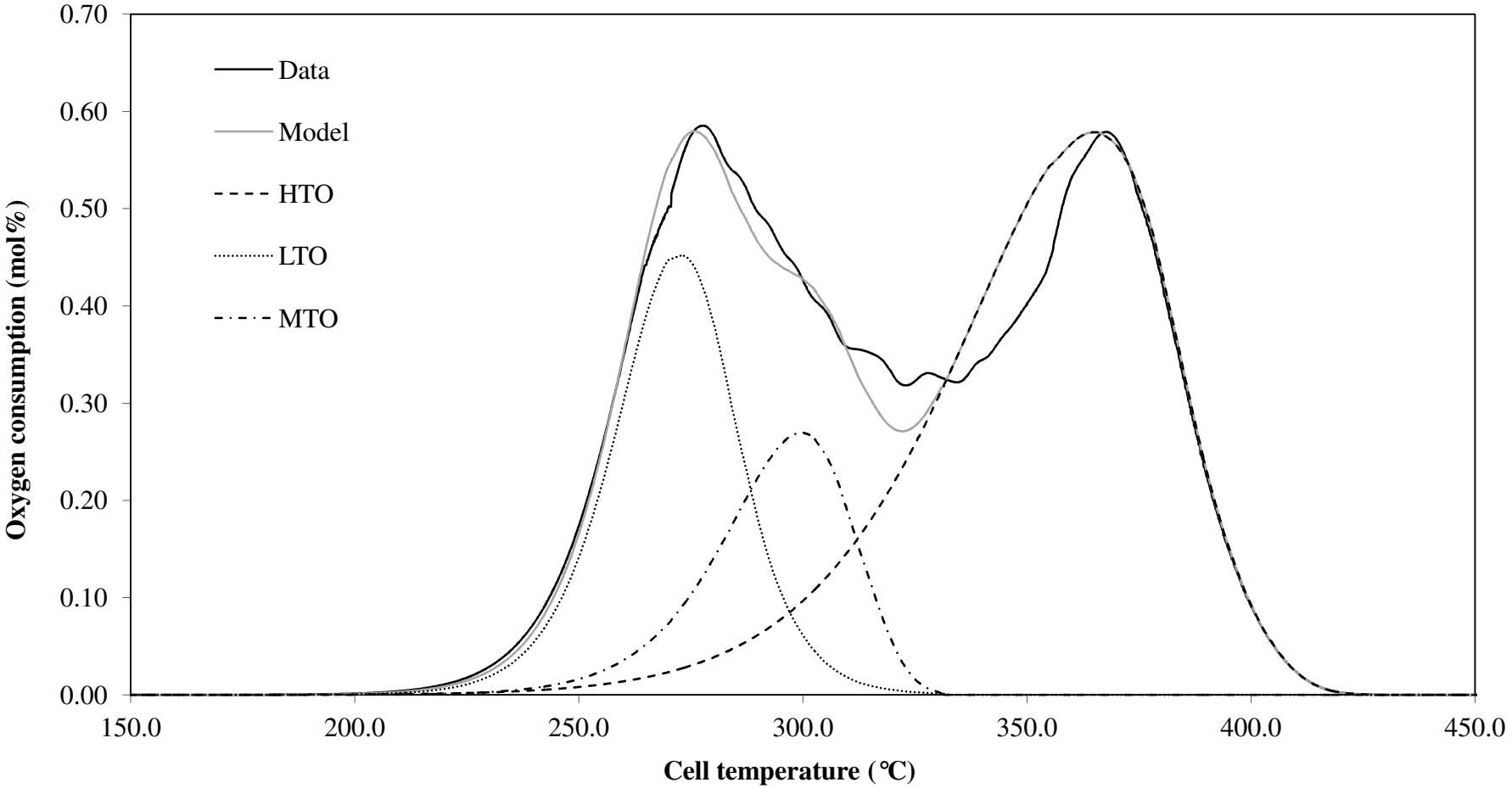

Figure 6.40 - Comparison of the oxygen consumption data and the model prediction with respects to the cell temperature for the oxidation of palm fibre with 15.10 mol% oxygen concentration in feed gas, an absolute total system pressure of 500kPa, an oxygen partial pressure of 76kPa, a flow rate of 400smL/min and a heating rate of 50°C/h (Experiment F11).

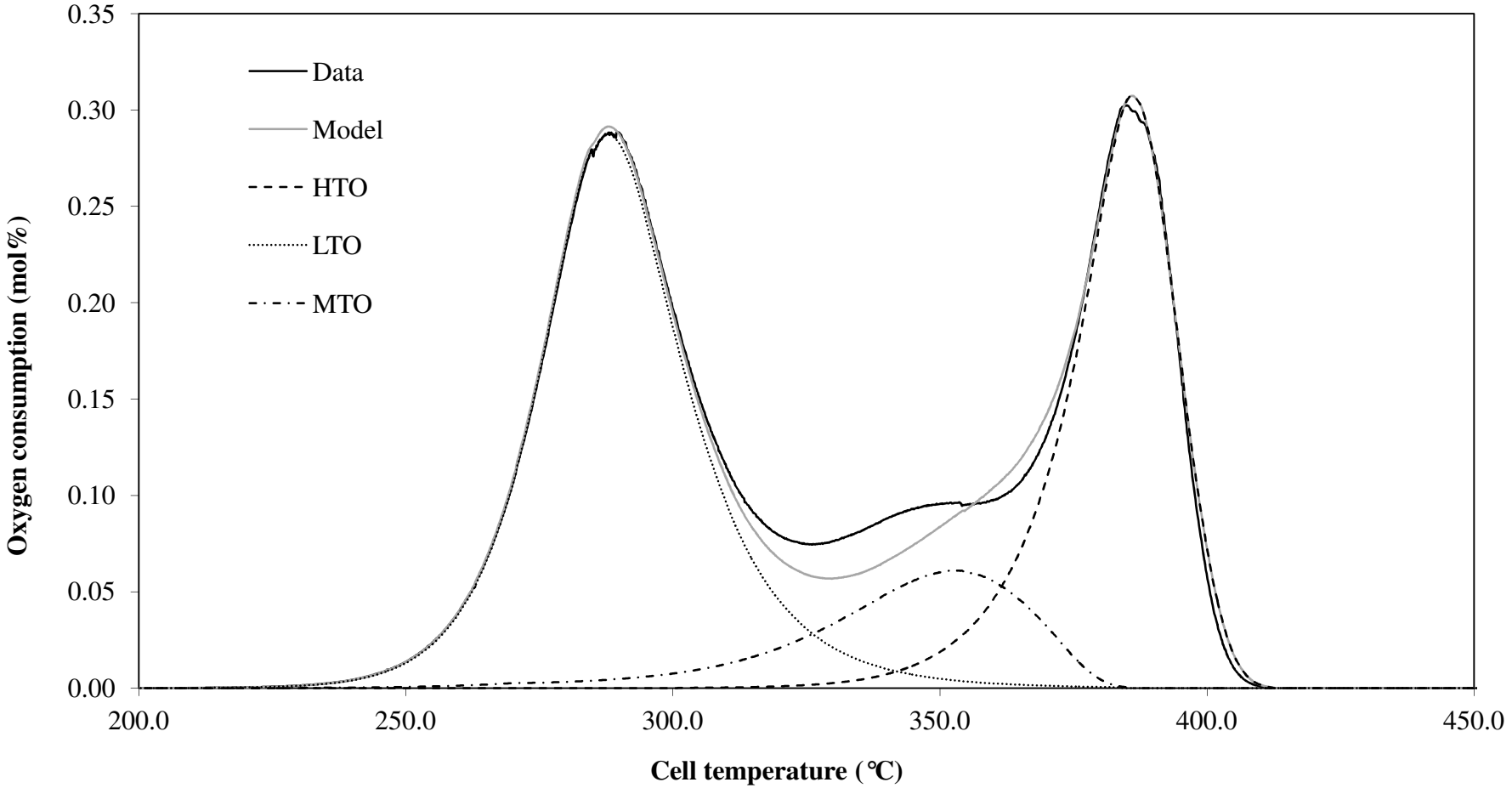

Figure 6.41 - Comparison of the oxygen consumption data and the model prediction with respects to the cell temperature for the oxidation of palm fibre with air as the oxidising gas, an absolute total system pressure of 200kPa, an air flow rate of 400smL/min and a heating rate of 50°C/h (Experiment F12).

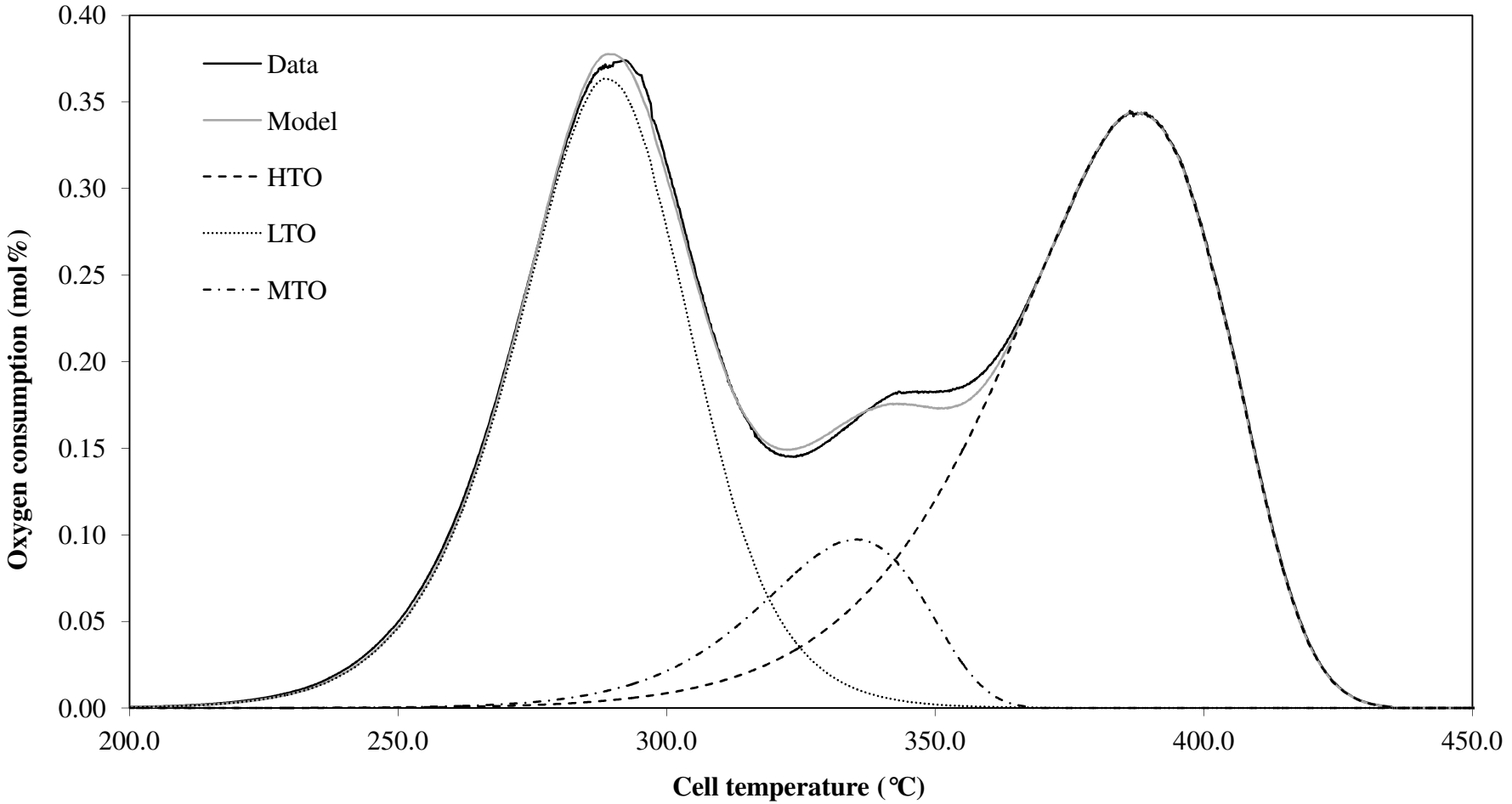

Figure 6.42 - Comparison of the oxygen consumption data and model prediction with respects to the cell temperature for the oxidation of palm fibre with 15.10 mol% oxygen concentration in feed gas, an absolute total system pressure of 278kPa, an oxygen partial pressure of 42kPa, a flow rate of 400smL/min and a heating rate of 50°C/h (Experiment F13).

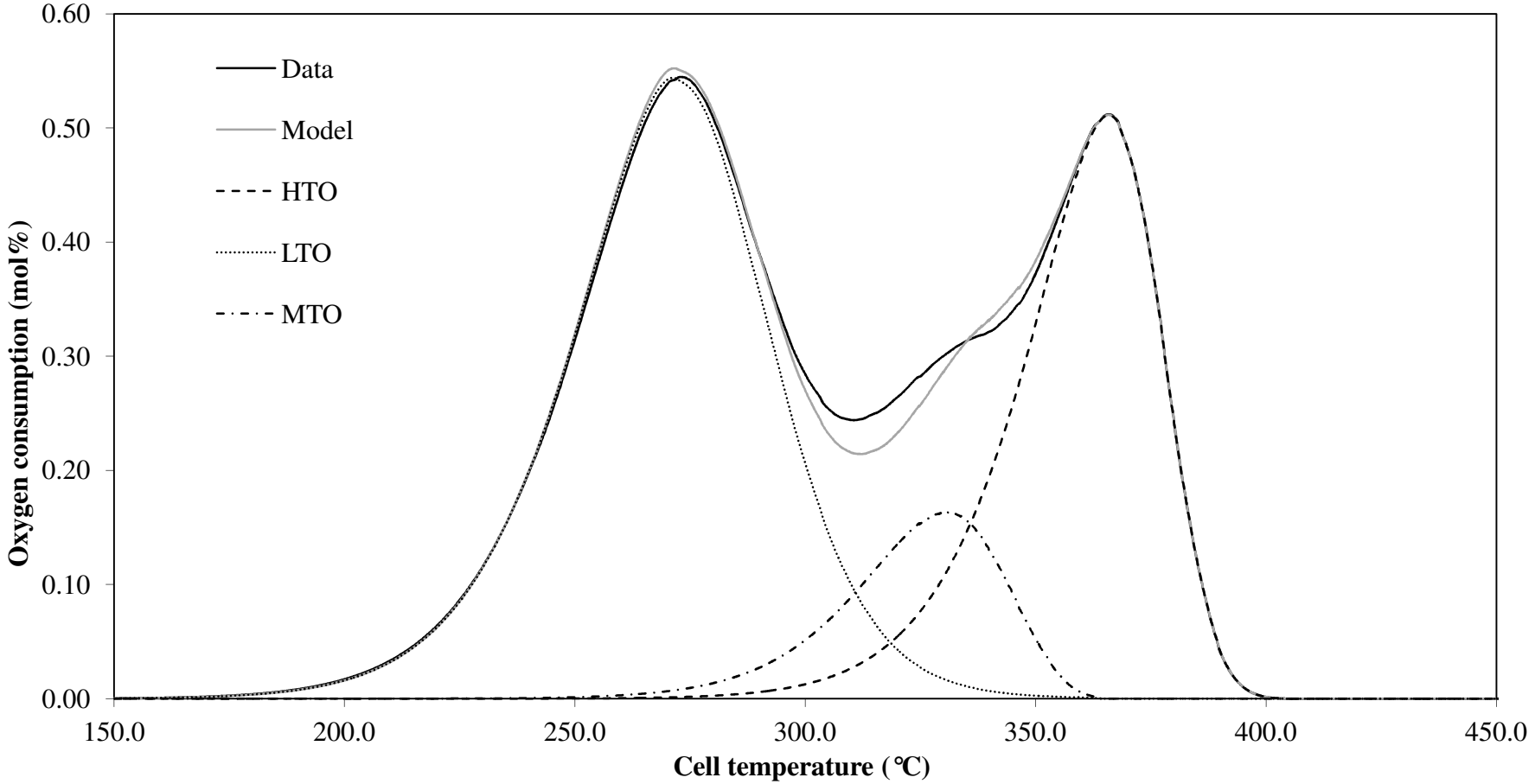

Figure 6.43 - Comparison of the oxygen consumption data and the model prediction with respects to the cell temperature for the oxidation of palm fibre with 18.10 mol% oxygen concentration in feed gas, an absolute total system pressure of 420kPa, an oxygen partial pressure of 76kPa, a flow rate of 400smL/min and a heating rate of 50°C/h (Experiment F18).

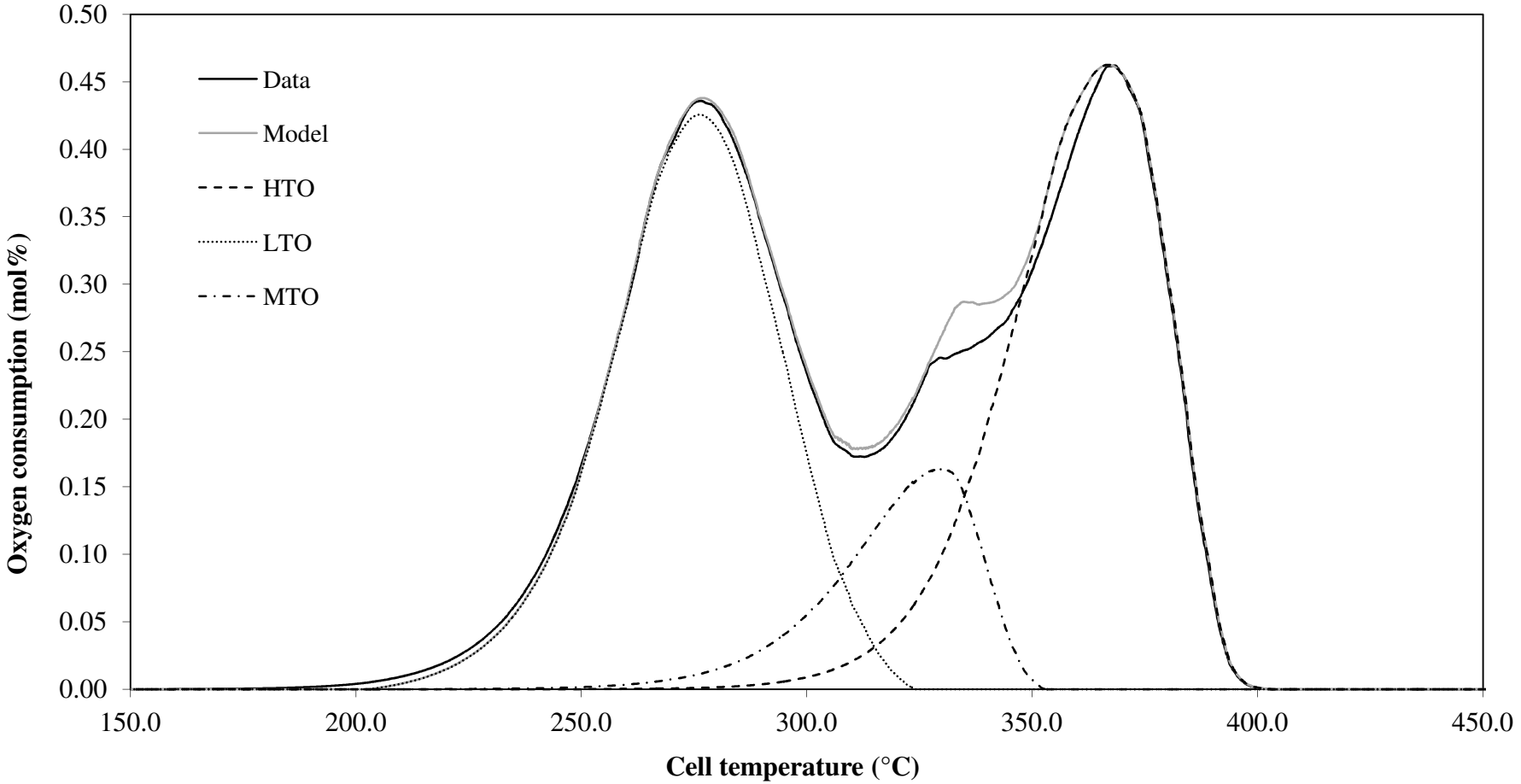

Figure 6.44 - Comparison of the oxygen consumption data and the model prediction with respects to the cell temperature for the oxidation of palm fibre with air as the oxidising gas, an absolute total system pressure of 362kPa, an air flow rate of 400smL/min and a heating rate of 50°C/h (Experiment F19).

As observed in Table 6.4, the activation energy for the high temperature oxidation (HTO) reaction reduced by 67.7% from 34.0 × 10^3K to 11.0 × 10^3K as the pressure increased from 200kPa to 700kPa. The ln β for the HTO reaction also reduced by 63.7% from 36.4 to 13.2 as the pressure increased. However, the reaction order of the HTO reaction displays an opposing trend. As the pressure increased from 200kPa to 700kPa, the reaction order increased by 0.06. A similar trend is observed for the medium temperature oxidation (MTO) and the low temperature oxidation (LTO) reactions. The activation energy decreases for the MTO and LTO reactions were in the range of 41% to 54% as the pressure increased from 200kPa to 700kPa. The ln β for the MTO and LTO reactions also recorded a reduction in the range of 38% to 56% as the pressure increased. Similarly, the reaction order of the MTO and LTO reactions was also increased as the pressure increased from 200kPa to 700kPa and was more obvious for the LTO reaction.

A comparison of experiments F9, F12 and F14 to F17 determines whether the total system pressure initiates the changes in the calculated kinetic parameters as the pressure increased from 200kPa to 700kPa. Experiments F10, F12 and F13 were conducted at the same oxygen partial pressure of 42kPa but at the various total system pressures. Experiments F11, F18 and F19 were performed at the various total system pressures but at the same oxygen partial pressure of 76kPa. Figures 6.45 to 6.47 present a plotted of the kinetic parameters of the activation energy (E/R) and the ln β with respect to the total system pressure for the HTO, LTO and MTO reactions, respectively.

By comparison of the experiments F10, F12 and F13 conducted at the same oxygen partial pressure of 42kPa but at the various total system pressures, there are no significant differences in the calculated kinetic parameters observed for the HTO, MTO and LTO reactions (see Figures 6.45 to 6.47). A comparison of the calculated kinetic parameters for the experiments F11, F18 and F19 conducted at the various total system pressures but at the same oxygen partial pressure of 76kPa shows that there are also no significant differences.

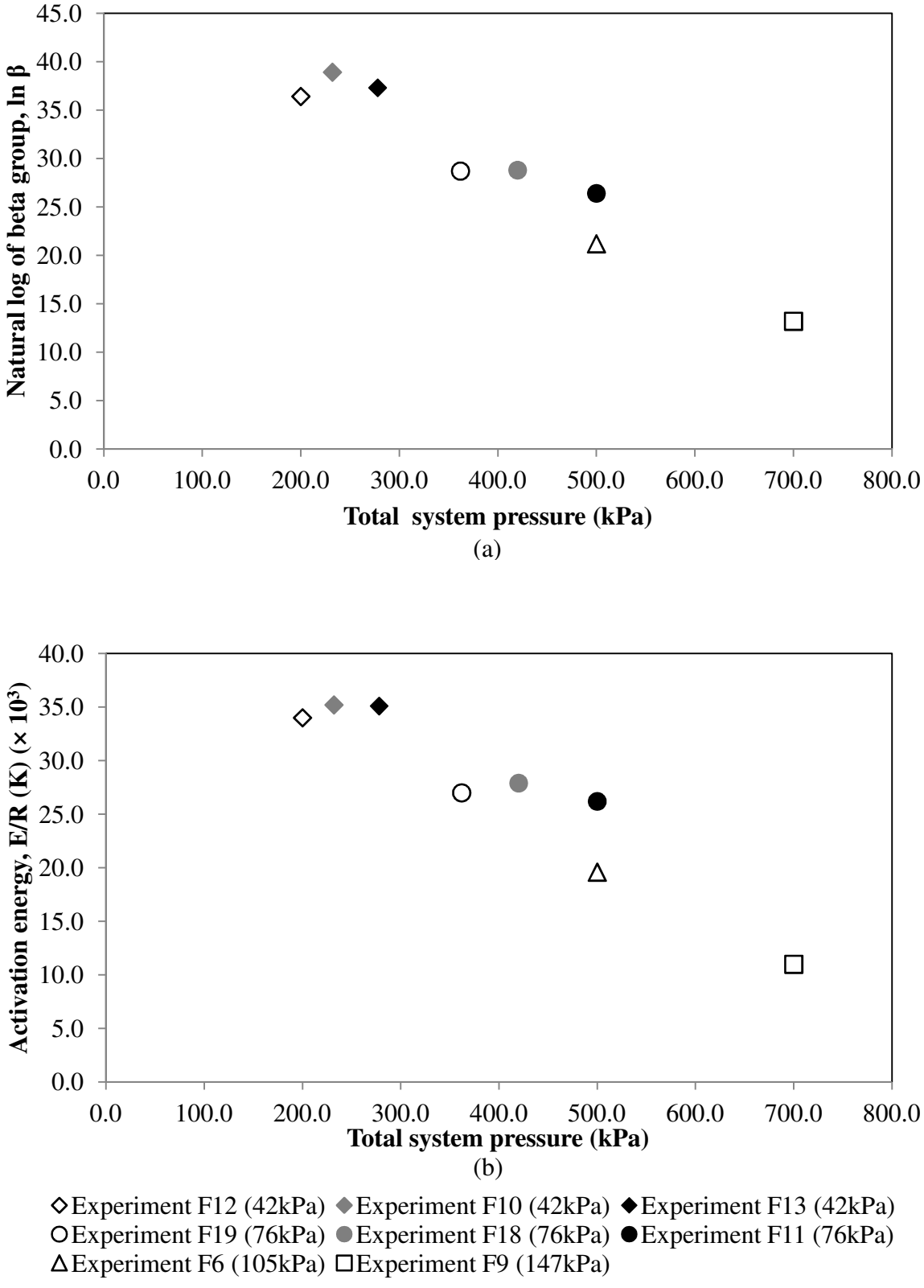

Figure 6.45 - Effect of the total system pressure on (a) the natural log of beta group, ln β (b) the activation energy, E/R for the high temperature oxidation, HTO. The pressure shown refer to the oxygen partial pressure.

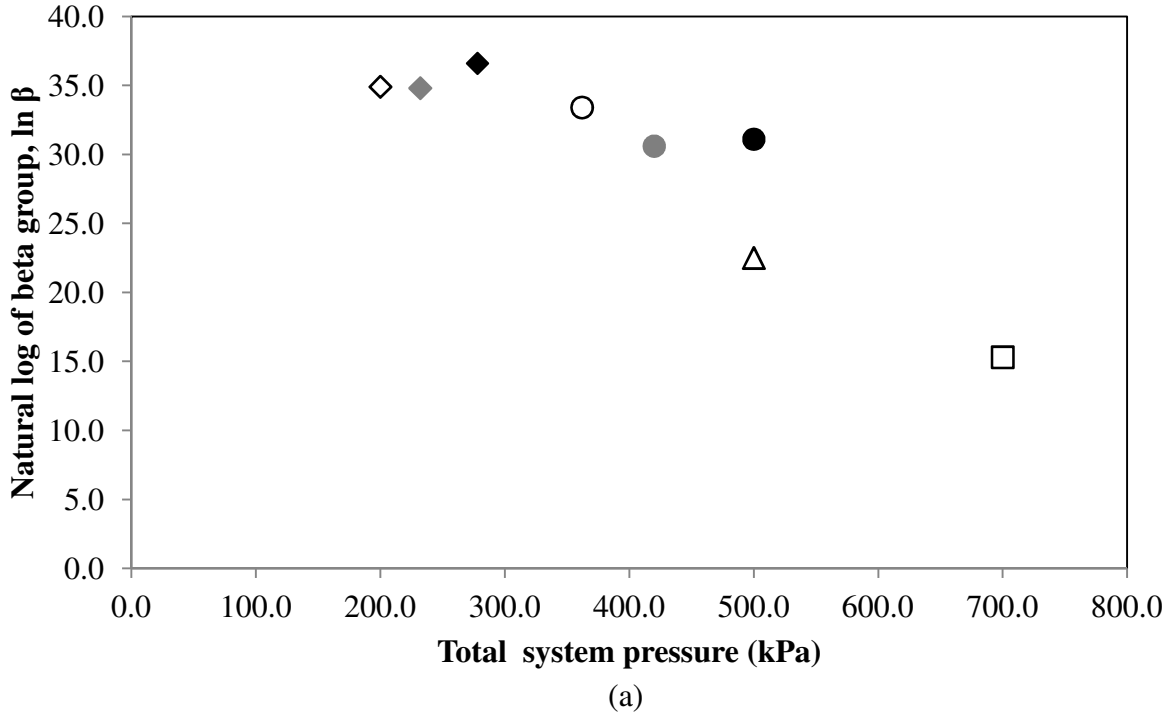

(a)

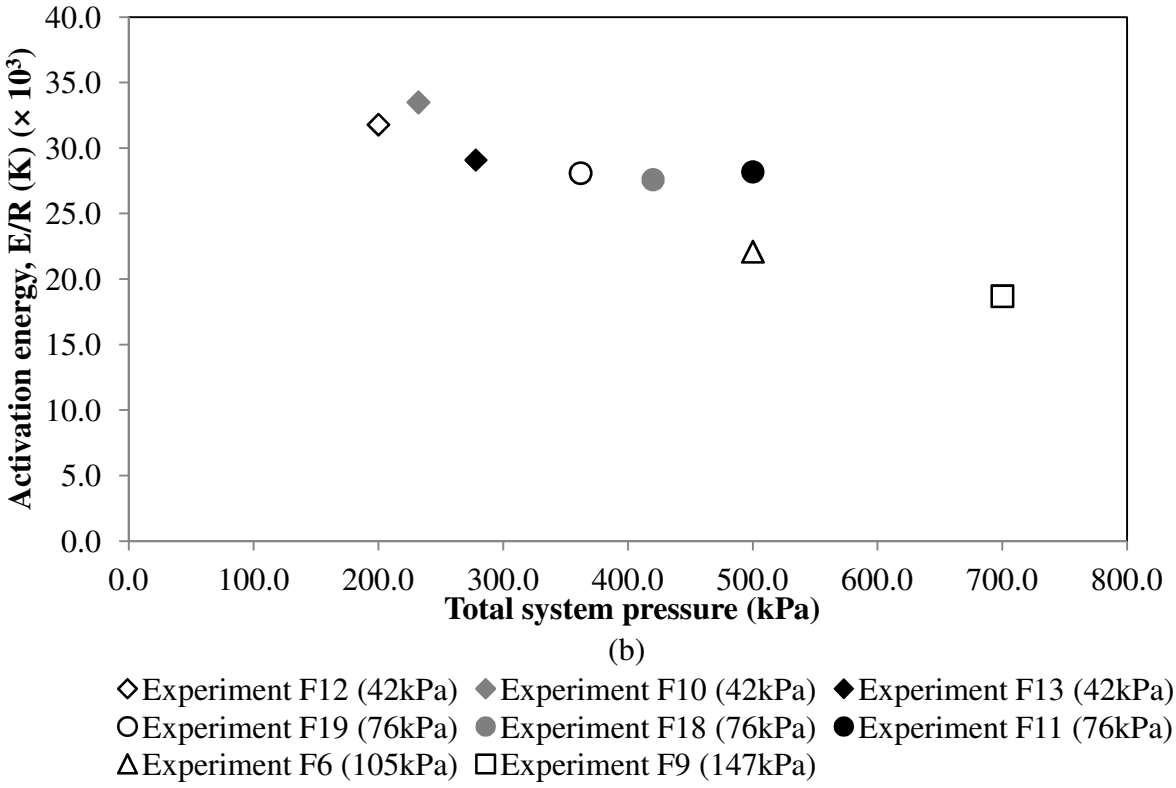

(b)

◇Experiment F12 (42kPa) ◆Experiment F10 (42kPa) ◆Experiment F13 (42kPa)
○Experiment F19 (76kPa) ●Experiment F18 (76kPa) ●Experiment F11 (76kPa)
△Experiment F6 (105kPa) □Experiment F9 (147kPa)

Figure 6.46 - Effect of the total system pressure on (a) the natural log of beta group, ln β (b) the activation energy, E/R for the medium temperature oxidation, MTO. The pressure shown refer to the oxygen partial pressure.

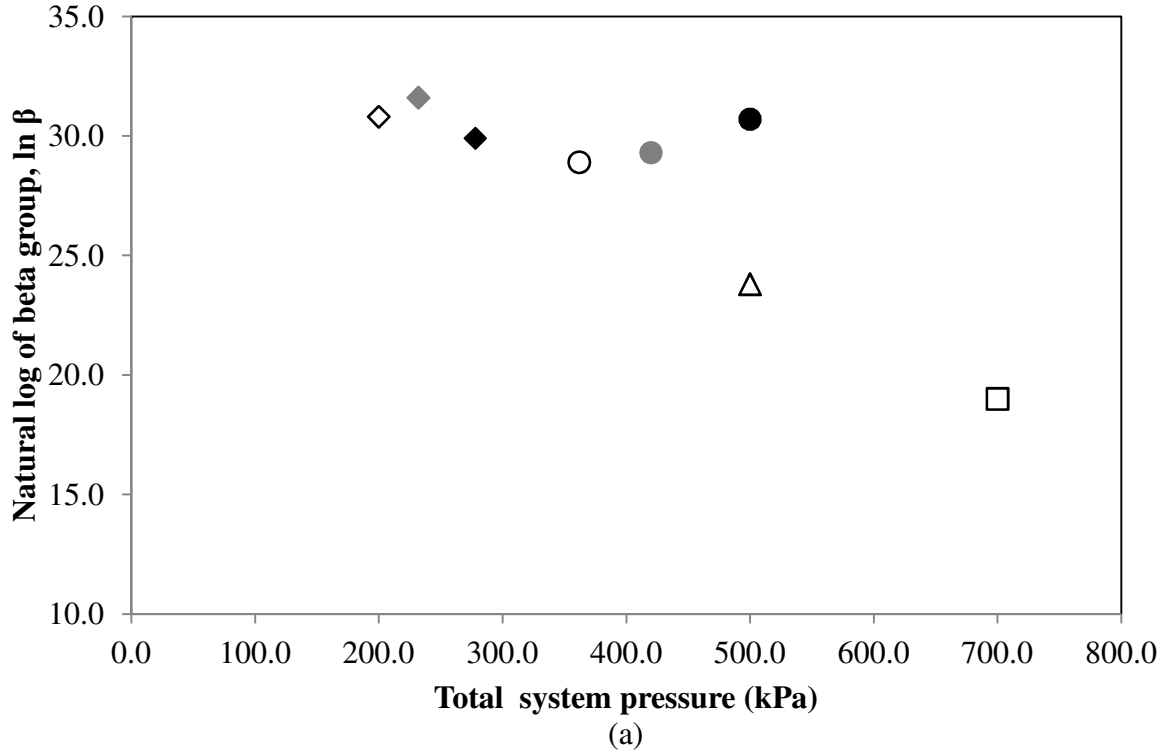

(a)

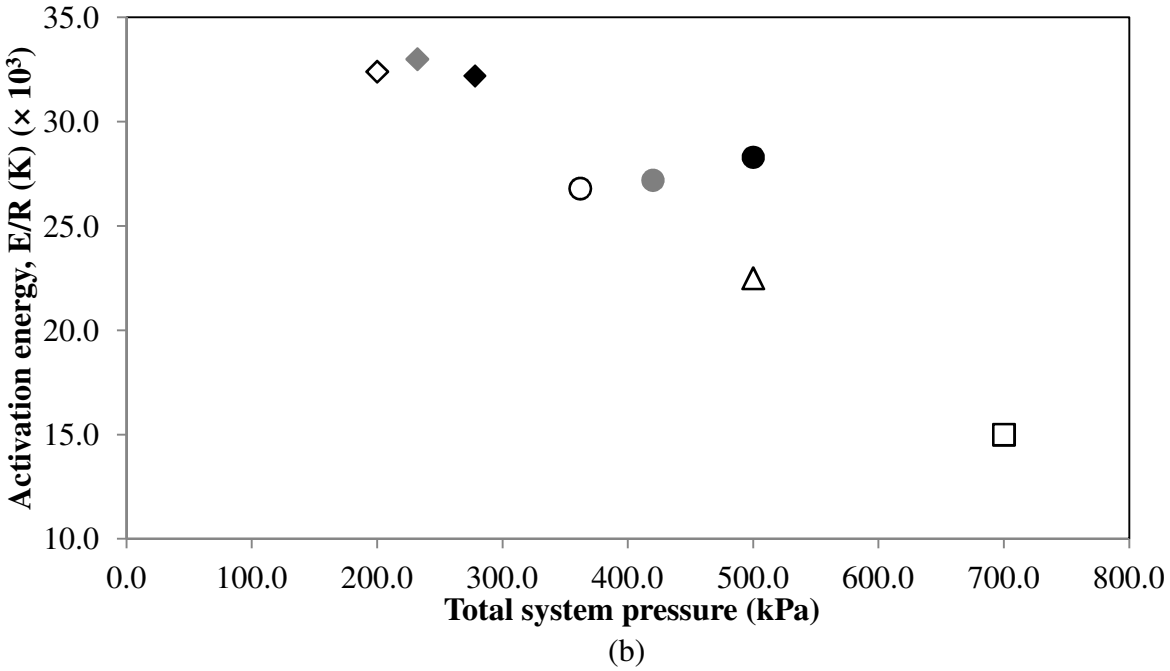

(b)

◇Experiment F12 (42kPa) ◆Experiment F10 (42kPa) ◆Experiment F13 (42kPa)
○Experiment F19 (76kPa) ●Experiment F18 (76kPa) ●Experiment F11 (76kPa)
△Experiment F6 (105kPa) □Experiment F9 (147kPa)

Figure 6.47 - Effect of the total system pressure on (a) the natural log of beta group, ln β (b) the activation energy, E/R for the low temperature oxidation, LTO. The pressure shown refer to the oxygen partial pressure.

From this observation, it is concluded that the reaction regimes representing the HTO, MTO and LTO reactions are not influenced by the total system pressure. Instead it is the oxygen partial pressure that controls the reactions. These findings was consistent with the palm fibre experimental data discussed in the previous Section 6.5.1 and the observations for the rice husk combustion characteristics.

In summary, pressure has a significant influence on the palm fibre combustion characteristics. As the pressure increases, all the exit gas oxygen, carbon dioxide and carbon monoxide composition peak temperatures decreases but the peak height increases. The oxygen partial pressure initiates the changes because there are no significant differences observed for both the hemicellulose and cellulose peak temperatures at the same oxygen partial pressure but various total system pressures for all the exit gas compositions. However, the peak height increases as the total system pressure increases. The calculated kinetic parameters of the activation energy and the ln β decrease as the pressure increases. However, the reaction order shows an opposing trend. The reaction order increases as the pressure increases. The calculated kinetic parameters show that the total system pressure has no significant influence on the palm fibre combustion characteristics study.

6.6 Effect of the oxygen partial pressure

This Section examines the influences of the oxygen partial pressure on the palm fibre combustion characteristics. Experiments F9, F14 and F9 were conducted at the various oxygen partial pressures but at the same total system pressure of 700kPa. Experiments F12, F16 and F17 were performed at the same total system pressure of 200kPa but at the various oxygen partial pressures.

The experimental conditions of these experiments are presented in Table 6.1. The evolved gas analysis (EGA) experimental results of these experimental runs are provided in Table 6.3. The variation in the exit gas compositions with respects to the cell temperature for the experiments F9 and F12 are shown previously in Figures 6.24 and 6.27, respectively.

Figures 6.48 to 6.51 present a plot of the exit gas composition curves with respect to the cell temperature for the experiments F14 to F17, respectively.

Figures 6.48 to 6.51, exhibit similar features to those observed for the typical palm fibre of experiment F6 exhibiting two main peaks referred to the hemicellulose and the cellulose peaks. However, there are variations in the peak temperatures and heights between these experimental runs. Figure 6.52 presents the comparison of the oxygen consumptions for the experiments F9, F12 and F14 to F17. Figures 6.53 and 6.54 show the corresponding information for the carbon dioxide production and the carbon monoxide production curves.

Considering Figures 6.52 to 6.54, the peak temperatures for all the exit gas composition curves shifted to lower temperatures as the oxygen partial pressure increased at the same total system pressure. Figure 6.55 shows the influences of the oxygen partial pressure at the same total system pressure on the hemicellulose peak temperature and height of the oxygen consumption curve. Figure 6.56 presents the corresponding information for the cellulose peak temperature and height. Figure 6.57 and 6.58 present the influences of the oxygen partial pressure at the same total system pressure on the hemicellulose and cellulose peak temperatures for the both carbon oxides, respectively.

Referring to Figures 6.55 and 6.58, the peak temperatures for both the hemicellulose and cellulose peaks decreased with the increasing of the oxygen partial pressure for the oxygen consumption curve. Likewise, the carbon dioxide production and the carbon monoxide production curves of both the hemicellulose and the cellulose were also decreased as the oxygen partial pressure increased. However, the peak height shows an opposing trend to the peak temperature. The peak height for the effluent gas oxygen, carbon dioxide and carbon monoxide composition curves increased with the increasing of the oxygen partial pressure.

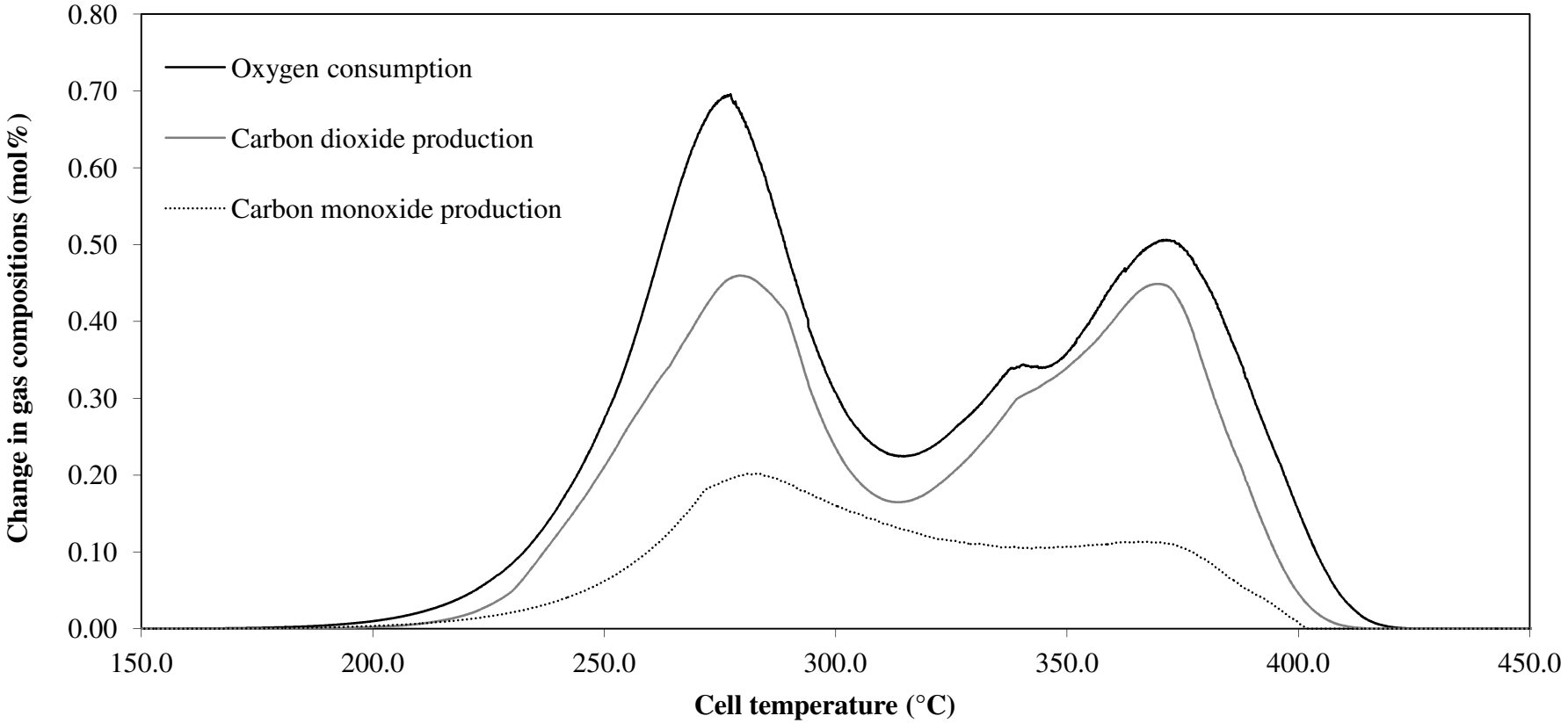

Figure 6.48 - Evolved gas analysis data with respects to the cell temperature for the oxidation of palm fibre with 15.10 mol% oxygen concentration in feed gas, an absolute total system pressure of 700kPa, an oxygen partial pressure of 106kPa, a flow rate of 400smL/min and a heating rate of 50°C/h (Experiment F14).

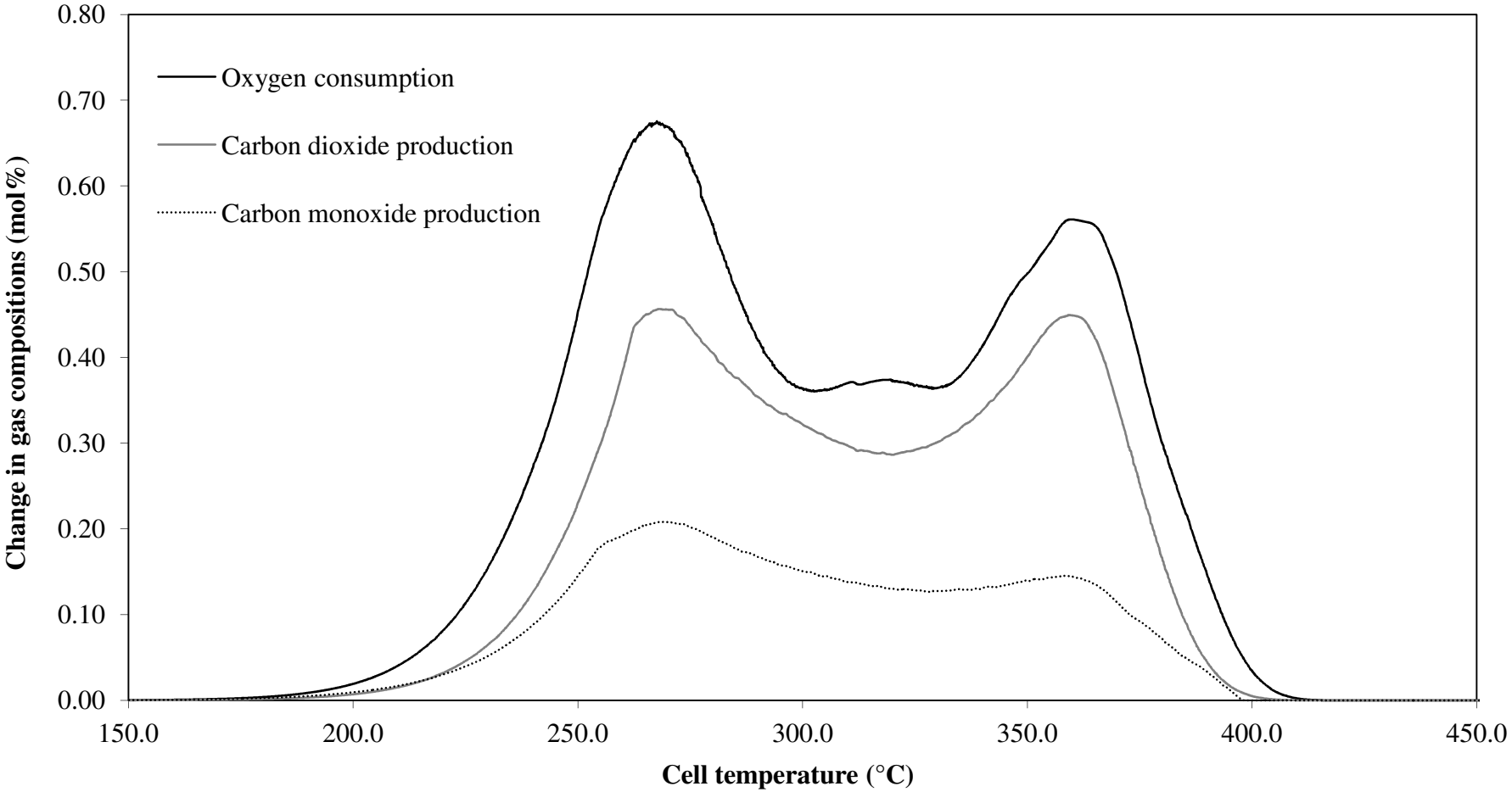

Figure 6.49 - Evolved gas analysis data with respects to the cell temperature for the oxidation of palm fibre with 18.10 mol% oxygen concentration in feed gas, an absolute total system pressure of 700kPa, an oxygen partial pressure of 127kPa, a flow rate of 400smL/min and a heating rate of 50°C/h (Experiment F15).

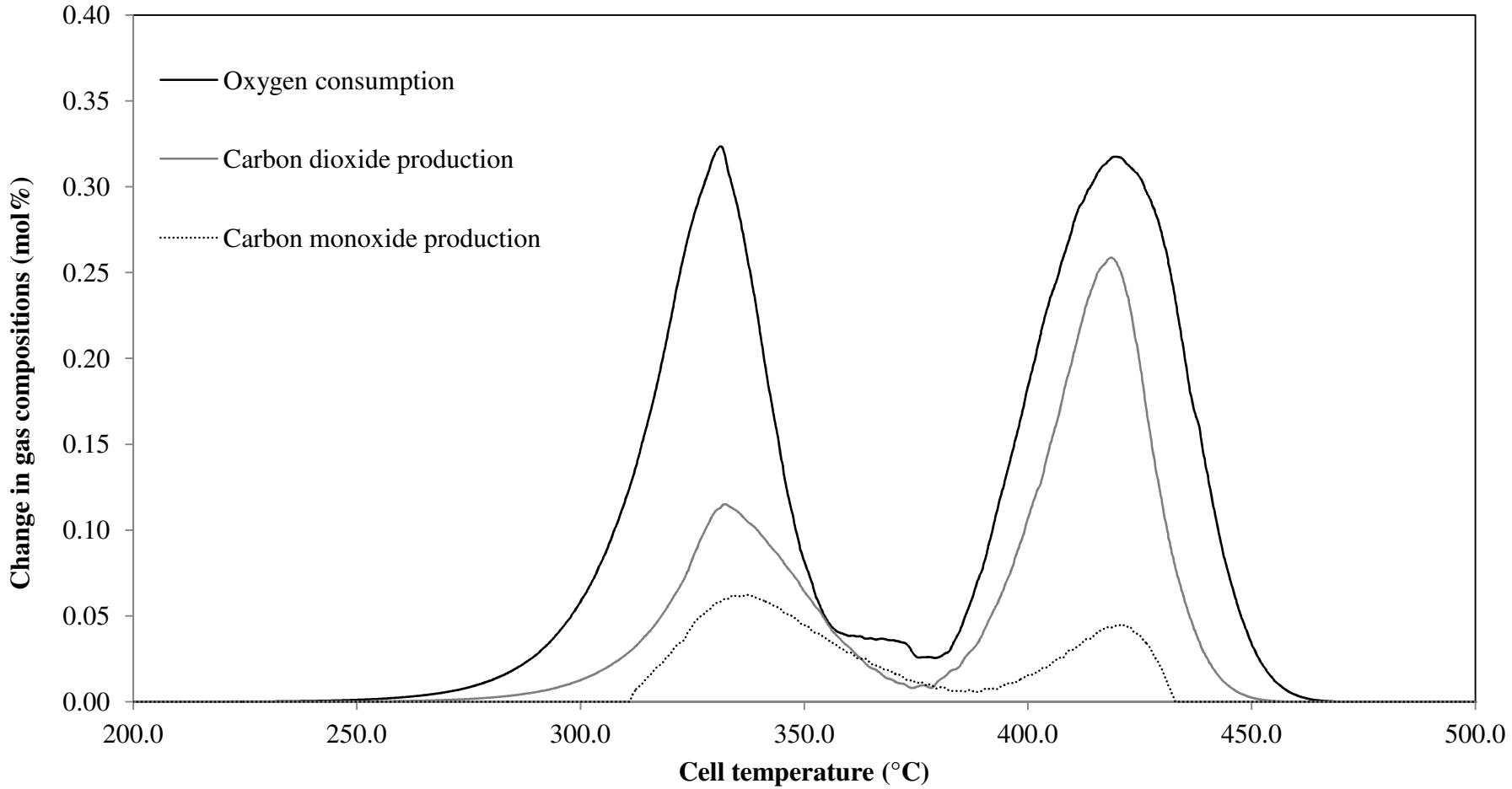

Figure 6.50 - Evolved gas analysis data with respects to the cell temperature for the oxidation of palm fibre with 15.10 mol% oxygen concentration in feed gas, an absolute total system pressure of 200kPa, an oxygen partial pressure of 30kPa, a flow rate of 400smL/min and a heating rate of 50°C/h (Experiment F16).

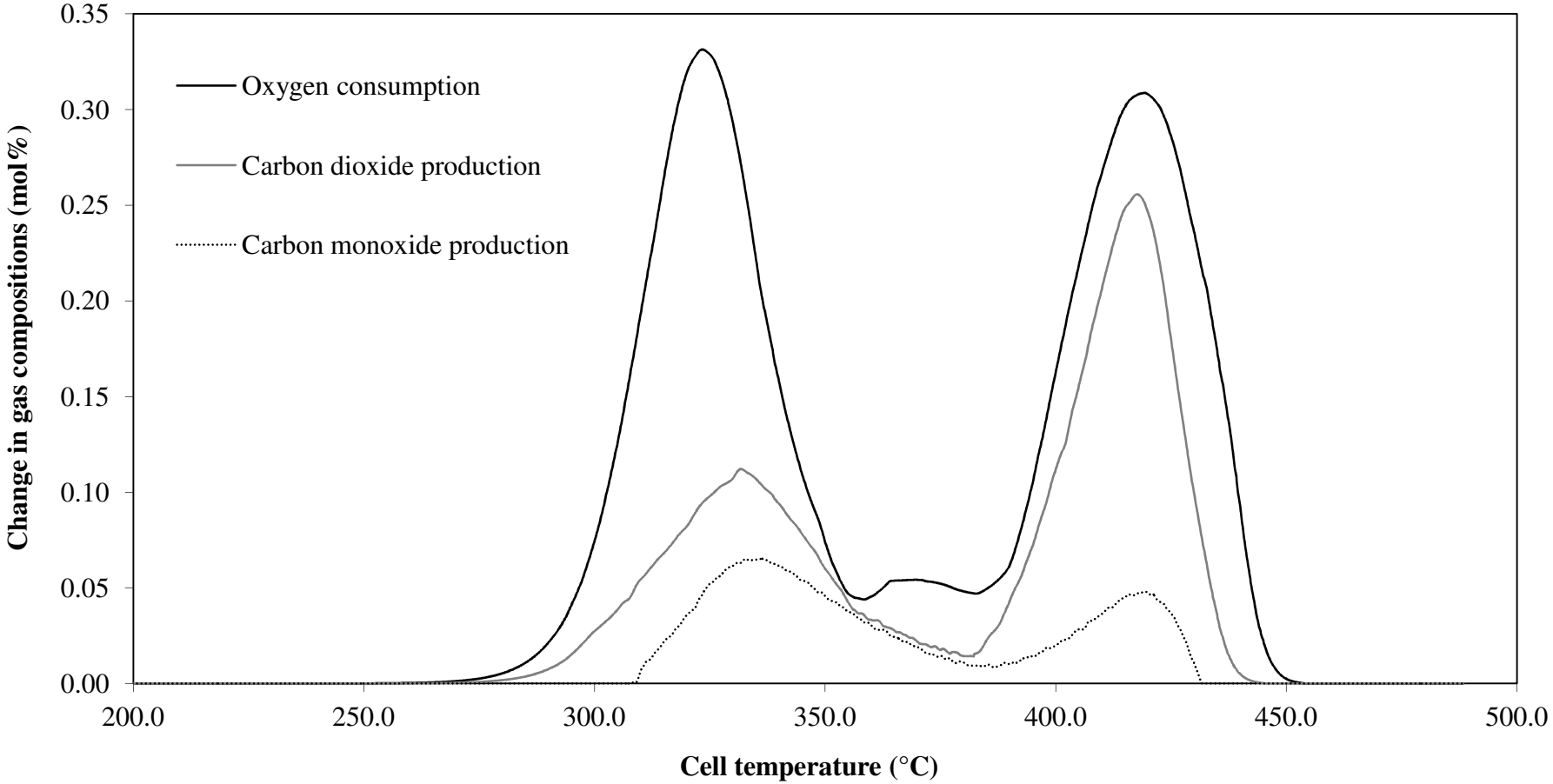

Figure 6.51 - Evolved gas analysis data with respects to the cell temperature for the oxidation of palm fibre with 18.10 mol% oxygen concentration in feed gas, an absolute total system pressure of 200kPa, an oxygen partial pressure of 36kPa, a flow rate of 400smL/min and a heating rate of 50°C/h (Experiment F17).

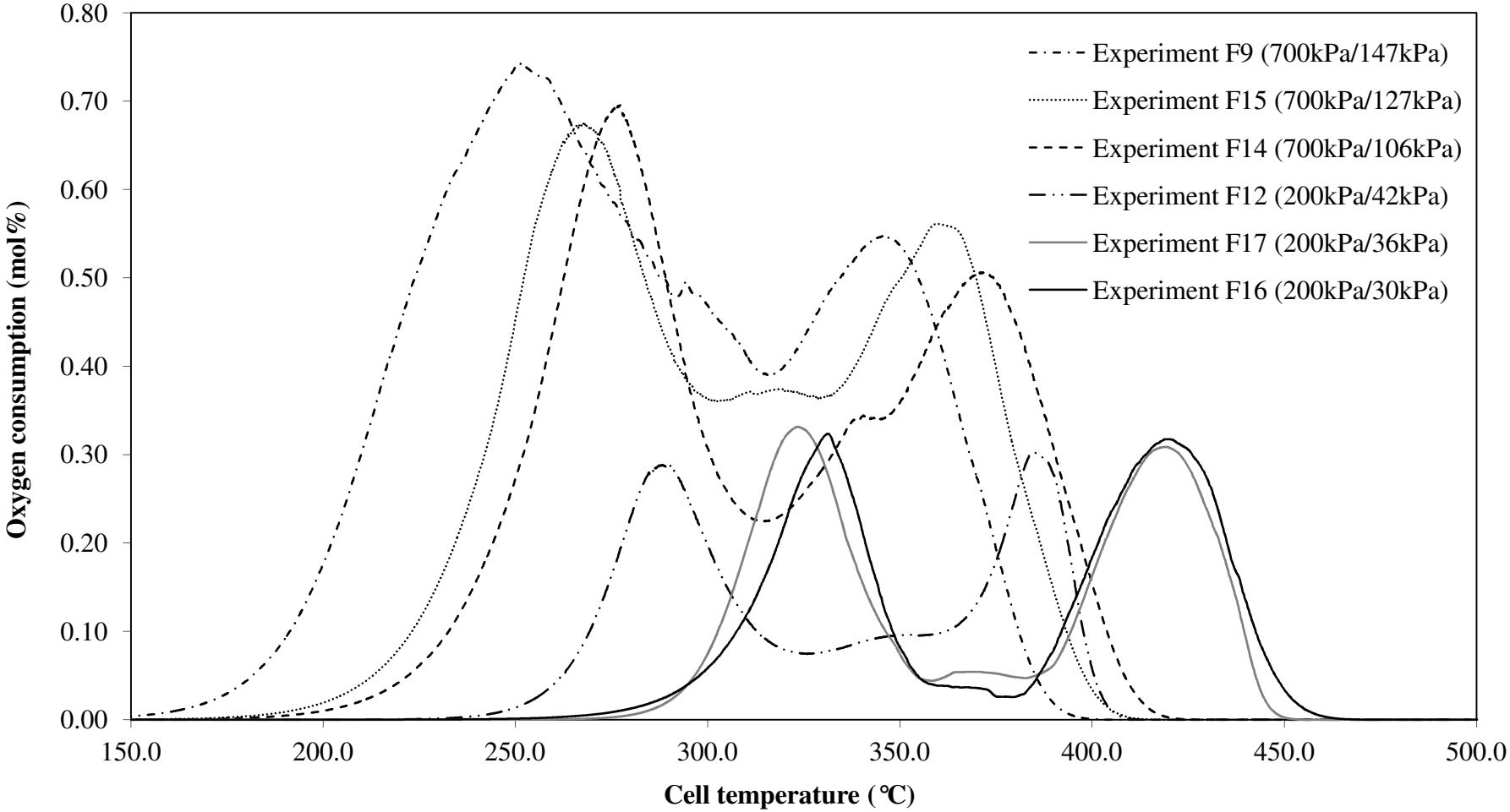

Figure 6.52 - The influences of the oxygen partial pressure on the oxygen consumption data with respects to the cell temperature conducted at heating rate of 50°C/h and gas flow rate of 400smL/min. The pressures shown refer to the absolute total system pressure and oxygen partial pressure, respectively.

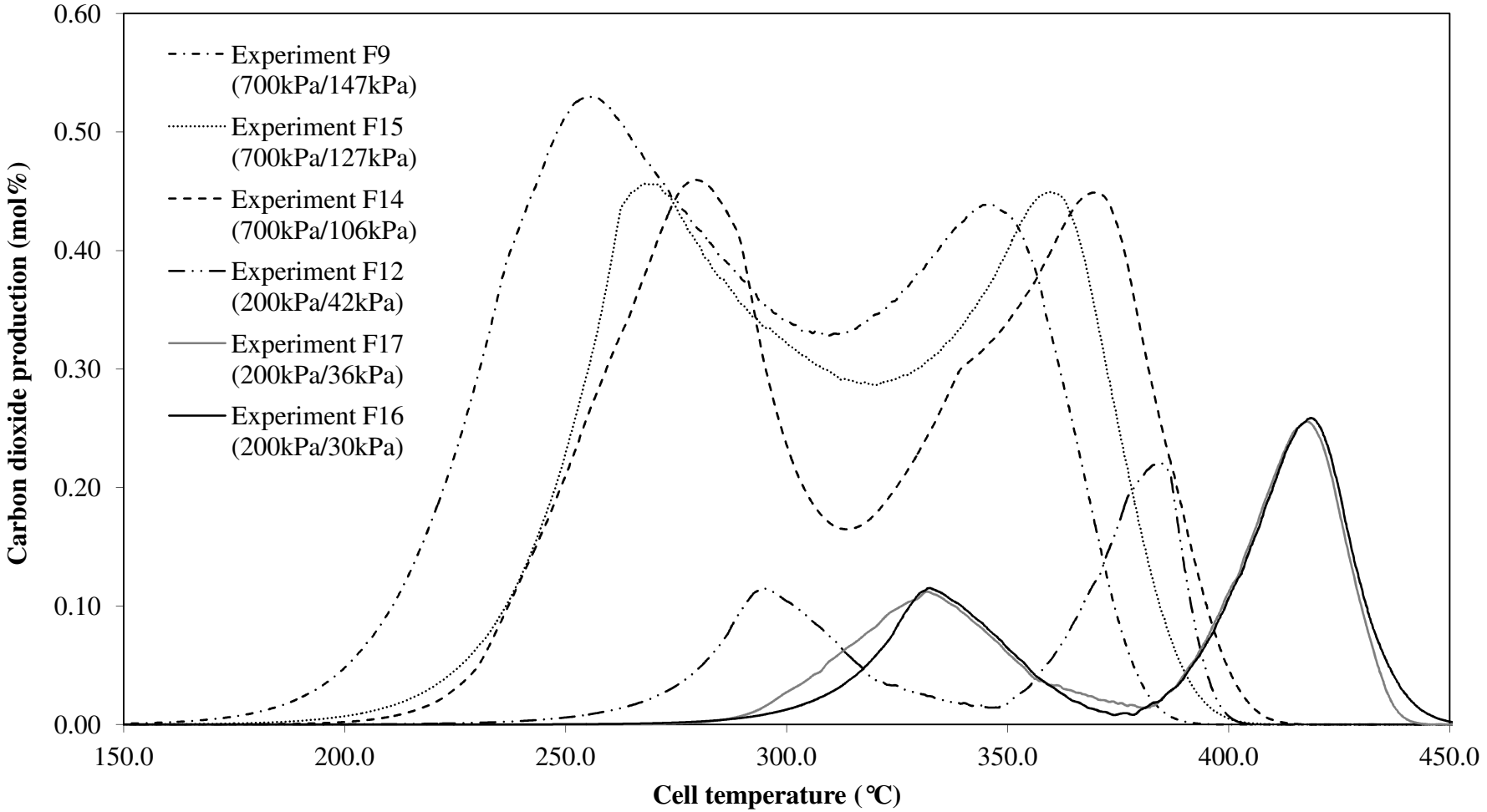

Figure 6.53 - The influences of the oxygen partial pressure on the carbon dioxide production data with respects to the cell temperature conducted at heating rate of 50°C/h and gas flow rate of 400smL/min. The pressures shown refer to the absolute total system pressure and oxygen partial pressure, respectively.

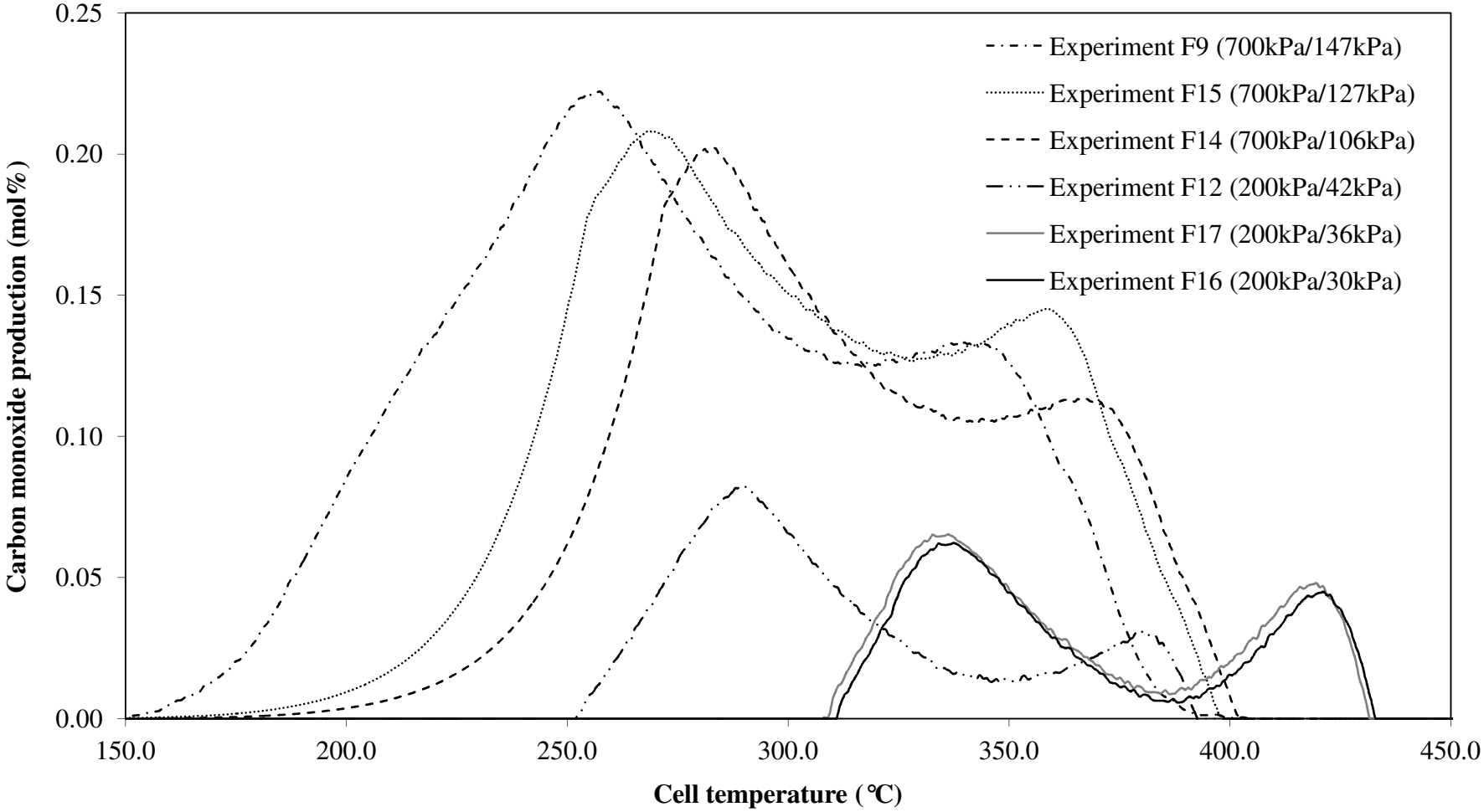

Figure 6.54 - The influences of the oxygen partial pressure on the carbon monoxide production data with respects to the cell temperature conducted at heating rate of 50°C/h and gas flow rate of 400smL/min. The pressures shown refer to the absolute total system pressure and oxygen partial pressure, respectively.

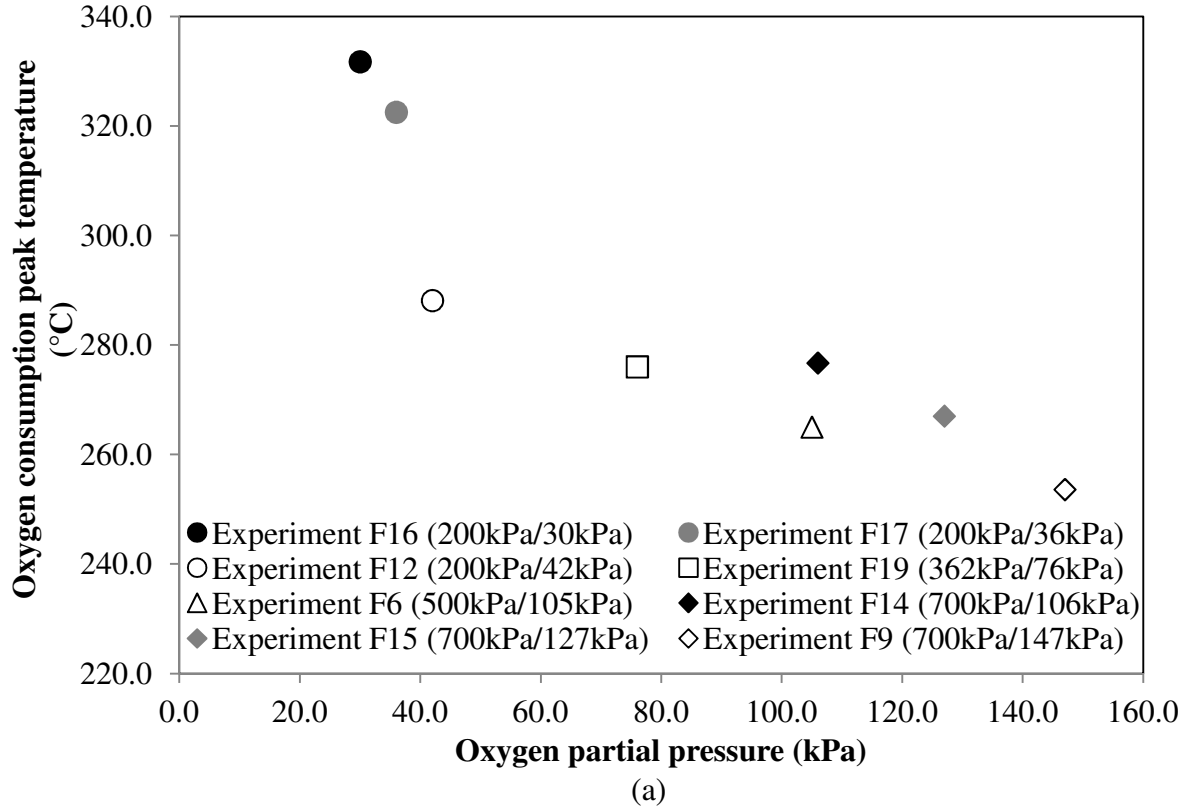

(a)

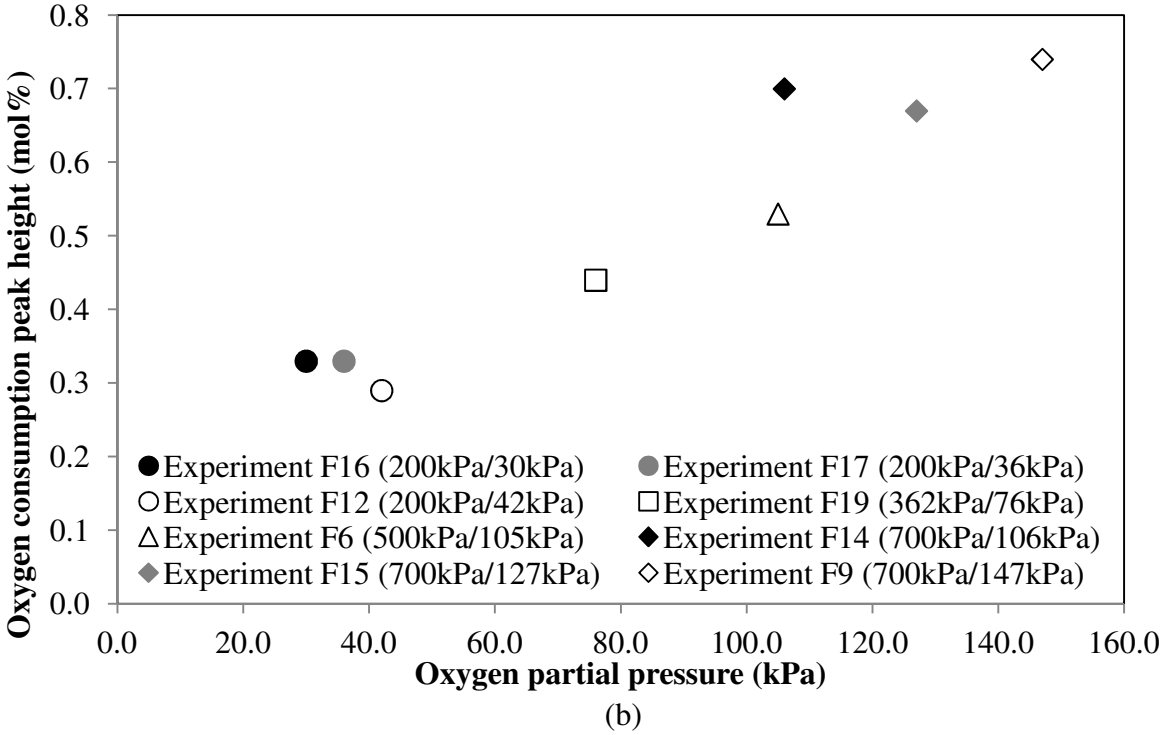

(b)

Figure 6.55 - Effect of the oxygen partial pressure of the hemicellulose (a) peak temperature (b) peak height of the oxygen consumption. The pressures shown refer to the total system pressure and the oxygen partial pressure, respectively.

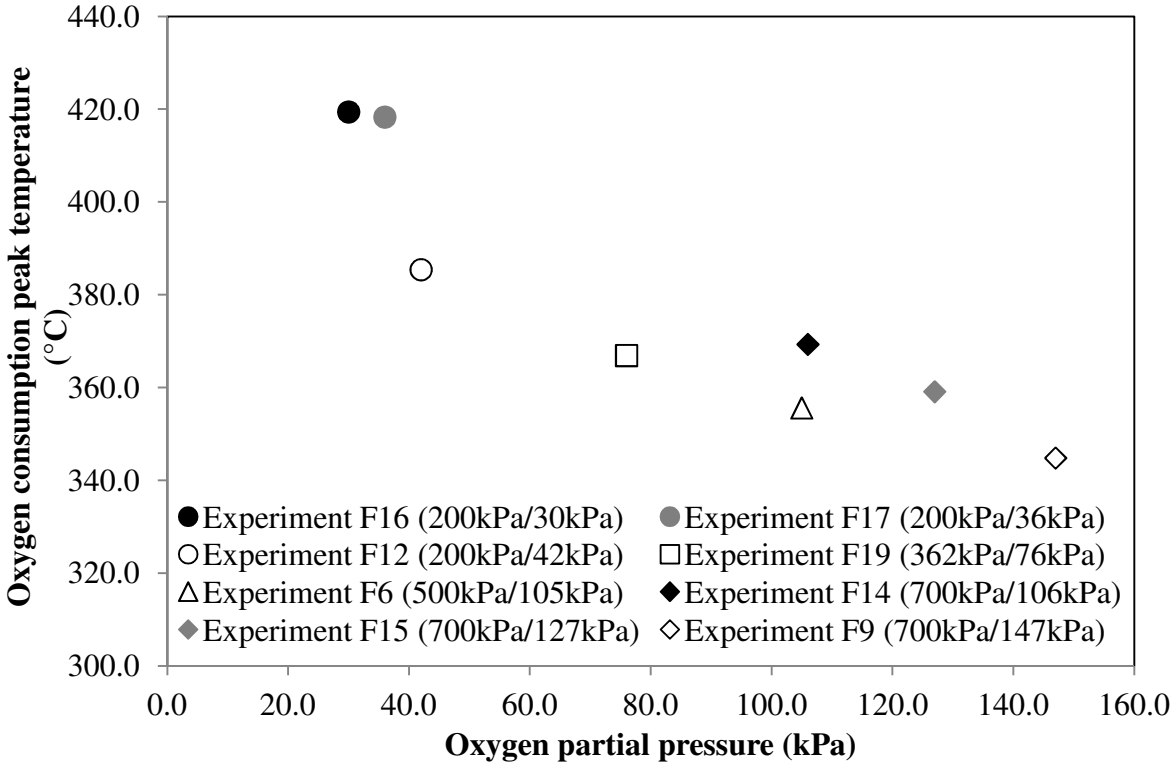

(a)

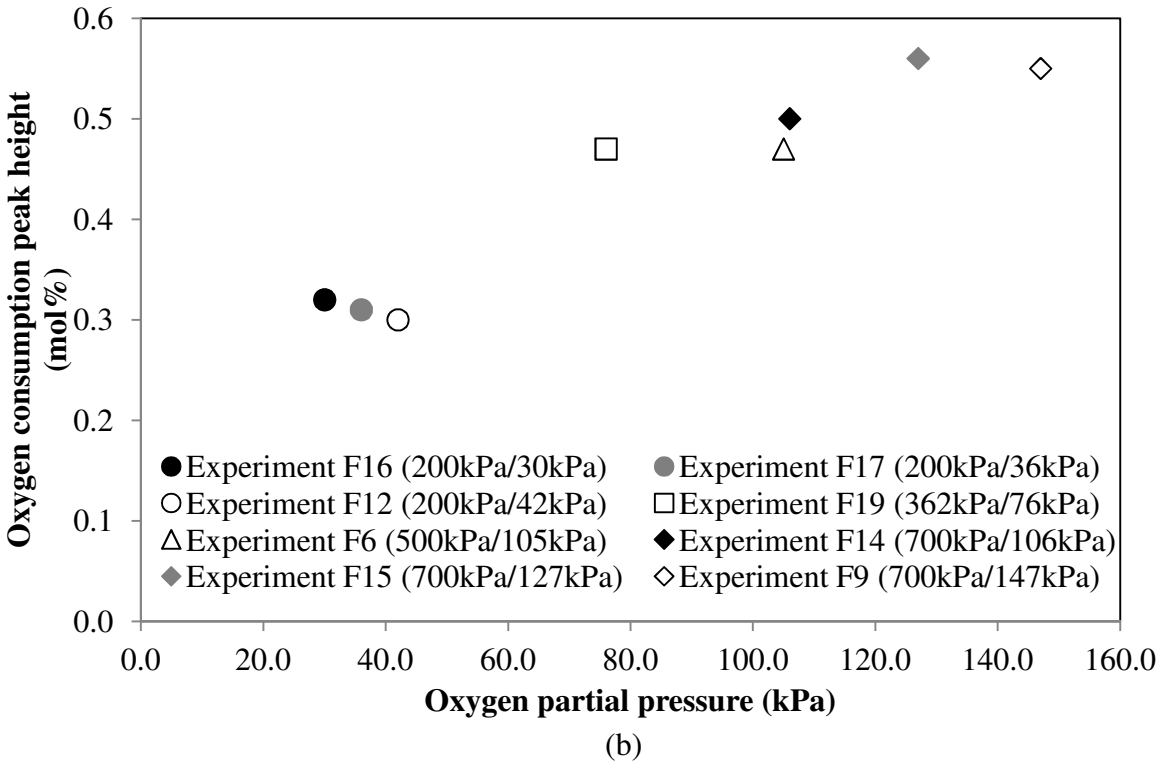

(b)

Figure 6.56 - Effect of the oxygen partial pressure of the cellulose (a) peak temperature (b) peak height of the oxygen consumption. The pressures shown refer to the total system pressure and the oxygen partial pressure, respectively.

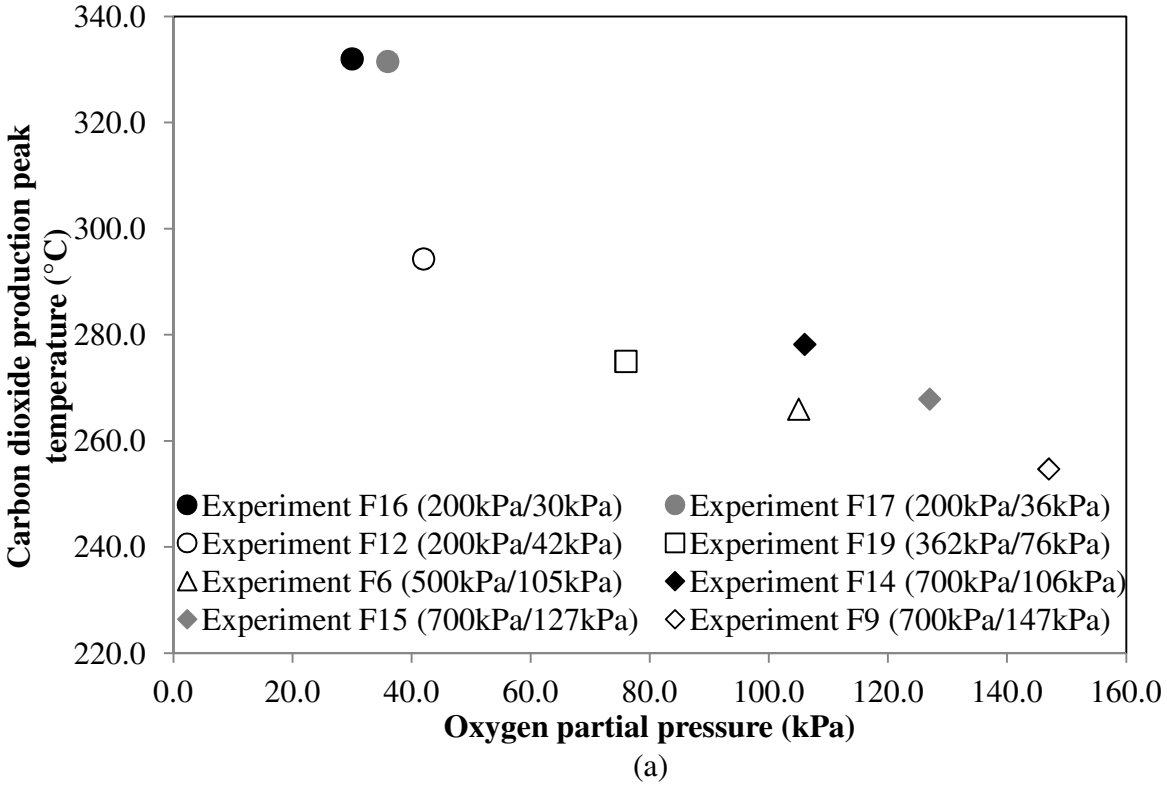

(a)

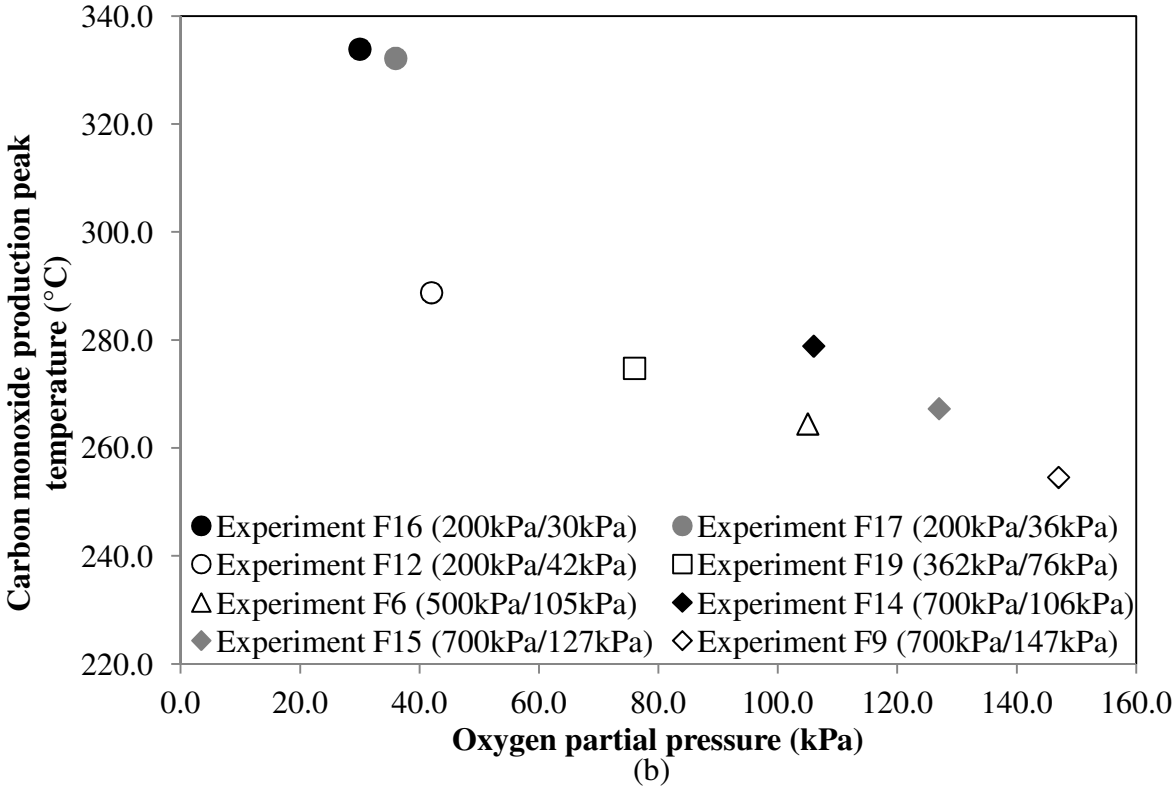

(b)

Figure 6.57 - Effect of the oxygen partial pressure on the hemicellulose peak temperatures of the (a) carbon dioxide production (b) carbon monoxide production. The pressure shown refer to the total pressure and the oxygen partial pressure.

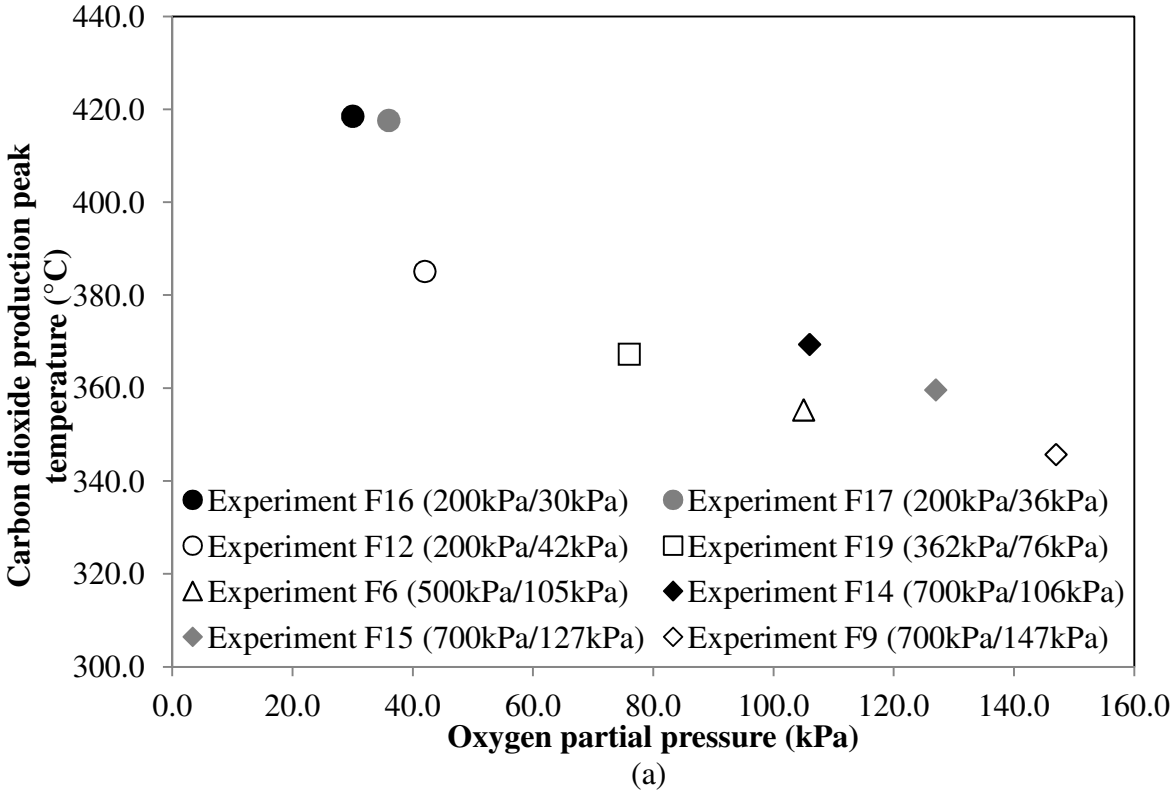

(a)

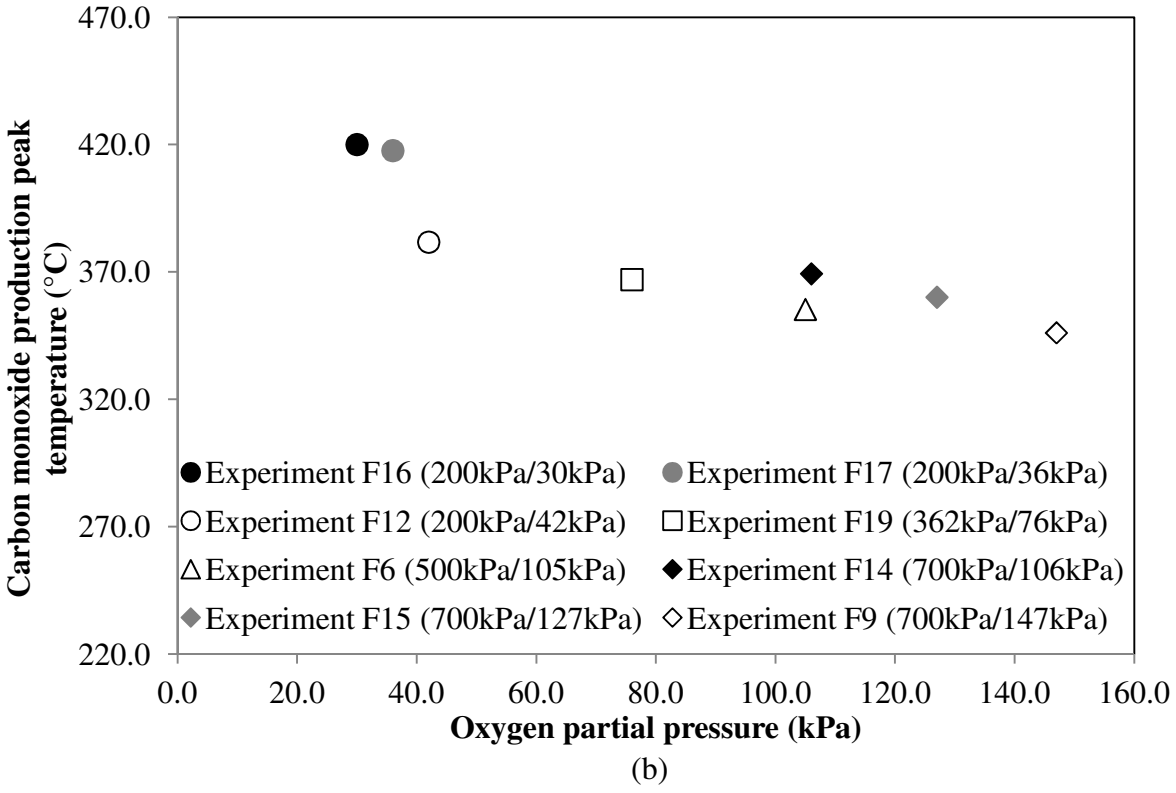

(b)

Figure 6.58 - Effect of the oxygen partial pressure on the cellulose peak temperatures of the (a) carbon dioxide production (b) carbon monoxide production. The pressure shown refer to the total pressure and the oxygen partial pressure.

Experiments F9, F14 and F15 were conducted at different oxygen partial pressures but at the same total system pressure of 700kPa. Experiments F12, F16 and F17 were conducted at the same total system pressure of 200kPa but at different oxygen partial pressures. Amongst these experiments, there are significant differences observed for both peak temperatures and heights for all the exit gas composition curves. This confirms that the oxygen partial pressure influences the changes in the combustion characteristics of palm fibre. The observation was found in agreement with the previous observation for the rice husk combustion characteristics study. The same observation was also reported by Bridgwater and Boocock (1997) in their rice husk decomposition study using evolved gas analysis (EGA) technique. The oxidation reactions are predominantly gas phase reactions until the efflux of volatile, combustible decomposition products from the palm fibre fall to a fairly low level which is after the cellulose decomposition products have been evolved. The effect of varying the oxygen partial pressure may be inferred to reflect a change in the rate of the gas phase oxidation reactions. It is suggested that the oxygen partial pressure or the oxygen concentration reflects the amount of oxygen presence during the reaction. More oxygen would enhance the reaction to a certain limit and increase the reaction rate.

Experiments F9, F14 and F15 were conducted at different oxygen partial pressures but at the same total system pressure of 700kPa. Experiments F12, F16 and F17 were performed at the same total system pressure of 200kPa but at different oxygen partial pressures. The calculated kinetic parameters of these experimental runs are presented in Table 6.4. The predicted oxygen consumption curve in comparison to the actual oxygen consumption curve of the experimental data for experiments F9 and F12 are presented in Figures 6.38 and 6.41. Figures 6.59 to 6.62 plot the oxygen consumption data and the model prediction of the experiments F14 to F17, respectively.

Considering Table 6.4 and Figures 6.59 to 6.62, all figures show a good fit between the predicted curve and the actual oxygen consumption experimental data with the calculated variance are well under 0.001. The calculated variance obtained for the experiments F14, F16 and F17 were 0.0001 and for the experiment F15 was 0.0002.

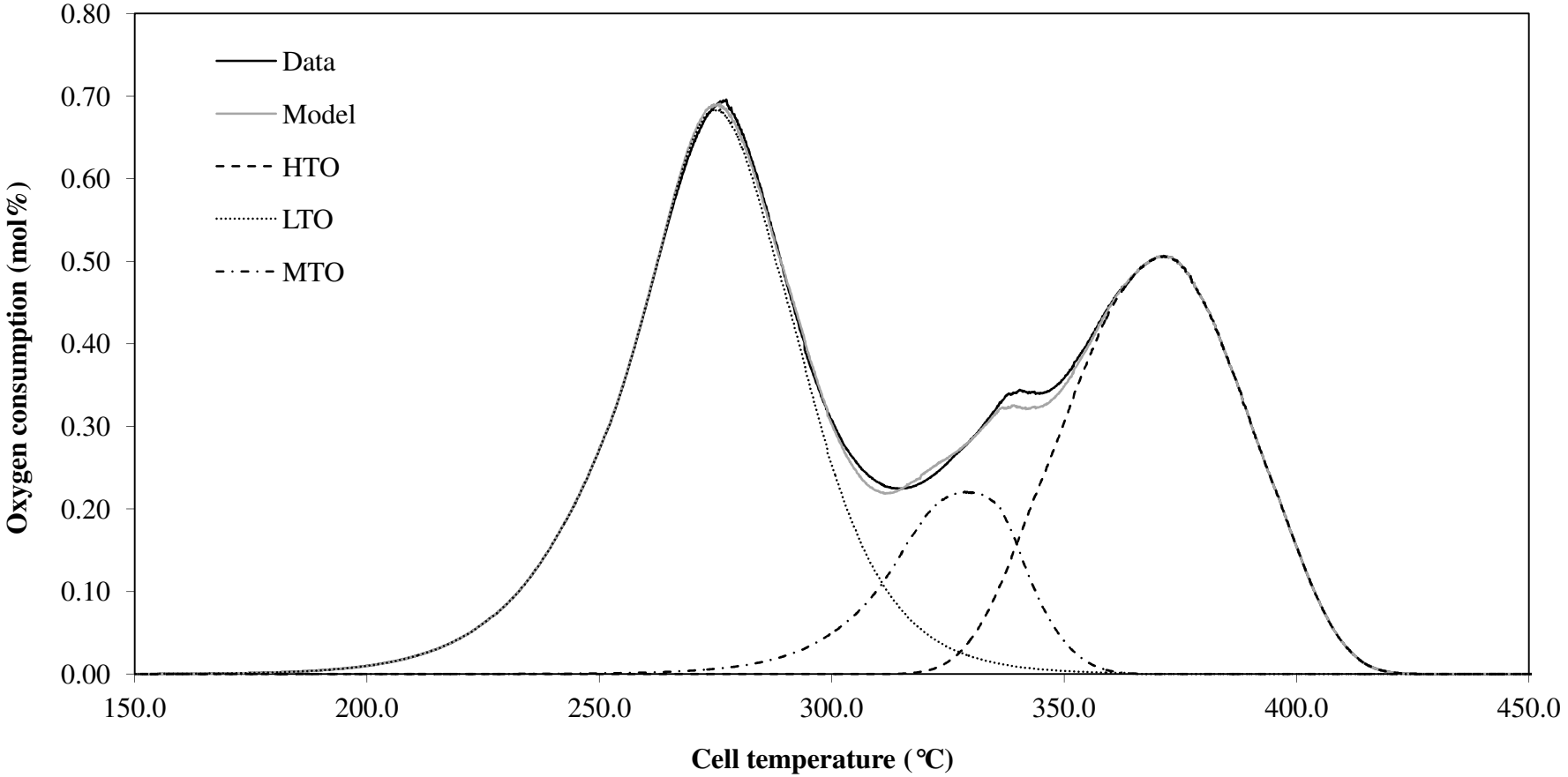

Figure 6.59 - Comparison of the oxygen consumption data and the model prediction with respects to cell temperature for the oxidation of palm fibre with 15.10 mol% oxygen concentration in feed gas, an absolute total system pressure of 700kPa, an oxygen partial pressure of 106kPa, a flow rate of 400smL/min and a heating rate of 50°C/h (Experiment F14).

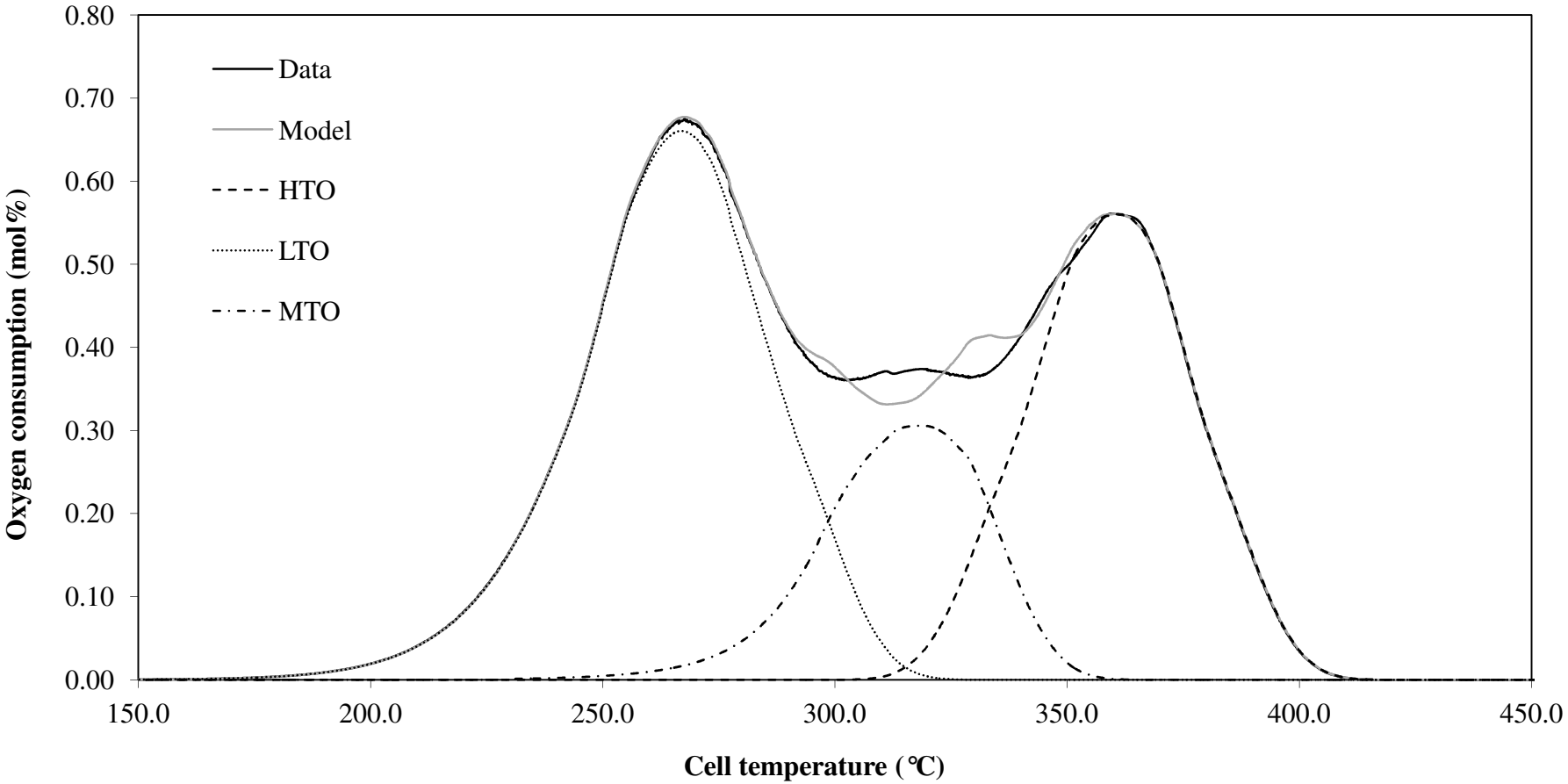

Figure 6.60 - Comparison of the oxygen consumption data and the model prediction with respects to the cell temperature for the oxidation of palm fibre with 18.10 mol% oxygen concentration in feed gas, an absolute total system pressure of 700kPa, an oxygen partial pressure of 127kPa, a flow rate of 400smL/min and a heating rate of 50°C/h (Experiment F15).

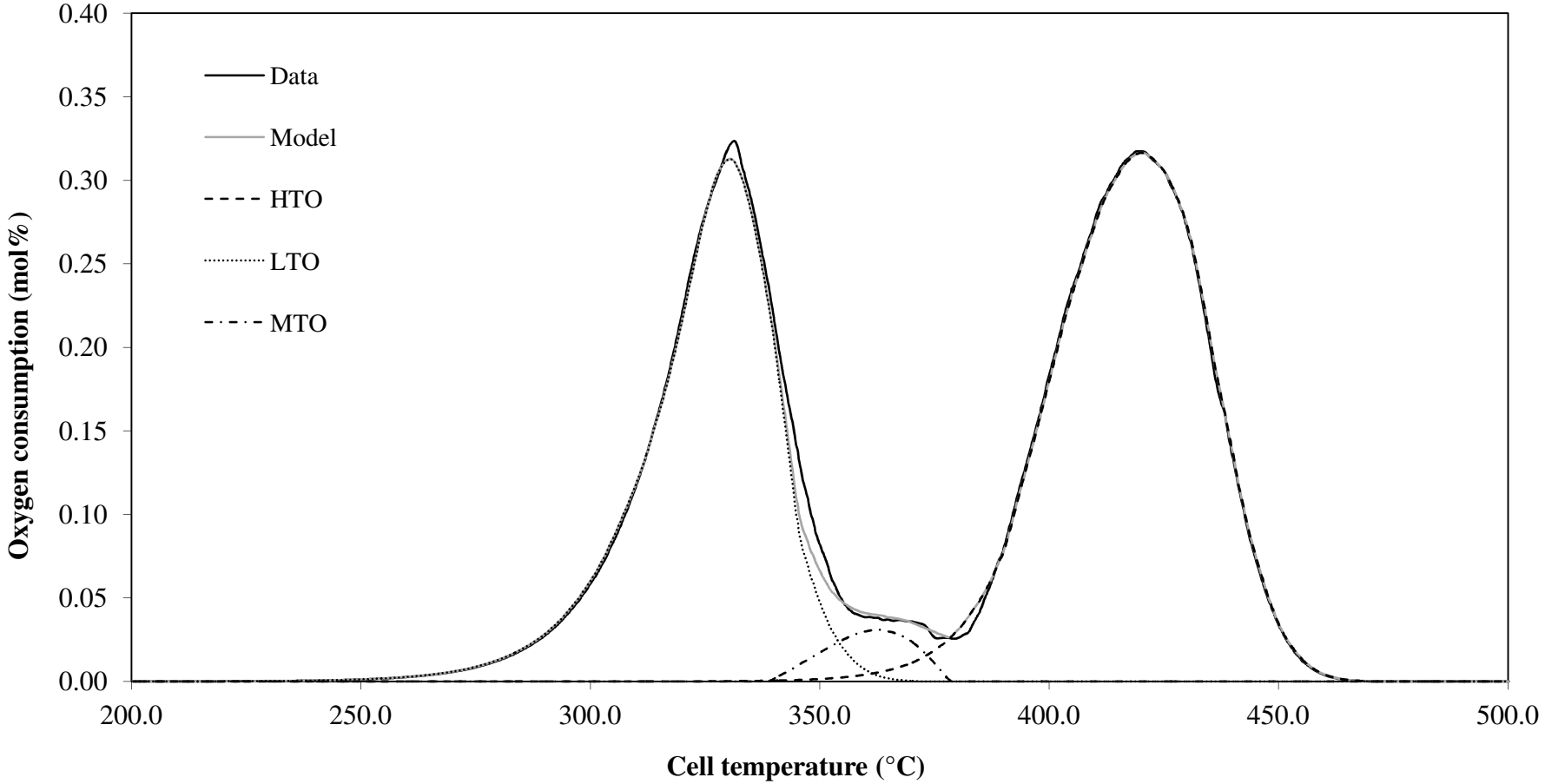

Figure 6.61 - Comparison of the oxygen consumption data and the model prediction with respects to the cell temperature for the oxidation of palm fibre with 15.10 mol% oxygen concentration in feed gas, an absolute total system pressure of 200kPa, an oxygen partial pressure of 30kPa, a flow rate of 400smL/min and a heating rate of 50°C/h (Experiment F16).

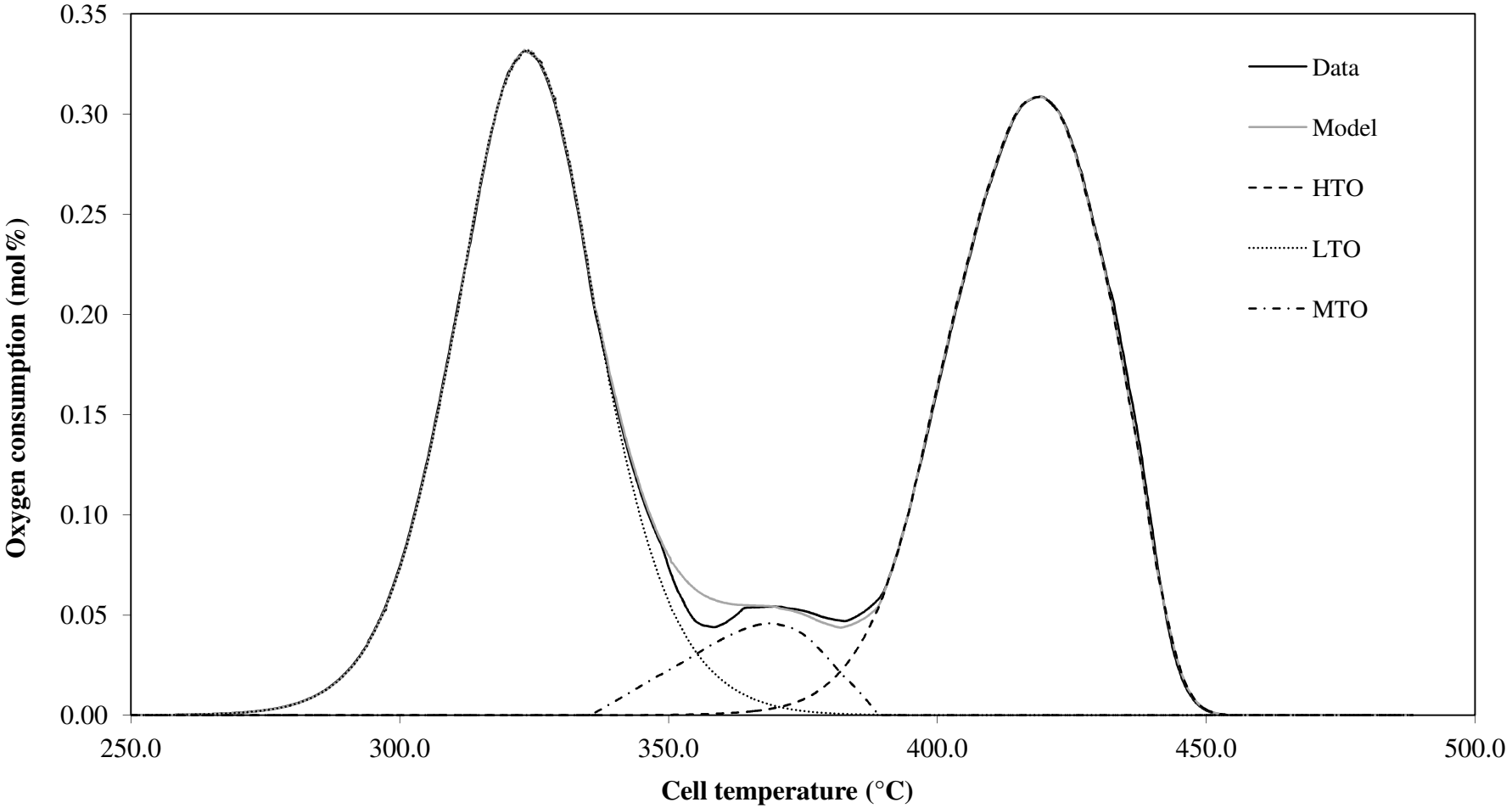

Figure 6.62 - Comparison of the oxygen consumption data and the model prediction with respects to the cell temperature for the oxidation of palm fibre with 18.10 mol% oxygen concentration in feed gas, an absolute total system pressure of 200kPa, an oxygen partial pressure of 36kPa, a flow rate of 400smL/min and a heating rate of 50°C/h (Experiment F17).

Similar to the typical palm fibre run of experiment F6, the discrepancy is obvious at the medium temperature regime. This was due to the overlapping of the LTO, MTO and HTO reactions that can make it difficult to obtain a good fit.

A comparison of experiments F9, F12, F14 to F17 permits the influence of the oxygen partial pressure on the palm fibre combustion characteristics to be studied. Figures 6.63 to 6.65 present a plotted of the calculated kinetic parameters of the activation energy (E/R) and the $\ln \beta$ with respect to the oxygen partial pressure for the HTO, MTO and LTO reactions, respectively. Considering Figure 6.63, the activation energy and the $\ln \beta$ for the high temperature oxidation (HTO) reaction decrease linearly with increasing oxygen partial pressure. Similarly to the HTO reaction, the activation energy and the $\ln \beta$ of the medium temperature oxidation (MTO) and the low temperature oxidation (LTO) reactions also decreased as the oxygen partial pressure increased. The activation energy and the $\ln \beta$ for the HTO, MTO and LTO reactions show significant changes over the oxygen partial pressure despite having a similar total system pressure (see experiments F9, F14 and F15 conducted at the various oxygen partial pressures but similar total system pressure of 700kPa, and experiments F12, F16 and F17 conducted at the various oxygen partial pressures but at the same total system pressure of 200kPa). From this we infer that all the reaction regimes are controlled by the oxygen partial pressure rather than by the total system pressure. These findings are consistent with the experimental data discussed in the previous Section 6.6.1 and the observation for the rice husk combustion characteristics study. This is well expected since the reaction model derived in Chapter 4 is based on the assumption that the reaction rate is proportional to the oxygen partial pressure and the fuel concentration.

In summary, the oxygen partial pressure significantly affects the palm fibre combustion characteristics. The peak temperatures of the oxygen consumption, the carbon dioxide production and the carbon monoxide production curves decrease significantly with increasing oxygen partial pressure. The peak height increases with increasing oxygen partial pressure. The calculated kinetic parameters for all the reaction regimes representing HTO, MTO and LTO were influenced by the oxygen partial pressure.

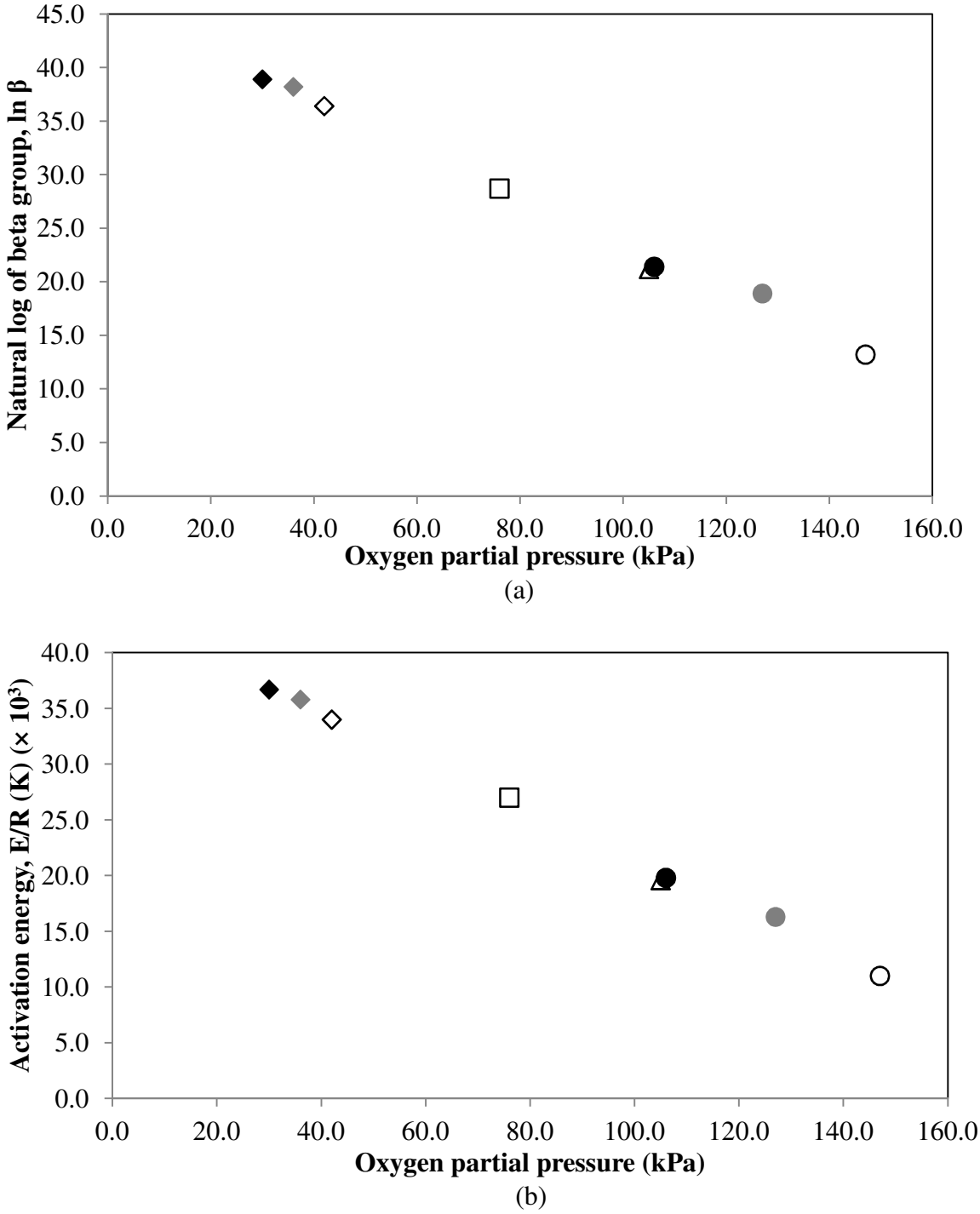

Figure 6.63 - Effect of the oxygen partial pressure on (a) the natural log of beta group, ln β (b) the activation energy, E/R for the high temperature oxidation, HTO. The pressure shown refer to the total system pressure.

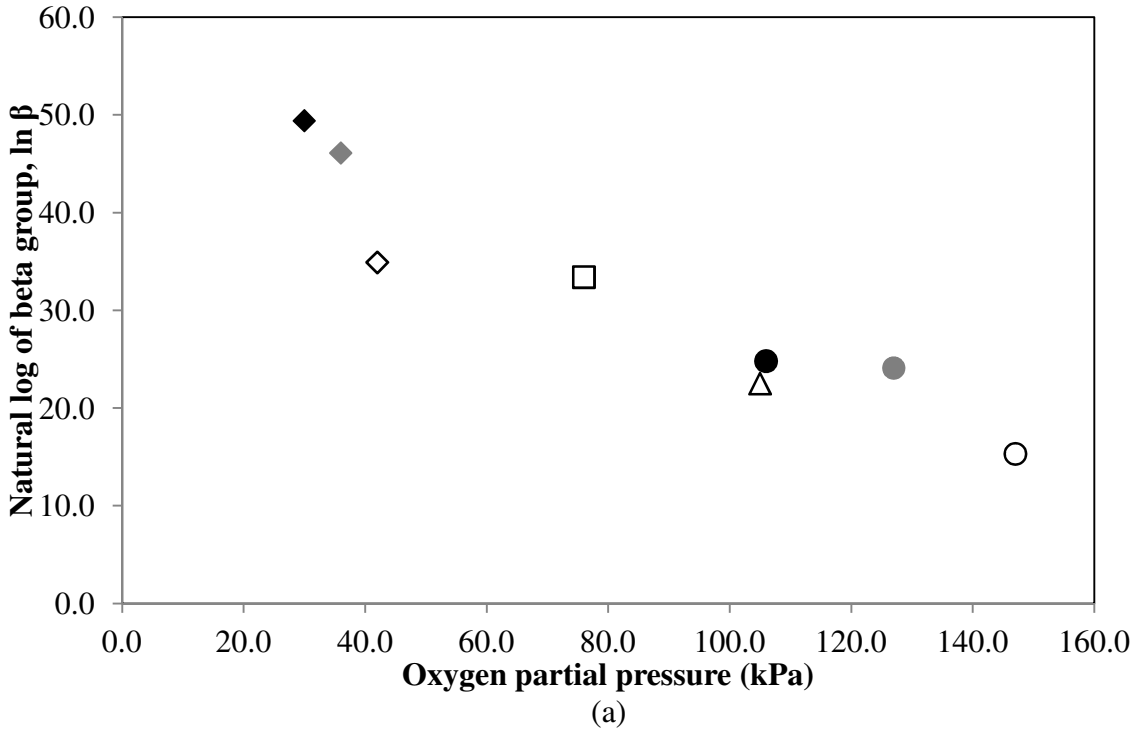

(a)

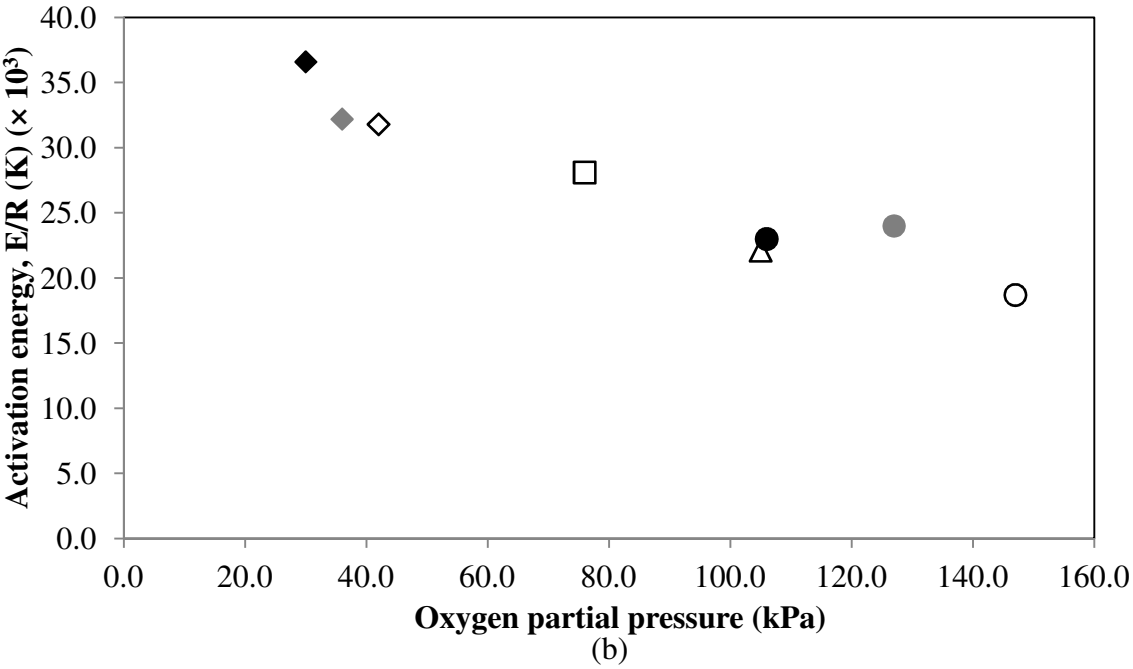

(b)

◆Experiment F16 (200kPa) ◆Experiment F17 (200kPa) ◇Experiment F12 (200kPa)
□Experiment F19 (362kPa) △Experiment F6 (500kPa) ●Experiment F14 (700kPa)
●Experiment F15 (700kPa) ○Experiment F9 (700kPa)

Figure 6.64 - Effect of the oxygen partial pressure on (a) the natural log of beta group, ln β (b) the activation energy, E/R for the medium temperature oxidation, MTO. The pressure shown refer to the total system pressure.

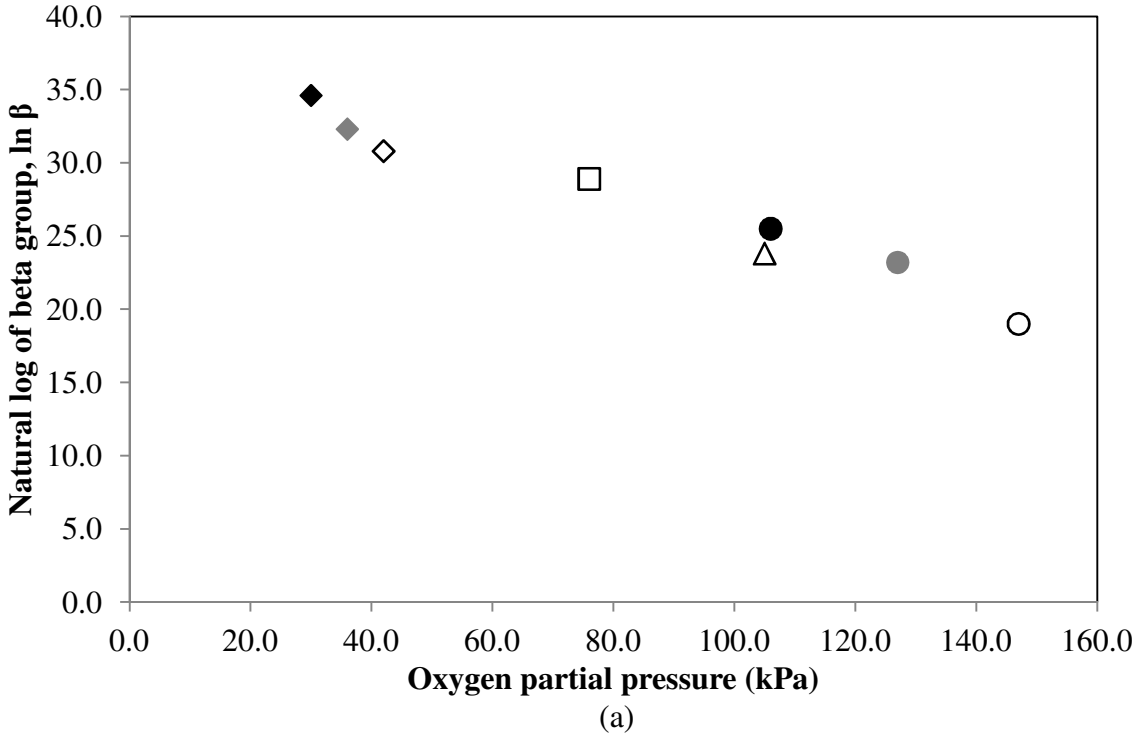

(a)

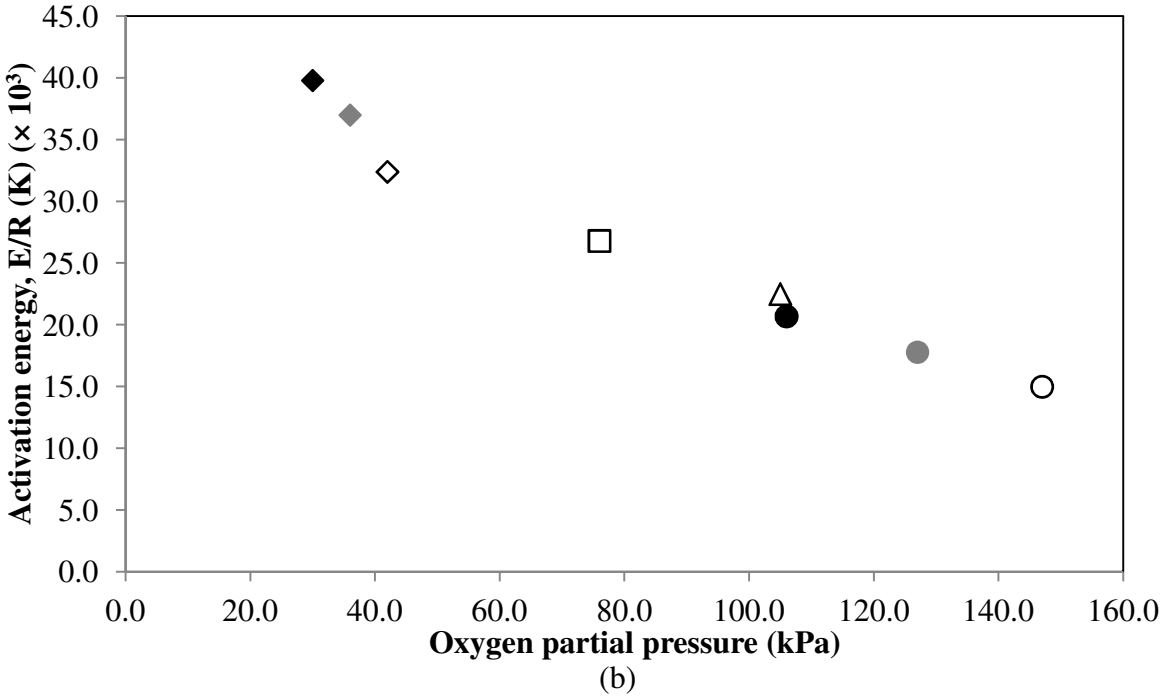

(b)

◆Experiment F16 (200kPa) ◆Experiment F17 (200kPa) ◇Experiment F12 (200kPa)
□Experiment F19 (362kPa) △Experiment F6 (500kPa) ●Experiment F14 (700kPa)
●Experiment F15 (700kPa) ○Experiment F9 (700kPa)

Figure 6.65 - Effect of the oxygen partial pressure on (a) the natural log of beta group, ln β (b) the activation energy, E/R for the low temperature oxidation, LTO. The pressure shown refer to the total system pressure.

There are significant differences in the calculated kinetic parameters over the various oxygen partial pressure that share a similar total system pressure. The activation energy and the ln β decrease linearly with increasing oxygen partial pressure for the HTO, MTO and LTO reactions.

6.7 Effect of pressure on the palm fibre - clump fibre

Experiments F1, F2, F20 and F21 were conducted using the clump fibre at various pressures with air as the oxidising gas, an air flow rate of 400smL/min and a heating rate of 50°C/h. The experimental conditions for these experimental runs are shown in Table 6.1. The evolved gas analysis (EGA) experimental results for these runs are presented in Table 6.3. The variations in the exit gas compositions with respect to the cell temperature for the typical clump fibre of the experiment F1 are shown in Figure 6.1. Figures 6.66 to 6.68 present a plots of the exit gas composition curves with respect to the cell temperature for experiments F2, F20 and F21, respectively.

Figures 6.66 to 6.68, exhibit similar features to those observed for the typical clump fibre of experiment F1 exhibiting two main peaks identified as the hemicellulose and the cellulose peaks. However, the variations in the peak temperatures and heights were observed as pressure is applied. Figure 6.69 presents the comparison of the oxygen consumption curves for experimental runs F1, F2, F20 and F21. Figures 6.70 and 6.71 show the corresponding information for the carbon dioxide production and the carbon monoxide production curves. As observed in Figures 6.69 to 6.71, the peak temperatures for the three curves shifted to lower temperatures as the pressure increased.

Referring to Table 6.3, the hemicellulose and the cellulose peak temperatures for the oxygen consumption curve decreased in the range of 0.12 mol% to 0.33 mol% oxygen as the pressure increased from 362kPa to 700kPa. A similar reduction of the hemicellulose and the cellulose peak heights were observed for the both carbon dioxide production and carbon monoxide production curves as the pressure increased. The peak height increased with the increasing pressure.

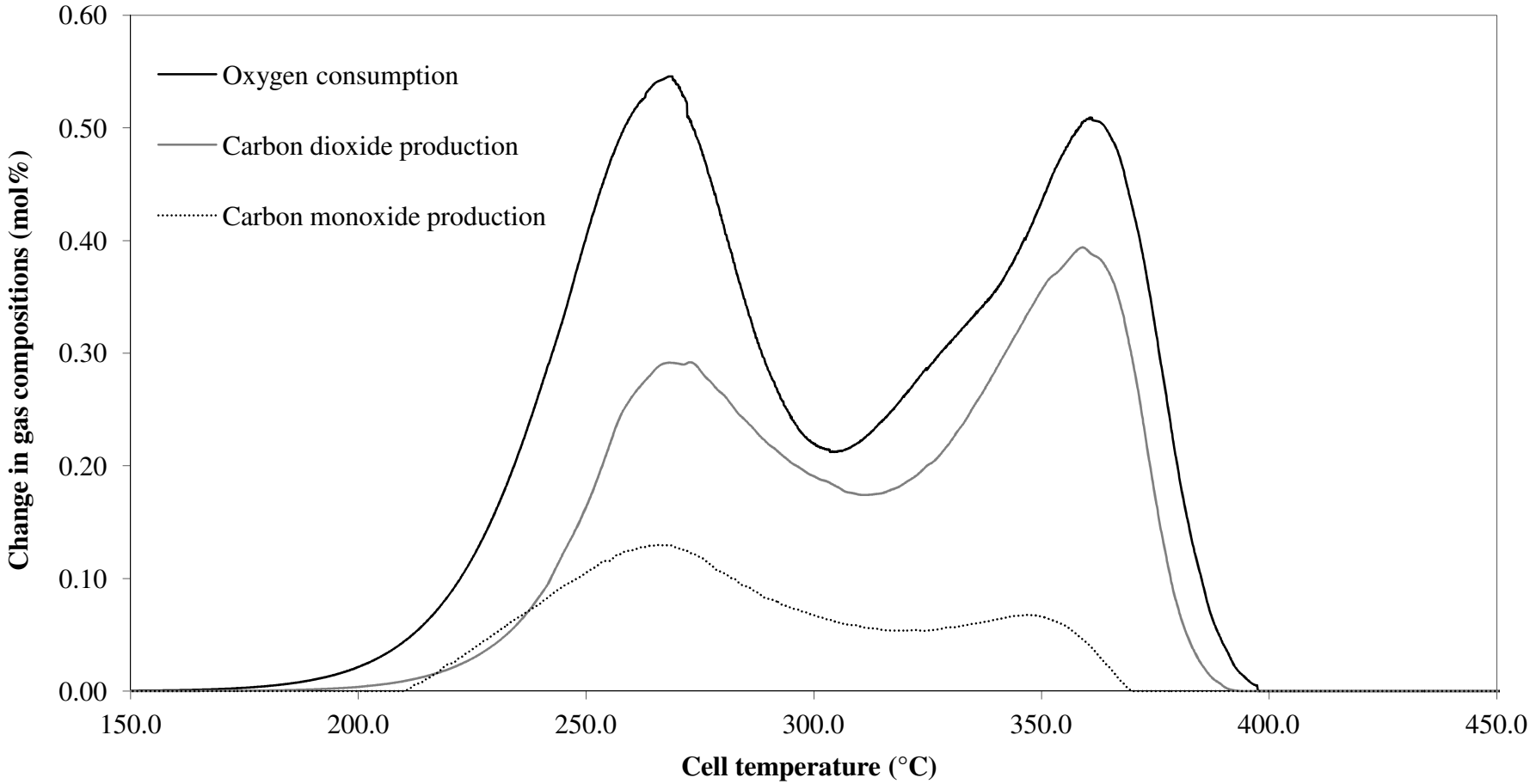

Figure 6.66 - Evolved gas analysis data with respects to the cell temperature for oxidation of palm fibre - clump fibre with air as the oxidising gas, an absolute total system pressure of 500kPa, an air flow rate of 400smL/min and a heating rate of 50°C/h (Experiment F2).

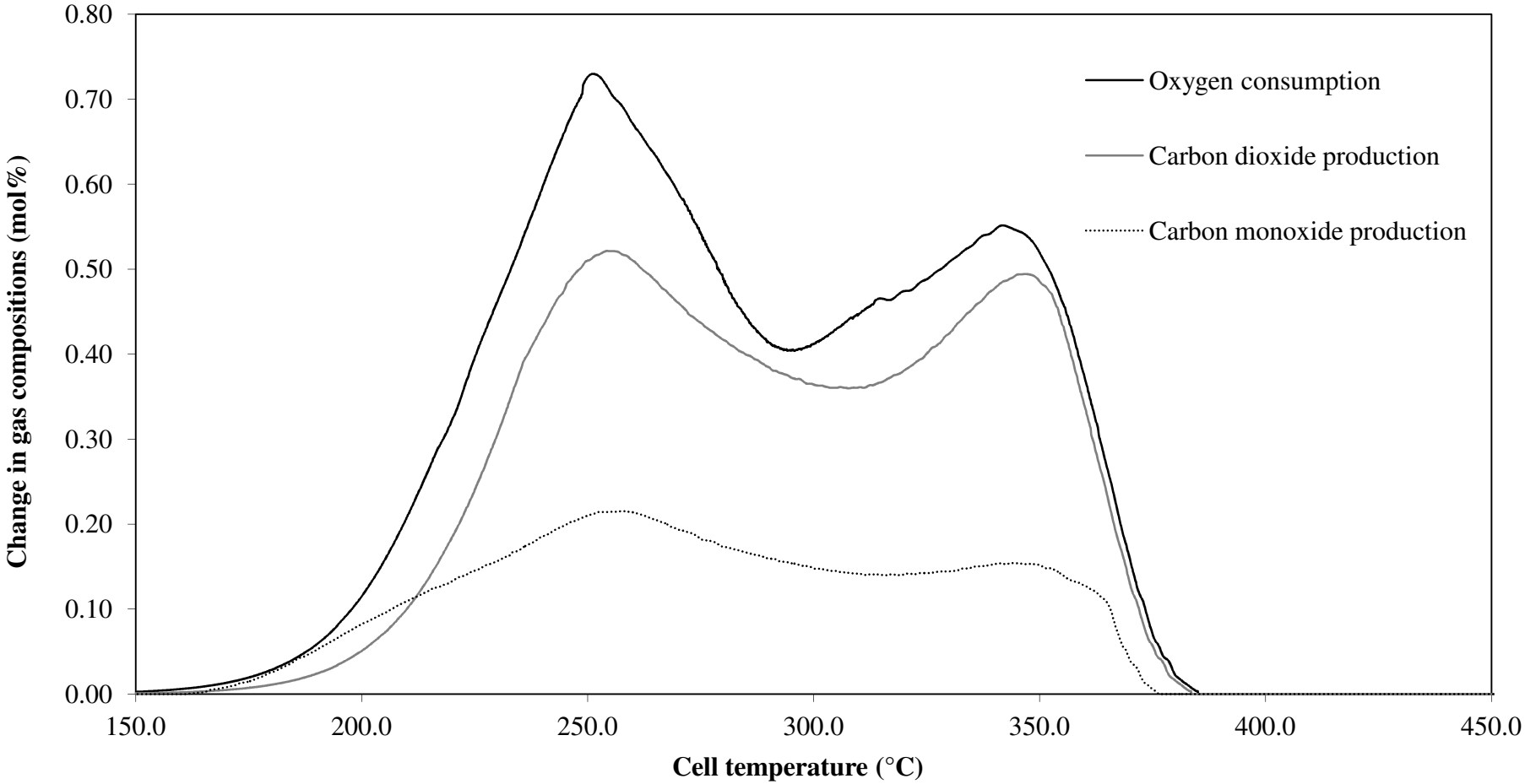

Figure 6.67 - Evolved gas analysis data with respects to the cell temperature for the oxidation of palm fibre - clump fibre with air as the oxidising gas, an absolute total system pressure of 700kPa, an air flow rate of 400smL/min and a heating rate of 50°C/h (Experiment F20).

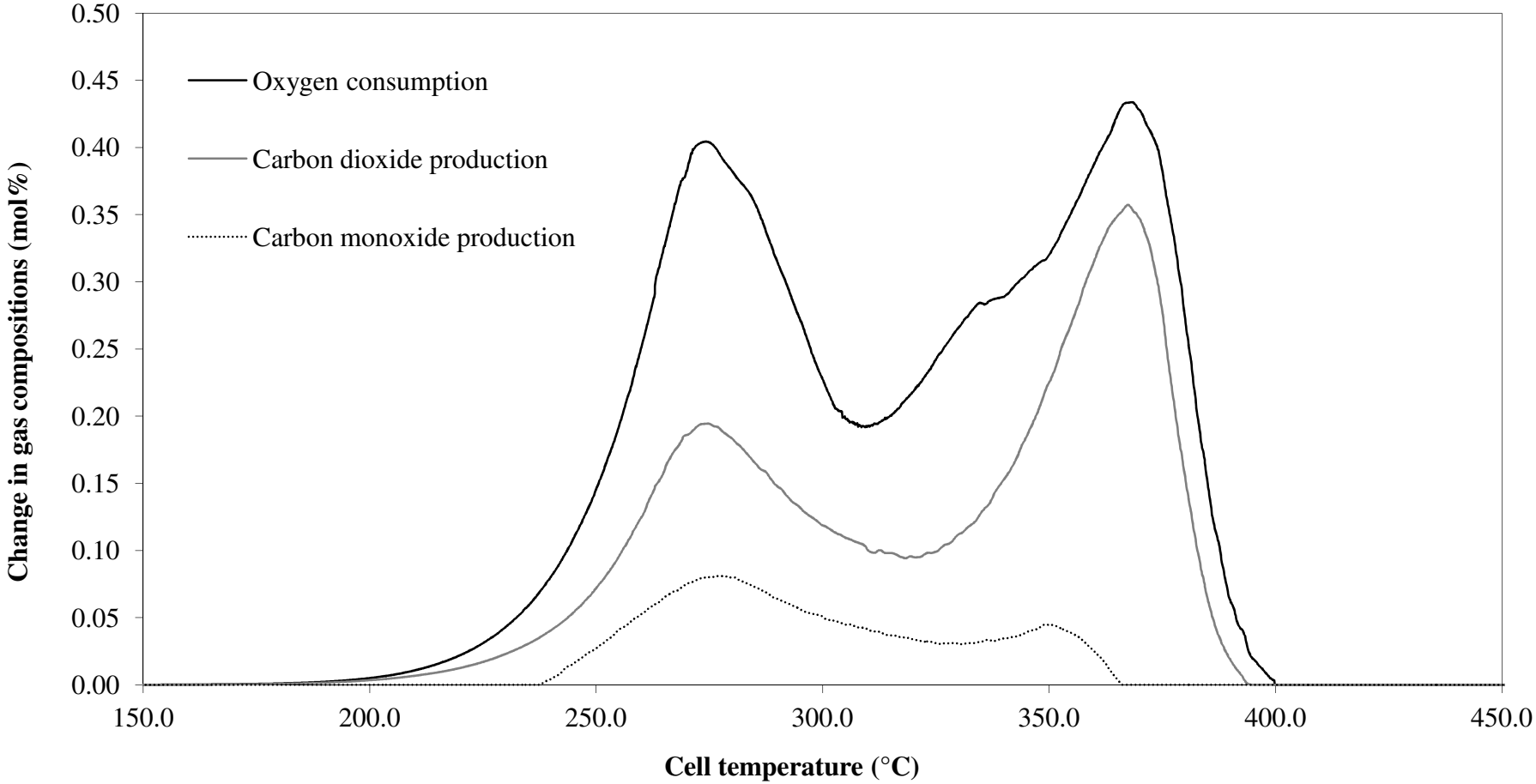

Figure 6.68 - Evolved gas analysis data with respects to the cell temperature for the oxidation of palm fibre - clump fibre with air as the oxidising gas, an absolute total system pressure of 363kPa, an air flow rate of 400smL/min and a heating rate of 50°C/h (Experiment F21).

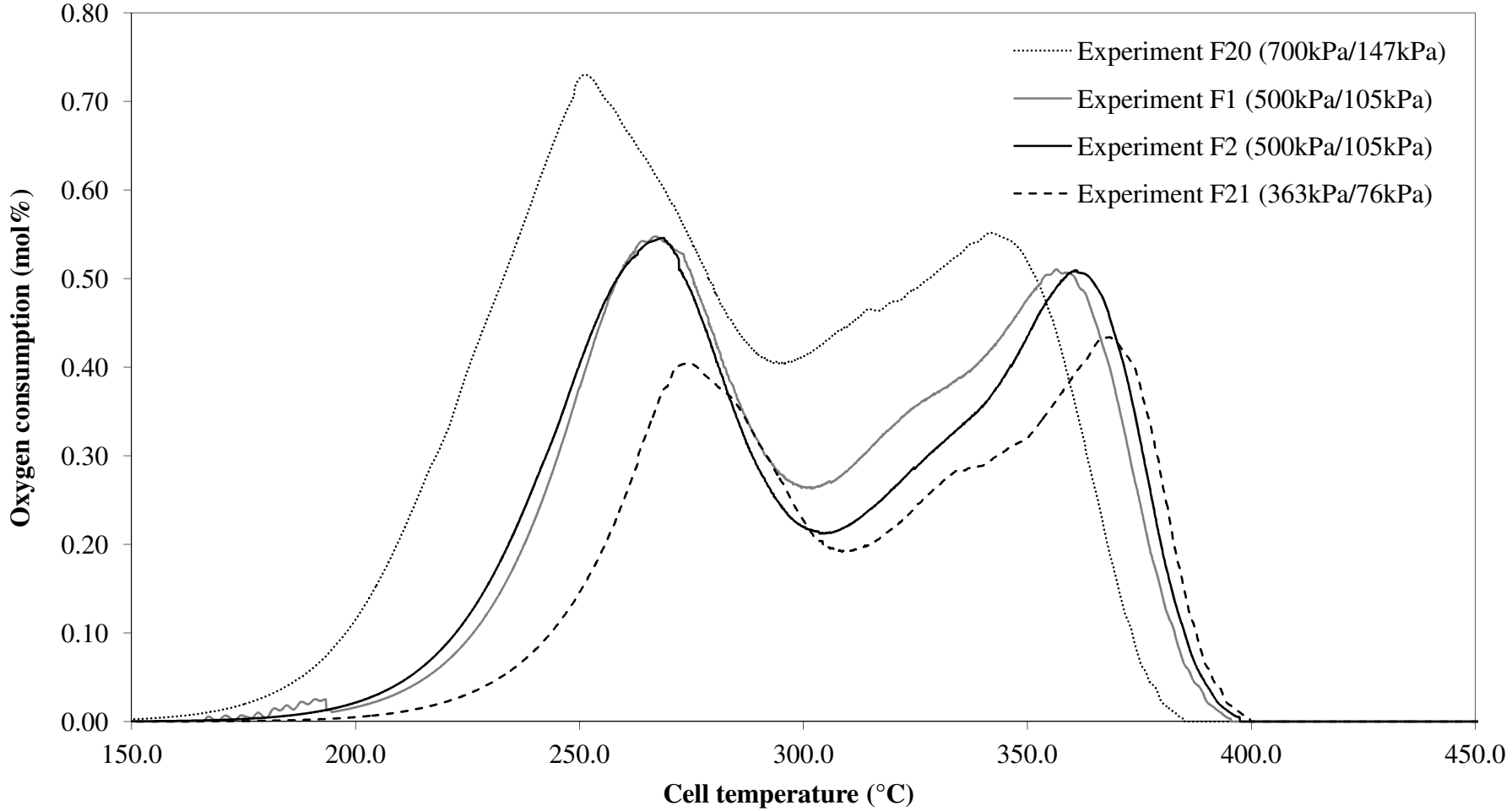

Figure 6.69 - Comparison of the oxygen consumption data with respects to the cell temperature for various pressures using clump fibre conducted at a heating rate of 50°C/h and a gas flow rate of 400smL/min. The pressures shown refer to the absolute total system pressure and oxygen partial pressure, respectively.

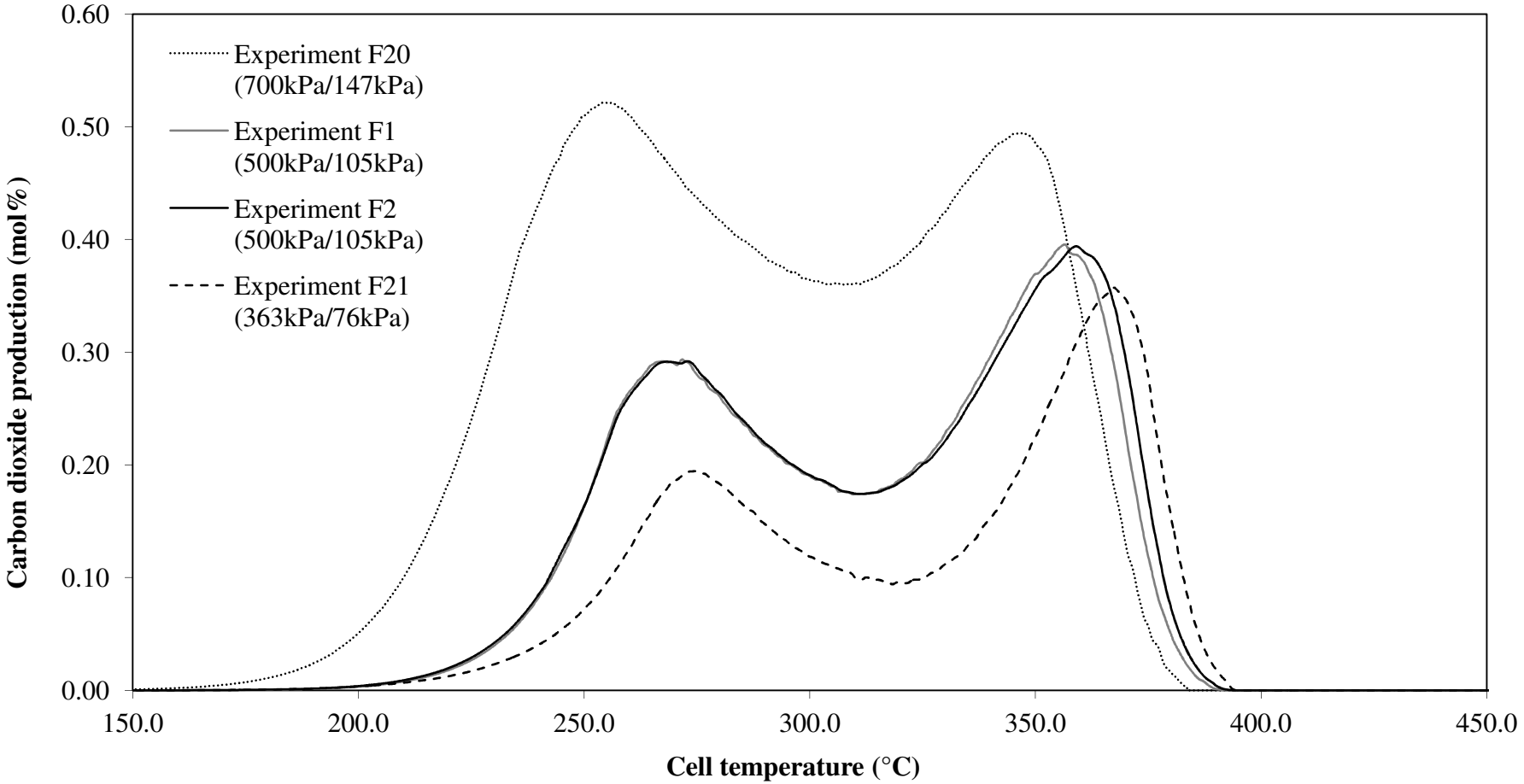

Figure 6.70 - Comparison of the carbon dioxide production data with respects to the cell temperature for various pressures using clump fibre conducted at a heating rate of 50°C/h and a gas flow rate of 400smL/min. The pressures shown refer to the absolute total system pressure and oxygen partial pressure, respectively.

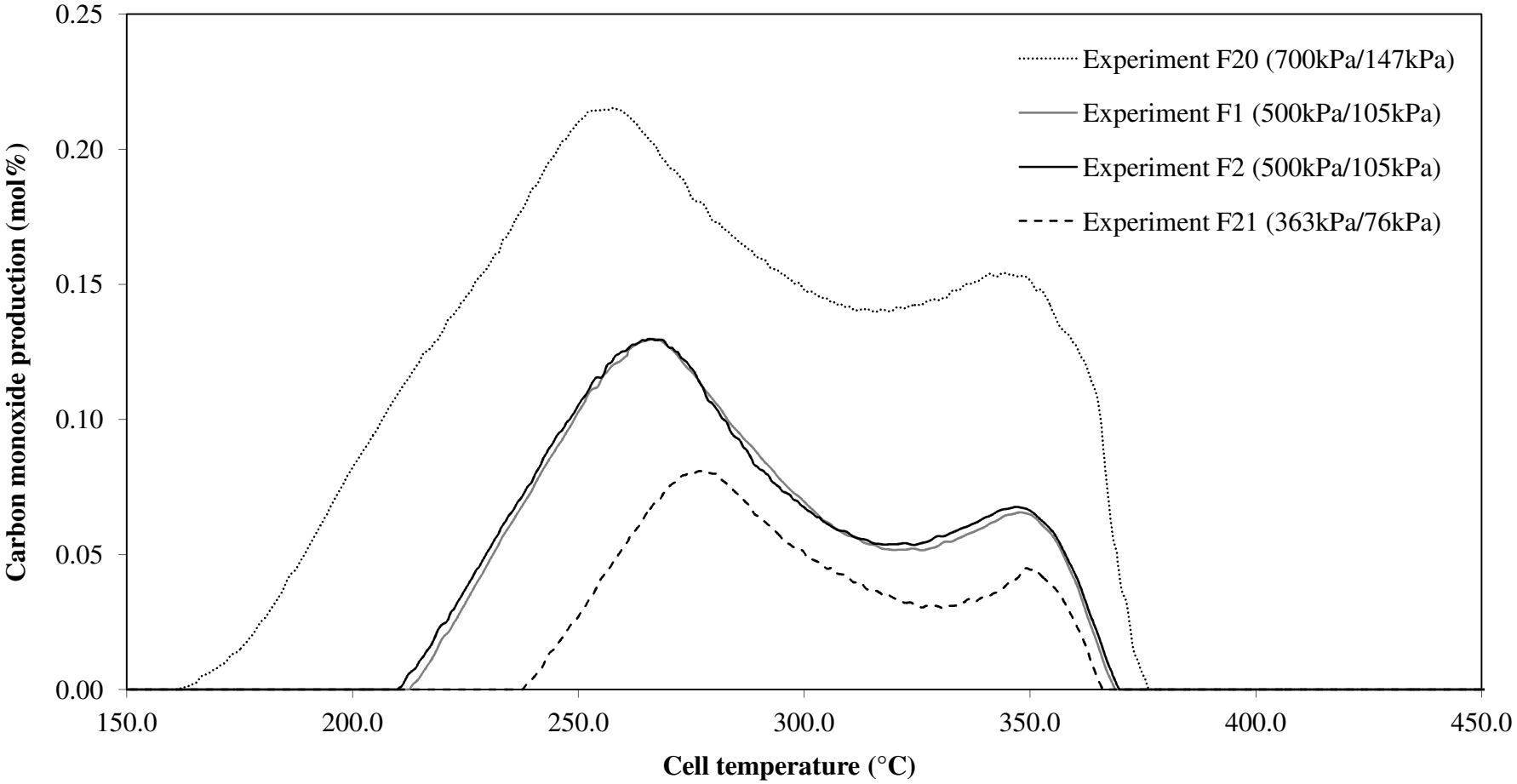

Figure 6.71 - Comparison of the carbon monoxide production data with respects to the cell temperature for various pressures using clump fibre conducted at a heating rate of 50°C/h and a gas flow rate of 400smL/min. The pressures shown refer to the absolute total system pressure and oxygen partial pressure, respectively.

The observation was found in agreement to the previous observations for the effect of pressure on palm fibre - loose fibre combustion characteristics study. By comparison of experiment F21 with experiment F19 and experiment F9 with experiment F20 conducted under similar conditions but using the loose and clump fibres, respectively, there are no significant differences in the measured peak temperatures and heights. This further confirms that the clump and loose fibres were comparatively similar samples.

The calculated kinetic parameters of the clump fibre samples of experiments F1, F2, F20 and F21 are provided in Table 6.4. The predicted oxygen consumption curve in comparison to the actual oxygen consumption curve of the experimental data for the typical clump fibre of experiment F1 is presented in Figure 6.7. Figures 6.72 to 6.74 present plots of the oxygen consumption data and the model prediction for experiments F2, F20 and F21, respectively. As observed in Table 6.4 and Figures 6.72 to 6.74, the experiments F2, F20 and F21 present a good fit between the predicted curve and the actual oxygen consumption experimental data with the calculated variance was below 0.001. The calculated variance obtained were 0.0001 for experiment F2 and 0.0002 for experiment F20. The calculated variance for the experiment F21 is 0.0005. Similar to the typical palm fibre experiment, most of the discrepancies were observed at the medium temperature range due to the overlapping of the MTO, LTO and HTO reactions. The discrepancy was also observed for the LTO reaction. The activation energy and the ln β for the high temperature oxidation (HTO) reaction decreased from 27.2×10^3K to 11.7×10^3K and from 28.0 to 13.5, respectively as the pressure increased from 362kPa to 700kPa (see Table 6.4). Likewise, the activation energy and the ln β for the medium temperature oxidation (MTO) and low temperature oxidation (LTO) reactions were also decreased as the pressure increased. The activation energy and the ln β for the MTO reaction decreased from 28.8×10^3K to 19.2×10^3K and 33.1 to 15.3, respectively. For the LTO reaction, the activation energy and the ln β were reduced from 26.6×10^3K to 14.9×10^3K and 28.5 to 19.2, respectively as the pressure increased from 363kPa to 700kPa. The reaction order also increased as the pressure increased for the HTO and LTO reactions but for the MTO reaction where the reaction order remains the same. These observations were found in agreement to the previous EGA experiments using the loose fibre discussed in previous Sections 6.5 and 6.6.

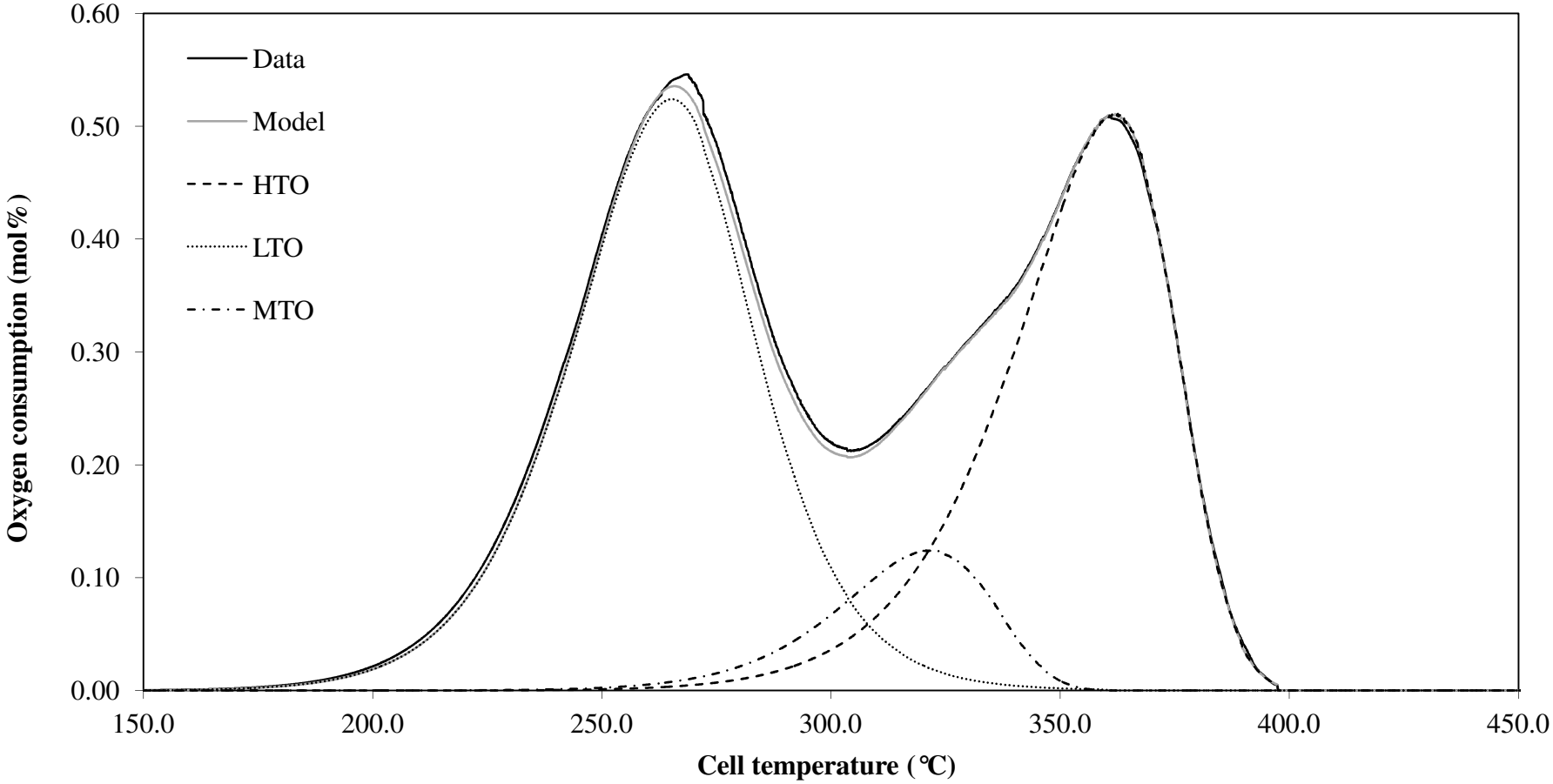

Figure 6.72 - Comparison of the oxygen consumption data and the model prediction with respects to the cell temperature for the oxidation of palm fibre - clump fibre with air as the oxidising gas, an absolute total system pressure of 500kPa, an air flow rate of 400smL/min and a heating rate of 50°C/h (Experiment F2).

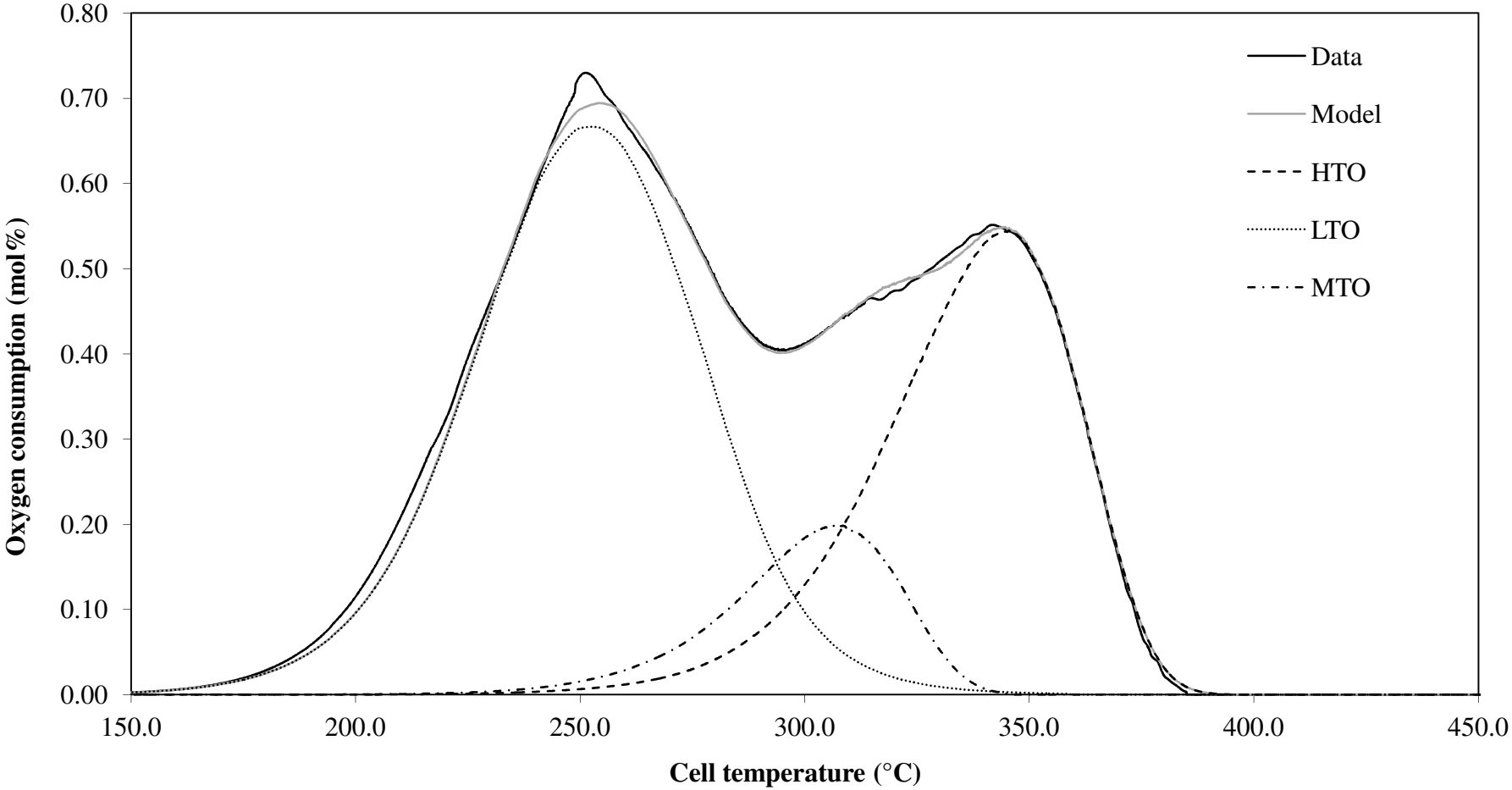

Figure 6.73 - Comparison of the oxygen consumption data and the model prediction with respects to cell temperature for the oxidation of palm fibre - clump fibre with air as the oxidising gas, an absolute total system pressure of 700kPa, an air flow rate of 400smL/min and a heating rate of 50°C/h (Experiment F20).

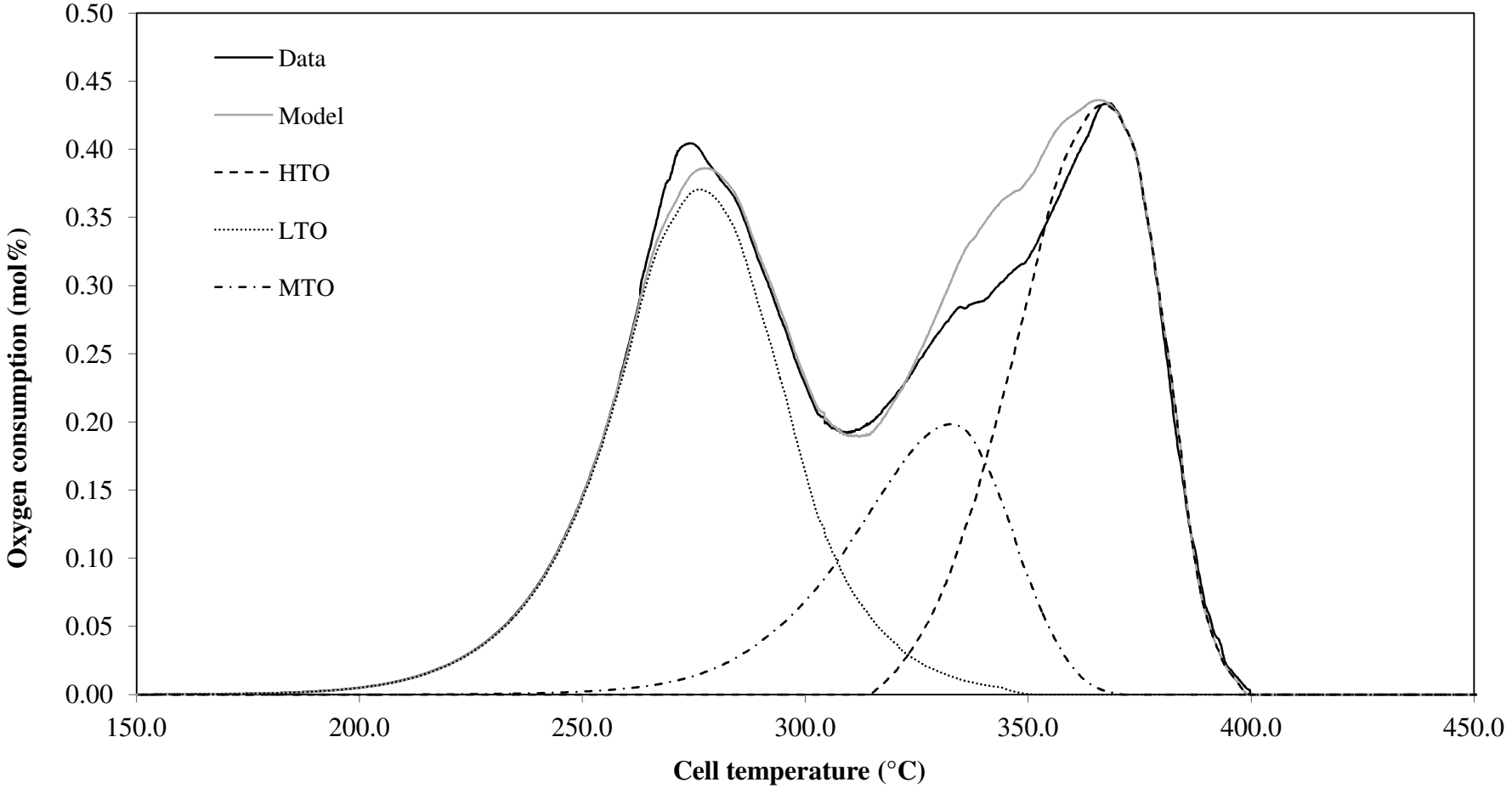

Figure 6.74 - Comparison of the oxygen consumption data and the model prediction with respects to the cell temperature for the oxidation of palm fibre - clump fibre with air as the oxidising gas, an absolute total system pressure of 362kPa, an air flow rate of 400smL/min and a heating rate of 50°C/h (Experiment F21).

By comparison of experiment F21 with experiment F19 and experiment F9 with experiment F20 conducted under similar conditions but using the loose and clump fibres, respectively, the calculated kinetic parameters show no significant differences.

In conclusion, the clump fibre and the loose fibre are similar samples. This findings is based on the EGA experimental results and the calculated kinetic parameters obtain for the loose and clump fibres. There are no significant differences obtained for both the peak temperatures and heights of the exit gas oxygen, carbon dioxide and carbon monoxide composition curves as well as the calculated kinetic parameters. As the pressure increases, all the exit gas composition peak temperatures reduce but the peak height increase. The calculated kinetic parameters of the activation energy and the ln β reduce as the pressure increases. The reaction order increases as the pressure increases for the HTO and LTO reactions with the MTO reaction as the exception where the reaction order remains the same.

6.8 Effect of particle size

If the internal diffusion is rate-controlling for the process of palm fibre combustion, then grinding the palm fibre sample could be expected to affect the EGA results. Experiment F22 was conducted using a ground sample of palm fibre and heated under conditions similar to those used for the typical palm fibre experiment F6. Figure 6.75 presents the variations in the exit gas compositions with respect to the cell temperature for experiment F22. The evolved gas analysis (EGA) experimental results are presented in Table 6.3. As shown in Figure 6.75, the plots were all in the same forms of having two peaks of hemicellulose and cellulose decompositions in the region of 250°C to 270°C and 340°C to 370°C, respectively. The peak temperatures were accurately determine at 263.1°C ± 1°C and 353.0°C ± 3°C for hemicellulose and cellulose, respectively. Figure 6.76 presents the comparison of the oxygen consumption curves for the experiment F22 using ground fibre with typical experiment F6 using the original size fibre conducted under similar conditions. Figures 6.77 and 6.78 present the corresponding information for the carbon dioxide production and carbon monoxide production curves.

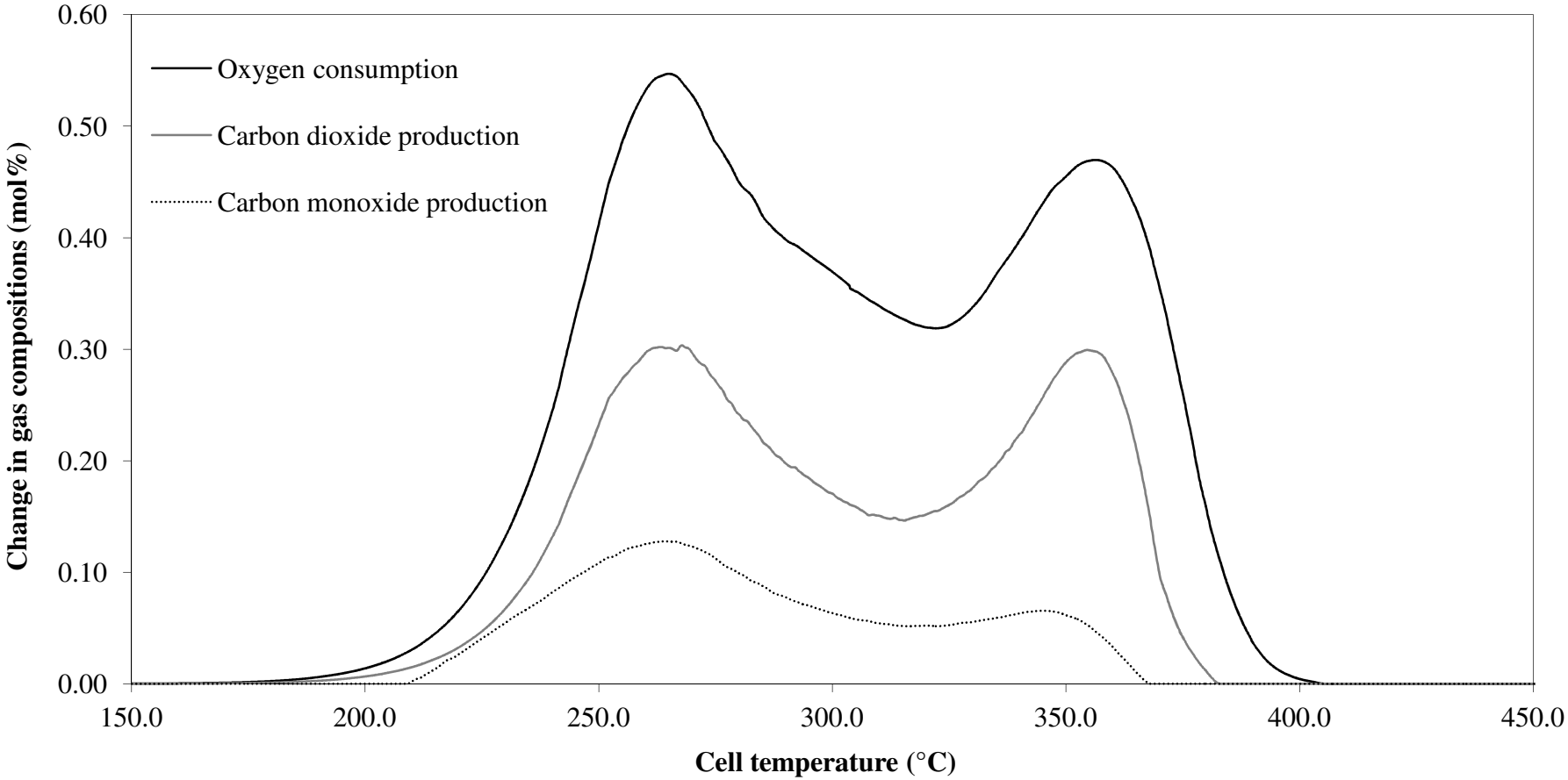

Figure 6.75 - Evolved gas analysis data with respect to the cell temperature for the oxidation of pulverised palm fibre with air as the oxidising gas, an absolute total system pressure of 500kPa, an air flow rate of 400smL/min and a heating rate of 50°C/h (Experiment F22).

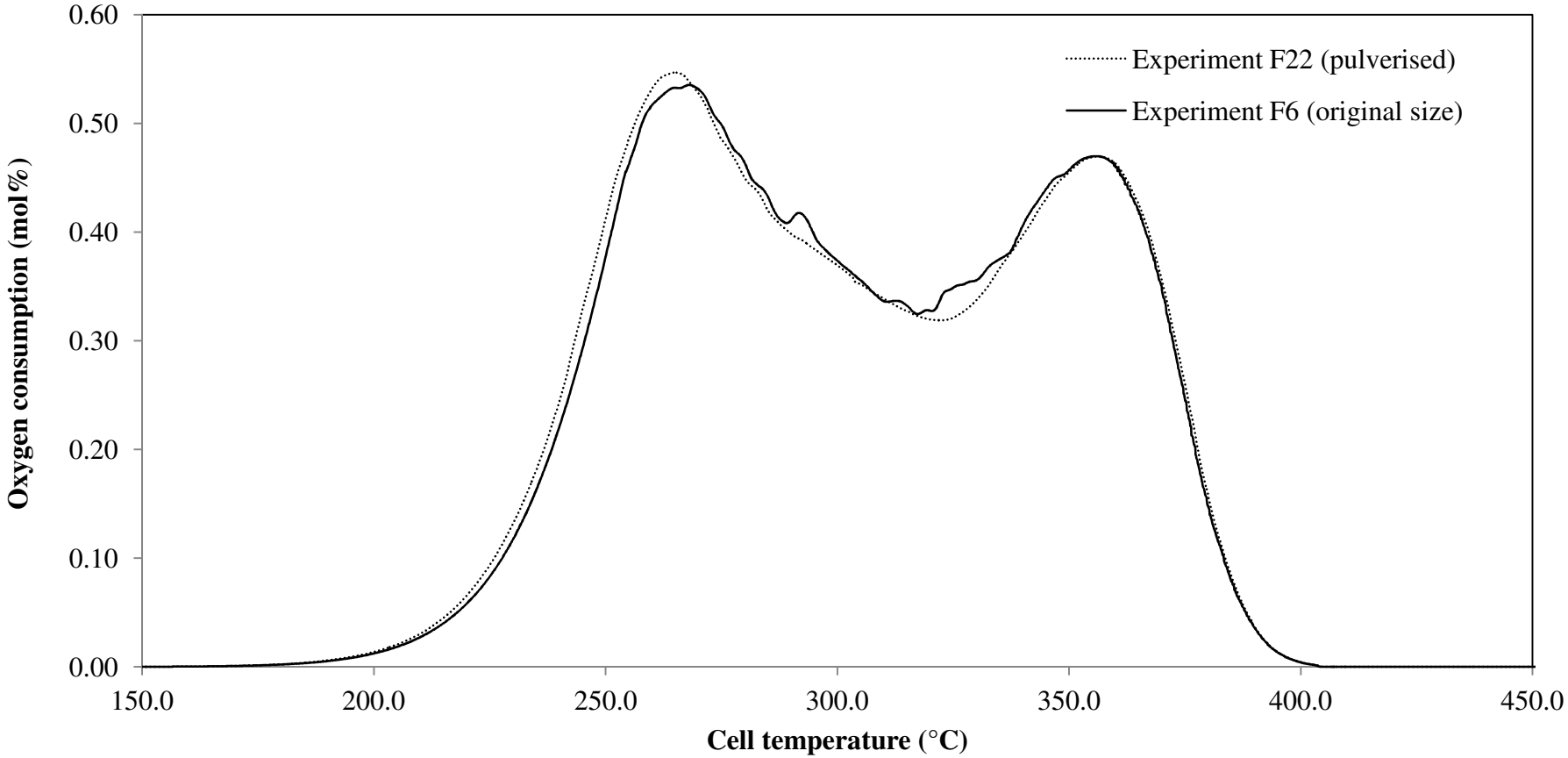

Figure 6.76 - Comparison of the oxygen consumption data with respect to the cell temperature of the pulverised and original size palm fibre experiments with air as the oxidising gas, an absolute total system pressure of 500kPa, an air injection flow rate of 400 smL/min and a heating rate of 50°C/h.

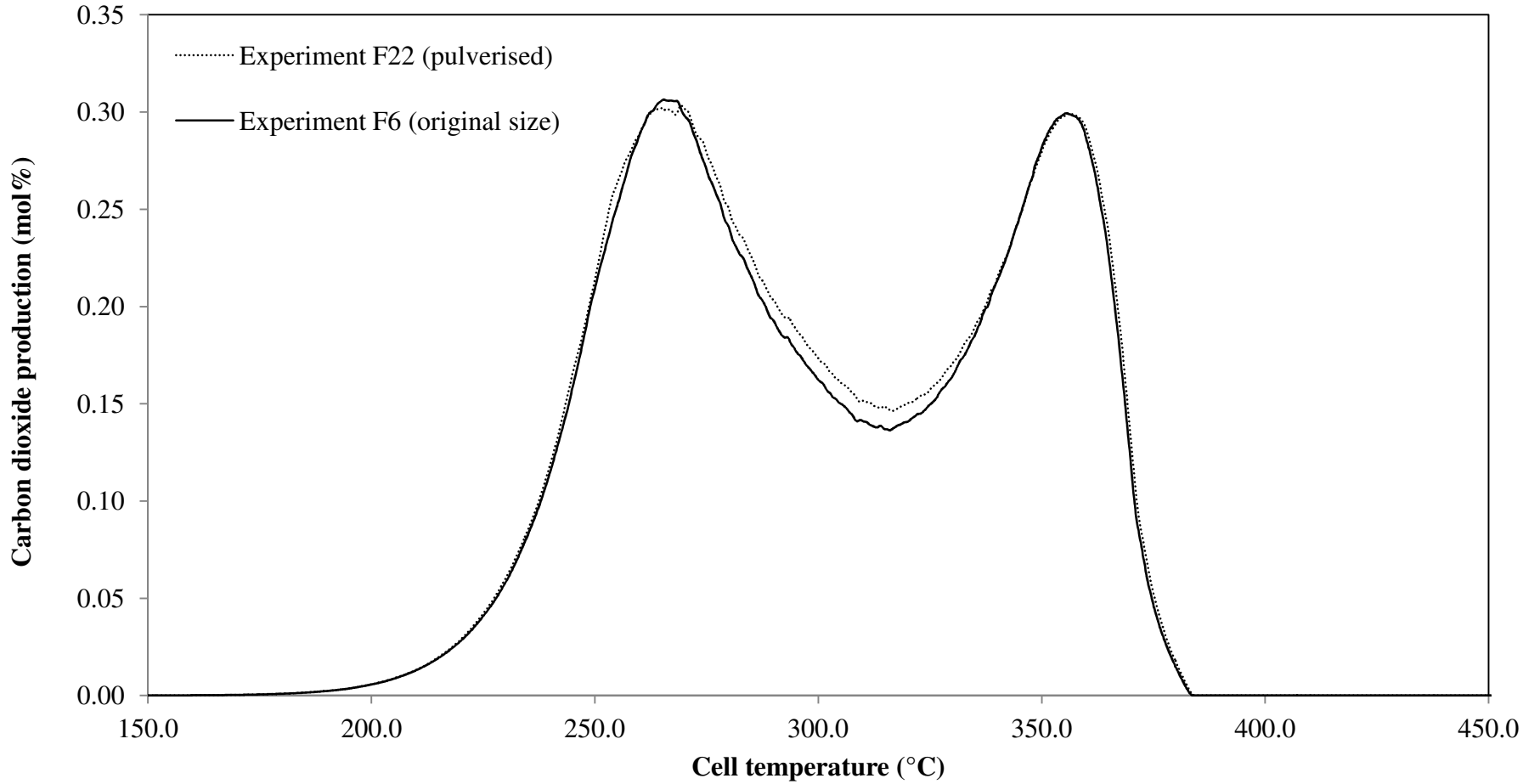

Figure 6.77 - Comparison of the carbon dioxide production data with respect to the cell temperature of the pulverised and original size palm fibre experiments with air as the oxidising gas, an absolute total system pressure of 500kPa, an air injection flow rate of 400 smL/min and a heating rate of 50°C/h.

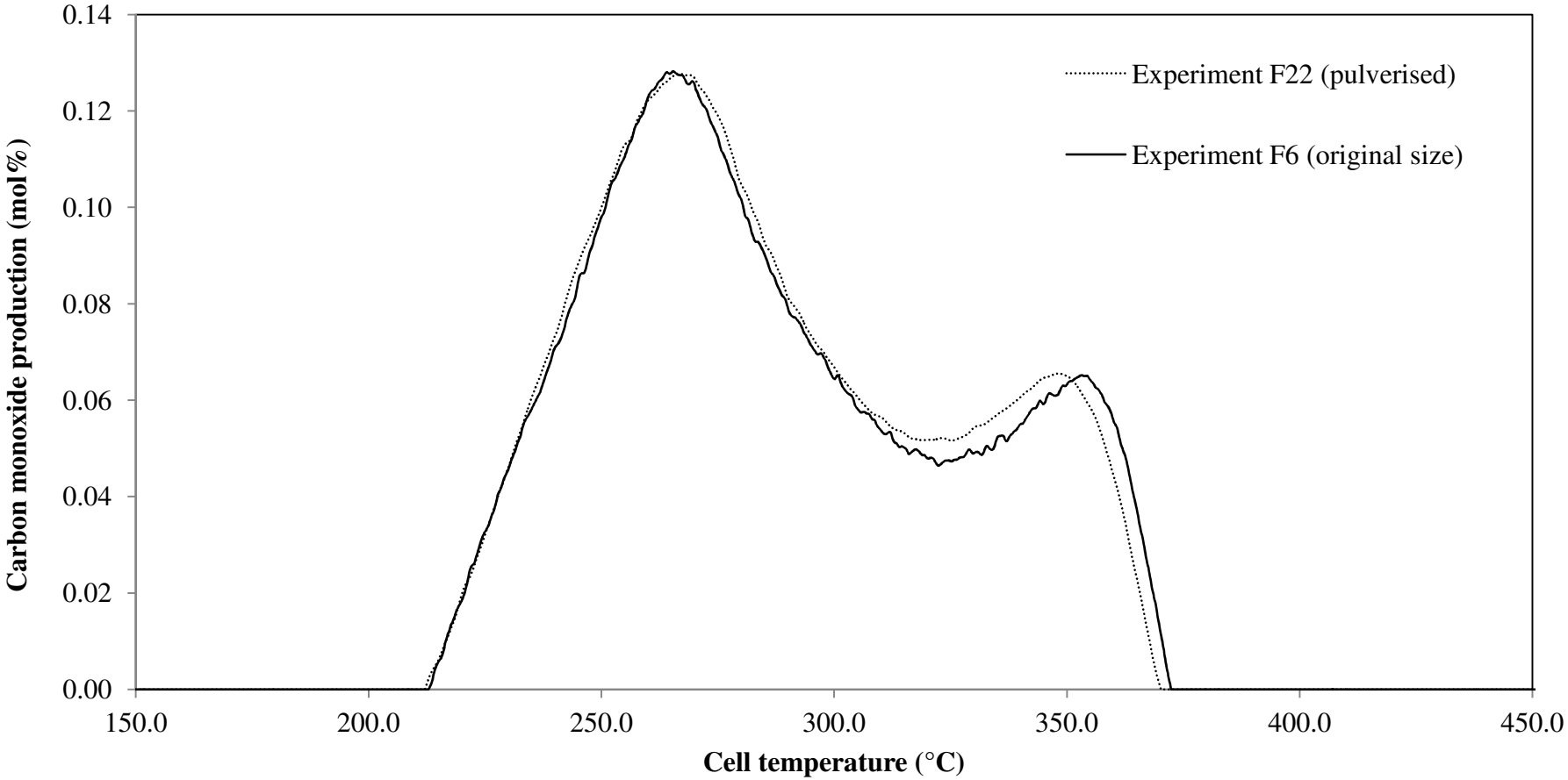

Figure 6.78 - Comparison of the carbon dioxide production data with respect to the cell temperature of the pulverised and original size palm fibre experiments with air as the oxidising gas, an absolute total system pressure of 500kPa, an air injection flow rate of 400 smL/min and a heating rate of 50°C/h.

As observed in Figures 6.76 to 6.78, there are small and almost negligible differences in the measured peak temperatures between both experiments F22 and F6. The peak heights of the exit gas oxygen, carbon dioxide and carbon monoxide also show no significant differences between experiments F22 and F6. The peak temperatures for the exit gas compositions of oxygen, carbon dioxide and carbon monoxide for experiment F22 were decreased by 1°C to 3°C for hemicellulose peak. The cellulose peak temperature show no significant differences between the two experiments. The small changes in peak temperatures show that grinding the palm fibre may facilitates the transfer of heat into the palm fibre interior and increase the rate at which volatile products from within the palm fibre to the palm fibre surface. These volatiles will escape and reacts with oxygen in the surrounding gases that eventually tend to reduce the peak temperature. However, the small decrease was within the Table 6.3 agreement of ± 3.1°C. Hence, this suggest that the palm fibre combustion process was not controlled by the internal diffusion. It would appear to confirm that the reaction is the rate-controlling step rather than the internal diffusion.

The summary of the calculated kinetic parameters for experiment F22 are shown in Table 6.4. Figure 6.79 presents the predicted oxygen consumption curve with the actual experimental data for experiment F22. Considering Figure 6.79 and Table 6.4 for experiment F22, a good fit between the predicted oxygen consumption and the actual experimental data was obtained with the calculated variance of 0.0001. The discrepancies are mainly observed at the medium temperature range of 270°C to 340°C due to overlaps of the MTO, LTO and HTO reactions. Considering Table 6.4 and by comparing experiment F22 (ground fibre) with experiments F4 to F6 (original size fibre), there are no significant differences observed in the calculated kinetic parameter values. This is well expected since the model does not considers the mass transfer resistance (if any).

In conclusion, there are no significant differences in the peak temperatures and peak heights observed for experiment conducted at smaller particle size in comparison to the original size of palm fibre.

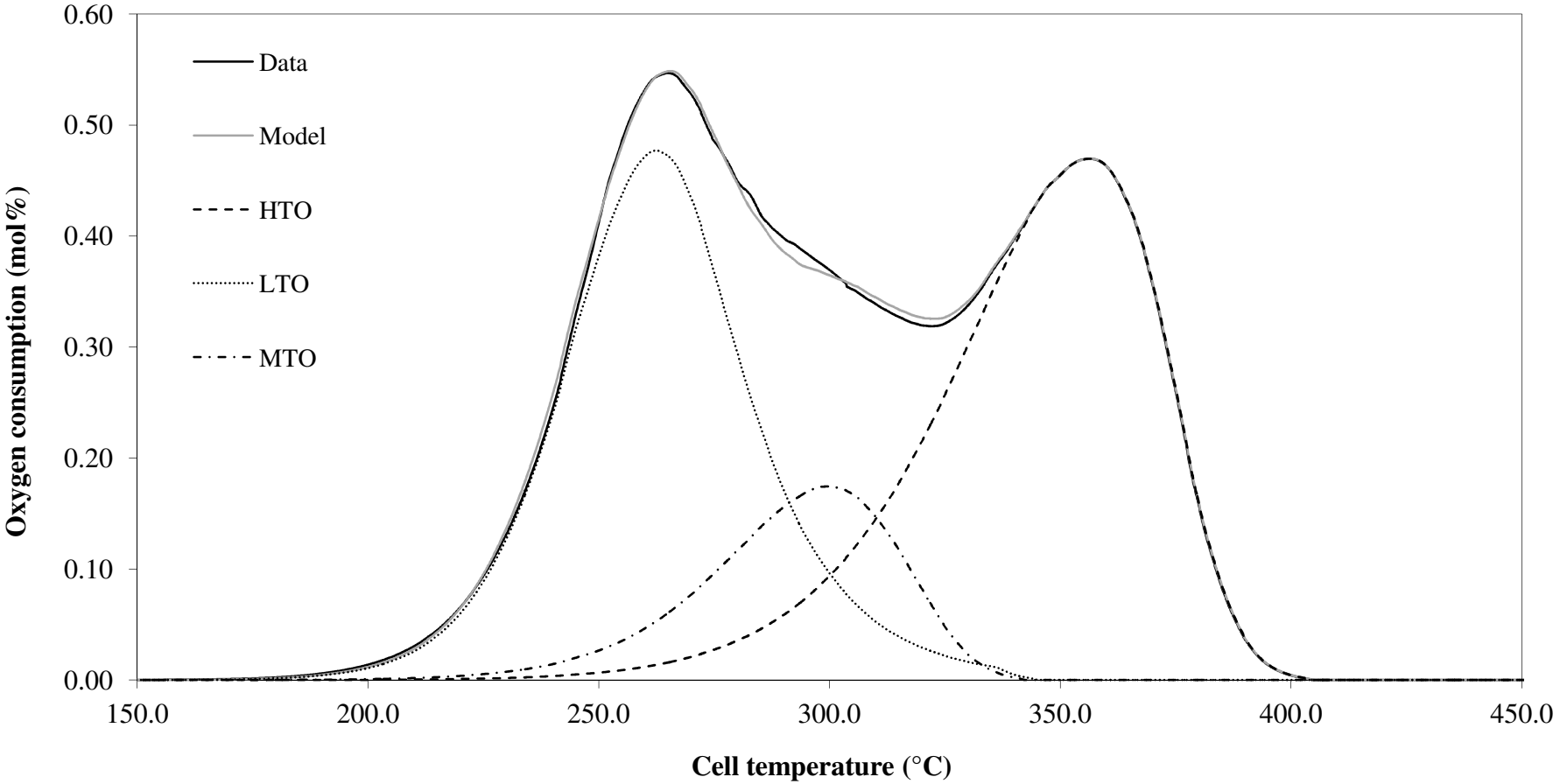

Figure 6.79 - Comparison of the oxygen consumption data and the model prediction with respect to the cell temperature for the palm fibre (ground sample) oxidation with air as the oxidising gas, an absolute total system pressure of 500kPa, an air injection flow rate of 400smL/min and a heating rate of 50°C/h (Experiment F22).

The finding confirms that the reaction is the rate-controlling step rather than the internal diffusion rate. The small differences are consistent with the level of accuracy of the palm fibre experiments. The calculated kinetic parameter values also show no significant differences as particle size reduces due to the proposed reaction model are not considering the mass transfer resistance.

6.9 Analysis of error in calculating the palm fibre kinetic parameters

The data obtained from an evolved gas analysis (EGA) experiments was used in the modeling procedure developed in Chapter 4. The accuracy of the raw data contributes to the range of confidence limits for the calculated kinetic parameters. The confidence limits may be determined by considering the contributions made by the various data points and the uncertainty associated with each data point. The calculation steps of the uncertainties in the experimental data and the sources of error for the EGA experiments were discussed in Section 5.6 previously. The same uncertainties calculation procedure was applied for the palm fibre. Table 6.5 presents the uncertainty in the calculated kinetic parameter values of the palm fibre for the high temperature oxidation (HTO) peak temperatures. The HTO reaction was chosen since the EGA results are most accurate at the high temperature. The absolute error was obtained by considering the change in the variable between each data reading of 10 seconds intervals.

Considering Table 6.5, the level of uncertainty in the activation energy was in the range of 2.0% to 6.4% for all the palm fibre experiments. The error in the calculated ln β were in the range of 3.3% to 9.9%. Hence, the level of uncertainty in the activation energy is about ±6.4% while the error for the ln β is approximately ±9.9% for all the palm fibre experiments.

The activation energy and the ln β for the typical clump fibre of experiment F1 obtained for the HTO reaction were 20.0×10^3K and 21.2, respectively. With the inclusion of the values for the uncertainty, the activation energy for the typical experiment F1 is therefore between 18.7×10^3K to 21.3×10^3K.

Table 6.5 - Uncertainty in the calculated values for the palm fibre EGA experiments. The relative error is refer to the peak temperature of the high temperature oxidation (HTO) reaction.

Variable	Absolute error	Relative error (%)							
		F1	F2	F3	F4	F5	F6	F7	F8
ΔO_2 (mol%)	0.004	0.78	0.78	0.46	0.87	0.85	0.85	0.70	1.29
Inverse temperature (K^{-1})	0.000001	0.04	0.04	0.04	0.04	0.04	0.04	0.04	0.03
Integral (ΔO_2 vs t)	6	0.15	0.16	0.16	0.15	0.15	0.15	0.22	0.30
Ln (RRR)	0.009	0.13	0.13	0.13	0.12	0.12	0.12	0.14	0.13
E_i/R	700	3.50	3.54	2.87	3.50	3.54	3.57	3.42	3.45
ln β_i	1.3	6.13	6.19	4.22	6.19	6.05	6.13	5.96	6.02

Table 6.5 (continued) - Uncertainty in the calculated values for the palm fibre EGA experiments. The relative error is refer to the peak temperature of the high temperature oxidation (HTO) reaction.

Variable	Absolute error	Relative error (%)							
		F9	**F10**	**F11**	**F12**	**F13**	**F14**	**F15**	**F16**
ΔO_2 (mol%)	0.004	0.73	1.29	0.69	1.33	1.18	0.80	0.71	1.25
Inverse temperature (K^{-1})	0.000001	0.03	0.04	0.04	0.04	0.04	0.04	0.04	0.04
Integral (ΔO_2 vs t)	6	0.10	0.27	0.14	0.40	0.24	0.13	0.12	0.35
Ln (RRR)	0.009	0.12	0.13	0.12	0.13	0.12	0.12	0.12	0.13
E_i/R	700	6.36	1.99	2.67	2.06	1.99	3.54	4.29	1.91
ln β_i	1.3	9.85	3.34	4.92	3.57	3.49	6.08	6.88	3.34

Table 6.5 (continued) - Uncertainty in the calculated values for the palm fibre EGA experiments. The relative error is refer to the peak temperature of the high temperature oxidation (HTO) reaction.

Variable	Absolute error	Relative error (%)					
		F17	**F18**	**F19**	**F20**	**F21**	**F22**
ΔO_2 (mol%)	0.004	1.29	0.78	0.85	0.73	0.93	0.85
Inverse temperature (K^{-1})	0.000001	0.04	0.04	0.04	0.03	0.04	0.04
Integral (ΔO_2 vs t)	6	0.36	0.15	0.20	0.11	0.20	0.15
Ln (RRR)	0.009	0.13	0.13	0.13	0.12	0.13	0.12
E_i/R	700	1.96	2.51	2.59	5.98	2.57	3.56
ln β_i	1.3	3.40	4.51	4.53	9.63	4.64	6.10

The ln β is between 19.1 to 23.3. The activation energy and the ln β for the typical kernel of experiment F3 were 24.4 × 10^3K and 30.8, respectively. By including the uncertainty values, the activation energy for the typical experiment F3 yields in between 22.8 × 10^3K to 26.0 × 10^3K. The ln β was in the range of 27.8 to 33.9. Considering the typical loose fibre of experiment F6, the activation energy and the ln β obtained for the HTO reaction were 19.6 × 10^3K and 21.2. After the inclusion of the uncertainty, the activation energy for experiment F6 was in the range of 18.4 × 10^3K to 20.9 × 10^3K. The ln β for the experiment F6 yields in between 19.1 to 23.3. From this, we infer that the activation energy and the ln β for the clump and loose fibres overlaps in the same range. However, the activation energy and the ln β for the kernel sample were higher than both the clump and loose fibre samples.

Vuthaluru (2004) investigated the pyrolytic behaviour of wood waste and wheat straw using the thermogravimteric analysis (TGA). The author found that the activation energy for the wood waste and the wheat straw decompositions were 118 kJ/mol (12 100K) and 115 kJ/mol (11 800K), respectively. Idris *et al.* (2010) calculated the activation energy of palm fibre to be of 216.1 kJ/mol (22 200K) and palm kernel shell of 277.11 kJ/mol (28 500K) in their work of the thermocehemical behaviour of the oil palm biomass using the thermogravimteric analysis (TGA). The calculated activation energy values observed for those previous researchers were comparatively similar to the activation energy values found for this study of palm fibre this study using an evolved gas analysis (EGA) technique.

6.10 Concluding remarks

The clump and loose fibre are comparatively similar sample as indicated by the evolved gas analysis (EGA) experimental results and the calculated kinetic parameters. However, the kernel sample is different from the loose and clump fibres. The evidence of these three samples of palm fibre shows that it is a very heterogeneous materials. This also confirms that the EGA experiments is able to handle various kind of samples accurately. Likewise, the suggested model of the oxygen consumption is also successfully able to fit with the experimental data of the palm fibre experiments.

The evolved gas analysis (EGA) experiments for the palm fibre are reproducible. There are no significant differences in the peak temperatures and heights observed for all the exit gas composition curves of the three experiments conducted under similar conditions. Further, there are also no significant differences on the calculated kinetic parameters of the reaction order, the activation energy and the natural log of beta group of these three identical experiments.

The heating rate of the combustion cell has a significant influence on both the peak temperatures and heights for all the exit gas composition curves. The peak temperatures and heights of all the exit gas composition curves increase as the heating rate increases. However, there are no significant differences in the calculated kinetic parameters observed since the calculation procedure allows for changes in the heating rate.

The pressure has a significant influence on the palm fibre combustion characteristics. The EGA experiments both on the loose and clump fibres confirm these findings. As the pressure increases, all the exit gas composition peak temperatures decrease but the peak height increases. The calculated kinetic parameters of the activation energy and the ln β decrease as the pressure increases.

The total system pressure has no significant influence on the peak temperature for the exit gas oxygen, carbon dioxide and carbon monoxide composition curves. However, the peak height increases as the total system pressure increases. The calculated kinetic parameters show that the total system pressure has no significant influence in the palm fibre combustion characteristics study. However it is the oxygen partial pressure that has a significant effect to the palm fibre combustion characteristics. The peak temperatures for the effluent gas oxygen, carbon dioxide and carbon monoxide composition curves decrease with the increasing oxygen partial pressure. The peak height for the exit gas oxygen, carbon dioxide and carbon monoxide composition curves increase to the increasing oxygen partial pressure. As for the calculated kinetic parameters, the reaction regimes of the HTO, MTO and LTO are influenced by the oxygen partial pressure. There are significant differences in the calculated kinetic parameters over a range of oxygen partial pressures that has a similar total system

pressure. The activation energy and the ln β decrease with increasing oxygen partial pressure for the HTO, MTO and LTO reactions.

The activation energy and the ln β for the typical clump and loose fibres falls comparatively within the same range. The activation energy and the ln β for the clump fibre are within the range of 18.7×10^3K to 21.3×10^3K and 19.1 to 23.3, respectively. As for the loose fibre, the activation energy and the ln β are within the range of 18.4×10^3K to 20.9×10^3K and 19.1 to 23.3, respectively. Further, the activation energy and the ln β for the typical kernel sample yields in between 22.8×10^3K to 26.0×10^3K and 27.8 to 33.9, respectively.

Of all the conditions tested, the best set of conditions tested is for the absolute total system pressure of 700kPa and the oxygen partial pressure of 147kPa. At this best condition, the activation energy and the peak temperatures recorded at their lowest values of within 10.3×10^3K to 11.7×10^3K and 253.6°C, respectively. The peak height of the oxygen consumption curve also reveals that at this condition, the oxygen consumed is at the optimum of 0.74 mol% oxygen. Hence, this would lead to a higher carbon conversion efficiency. The use of higher oxygen concentrations would lead to the increase of the oxygen partial pressure and results in higher carbon conversion efficiency. This observations will be useful in subsequent biomass combustion design studies. The next Chapter 7 examines the combustion characteristics of the palm fibre char and may provides an excellence comparison to the raw samples.

CHAPTER 7

PALM FIBRE CHAR OXIDATION

7.1 Introduction

Palm fibre char is an alternative fuel obtained from the carbonisation of the palm fibre. The carbon rich material may be used as a fuel that has desirable properties and is potentially a good solution to the high transport costs and poor grind-ability associated with the direct use of the biomass as a fuel. The combustion of carbon in air occurs in two reactions with the oxygen reacting to form both carbon oxides:

$$C + O_2 \rightarrow CO_2 \tag{7.1}$$

$$C + \frac{1}{2}O_2 \rightarrow CO \tag{7.2}$$

This Chapter reports the results of an evolved gas analysis (EGA) experimental investigation into the combustion characteristics of palm fibre char. First a discussion is presented on the typical experimental results of the palm fibre char and this is followed by the discussion of the calculated kinetic parameters. A discussion on the reproducibility study and the effect of the total system pressure and the oxygen partial pressure on the palm fibre char experiments is then presented. This discussion covers both the experimental and the calculated kinetic parameters result. Next an analysis of error in calculating kinetic parameters of the palm fibre char experiments is presented.

7.2 Typical palm fibre char experimental and kinetic parameter results

A total of nine experimental runs were conducted using the palm fibre char. The summary of the experimental conditions for the palm fibre char experiments is presented in Table 7.1. Table 7.2 presents the results of the ultimate and proximate analyses of the palm fibre char. As shown in Table 7.2, the calorific value for the palm fibre char is approximately 80% higher (from 19.0MJ/kg to 34.2MJ/kg) than the calorific value of the raw palm fibre. This is expected as the volatile matter has been discharged during the pyrolysis process at 400°C increasing the calorific value (Park and Jang, 2012). The typical palm fibre char evolved gas analysis (EGA) experimental results for experiment C1 is shown in Figure 7.1. In this Figure 7.1, the oxygen consumption curve is plotted with the actual carbon monoxide and carbon dioxide production curves against the cell temperature. As observed in Figure 7.1, the plots were all in the same forms; exhibiting one peak in the region of 350°C to 370°C. The peak temperatures for the exit gas oxygen, carbon dioxide and carbon monoxide compositions were in agreement being 360.5°C within ±0.2°C. A similar observation was also reported by Park and Jang (2012) in their fuel characteristics study of the biomass char (rice husks, wood chips and wood pellets) using a thermogravimetric analysis (TGA) technique. They observed that the rice husks, wood chips and wood pellets chars displayed only one peak in their char combustion decomposition.

The typical palm fibre char experiment C1 may be modeled against the three overlapping reaction regimes representing the high temperature oxidation (HTO), the low temperature oxidation (LTO) and the medium temperature oxidation (MTO). For each of the oxidation regimes, the calculated kinetic parameters are obtained. The kinetic parameters calculated for each of the oxidation regimes are the natural log of beta group (ln β), the activation energy expressed as the activation energy divided by the Universal gas constant (E/R) and the reaction order (n). The procedure as described in detail in the previous Chapter 4 was used to calculate the kinetic parameters. Values obtained for the kinetic parameters from these experiments indicate the accuracy of the experimental technique and the data analysis procedure.

Table 7.1 - Experimental conditions for palm fibre char experimental runs. M1 is gas mixture 1 that consists of 15.10 mol% O_2, 2.01 mol% CO_2, 0.983 mol% CO and balance nitrogen. M2 is gas mixture 2 that contains of 18.10 mol% O_2, 4.99 mol% CO_2, 2.51 mol% CO and balance nitrogen.

Experiment	**C1**	**C2**	**C3**	**C4**	**C5**	**C6**	**C7**	**C8**	**C9**
Absolute total system pressure (kPa)	500	500	500	700	300	500	500	695	580
Oxygen partial pressure (kPa)	105	105	105	147	63	76	91	105	105
Injection gas (mol% Oxygen)	20.96 (Air)	20.96 (Air)	20.96 (Air)	20.96 (Air)	20.96 (Air)	15.10 (M1)	18.10 (M2)	15.10 (M1)	18.10 (M2)
Injection flow rate (smL/min)	400	400	400	400	400	400	400	400	400
Heating rate (°C/h)	50	50	50	50	50	50	50	50	50

Table 7.2 - Ultimate and proximate analyses of palm fibre char. Note that db is dry basis and daf is dry ash free.

Analyses	Palm fibre char
Proximate analysis (db) (wt.%)	
Volatile matter	36.3
Fixed carbon	45.2
Ash	18.4
Ultimate analysis (daf) (wt.%)	
Carbon	60.90
Hydrogen	2.82
Nitrogen	1.43
Sulphur	-
Oxygen	34.85
Calorific value (MJ/kg)	34.20

The level of agreement between the predicted and the actual oxygen consumption curves was based on the calculated variance. The variance is calculated by:

$$\sigma^2 = \frac{\sum_{j=1}^{m} \left(\Delta O_{2\,j} - \Delta O_{2\,calc} \right)^2}{(m-2)} \tag{7.3}$$

where, σ^2 is the variance,

m is the number of data points used in the regression, first point at time t_1 , and last point at time t_m,

and, m-2 is the degree of freedom.

Similar to the rice husks and the palm fibre oxidation studies, we define a good fit to be when the value of the variance is below than 0.001 whereas if the value of the variance in between 0.001 and 0.003, we define this to be an acceptable fit. A poor fit is defined if the value of variance is higher than 0.003. Figure 7.2 shows the predicted oxygen consumption curve together with the actual oxygen consumption curve with respect to the cell temperature.

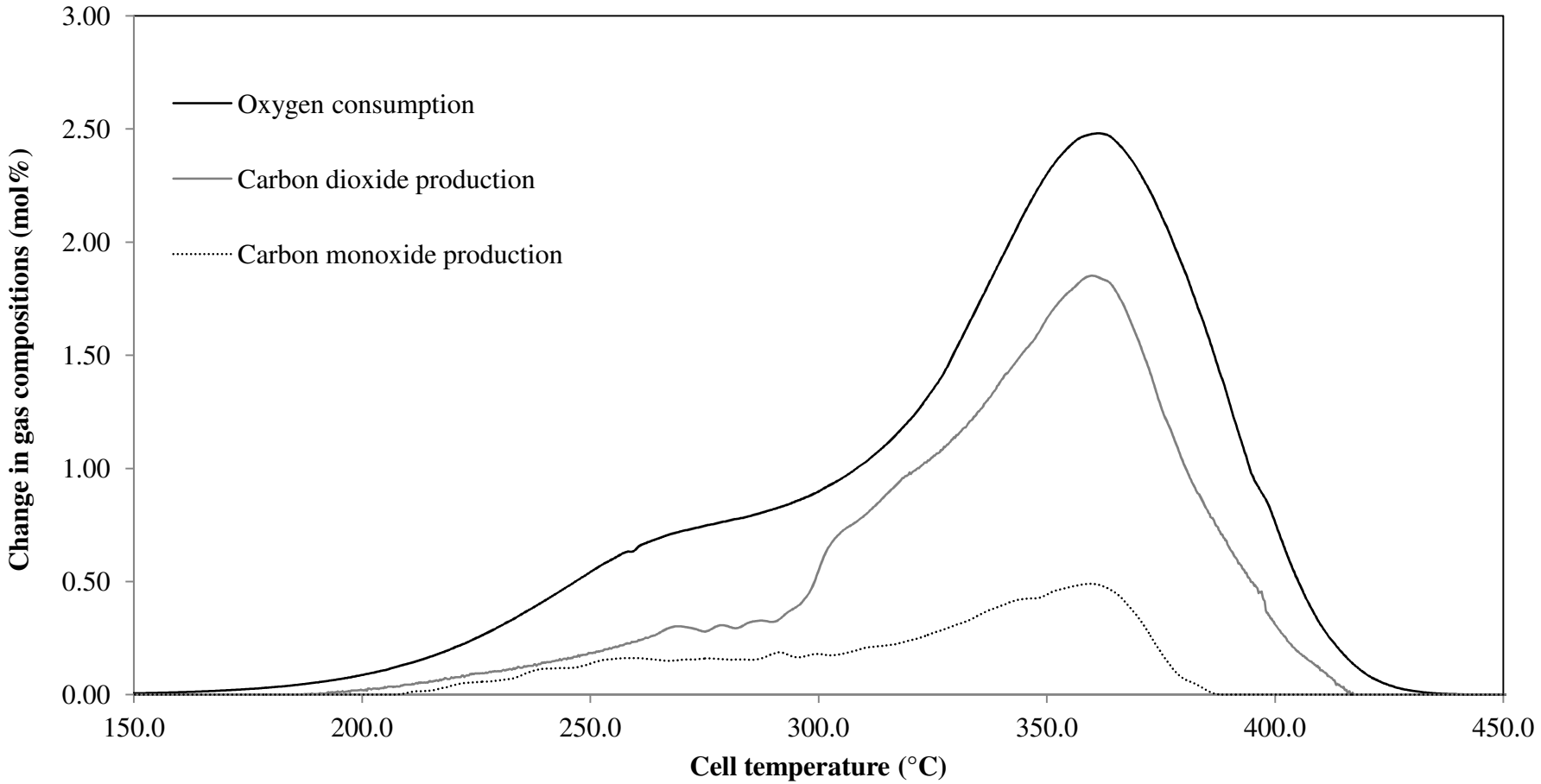

Figure 7.1 - Typical palm fibre char evolved gas analysis (EGA) experimental results with air as the oxidising gas, an absolute total system pressure of 500kPa, an air flow rate of 400smL/min and a heating rate of 50°C/h (Experiment C1).

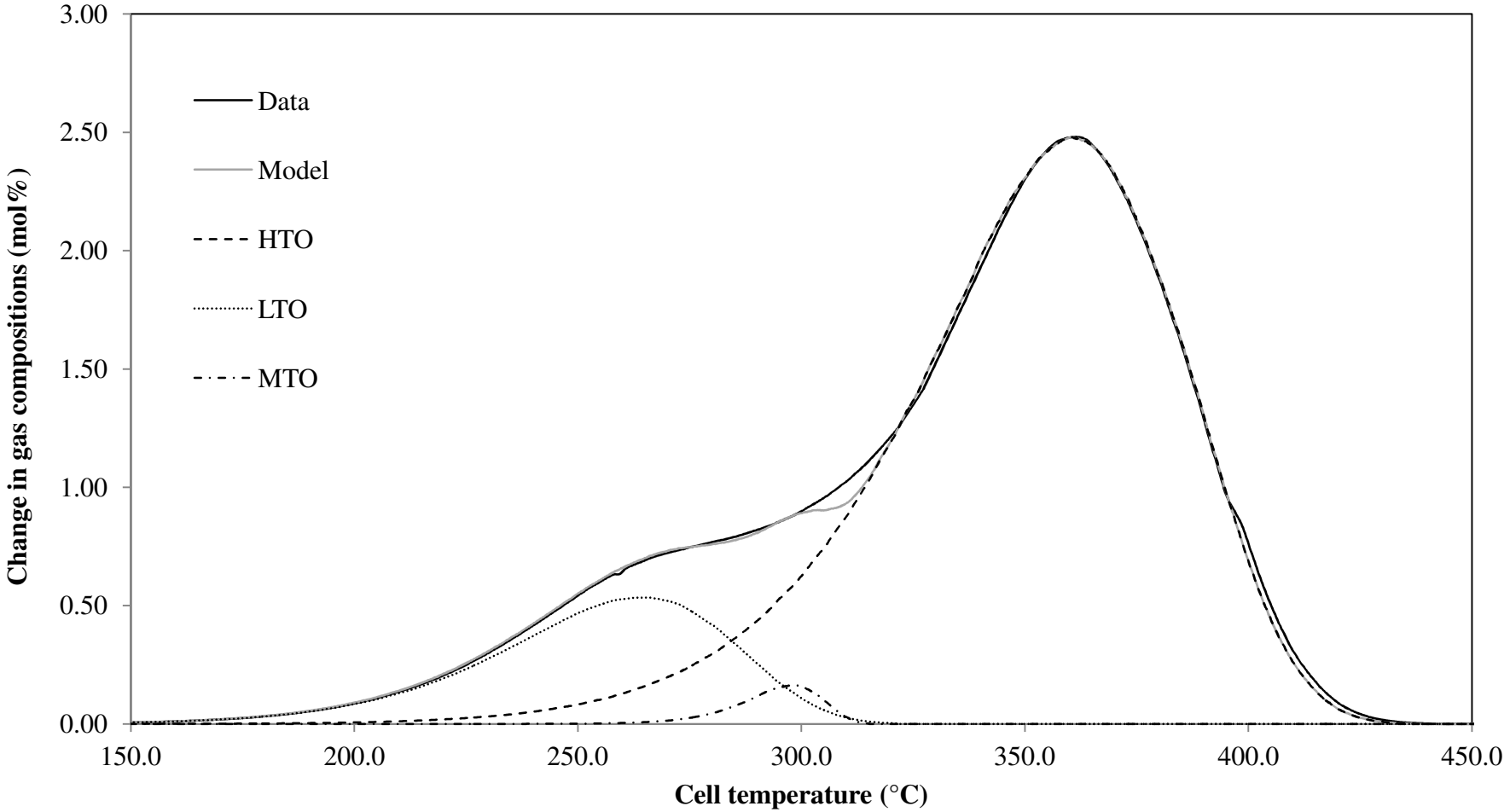

Figure 7.2 - Typical palm fibre char decoupled evolved gas analysis for the oxidation of experiment C1. The oxygen consumption curve was decoupled using the three regimes (HTO, MTO and LTO) model. The LTO and MTO reactions were decoupled simultaneously.

Considering Figure 7.2, a good fit between the predicted oxygen consumption curves and the experimental data was obtained for experiment C1. The calculated variance obtained was 0.0009. There are small disagreements in the high temperature region between 390°C and 430°C and in the medium temperature range between 290°C and 330°C. Unlike the rice husks and palm fibre combustion characteristic studies, there is a good agreement between the predicted and the actual oxygen consumption curves at the LTO reaction. The disagreement in the high temperature range of 390°C to 430°C is due to the instability of the experimental data at very high temperature that leads to the poor match to the predicted oxygen consumption curve. The disagreement in the medium temperature range between 290°C and 330°C is due to the overlapping between the HTO and the MTO regimes that makes it difficult to obtain a good fit. Further, the errors that been transferred from the HTO and the LTO calculations also contribute to the disagreement in the medium temperature range between 290°C and 330°C. Also, the magnitude of the MTO reaction was relatively very small for a typical palm fibre char experiment C1. This may be due to the fact that most of the volatile matter escaped during the pyrolysis of the raw samples.

7.3 Palm fibre char reproducibility study

Three palm fibre char evolved gas analysis (EGA) experiments, C1 to C3, were conducted under identical conditions to examine the reproducibility of the experiments. The experiments C1 to C3 were conducted with air as the oxidising gas, an absolute total system pressure of 500kPa, an air flow rate of 400smL/min and a heating rate of 50°C/h. The experimental conditions of these runs are presented in Table 7.1. The results of these three experiments are presented in Table 7.3. Figure 7.1 shows the variations in the exit gas compositions with respects to the cell temperature for experiment C1. Figures 7.3 and 7.4 are plotted showing the variations in the exit gas compositions with respect to the cell temperature for experiments C2 and C3, respectively.

Table 7.3 - Summary of the evolved gas analysis (EGA) experimental results of palm fibre char. The $\Delta O_{2,\,max}$, $\Delta CO_{2,\,max}$ and $\Delta CO_{,\,max}$ (in mol%) is the peak height and the T (in °C) is cell temperature at which the peak occurs. M1 is gas mixture 1 that consists of 15.10 mol% O_2, 2.01 mol% CO_2, 0.983 mol% CO and balance nitrogen. M2 is gas mixture 2 that contains of 18.10 mol% O_2, 4.99 mol% CO_2, 2.51 mol% CO and balance nitrogen.

Experiment		**C1**	**C2**	**C3**	**C4**	**C5**	**C6**	**C7**	**C8**	**C9**
Absolute total system pressure (kPa)		500	500	500	700	300	500	500	695	580
Oxygen partial pressure (kPa)		105	105	105	147	63	76	91	105	105
Oxygen concentration in feed gas (mol%)		20.96 (Air)	20.96 (Air)	20.96 (Air)	20.96 (Air)	20.96 (Air)	15.10 (M1)	18.10 (M2)	15.10 (M1)	18.10 (M2)
Heating rate (°C/h)		50	50	50	50	50	50	50	50	50
Oxygen consumption peak										
Peak	$\Delta O_{2,\,max}$ (mol%)	2.48	2.37	2.45	2.85	2.15	2.39	2.42	2.74	2.55
	T (°C)	360.7	361.9	360.8	342.4	380.8	374.4	367.4	363.1	362.7
Carbon dioxide production peak										
Peak	$\Delta CO_{2,\,max}$ (mol%)	1.95	1.94	1.94	2.15	1.69	1.85	1.72	2.03	1.95
	T (°C)	360.3	361.5	360.5	342.7	381.0	374.0	367.9	362.4	362.2
Carbon monoxide production peak										
Peak	$\Delta CO_{,\,max}$ (mol%)	0.49	0.50	0.50	0.86	0.36	0.60	0.63	0.81	0.77
	T (°C)	360.5	361.2	360.8	342.9	381.4	373.8	367.6	362.2	363.1

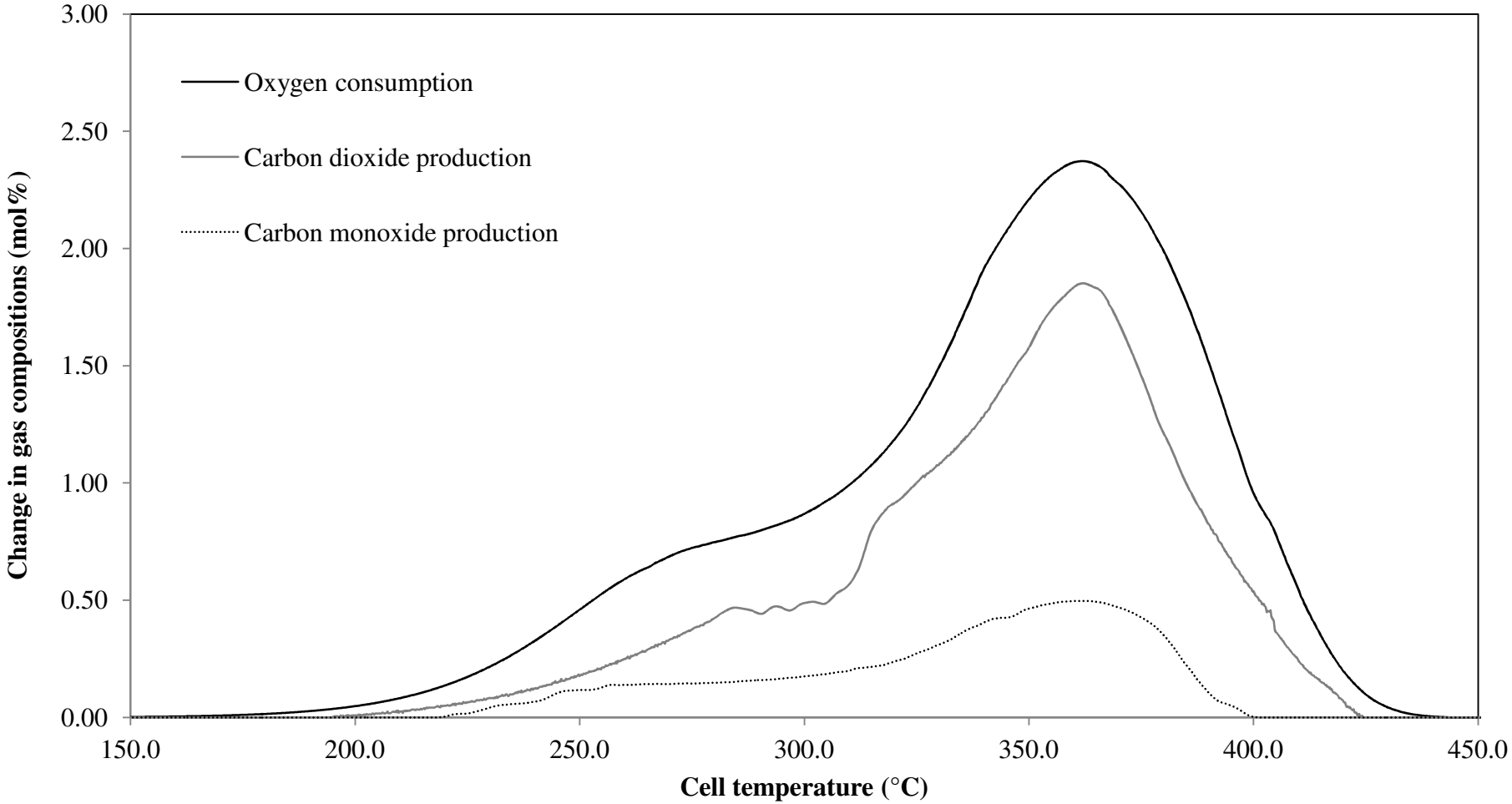

Figure 7.3 - Evolved gas analysis data with respects to the cell temperature for the oxidation of palm fibre char with air as the oxidising gas, an absolute total system pressure of 500kPa, an air flow rate of 400smL/min and a heating rate of 50°C/h (Experiment C2).

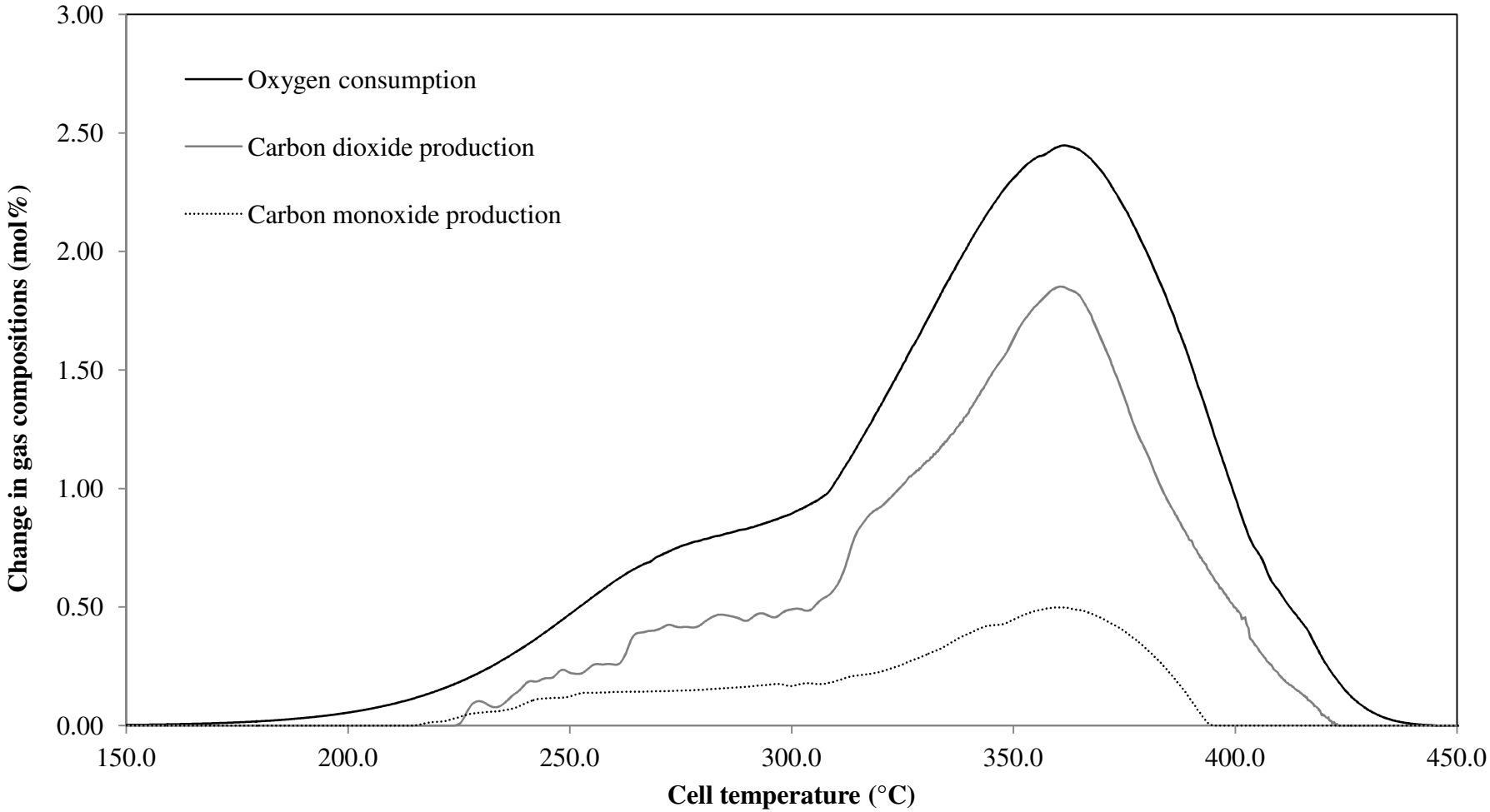

Figure 7.4 - Evolved gas analysis data with respects to the cell temperature for the oxidation of palm fibre char with air as the oxidising gas, an absolute total system pressure of 500kPa, an air flow rate of 400smL/min and a heating rate of 50°C/h (Experiment C3).

Figures 7.3 and 7.4 exhibit similar features to those observed for the typical palm fibre char of experiment C1, i.e., one peak in the cell temperature range of 350°C to 370°C for the exit gas oxygen, carbon dioxide and carbon monoxide compositions. Considering Table 7.3, the oxygen consumption peak temperature lies at an average peak temperature of 361.1°C ± 0.8°C for the three samples.

The average temperature at which the carbon dioxide production curves peak agree at 360.8°C ± 0.7°C for experiments C1 to C3. Similarly, the average temperature at which the carbon monoxide production curves peak is 360.8°C ± 0.4°C for the three runs. Table 7.3 indicates an agreement to within ±1°C for the palm fibre char experiments. For the remainder of the palm fibre char experiments, the level of the reproducibility may be taken as ±1°C. By comparison to the rice husk and the palm fibre experiments, the palm fibre char experiment shows a higher reproducibility. This is well expected since palm fibre char sample are less heterogeneous in comparison to the raw rice husk and palm fibre samples.

Figure 7.5 presents a comparison of the oxygen consumption curves with respect to the cell temperature for the experiments C1 to C3. Figures 7.6 and 7.7 show the corresponding information for the carbon dioxide production and the carbon monoxide production curves. Considering Figure 7.5, the oxygen consumption peak height shows a close agreement between the three identical runs. The oxygen consumption peak height ranges from 2.37 mol% to 2.48 mol% oxygen. The carbon dioxide production peak heights ranged between 1.94 mol% and 1.95 mol% carbon dioxide (see Figure 7.6). There are similarities in the shapes of the sudden change in the carbon dioxide concentration in the temperature range between 270°C and 320°C. The reasons behind these bumps are not fully understood and may be due to the balance volatile matters that have not fully escaped during the pyrolysis process of the raw samples. For the carbon monoxide production curve, the peak height ranged from 0.49 mol% to 0.50 mol% carbon monoxide (see Figure 7.7).

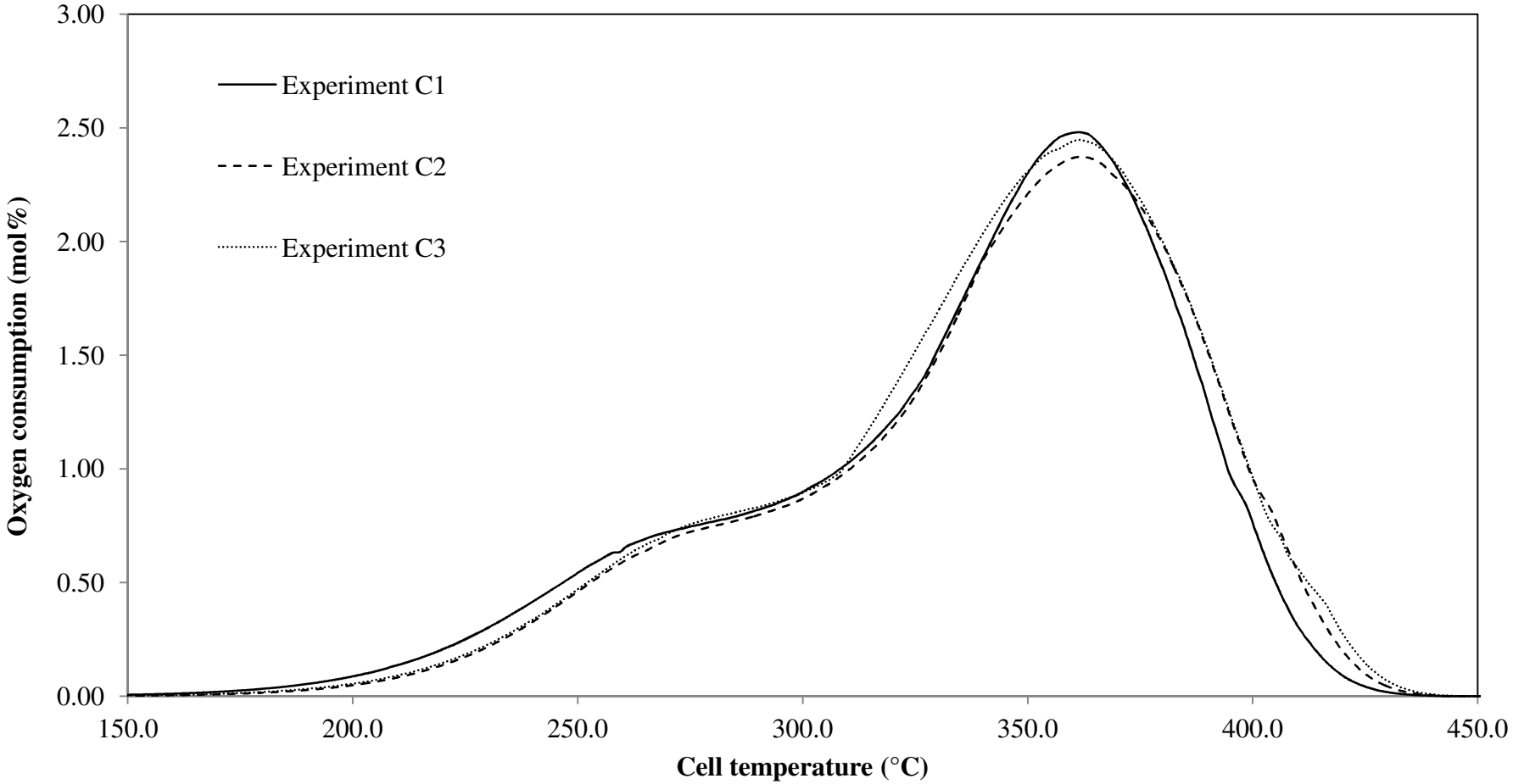

Figure 7.5 - Comparison of the oxygen consumption data with respects to the cell temperature for the three palm fibre char experiments conducted under identical conditions with air as the oxidising gas, an absolute total system pressure of 500kPa, an air flow rate of 400smL/min and a heating rate of 50°C/h.

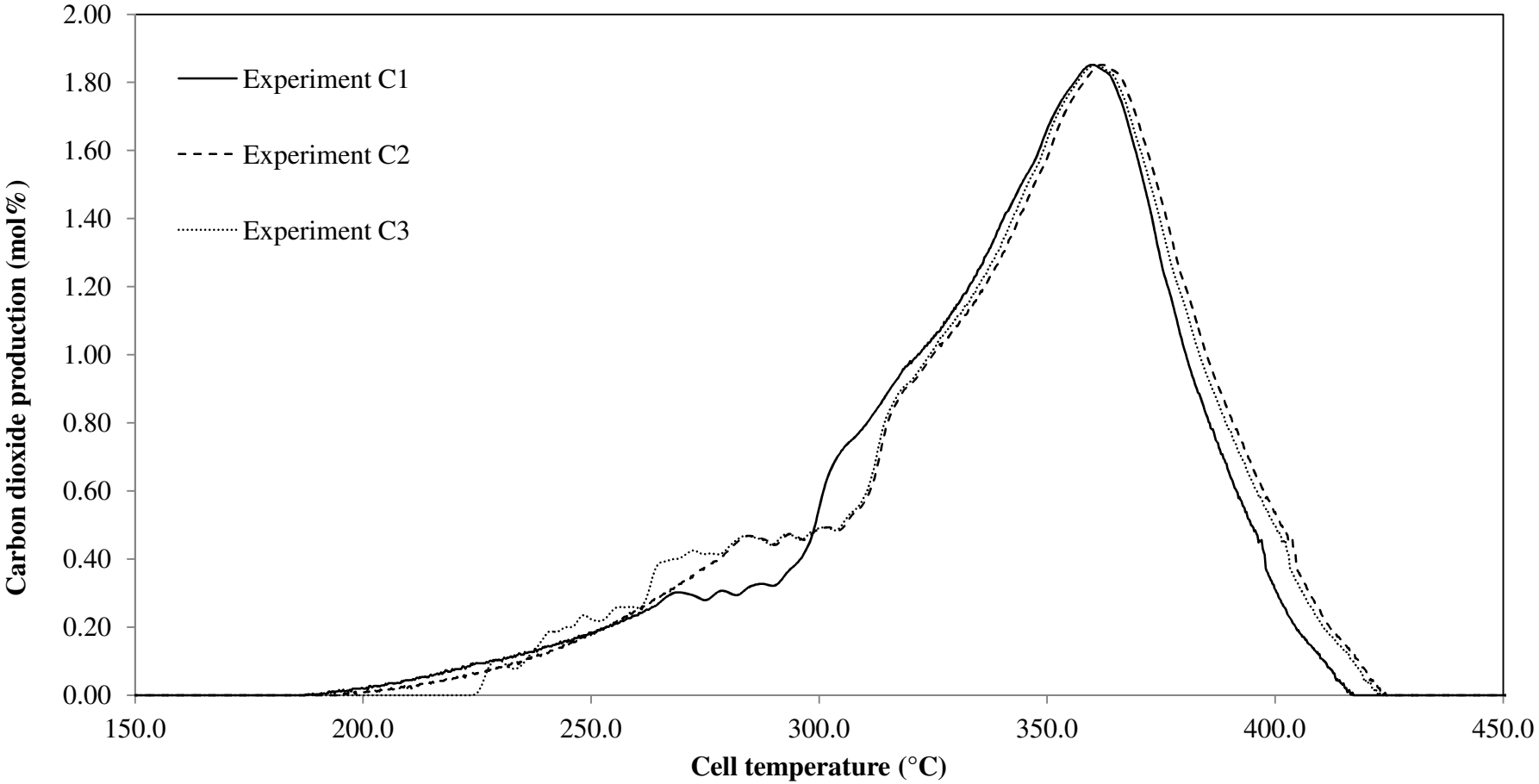

Figure 7.6 - Comparison of the carbon dioxide production data with respects to the cell temperature for the three palm fibre char experimental runs conducted under identical conditions with air as the oxidising gas, an absolute total system pressure of 500kPa, an air flow rate of 400smL/min and a heating rate of 50°C/h.

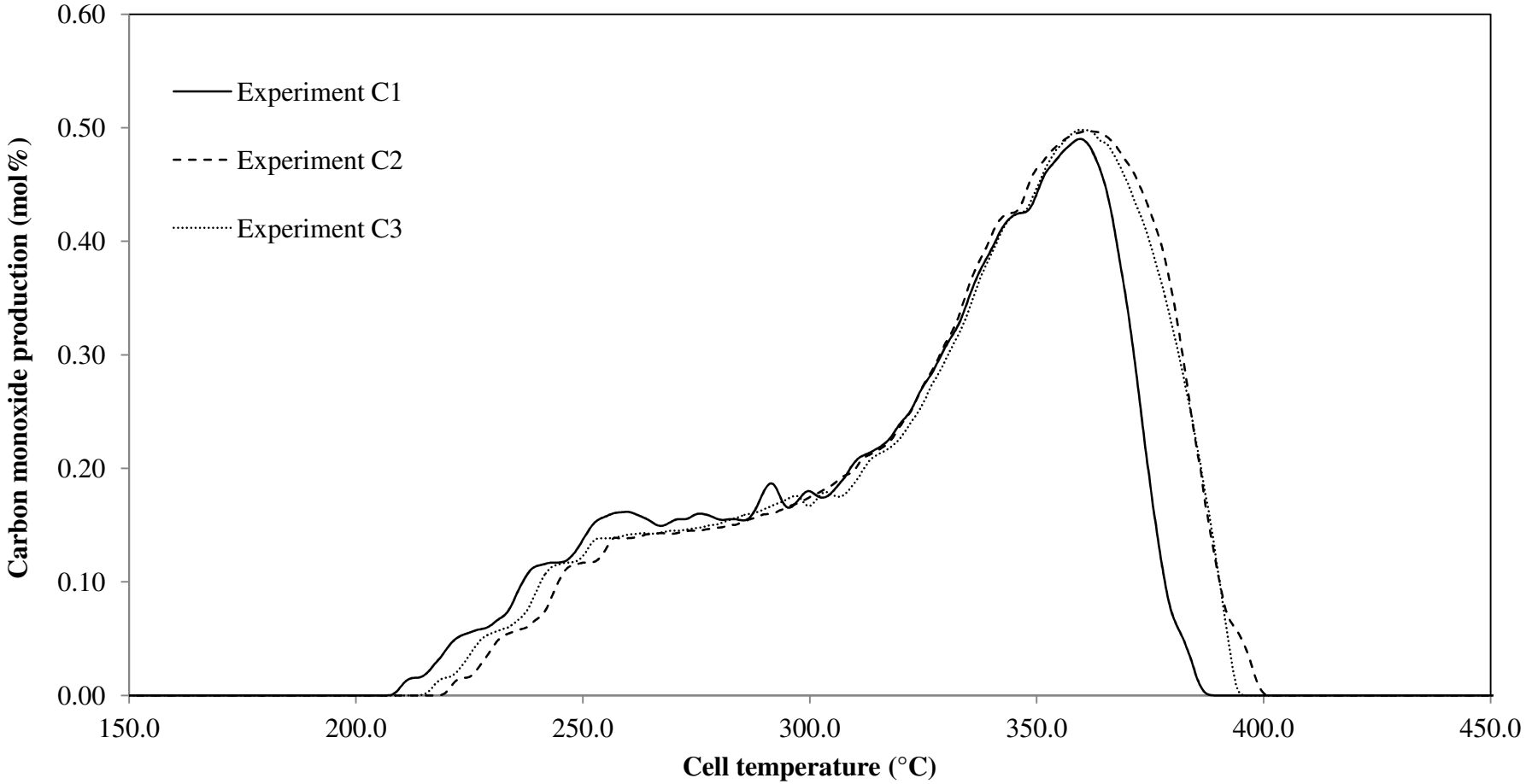

Figure 7.7 - Comparison of the carbon monoxide production data with respects to the cell temperature for the three palm fibre char experiments conducted under identical conditions with air as the oxidising gas, an absolute total system pressure of 500kPa, an air flow rate of 400smL/min and a heating rate of 50°C/h.

The overall comparison of the peak height in Table 7.3 presents an agreement to within ±5% for the palm fibre char experiments. As in Chapter 5 and 6, the peak height was much depending on the quantity of sample presents in each of the experimental runs. The small differences observed for the three runs may be due to the amount of palm fibre char initially present in the reaction cell. A significant error during the preparation of the sample would contribute to a variation in the results. In this case, the sample weight of the three identical palm fibre char experimental runs were varied by ±2%.

By comparison to the raw samples of the rice husk and the palm fibre, the palm fibre char shows a smaller variation. The fact that the palm fibre char samples are less heterogeneous, the smaller variations of the peak temperatures and heights of the effluent gas oxygen, carbon dioxide and carbon monoxide composition curves in comparison to the raw samples are expected.

Table 7.4 presents the calculated kinetic parameters of the three experiments, C1 to C3, conducted under identical conditions. The predicted oxygen consumption curve together with the actual experimental data for the experiment C1 was presented earlier in Figure 7.2. Figures 7.8 and 7.9 present the predicted oxygen consumption curve and the actual experimental data for experiments C2 and C3.

Experiments C2 and C3 show an acceptable fit between the predicted oxygen consumption curve and the experimental data with the calculated variance of 0.0012 and 0.0021, respectively. Similar to experiment C1, there are a few disagreements observed between predicted oxygen consumption at the medium temperature range between 290°C and 330°C and at the high temperature range between 370°C and 420°C. The reasons for the discrepancies as explained earlier for the typical palm fibre char experiment of C1 may also be applied to the experiments C2 and C3. For the calculated kinetic parameters of the reaction order, the activation energy and the natural log of beta group for the HTO, MTO and LTO reactions, there are no significant differences were observed for all the three identical experiments (see Table 7.4).

Table 7.4 - Summary of the calculated kinetic parameters of the palm fibre char oxidation. The E/R is the activation energy (in K) and the ln β is the natural log of beta group (dimensionless). M1 is gas mixture 1 that consists of 15.10 mol% O_2, 2.01 mol% CO_2, 0.983 mol% CO and balance nitrogen. M2 is gas mixture 2 that contains of 18.10 mol% O_2, 4.99 mol% CO_2, 2.51 mol% CO and balance nitrogen.

Experiment		**C1**	**C2**	**C3**	**C4**	**C5**	**C6**	**C7**	**C8**	**C9**
Absolute total system pressure (kPa)		500	500	500	700	300	500	500	695	580
Oxygen partial pressure (kPa)		105	105	105	147	63	76	91	105	105
Oxygen concentration in feed gas (mol%)		20.96 (Air)	20.96 (Air)	20.96 (Air)	20.96 (Air)	20.96 (Air)	15.10 (M1)	18.10 (M2)	15.10 (M1)	18.10 (M2)
Heating rate (°C/h)		50	50	50	50	50	50	50	50	50
HTO	Reaction order, n	0.99	0.98	0.98	0.99	0.97	0.97	0.98	1.00	0.98
	E/R ($\times 10^{-3}$)	12.8	12.6	12.5	8.5	16.7	15.2	14.0	13.5	13.7
	ln β	13.0	12.9	12.8	8.6	18.5	16.4	14.8	13.5	14.0
MTO	Reaction order, n	0.98	0.99	0.97	0.83	1.11	0.93	0.93	0.99	0.99
	E/R ($\times 10^{-3}$)	18.5	19.5	19.2	14.2	24.8	23.7	20.0	19.2	19.9
	ln β	20.9	21.5	21.1	10.0	29.3	28.4	23.2	21.8	21.3
LTO	Reaction order, n	0.97	0.96	0.96	1.10	0.77	0.93	0.96	0.96	0.94
	E/R ($\times 10^{-3}$)	11.9	12.0	11.9	13.1	10.4	10.8	11.3	12.2	12.3
	ln β	16.2	16.5	16.3	19.3	12.3	14.0	15.5	17.4	17.9
Variance, σ^2		0.0009	0.0012	0.0021	0.0115	0.0004	0.0003	0.0003	0.0018	0.0006

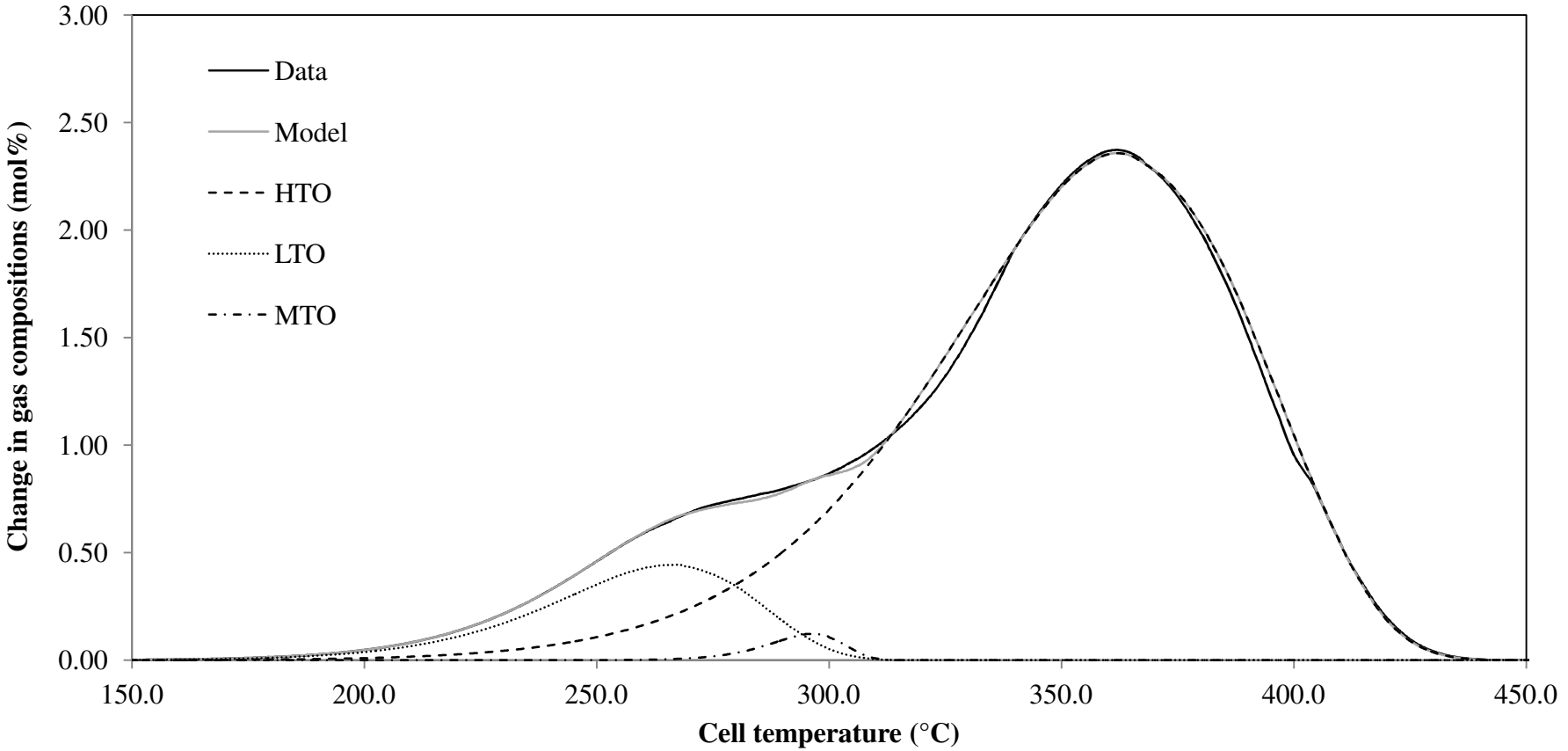

Figure 7.8 - Comparison of the oxygen consumption data and the model prediction with respects to the cell temperature for the palm fibre char oxidation with air as the oxidising gas, an absolute total system pressure of 500kPa, an air flow rate of 400smL/min and a heating rate of 50°C/h (Experiment C2).

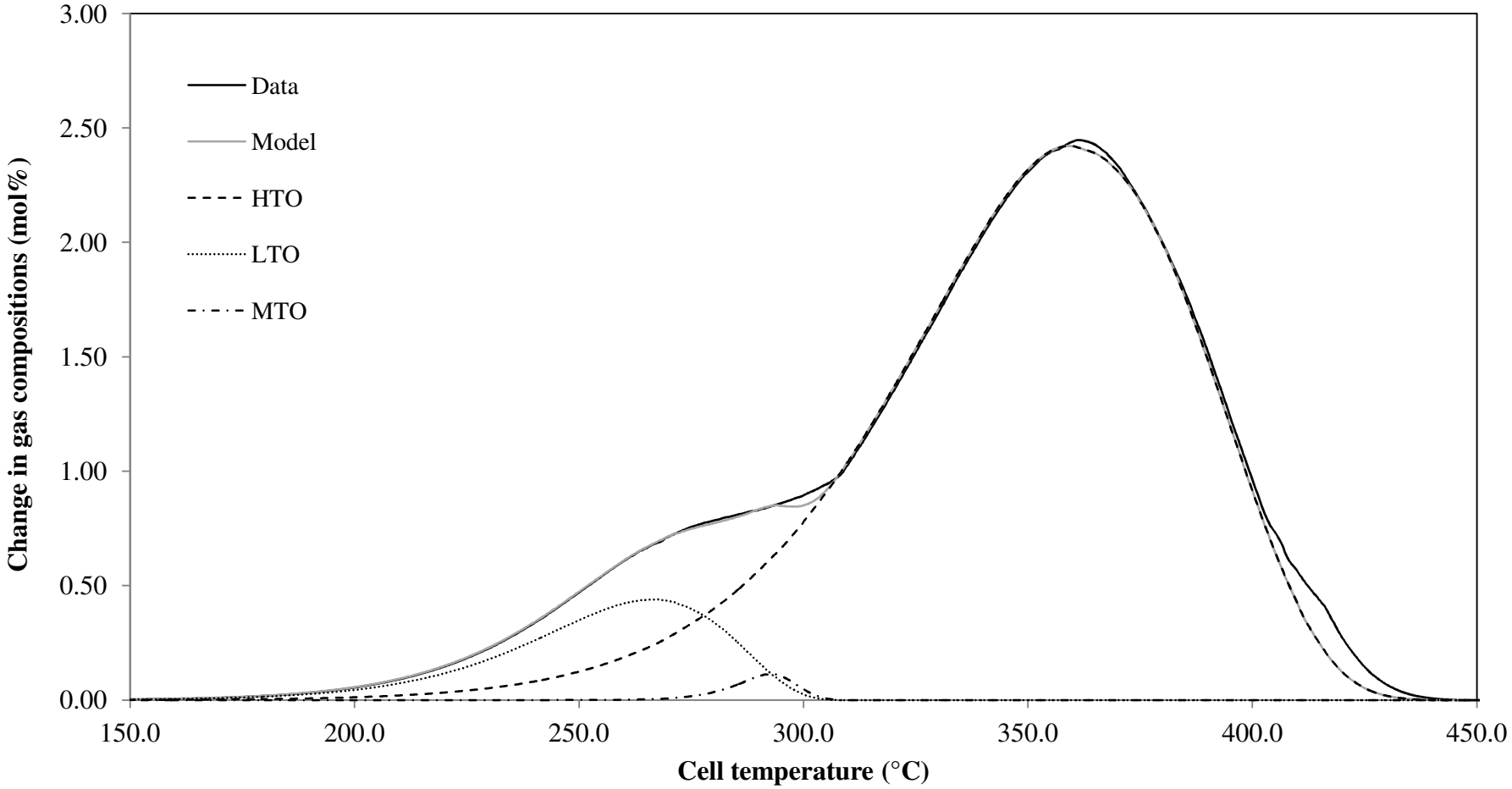

Figure 7.9 - Comparison of the oxygen consumption data and the model prediction with respects to the cell temperature for the palm fibre char oxidation with air as the oxidising gas, an absolute total system pressure of 500kPa, an air flow rate of 400smL/min and a heating rate of 50°C/h (Experiment C3).

Considering the high temperature oxidation (HTO) reaction, the reaction order varied 0.01 for all the three identical runs. The activation energy was varied only slightly from 12.5×10^3K to 12.8×10^3K while the ln β varied in the range from 12.8 to 13.0 for all the three identical palm fibre char experiments of C1 to C3. For the medium temperature oxidation (MTO) reaction, the reaction order varied by only 0.02. The activation energy fell in the range from 18.5×10^3K to 19.5×10^3K and the ln β varied in the range of 20.9 to 21.5 for the three runs.

The variation in the reaction orders for the low temperature oxidation (LTO) reaction is 0.01. The activation energy and the ln β for the LTO reaction varied in the ranges of 11.9×10^3K to 12.0×10^3K and 16.2 to 16.5, respectively for the three identical palm fibre char experiments. Table 7.4 shows an agreement to 2% of the reaction order, 5% of the activation energy and 3% of the ln β.

In conclusion, there are no significant differences in the peak temperatures and heights observed for the oxygen consumption, the carbon dioxide production and the carbon monoxide production curves of the three palm fibre char experiments conducted under similar conditions. The level of the reproducibility for the palm fibre char experiments may be taken as agreement to within ±1°C of the peak temperature and 5% of the peak height. Further, there are no significant differences in the calculated kinetic parameters of the reaction order, the activation energy and the natural log of beta group of the three palm fibre char experiments conducted under similar conditions. The palm fibre char experiments show an agreement to within 2% of the reaction order, 5% of the activation energy and 3% of the ln β. Overall, the evolved gas analysis (EGA) experiments for the palm fibre char are reproducible.

7.4 Effect of the total system and the oxygen partial pressures

The absolute total system pressure ranging from 300kPa to 700kPa and the oxygen partial pressure in between 63kPa to 147kPa were investigated for the palm fibre char combustion characteristics. The oxygen concentrations of the inlet gas were varied

appropriately in order to study the influences of the oxygen partial pressures on the palm fibre char combustion characteristics.

Experiments C4 to C9 were conducted at various total system pressures, oxygen partial pressures and the oxygen concentrations in the feed gas at a heating rate of 50°C/h and a flow rate of 400smL/min. Experiments C4 and C5 were conducted at a high and a low pressures with air as the oxidising gas. Experiments C6 and C7 were conducted at the same absolute total system pressure of 500kPa but with different oxygen partial pressure allows the effect of the oxygen partial pressure to be observed.

Experiments C8 and C9 were conducted at the same oxygen partial pressure of 105kPa but with different total system pressure allowing the influences of the total system pressures to be examined. A summary of the experimental conditions is presented in Table 7.1. The evolved gas analysis (EGA) experimental results are presented in Table 7.3. Figures 7.10 to 7.15 present the variations in the exit gas compositions with respect to the cell temperature for experiments C4 to C9, respectively. These figures exhibit similar features to those observed for experiments C1 to C3. The oxygen consumption, carbon dioxide production and carbon monoxide production curves of experiments C4 to C9 have a single peak. However, the peak temperatures and the peak heights varied between the runs.

Figure 7.16 presents the comparison of the oxygen consumption curves for the palm fibre char experiments conducted at the various total system pressures and the oxygen partial pressures. Figures 7.17 and 7.18 present the corresponding information for the carbon dioxide production and the carbon monoxide production curves. As shown in Figure 7.16 and Table 7.3 for the experiments C1, C4 and C5, as the pressure increased, the oxygen consumption curve shifted to lower peak temperatures. Experiments C1, C4 and C5 were conducted using air as the oxidising gas. The oxygen consumption peak temperature was reduced approximately 38.4°C as the pressure increased from 300kPa to 700kPa.

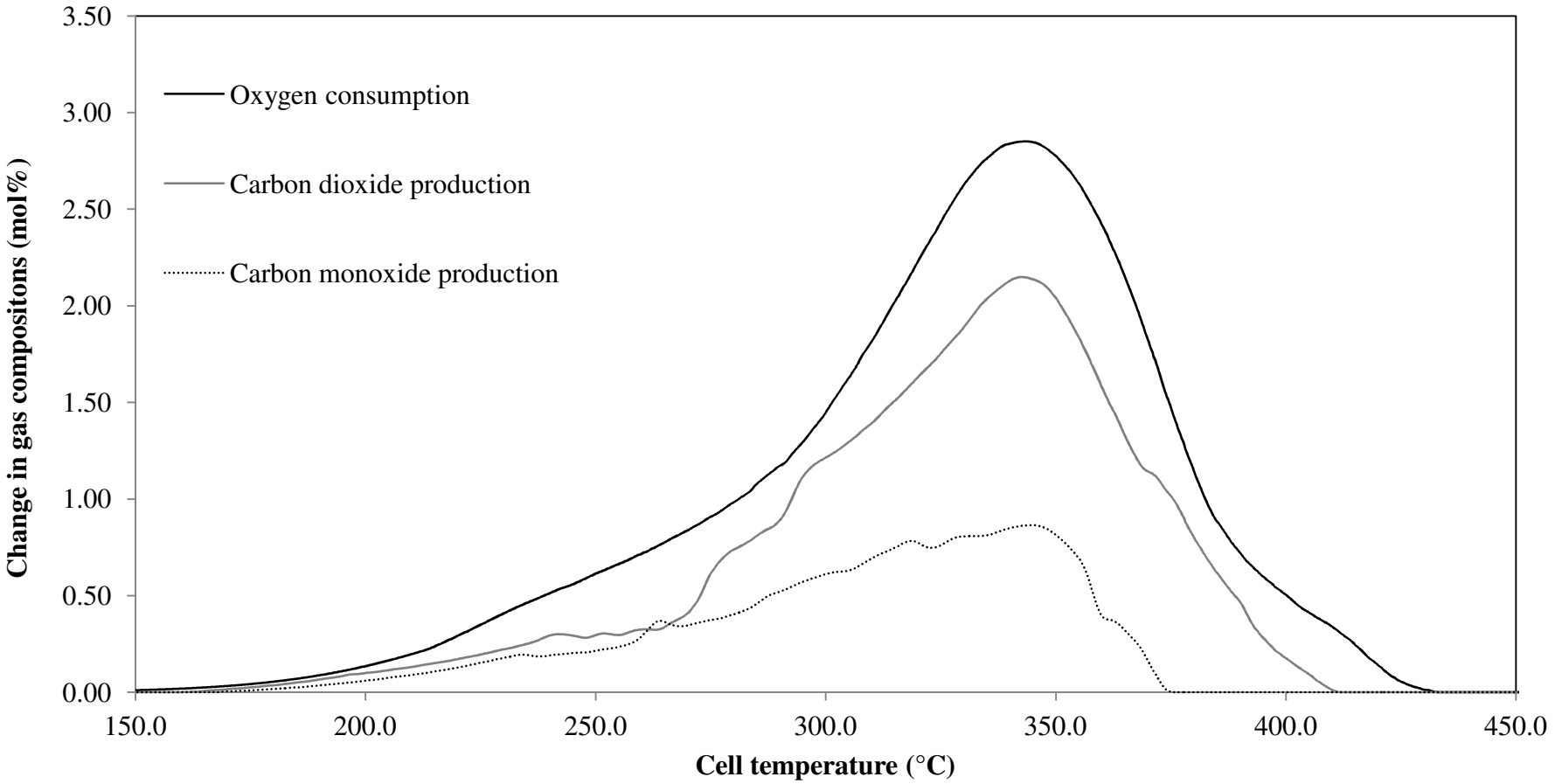

Figure 7.10 - Evolved gas analysis data with respects to the cell temperature for the oxidation of palm fibre char with air as the oxidising gas, an absolute total system pressure of 700kPa, an air flow rate of 400smL/min and a heating rate of 50°C/h (Experiment C4).

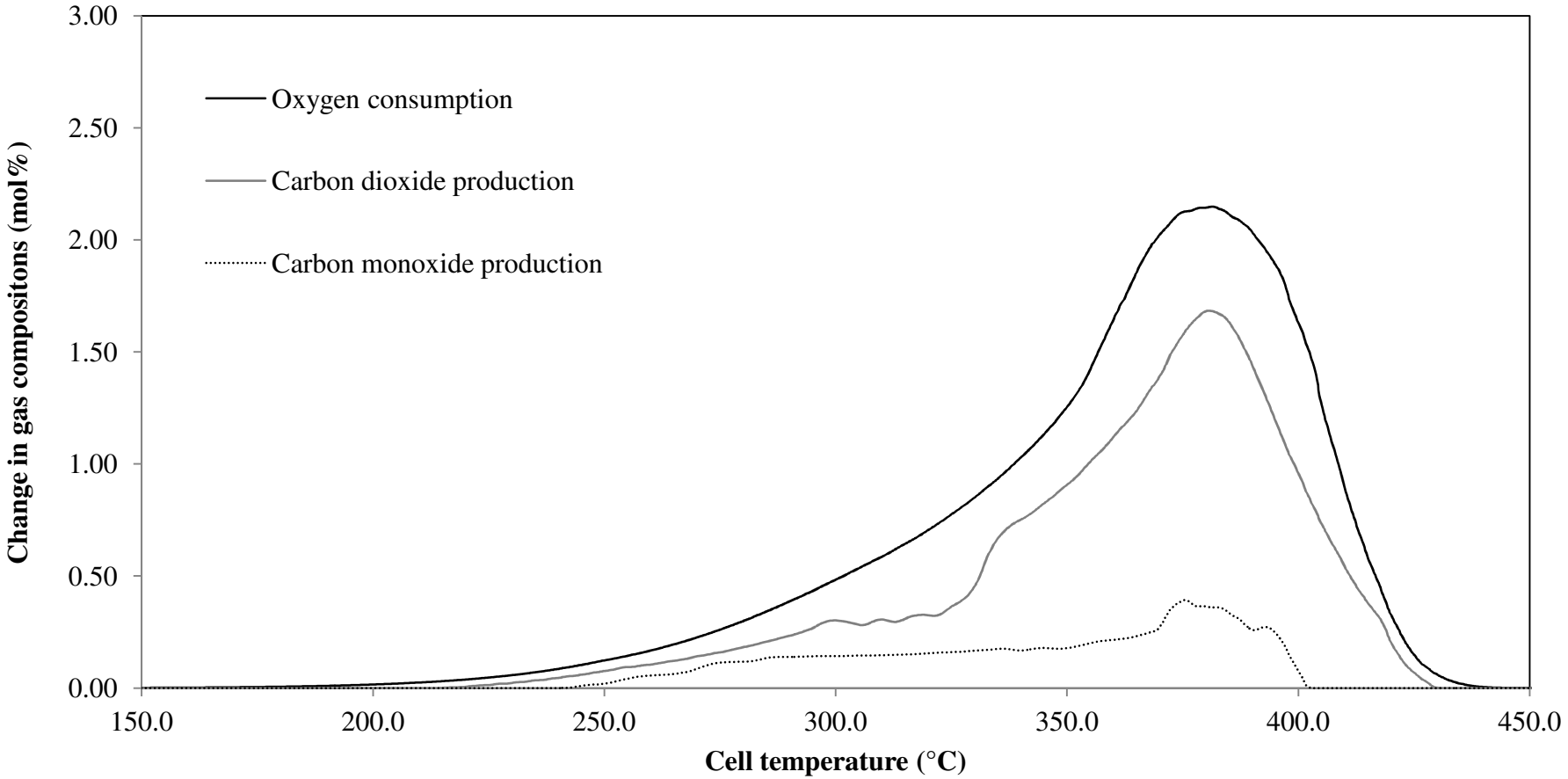

Figure 7.11 - Evolved gas analysis data with respects to the cell temperature for the oxidation of palm fibre char with air as the oxidising gas, an absolute total system pressure of 300kPa, an air flow rate of 400smL/min and a heating rate of 50°C/h (Experiment C5).

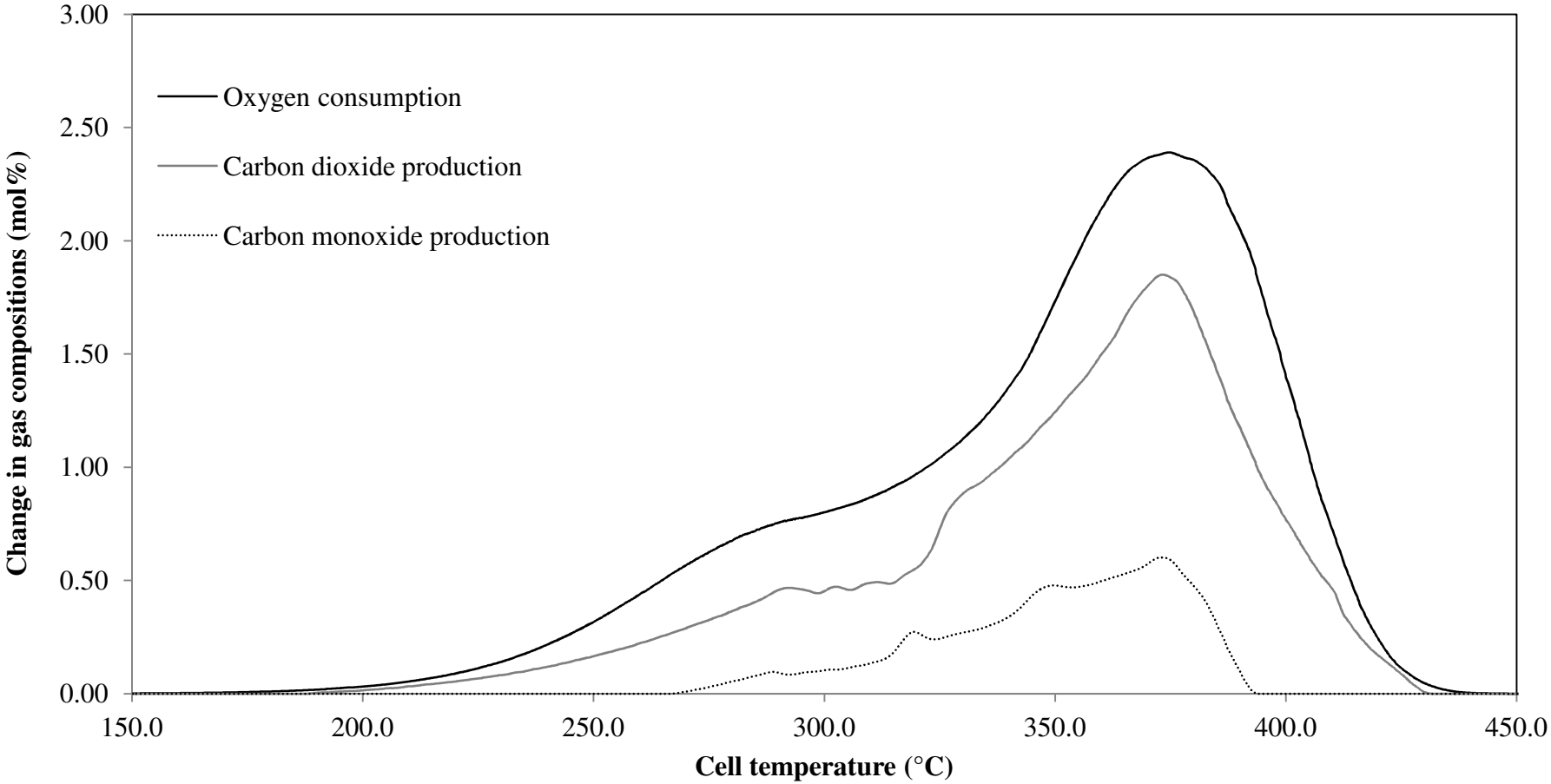

Figure 7.12 - Evolved gas analysis data with respects to the cell temperature for the oxidation of palm fibre char with 15.10 mol% oxygen concentration in the feed gas, an absolute total system pressure of 500kPa, an oxygen partial pressure of 76kPa, a flow rate of 400smL/min and a heating rate of 50°C/h (Experiment C6).

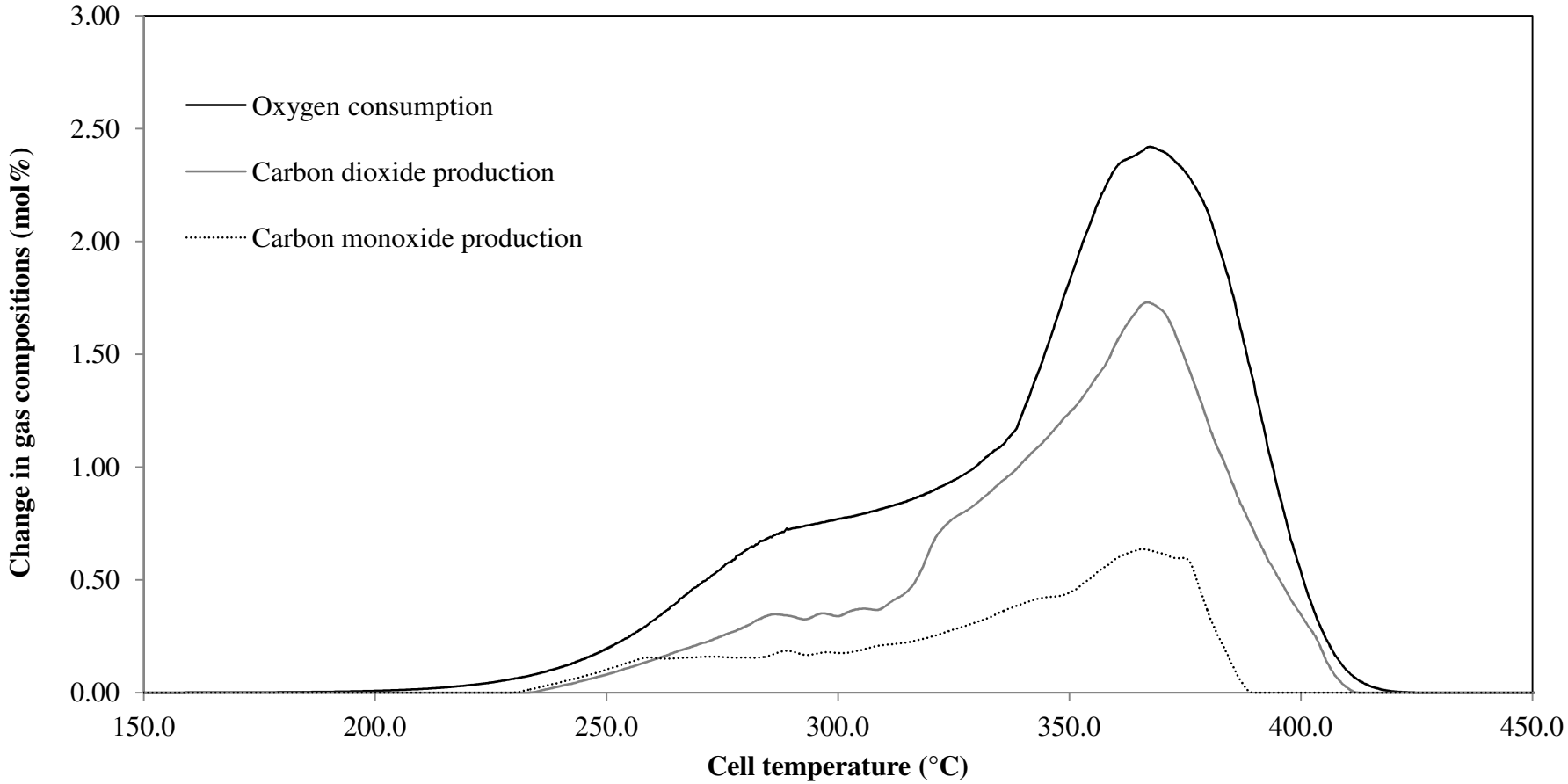

Figure 7.13 - Evolved gas analysis data with respects to the cell temperature for the oxidation of palm fibre char with 18.10 mol% oxygen concentration in the feed gas, an absolute total system pressure of 500kPa, an oxygen partial pressure of 91kPa, a flow rate of 400smL/min and a heating rate of 50°C/h (Experiment C7).

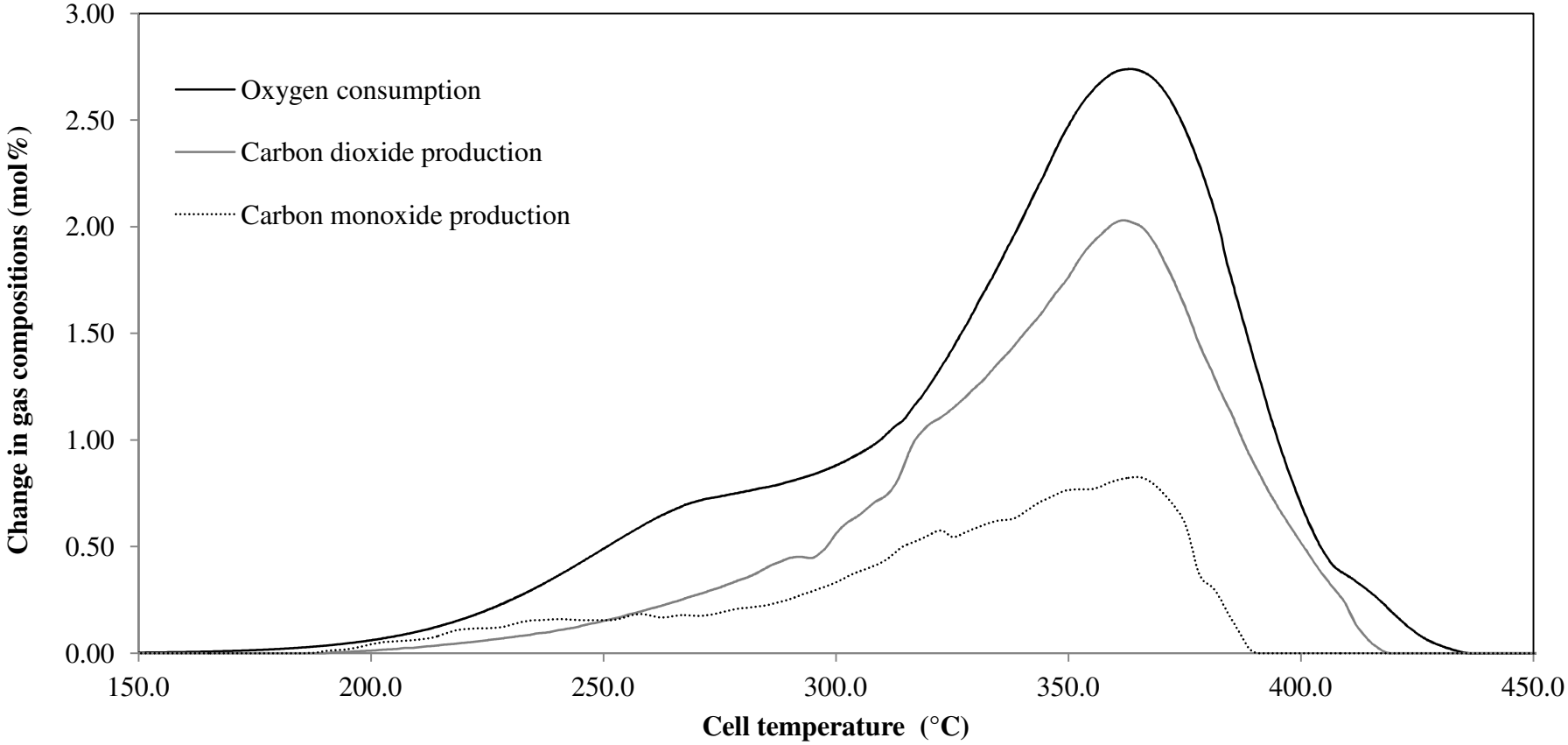

Figure 7.14 - Evolved gas analysis data with respects to the cell temperature for oxidation of the palm fibre char with 15.10 mol% oxygen concentration in the feed gas, an absolute total system pressure of 695kPa, an oxygen partial pressure of 105kPa, a flow rate of 400smL/min and a heating rate of 50°C/h (Experiment C8).

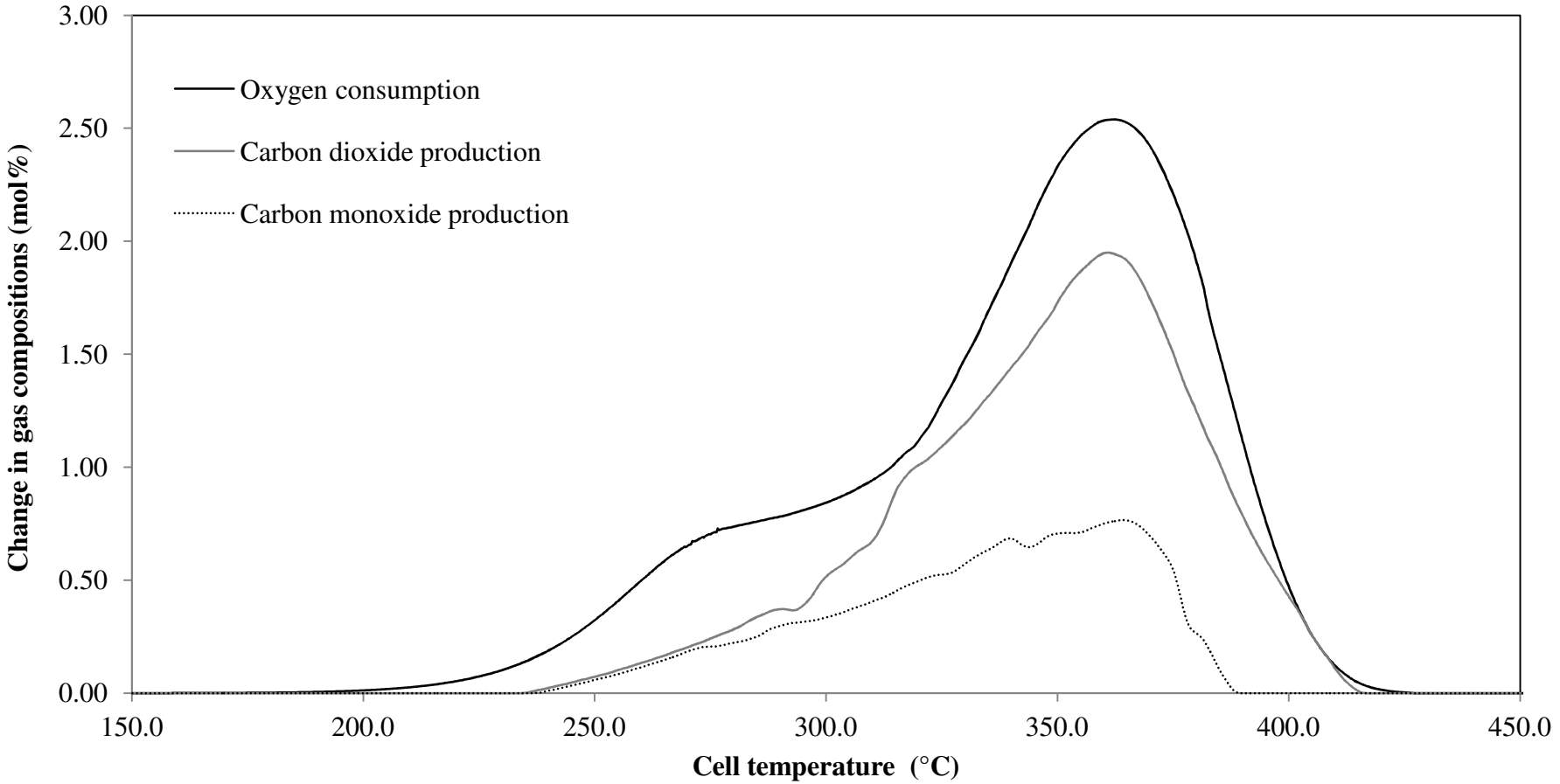

Figure 7.15 - Evolved gas analysis data with respects to the cell temperature for the oxidation of palm fibre char with 18.10 mol% oxygen concentration in the feed gas, an absolute total system pressure of 580kPa, an oxygen partial pressure of 105kPa, a flow rate of 400smL/min and a heating rate of 50°C/h (Experiment C9).

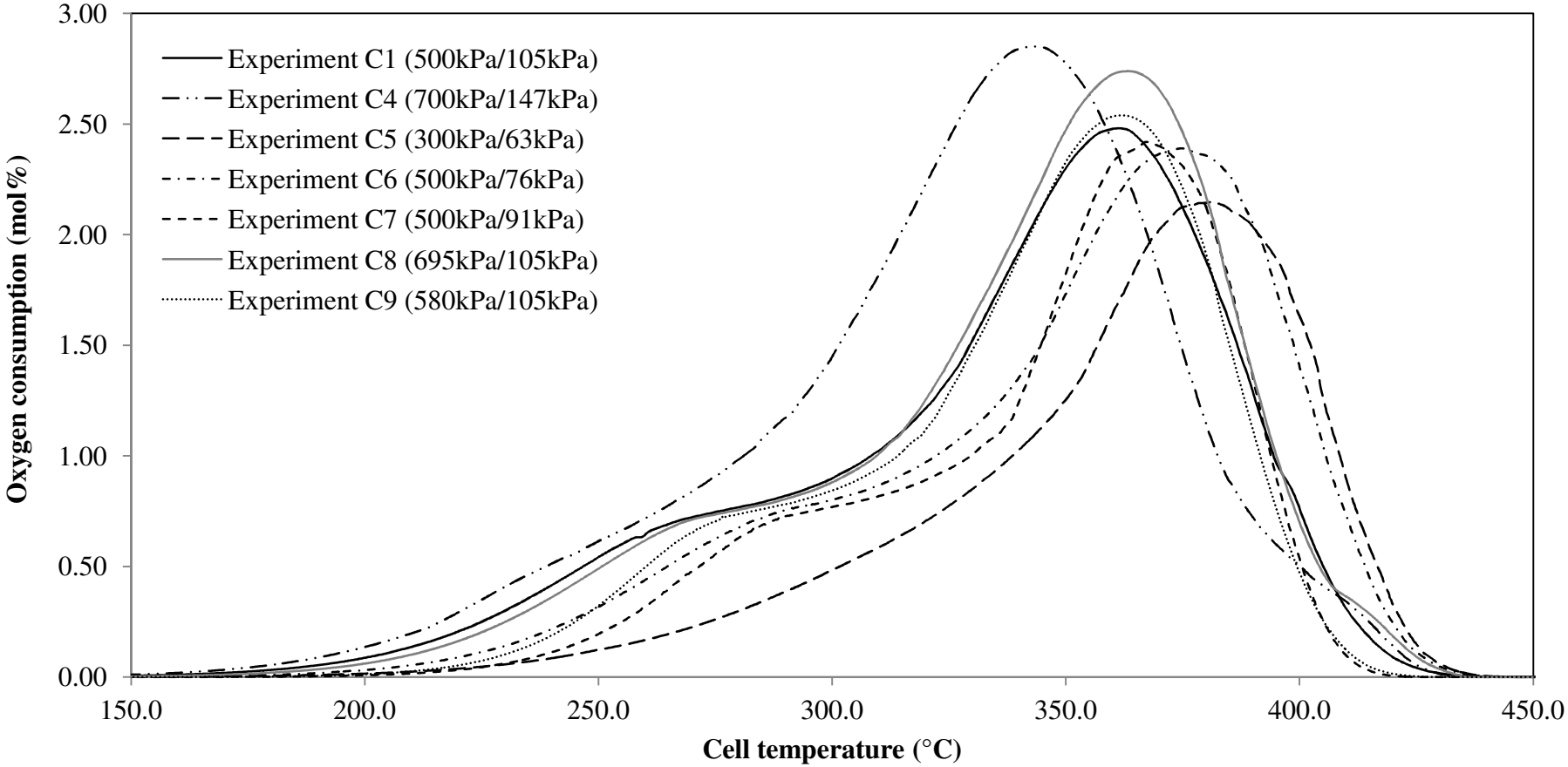

Figure 7.16 - Comparison of the oxygen consumption data with respects to the cell temperature for the palm fibre char experimental runs conducted at the various total system and oxygen partial pressures at a feed gas flow rate of 400smL/min and a heating rate of 50°C/h. The pressures shown refer to the absolute total system pressure and oxygen partial pressure, respectively.

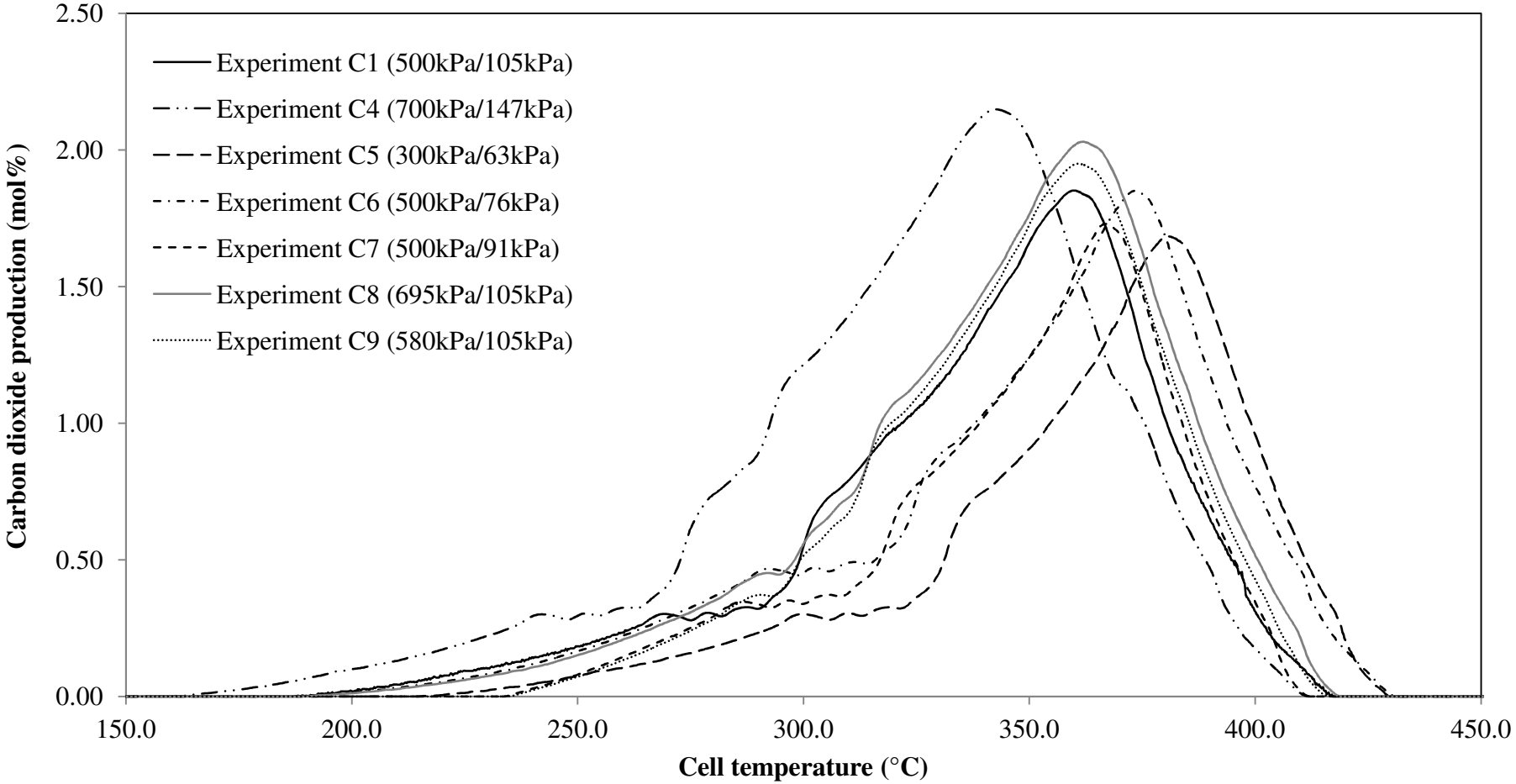

Figure 7.17 - Comparison of the carbon dioxide production data with respects to the cell temperature for the palm fibre char experimental runs conducted at the various total system and oxygen partial pressures at a feed gas flow rate of 400smL/min and a heating rate of 50°C/h. The pressures shown refer to the absolute total system pressure and oxygen partial pressure, respectively.

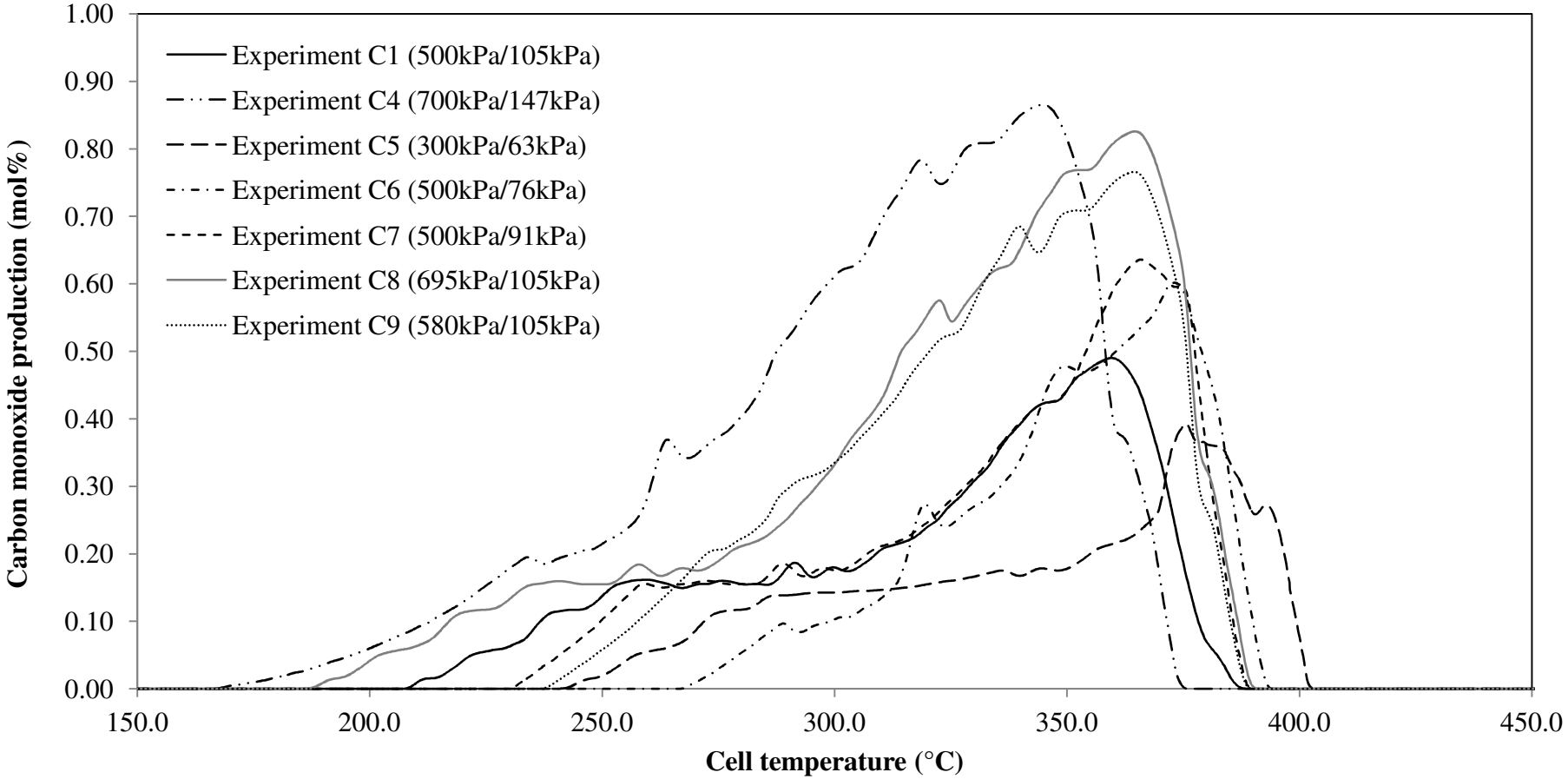

Figure 7.18 - Comparison of the carbon monoxide production data with respects to the cell temperature for the palm fibre char experimental runs conducted at the various total system and oxygen partial pressures at a feed gas flow rate of 400smL/min and a heating rate of 50°C/h. The pressures shown refer to the absolute total system pressure and oxygen partial pressure, respectively.

Likewise, the carbon dioxide production and the carbon monoxide production curves also show a similar trend as the oxygen consumption curve (see experiments C1, C4 and C5 of Figures 7.17 and 7.18 and Table 7.3). The reduction of the carbon dioxide production peak temperature was 38.3°C and the carbon monoxide production peak temperature was around 38.5°C as the pressure the increased from 300kPa to 700kPa. Considering the oxygen consumption peak height, as the pressure increased from 300 to 700kPa, the peak height increased by 32.6% from 2.15 mol% to 2.85 mol% oxygen. The carbon dioxide production peak height increased 27.2% from 1.69 mol% to 2.15 mol% carbon dioxide and the carbon monoxide production peak height increased from 0.36 mol% to 0.86 mol% carbon monoxide as the pressure increased from 300kPa to 700kPa.

A comparison of experiments C1, C6 and C7 permits an examination of the influence of the oxygen partial pressures at the same absolute total system pressure of 500kPa. Figure 7.19 presents the effect of the oxygen partial pressure on the peak temperatures and peak heights of the oxygen consumption curve. Figure 7.20 presents the effect of the oxygen partial pressure on the peak temperatures for the both carbon oxide curves. As observed in Figure 7.19, the peak temperature decreases with increasing oxygen partial pressure. The oxygen consumption peak temperature decreases around 13.6°C as the oxygen partial pressure increases from 76kPa to 105kPa but with the same total system pressure of 500kPa. However, the peak height reveals an opposing trends. As the oxygen partial pressure increases from 76kPa to 105kPa with the total system pressure held constant at 500kPa, the oxygen consumption peak height slightly increases from 2.39 mol% to 2.48 mol% oxygen. The carbon dioxide production and carbon monoxide production peak temperatures and heights exhibit similar trends to those observed for the oxygen consumption peak temperature and height as the oxygen partial pressure increased from 76kPa to 105kPa (see Figure 7.20 for experiments C1, C6 and C7). The observation was found in agreement with the previous observations for the rice husks and the palm fibre combustion characteristic studies.

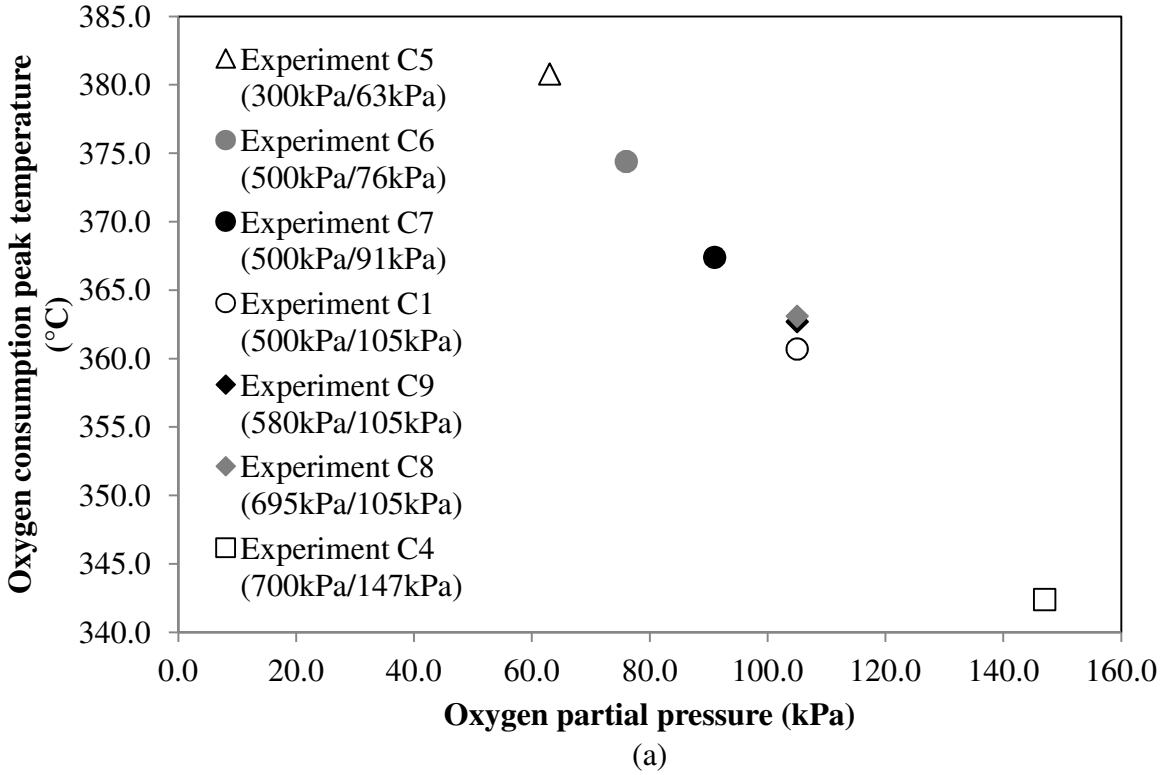

(a)

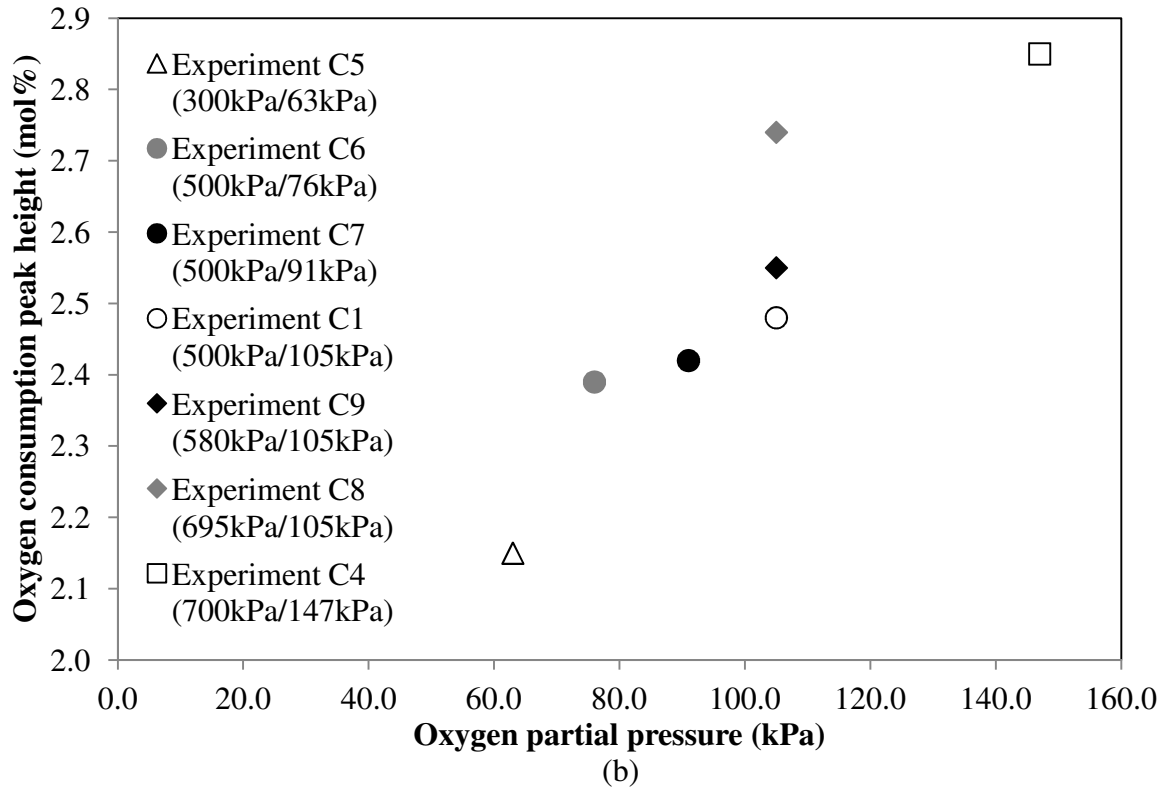

(b)

Figure 7.19 - Effect of the oxygen partial pressure on (a) the peak temperatures (b) the peak heights of the oxygen consumption curve. The pressures shown refer to the absolute total system pressure and oxygen partial pressure, respectively.

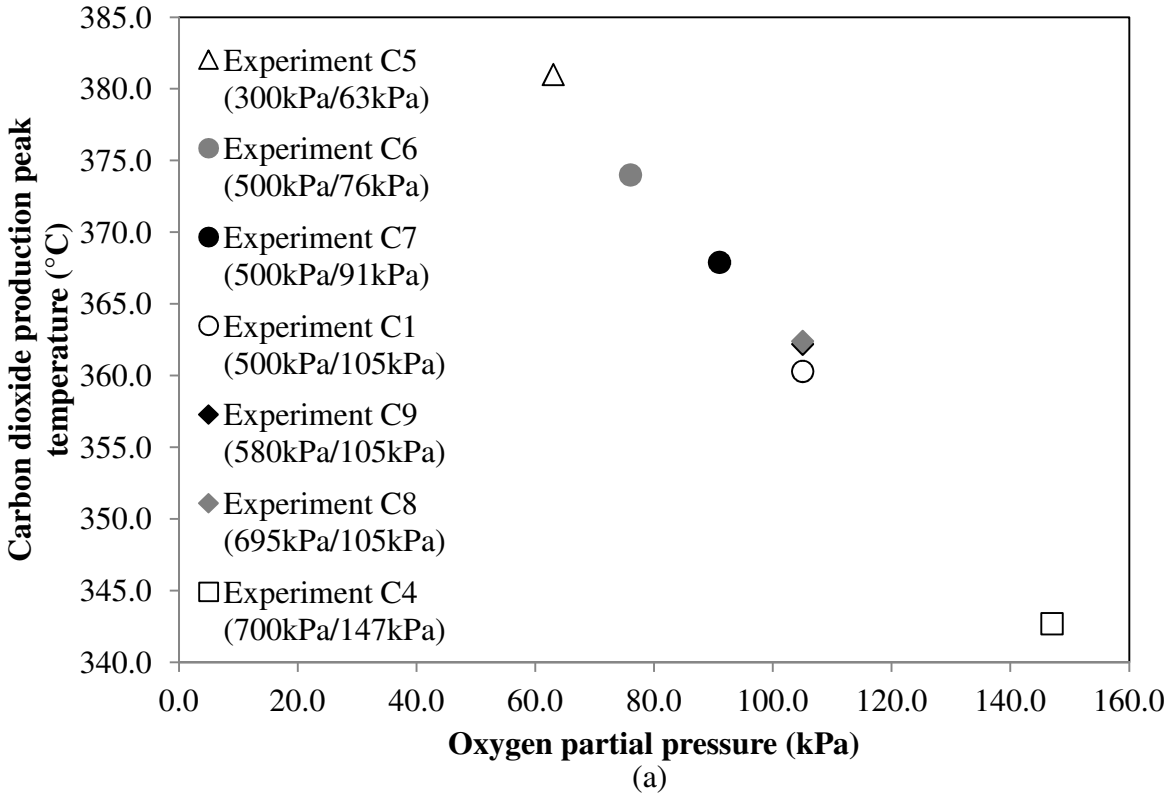

(a)

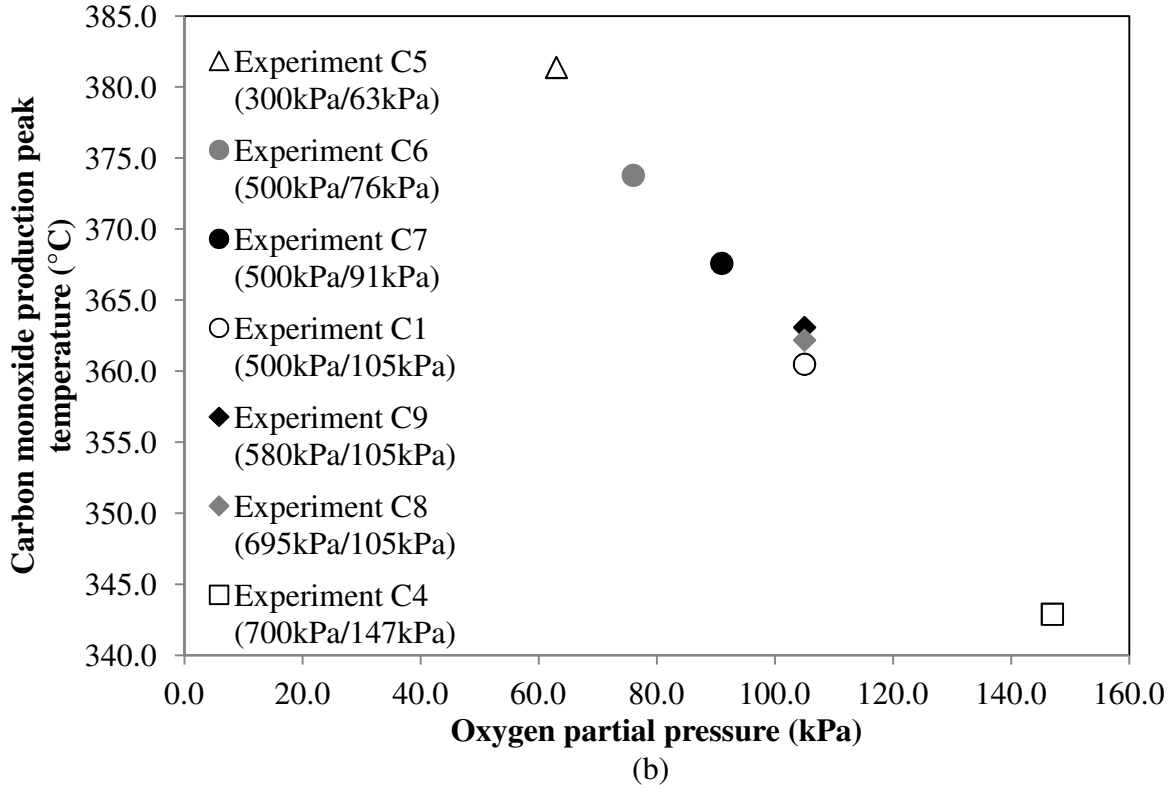

(b)

Figure 7.20 - Effect of the oxygen partial pressure on the peak temperatures of (a) the carbon dioxide production (b) the carbon monoxide production curves. The pressures shown refer to the absolute total system pressure and oxygen partial pressure, respectively.

A similar observation has also been reported by Daood *et al.* (2010) in their sugar cane bagasse char decompositions study using TGA technique. They observed that reaction rate is controlled by both the chemical reaction rate and the rate of pore diffusion. However, the oxygen pore diffusion is a limiting factor. According to the Fick's law, diffusion is proportional to the concentration gradient, and in the gaseous phase the concentration is dependent on the partial pressure. hence, an increase in oxygen partial pressure may significantly enhance the rate of weight loss. Meng *et al.* (2012) also reported the same observation in their TGA experiments of willow char. They found that the char weight loss increased with increasing oxygen concentration. An increase in oxygen concentration could increase available reactant concentration. In this study, the palm fibre char consist of mainly carbon and very low distillation due to most of the volatiles has escaping during the pyrolysis process. The less volatiles make it easier for carbon to vaporise at certain temperature and reacts with oxygen. This would reflect the higher oxygen consumption and the lower activation energy obtained for palm fibre char.

A comparison of experiments C1, C8 and C9 allows the effect of the total system pressure to be observed. These experiments were conducted at the various total system pressures with the same oxygen partial pressure of 105kPa. Figure 7.21 presents the influence of the total system pressure with the same oxygen partial pressure on the peak temperatures and heights of the oxygen consumption curve. Figure 7.22 shows the influence of the total system pressure on the peak temperature for the both carbon oxide curves. As shown in Figure 7.21, there are no significant differences for the measured peak temperatures as the total system pressure increased from 500kPa to 695kPa with the same oxygen partial pressure of 105kPa. The differences were only 1°C to 3°C of the measured peak temperatures between the experiments C1, C8 and C9. However, as the total system pressure increased from 500kPa to 695kPa at the same oxygen partial pressure of 105kPa, the oxygen consumption peak height increased from 2.48 mol% to 2.74 mol% oxygen. The carbon dioxide production and carbon monoxide production curves were also revealed a similar trend as the oxygen consumption curve with the increasing of the total system pressure from 500kPa to 695kPa with the same oxygen partial pressure of 105kPa (see Figure 7.22 for experiments C1, C8 and C9).

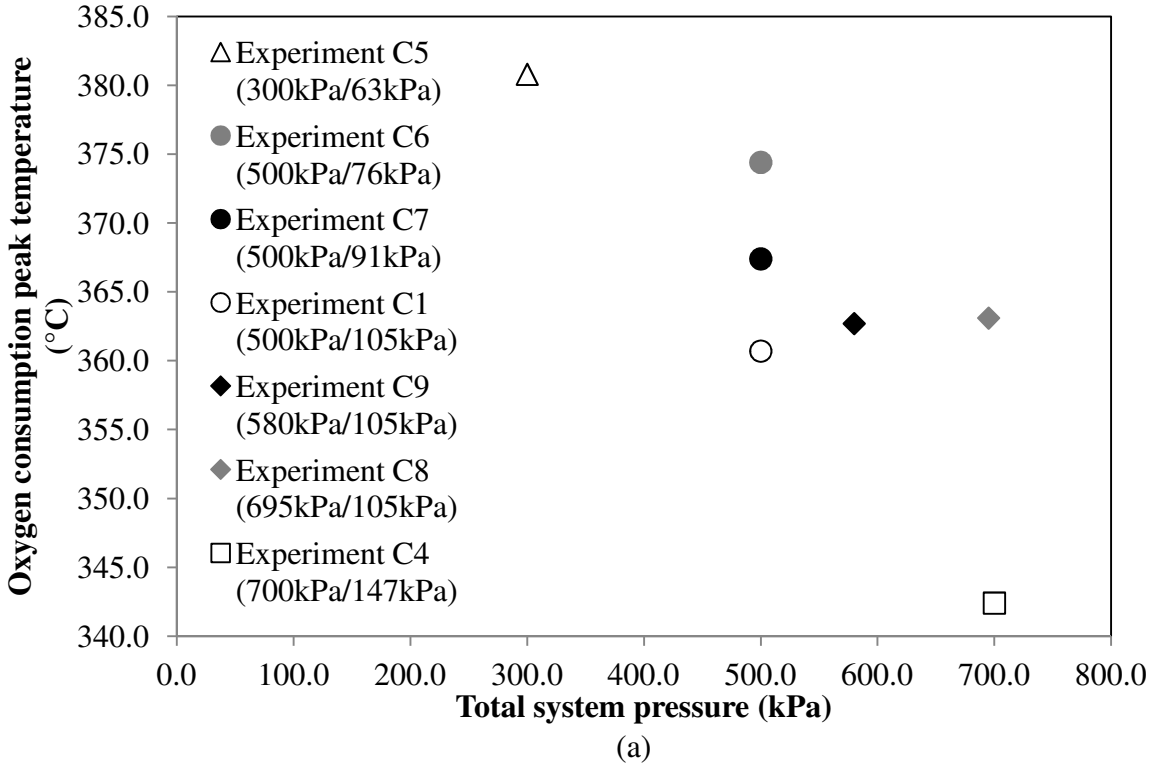

(a)

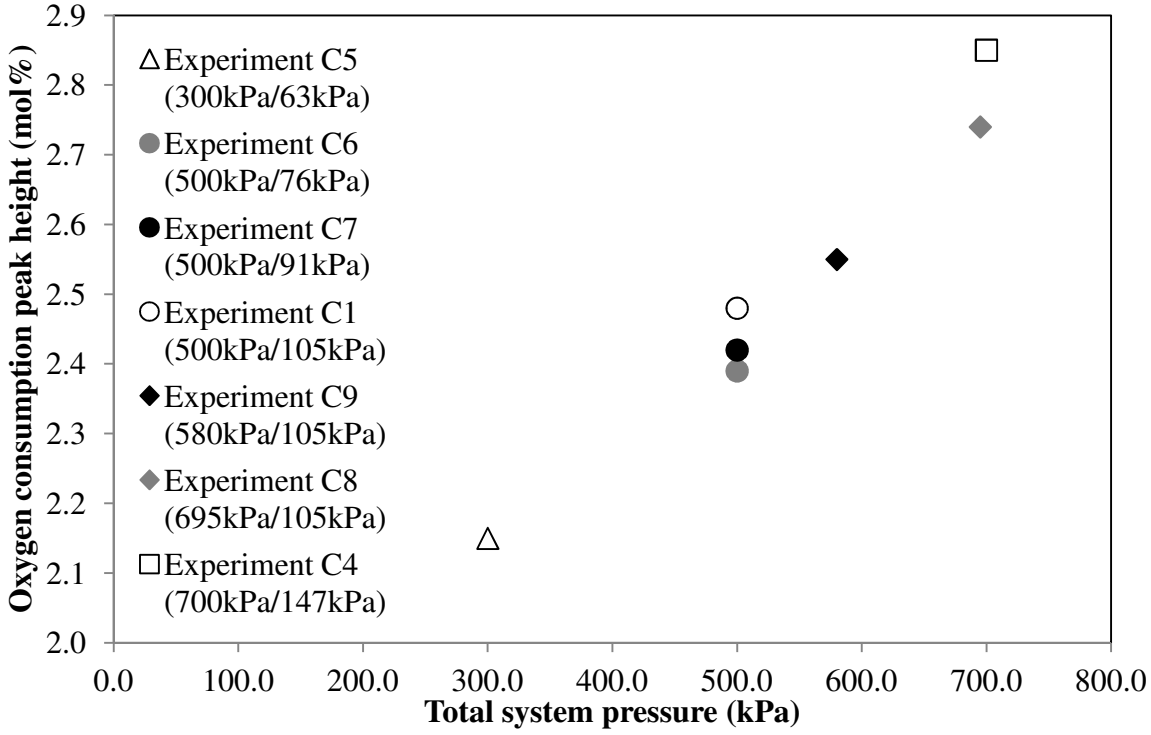

(b)

Figure 7.21 - Effect of the total system pressure on (a) the peak temperatures (b) the peak heights of the oxygen consumption curve. The pressures shown refer to the absolute total system pressure and oxygen partial pressure, respectively.

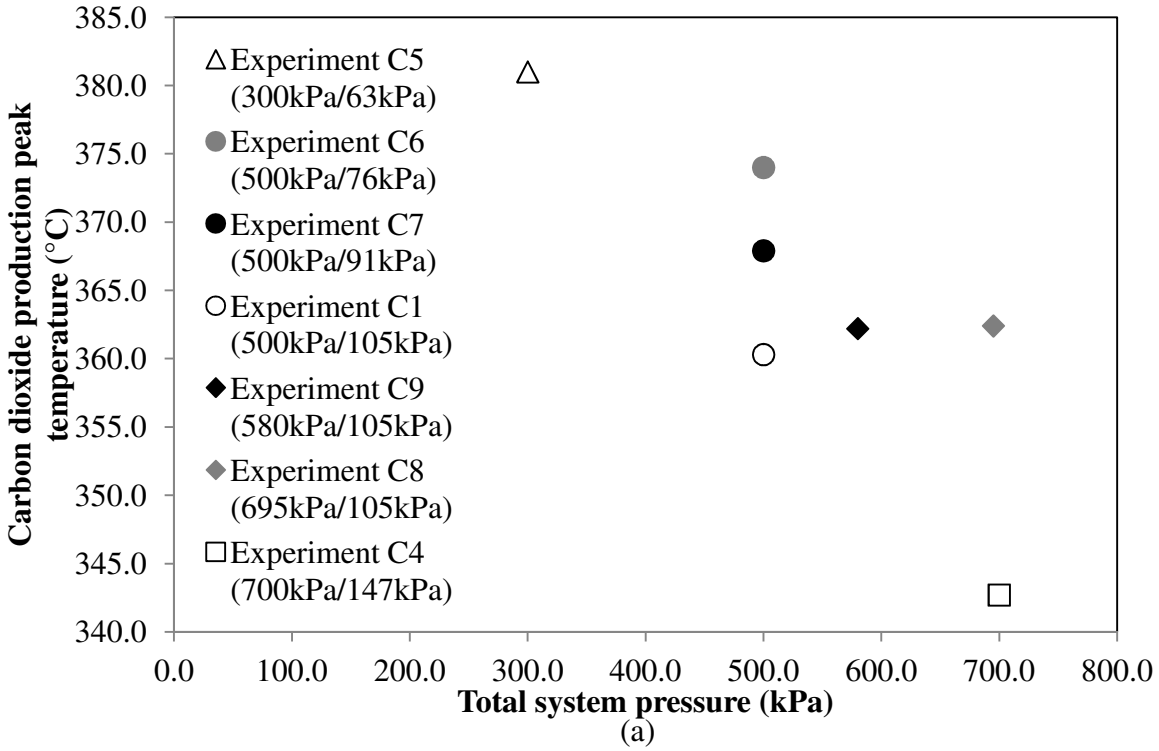

(a)

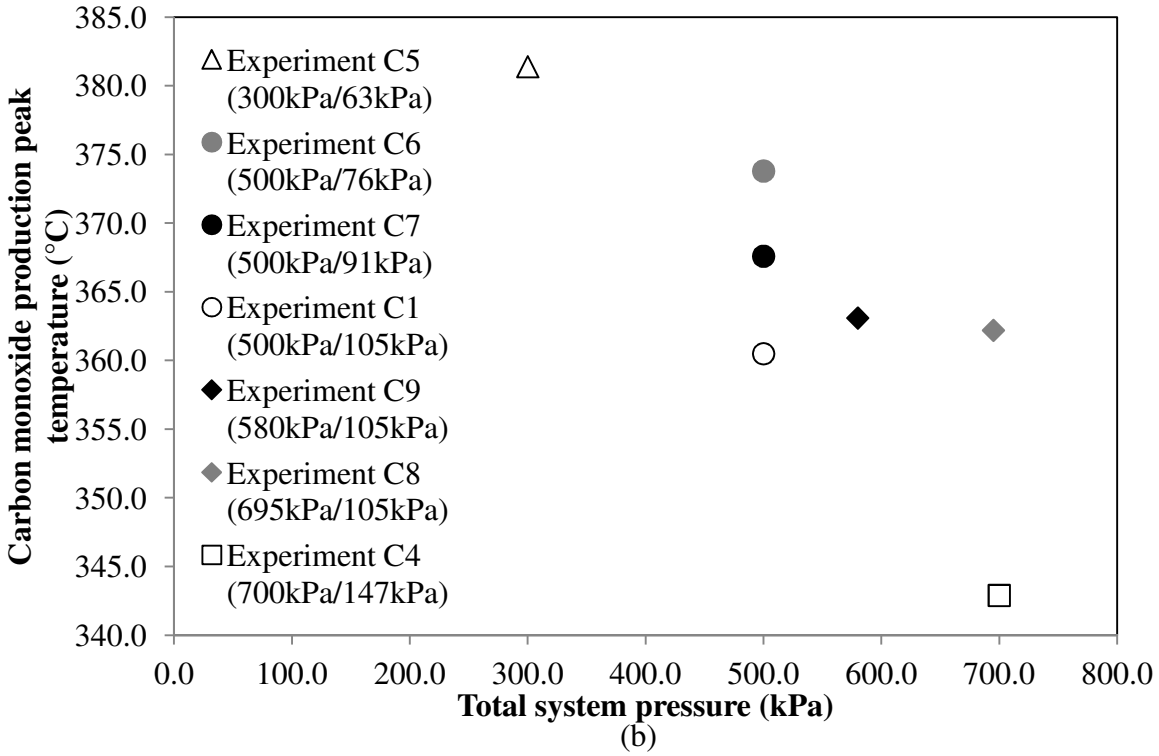

(b)

Figure 7.22 - Effect of the total system pressure on the peak temperatures of (a) the carbon dioxide production (b) the carbon monoxide production curves. The pressures shown refer to the absolute total system pressure and oxygen partial pressure, respectively.

The observations are in an agreement with the EGA experimental results discussed for the rice husk and the palm fibre combustion characteristic studies.

Table 7.4 provides the summary of the calculated kinetic parameters for experiments C4 to C9 on the effect of the total system and oxygen partial pressures of the palm fibre char. Figures 7.23 to 7.28 show a plots of oxygen consumption data and the model predictions for experiments C4 to C9, respectively. Considering Figures 7.23 to 7.28, all experiments except for experiments C4 and C8 show a good fit between the predicted oxygen consumption curve and the actual experimental data with the calculated variance of below 0.001. The variance observed for experiments C5 to C7 were 0.0004, 0.0003 and 0.0003, respectively. The experiment C9 calculated variance is 0.0006. As shown in Figure 7.27, the experiment C8 display an acceptable fit between the predicted modeled and the actual experimental data of the oxygen consumption. The disagreement between the predicted and observed oxygen consumption levels are obvious at the very high temperature range of 400°C to 430°C. This may be due to the instability of the oxygen consumption experimental data at the ends of the experiment which makes it difficult to obtain a good fit with the predicted curve. Referring to the Figure 7.23 for the experiment C4, a poor fit between the predicted curve and the actual oxygen consumption experimental data was observed with the calculated variance of 0.0115.

The discrepancies were obvious at the very high temperature range of 370°C to 420°C and at the medium temperature range of 250°C to 300°C. The disagreement at the very high temperature range of 370°C to 420°C was due to the instability of the oxygen consumption experimental data at the ends of the experiment. The disagreement in medium temperature range of 250°C to 300°C was due to the overlapping of the LTO, MTO and HTO peaks.

Experiments C1 to C5 were conducted using air as the oxidising gas. As observed in Table 7.4 for experiments C1 to C5, as the pressure increased from 300kPa to 700kPa, the activation energy of the high temperature oxidation (HTO) reaction decreased from 16.7×10^3K to 8.5×10^3K and the ln β decreased from 18.5 to 8.6.

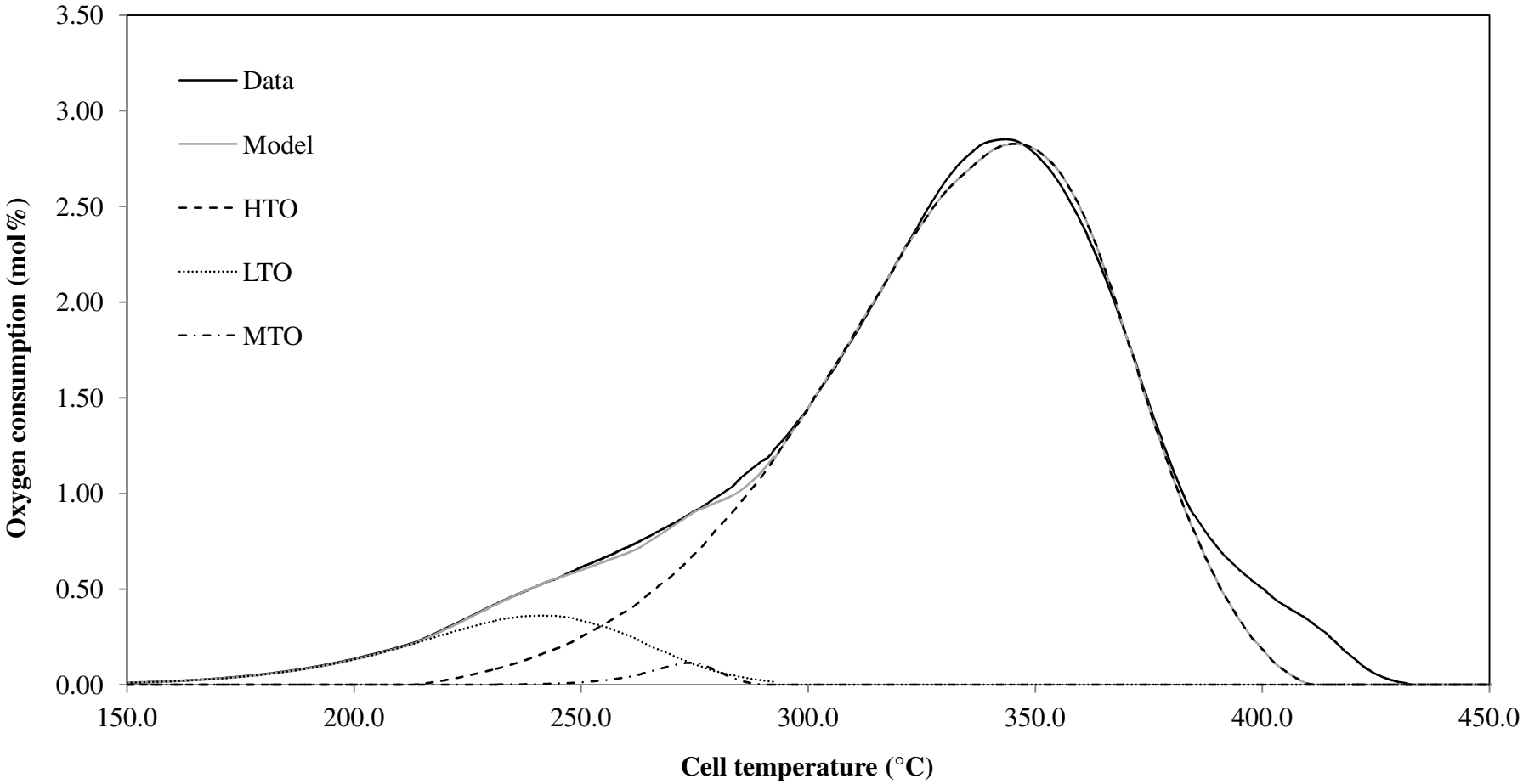

Figure 7.23 - Comparison of the oxygen consumption data and the model prediction with respects to the cell temperature for the palm fibre char oxidation with air as the oxidising gas, an absolute total system pressure of 700kPa, an air flow rate of 400smL/min and a heating rate of 50°C/h (Experiment C4).

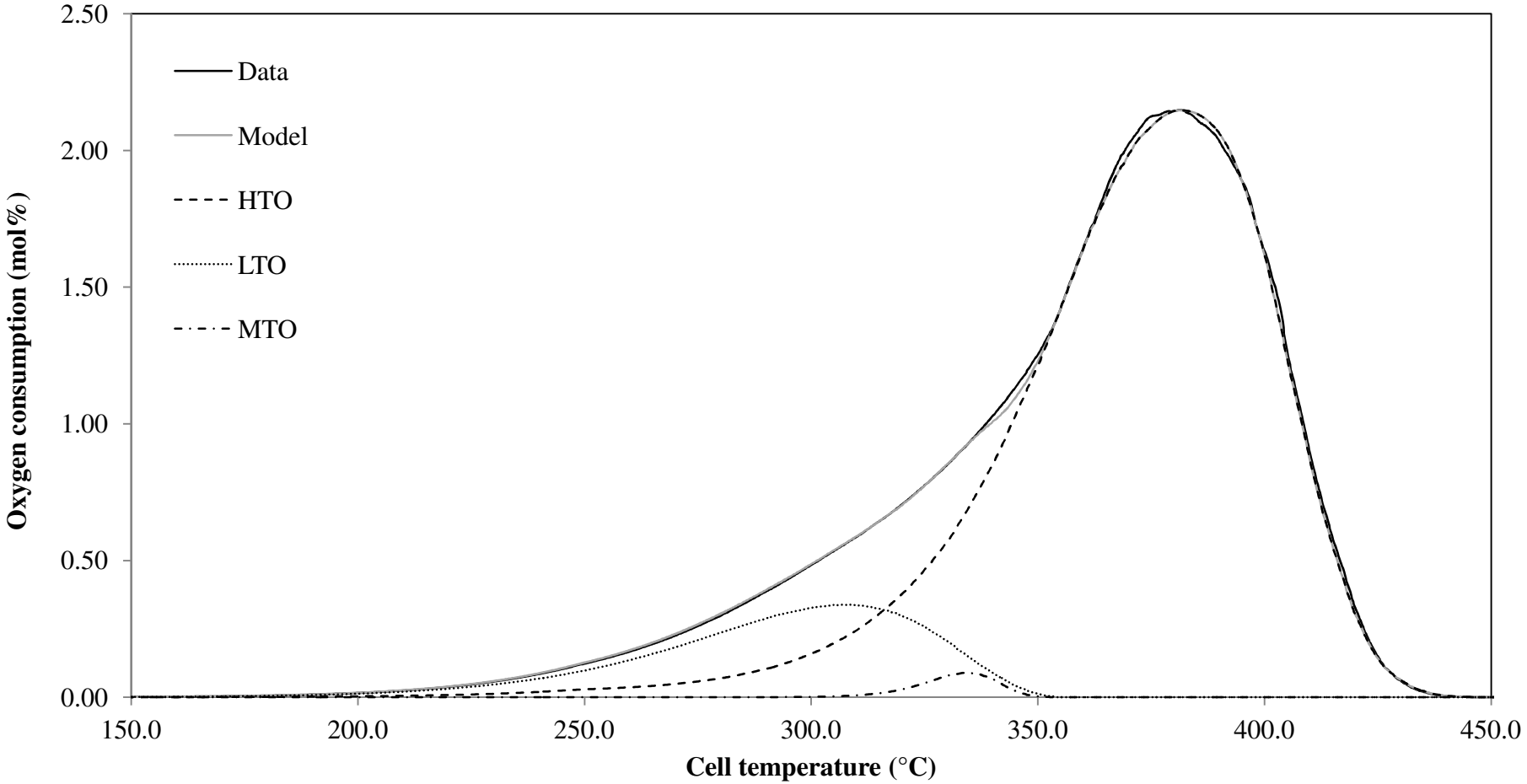

Figure 7.24 - Comparison of the oxygen consumption data and the model prediction with respects to the cell temperature for the palm fibre char oxidation with air as the oxidising gas, an absolute total system pressure of 300kPa, an air flow rate of 400smL/min and a heating rate of 50°C/h (Experiment C5).

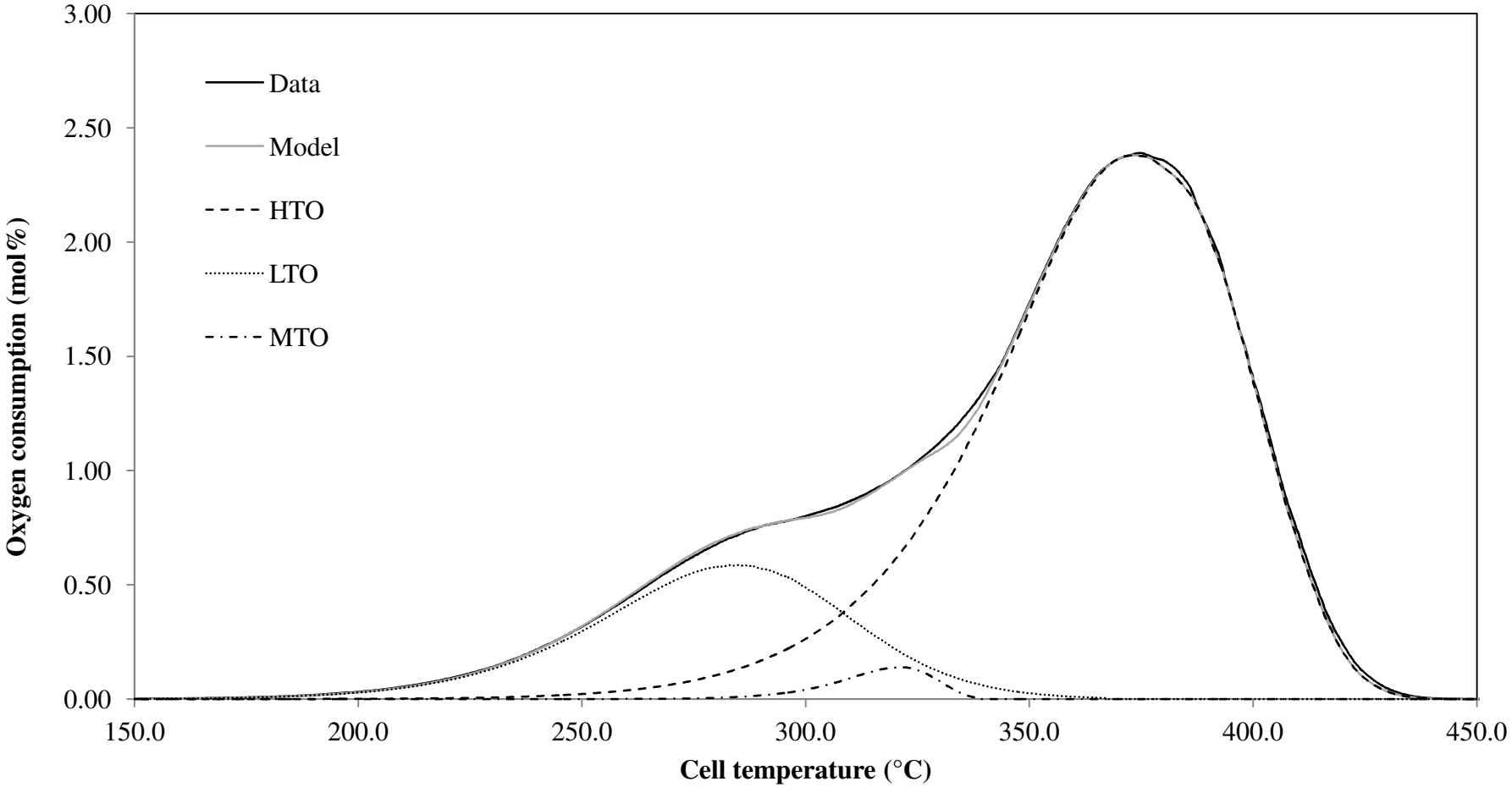

Figure 7.25 - Comparison of the oxygen consumption data and the model prediction with respects to the cell temperature for the palm fibre char oxidation with an oxygen partial pressure of 76kPa, an absolute total system pressure of 500kPa, a feed gas flow rate of 400smL/min and a heating rate of 50°C/h (Experiment C6).

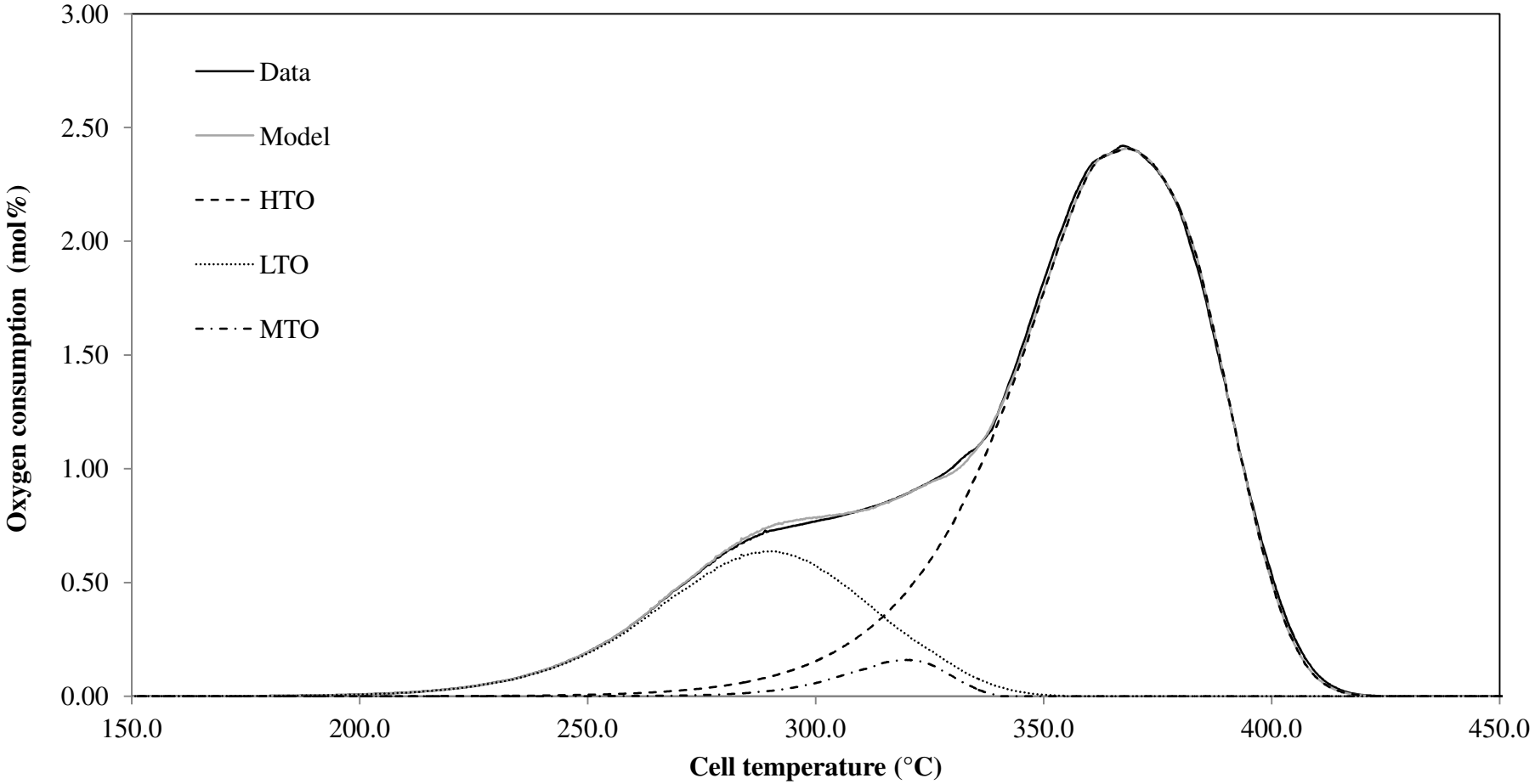

Figure 7.26 - Comparison of the oxygen consumption data and the model prediction with respects to the cell temperature for the palm fibre char oxidation with an oxygen partial pressure of 91kPa, an absolute total system pressure of 500kPa, a feed gas flow rate of 400smL/min and a heating rate of 50°C/h (Experiment C7).

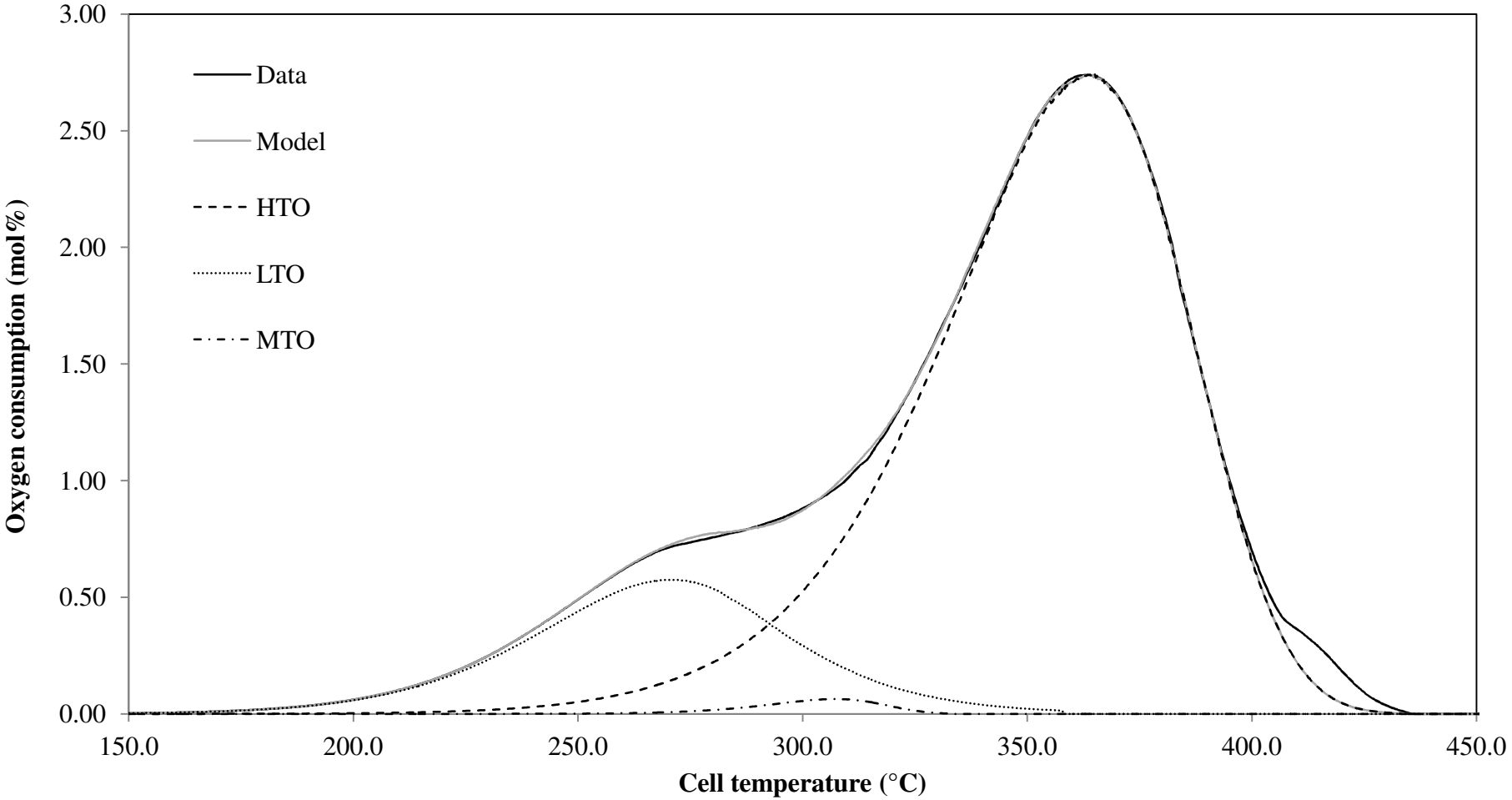

Figure 7.27 - Comparison of the oxygen consumption data and the model prediction with respects to the cell temperature for the palm fibre char oxidation with an oxygen partial pressure of 105kPa, an absolute total system pressure of 695kPa, a feed gas flow rate of 400smL/min and a heating rate of 50°C/h (Experiment C8).

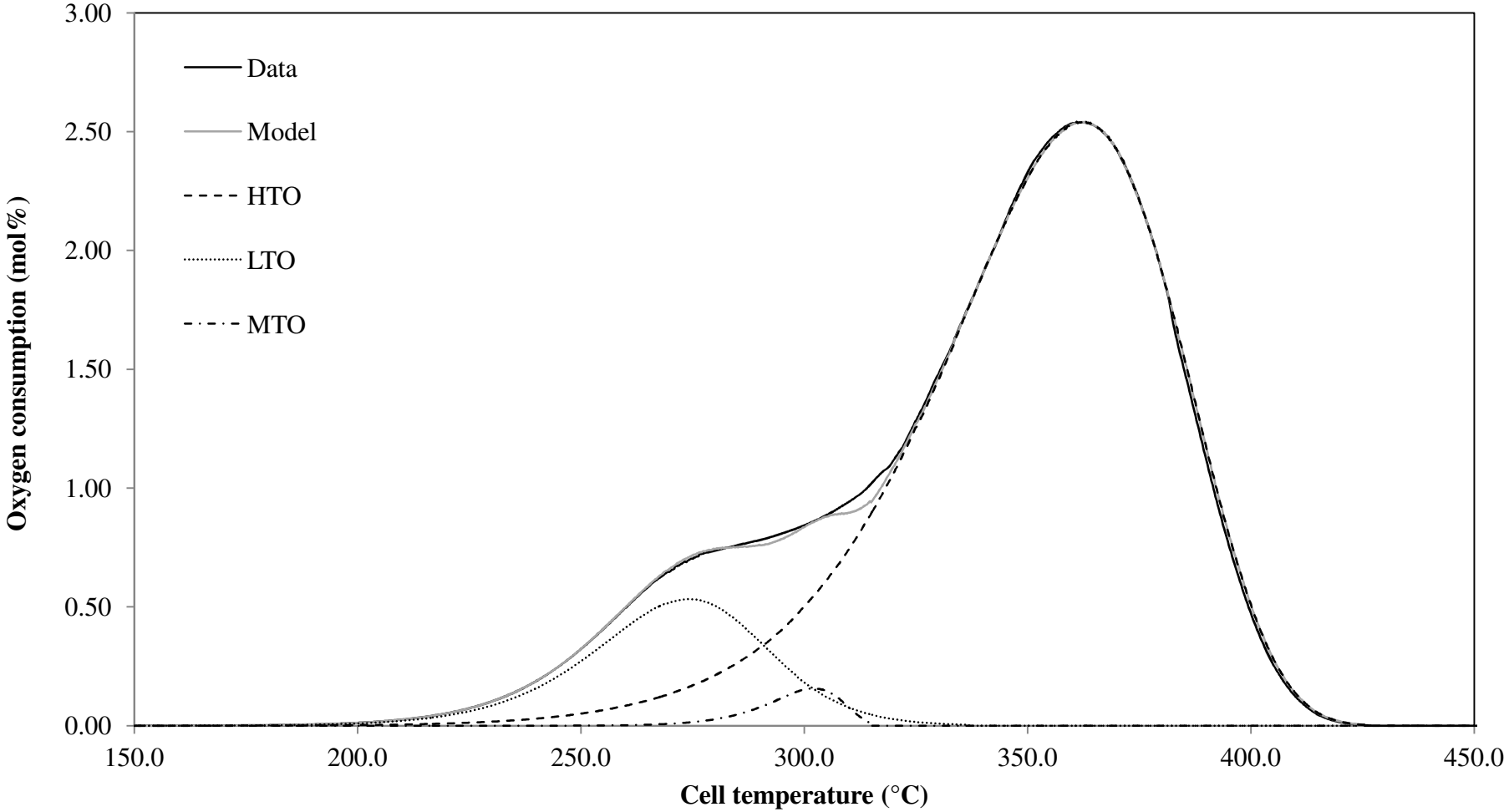

Figure 7.28 - Comparison of the oxygen consumption data and the model prediction with respects to the cell temperature for the palm fibre char oxidation with an oxygen partial pressure of 105kPa, an absolute total system pressure of 580kPa, a feed gas flow rate of 400smL/min and a heating rate of 50°C/h (Experiment C9).

For the reaction order a slight increase of 0.02 was observed as the pressure increased from 300kPa to 700kPa. A similar trend was also observed for the medium temperature oxidation (MTO) reaction. The activation energy of the MTO reaction decreased from 24.8×10^3K to 14.2×10^3K. The ln β for the MTO reaction was also recorded a decrease from 29.3 to 10.0 as the pressure increased from 300kPa to 700kPa. Unlike the HTO reaction, the reaction order of the MTO reaction decreased by 0.28 as the pressure increased from 300kPa to 700kPa. For the low temperature oxidation (LTO) reaction, an opposite trend from the HTO and the MTO was observed. The reaction order, the activation energy and the ln β of the LTO reaction increased as the pressure increased from 300kPa to 700kPa. The activation energy and the ln β increased from 10.4×10^3K to 13.1×10^3K and from 12.3 to 19.3, respectively as the pressure increased from 300kPa to 700kPa. An increase from 0.77 to 1.10 was observed for the reaction order of the LTO reaction as the pressure increased. In order to examine whether it is the total system pressure or the oxygen partial pressure that has the more significant influence on the palm fibre char combustion characteristics, a comparison of experiments C1 to C3, C6 and C7 may be made. Further, a comparison of the experiments C1 to C3, C8 and C9 allows the effect of the total system pressure but with the same oxygen partial pressure of 105kPa to be examined.

Figures 7.29 to 7.31 present a plot of the kinetic parameters of the activation energy (E/R) and the ln β with respect to the oxygen partial pressure for the HTO, LTO and MTO reactions, respectively. Figure 7.29 for the HTO reaction shows that the activation energy and the ln β decrease with increasing oxygen partial pressure. By comparison of the experiments C1, C6 and C7 conducted at the same total system pressure of 500kPa but with various oxygen partial pressures, there are a changes in the activation energy and the ln β of the HTO reaction.

A similar trend is observed for the LTO reaction (see Figure 7.31). The activation energy and the ln β decreased with increasing oxygen partial pressures. However, the MTO reaction shows an opposing trend to the HTO and the LTO reactions.

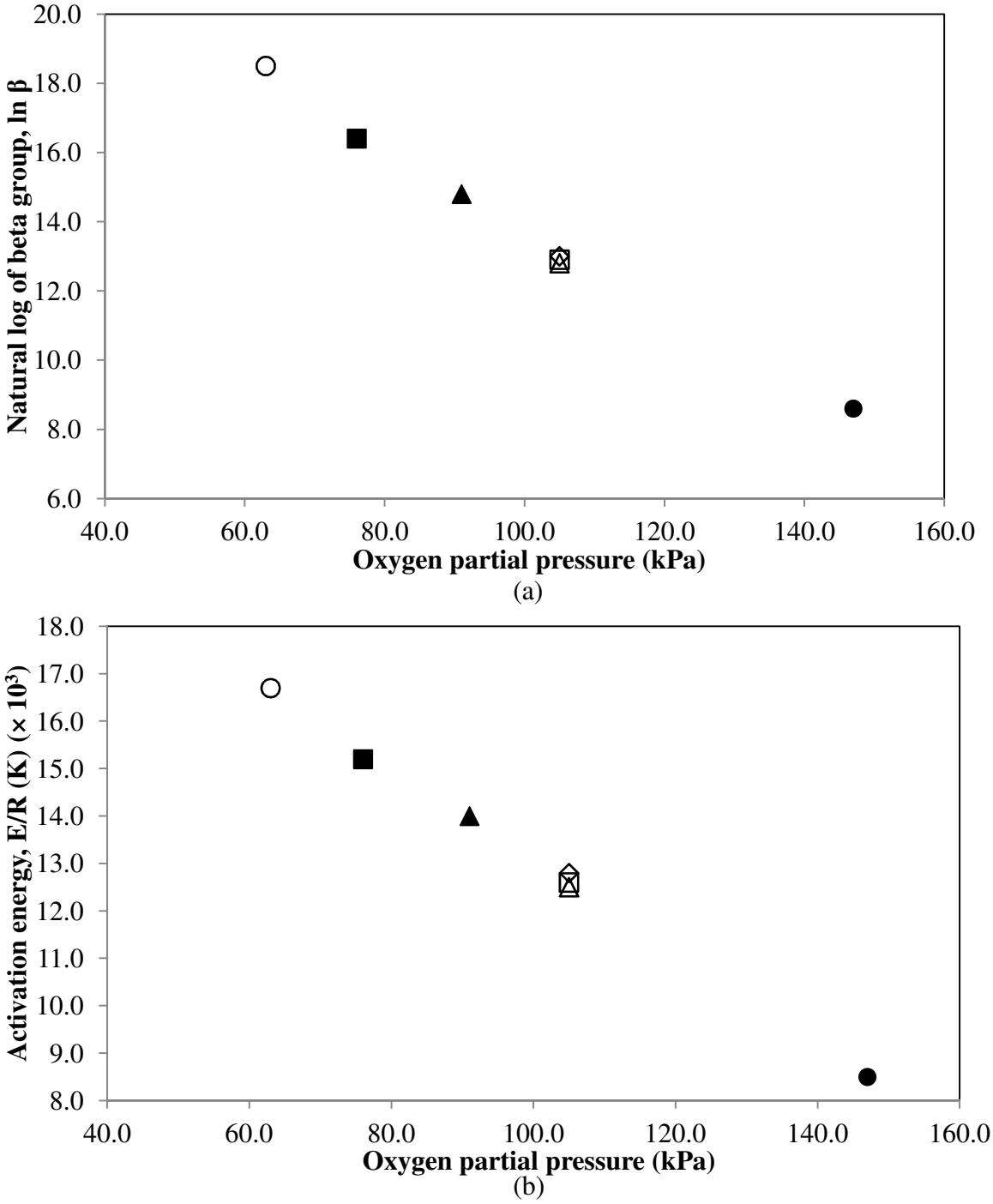

Figure 7.29 - Effect of the oxygen partial pressure on (a) the natural log of beta group, ln β (b) the activation energy, E/R for the high temperature oxidation, HTO. The pressure shown refer to the total system pressure.

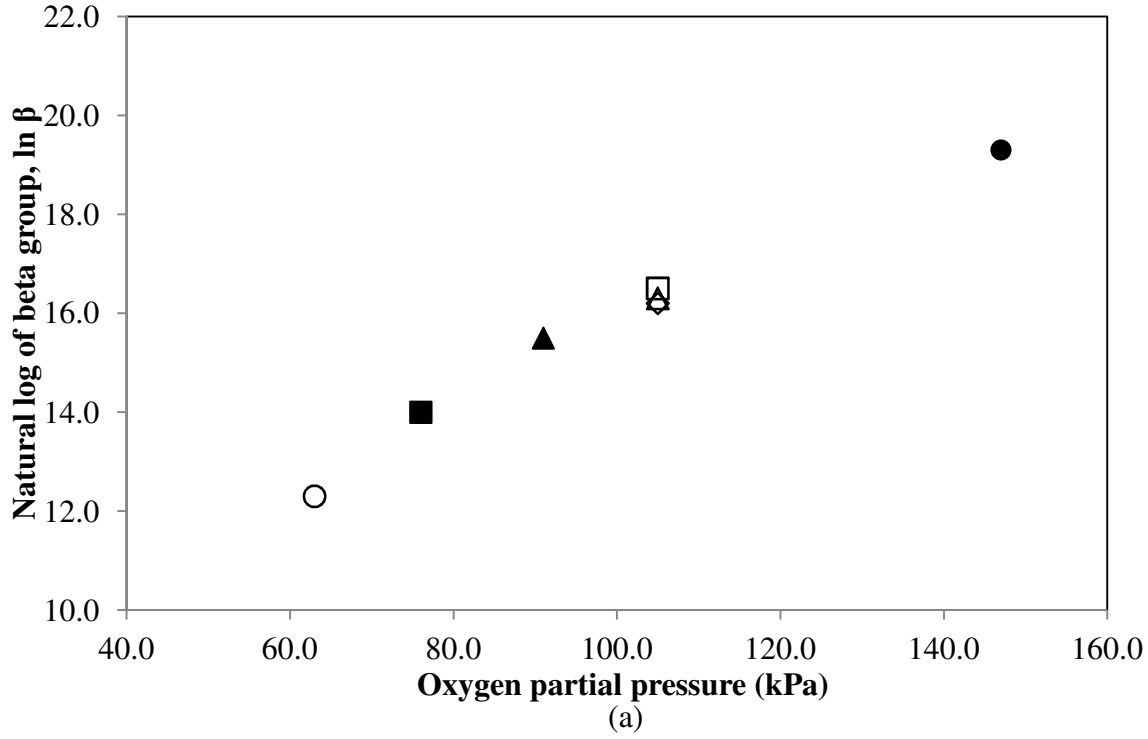

(a)

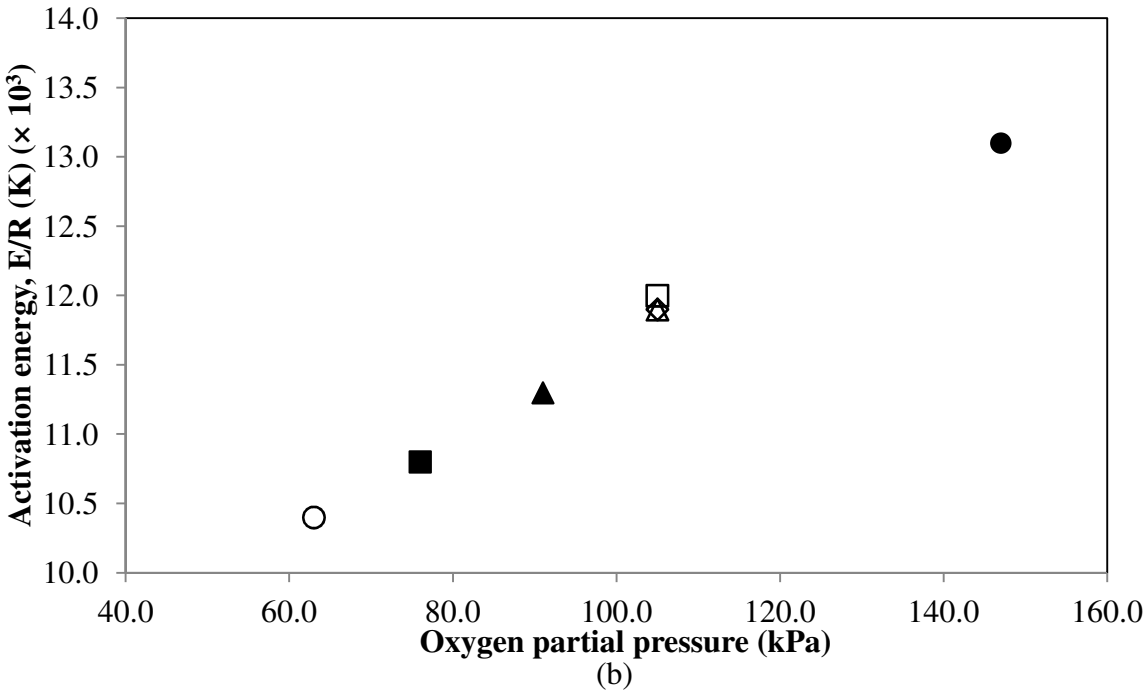

(b)

○ Experiment C5 (300kPa) ■ Experiment C6 (500kPa) ▲ Experiment C7 (500kPa)
◇ Experiment C1 (500kPa) □ Experiment C2 (500kPa) △ Experiment C3 (500kPa)
● Experiment C4 (700kPa)

Figure 7.30 - Effect of the oxygen partial pressure on (a) the natural log of beta group, ln β (b) the activation energy, E/R for the low temperature oxidation, LTO. The pressure shown refer to the total system pressure.

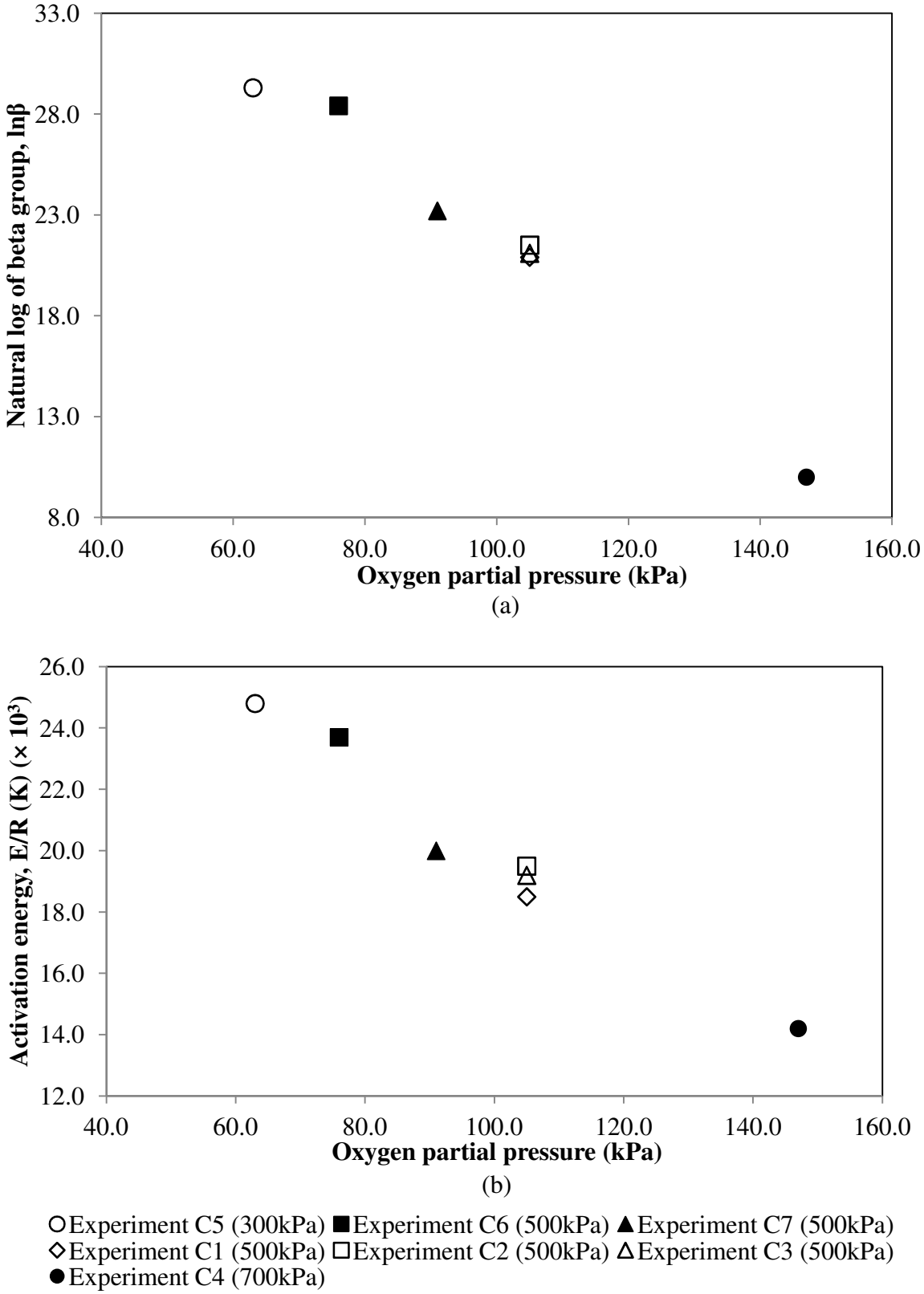

Figure 7.31 - Effect of the oxygen partial pressure on (a) the natural log of beta group, ln β (b) the activation energy, E/R for the medium temperature oxidation, MTO. The pressure shown refer to the total system pressure.

The activation energy and the ln β increased with increasing oxygen partial pressure (see Figure 7.30). This is well expected since the reaction model derived in Chapter 4 assumed that the reaction rate was proportional to the oxygen partial pressure and the fuel concentration.

Figures 7.32 to 7.34 show a plots of the kinetic parameters of activation energy (E/R) and ln β with regards to the total system pressure for the three regimes HTO, LTO and MTO, respectively. As observed in Figures 7.32 to 7.34 and by comparison of the experiments C1 to C3, C8 and C9, there are no significant differences in the calculated kinetic parameters of the activation energy and the ln β for the HTO, LTO and MTO reactions. From this, we infer that all the reaction regimes are influenced by the oxygen partial pressure rather than by the total system pressure. These findings are consistent with the experimental data discussed in the previous Section 7.4.1 and the observations found for the rice husk and the palm fibre combustion characteristic studies.

In summary, the oxygen partial pressure has a significant influence on the palm fibre char combustion characteristics. The peak temperatures of the oxygen consumption, the carbon dioxide production and the carbon monoxide production curves decrease with increasing oxygen partial pressures. However, the peak heights for the exit gas oxygen, carbon dioxide and carbon monoxide composition curves increase with increasing oxygen partial pressure.

The total system pressure has no significant effect on the peak temperature. However, the peak height increases with increasing total system pressure. All the reaction regimes are influenced by the oxygen partial pressure rather than by the total system pressure. The activation energy and the ln β decrease with increasing oxygen partial pressure for the HTO and LTO reactions. However, the activation energy and the ln β of the MTO reaction increase with increasing oxygen partial pressure. There are no significant changes in the calculated kinetic parameters over the various total system pressures but with the same oxygen partial pressure.

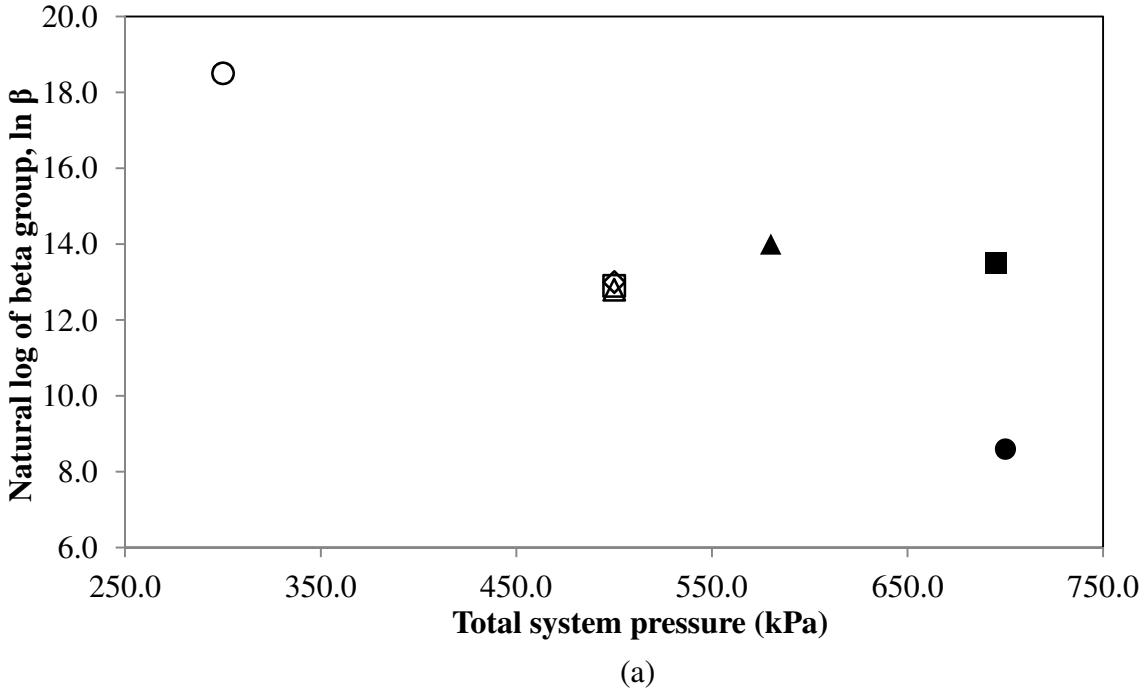

(a)

.

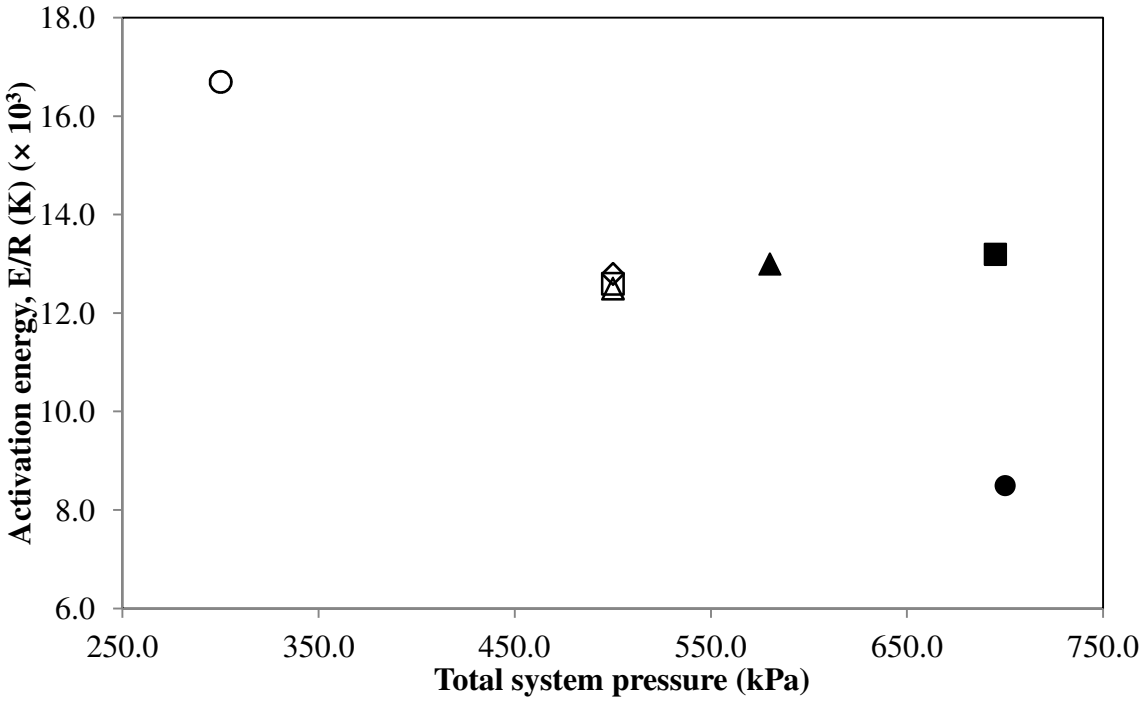

(b)

○Experiment C5 (63kPa) ◇Experiment C1 (105kPa) □Experiment C2 (105kPa)
△Experiment C3 (105kPa) ▲Experiment C9 (105kPa) ■Experiment C8 (105kPa)
●Experiment C4 (147kPa)

Figure 7.32 - Effect of the total system pressure on (a) the natural log of beta group, ln β (b) the activation energy, E/R for the high temperature oxidation, HTO. The pressure shown refer to the oxygen partial pressure.

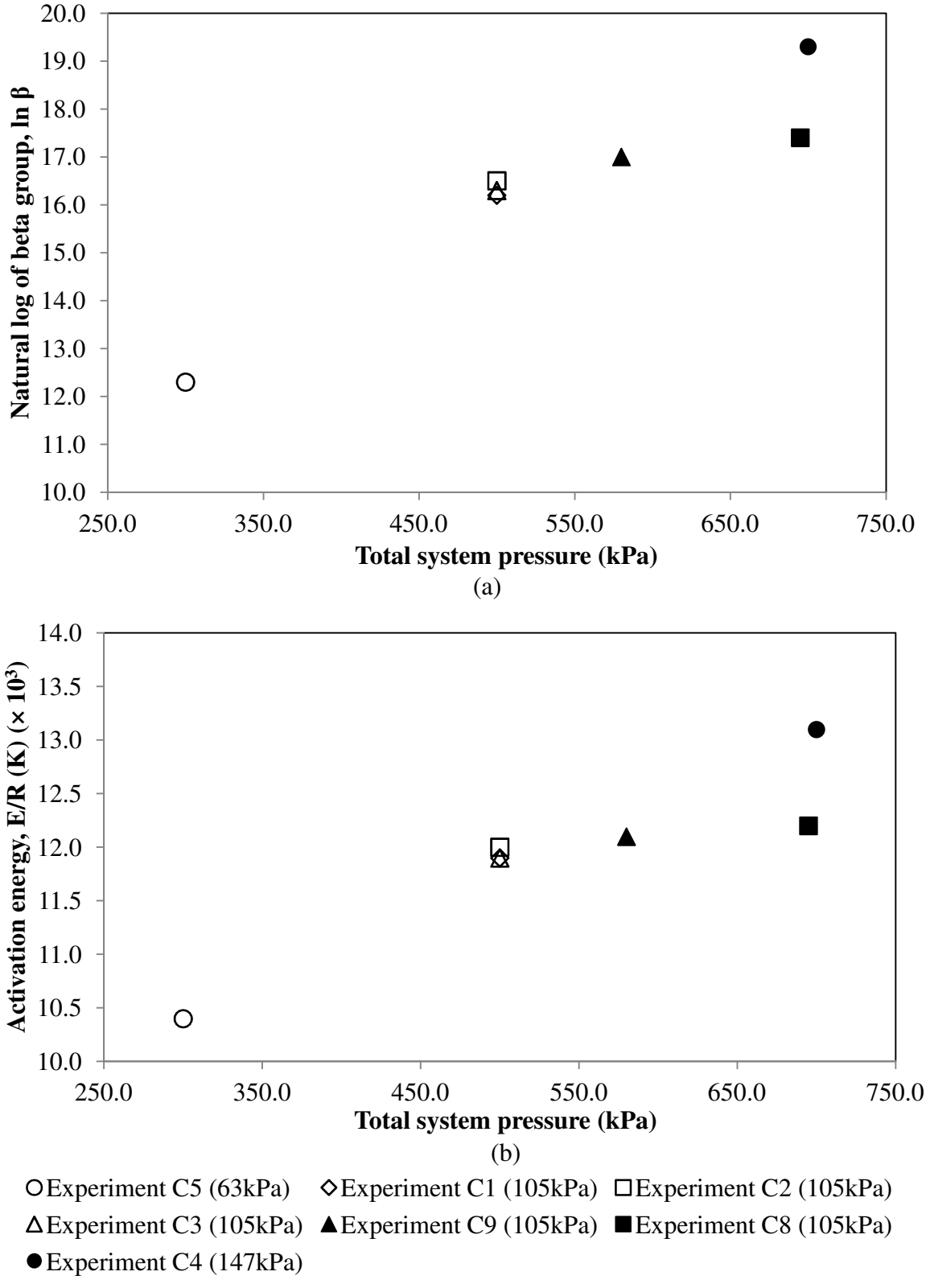

Figure 7.33 - Effect of the total system pressure on (a) the natural log of beta group, ln β (b) the activation energy, E/R for the low temperature oxidation, LTO. The pressure shown refer to the oxygen partial pressure.

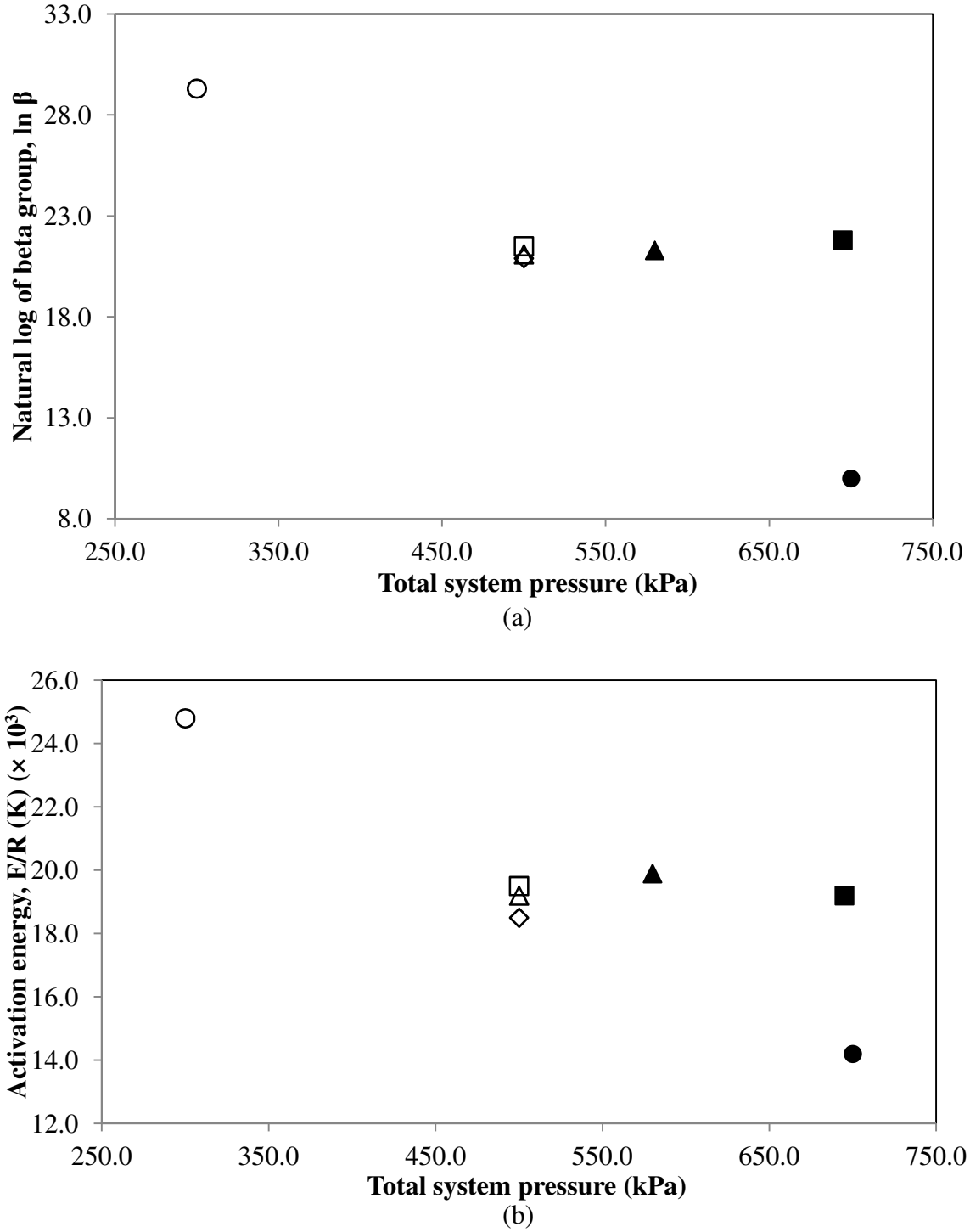

Figure 7.34 - Effect of the total system pressure on (a) the natural log of beta group, ln β (b) the activation energy, E/R for the medium temperature oxidation, MTO. The pressure shown refer to the oxygen partial pressure.

7.5 Analysis of error in calculating the palm fibre char kinetic parameters

Any uncertainty in the raw experimental data will be passed on to the values calculated for the kinetic parameters. The calculated kinetic parameters from the evolved gas analysis (EGA) data falls within a range of confidence limits. The confidence limits are dependent on the accuracy of the raw data. The confidence limits may be determined by considering the contributions made by the various data points and the uncertainty associated with each data point. The calculation steps for the uncertainties of the experimental data was discussed previously in Section 5.6 of the rice husks oxidation study. The same uncertainties calculation procedure was applied for the palm fibre char.

Table 7.5 presents the uncertainty in the calculated kinetic parameter values of the palm fibre char for the high temperature oxidation (HTO) peak temperature. The absolute error was obtained by considering the change in the variable between each data reading of 10 seconds intervals. Considering Table 7.5, the level of uncertainty in the activation energy was in the range of 5.7 to 6.7% for all the palm fibre char oxidation reactions. The error in the calculated ln β for all the palm fibre char oxidation reactions were in the range of 7.0% to 15.1%. Hence, the level of uncertainty in the activation energy is about ±6.7% while the error for the ln β is approximately ±15.1% for all the palm fibre char oxidation reactions.

The activation energy and the ln β for the typical experiment C1 were calculated to be of 12.8×10^3K and 13.0, respectively. By including the value for the uncertainty, the activation energy for a typical experiment C1 yields in between 11.9×10^3K to13.7×10^3K. The natural log of beta group, ln β was in the range of 11.0 to 15.0. There is a limited number of studies on the carbon combustion characteristics using an evolved gas analysis (EGA) experiments. Kisler (1995) calculated the activation energy of 26.1×10^3K and ln β of 30.8 in the work of finely ground activated carbon with sand and water using EGA experiments. The reaction order is between zero and one with respect to the oxygen. Mamora *et al.* (1993) investigated the carbon combustion using an EGA experiments. They found that the activation energy was 19×10^3K with the reaction order of 0.75 with respect to the carbon.

Table 7.5 - Uncertainty in the calculated values for the palm fibre char EGA experiments. The relative error is refer to the peak temperature of the high temperature oxidation (HTO) reaction.

Variable	Absolute error	Relative error (%)								
		C1	C2	C3	C4	C5	C6	C7	C8	C9
ΔO_2 (mol%)	0.004	0.16	0.17	0.16	0.14	0.19	0.17	0.17	0.15	0.16
Inverse temperature (K^{-1})	0.000001	0.04	0.04	0.04	0.03	0.04	0.04	0.04	0.04	0.04
Integral (ΔO_2 vs t)	6	0.07	0.06	0.07	0.05	0.09	0.07	0.08	0.06	0.08
Ln (RRR)	0.009	0.13	0.12	0.13	0.12	0.13	0.13	0.13	0.16	0.13
E_i/R	700	5.88	5.83	5.88	5.34	6.73	6.48	6.20	5.74	5.93
ln β_i	1.3	10.00	10.08	10.16	15.12	7.03	7.93	8.78	9.63	9.29

Recently, Park and Jang (2012) investigated the changes in the fuel properties of the rice husk char and the wood pellet char using thermogravimetric analysis (TGA) technique. They found that the activation energy for the rice husk char and the wood pellet char were 105 kJ/mol (10.8×10^3K) and 137 kJ/mol (14.1×10^3K), respectively. The values were comparatively similar to the activation energy found for this present study of palm fibre char. Essenhigh (1981) reported that the activation energy of the carbon combustion varies widely depending on the carbon structure, the experimental technique and the reaction order.

7.6 Concluding remarks

The evolved gas analysis (EGA) experiments of the palm fibre char are found to be reproducible based on the peak temperature and height of the runs under identical conditions. The calculated kinetic parameters of the runs under identical conditions also reveal that the experiments are reproducible with no significant changes in the kinetic parameter values. The series of experimental runs conducted at the various total system pressures and oxygen partial pressures show that the oxygen partial pressure has a significant influence on the palm fibre char oxidation reactions. The peak temperature for the oxygen consumption, the carbon dioxide production and the carbon monoxide production curves decrease with increasing oxygen partial pressure. However, the peak height shows an opposing trend. The total system pressure has no significant influence on the peak temperature but the peak height increases with increasing total system pressure. The calculated kinetic parameters for experiments at various total system and oxygen partial pressures also show that all the reaction regimes representing HTO, MTO and LTO are influenced by the oxygen partial pressure rather than by the total system pressure.

The calculated activation energy for a typical experiment C1 is in the range of 11.9×10^3K to 13.7×10^3K. Further, the natural log of beta group, ln β is between 11.0 and 15.0. From the findings we infer that the best combustion parameters for the palm fibre char is at an absolute total system pressure of 700kPa, an oxygen partial pressure of 147kPa, a flow rate of 400smL/min and at a heating rate of 50°C/h.

At this condition the activation energy and the measured peak temperature are at its lowest and may improve the carbon conversion efficiency of the combustion process. The use of higher concentration of oxygen may also contributes to the low activation energy and the higher carbon conversion efficiency.

This Chapter gives an insight on the combustion characteristics of the palm fibre char. The findings could be useful for the biomass char combustion reactor design. Next Chapter 8 will compare the results of the combustion characteristics for the three biomasses of rice husk, palm fibre and palm fibre char using an EGA technique.

CHAPTER 8

COMPARISON STUDY

8.1 Introduction

This Chapter compares the results of the evolved gas analysis (EGA) experimental investigation into the combustion characteristics of rice husk, palm fibre and palm fibre char. The first section provides a comparison between typical rice husk, palm fibre and palm fibre char experimental results. Next a discussion on the calculated kinetic parameters result of the three biomass materials is presented. Both discussions cover the effect of pressure on the experimental results and the calculated kinetic parameters of the three biomass materials.

8.2 Comparison of typical experimental combustion results for rice husk, palm fibre and palm fibre char

To allow a comparison between the three different biomasses studied three experiments conducted under identical conditions have been selected for review: experiments R4, F6 and C1. Each of these runs were performed under identical conditions with air as the oxidising gas, an absolute total system pressure of 500kPa, an injection air flow rate of 400smL/min and a heating rate of 50°C/h. Table 8.1 presents a summary of the experimental conditions of these experiments. Table 8.2 presents the results of the ultimate and proximate analyses of the rice husk, palm fibre and palm fibre char samples.

Table 8.1 - Experimental conditions for typical rice husk, palm fibre and palm fibre char samples.

Experiment	**R4**	**F6**	**C1**
Sample	Rice husk	Palm fibre	Palm fibre char
Absolute total system pressure (kPa)	500	500	500
Oxygen partial pressure (kPa)	105	105	105
Injection gas (mol% Oxygen)	20.96 (Air)	20.96 (Air)	20.96 (Air)
Injection flow rate (smL/min)	400	400	400
Heating rate (°C/h)	50	50	50

Table 8.2 - Ultimate and proximate analyses of rice husk, palm fibre and palm fibre char. (Note that db is dry basis and daf is dry ash free basis).

Analyses	**Rice husk**	**Palm fibre**	**Palm fibre char**
Proximate analysis (db) (wt.%)			
Volatile matter	64.2	68.8	36.3
Fixed carbon	17.4	15.2	45.2
Ash	18.4	10.2	18.4
Ultimate analysis (daf) (wt.%)			
Carbon	40.90	43.19	60.90
Hydrogen	4.82	5.24	2.82
Nitrogen	0.43	1.59	1.43
Sulphur	0.17	0.19	-
Oxygen	53.68	49.79	34.85
Calorific value (MJ/kg)	15.50	19.00	34.20

As shown in Table 8.2, the volatile matter value for the rice husk and the palm fibre samples were almost double the values for the palm fibre char sample. This is well expected since most of the volatile content had already escaped during the pyrolysis process used to produce the char. However, the fixed carbon content of the raw samples of rice husk and palm fibre were less than half the content of the palm fibre char sample. The carbon content for the char sample is higher than the rice husk and palm fibre samples being 60.9 wt% in comparison to 40.9 wt% (rice husk) and 43.2 wt% (palm fibre). This results in the higher calorific value obtained for the palm fibre char sample compared to the rice husk and palm fibre samples.

The palm fibre sample had slightly higher volatile matter, carbon content and calorific values than the rice husk sample. The slight differences are due to the nature of the biomass used. Different biomasses gives different ultimate and proximate analyses results. The results agree very well with the previous studies by Biagini *et al.* (2008) and Fernandez *et al.* (2012) in their rice husk combustion characteristics study using TGA technique. The same observations were also reported by Idris *et al.* (2010) and Park and Jang (2012) in their combustion characteristics studies by TGA technique using oil palm biomass and biomass char, respectively.

Figures 8.1 to 8.3 present data for typical evolved gas analysis (EGA) experiments of rice husk, palm fibre and palm fibre char, respectively. The actual carbon monoxide and carbon dioxide levels in the evolved gas are shown together with the oxygen consumption curves. As observed in Figures 8.1 and 8.2, the plots are of similar forms, exhibiting two main peaks, one in the 240°C to 280°C temperature range and the other in the 330°C to 380°C temperature range except for the carbon monoxide production curve for the rice husk sample. The carbon monoxide production curve for a rice husk sample appears to have only one peak in the 260°C to 280°C region.

The first and second peaks for the rice husk and palm fibre samples may be referred to as the hemicellulose and cellulose peaks, respectively (Biagini *et al.*, 2008 and Idris *et al.*, 2010). Considering Figure 8.3, the typical palm fibre char experiment has one peak in the 350°C to 370°C region. This peak is referred to as the lignin decomposition peak.

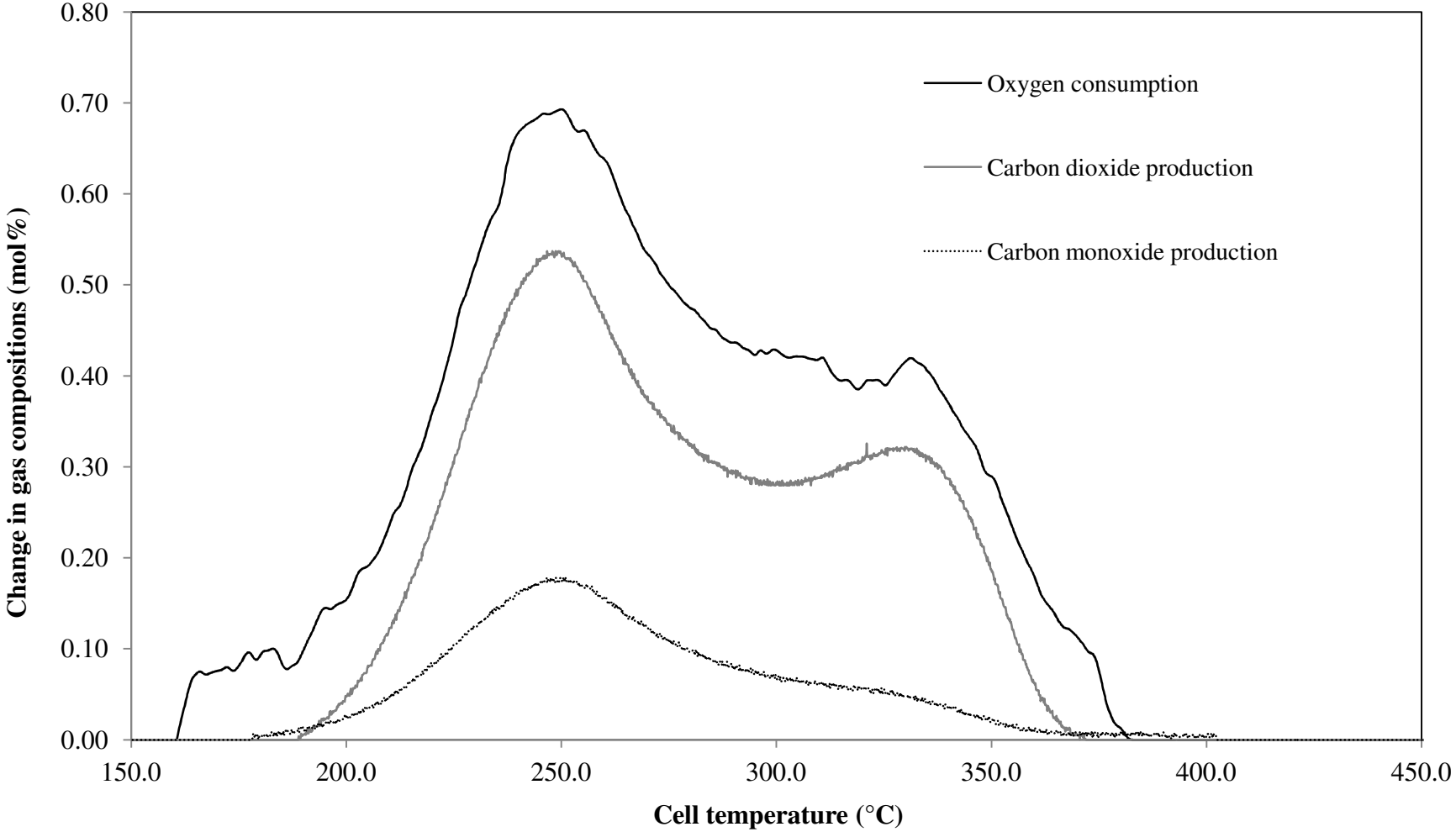

Figure 8.1 - Typical rice husk evolved gas analysis (EGA) experimental results with air as the oxidising gas, an absolute total system pressure of 500kPa, an air flow rate of 400smL/min and a heating rate of 50°C/h (Experiment R4).

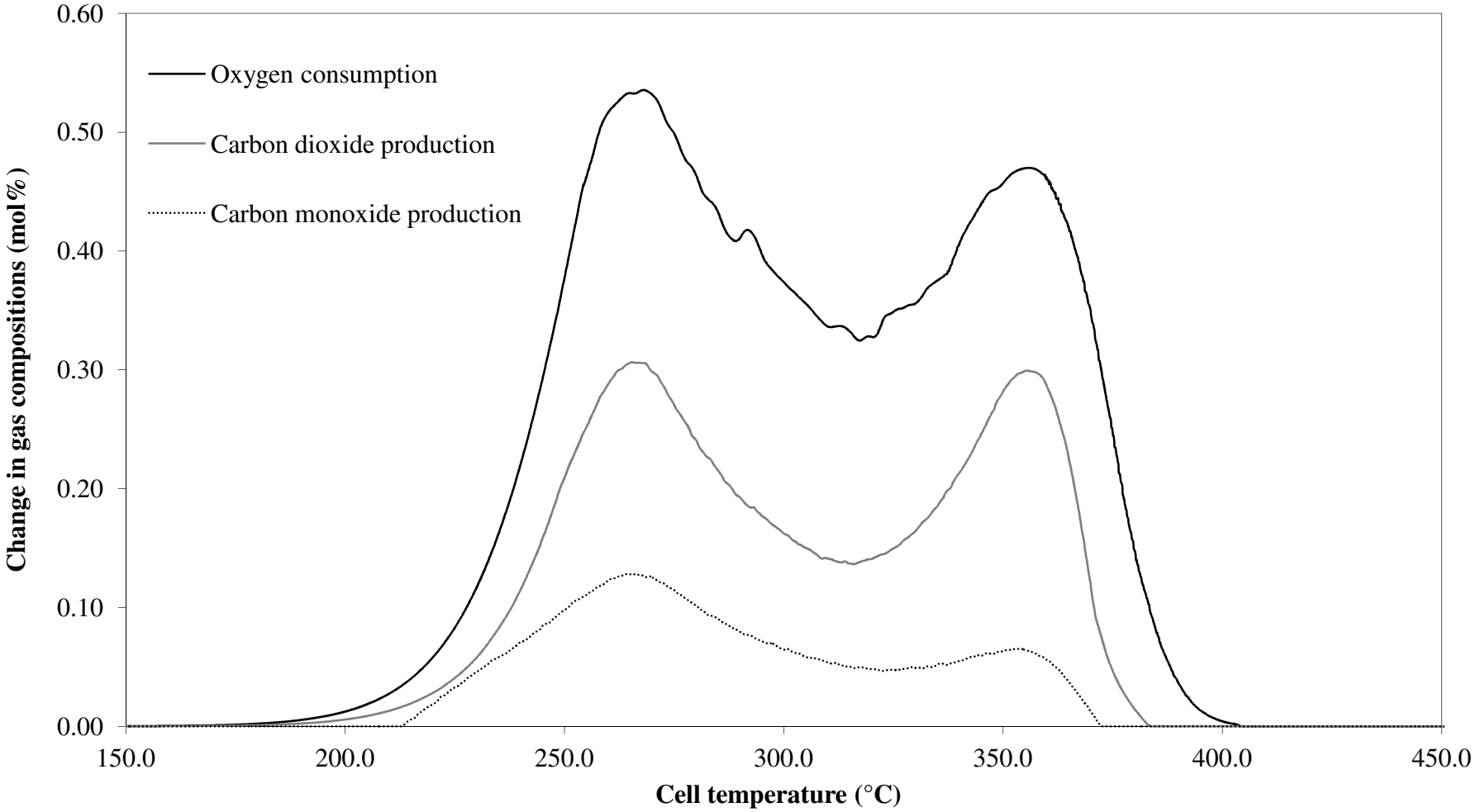

Figure 8.2 - Typical palm fibre evolved gas analysis (EGA) experimental results with air as the oxidising gas, an absolute total system pressure of 500kPa, an air flow rate of 400smL/min and a heating rate of 50°C/h (Experiment F6).

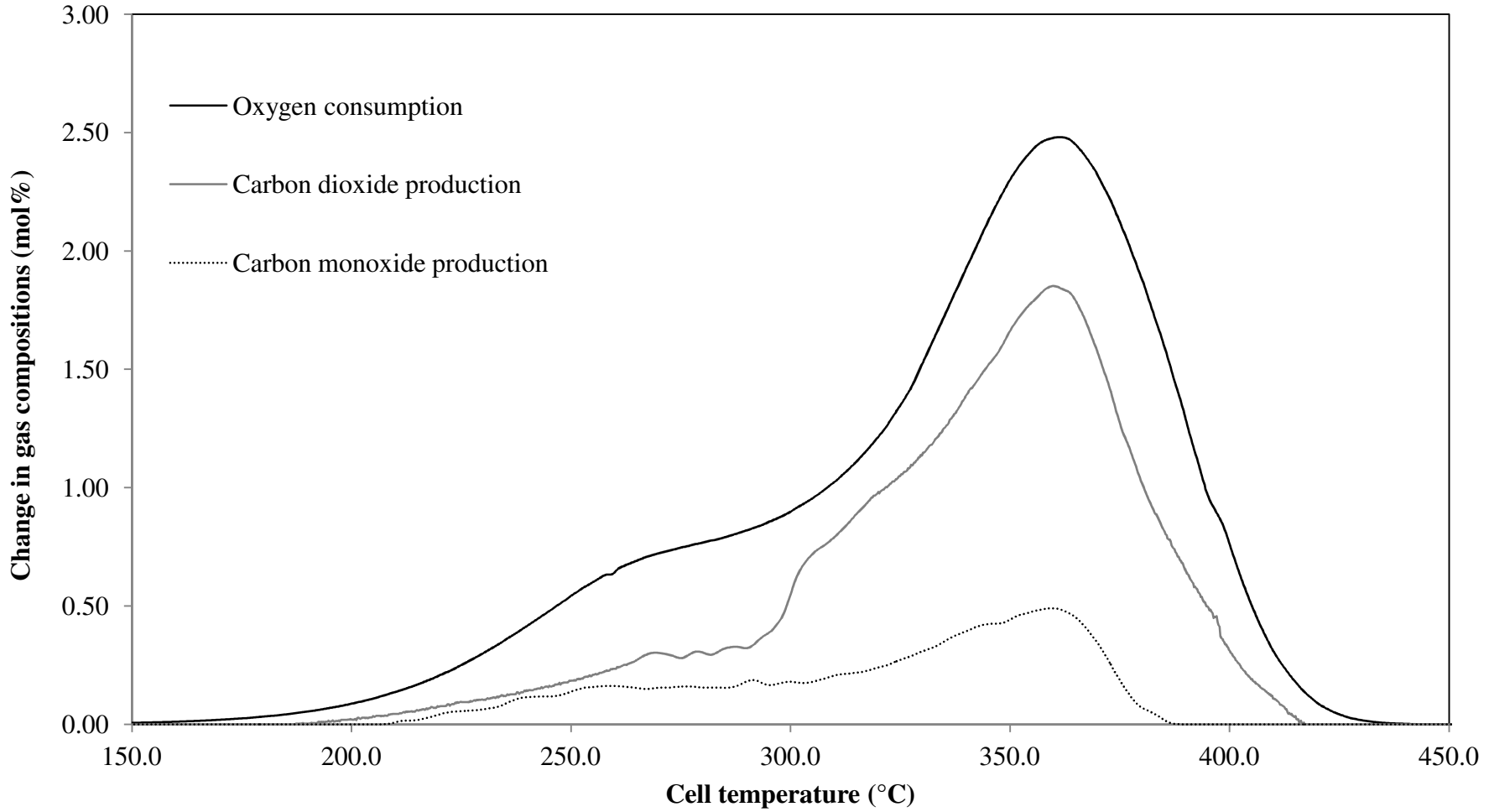

Figure 8.3 - Typical palm fibre char evolved gas analysis (EGA) experimental results with air as the oxidising gas, an absolute total system pressure of 500kPa, an air flow rate of 400smL/min and a heating rate of 50°C/h (Experiment C1).

Table 8.3 presents the evolved gas analysis (EGA) results for the three typical experimental runs. As observed in Table 8.3, the hemicellulose peak for the rice husk sample occurred at a temperature of 249.8°C ± 1.0°C for all the exit gas oxygen, carbon dioxide and carbon monoxide curves. The cellulose peak temperature for the oxygen consumption and the carbon dioxide production curves coincide at 331.2°C ± 1.0°C for the rice husk sample. For the palm fibre sample, the hemicellulose peak temperature for all the exit gas composition curves was at an average temperature of 265.2°C ± 0.8°C and the cellulose peak temperature was at average of 355.4°C ± 0.2°C. For the palm fibre char sample, the single peak temperature for the exit gas oxygen, carbon dioxide and carbon monoxide compositions was in agreement being 360.5°C within ±0.2°C.

Figure 8.4 allows a comparison between the oxygen consumption curves as functions of cell temperature for the three typical experiments R4, F6 and C1. Figures 8.5 and 8.6 allow similar comparisons to be made for carbon dioxide production and carbon monoxide production curves, respectively. As observed in Figures 8.4 to 8.6, the rice husk sample occurred at the lowest temperatures with the palm fibre char sample yielding the highest peak temperatures. The rice husk and palm fibre samples exhibit similar trends with the rice husk sample occurred at slightly 17°C to 18°C lower temperature compared to the palm fibre sample for all the exit gas composition curves. This is due to the difference nature of the both biomasses. The peak height of the hemicellulose peak was greater for the rice husk sample than for the palm fibre sample. However, the peak height of the cellulose peak was similar for the rice husk and palm fibre samples. This is due to the rice husk sample used in the present study having a larger amount of hemicellulose compared to the palm fibre sample.

For the palm fibre char sample, all the exit gas composition curves for the oxygen, carbon dioxide and carbon monoxide peak heights were higher in comparison to the corresponding ones for the rice husk and palm fibre samples. The palm fibre char sample exhibits a well defined single main peak, a shoulder in the lower temperature region of 250°C to 310°C and a short tail zone. The decomposition of the palm fibre char sample occurred at a very broad temperature range from 190°C to 420°C.

Table 8.3 - Summary of the evolved gas analysis (EGA) experimental results of a typical rice husk, palm fibre and palm fibre char. The $\Delta O_{2,\,max}$, $\Delta CO_{2,max}$ and $\Delta CO_{,\,max}$ (in mol%) is the peak height and the T (in °C) is cell temperature at which the peak occurs.

Experiment		**R4**	**F6**	**C1**
Sample type		Rice husk	Palm fibre	Palm fibre char
Absolute total system pressure (kPa)		500	500	500
Oxygen partial pressure (kPa)		105	105	105
Oxygen concentration in feed gas (mol%) and balance Nitrogen		20.96 (Air)	20.96 (Air)	20.96 (Air)
Heating rate (°C/h)		50	50	50
Oxygen consumption peaks				
First peak	$\Delta O_{2,\,max}$ (mol%)	0.69	0.53	2.48
	T (°C)	247.8	265.0	360.7
Second peak	$\Delta O_{2,\,max}$ (mol%)	0.42	0.47	-
	T (°C)	329.5	355.6	-
Carbon dioxide production peaks				
First peak	$\Delta CO_{2,\,max}$ (mol%)	0.54	0.30	1.95
	T (°C)	247.9	266.0	360.3
Second peak	$\Delta CO_{2,\,max}$ (mol%)	0.32	0.30	-
	T (°C)	330.2	355.3	-
Carbon monoxide production peaks				
First peak	$\Delta CO_{,\,max}$ (mol%)	0.16	0.13	0.49
	T (°C)	248.3	264.5	360.5
Second peak	$\Delta CO_{,\,max}$ (mol%)	-	0.06	-
	T (°C)	-	355.3	-

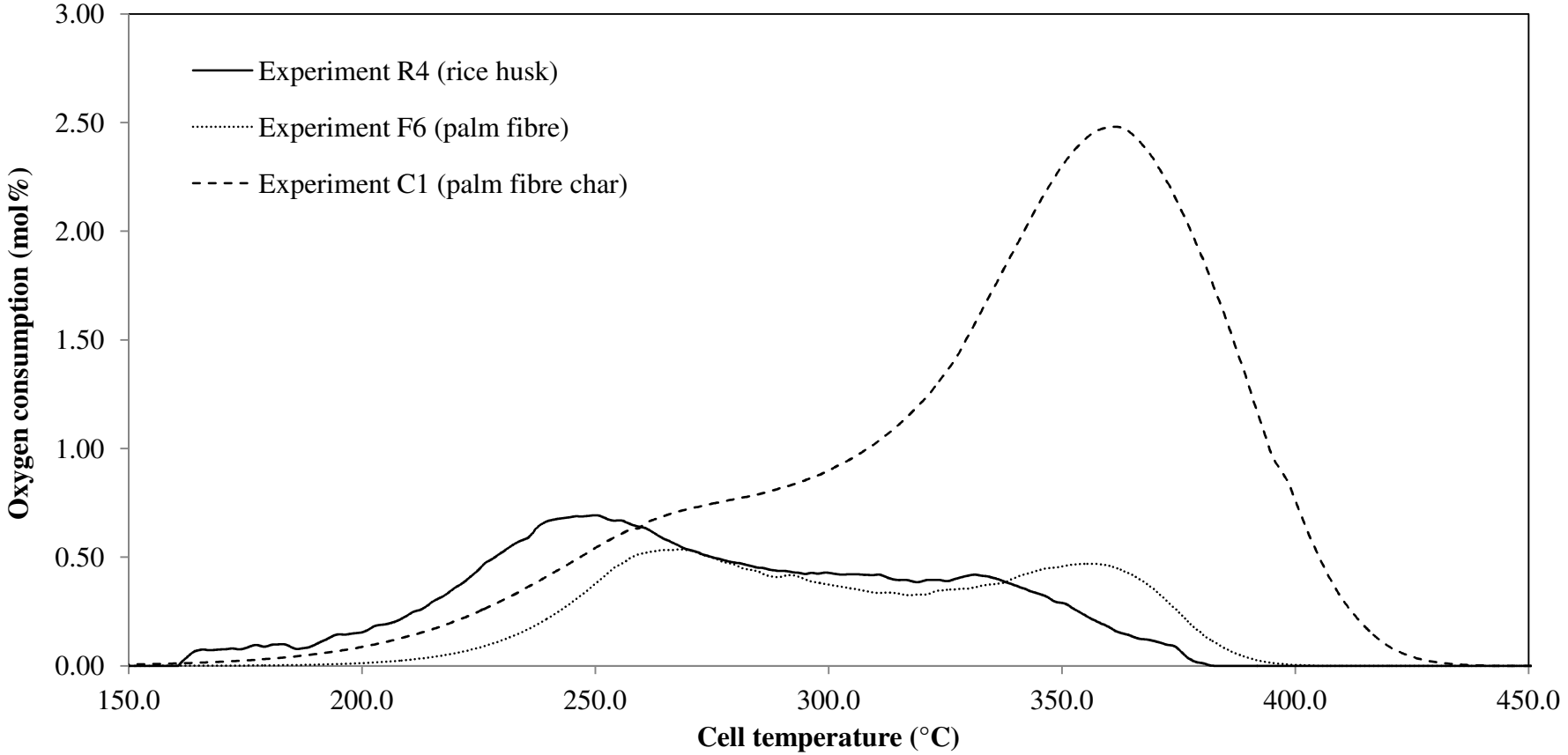

Figure 8.4 - Comparison of the oxygen consumption data with respect to the cell temperature for a typical rice husk, palm fibre and palm fibre char experiments conducted with air as the oxidising gas, an absolute total system pressure of 500kPa, an air flow rate of 400smL/min and a heating rate of 50°C/h.

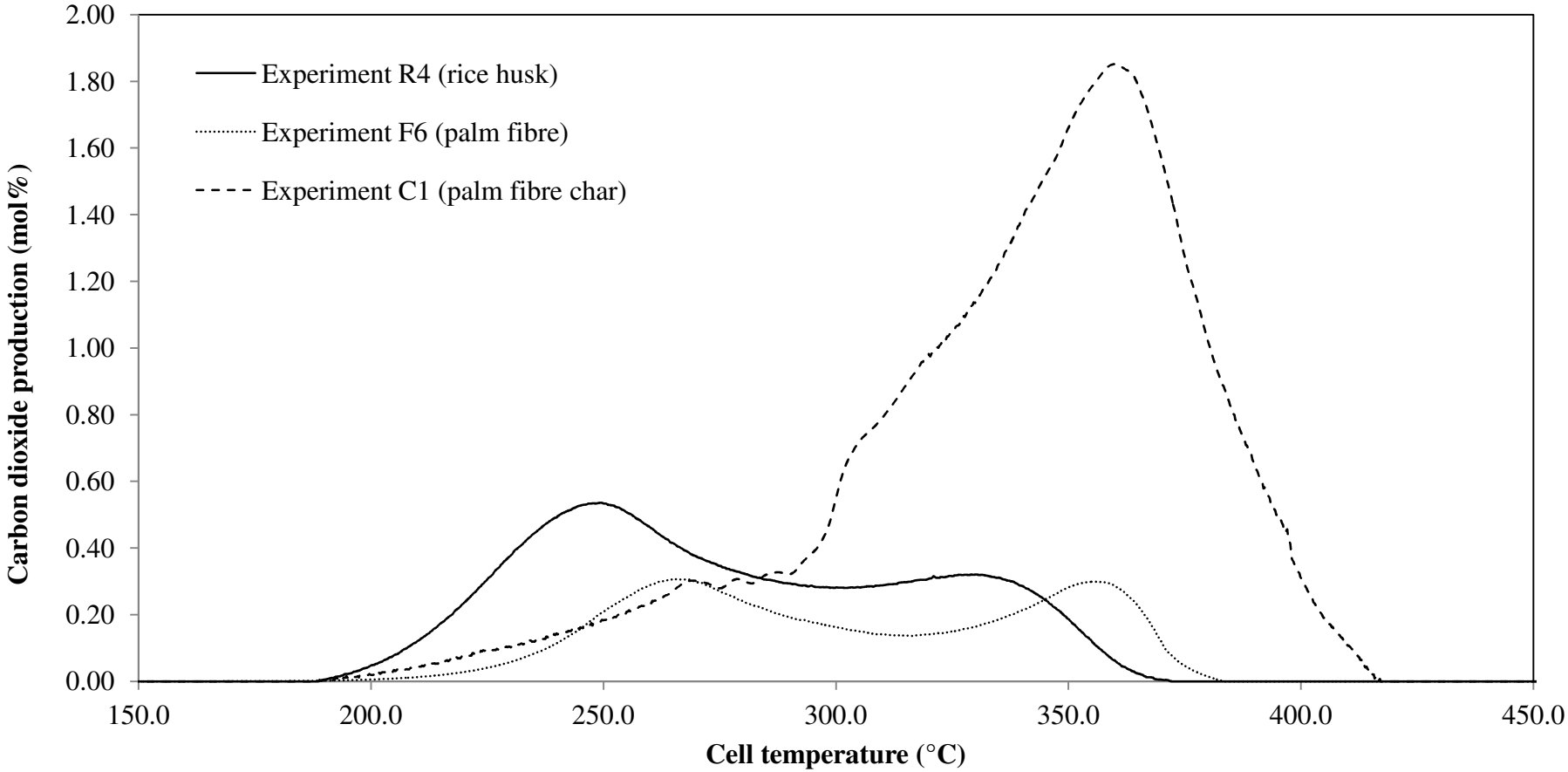

Figure 8.5 - Comparison of the carbon dioxide production data with respect to the cell temperature for a typical rice husk, palm fibre and palm fibre char experiments conducted with air as the oxidising gas, an absolute total system pressure of 500kPa, an air flow rate of 400smL/min and a heating rate of 50°C/h.

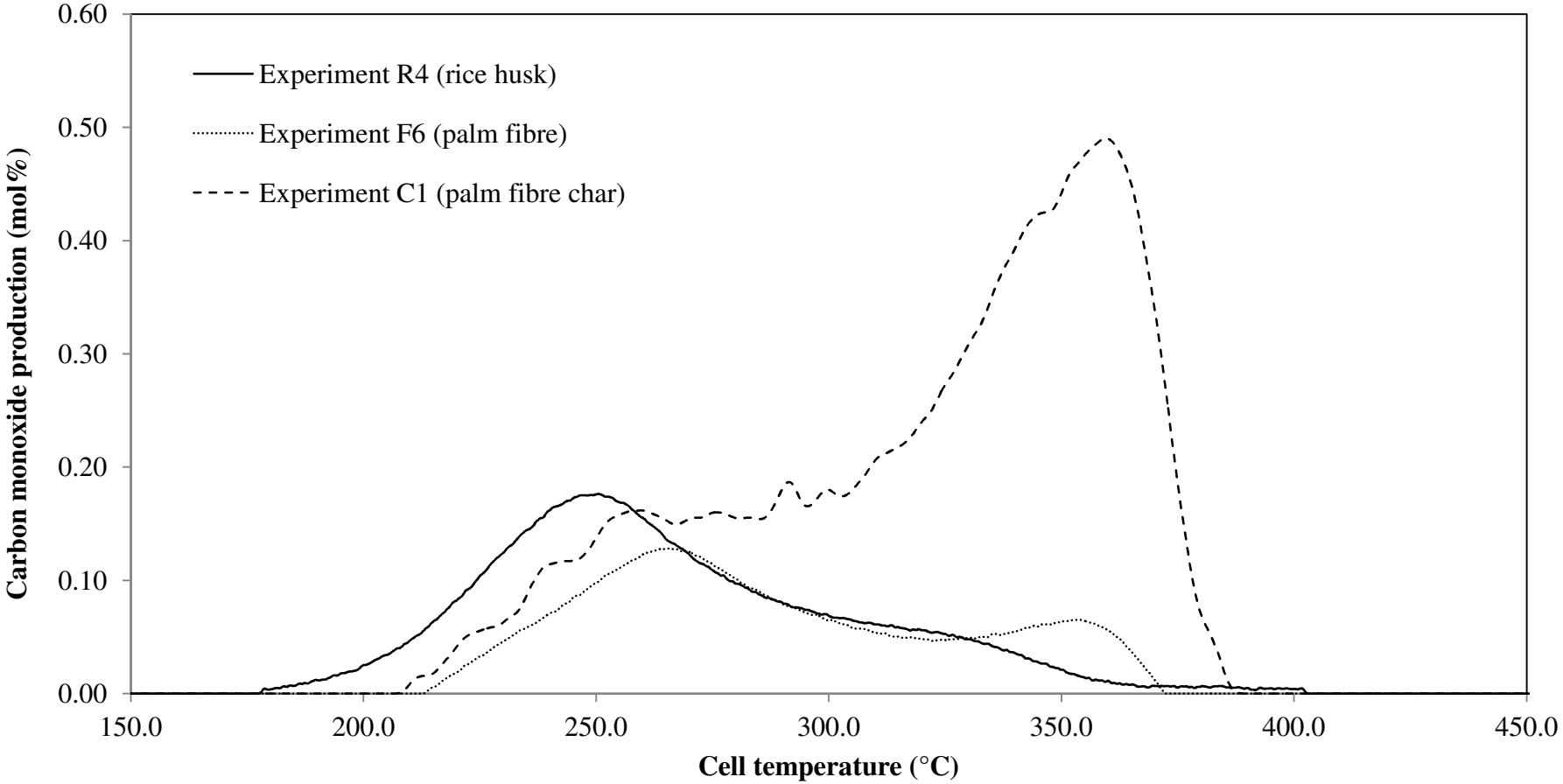

Figure 8.6 - Comparison of the carbon monoxide production data with respect to the cell temperature for a typical rice husk, palm fibre and palm fibre char experiments conducted with air as the oxidising gas, an absolute total system pressure of 500kPa, an air flow rate of 400smL/min and a heating rate of 50°C/h.

This is well expected since the decomposition of the palm fibre char is mainly due to the decomposition of lignin. The decomposition of lignin decomposes very slowly over a broad temperature range (Darvell *et al*., 2010). This might explains the broad temperature range for the palm fibre char sample.

As observed in Chapters 5 to 7, pressure has a significant influence on the rice husk, palm fibre and palm fibre char combustion characteristics studies. The oxygen partial pressure initiated the changes rather than the total system pressure. The peak temperatures of the effluent gas oxygen, carbon dioxide and carbon monoxide composition curves decreased with increasing oxygen partial pressures and the peak heights increased with increasing oxygen partial pressures. Figure 8.7 allows the comparison to be made between the first peak temperatures in the oxygen consumption curve with respect to the oxygen partial pressure for the rice husk, palm fibre and palm fibre char samples. Figure 8.8 allows a similar comparison to be made for the first peak height of the oxygen consumption curve.

As shown in Figure 8.7, the temperature at which the first oxygen consumption peaks occurs decreases linearly with increasing oxygen partial pressure for the three typical rice husk, palm fibre and palm fibre char samples. The peaks for the palm fibre char sample occurs at higher temperatures and followed by the palm fibre and rice husk samples. Considering Figure 8.8, the first peak height of the oxygen consumption curve increased linearly with increasing oxygen partial pressure for the rice husk, palm fibre and palm fibre char samples. However, the rice husk sample shows a slight increment compared to the both palm fibre and palm fibre char samples. This may be due to the nature of the rice husk that is different from the palm fibre and palm fibre char biomass material. Note that a similar trend was also observed for the carbon dioxide and carbon monoxide production curves and also for the second peak of the palm fibre and rice husk samples.

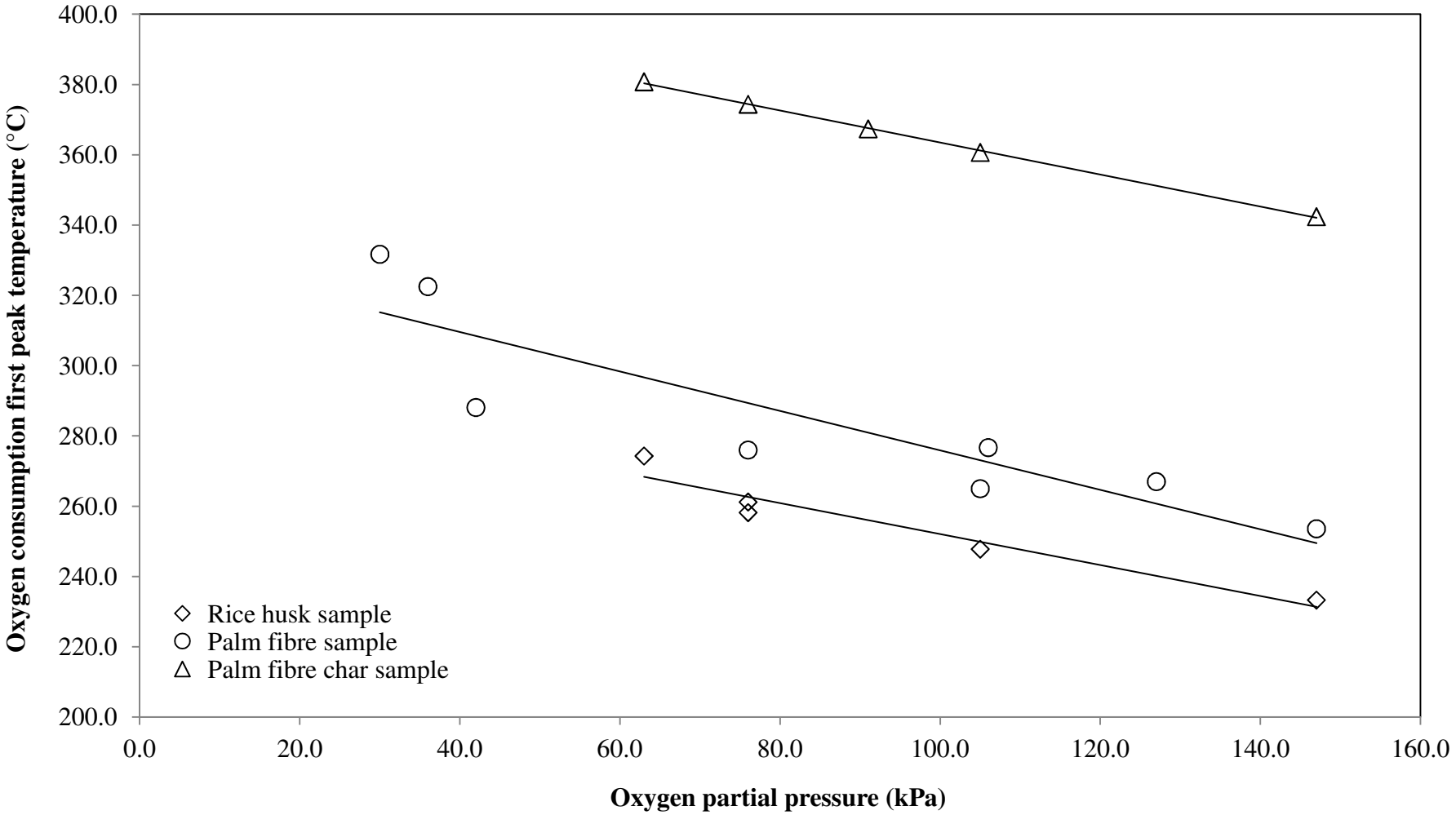

Figure 8.7 - Comparison of the first peak temperature of the oxygen consumption curve with respect to the oxygen partial pressure for a typical rice husk, palm fibre and palm fibre char experiments.

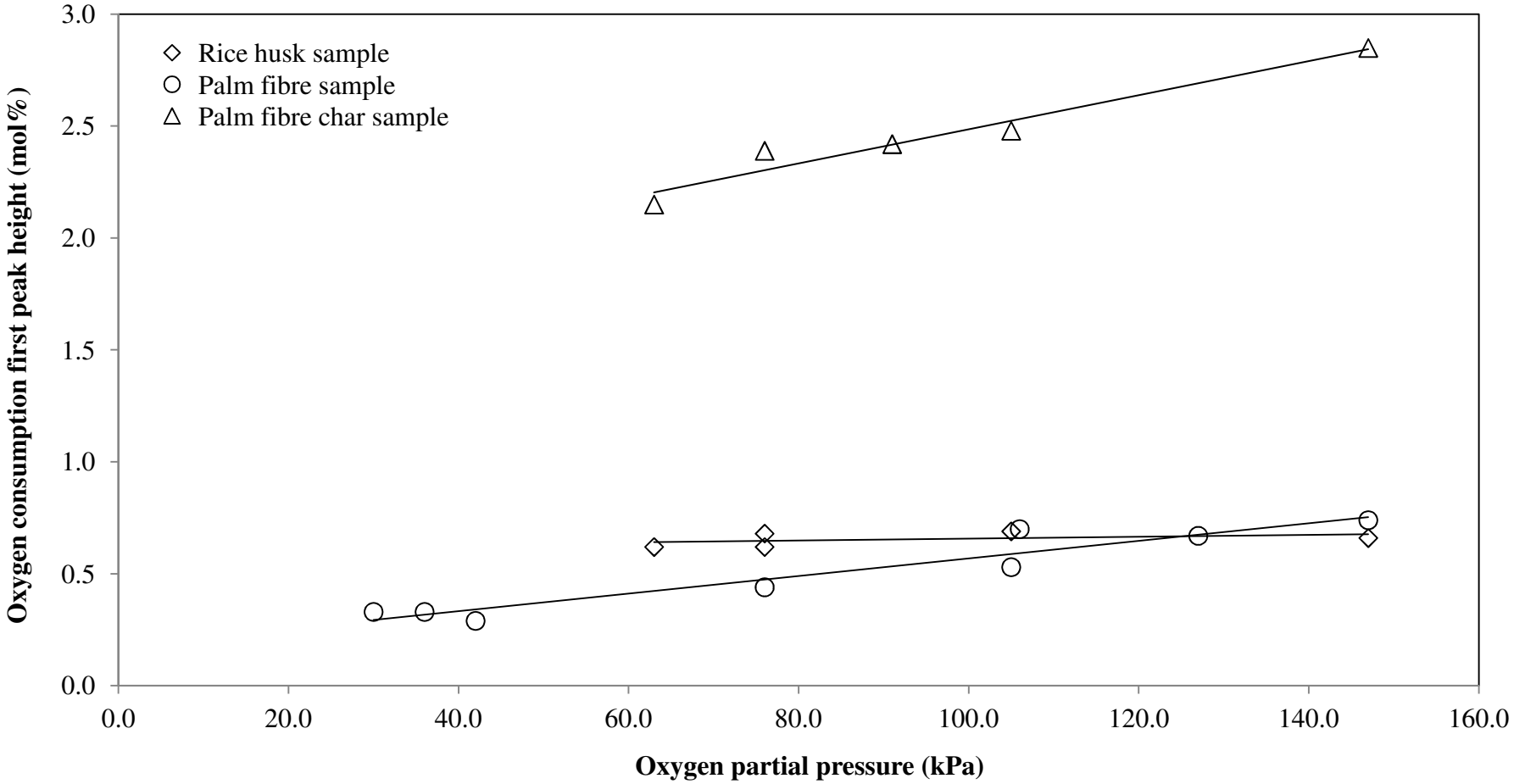

Figure 8.8 - Comparison of the first peak height of the oxygen consumption curve with respect to the oxygen partial pressure for a typical rice husk, palm fibre and palm fibre char experiments.

8.3 Comparison of the typical rice husk, palm fibre and palm fibre char data calculated kinetic parameter results

The typical rice husk (experiment R4), palm fibre (experiment F6) and palm fibre char (experiment C1) experimental results are modeled against the three overlapping reaction regimes of the high temperature oxidation (HTO), medium temperature oxidation (MTO) and low temperature oxidation (LTO). Each of the experimental data are decoupled into their constituent oxidation reactions and kinetic parameters such as activation energy are calculated for each reaction regime. The LTO and MTO regimes are considered simultaneously.

The calculated kinetic parameters of these three typical experiments, R4, F6 and C1, are presented in Table 8.4. Figure 8.9 presents the predicted oxygen consumption curve in comparison with the actual oxygen consumption curve of the typical rice husk experimental data of experiment R4. Figures 8.10 to 8.11 present similar information for the typical palm fibre (experiment F6) and palm fibre char (experiment C1) experiments, respectively.

As observed in Figure 8.9, the peak height of the LTO reaction was the greatest and followed by the peak height of the HTO reaction and lastly, the MTO reaction for the rice husk sample. Nevertheless, the peak heights of the HTO and LTO reactions were comparatively similar for the palm fibre sample (see Figure 8.10). For the palm fibre char sample, the peak height of the HTO reaction was the highest and followed by the LTO reaction and lastly the MTO reaction (see Figure 8.11). The peak height of the MTO reaction for the palm fibre char sample was obviously the lowest in comparison to the rice husk and palm fibre samples. This may be because most of the volatile components had escaped during the pyrolysis process to produce palm fibre char and hence lowered the peak height of the MTO reaction and as well as the LTO reaction compared to the raw sample. The differences in the peak height of the raw samples of rice husk and palm fibre samples were due to the nature of the biomass and the volatile matter content in each of biomasses.

Table 8.4 - Summary of the calculated kinetic parameters of a typical rice husk, palm fibre and palm fibre char. The E/R is the activation energy (in K) and the ln β is the natural log of beta group (dimensionless).

Experiment		**R4**	**F6**	**C1**
Sample type		Rice husk	Palm fibre	Palm fibre char
Absolute total system pressure (kPa)		500	500	500
Oxygen partial pressure (kPa)		105	105	105
Oxygen concentration in feed gas (mol%)		20.96 (Air)	20.96 (Air)	20.96 (Air)
Heating rate (°C/h)		50	50	50
HTO	Reaction order, n	1.01	1.01	0.99
	E/R ($\times 10^{-3}$)	17.5	19.6	12.8
	ln β	21.3	21.2	13.0
MTO	Reaction order, n	0.98	0.99	0.98
	E/R ($\times 10^{-3}$)	19.5	22.1	18.5
	ln β	26.1	22.5	20.9
LTO	Reaction order, n	1.35	1.36	0.97
	E/R ($\times 10^{-3}$)	14.8	22.5	11.9
	ln β	16.2	23.8	16.2
Variance, σ^2		0.0006	0.0001	0.0009

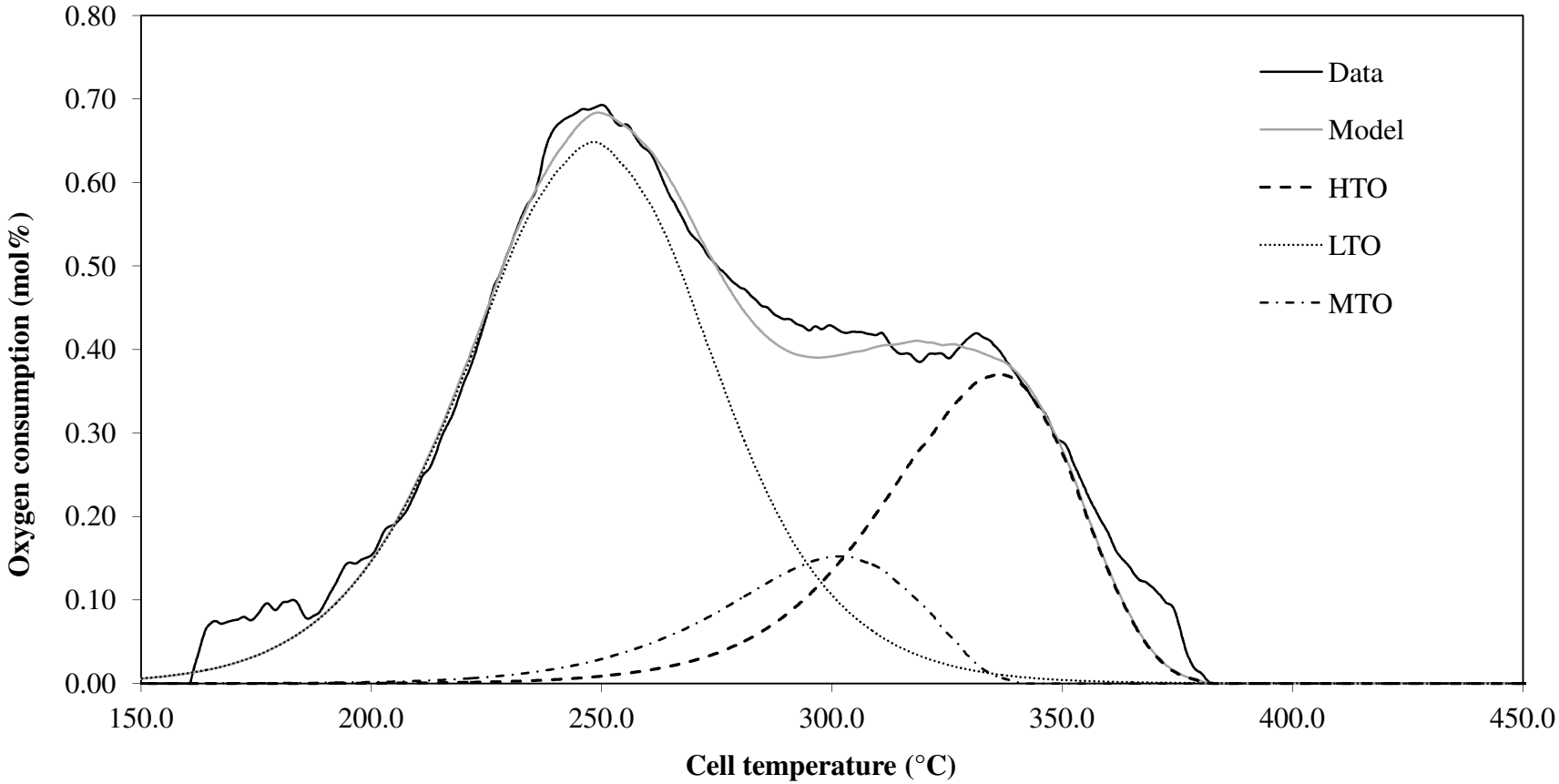

Figure 8.9 - Typical rice husk decoupled evolved gas analysis for the oxidation of rice husk (Experiment R4). The oxygen consumption curve was decoupled using the three regimes (HTO, MTO and LTO) model. The LTO and the MTO reactions were decoupled simultaneously.

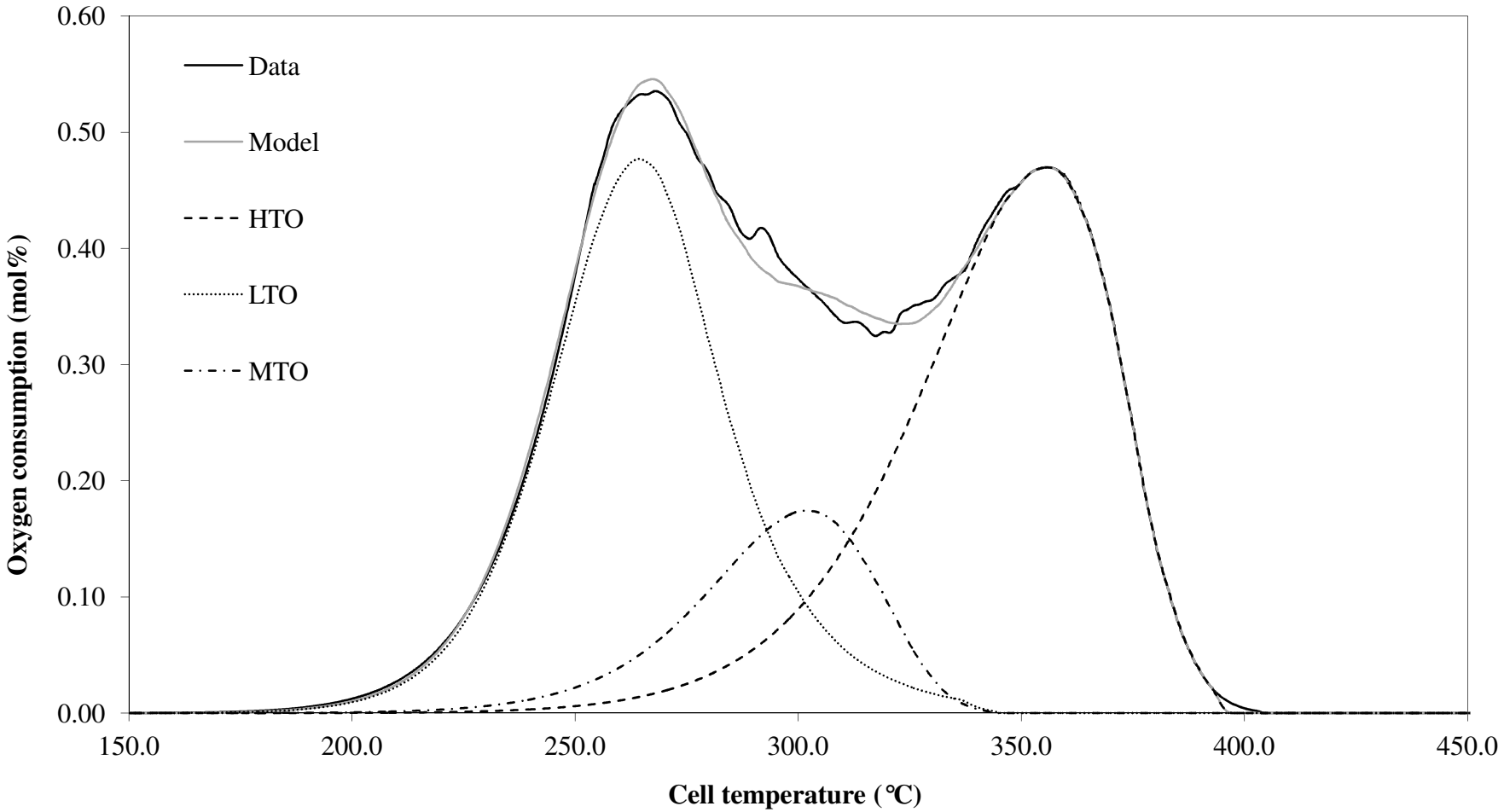

Figure 8.10 - Typical palm fibre decoupled evolved gas analysis for the oxidation of experiment F6. The oxygen consumption curve was decoupled using the three regimes (HTO, MTO and LTO) model. The LTO and MTO reactions were decoupled simultaneously.

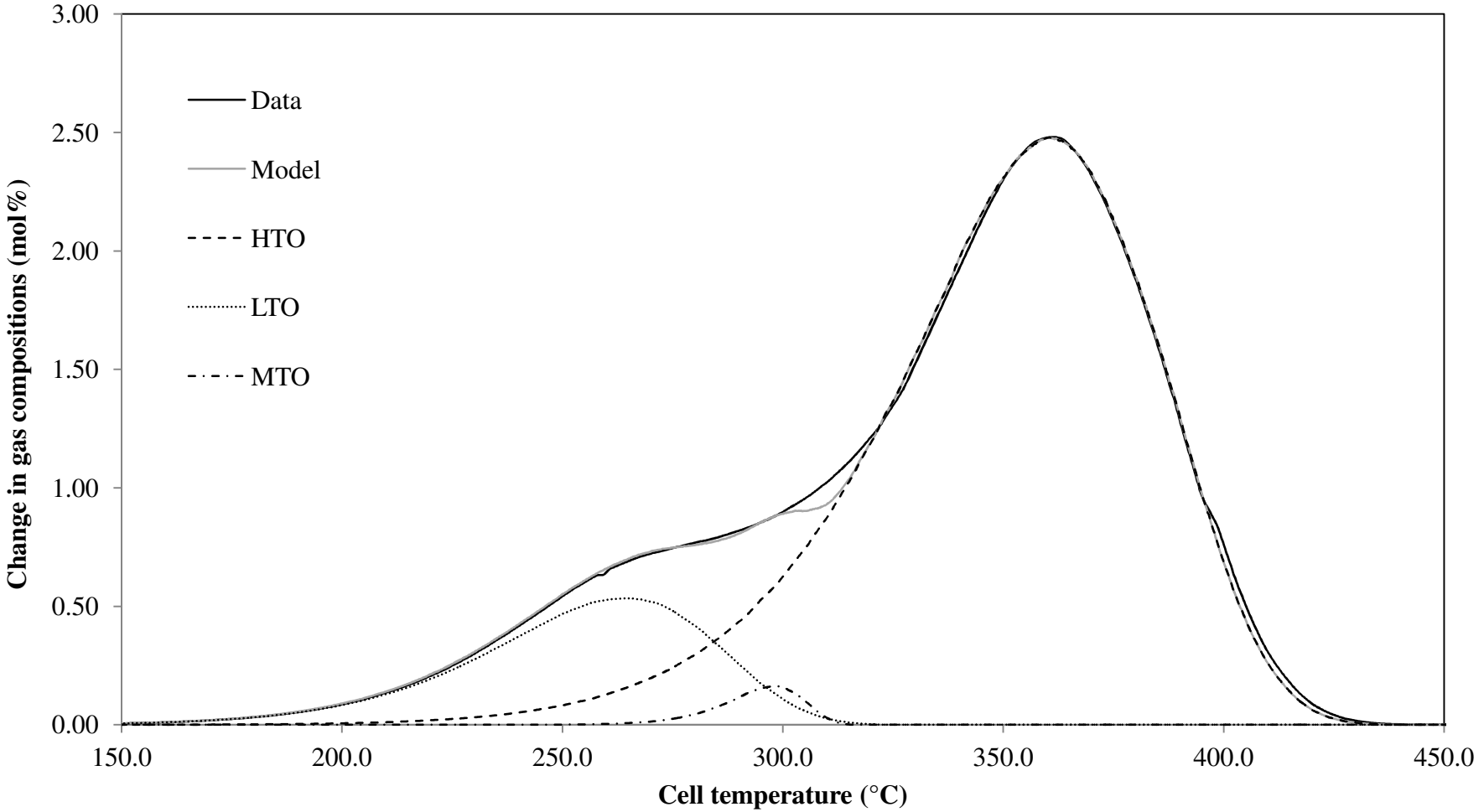

Figure 8.11 - Typical palm fibre char decoupled evolved gas analysis for the oxidation of experiment C1. The oxygen consumption curve was decoupled using the three regimes (HTO, MTO and LTO) model. The LTO and MTO reactions were decoupled simultaneously.

Considering Table 8.4, for the high temperature oxidation (HTO) reaction, the reaction order for the rice husk and palm fibre samples was the same at 1.01 but the reaction order of the palm fibre char sample was 0.02 lower than the typical raw samples. The activation energy for the palm fibre char sample was the lowest with 12.8×10^3K and followed by the rice husk sample (17.5×10^3K) and lastly the palm fibre sample (19.6×10^3K). Similarly, the value for the ln β for the palm fibre char sample was the lowest with 13.0 in comparison to the typical raw samples. For the medium temperature oxidation (MTO) reaction of the three typical samples, the reaction order varied by 0.01. The activation energy and the value for the ln β for the palm fibre char sample were the lowest with 18.5×10^3K and 20.9, respectively in comparison to the typical raw samples. By comparison of the rice husk and palm fibre samples, the rice husk has a lower activation energy (19.5×10^3K) compared to the palm fibre sample (22.1×10^3K).

However, the value for the ln β for the palm fibre sample was lower than the corresponding value for the rice husk sample. For the low temperature oxidation (LTO) reaction, there is an obvious difference in terms of the reaction order observed for the palm fibre char sample. The reaction order for the palm fibre char sample was the lowest with 0.97 compared to the typical raw samples. The reaction orders for the rice husk and palm fibre samples were comparatively similar being 1.35 and 1.36, respectively. The palm fibre char sample has the lowest activation energy with 11.9×10^3K and followed by the rice husk sample (14.8×10^3K) and palm fibre sample (22.5×10^3K). The value for the ln β for the palm fibre char and the rice husk samples was similar with 16.2. The value for the ln β for the palm fibre sample was 23.8. Generally, the palm fibre char sample has higher oxygen consumption and lower activation energy compared to the raw samples. This is because most of the volatile components had escaped during the pyrolysis process. With the low volatiles, make it easier for carbon mainly to vaporise at certain temperature and reacts with oxygen. This would explain the higher oxygen consumption and the lower activation energy obtained for the palm fibre char sample.

The oxygen partial pressure of the evolved gas analysis (EGA) experiments using rice husk, palm fibre and palm fibre char were seen to have a significant influence on the calculated kinetic parameters of the reaction regimes of the HTO, MTO and LTO as revealed in Chapters 5 to 7. It appears that all the reaction regimes are influenced by the oxygen partial pressure rather than by the total system pressure. Figures 8.12 to 8.14 allow comparisons of the activation energy with respect to the oxygen partial pressure to be made between the typical rice husk, palm fibre and palm fibre char samples for the HTO, MTO and LTO reactions, respectively. Figures 8.15 to 8.17 allow similar comparisons for the natural log of beta group, ln β, to be made.

As shown in Figure 8.12, the activation energy for the HTO reaction decreases linearly with increasing oxygen partial pressure for the three biomass studied: rice husk, palm fibre and palm fibre char samples. Similarly, the activation energy for the MTO reaction decreases linearly with increasing oxygen partial pressure for the palm fibre and palm fibre char samples (see Figure 8.13). For the rice husk sample, an opposite trend is displayed for the activation energy for the MTO reaction. As observed in Figure 8.14, the LTO reaction activation energy for the rice husk and palm fibre samples decreases linearly with increasing oxygen partial pressure. The corresponding data for the char sample has a slightly reversed gradient. Biomass combustion consists of many completing reactions but these may be grouped into three regimes of HTO, MTO and LTO. The difference in the curve trends of the three biomasses for the three regimes may be due to differences in the biomass structure and hence, contribute to the variations in the reactions occurring during the biomass combustion.

Similarly to the activation energy trends, the values for the ln β for the HTO reaction decrease linearly with increasing oxygen partial pressure for the three biomasses (see Figure 8.15). The values for the MTO reaction ln β decrease linearly with increasing oxygen partial pressure for both the palm fibre and palm fibre char samples. Again for the MTO reaction, the rice husk sample data displayed an opposite trend (see Figure 8.16).

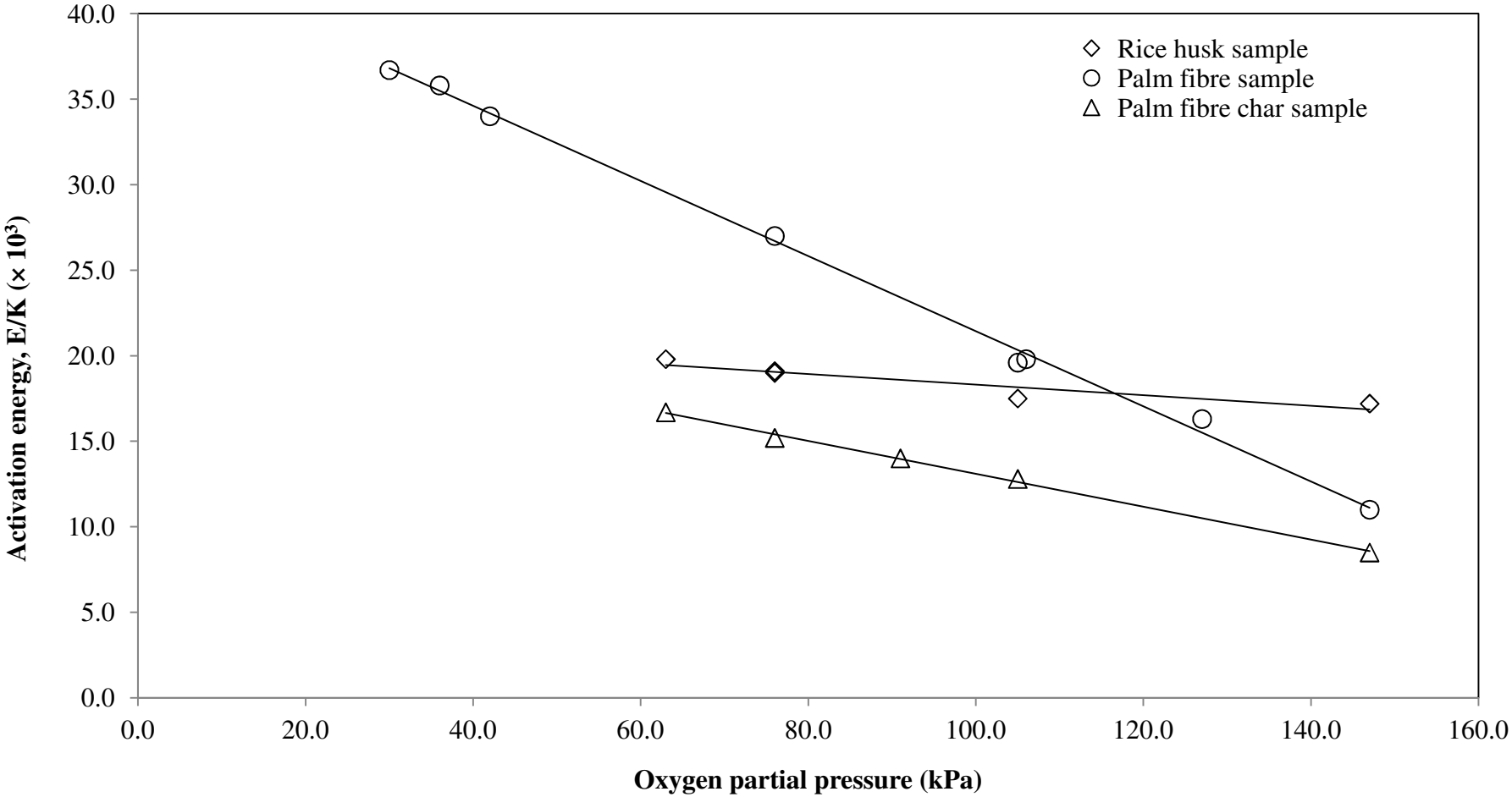

Figure 8.12 - Comparison of the calculated values for activation energy of the HTO reaction with respect to the oxygen partial pressure for rice husk, palm fibre and palm fibre char samples.

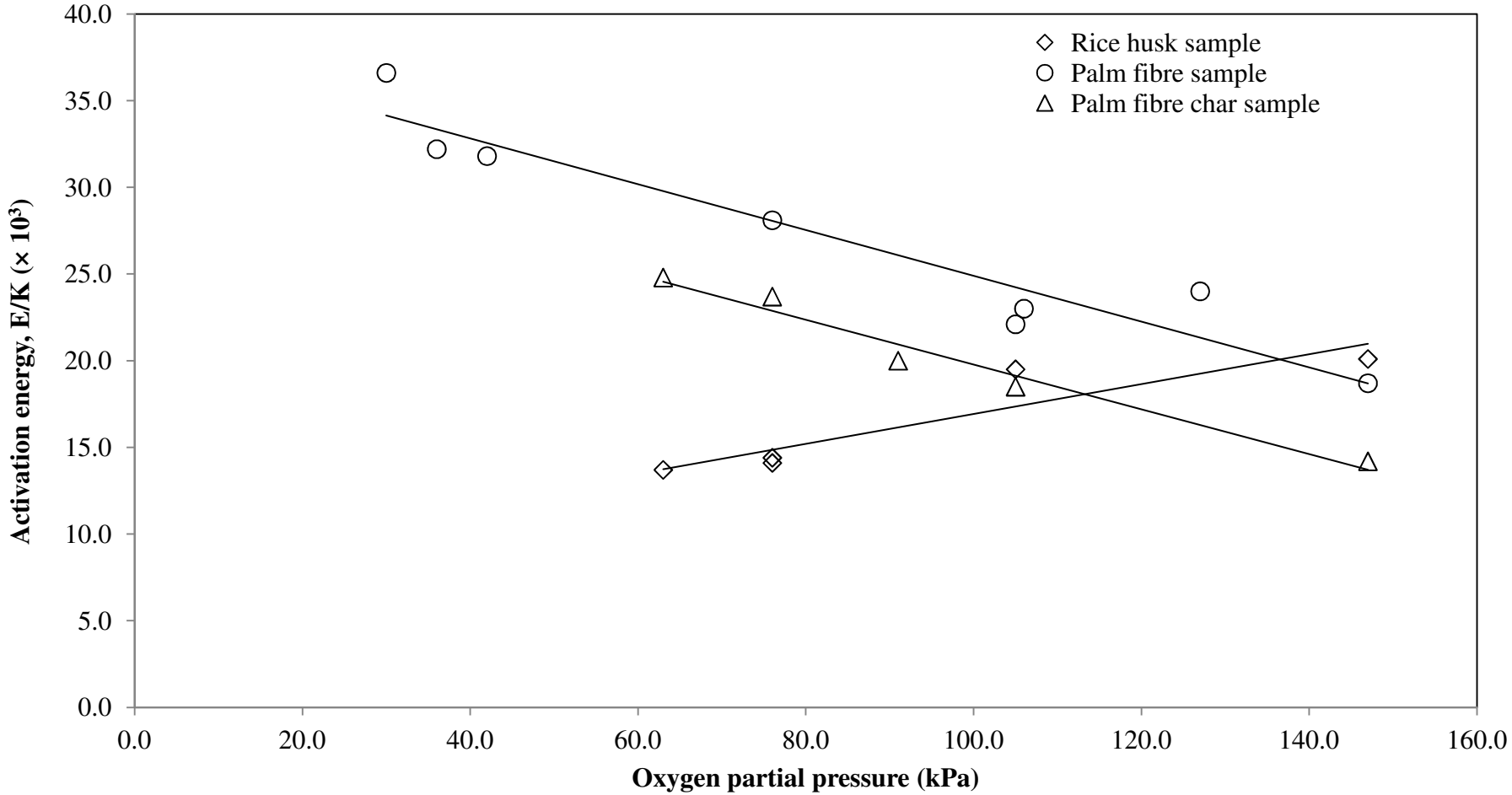

Figure 8.13 - Comparison of the calculated values for activation energy of the MTO reaction with respect to the oxygen partial pressure for rice husk, palm fibre and palm fibre char samples.

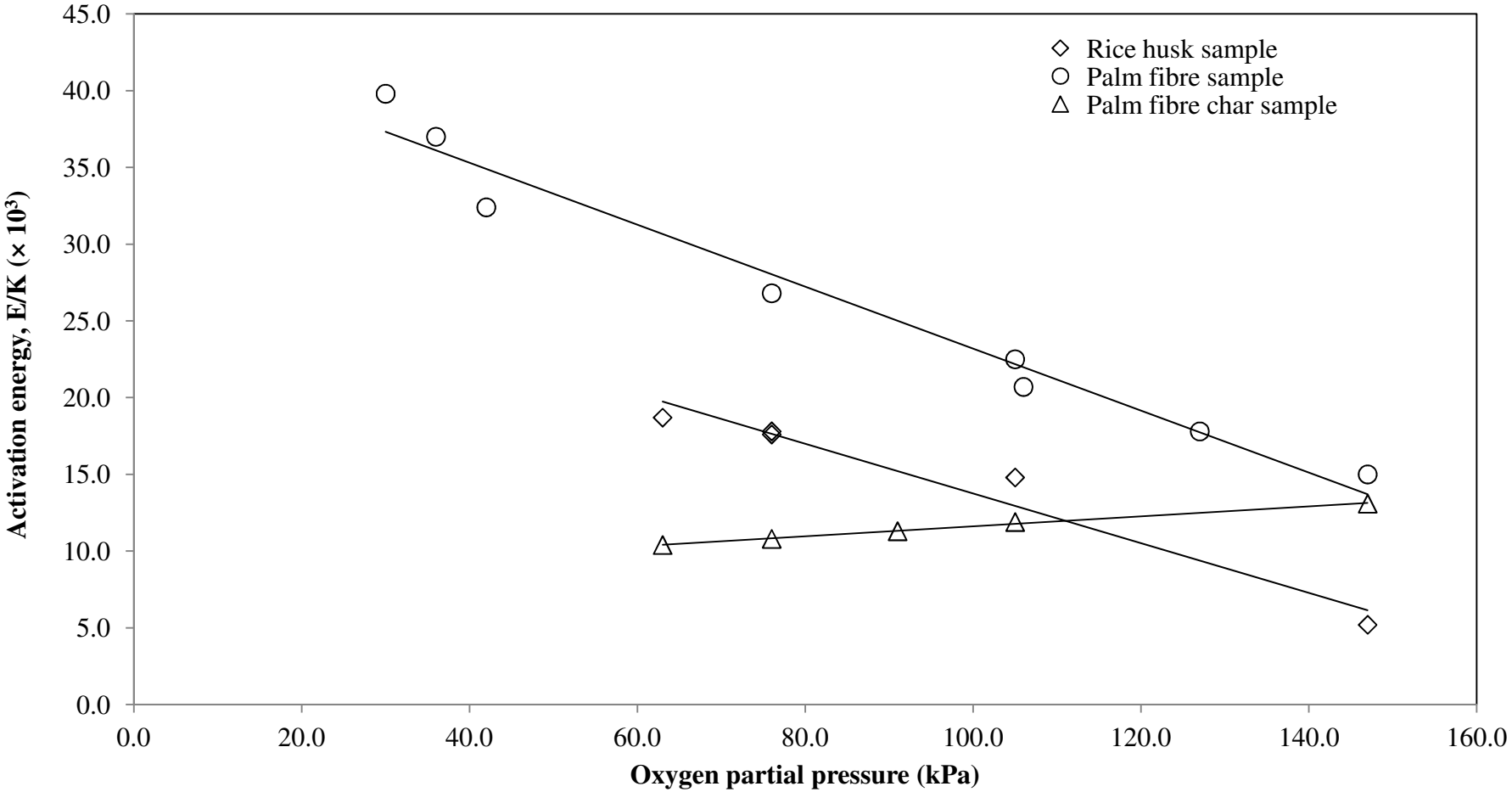

Figure 8.14 - Comparison of the calculated values for activation energy of the LTO reaction with respect to the oxygen partial pressure for rice husk, palm fibre and palm fibre char samples.

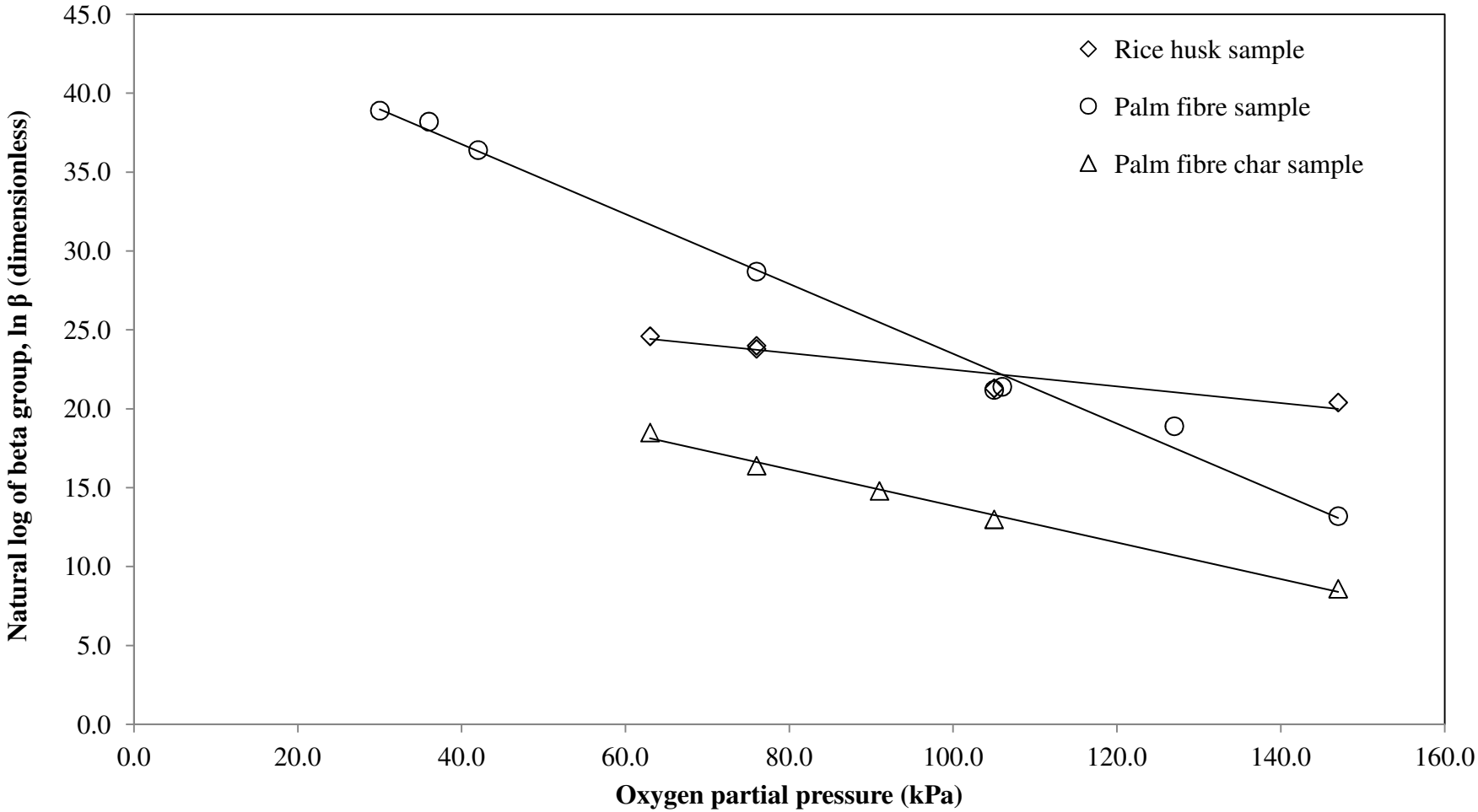

Figure 8.15 - Comparison of the natural log of beta group, ln β for the HTO reaction with respect to the oxygen partial pressure for rice husk, palm fibre and palm fibre char samples.

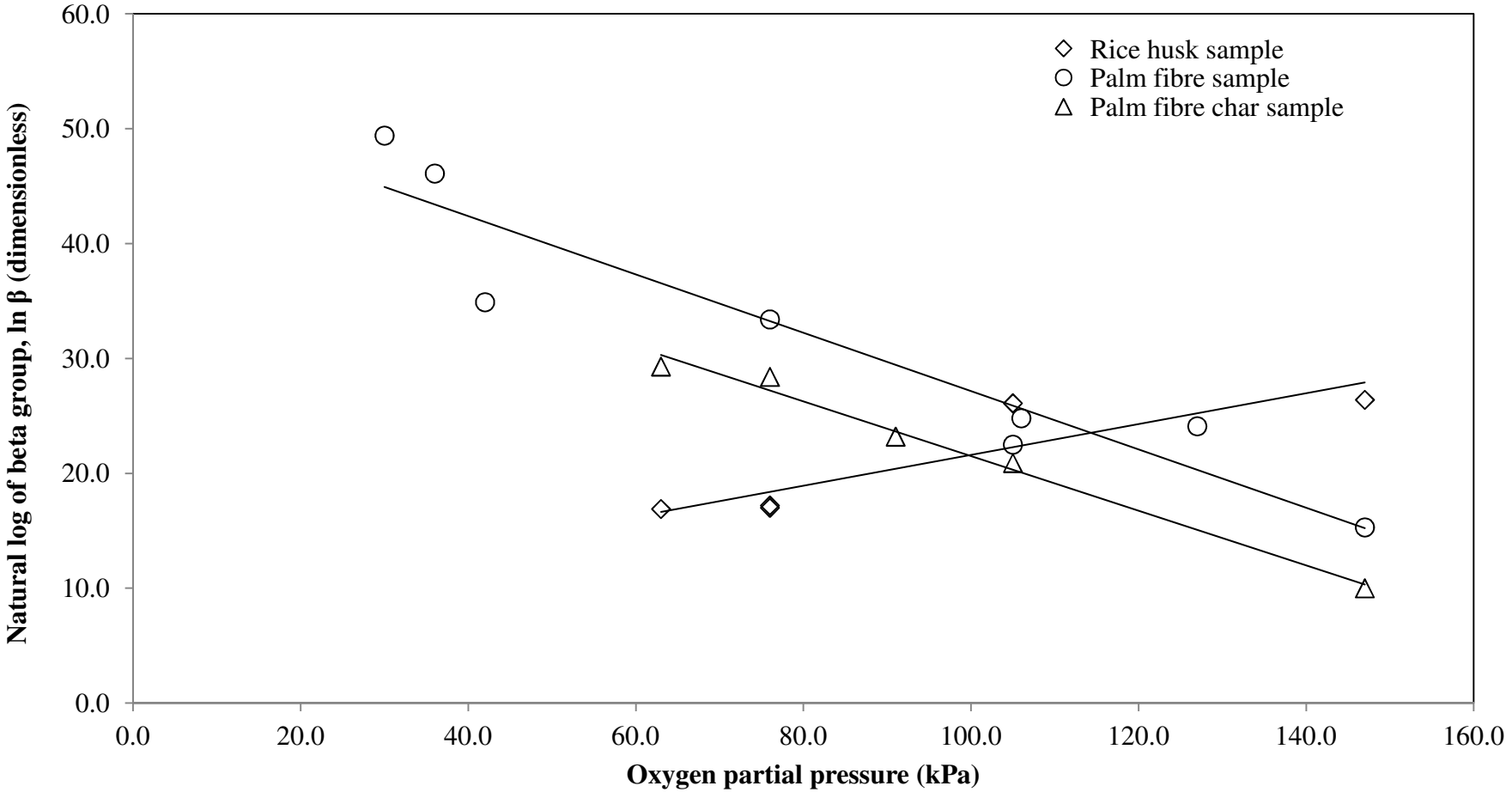

Figure 8.16 - Comparison of the natural log of beta group, ln β for the MTO reaction with respect to the oxygen partial pressure for rice husk, palm fibre and palm fibre char samples.

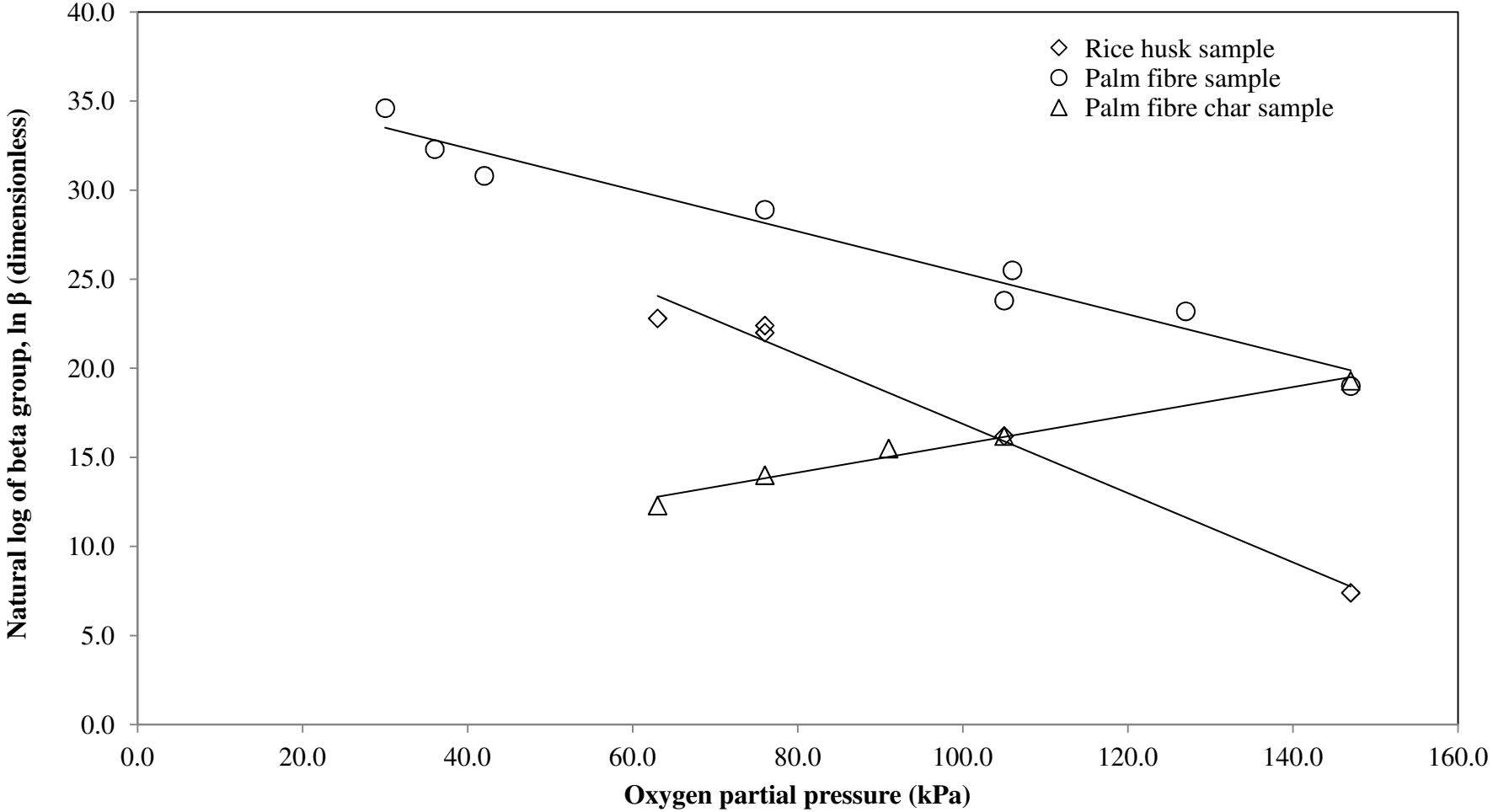

Figure 8.17 - Comparison of the natural log of beta group, ln β for the LTO reaction with respect to the oxygen partial pressure for rice husk, palm fibre and palm fibre char samples.

For the LTO reaction, the values for the ln β for both the rice husk and palm fibre biomasses tested decrease linearly with increasing oxygen partial pressure. However, the values for the LTO reaction ln β for the typical palm fibre char biomass increase linearly with increasing pressure. Generally, for the three biomasses studied, both activation energy and values for the ln β trend together with changing temperature. The ln β represents the total number of molecules collision that may or may not leads to reactions. Since the activation energy and the ln β trends together, it may be concluded that the ln β increases with increasing activation energy. Hence, the higher molecule collision during biomass combustion may not leads to reaction due to higher value of activation energy observed.

By comparing the oxygen consumption and the activation energy of the three biomasses, obviously it can be seen that as the oxygen consumption increased, the activation energy decreased. This is well expected because as the biomass consumed higher oxygen, the lower energy to start the reactions. Further, the oxygen consumption for the three biomasses increases with increasing pressure. The pressures may suppress the amount of distillation occurring and hence more fuel remains for combustion.

No studies have been reported on the effect of the oxygen partial pressure on the calculated kinetic parameters of the biomass and biomass char combustion characteristics. However, many authors have reported the effect of the oxygen partial pressure on the various types of crude oil oxidations (Nguyen, 2004, Al-Saffar *et al.*, 2000, Kisler, 1995, Shallcross, 1991).

Shallcross (1991) conducted an EGA experiments with a heavy crude oil. He found that the natural log of beta group increased with oxygen partial pressure for the LTO and MTO reactions but decreased for the HTO reaction. Nguyen (2004) reported that the LTO reaction was influenced by the oxygen partial pressure rather than by the total system pressure while the MTO reaction was affected by the total system pressure in her oxidation kinetics study of Vietnamese crude oil. For the HTO reaction, an increase in the calculated kinetic parameters is observed with a rise in both the total system and the oxygen partial pressures. Hence, the HTO reaction is influenced by both pressures.

In this study, it is believed that pressure may suppress the amount of distillation occurring and hence more fuel remains for oxidation.

Kisler (1995) reported that the LTO and MTO reactions were influenced by the oxygen partial pressure while HTO reaction was dependant on the total system pressure in his light crude oil oxidation study. Al-Saffar *et al.* (2000) found that the total system pressure influences the calculated activation energy in their crude oil oxidation study. The variation of findings are due to the different types of oil used in each of the study. Similarly, in the present study, the differences in the findings are due to the different types of biomass used.

8.4 Concluding remarks

The combustion characteristic results are dependent on the nature of the biomass. Different biomass shows different experimental and calculated kinetic parameter results. For the three biomasses studied, both activation energy and values for the ln β trend together with changing temperature. The activation energy decreases with increasing oxygen consumption for the three biomasses. Further, the oxygen consumption for the biomasses studied increases with increasing pressure.

The best conditions obtained using the present EGA rig for the biomasses (rice husk, palm fibre and palm fibre char) experiments are when the absolute total system pressure is 700kPa, the oxygen partial pressure is 147kPa, the heating rate is 50°C/h and the flow rate is 400smL/min.

This Chapter offers comparisons of the combustion characteristics between the three types of biomasses using an EGA technique. The relationship between the activation energy, the values of ln β and the oxygen consumption with changing temperature and pressure reported in this Chapter could be useful for the biomass and biomass char combustion reactor design. The amount of exit gases carbon monoxide and carbon dioxide obtained in this study may contribute to the design and optimisation of the flue gas treatment of the biomass combustor. The combustion temperatures and the

activation energies for the three biomasses suggested in this study may be useful in the optimising the biomass combustor hence may reduce the cost. The information on the effect of the oxygen partial pressure and the oxygen concentration for the three biomasses will benefit the design in enabling the best selection of the oxidising gas and the pressure drop of the combustor bed. The fact that the reaction is the rate-controlling step rather than the internal diffusion, will avoid having to grind the biomass before combustion. This will allow savings in cost by avoiding the grinding process.

CHAPTER 9

CONCLUSIONS AND RECOMMENDATIONS

9.1 Conclusions

The present study examines the combustion characteristics of rice husk, palm fibre and palm fibre char using an evolved gas analysis (EGA) technique. This study provides insights into the oxidation behaviour, the results of which will be useful in subsequent biomass combustion reactor design work. The following conclusions may be drawn from this study:

1. The evolved gas analysis (EGA) technique has been successfully used to study the oxidation kinetics of rice husk, palm fibre and palm fibre char.

2. Experimental runs with rice husk, palm fibre and palm fibre char may be adequately modeled by grouping the many competing oxidation reactions occurring during the combustion process into just three simultaneous and competing reaction regimes. The three reaction regimes are known as high temperature oxidation (HTO) reaction, the medium temperature oxidation (MTO) reaction and the low temperature oxidation (LTO) reaction.

3. A new calculation approach of solving the MTO and LTO reactions simultaneously is developed and further improved the curve fitting between the predicted oxygen consumption curve and the actual experimental data.

4. The EGA results for the rice husk and palm fibre samples show two peaks in the oxygen consumption curve whereas for palm fibre char features a single peak.

5. The palm fibre sample is segregated into three types of samples namely the clump fibre, the kernel and the loose fibre. The EGA results and the calculated kinetic parameters of these samples reveal that the clump and the loose fibres are similar. The loose fibre is chosen to represents the palm fibre in this study.

6. The EGA experiments using the rice husk, palm fibre and palm fibre char are reproducible. Three experimental runs of each rice husk, palm fibre and palm fibre char were conducted under similar conditions. The EGA results of these runs show that there are no significant differences in the peak temperatures and heights observed for the effluent gas oxygen, carbon dioxide and carbon monoxide composition curves. The calculated kinetic parameters of these identical runs for the rice husk, palm fibre and palm fibre char also show no significant differences.

7. The heating rate of the combustion cell has a significant influence on the oxidation peak temperatures and heights of the exit gas oxygen, carbon dioxide and carbon monoxide composition curves. The peak temperatures shift to higher temperatures as the heating rate increases. The peak heights increase with increasing heating rates. However, the calculated kinetic parameters are found to be independent of the heating rates as the calculation procedure allows for changes in the heating rate. Slower heating rates may ensure the entire cell is always at a uniform temperature so avoiding the exothermic peaks.

8. Particle size has no significant effect on the biomass combustion characteristics study. No significant differences were observed in the peak temperatures and

heights between the ground and the original size samples. This finding confirms that the reaction is the rate controlling step rather than the internal diffusion rate. The model does not consider the mass transfer resistance hence, shows no significant differences between the ground and the original size samples.

9. Pressure has a significant influence on the rice husk, palm fibre and palm fibre char combustion characteristics studies. As the pressure increases, the three exit gas composition peak temperatures decrease but the peak heights increase. The calculated kinetic parameters of the activation energy and the natural log of beta group decrease as the pressure increases.

10. The total system pressure has no significant influence on the peak temperatures but it does influence the peak heights. The peak heights of all the exit gas oxygen, carbon dioxide and carbon monoxide composition curves increase as the total system pressure increases. However, the total system pressure has no significant influence on the calculated kinetic parameters.

11. The combustion characteristic results are dependent on the nature of the biomass. Different biomass produce different evolved gas analysis (EGA) results. Comparison of the typical samples of rice husk, palm fibre and palm fibre char EGA results reveal that the decomposition of the palm fibre char sample occurs at higher temperatures compares to the rice husk and palm fibre samples. The rice husk and palm fibre decompositions are almost similar, exhibiting similar curves with the rice husk sample occurring at a slightly lower temperature compared to the palm fibre sample for all the exit gas composition curves.

12. For typical rice husk and palm fibre samples, the peak heights of the hemicellulose peak appear greater for the rice husk sample in comparison to the palm fibre sample. However, the peak heights of the cellulose peaks are almost similar between the rice husk and palm fibre samples. The exit gas composition curves of the oxygen, carbon dioxide and carbon monoxide peak heights for the

palm fibre char sample are relatively higher in comparison to the rice husk and palm fibre samples.

13. The magnitude of the LTO reaction is higher than the HTO and the MTO reactions for the typical rice husk sample. However, the magnitude of the HTO and LTO reactions for the palm fibre sample are comparatively similar. For the palm fibre char sample, the magnitude of the HTO reaction is the highest and follow by the LTO and MTO reactions. The magnitude of the MTO reaction for the palm fibre char sample is obviously the lowest in comparison to the rice husk and palm fibre samples.

14. The oxygen partial pressure has a significant influence on the rice husk, palm fibre and palm fibre char combustion characteristics studies rather than the total system pressure. The peak temperatures of the effluent gas oxygen, carbon dioxide and carbon monoxide composition curves decrease linearly with increasing oxygen partial pressures and the peak heights increase linearly with increasing oxygen partial pressures. However, the peak heights for the rice husk samples show a slight increment compared to the both palm fibre and palm fibre char samples.

15. The calculated kinetic parameters for the reaction regimes, HTO, MTO and LTO, are influenced by the oxygen partial pressure for the rice husk, palm fibre and palm fibre char samples. The activation energy and the values for the ln β for the HTO reaction decrease linearly with increasing oxygen partial pressures for the three biomasses. For the MTO reaction, the activation energy and the values for the ln β decrease linearly with increasing oxygen partial pressures for the palm fibre and palm fibre char samples with exception to the rice husk sample. The activation energy and the ln β for the rice husk sample increase linearly with increasing oxygen partial pressures for the MTO reaction. For the LTO reaction, the activation energy and the ln β decrease linearly with increasing oxygen partial pressures for the palm fibre and rice husk samples.

The activation energy and the ln β increase linearly with increasing oxygen partial pressures for the palm fibre char sample.

16. The activation energy obtained for a typical rice husk sample is within the range of 16.8 × 10^3K to 18.2 × 10^3K whereas for the typical palm fibre sample is within the range of 18.4 × 10^3K to 20.9 × 10^3K. The activation energy for the typical palm fibre char sample is calculated to be within the range of 11.9 × 10^3K to 13.7 × 10^3K.

17. For the three biomasses studied, both the activation energy and values for the ln β trend together with changing temperature. The activation energy decreases with increasing oxygen consumption and pressure.

18. The best combustion parameters obtained for this study using the present EGA rig for the rice husk, palm fibre and palm fibre char samples are at the absolute total system pressure of 700kPa, an oxygen partial pressure of 147kPa with an injection flow rate of 400smL/min and a heating rate of 50°C/h.

19. The peak temperatures and the activation energies for the three biomasses examined in this study may be useful in the optimising the biomass combustor and reducing the cost. The biomass combustion is predominantly control by the reaction rather than the internal diffusion. This will further reduce the cost by avoiding the biomass grinding process before combustion. The information on the exit gas carbon monoxide and carbon dioxide may be useful in the designing of the flue gas treatment of the biomass combustion.

9.2 Recommendations

The work performed in this study has been limited to the evolved gas analysis (EGA) experiments using the rice husk, palm fibre and palm fibre char. The following areas are recommended for further study:

1. Further EGA experiments with rice husk, palm fibre and palm fibre char may be conducted at higher operating pressures. The operating pressure of the present study is limited by the design of the experimental rig to a maximum absolute pressure of 800kPa.

2. The EGA work should be applied to the other biomass and biomass char such as sugarcane bagasse, pine, wood char and rice char. Further, the EGA work may also be applied to the various industrial solid wastes (i.e. refuse derived fuels (RDF) and industrial wood waste).

3. Further EGA work with biomass and biomass char may be conducted to investigate the effect of catalyst or the effect of biomass and biomass char pretreatment on the oxidation behaviour (i.e. effect of soaking biomass in water and chemicals such as alkali or acid treatments)

4. The present work only considers the combustion characteristics of a single biomass fuel at a time. A co-combustion characteristics study of an EGA experiments may be conducted using a fuel mixtures of coal: biomass, char: biomass, biomass: biomass or coal: char: biomass.

5. Further EGA work on the model that may consider the carbon oxides production data might improve the model.

6. The model only considers the oxygen partial pressure of the inlet stream into the combustion cell. Further work on the model may consider the inclusion of the oxygen partial pressure of the outlet stream of the combustion cell. The oxygen

partial pressure of the inlet and outlet streams will be different across the reaction bed due to the oxygen being consumed by the combustion process.

7. Further experiments should be conducted to study the pore size of the biomass and the gas diffusion to further investigate the existence of the mass transfer resistance.

8. Further work may also include modeling a combustor in order to know in detail the contribution of the combustion characteristics into a combustor design.

REFERENCES

Abramowitz, M., Stegun, I.A., (1972), 'Handbook of Mathematical Functions', Dover Publications Inc. New York.

Alexander, J.D., Martin, W.L., Dew, J.N., (1962), 'Factors affecting fuel availability and composition during in situ combustion', *Journal of Petroleum Technology*, **14(10)**, pp. 1154-1162

Al-Saffar, H., Price, D., Soufi, A., Hughes, R., (2000), 'Distinguishing between overlapping low temperature and high temperature oxidation data obtained from a pressurized flow reactor system using consolidated core material', *Fuel*, **79**, pp. 723-732

Armesto, L., Bahillo, A., Veijonen, K., Cabanillas, A., Otero, J., (2002), 'Combustion behaviour of rice husk in a bubbling fluidised bed', *Biomass and Bioenergy*, **23**, pp. 171-179

ASTM Standard D2015-96, (1996), 'Standard test method for gross calorific value of coal and coke by the adiabatic bomb calorimeter', ASTM International, West Conshohocken, Pennsylvania.

ASTM Standard D5373-02, (2002), 'Standard test methods for instrumental determination of carbon, hydrogen and nitrogen in laboratory samples of coal and coke', ASTM International, West Conshohocken, Pennsylvania.

ASTM Standard D5142-02a, (2002), 'Standard test methods for proximate analysis of the analysis sample of coal and coke by instrumental procedures', ASTM International, West Conshohocken, Pennsylvania.

Biagini, E., Fantei, A., Tognotti, L., (2008), 'Effects of the heating rate on the devolatilization of biomass residues', *Thermochimica Acta*, **472**, pp. 55-63

Blasi, C.D., (2008), 'Modeling chemical and physical processes of wood and biomass pyrolysis', *Progress in Energy and Combustion Science*, **34**, pp. 47-90

Blazej, A., Kosik, M., Nevell, T.P., (1993), 'Phytomass: A Raw Material for Chemistry and Biotechnology (Ellis Horwood Series in Polymer Science and Technology)', Ellis Horwood, New York.

Boateng, A.A., Cooke, P.H., Hicks, K.B., (2007), 'Microstructure development of chars derived from high-temperature pyrolyis of barley (*Hordeum vulgare L.*) hulls', *Fuel*, **86**, pp. 735-742

Bridgwater, A.V., Boocock, D.G.B., (1997), 'Developments in thermochemical biomass conversion', Chapman & Hall, **1**, pp. 67-81

Brown, R.A., Krecher, A.K., Nguyen, T.H., Nagle, D.C., Ball, W.P., (2006), 'Production and characterization of synthetic wood chars for use as surrogates for natural sorbents', *Organic Geochemistry*, **37(3)**, pp. 321-333

Burger, J.P., Sahuquest, B.C., (1972), 'Chemical aspects of in situ combustion - heat of combustion and kinetics', *Society of Petroleum Engineers Journal*, **12(5)**, pp. 410-422

Cao, X., Ma, L., Gao, B., Harris, W., (2009), 'Dairy-manure derived biochar effectively sorbs lead and atrazine', *Environment Science Technology*, **43(9)**, pp. 3285-3291

Chuah, T.G., Azlina, A.G.K.W., Robiah, Y., Omar, R., (2006), 'Biomass as the renewable energy sources in Malaysia: an overview', *International Journal of Green Energy*, **3**, pp. 323-346

Dabbous, M.K., Fulton, P.F., (1974), 'Low temperature oxidation kinetics and effects on the in situ combustion process', *Society of Petroleum Engineers Journal*, **14(3)**, pp. 252-263

Daood, S.S., Munir, S., Nimmo, W., Gibbs, B.M., (2010), 'Char oxidation study of sugar cane bagasse, cotton stalk and Pakistani coal under 1% and 3% oxygen concentrations', *Biomass and Bioenergy*, **34**, pp. 263-271

Darvell, L.I., Jones, J.M., Gudka, B., Baxter, X.C., Saddawi, A., Williams, A., Malmgren, A., (2010), 'Combustion properties of some power station biomass fuels', *Fuel*, **89**, pp. 2881 - 2890

Das, K.C., Garcia-Perez, M., Bibens, B., Melear, N., (2008), 'Slow pyrolysis of poultry litter and pine woody biomass: Impact of chars and bio-oils on microbial growth', *Journal of Environmental Science and Health: Part A*, **43**, pp. 714-724

de los Rios, C.F., Brigham, W.E., Castanier, L.M., (1988), 'The effect of metallic additives on the kinetic of oils oxidation reaction in in-situ combustion.' U.S. Department of Energy, Report DOE/BC/14126-4

Demirbas, A., (2004), 'Effects of temperature and particle size on bio-char yield from pyrolysis of agricultural residues', *Journal of Analytical and Applied Pyrolysis*, **72**, pp. 243-248

Demirbas, A., (2005), 'Potential applications of renewable energy sources, biomass combustion problems in boiler power systems and combustion related environmental issues', *Progress in Energy and Combustion Science*, **31(2)**, pp. 171-192

Essenhigh, R.H. (1981), 'Chemistry of coal utilization', Editor: M.A. Elliot, Second Supplementary Volume, Wiley Interscience, New York.

Fassihi, M.R., Brigham, W.E., Ramey, H.J.J., (1984), 'Reaction kinetics of in situ combustion: Part 1 – Observation', *Society of Petroleum Engineers Journal*, **24(4)**, pp. 399-407

Fernandez, R.G., Garcia, C.P., Lavin, A.G., de las Heras, J.L.B., (2012), 'Study of main combustion characteristics for biomass fuels used in boilers', *Fuel Processing Technology*, **103**, pp. 16-26

Ghani, W.A.W.A.K., Idris, A., Rebitanim, N.Z., Salleh, M.A.M., (2011), 'Towards CO_2 reduction: The role of biochar', Symposium on Climate Change Adaptation, 16-17 November 2011, Putrajaya, Malaysia

Gokcol, C., Dursun, B., Alboyaci, B., Sunan, E., (2009), 'Importance of biomass energy as alternative to other sources in Turkey', *Energy Policy*, **37(2)**, pp. 424-431

Guan, C.T., (2003), 'Technical Update: Biomass: Renewable Energy Sources in Malaysia.' *Quarterly Bulletin of the Department of Environment Malaysia (MOSTE)*, Vol. 2: 15-16

Haykiri-Acma, H., Yaman, S., Kucukbayrak, S., (2012), 'Combustion characteristics of sodium-free pyrolytic char from hazelnut shell', *Fuel Processing Technology*, **96**, pp. 169-174

Idris, S.S., Rahman, N.A., Ismail, K., Alias, A.B., Rashid, Z.A., Aris, M.J., (2010), 'Investigation on thermochemical behaviour of low rank Malaysian coal, oil palm biomass and their blends during pyrolysis via thermogravimetric analysis (TGA)', *Bioresource Technology*, **101**, pp. 4584-4592

Kadir, S.A.S.A., (1995), 'Prediction of heavy fuel oil spray combustion and particulate emissions in a cylindrical furnace.' Department of Chemical Engineering, PhD. Thesis, University of Leeds: United Kingdom.

Kaer, S.K., (2005), 'Straw combustion on slow-moving grates - a comparison of model predictions with experimental data', *Biomass and Bioenergy*, **28**, pp. 307-320

Kastanaki, E., Vamvuka, D., Grammelis, P., Kakaras, E., (2002), 'Thermogravimetric studies of the behaviour of lignite-biomass blends during devolatilization', *Fuel Processing Technology*, **77-78**, pp. 159-166

Kastanaki, E., Vamvuka, D., (2006), 'A comparative reactivity and kinetic study on the combustion of coal-biomass char blends', *Fuel*, **85**, pp. 1186-1193

Kelly-Yong, T.L., Lee, K.T., Mohamed, A.R., Bhatia, S., (2007), 'Potential of hydrogen from oil palm biomass as a source of renewable energy worldwide', *Energy Policy*, **11**, pp. 5692-5701

Kheang, L.S., Subramaniam, V., Ngatiman, M., (2012), 'Oil palm biomass energy resource data', Malaysian Palm Oil Board (MPOB) Publications, Malaysia

Kisler, J., (1995), 'The application of in situ combustion to light Australian oils.' Department of Chemical & Biomolecular Engineering, PhD. Thesis, University of Melbourne: Melbourne.

Kisler, J.P., Shallcross, D.C., (1997), 'An Improved model for the oxidation processes of light crude oil', *Chemical Engineering Research & Design*, **75**, pp. 392-400

Maiti, S., Dey, S., Purakayastha, S., Ghosh, B., (2006), 'Physical and thermochemical characterization of rice husk char as potential biomass energy source', *Bioresource Technology*, **97**, pp. 2065-2070

Mamora, D.D., Ramey, H.J., Brigham, W.E., Castanier, L.M., (1993), 'Kinetics of in situ combustion', Standford University Petroleum Research Institute, Standford, California, Topical Report, **91**, May

Mansaray, K.G., Ghaly, A.E., (1998), 'Thermal degradation of rice husks in nitrogen atmosphere', *Bioresource Technology*, **65**, pp. 13-20

Masek, O., Brownsort, P., Cross, A., Sohi, S., (2011), 'Influence of production conditions on the yield and environmental stability of biochar', *Fuel*, doi:10.1016/j.fuel.2011.08.044

Meng, X., de Jong, W., Badri, F.S., Benito, P., Basile, F., Verkooijen, A.H.M., (2012), 'Combustion study of partially gasified willow and DDGS chars using TG analysis and COMSOL modeling', *Biomass and Bioenergy*, pp. 1-14

Natarajan, E., Nordin, A., Rao, A.N., (1998), 'Overview of combustion and gasification of rice husk in fluidized bed reactors', *Biomass and Bioenergy*, **14(5-6)**, pp. 533-546

Nguyen, T.T., (2004), 'Oxidation kinetics of Vietnamese crude oil.' Department of Chemical & Biomolecular Engineering, MSc. Thesis, University of Melbourne: Melbourne.

Park, S., Jang, C., (2012), 'Effects of pyrolysis temperature on changes in fuel characteristics of biomass char', *Energy*, **39**, pp. 187-195

Purevsuren, B., Tesche, B., Davajaav, (2003), 'A biochar from casein and its properties', *Journal of Material Science*, **38**, pp. 2347-2351

Sahu, S.G., Sarkar, P., Chakraborty, N., Adak, A.K., (2010), 'Thermogravimetric assessment of combustion characteristics of blends of a coal with different biomass chars', *Fuel Processing Technology*, **91**, pp. 369-378

Sami, M., Annamalai, K., Wooldridge, M., (2001), 'Co-firing of coal and biomass fuel blends', *Progress in Energy and Combustion Science*, **27(2)**, pp. 171-214

Shackley, S., Carter, S., Knowles, T., Middelink, E., Haefele, S., Sohi, S., Cross, A., Haszeldine, S., (2012), 'Sustainable gasification-biochar systems? A case study of rice husk gasification in Cambodia. Part I: Context, chemical properties, environmental and health and safety issues', *Energy Policy*, **42**, pp. 49-58

Shallcross, D.C., (1991), 'Oxidation kinetics of very light Australian Crude Oils: Preliminary Results.' IEA Collaborative Project on EOR, 12th International Workshop and Symposium, Guildhall U.K., October

Shinogi, Y., Yoshida, H., Koizumi, T., Yamaoka, M., Saito, T., (2002), 'Basic characteristics of low-temperature carbon products from waste sludge', *Advances in Environmental Research*, **7**, pp. 661-665

Shuit, S.H., Tan, K.T., Lee, K.T., Kamaruddin, A.H., (2009), 'Oil palm biomass as a sustainable energy source: A Malaysian case study', *Energy*, **34(9)**, pp. 1225-1235

Skreiberg, A., Skreiberg, O., Sandquist, J., Sorum, L., (2011), 'TGA and macro-TGA characterisation of biomass fuels and fuel mixtures', *Fuel*, **90**, pp. 2182-2197

Sohi, S.P., Krull, E., Lopex-Capel, E., Bol, R., (2010), 'Chapter 2: A review of biochar and its use and function in soil', *Advances in Agronomy*, **105**, pp. 47-82

Sung, Y.J., Seo, Y.B., (2009), 'Thermogravimetric study on stem biomass of Nicotiana tabacum', *Thermochimica Acta*, **486**, pp. 1-4

Tewfik, S., (2004), 'Biomass utilization facilities and biomass processing technologies', *Energy Education Science Technology* **14**, pp. 1-19

Vuthaluru, H.B., (2004), 'Investigations into the pyrolytic behaviour of coal/biomass blends using thermogravimetric analysis', *Bioresource Technology*, **92**, pp. 187-195

Wahid, M. B., May, C.Y., Soon, L.W., Aziz, A.A., Mokhtar, A., Ibrahim, Z., Hassan, K., Bakar, N.A., Ramli, R., Soom, R.M., Hassan, W.H.W., Mamat, R., Wahab, N.S.A., Sulong, M., (2009), 'MPOB biomass technology centre road to zero waste', Malaysian Palm Oil Board (MPOB) Publications, Malaysia

Wan Rosli, W.D., Law, K.N., Zainuddin, Z., Asro, R., (2004), 'Effect of pulping variables on the characteristics of oil-palm frond-fiber', *Bioresource Technology*, **93**, pp. 233-240

Xu, R., Ferrante, L., Hall, K., Briens, C., Berruti, F., (2011), 'Thermal self-sustainability of biochar production by pyrolysis', *Journal of Analytical and Applied Pyrolysis*, **91**, pp. 55-66

Yaman, S., (2004), 'Pyrolysis of biomass to produce fuels and chemical feedstocks', *Energy Conversion and Management*, **45**, pp. 651-671

Yang, H., Yan, R., Chin, T., Liang, D.T., Chen, H., Zheng, C., (2004), 'Thermogravimetric anaysis-Fourier transform infrared analysis of palm oil waste pyrolysis', *Energy and fuel*, **18(6)**, pp. 1814-1821

Yang, H., Yan, R., Chen, H., Lee, D.H., Liang, D.T., Zheng, C., (2006), 'Pyrolysis of palm oil wastes for enhanced production of hydrogen rich gases', *Fuel Processing Technology*, **87**, pp. 935-942

Yorulmaz, S. Y., Atimtay, A.T., (2009), 'Investigation of combustion kinetics of treated and untreated waste wood samples with thermogravimteric analysis', *Fuel Processing Technology*, **90**, pp. 939-946

Yusoff, S., (2006), 'Renewable energy from palm oil - innovation on effective utilization of waste', *Journal of Cleaner Production*, **14(1)**, pp. 87-93

Zheng, G., Kozinski, J.A., (2000), 'Thermal events occurring during the combustion of biomass residue', *Fuel*, **79**, pp. 181-192

Zhou, H., Jensen, A.D., Glarborg, P., Jensen, P.A., Kavaliauskas, A., (2005), 'Numerical modeling of straw combustion in a fixed bed', *Fuel*, **84(4)**, pp. 389-403

APPENDIX A

CALIBRATION

A.1 Introduction

Several items of the experimental apparatus must be calibrated in order to obtain the calibration equation for the conversion of their voltage outputs into physical quantities. The calibration equations were determined by the linear regression of the experimentally determined data points. In all of the cases, the correlation coefficient of the linear regression (r^2) was greater than 0.999. This indicates that the data is well represented by a linear relationship and high order equations are not required. The K-type thermocouple signal was readily converted from a voltage to °C by the data logging software.

A.2 Calibration of pressure transducer

The pressure transducer, which measures the cell pressure, was calibrated with an accurate pressure gauge and a constant flow rate of air. Table A.1 and Figure A.1 show the calibration data and the fitted line. The linear relationship between the gauge pressure (P in kPa) and the transducer voltage (V in millivolts) is:

$$P = 7.019\ V - 18.67 \qquad (A.1)$$

Table A.1 - The pressure transducer calibration.

Gauge pressure (kPa)	Voltage (mV)
0	4.22
50	9.55
100	16.47
150	23.88
200	30.89
250	37.73
300	45.09
350	52.28
400	59.43
450	66.54
500	74.23
550	81.66
600	88.21
650	95.09
700	102.04
750	109.76
800	116.84

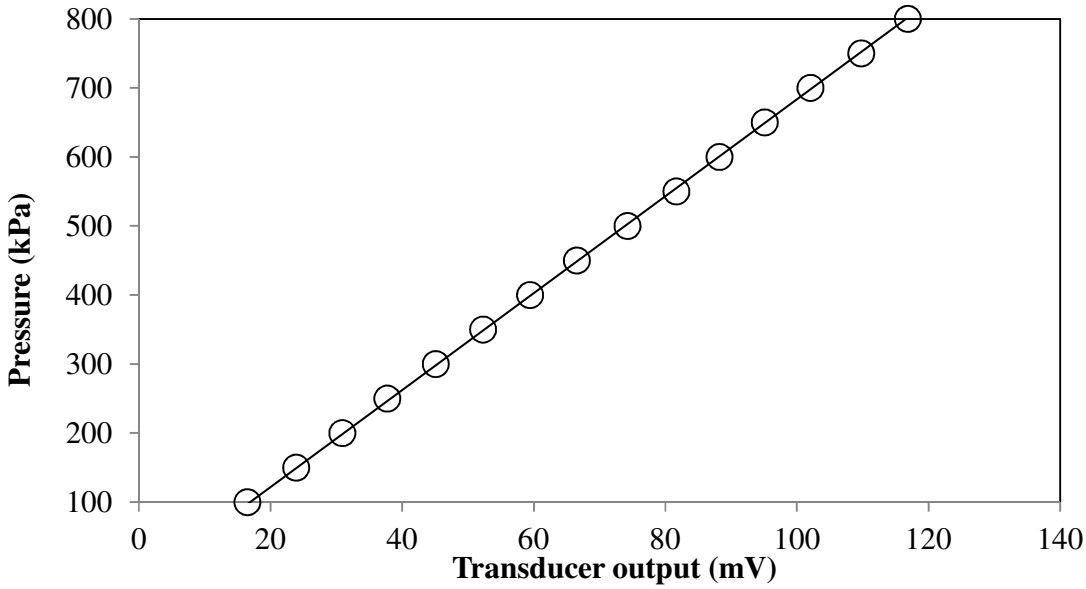

Figure A.1 - Gauge pressure in the combustion cell versus pressure transducer output voltage.

A.3 Calibration of K-type thermocouple

The thermocouples were calibrated using an ice point method and a boiling point method. For the ice point method, a crushed ice was placed in a container flask and the container flask was filled with cold water. The thermometer was placed at the centre of the container to a depth at least 2 inches from the bottom of container. The temperature should be noted after the reading has stabilised after five minutes. The temperature reading was observed in between -0.5°C to 0.5°C. As for the boiling point method, a boiling water was placed in a container flask and the thermocouple was placed at the centre of the container. The temperature should be noted after the reading has stabilised after five minutes. The temperature reading was observed to be within 99.5°C to 100.5°C. Throughout the experiment, the temperature would reached 500°C. Since type K thermocouple has a wide temperature range of -200°C to 1250°C, it is assumed that the temperature reading deviation would be similar at 500°C.

A.4 Gas analyser calibration

The gas analysers were calibrated before and after each experiment with the high and the low scale gas mixtures at conditions of pressure and flow rate similar to those found during the experiment.

The calibration was conducted bypassing the cell to prevent any interaction between the biomass materials and the calibration gases that could influence the calibration procedure or promote reactions within the cell. A total of four gas cylinders were used during the calibration. There were:

- Air (20.96 mol% oxygen and balance nitrogen)
- Nitrogen (100 mol%)
- Gas mixture 1 (15.10 mol% O_2, 2.01 mol% CO_2, 0.983 mol% CO and balance nitrogen)

- Gas mixture 2 (18.10 mol% O_2, 4.99 mol% CO_2, 2.51 mol% CO and balance nitrogen)

Calibration equations for the analysers are calculated from the calibration data gathered before and after the run. For the carbon dioxide and carbon monoxide calibrations, air was used as the zero basis gas since a typical run starts and finishes with air. Nitrogen was used as the zero basis gas for the oxygen calibration. Data from a typical gas analyser is shown in Table A.2 and Figures A.2, A.3 and A.4. The two calibrations were performed 10.5 hours apart. The calibration equation is in the form of Equation (A.2).

$$Gas = (a + bt)V + (c + dt) \quad (A.2)$$

Table A.2 - Calibration of gas analyser for experiment F6 conducted at the operating absolute pressure of 500kPa and an injection flow rate of 400smL/min. The two calibrations were conducted 10.5 hours apart.

Gas	Concentration (%)	First calibration	Second calibration
O_2	0	1.93	1.96
	15.100	5.83	5.42
	18.100	6.59	6.07
	20.960	7.29	6.76
	Calibration equation	$\%O_2 = 3.898V - 7.550$	$\%O_2 = 4.378V - 8.579$
CO	0	0.08	0.08
	0.983	1.46	1.47
	2.510	3.48	3.49
	Calibration equation	$\%CO = 0.740V - 0.073$	$\%CO = 0.738V - 0.075$
CO_2	0	1.88	1.88
	2.01	2.66	2.66
	4.99	3.74	3.74
	Calibration equation	$\%CO_2 = 2.688V - 5.084$	$\%CO_2 = 2.688V - 5.084$

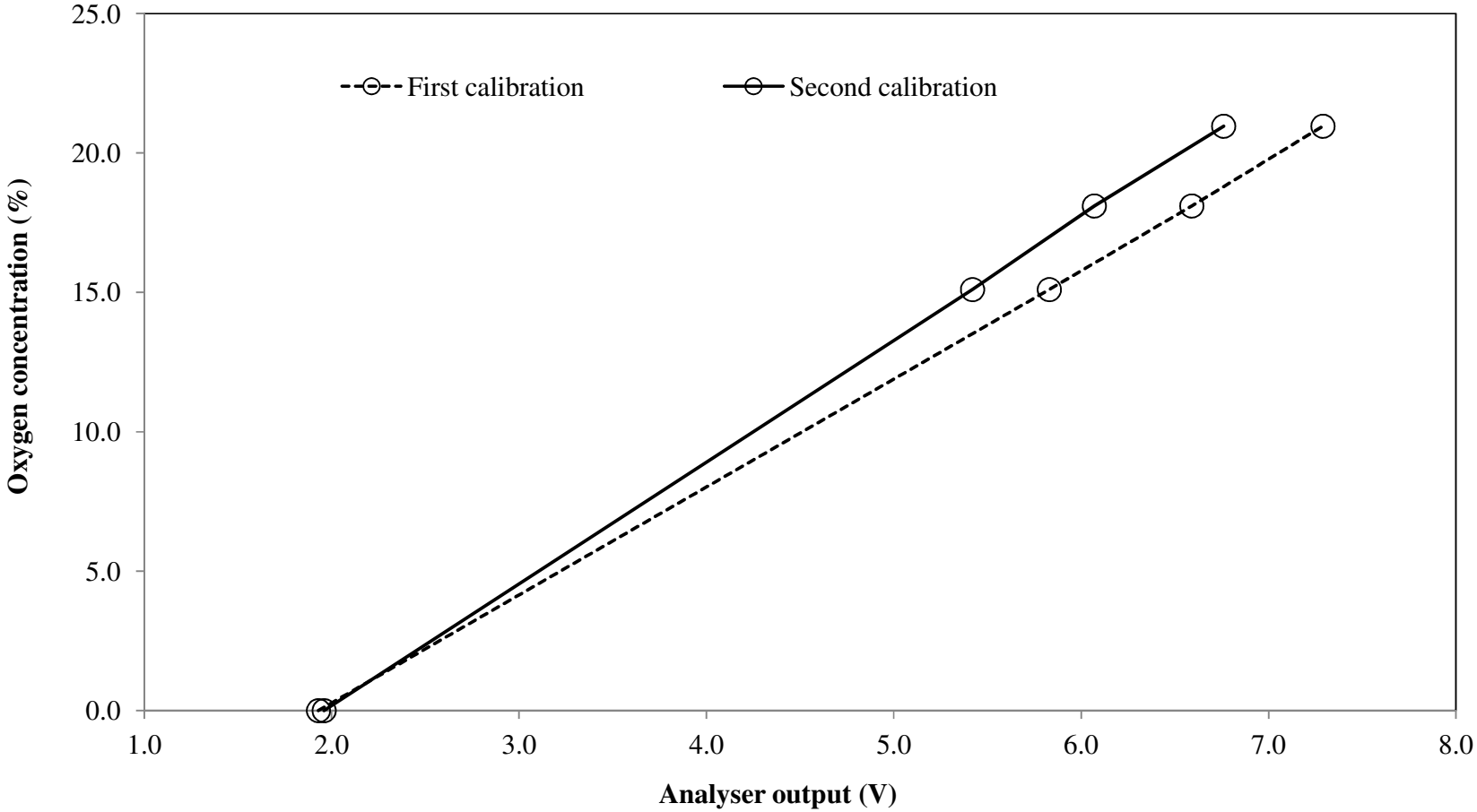

Figure A.2 - Calibration curves for the oxygen analyser of experiment F6. The two calibrations were conducted 10.5 hours apart. There seems to be a significant different between the regression parameters in the two linear regressions performed on the first and second calibrations.

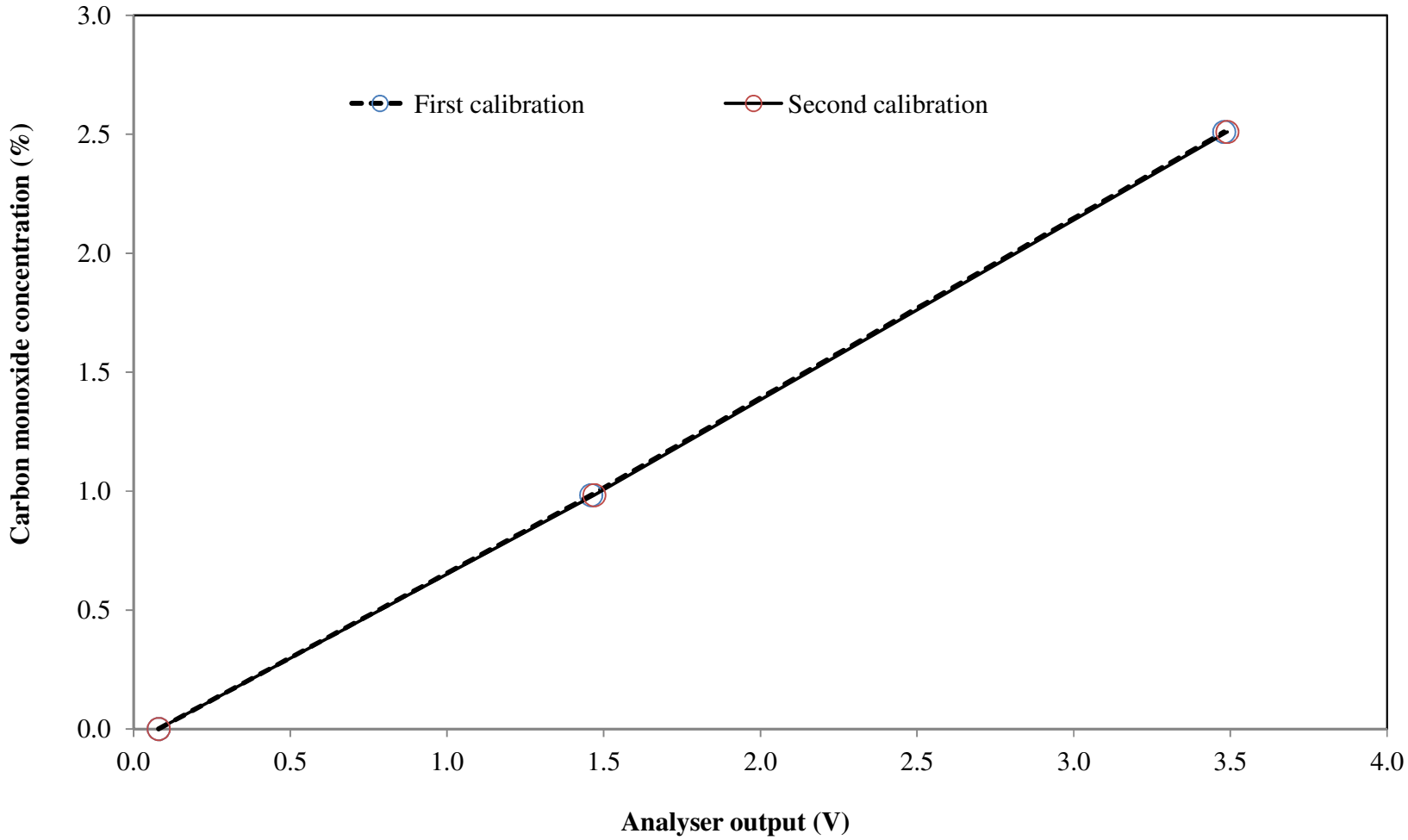

Figure A.3 - Calibration curves for the carbon monoxide analyser of experiment F6. The two calibrations were conducted 10.5 hours apart. There was negligible analyser drift between the two calibrations.

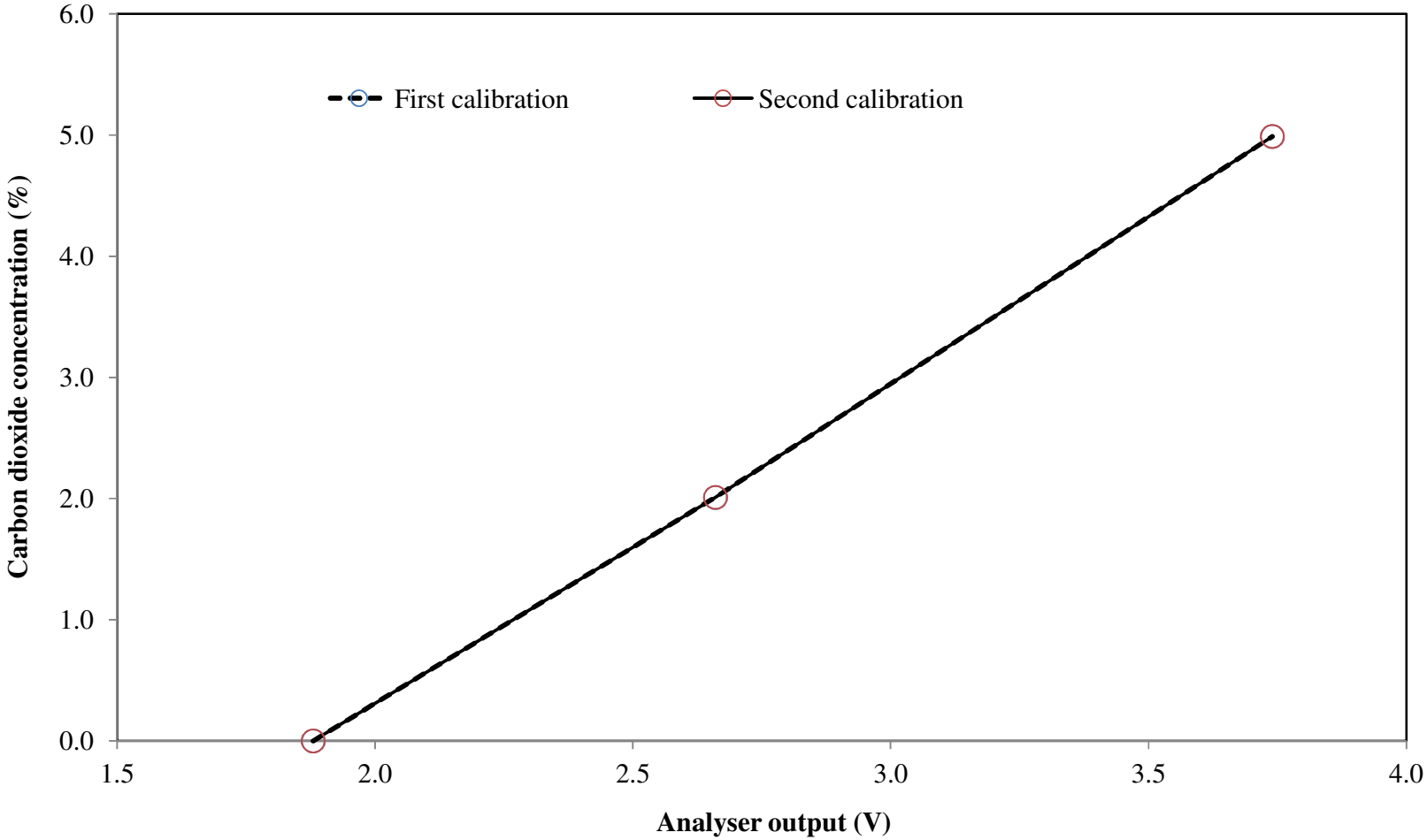

Figure A.4 - Calibration curves for the carbon dioxide analyser of experiment F6. The two calibrations were conducted 10.5 hours apart. There was negligible analyser drift between the two calibrations.

In all cases, the correlation coefficient of the linear regression was greater than 0.999. However, there seems to be a significant different between the regression parameters in the two linear regressions performed on the pre and post calibrations for the oxygen analyser (see Figure A.2). Hence, a linear model using only V, volts as a predictor is inadequate. It is proposed that time, t be included as the second predictor for the mol% oxygen calibration. The mol% carbon dioxide and mol% carbon monoxide calibrations do not require the addition of time as a second predictor because the parameters of the corresponding linear equations are almost identical for both the pre and post calibrations.

The suggested model for the mol% oxygen calibration is:

$$\text{mol\% } O_2 = a_o + a_1(V) + a_2(t) \qquad \text{(A.3)}$$

A multiple linear regression was performed on the calibration data is presented in Table A.3. Considering Table A.3, the adjusted R^2 is 0.995. The overall fit seems to be very good as the adjusted R^2 is close to one. Table A.4 shows the regression parameters of the multiple linear regression performed for the mol% oxygen calibration. As observed in Table A.4, all of the parameters are significant (p-value < 0.05). Hence the suggested model for the mol% oxygen calibration is:

$$\text{mol\% } O_2 = -8.7 + 4.11(V) + 0.14(t) \qquad \text{(A.4)}$$

Initial work found that the gas analysers gave a slightly different reading depending whether the cell was by-passed or not. The cause of this is the analysers sensitivity to temperature and pressure.

Table A.3 - The calibration data for the oxygen concentration of the typical EGA experiment F6 conducted with air as the oxidising gas, an absolute system pressure of 500kPa, an injection air flow rate of 400smL/min and a heating rate of 50°C/h.

Time, t (hrs)	Volt, V (V)	Oxygen concentration (mol%)
0	1.93	0
0	5.83	15.10
0	6.59	18.10
0	7.29	20.96
10.5	1.96	0
10.5	5.42	15.10
10.5	6.07	18.10
10.5	6.76	20.96

Table A.4 - The regression parameters for the multiple regression performed for the oxygen calibration of experiment F6.

	Coefficients	P-value
Intercept	-8.70	4.3×10^{-05}
t (hrs)	0.14	0.018
V (V)	4.11	2.3×10^{-07}

A.4.1 Gas analyser lag time determination

Gas analyser lag time is determined by observing the analyser response to a step change in the concentration of the gas flowing through the cell. The lag time for the system was taken as the time from the start of the step change until the gas analyser registered 95% of its final value.

The process is applied to all the analysers. Apart from that, the residence times of other operating pressure were also determined experimentally. Figure A.5 shows the relationship between the cell residence time and the pressure for the oxygen analyser. Theoretically the residence time should consist of two parts. Firstly, a non-zero but constant corresponding to the dead volume downstream of the back pressure regulator since this part of the rig is always at the atmospheric pressure. Secondly, the residence time should be proportional to the operating pressure to represent the dead volume upstream of the back pressure regulator. Table A.5 displays the cell residence times for a variety of total system pressures (absolute). The residence times have been rounded to the nearest 10 seconds interval to correspond with the regularity of data logging.

Table A.5 - Combustion cell residence time at injection flow rate of 400smL/min.

Total system pressure (kPa) (absolute)	**Residence time for oxygen analyser (seconds)**	**Residence time for carbon monoxide analyser (seconds)**	**Residence time for carbon dioxide analyser (seconds)**
200	59	36	39
300	88	66	69
500	138	115	118
700	195	135	140

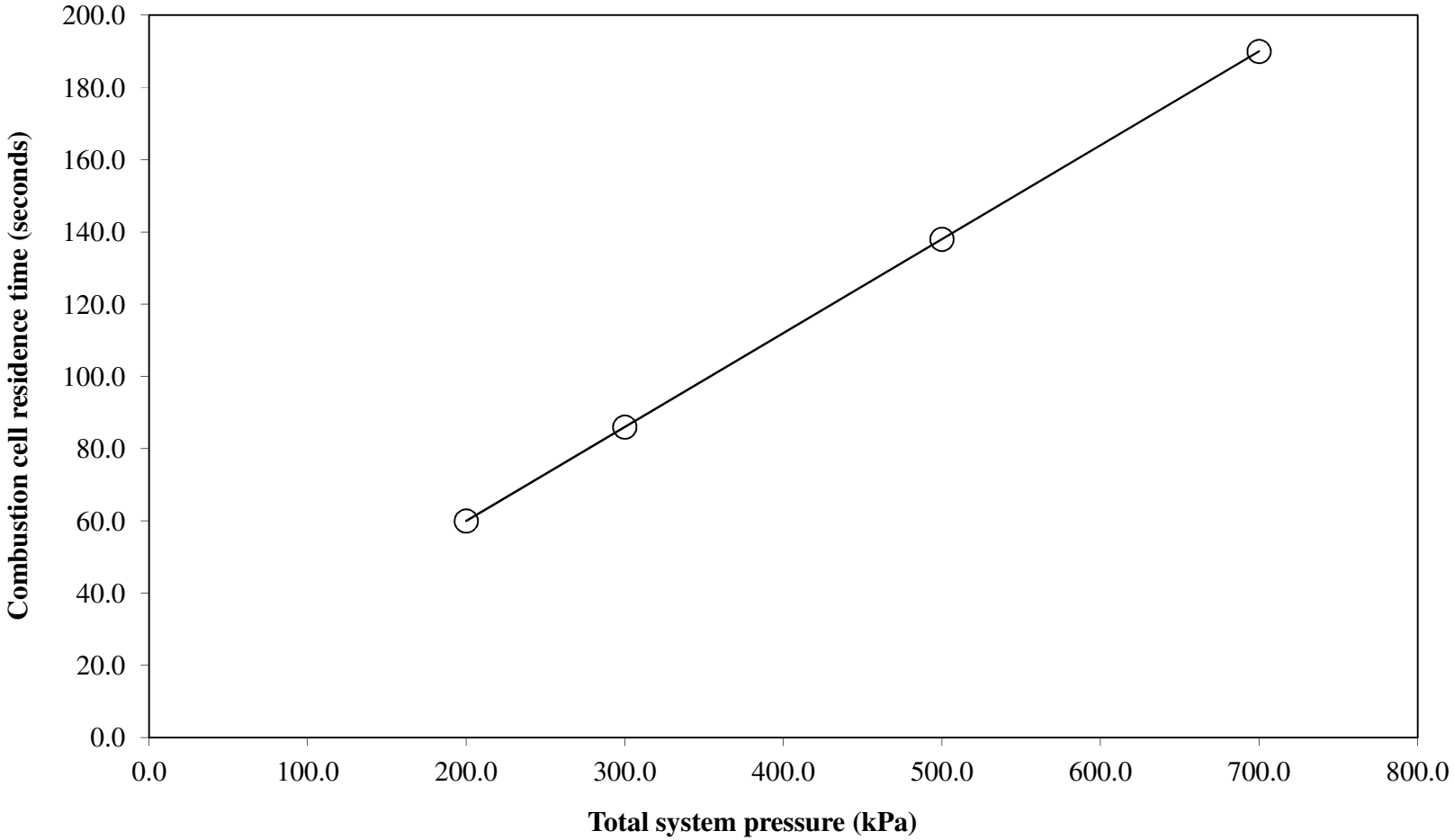

Figure A.5 - Combustion cell residence time with respect to the absolute total system pressure for the oxygen analyser. The line of best fit was obtained by the linear regression of the data.

APPENDIX B

MODELING PROGRAMS

B.1 Introduction

The experimental data analysis was performed using programs written in the Visual Basic 6.0 language. The PO2CONS programs are designed to be compatible with Microsoft Windows operating system (95, 98, XP, 7, Microsoft Vista and Microsoft 2007). The programs are developed to analyse the effluent gas analysis data for biomass oxidation study. There are two programs developed in the PO2CONS software. For each of the programs, a flowchart is presented.

The first program is used to calculate the kinetic parameters by linear regression. This involves weighted linear regression calculations based on the relative reaction rate data. This program uses the calculation technique of working from high to low temperatures. This calculation technique implied for the high temperature oxidation (HTO) and medium temperature oxidation (MTO) reactions.

The second program under the PO2CONS software is similar to the first program except that it employs the calculation technique of working from low to high temperatures. This technique requires an estimate for the total integral under the oxygen consumption curve. The second program is used for calculation for the low temperature oxidation (LTO) reaction.

B.2 The first program

This program is used to calculate the predicted oxygen consumption data for the HTO and MTO reactions. The program employs the calculation technique of working from high to low temperatures. Figure B.1 shows the flowchart of the program.

The general interface is used to obtain selections for the user to choose the experimental runs to be evaluated. The general interface consists of a file menu (see Figure B.2). Further menus can be easily added in the future based on system requirements. The file menu consists of several submenus; (open, save and exit). The submenus are made visible by the clicking event procedure of the main menus. For example, “Open” submenu will open the screen form. The “Save” submenu is used to save the current application under its existing name. The “Exit” submenu terminates the running application.

Figure B.3 shows the interface output format for experiment F6 of the HTO reaction. Based on Figure B.3, the interface displayed the input data of temperature (in °C), 1/T, O_2 exp (oxygen consumption experimental data) and the data for Ln RRR (relative reaction rate). The interface also displayed the plot of relative reaction rate with respect to 1/T and the plot of oxygen consumption of the predicted and the experimental data with regards to the cell temperature. The output data are stored in a separate file for easy access. The time taken to complete the HTO model on one experiment is around 24 hours depending on the selected data points for regression. In order to speed up the program, de-selecting "show Fig" and the program will not display the plots continuously. The plots will appear at the end of the process taken at the minimum variance. By doing this, the time taken to complete the HTO model is less than 24 hours. Similar steps are applied to the calculation of the MTO reaction.

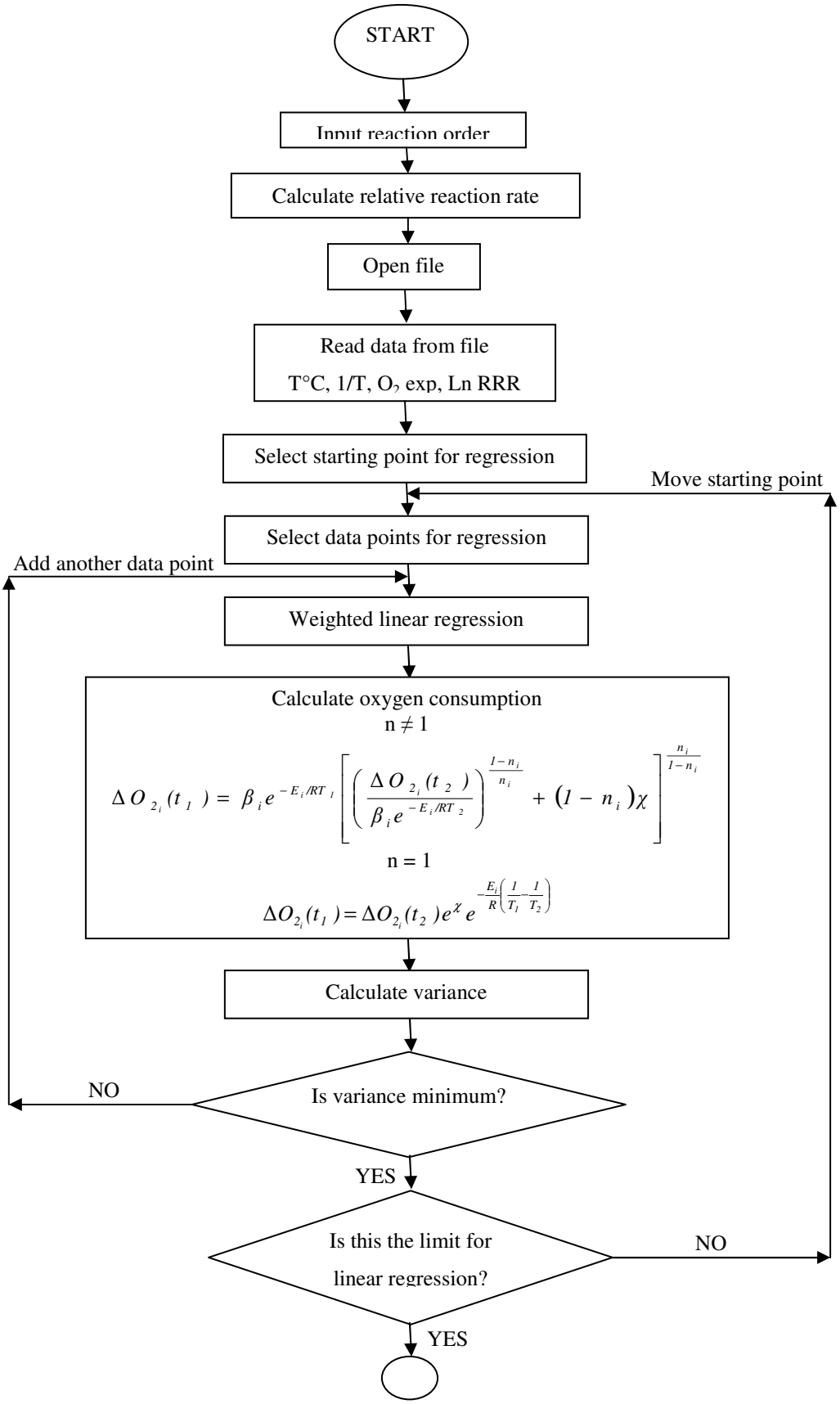

Figure B.1 - Flowchart for the first program model of PO2CONS software.

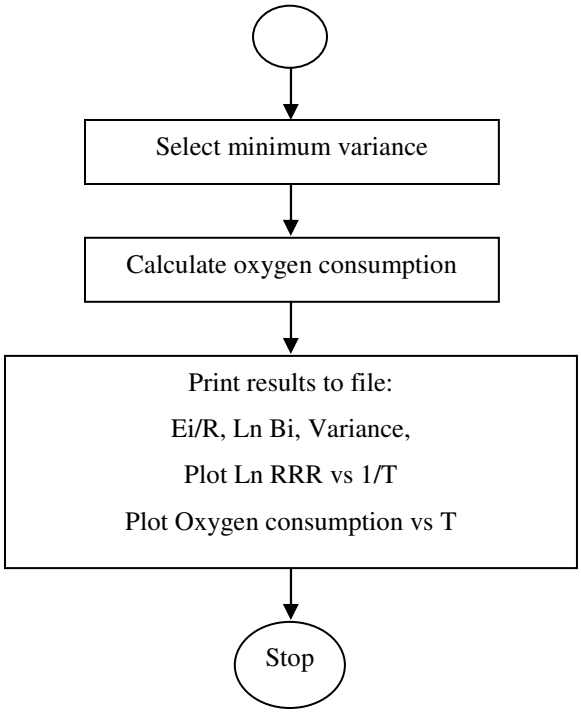

Figure B.1 (Continued) - Flowchart for the first program model of PO2CONS software.

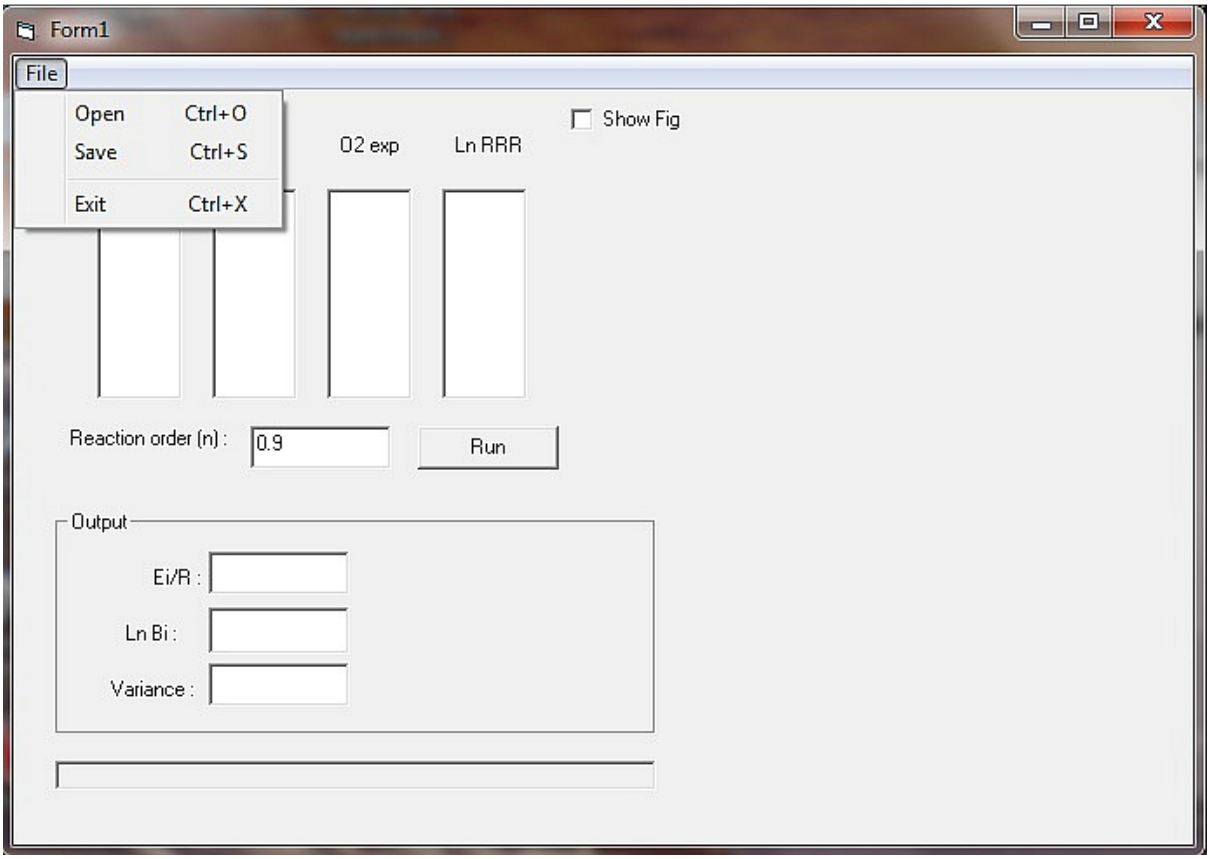

Figure B.2 - The general interface of file submenus for the first program.

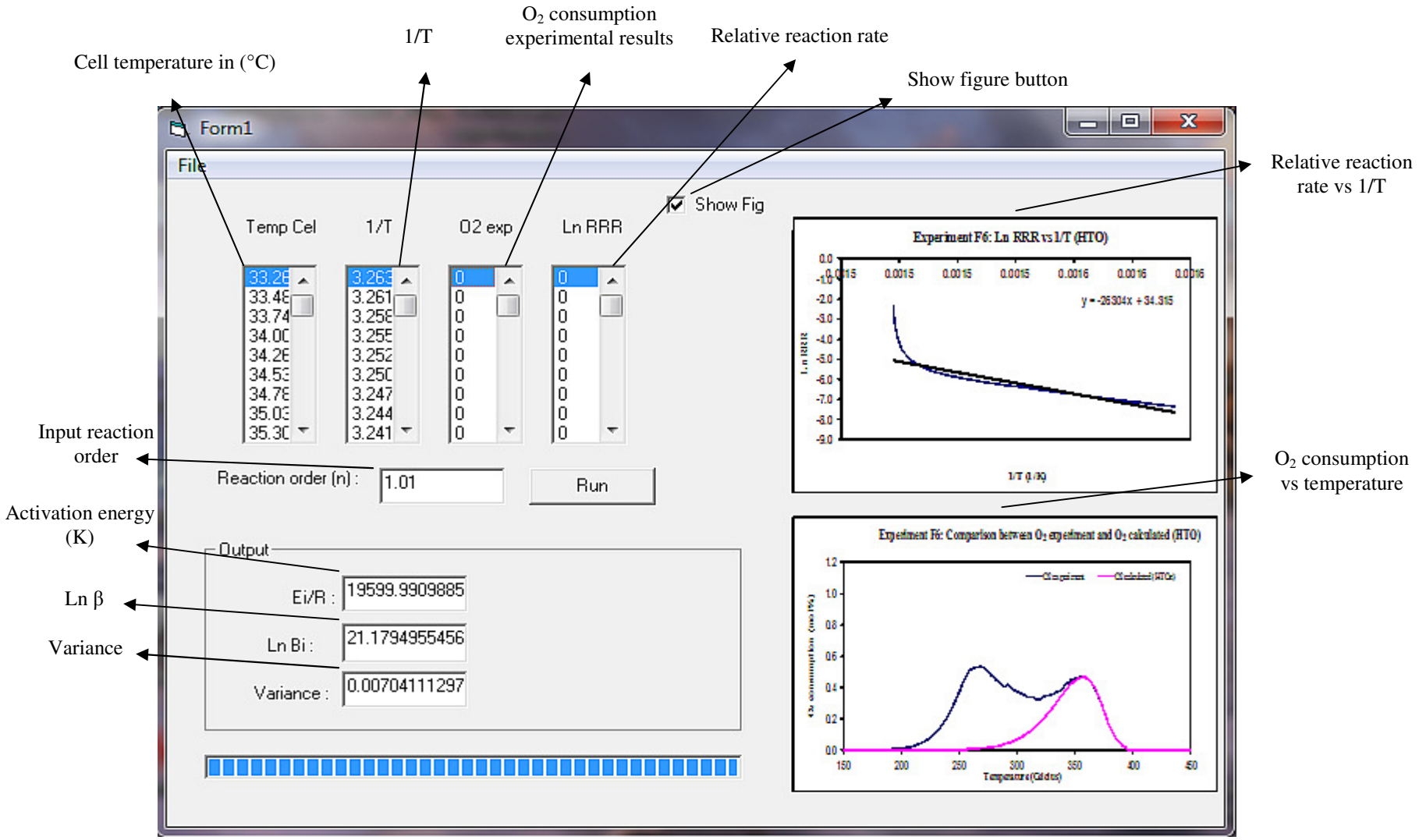

Figure B.3 - The interface output format for experiment F6 (HTO reaction).

B.3 The second program

The second program is used to calculate the predicted oxygen consumption data using the calculation technique of working from low to high temperature. This technique is applied to the LTO reaction only. The only difference from the first program is the inclusion of the ILTO (an estimation of the total integral under the oxygen consumption curve). The calculation procedure has been discussed previously in Chapter 4. Figure B.4 shows the flowchart of the second program.

The general interface for the second program is similar to the first program except that instead of inputting only the reaction order, the user must also input the estimate for the total integral under the oxygen consumption curve, ILTO. Figure B.5 shows the general interface for the second program.

Figure B.6 shows the sample of the interface output format for experiment F6 (LTO reaction) using the second program. Similar to the first program, there are two plots that may be displayed on the interface. There are a plot of relative reaction rate with respect to the 1/T and a plot of oxygen consumption of the predicted and the actual experimental data with respect to the cell temperature. Further, the values of the activation energy (E/R), ln β and variance will also be displayed in the final output format.

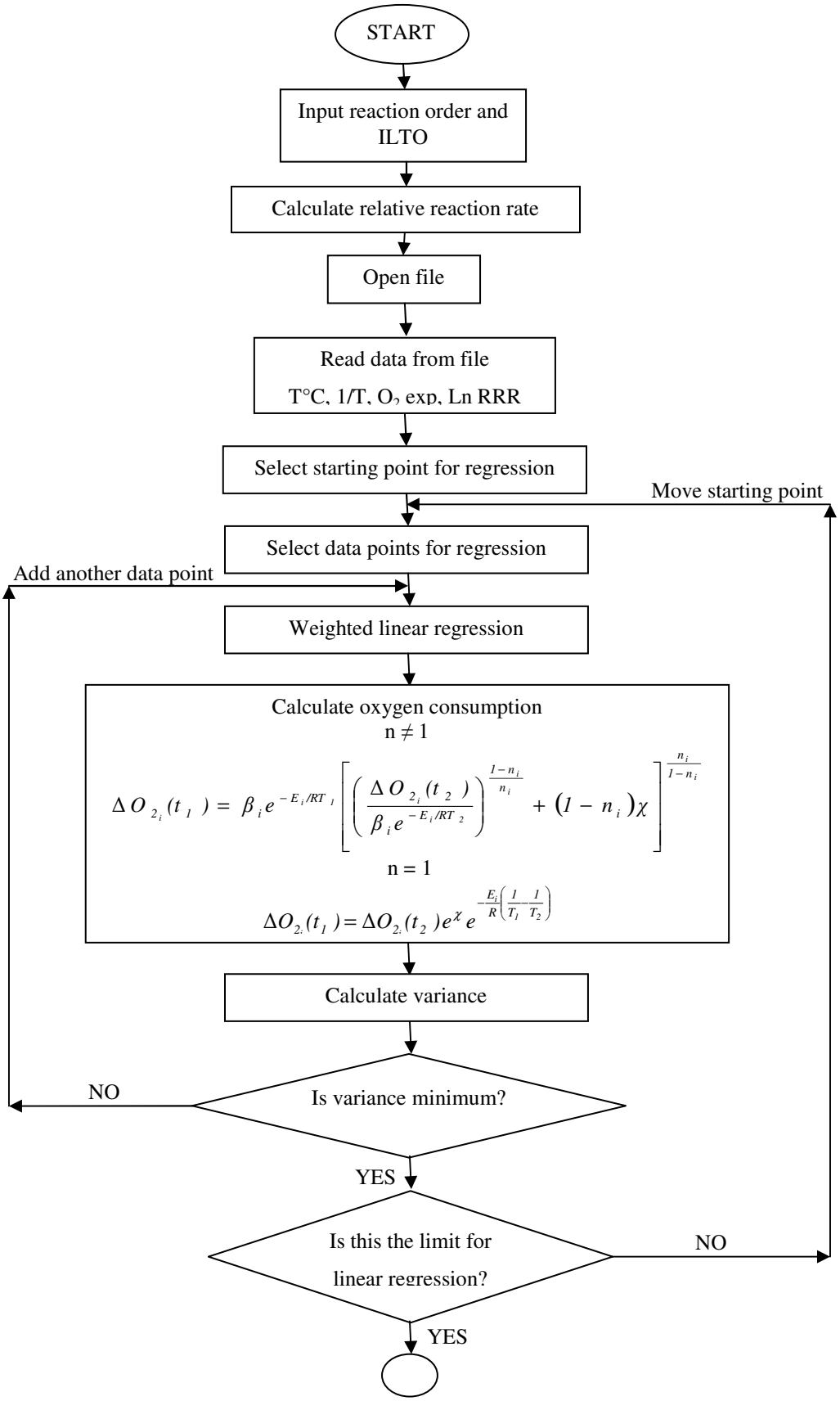

Figure B.4 - Flowchart for the second program model of PO2CONS software.

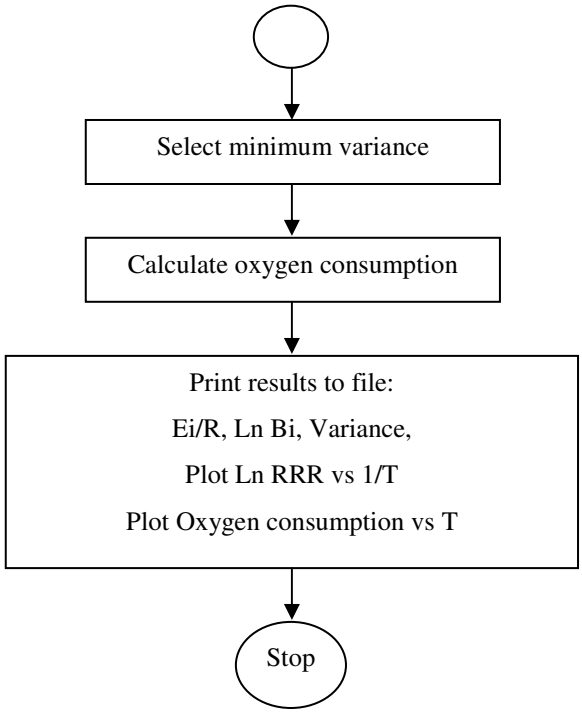

Figure B.4 (Continued) - Flowchart for the second program model of PO2CONS software.

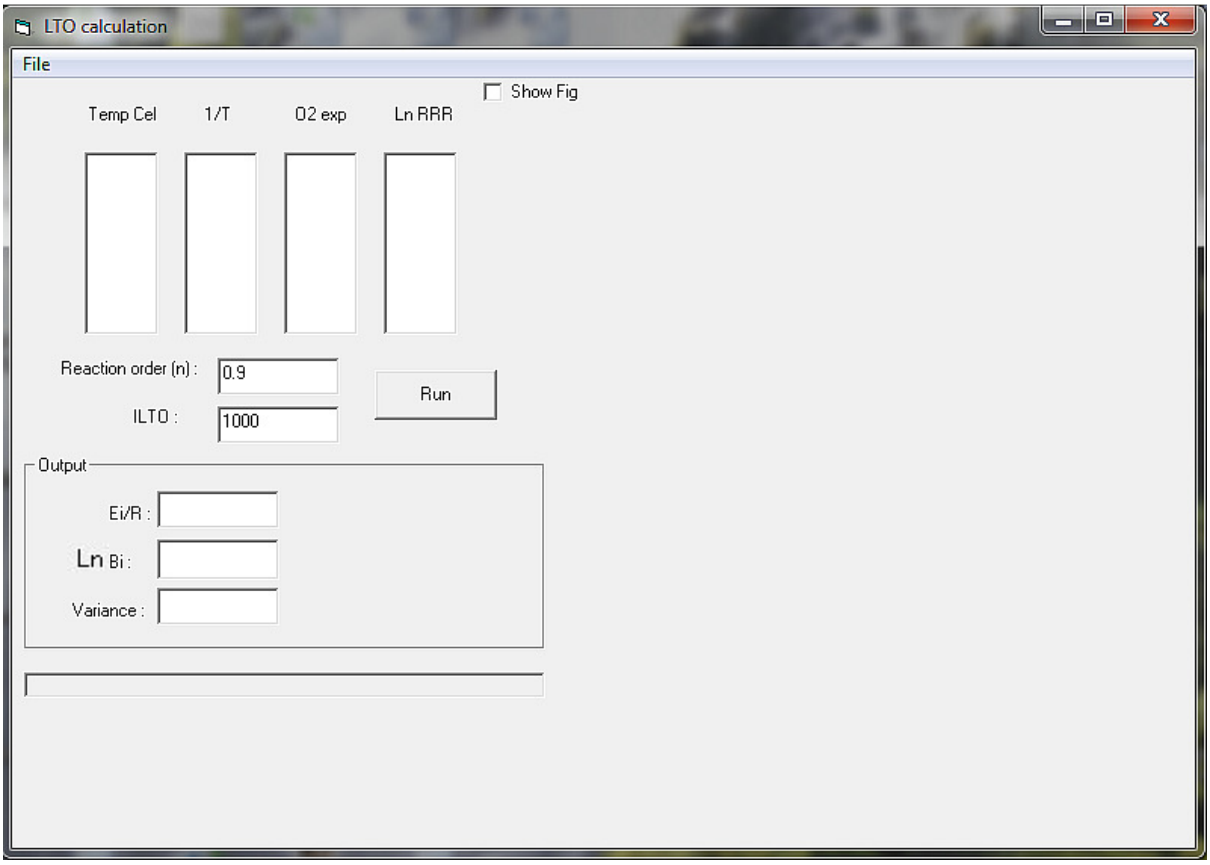

Figure B.5 - The general interface of file submenus for the second program.

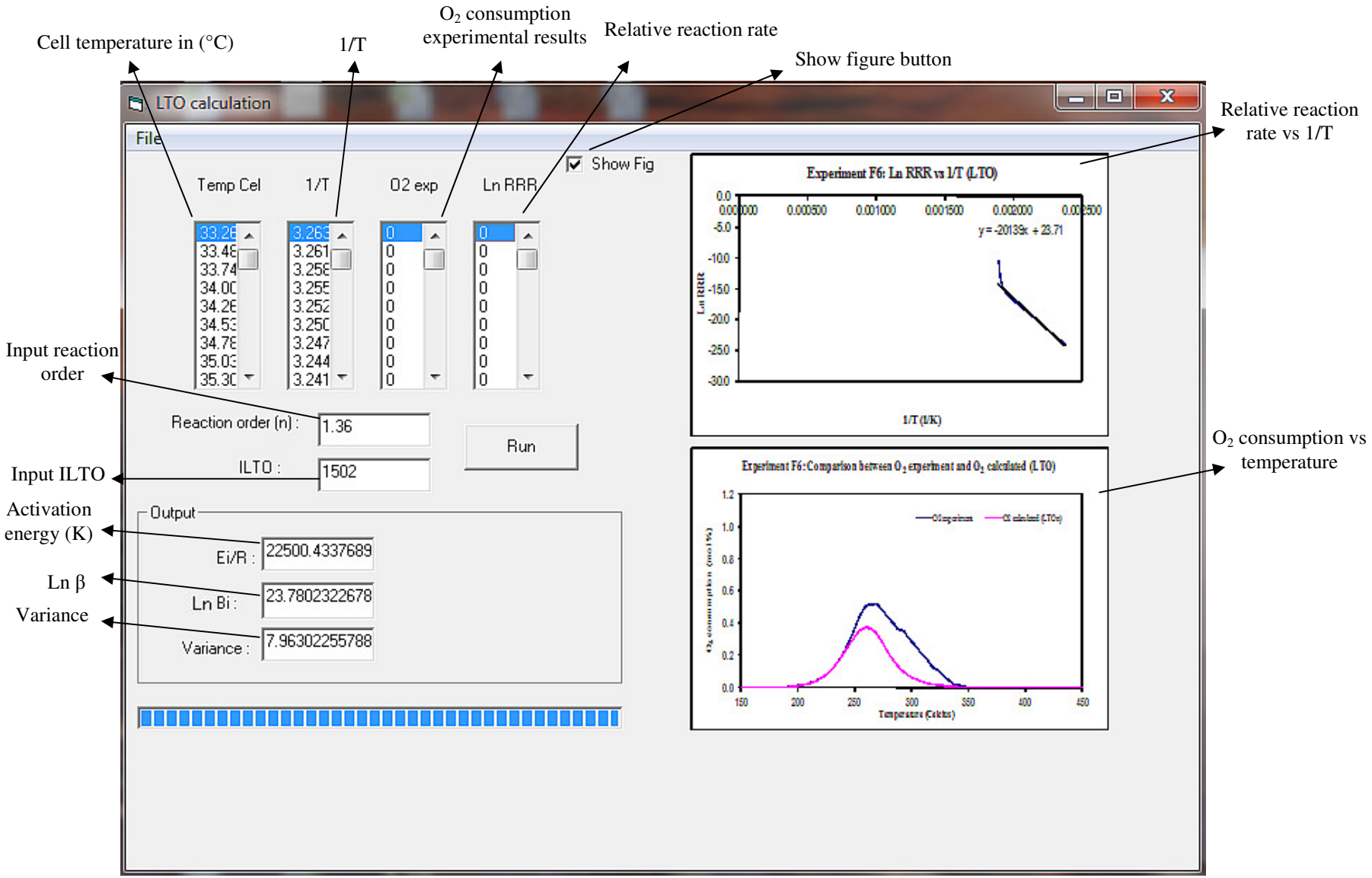

Figure B.6 - The interface output format for experiment F6 (LTO reaction).

APPENDIX C

PUBLISHED WORK

Azil Bahari Alias, David Shallcross, Sharifah Aishah Syed A. Kadir (2010). 'Combustion characteristics of Australian rice husk and Malaysian palm fibre', In: Proceeding of the Australasian Conference on Chemical Engineering, CHEMECA 2010, 26 - 29 September 2010, Adelaide, Australia

COMBUSTION CHARACTERISTICS OF AUSTRALIAN RICE HUSK AND MALAYSIAN PALM FIBRE

Azil Bahari Alias* [1,2], David C. Shallcross [1], Sharifah Aishah Syed Abd Kadir [2]

[1] Department of Chemical & Biomolecular Engineering, University of Melbourne, Victoria 3010 Australia
[2] Faculty of Chemical Engineering, Universiti Teknologi MARA Malaysia, 40450 Shah Alam, Malaysia
*Email:a.aliasales@pgrad.unimelb.edu.au

ABSTRACT

The combustion characteristics of Australian rice husks and Malaysian palm fibre have been investigated using an evolved gas analysis (EGA) technique. Air is passed through a bed containing the biomass while the temperature of the bed is gradually increased from 100°C to 500°C at a constant rate. The gas effluent is then analysed for its oxygen, carbon monoxide and carbon dioxide contents. By studying how the effluent gas composition varies with temperature the many oxidation reactions occurring within the bed may be grouped into three simultaneous and competing reaction regimes. The different reaction regimes may be decoupled and the key kinetic parameters estimated. This work reports the results of a series of EGA experiments using the rice husks and palm fibres as the biomass material. The results clearly show the variation in oxidation behaviour with system pressure and oxygen partial pressure.

Keywords: Combustion characteristics; oxidation; evolved gas analysis; biomass.

INTRODUCTION

Depletion of fossil fuel and tighter environmental regulations have forced the world to adopt alternative renewable fuel sources such as solar, hydro, wind and biomass (Guan, 2003). The energy and oil crisis worldwide will increase demands for renewable energy resources for power and transportation into the future. Hence, due to current demands for fuel and with recent developments in the energy sector, alternative renewable fuels such as biomass must be recognised as an important energy source for the foreseeable future. Palm oil wastes (empty fruit bunch, fibre and palm oil shell) and rice husks are the main biomass resources in ASEAN countries. In Malaysia, the second largest palm oil producing country in the world, 30 million tonnes of palm oil wastes were generated in year 2000 with the rate of palm oil waste production increasing rapidly due to the expansion of food and manufacturing industries (Yang et al., 2006). In year 2010, approximately 368 palm oil mills operated in the country, which produced substantial amount of lignocellulosic biomass in the form of fibre, empty fruit bunches (EFB) and palm kernel shell. It was estimated that the amount of solid waste produced could reach 39 million tonnes by the year 2020 (Yusoff, 2006). Meanwhile, worldwide annual production of rice husks is around 100 million tonnes, 90% of which is generated in developing countries (Bridgwater & Boocock, 1997). Currently most of the biomass wastes (palm oil wastes and rice husks) are incinerated or utilised as boiler fuels for

steam generation. They have also been used as medium density fibre board in furniture and material for insulation and construction industries (Kelly-Yong et al., 2007). Even though there are a number of researches investigating the ways of utilising these wastes there is still a large fraction of these residues abundantly unattended (Yusoff, 2006). Perhaps these residues can be better utilised as biomass fuel. Nevertheless, in order to get an efficient combustion process of burning biomass, a better understanding of the oxidation process is needed.

The promising thermal approach that has been used for the laboratory scale study of biomass combustion or oxidation is EGA technique. EGA experiments involve subjecting a mixture of the fuel sample and sand to a programmed heating rate under a constant flow of an oxidising gas. The produced gas is continuously analysed for its carbon monoxide (CO), carbon dioxide (CO_2) and oxygen (O_2) contents. EGA runs provide information on the types of reactions occurring by comparing the carbon oxides (CO and CO_2) production to oxygen consumption. EGA is the most useful technique to determine the nature and amount of volatile products formed during the thermal degradation of materials (Materazzi et al., 2006). Bridgwater & Boocock (1997) studied the pyrolytic decomposition and subsequent combustion of rice husks using EGA technique. They found that the total system pressure has no effect on patterns of rice husk decomposition whereas varying the oxygen partial pressure affects the decomposition patterns. Except for the study by Bridgwater & Boocok (1997), a limited study has been reported on the use of EGA technique on the decomposition of biomass (i.e. cellulose and lignin contents). By using the EGA technique, most of the researchers only concentrate on investigating the emission gases of the biomass combustion for example study by Harimi et al. (2005) on the numerical analysis of emission component from incineration of palm oil wastes (fibre and shell). They revealed that gaseous emissions of SOx, NOx and CO generated from burning palm oil waste biomass fuels such as shell and fibre are much lower in comparison with heavy fuel oil. Recently, Porteiro et al. (2010) investigated the experimental analysis of the ignition front propagation of wood, Refuse Derived Fuel (RDF) and pine in a fixed bed combustor. They revealed that the RDF pellet presents the poorest velocities due to its low calorific value, high moisture and ash content and large particle size. Furthermore, the bigger the particles, the lower the surface area per volume ratio, lessening inter-particle heat transfer.

To date only limited studies have been undertaken of the fundamentals aspects (i.e. combustion characteristics) of Malaysian palm fibres and Australian rice husks decomposition on heating; most of the research carried out has been concerned with practical aspects of biomass gasification, pyrolysis or combustion. The few fundamental works that has been carried are using thermogravimetric analysis (TGA) technique to determine patterns of weight loss from a very small sample of biomass. Fundamental studies of the oxidation kinetics of biomass by Bridgwater & Boocok (1997) and crude oil by Kisler (1995) and Nguyen (2004) suggested that the EGA technique offer several advantages as it could provide information both supplementary and complementary to that obtained in TGA. Furthermore, it uses a larger sample size and longer experimental running time hence reduces the impact of short term fluctuations in the data. The aim of this work is therefore to investigate the combustion characteristics of Malaysian palm fibres and Australian rice husks using a series of EGA experiments. The effect of

varying system pressure and oxygen partial pressure on the biomass materials will be reported.

EXPERIMENTAL APPARATUS AND PROCEDURE

Biomass and sand

Australian rice husks originated from New South Wales and Malaysian palm fibres obtained from oil palm mill located in Nilai, Negeri Sembilan, were selected in this study. The characterisations of biomass materials are shown in Tab. 1. Fig. 1 (a) and (b) show the photograph of the Malaysian palm fibre and Australian rice husks, respectively. Proximate analysis was carried out according to ASTM standards (ASTM D5142 – 02a) using thermobalance TGA/SDRA51e manufactured by Mettler Toledo, while ultimate analysis was performed using a Thermo Finnigan Flashed 1112 analyser according to ASTM D5373 – 02. The calorific value was achieved based on ASTM D2015 – 96 via Ika-works C5000 calorimeter. Quartz sand was obtained from Commercial Minerals, of Victoria, Australia. This sand was nominal grade 300 µm to 600 µm (i.e. 300 µm < Grain size < 600 µm) and typically experiments were conducted using sand from 425-500 µm size range. Using a density flask the sand was experimentally determined to be 2.641 g/cm^3 (Kisler, 1995).

Experimental apparatus

A schematic flow diagram of the EGA apparatus is presented in Fig. 2 (a). On leaving the cylinder, the oxidising gas flows through a mass flow controller and into the combustion cell via a preheating coil. This arrangement allows the gas flowrate to the combustion cell inlet to be held constant independent of pressure within the cell. The combustion cell and preheating coil are both located inside a tube furnace. Effluent gases from the cell are passed through a water-cooled condenser and dryer system. The cooled and dried gases then flow to a back pressure regulator which is used to control the pressure within the combustion cell. The gases then pass through three gas analysers (O_2, CO and CO_2) connected in series. Finally the gases are vented to the atmosphere. Fig. 2 (b) shows a cross-section of the combustion cell. The combustion cell and preheating coil are placed in the centre of the tube furnace with the water-cooled condenser above and to one side. The stainless steel preheating coil of nominal 3-mm diameter is wound in a spiral coil. Gas passes through the preheating coil and then into the base of the cell. The function of the preheating coil is to ensure that the gas entering the cell is preheated to the same temperature as the cell. The combustion cell is a cylindrical steel vessel, designed to withstand pressures in excess of 900kPa, closed at both ends with plugs, O-rings and screwed on end caps. The O-rings are made of copper to provide an effective high temperature pressure seal. Within the cell are two thin-walled stainless steel cups with perforated bases to allow gas to pass through. The bottom cup is filled with sand and acts as both a flow distributor and a final preheater for the gas passing through the cell. The upper cup is 27.0mm in diameter and 70.7mm high. This is the sample cup which holds the mixture of biomass material and sand used in the study.

Tab.1: Ultimate and proximate analyses of Malaysian palm fibres and Australian rice husks.

Analyses	Malaysian palm fibre	Australian rice husks
Proximate analysis (db) (wt.%)		
Volatile matter	68.8	64.2
Fixed carbon	15.2	17.4
Ash	10.2	18.4
Ultimate analysis (daf) (wt.%)		
Carbon	43.19	40.90
Hydrogen	5.24	4.82
Nitrogen	1.59	0.43
Sulphur	0.19	0.17
Oxygen[a]	49.79	53.68
Calorific value (MJ/kg)	19.00	15.50

db – Dry basis; daf – dry ash free basis.

[a] Calculated by difference

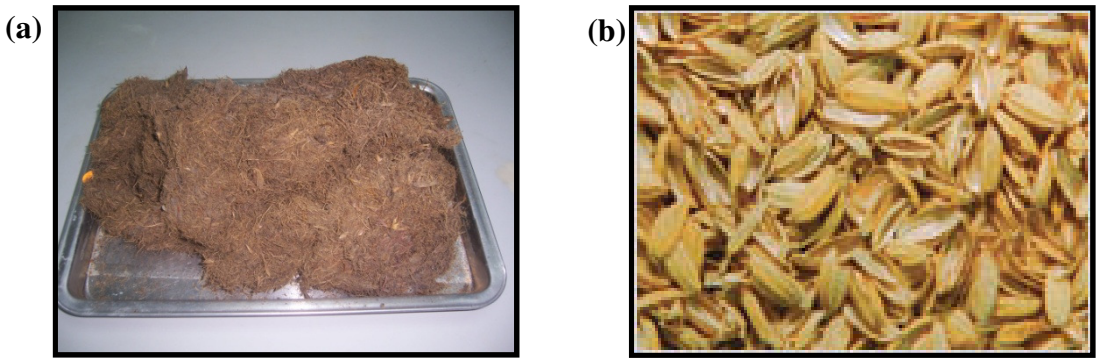

Fig.1: Photographs showing (a) Malaysian palm fibres (b) Australian rice husks

The sand functions both as a flow distributor and as a thermal capacitance, damping out temperature fluctuations associated with endothermic and exothermic decomposition or oxidation reactions ensuring that there are no localised temperature spikes. Quartz sand with a size range of 425-500µm and the bed porosity of 40 ± 0.5% is used. Screens of wire mesh are placed on the bottoms of both cups and on top of the sample cup to contain the sand. Seven variables are logged; cell temperature, furnace temperature, cell pressure, inlet gas flow rate and outlet gas composition (O_2, CO_2 and CO). Data readings are taken every 10 seconds. The injection gas flow rate was held at 400sml/min. A total of four gases were tested although air injection was used for the majority of the runs. The heating program involved heating at 50°C/hour from room temperature to 500°C. It was found that below 160°C to above 500°C no noticeable oxidation reactions occurred.

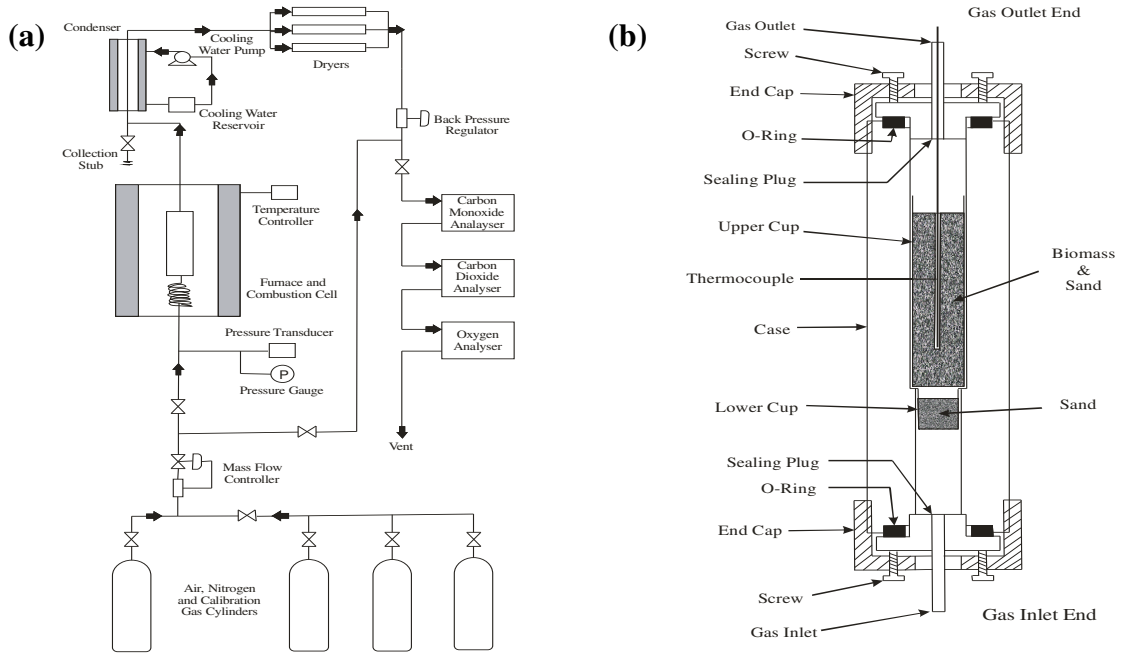

Fig.2: (a) Schematic flow diagrams of the EGA apparatus (b) Cross-section of the combustion cell.

Experimental procedure

The cell is loaded with the sample and placed in the furnace. The rig is then pressure tested to ensure that all connections are leak-tight. The furnace heater is switched on and the heating program and the pressure regulator are adjusted to give the desired heating rate and cell pressure. While the furnace is heating, the gas analysers are calibrated. Once the gas analyser has been calibrated and the cell temperature reaches 160°C, flow of gas through the cell commences at this point and the experimental run begins. The run is allowed to continue until gas composition readings of carbon oxides have ceased (500°C). Thereupon the gas heater is turned off, the cell allowed to cool and the gas analysers recalibrated.

Experimental program

A total of sixteen rice husk and palm fibre combustion experiments were carried out (eight runs each on rice husk and palm fibre). The first experiment of each rice husk and palm fibre was a preliminary experiment used to determine appropriate biomass to sand ratio. This experiment showed that if too much biomass were present, CO levels in the effluent gas could exceed the upper limit of the range set on the measuring instruments. In addition, during periods when exothermic reactions were occurring, cell temperatures could rise above the desired level subsequently increasing reaction rates, further accelerating rates of heat generation and leading to unwanted temperature and carbon oxide concentration “spikes”. On the other hand, too low a biomass content was found to give very low CO readings on the measuring instrument, thereby introducing

larger than desirable inaccuracies into measured gas compositions. As a result of Run 1 (rice husk) and Run 9 (palm fibre) experiments, a mixture of 0.5g of biomass in 40g of sand was settled on; for this mixture the rate of temperature increase in the cell remained linear while at the same time effective use was made of the measuring instrument ranges. The remaining experiments were performed firstly to establish the reproducibility of the results obtained using the evolved gas analysis (EGA) technique and secondly to investigate the effect of system pressure and oxygen partial pressure of the biomass materials.

RESULTS AND DISCUSSION

Fig. 3 and 4 show the gas compositions at pressure of 500kPa, heating rate of 80°C/hour and flow rate of 400sml/min temperature of rice husk and palm fibre combustions, respectively. Actual carbon monoxide and carbon dioxide levels in the effluent gas are shown together with the difference between the oxygen levels in the influent and effluent gases. These plots were all of similar forms, having two main peaks, one in the 260°C to 280°C region and the other in the 340°C to 380°C region except for CO curve that only appear to have only one peak for rice husk combustion. This experiment was conducted of the slow heating rate and the high frequency in which gas composition measurements were recorded once in every ten seconds. As a result, peak temperatures of all gas compositions could be very accurately determined which were 271.4°C for the first peak and 357.9°C for the second peak for rice husk combustion within 0.3°C (see Fig. 3). As for palm fibre combustion, the first and second peak temperatures are 265.3°C and 355.5°C within 0.3°C, respectively (see Fig. 4). The results agree reasonably well with those of similar studies of rice husk decomposition study using EGA technique by Bridgwater & Boocok (1997) and wood, RDF and pine combustion in a fixed bed combustor by Porteiro et al. (2010). On the basis of these similarities, the above two peaks may be taken to define periods during which decompositions of first hemicellulose and then cellulose escape from the rice husks and undergo combustion. Those peaks may be referred to as the hemicellulose and cellulose peaks, respectively.

Reproducibility of results

The reproducibility results of the evolved gas analysis (EGA) technique was validated by comparing the values of the peak temperature and peak height obtained for runs performed under similar sets of operating conditions. Tab. 2 shows the results of runs perform under identical conditions for rice husk and palm fibre combustions. As may be seen in Tab. 2, the hemicellulose and cellulose peaks lay almost exactly at the same peak temperature of 271.2°C and 358.1°C within 3°C for all three runs of carbon oxides production and O_2 consumed curves of rice husk combustion. Likewise, as for palm fibre combustion the two runs revealed the hemicellulose and cellulose peak temperatures of 266.1°C and 353.3°C within 2°C for all the gas compositions, respectively. From the results in Tab. 2, it was concluded that good reproducibility of the hemicellulose and cellulose peaks provided that a consistent biomass sample and weight were used.

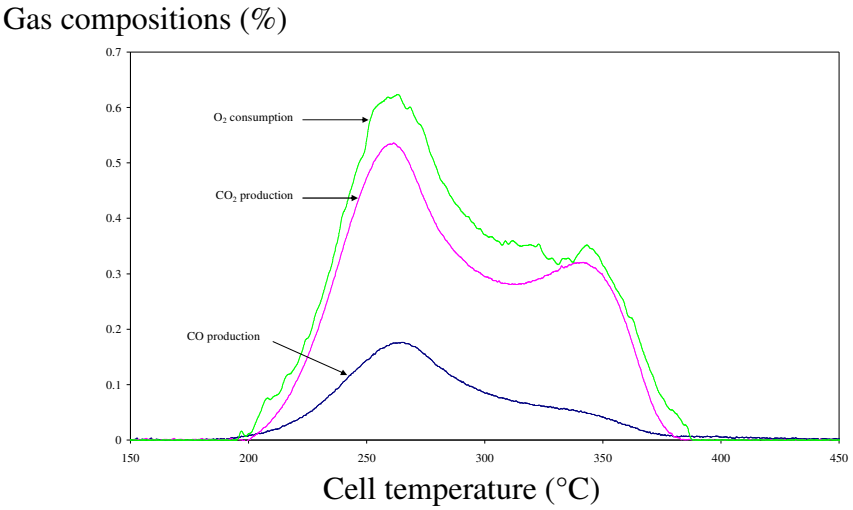

Fig. 3: Rice husk combustion characteristics at pressure of 500kPa, heating rate of 50°C/hour and flow rate of 400sml/min.

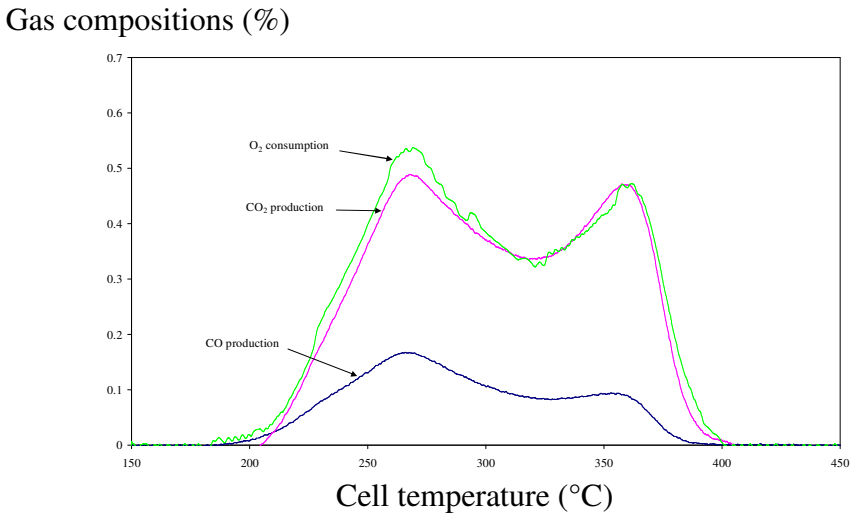

Fig. 4: Palm fibre combustion characteristics at pressure of 500kPa, heating rate of 50°C/hour and flow rate of 400sml/min.

Tab. 2: Results of runs perform under identical conditions of each biomass materials.

Sample	Run no.	Heating Rate (°C/h)	CO production Peak temperature (°C)		CO_2 production Peak temperature (°C)		O_2 consumption Peak temperature (°C)	
			Peak 1	Peak 2	Peak 1	Peak 2	Peak 1	Peak 2
Rice husk	2	80	271.6	-	271.1	355.0	271.1	360.8
	3	80	271.2	-	270.7	360.8	270.7	361.2
	4	80	271.4	-	270.9	356.7	270.7	357.7
Palm fibre	10	50	264.3	350.9	265.1	352.8	267.8	353.0
	11	50	264.5	355.3	266.0	355.3	265.0	355.6

Effect of system and oxygen partial pressures

A major advantage of EGA technique in comparison of TGA technique is the ease to study the influence of pressure and O_2 partial pressure on the combustion characteristics of biomass materials. The system pressure ranging from 363 to 700kPa and O_2 partial pressure of 76 to 147kPa were investigated for rice husk and palm fibre combustions. The oxygen concentrations of the inlet gas were varied appropriately in order to study the effects of system pressure and O_2 partial pressure. The results obtained are shown in Tab. 3. Fig. 5 and 6 illustrate the effect of system and O_2 partial pressures on the O_2 consumption of rice husk and palm fibre combustions, respectively. From Tab. 3 and Fig. 5 and 6 we may see that at the same O_2 partial pressure (76kPa), the system pressure has no significant effect on measured peak temperatures (only ~ 1 to 3°C) regardless of biomass materials and produced gases for both peaks (see Run 5 and 6 for rice husk combustion (Fig. 5) and Run 12 and 13 for palm fibre combustion (Fig.6)). The same observation was also reported by Bridgwater & Boocock (1997) in their rice husk decomposition study using EGA technique. This may be due to the fact that heat transfer into the rice husk is not materially affected by a change of gas pressure whereby heat transfer occurring predominantly by conduction through the solid portion of the biomass rather than by conduction and convection through the gases in the internal pores. Further, the evolution of volatiles from the surface of the biomass into the surrounding gas phase is not affected by the external pressure which implies that internal mass transfer resistances are small compared to the quantities of gas seeking to migrate to the surface. This would be consistent with rates of decomposition within the biomass being heat transfer-limited (Bridgwater & Boocock, 1997). As O_2 partial pressure increases, the peak temperatures decrease regardless of biomass materials and produced gases for both peaks (see Run 7 and 8 for rice husk combustion (Fig. 5) and Run 14 and 15 for palm fibre combustion (Fig. 6)). Again, the results agree reasonably well with Bridgwater & Boocock (1997). Oxidation reactions would be predominantly gas phase reactions until the efflux of volatile, combustible decomposition products from the biomass fell to a fairly low level which is after the cellulose decomposition products had been evolved. The effect of varying the O_2 partial pressure may be inferred to reflect a change in the rate of the gas phase oxidation reactions. For such a change to manifest itself as a change in peak temperature, maybe some of the combustible products of biomass must be escaping unburned (Bridgwater & Boocock, 1997). However, further studies have to be carried out in order to understand this behaviour.

CONCLUSION

Combustion characteristics of Australian rice husk and Malaysian palm fibre have been investigated using EGA technique. Evidently, the EGA experiments described here were sufficient to show that the results are reproducible provided that a consistent biomass sample and weight were used. Apparently, system pressure has no effect on patterns of both biomass decompositions whereas higher O_2 partial pressure shifted the peak temperatures towards lower temperatures regardless of biomass materials and produced gases for both of the peaks. Nevertheless, future studies will be conducted in order to further understand the behaviour of the biomass decompositions using EGA technique.

Tab.3: The effect of system and oxygen partial pressure on peak temperatures of rice husk and palm fibre combustions.

Run no.	P (kPa)	O_2 conc. in gas (mol %)	O_2 partial pressure (kPa)	CO production Peak temperature (°C)		CO_2 production Peak temperature (°C)		O_2 consumption Peak temperature (°C)	
				Peak 1	Peak 2	Peak 1	Peak 2	Peak 1	Peak 2
Rice husk									
5	362	20.96	76	262.4	-	261.5	346.8	261.2	342.5
6	500	15.10	76	260.2	-	258.0	345.8	258.2	347.5
7	500	20.96	105	248.3	-	247.9	330.2	247.8	329.5
8	700	20.96	147	233.3	-	233.3	314.9	233.3	316.5
Palm fibre									
12	362	20.96	76	274.8	367.0	275.0	367.3	276.0	366.9
13	420	18.10	76	274.5	366.0	275.0	364.2	273.0	365.9
14	500	20.96	105	264.5	355.3	266.0	355.3	265.0	355.6
15	700	20.96	147	254.6	346.1	254.7	345.7	253.6	344.8

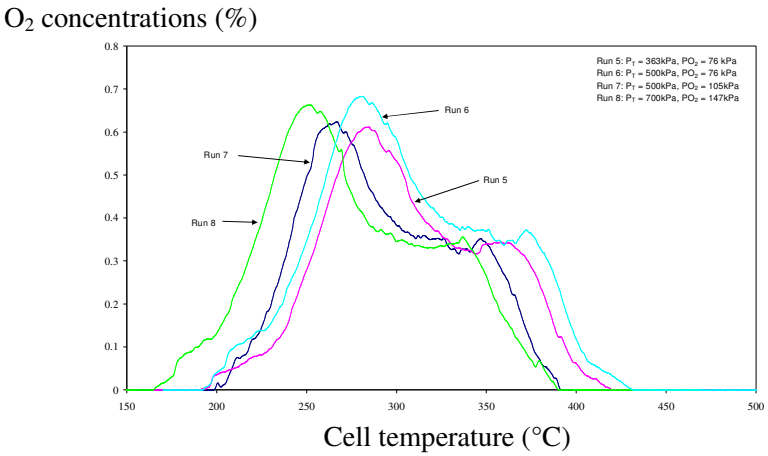

Fig. 5: The effect of O_2 consumptions of rice husk combustion at various system pressures and O_2 partial pressures.

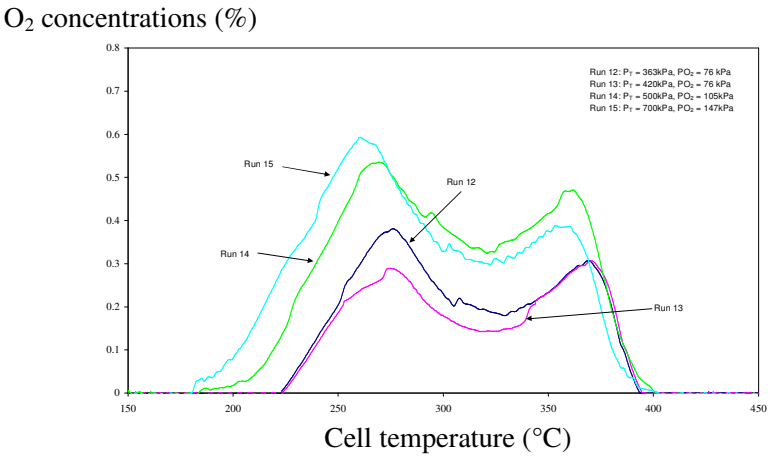

Fig. 6: The effect of O_2 consumptions of palm fibre combustion at various system pressures and O_2 partial pressures.

ACKNOWLEDGEMENTS

The authors would like to thank The University of Melbourne, University Technology MARA and Ministry of Higher Education Malaysia for their support.

REFERENCES

Bridgwater, A.V., Boocock, D.G.B. 1997. 'Developments in thermochemical biomass conversion.' Vol. 1: 67-81. Chapman & Hall.

Guan, C.T. 2003. 'Technical Update: Biomass: Renewable Energy Sources in Malaysia.' *Quarterly Bulletin of the Department of Environment Malaysia (MOSTE)*, Vol. 2: 15-16.

Harimi, M., Megat Ahmad, M.M.H., Sapuan, S.M., Idris, A., (2005), 'Numerical analysis of emission component from incineration of palm oil wastes', *Biomass and Bioenergy*, **28(3)**, pp. 339-345.

Kelly-Yong, Lee, T.L., Mohamed, A.R., Bhatia, S., (2007), 'Potential of hydrogen from oil palm biomass as a source of renewable energy worldwide', *Energy policy*, **11**, pp. 5692-5701.

Kisler, J. 1995. 'The application of in situ combustion to light Australian oils.' *Department of Chemical & Biomolecular Engineering*, PhD Thesis, University of Melbourne: Melbourne.

Materazzi, S., Gentili, A., Curini, R., (2006), 'Applications of evolved gas analysis Part 2: EGA by mass spectrometry', *Talanta*, **69**, pp. 781-794.

Nguyen, T.T. 2004. 'Oxidation kinetics of Vietnamese crude oil.' *Department of Chemical & Biomolecular Engineering*, Masters Thesis, University of Melbourne: Melbourne.

Porteiro, J., Patino, D., Collazo, J., Granada, E., Moran, J., Miguez, J.L., (2010), 'Experimental analysis of the ignition front propagation of several biomass fuels in a fixed-bed combustor', *Fuel*, **89(1)**, pp. 26-35.

Yang, H., Yan, R., Chen, H., Lee, D.H., Liang, D.T., Zheng, C., (2006), 'Pyrolysis of palm oil wastes for enhanced production of hydrogen rich gases', *Fuel Processing Technology*, **87**, pp. 935-942.

Yusoff, S., (2006), 'Renewable energy from palm oil - innovation on effective utilization of waste', *Journal of Cleaner Production*, **14(1)**, pp. 87-93.